

# **Molecular Investigations of Ovarian Clear Cell Carcinoma – a Treatment Resistant Malignancy**

**by Yue Ma**

Thesis submitted in fulfilment of the requirements for  
the degree of

**Doctor of Philosophy**

under the supervision of

Professor Deborah Marsh,  
A/Professor Nham Tran

University of Technology Sydney  
Faculty of Sciences  
School of Life Sciences (SoLS)

August 2024

# CERTIFICATE OF ORIGINAL AUTHORSHIP

I, Yue Ma, declare that this thesis is submitted in fulfilment of the requirements for the award of *Doctor of Philosophy*, in the School of Life Sciences, Faculty of Science at the University of Technology Sydney.

This thesis is wholly my own work unless otherwise referenced or acknowledged. In addition, I certify that all information sources and literature used are indicated in the thesis.

This document has not been submitted for qualifications at any other academic institution.

This research is supported by the Australian Government Research Training Program.

Signature: Production Note:  
Signature removed prior to publication.

Date: 10. August. 2024

# Acknowledgements

I would like to express my sincerest thanks to all those who have provided me with support and assistance throughout this challenging four-year journey.

Firstly, I am deeply grateful to my supervisor, Professor Deborah Marsh, for your invaluable guidance, support, and encouragement throughout this process. Your expertise and insights have been crucial in shaping this thesis. I am especially thankful for the opportunity to be your first Honours student as well as your first PhD student at UTS. Your support in attending various academic conferences and presenting my research in the US has been greatly appreciated. Your care and attention have made me feel like I am with family during these years of study. I would also like to extend my heartfelt thanks to my co-supervisor, A/Professor Nham Tran, for your expert advice, guidance, and critical feedback, especially during my Stage 3.

I would like to thank the members of the Translational Oncology Group (TOG) for their assistance throughout the duration of my Ph.D. Special thanks to Mrs. Kristie Dickson, who taught me many of my experimental techniques and guided me based on the direction of my research. Your advice while I was writing this thesis was invaluable. I am also grateful to Dr. Christine Yee, a past member of our research group, for teaching me about 3D bioprinting and assisting with experiments during the COVID-19 pandemic. A special mention to your lovely dogs, Maccha and Mojo, for their positive influence. I would like to thank Dr. Amani Alghalayini and Dr. Amy Sarker for their help and encouragement throughout the years. Thank you to all the students in TOG: Tao Xie, Natisha Field, Tali Skipper, Kiara Heyward, and Phoebe Hunt, for your help and advice. I would also like to thank Sarina Briscas, a past student who worked alongside me in 3D bioprinting.

My gratitude also extends to Dr. Alen Faiz from the CRISPR facility for providing the CRISPR technology and resources, and to Mr. Kun Xiao for his assistance with flow cell sorting. I extend my gratitude to the UTS Faculty of Science Level-7 laboratory management team. Special thanks to Mercedes Ballesteros for reminding me to take breaks, Sarah Osvath for assisting with laboratory equipment, and Luke Beebe for helping me find a suitable chair,

allowing me to complete this thesis in comfort. I would also like to thank Dr. Alex Volkerling, formerly at INVENTIA Life Science and now with Franklin.ai, for your support with 3D bioprinting.

I am very grateful for the financial support provided by the UTS-CSC International Research Scholarship (IRS), which allowed me to focus on my research without being burdened by financial pressures.

Most importantly, I am deeply grateful to my family for their unwavering love and support. Your consistent encouragement has been a constant source of motivation throughout this journey.

Finally, thank you to my partner, Miss Weihsin Juan, for your unconditional love, for being by my side all the time, and for supporting me from the beginning to the end of this thesis.



# Abstract

Ovarian cancer (OC) is the eighth most common cancer and the eighth leading cause of cancer deaths in women worldwide. It is the deadliest of all gynaecological malignancies. Epithelial ovarian cancer (EOC) accounts for approximately 90% of these cases, with ovarian clear cell carcinoma (OCCC) representing the second most common subtype of EOC. OCCC exhibits unique biological characteristics and a poor prognosis, underscoring the urgent need for new therapeutic approaches. The chromatin remodelling complex Switch/Sucrose Non-Fermentable (SWI/SNF) regulates a number of processes, including cell development, proliferation, differentiation and DNA repair, which plays a crucial role in the differentiation of a wide range of cells. AT-rich interaction domain 1A (*ARID1A*) and *ARID1B* encode two subunits of SWI/SNF, and, especially *ARID1A*, has a high mutation rate in OCCC. The overall aim of this thesis was to identify new therapeutic compounds that could be repurposed to treat OCCC, as well as develop CRISPR-Cas9 engineered models of OCCC for future studies.

Initially, we confirmed that the seven OCCC cell lines used in this study (RMG-I, JHOC-5, OV207, OVTOKO, OVMANA, OVISe, and TOV-21G) displayed epithelioid features and characteristic cell shapes and nuclei as reported in the literature. Short tandem repeat (STR) analyses were used for cell line authentication, and Sanger sequencing verified the reported mutations in *ARID1A* and *ARID1B*. Some cell lines, including OVISe, OV207, OVMANA, and TOV-21G, exhibited heterozygous mutations in *ARID1A*, while OVISe and TOV-21G showed heterozygous mutations in *ARID1B*. Western blot analyses revealed ARID1A protein of the expected size in RMG-I, JHOC-5, and OV207 cells, with faint protein levels observed in OVTOKO and OVISe cells, and an absence of protein in OVMANA and TOV-21G cells. ARID1B protein was observed in all OCCC cell lines. Platinum sensitivity assays indicated that *ARID1A* and/or *ARID1B* mutation status did not influence sensitivity of cells to platinum compounds.

Seven OCCC cell lines and 3 non-OCCC cell lines (A2780.b1, COV434, and OVCAR-8) were screened using the Tocriscreen Epigenetics Library 3.0 consisting of 160 drug compounds targeting epigenetic readers, writers and erasers, as well as transcriptional modulators, at 5  $\mu$ M and 0.5  $\mu$ M concentrations. Results demonstrated that the Bruton's Tyrosine Kinase (BTK) inhibitor ibrutinib significantly reduced OCCC cell viability compared to non-OCCC cells, with lower ibrutinib IC<sub>50</sub> values observed in OCCC cell lines. The BTK target of ibrutinib was

detected in all seven OCCC cell lines. Three-dimensional (3D) cell line models, created using 3D bioprinting technology, identified the fibronectin tripeptide Arg-Gly-Asp (RGD) as the optimal matrix for OCCC cells. IC50 values of ibrutinib were higher in 3D models of OCCC cell lines compared to 2D models.

We used clustered regularly interspaced short palindromic repeats (CRISPR)-Cas9 technology to generate isogenic panels of ARID1A and/or ARID1B knockout (KO) in OCCC cell lines reported to be wild-type (WT) for *ARID1A* and *ARID1B*, specifically RMG-I and JHOC-5. A pipeline was established to generate and test these genetically engineered cell lines. We found that both ARID1A and ARID1B cannot be completely knocked out in a single cell line, supporting previous reports that dual loss of these paralogues is synthetic lethal in cells. Functional analyses of the isogenic ARID1A and ARID1B panels indicated that the proliferation rate of most engineered cells decreased compared to the WT cell line, with the exception of two RMG-I ARID1A engineered cells. Additionally, all JHOC-5 engineered cells, along with one ARID1A and one ARID1B engineered cell line originating from RMG-I cells, exhibited resistance to cisplatin. The other RMG-I engineered cells were sensitive to cisplatin compared to the WT cell line. Furthermore, ARID1A KO led to decreased expression of *STAG1*, the gene encoding the STAG1 Cohesin Complex Component in JHOC-5 cells and most RMG-I cells with roles in DNA replication and repair.

The major discovery of this thesis that ibrutinib shows potential as a new inhibitor of OCCC cell line viability will be further explored in pre-clinical and, if promising, ultimately clinical settings. Interestingly, ibrutinib has recently been used to treat two patients with low-grade serous ovarian cancer, with efficacious results. The CRISPR-Cas9 pipelines determined as part of this study will be used to knockout multiple proteins of interest in cancer cell lines into the future. The ARID1A isogenic cell line panels generated as part of this study will be used in future discovery science projects to elucidate roles for ARID1A, as well as in translational projects to identify promising drug candidates for *ARID1A*-mutated OCCC.

### Manuscripts arising from thesis

1. **Ma Y**, Field NR, Xie T, Briscas S, Kokinogoulis EG, Skipper TS, Alghalayini A, Sarker FA, Tran N, Bowden NA, Dickson K-A, and Marsh DJ. Aberrant SWI/SNF complex members are predominant in rare ovarian malignancies – therapeutic vulnerabilities in treatment resistant subtypes. *Cancers*. (Submitted, 9/8/2024).
2. Yee C, Dickson KA, Muntasir MN, **Ma Y**, Marsh DJ (2022). Three-Dimensional Modelling of Ovarian Cancer: From Cell Lines to Organoids for Discovery and Personalized Medicine. *Front Bioeng Biotechnol* 10:836984. PMID: 35223797.

### Manuscripts in preparation from this thesis

1. **Ma Y**, Dickson K-A, *et al.*, and Marsh DJ. Epigenetic compound library screen identifies ibrutinib as an inhibitor of ovarian clear cell carcinoma viability. (In preparation).

### Publication related to this thesis

1. Dickson KA, Field N, Blackman T, **Ma Y**, Xie T, Kurangil E, Idrees S, Rathnayake SNH, Mahbub RM, Faiz A, Marsh DJ (2023). CRISPR single base-editing: in silico predictions to variant clonal cell lines. *Hum Mol Genet* 32(17):2704-2716. PMID: 37369005.
2. Xie T, Dickson KA, Yee C, **Ma Y**, Ford CE, Bowden NA, Marsh DJ (2022). Targeting homologous recombination deficiency in ovarian cancer with PARP inhibitors: synthetic lethal strategies that Impact overall survival. *Cancers (Basel)* 14(19):4621. PMID: 36230543.
3. Dickson KA, Xie T, Evenhuis C, **Ma Y**, Marsh DJ (2021). PARP inhibitors display differential efficacy in models of BRCA mutant high-grade serous ovarian cancer. *Int J Mol Sci* 22(16):8506. PMID: 34445211.
4. Marsh DJ, **Ma Y**, Dickson KA (2020). Histone monoubiquitination in chromatin remodelling: focus on the histone H2B interactome and cancer. *Cancers (Basel)* 12(11):3462. PMID: 33233707.

## Conference abstracts associated with this thesis

1. **Ma Y**, Dickson KA, Field N, Xie T, Marsh DJ. Epigenetic compound library screen of ovarian clear cell carcinoma cell line models identifies decreased cell viability following treatment with the Bruton tyrosine kinase inhibitor ibrutinib. *American Association for Cancer Research (AACR) Special Conference in Cancer Research: Ovarian Cancer*, October 5th, 2023, Boston, USA. (Poster)
2. **Ma Y**, Dickson KA, Field N, Xie T, Marsh DJ. The Bruton tyrosine kinase inhibitor ibrutinib shows efficacy in the treatment of ovarian clear cell carcinoma cell line models. *European Molecular Biology Laboratory Australia Postgraduate Symposium (EAPS)*, November 1st, 2023, Sydney, Australia. (Poster)
3. **Ma Y**, Dickson KA, Field N, Xie T, Marsh DJ. Epigenetic compound library screen of ovarian clear cell carcinoma cell lines. *Australia and New Zealand Gynaecological Oncology Group (ANZGOG) Scientific Meeting*, March 22nd, 2023, Sydney, Australia. (Poster)
4. **Ma Y**, Dickson KA, Yee C, Faiz A, Tran N, Marsh DJ. Generating CRISPR knockout ARID1A/B SWI/SNF complex members in ovarian clear cell cancer cell lines. *Australian Society for Medical Research (ASM) National Scientific Conference*, November 10th, 2022, Sydney, Australia. (Poster)
5. **Ma Y**, Dickson KA, Yee C, Faiz A, Tran N, Marsh DJ. Generating CRISPR knockout ARID1A/B SWI/SNF complex members in ovarian clear cell cancer cell lines. *NSW Cancer Conference 2022*, September 15th, 2022, Sydney, Australia. (Poster)

**NOTE:** Bold and underlined name denotes the presenting author.

# List of Abbreviations

2D	Two-dimensional
3D	Three-dimensional
5-FU	Fluorouracil
AAV2 ITR	Adeno-associated virus 2 inverted terminal repeats
AIHW	Australian Institute of Health and Welfare
AKT	Protein kinase B
AKT1	AKT Serine/Threonine Kinase 1
ALDH1A1	Aldehyde Dehydrogenase 1 Family Member A1
AmpR	Ampicillin resistance gene
ARID1A	AT-rich interaction domain 1A
ARID1B	AT-rich interaction domain 1B
ATCC	American Type Culture Collection
ATP	Adenosine triphosphate
BAF	BRG1/BRM-associated factor
BbsI	Type IIS restriction enzyme site
BCA	Bicinchoninic Acid
BCR	B cell receptor
BER	Base excision repair
bGH poly(A)	Bovine growth hormone polyadenylation
BMI	Body mass index
BRAF	B-Raf Proto-Oncogene, Serine/Threonine Kinase
BRCA1	Breast cancer 1
BRCA2	Breast cancer 2
BSA	Bovine serum albumin
BTK	Bruton tyrosine kinase
CA-125	Cancer antigen 125
CAR	Chimeric antigen receptors
Cas9	CRISPR-associated protein 9
ccRCC	Clear cell renal cell carcinoma
CDKN1A	Cyclin-dependent kinase inhibitor 1A
CI	Confidence intervals
CLL	Chronic lymphocytic leukaemia

C <sub>max</sub>	Maximum plasma concentration
CMV	Cytomegalovirus
CR	Clinical remission
CRISPR	Clustered regularly interspaced short palindromic repeats
crRNA	CRISPR RNA
CSC	Cancer stem cell
CTG	CellTiter-Glo 3D Viability Assay
Cys-481	Cysteine at position 481 of the kinase structural domain
DBD	DNA binding domain
DepMap	Cancer Dependency Map Project at Broad Institute
dH <sub>2</sub> O	Distilled water
DH5α	5-alpha competent E. coli
DK	Double knockout
DMEM	Dulbecco's Modified Eagle's Medium
DMSO	Dimethyl sulfoxide
DNA	Deoxyribonucleic acid
DNMTs	DNA methyltransferases
DSBs	Double-strand breaks
DSMZ	Liebniz Institute
DTT	Dithiothreitol
DUSP4	Dual Specificity Phosphatase 4
E. coli	Escherichia coli
ECACC	European Collection of Authenticated Cell Cultures
ECCC	Endometrial clear cell carcinoma
ECM	Extracellular matrix
EcoRI	Restriction enzyme site EcoRI
EDTA	Ethylenediaminetetraacetic acid
EGFP	Enhanced green fluorescent protein
EGFR	Epidermal Growth Factor Receptor
EHMT2	Euchromatic histone-lysine N-methyltransferase 2
EnOC	Endometrioid ovarian cancer
EOC	Epithelial ovarian cancer
ErbB3	Erb-B2 receptor tyrosine kinase 3
ErbB4	Erb-B2 receptor tyrosine kinase 4

EU	European Union
EZH2	Enhancer of zeste homolog 2
FBS	Foetal bovine serum
FC $\gamma$ R	Fc- $\gamma$ receptor
FDA	US Food and Drug Administration
FIGO	International Federation of Gynaecology and Obstetrics
GCOC	Germ cell ovarian cancer
GCTs	Germ cell tumours
gDNA	Genomic DNA
GFP	Green fluorescent protein
GOF	Gain-of-function
H2Bub1	Histone H2B lysine 120
HBB	Haemoglobin Subunit Beta
HAT	Histone acetyltransferase
HbF	Fetal haemoglobin
HCS	High-content screening
HDAC	Histone deacetylases
HDR	Homology-directed repair
HE4	Human epididymis protein 4
HER2	Human epidermal growth factor receptor 2
HGSOC	High-grade serous ovarian cancer
HRR	Homologous recombination repair
HTS	High-throughput screening
IARC	International Agency for Research on Cancer
IC50	Half-maximal inhibitory concentration
IHC	Immunohistochemistry
IKVAV	Ile-Lys-Val-Ala-Val
IL-1	Interleukin-1
IL-18	Interleukin-18
IL-1 $\beta$	Interleukin 1 $\beta$
IP	Intraperitoneal
JCRB	Japanese Collection of Research Bioresources
kDa	Kilodaltons
KMTs	Histone lysine methyltransferase

KRAS	Kirsten rat sarcoma virus
LB	Luria-Bertani
LGSOC	Low-grade serous ovarian cancer
LOF	Loss-of-function
LSD	Lysine-specific histone demethylase
MCL	Mantle cell lymphoma
miRNA	MicroRNA
MOC	Mucinous ovarian cancer
MOPS	3-(N-morpholino) propanesulfonic acid
MRT	Malignant rhabdomyosarcoma
MSC	Mesenchymal stem cell
Mtor	Mammalian target of rapamycin
NARS	Asparaginyl-tRNA synthetase
ncBAF	Non-canonical BAF
NCI	National Cancer Institute
NHEJ	Non-homologous end joining
NHL	Non-Hodgkin lymphoma
NIR	Near infrared
NLRP3	Nucleotide-binding domain, leucine-rich-containing family, pyrin domain-containing-3
NLS	Nuclear localization signal
NRTK	Non-receptor tyrosine kinase
NSCLC	Non-small cell lung cancer
OCCC	Ovarian Clear Cell Carcinoma
ori	Origin of replication
OS	Overall survival
PAM	Protospacer-adjacent motif
PARP	Poly (ADP-ribose) polymerase
pBAF	Polybromo-associated BAF
PBS	Phosphate buffered saline
PCR	Polymerase Chain Reaction
PEG	Poly (ethylene glycol)
PEN/STREP	Penicillin-Streptomycin
PFS	Progression-free survival



PH	Pleckstrin homology
PI3K	Phosphatidylinositol-3-kinase
PIK3CA	Phosphatidylinositol-4,5-bisphosphate 3-kinase catalytic subunit alpha
PIK3IP1	Phosphoinositide-3-kinase-interacting protein 1
PNK	T4 Polynucleotide Kinase
polIII	RNA polymerase III
PRC2	Polycomb repressive complex 2
PRMT	Protein arginine N-methyltransferase
PTEN	Phosphatase and tensin homolog
PX458	pSpCas9(BB)-2A-GFP
qRT-PCR	Quantitative Real-Time Reverse Transcriptase PCR
RAD51C	RAD51 Recombinase C
RAD51D	RAD51 Recombinase D
RBP	RNA binding proteins
RGD	Arginine–glycine–aspartic acid
RLU	Relative light units
RNA	Ribonucleic acid
RNAi	RNA interference
RNAPII	RNA polymerase II
RNF	RING (Really Interesting New Gene) Finger Protein
RPMI	Roswell Park Memorial Institute Medium
SC	Subcutaneous
SCCOHT	Small Cell Carcinoma of the Ovary, Hypercalcemic Type
SCD	Sickle cell disease
SCSOC	Sex-cord stromal ovarian cancer
SDO	Standards Development Organization
SDS	Sodium Dodecyl Sulfate
sgRNA	Single guide RNA
SH2	SRC homology domain 2
SH3	SRC homology domain 3
siRNA	Small interfering RNAs
SMAD3	Mothers Against Decapentaplegic Homolog 3
SMARCA4	SWI/SNF Related, Matrix Associated, Actin Dependent Regulator Of Chromatin, Subfamily A, Member 4

SNP	STR include Single nucleotide polymorphisms
SOC	Serous ovarian cancer
SSBs	Single-strand breaks
STAG1	STAG1 Cohesin Complex Component
STR	Short tandem repeat
SV40	Simian Virus 40
SWI/SNF	SWItch/Sucrose Non-Fermentable
TBS	Tris-Buffered Saline
TFK	Tec kinase family
TGA	Therapeutic Goods Administration
TH	TEC homology
TLR	Toll-like receptor
T <sub>m</sub>	Melting temperatures
TMB	Tumour mutational burden
TNF $\alpha$	Tumour necrosis factor $\alpha$
TP53	Tumour Protein P53
tracrRNA	Trans-activated crRNA
TRIM11	Tripartite motif containing 11
tRNA	Transfer RNA
TVUS	Transvaginal ultrasonography
U6 promoter	U6 small nuclear RNA promoter
uHTS	Ultra-high throughput screening
USPs	Ubiquitin-specific proteases
UV	Ultraviolet
VEGF	Vascular endothelial growth factor
WHO	World Health Organisation
WT	Wild-type
YIGSR	Tyr-Ile-Gly-Ser-Arg

# List of Figures

Figure 1.1 Cancer rates per 100,000 population in Australia in 2023..	3
Figure 1.2 Global incidence and mortality of female cancers .....	4
Figure 1.3 Estimated number of Australian female cancer cases and deaths in 2023.....	5
Figure 1.4 Ovarian cancer rates per 100,000 population in Australia .....	6
Figure 1.5 Ovarian cancer subtypes and associated mutated genes.....	21
Figure 1.6 Percentage of different types of <i>TP53</i> somatic mutations found in human ovarian cancers.....	23
Figure 1.7. The haematoxylin and eosin (H&E) stained histology image of OCCC showing a predominantly papillary architecture .....	25
Figure 1.8 Schematic Representation of the interplay between EZH2, ARID1A, PIK3IP1, PI3K, AKT, mTOR, and PTEN in cell proliferation and survival .....	33
Figure 1.9 Information about CRISPR Knockout.....	36
Figure 3.1 Representative images of OCCC cell lines growing in 96-well plates captured with the IncuCyte S3 Live-Cell Imaging System with 10X objective.....	63
Figure 3.2 Allelic differences observed for the microsatellite marker D13S317 in our RMG-I cells compared to data held in the DMSZ database .....	64
Figure 3.3 DNA gel electrophoresis image of PCR amplified fragments containing mutation sites in different cell lines .....	65
Figure 3.4 Sanger sequencing of the four OCCC cell lines OVISE, OVTOKO, OVMANA and TOV-21G for <i>ARID1A</i> mutations .....	66
Figure 3.5 Sanger sequencing of two OCCC cell lines, OVISE and TOV-21G, for <i>ARID1B</i> mutations.....	67
Figure 3.6 <i>ARID1A</i> and <i>ARID1B</i> mRNA expression levels for all OCCC cells. ....	68
Figure 3.7 Protein expression levels of all OCCC cell lines.....	69
Figure 3.8 IC50 of cisplatin and carboplatin in OCCC cell lines. ....	70
Figure 3.9 Comparison of IC50 of cisplatin and carboplatin in seven OCCC cells. ....	71
Figure 4.1 Schematic diagram of the bioprinting process using the RASTRUM bioprinter...	78
Figure 4.2 Workflow of treating ovarian cancer cell lines with the Tocris drug screening library.....	80
Figure 4.3 Flow diagram summarising inclusion and exclusion criteria for drug compounds in the Tocriscreen Epigenetics Library 3.0 screened against ovarian cancer cell lines. ....	81

Figure 4.4 Layout of the RASTRUM 3D bioprinter cartridge .....	85
Figure 4.5 Workflow of 3D bioprinting with the RASTRUM platform to test cell viability after drug treatment.....	86
Figure 4.6 Scatter plot of cell viability in 10 ovarian cancer cell lines after treatment with the 160 drug compound screening library .....	88
Figure 4.7 Heatmap of cell viability in 10 ovarian cancer cell lines after treatment with the drug screening library .....	90
Figure 4.8 Result of selecting compounds of interest from the Tocriscreen epigenetics 3.0 library screening.....	92
Figure 4.9 Heatmap of Log (2) fold change in cell viability after treatment with ibrutinib (Drug 152) at 5 and 0.5 $\mu$ M concentrations in seven OCCC and three non-OCCC ovarian cancer cell lines.....	93
Figure 4.10 Bar chart of cell viability in seven OCCC and three non-OCCC ovarian cancer cell lines after treatment with the Drug 152 (ibrutinib) at (A) 5 $\mu$ M and (B) 0.5 $\mu$ M concentrations. ....	94
Figure 4.11 mRNA expression level of BTK in all OCCC cells normalised to HEK293 cells .....	95
Figure 4.12 Ibrutinib dose curves of 10 ovarian cancer cell lines .....	96
Figure 4.13 IC <sub>50</sub> of ibrutinib in 10 ovarian cancer cell lines. ....	97
Figure 4.14 Comparison of IC <sub>50</sub> of ibrutinib in seven OCCC cells in 2D.....	98
Figure 4.15 Bar chart of growth trends for matrix selection in 3D bioprinted OCCC cell lines RMG-I and JHOC-5.....	100
Figure 4.16 Bar chart of cell culture growth trends of seven 3D bioprinted OCCC models. ....	101
Figure 4.17 Ibrutinib dose curves of 7 bioprinted OCCC cell lines .....	103
Figure 4.18 IC <sub>50</sub> of ibrutinib in 7 bioprinted OCCC cell lines .....	104
Figure 4.19 Comparison of IC <sub>50</sub> of ibrutinib in seven OCCC cells in 3D.....	105
Figure 4.20 Summary of IC <sub>50</sub> of ibrutinib in 7 OCCC cell lines in 2D and 3D bioprinted models .....	105
Figure 4.21 Images of RMG-I and JHOC-5 3D bioprinted cell lines treated with ibrutinib or DMSO control and stained using the LIVE/DEAD viability assay.....	107
Figure 4.22 Schematic overview of the structure of Bruton's tyrosine kinase (BTK).....	109
Figure 4.23 Structures of BTK isoforms. BTK-C has a 34-amino acid extension of PH domain.....	111
Figure 5.1 Workflow for generating CRISPR KO cancer cell lines.....	119

Figure 5.2 Effect of ARID1A and ARID1B KO on cell lines .....	120
Figure 5.3 PX458 vector map .....	121
Figure 5.4 Representative images of three RMG-I clonal lines.....	133
Figure 5.5 Growth rate of RMG-I parental and clonal lines over 72h.....	134
Figure 5.6 IC50 cisplatin concentration of RMG-I parental and clonal lines b4, c9 and b10 determined by MTS assay 72 hours post treatment .....	135
Figure 5.7 Representative images of JHOC-5 parental and three JHOC-5 clonal lines. ....	136
Figure 5.8 Growth rate and cell viability of the JHOC-5 parental line and clonal cell lines.	137
Figure 5.9 Sequence confirmation of <i>ARID1A</i> sgRNA cloned into the CRISPR-Cas9 vector PX458 .....	138
Figure 5.10 Transfection of RMG-I.b4 clonal cells with <i>ARID1A</i> plasmid DNA using lipofectamine 3000 transfection reagent for 24 hours .....	139
Figure 5.11 Flow cytometry analysis of RMG-I.b4 clonal cells transfected with reagent control and <i>ARID1A</i> exon 1 or exon 2 targeting plasmid vectors.....	140
Figure 5.12 Representative alignment of Sanger sequencing of RMG-I CRISPR KO <i>ARID1A</i> Exon1 (RAE1AB5; upper panel) and Exon2 (RAE2BC9; lower panel) clones in Benchling .....	142
Figure 5.13 Protein levels of ARID1A in ARID1A CRISPR KO cells.....	144
Figure 5.14 Flow diagram summarising inclusion and exclusion criteria for the RMG-I.b4 CRISPR KO cell cohort. Single cells were flow sorted into 190 wells for each exon. ....	145
Figure 5.15 Transfection of JHOC-5.d12 cells with <i>ARID1A</i> CRISPR KO plasmid DNA using lipofectamine LTX reagent for 39 hours and flow cytometry analysis of JHOC-5.d12 transfected with reagent control (RC) and <i>ARID1A</i> CRISPR KO plasmid DNAs .....	146
Figure 5.16 Flow cytometry analysis of JHOC-5.d12 clonal cells transfected with reagent control and <i>ARID1A</i> exon 1 or exon 2 targeting plasmid vectors.....	147
Figure 5.17 Representative protein levels of ARID1A in ARID1A CRISPR JHOC-5 KO clones. ....	148
Figure 5.18 Representative alignment of Sanger sequencing of JHOC-5 CRISPR KO <i>ARID1A</i> Exon2 (RAE2BE10) clones in Benchling.....	148
Figure 5.19 Flow diagram summarising inclusion and exclusion criteria for CRISPR-Cas9 KO of ARID1A in the JHOC-5.d12 cell cohort .....	150
Figure 5.20 Sanger sequencing validated that sgRNA targeting A) <i>ARID1B</i> exon 6, and B) <i>ARID1B</i> exon 10, were successfully cloned into PX458.....	151

Figure 5.21 Transfection comparison between lipofectamine 3000 and X-tremeGENE HP in RMG-I.b4 cells transfected with the CRISPR-Cas9 KO plasmid targeting <i>ARID1B</i> exon 6.	152
Figure 5.22 Transfection of RMG-I.b4 clonal cells with CRISPR-Cas9 KO vectors targeting <i>ARID1B</i> using X-tremeGene HP reagent for 48 hours	153
Figure 5.23 Flow cytometry analysis of RMG-I.b4 clonal cells transfected with <i>ARID1B</i> CRISPR-Cas9 KO plasmid DNA (targeting exon 6 or exon 10) or reagent control (RC).	154
Figure 5.24 Flow cytometry analysis of the RMG-I <i>ARID1A</i> KO cell line RAE1AB5 transfected with RC and a CRISPR-Cas9 vector targeting <i>ARID1B</i>	155
Figure 5.25 Transfection of the RMG-I <i>ARID1A</i> KO cell line RAE1AB5 with a CRISPR-Cas9 vector targeting <i>ARID1B</i> using X-tremeGene HP reagent for 24 hours	156
Figure 5.26 Alignment of Sanger sequencing of RMG-I CRISPR KO <i>ARID1B</i> Exon6 (RBE6AB6) and Exon10 (RBE10BF3) clones in Benchling	157
Figure 5.27 Analysis of Sanger sequencing of <i>ARID1B</i> in ARID1A KO cells (RDKBE6AB5)	158
Figure 5.28 Protein expression of ARID1B in cells that had undergone attempts to KO this protein	159
Figure 5.29 Flow diagram summarising inclusion and exclusion criteria for the RMG-I.b4 ARID1B CRISPR KO cell cohort	160
Figure 5.30 Flow diagram summarising inclusion and exclusion criteria for identifying <i>ARID1B</i> CRISPR KO in a previously validated <i>ARID1A</i> KO RMG-I.b4 clone RAE1AB5 to attempt to isolate a double KO (DK) of both ARID1A and ARID1B in a single cell line	161
Figure 5.31 Transfection of the JHOC-5.d12 clonal cell line with CRISPR KO plasmids targeting <i>ARID1B</i> exons 6 and 10	162
Figure 5.32 Flow cytometry analysis of the JHOC-5.d12 transfected with RC and a CRISPR-Cas9 vector targeting <i>ARID1B</i>	163
Figure 5.33 Representative protein levels of ARID1B CRISPR KO cells. Whole cell protein lysate was quantitated and analysed via Western blotting	163
Figure 5.34 Representative analysis of Sanger sequencing of JHOC-5 CRISPR KO cell lines targeting <i>ARID1B</i> Exon6 and Exon10, visualised using the ICE CRISPR Analysis Tool	164
Figure 5.35 Flow diagram summarising inclusion and exclusion criteria for CRISPR-Cas9 KO of ARID1B in the JHOC-5.d12 clonal cell line	166
Figure 5.36 <i>ARID1A</i> mRNA expression levels for RMG-I CRISPR KO cell lines	167
Figure 5.37 <i>ARID1B</i> mRNA expression levels for the RMG-I isogenic panel of cell lines	168

Figure 5.38 Growth rate of RMG-I parental line and CRISPR KO clonal lines .....	169
Figure 5.39 IC <sub>50</sub> cisplatin concentration of RMG-I CRISPR KO cell lines.....	169
Figure 5.40 <i>ARID1A</i> mRNA expression levels for JHOC5 CRISPR-Cas9 KO cells.....	170
Figure 5.41 Growth rate of JHOC-5 parental line and CRISPR clonal lines .....	171
Figure 5.42 IC <sub>50</sub> cisplatin concentration of JHOC-5 CRISPR KO cell lines .....	172
Figure 5.43 <i>STAG1</i> mRNA expression levels for RMG-I and JHOC-5 CRISPR-Cas9 KO cells .....	173
Figure 6.1 Schematic outlining the process of identifying a molecular target therapy for <i>ARID1A</i> and/or <i>ARID1B</i> mutated OCCC .....	186

# List of Tables

Table 1.1 FIGO staging of Ovarian cancer (2021) .....	14
Table 2.1 Ovarian Clear Cell Carcinoma cell line specimen site of origin, <i>in vivo</i> growth in mice and commercial availability .....	42
Table 2.2 Cell culture conditions for growing cell lines.....	44
Table 2.3 Cell seeding density for cell viability assay.....	46
Table 2.4 Components of the PCR reaction.....	47
Table 2.5 Thermocycling conditions for PCR .....	48
Table 2.6 SuperScript reagents .....	49
Table 2. 7 PCR cycling conditions for cDNA synthesis.....	50
Table 2.8 Real-Time PCR reaction using TaqMan assays .....	50
Table 2.9 Taqman assay probe.....	51
Table 2.10 TaqMan assay PCR cycling conditions .....	51
Table 2.11 Serial dilutions used to create BCA assay standard curves with Bovine serum albumin (BSA) stock.....	53
Table 2.12 Primary and secondary antibody details and dilutions used for western blotting ..	54
Table 3.1 Cell seeding density .....	58
Table 3.2 Primer sequences used for cell line mutation verification. ....	60
Table 3.3 Concentration ranges of platinum drugs used to assess chemosensitivity in OCCC cell lines .....	61
Table 3.4 STR profiling results for the OCCC cell lines used this study .....	64
Table 4.1 Cell seeding density for use of the drug screening library .....	80
Table 4.2 Dilutions of the drug of interest^ to determine IC50 levels.....	82
Table 4.3 List of bioinks and activators for matrix selection using the RASTRUM 3D bioprinter.....	84
Table 4.4 Cell viability in OCCC cell lines post drug treatment with 160 compounds from the epigenetic screening library .....	91
Table 4.5 Cell viability in non-OCCC cell lines post drug treatment with 160 compounds from the epigenetic screening library .....	91
Table 4.6 IC50 comparisons (cell viability: MTS) for ibrutinib in 10 ovarian cancer cell lines grown in 2D .....	98



Table 4.7 IC50 comparisons (cell viability: CTG) for Ibrutinib in 10 ovarian cancer cell lines grown in 3D .....	104
Table 4.8 Clinical trials of ibrutinib in solid tumors.....	112
Table 5.1 sgRNA target sequences used for CRISPR KO of ARID1A or ARID1B.....	124
Table 5.2 Primers used for CRISPR KO screening.....	130
Table 5.3 Thermocycling conditions for PCR.....	131
Table 5.4 Thermocycling conditions for touchdown PCR .....	131
Table 5.5 Nomenclature for cell sorted CRISPR KO clones.....	141
Table 5.6 Summary of all RMG-I ARID1A CRISPR KO cells and mutation types.....	143
Table 5.7 Summary of all JHOC-5 ARID1A CRISPR knockout cells and mutation types..	149
Table 5.8 Summary of all JHOC-5 ARID1B CRISPR KO cells and mutation types .....	165

# Table of Contents

CERTIFICATE OF ORIGINAL AUTHORSHIP .....	i
Acknowledgements.....	ii
Abstract .....	iv
List of Abbreviations .....	viii
List of Figures .....	xiv
List of Tables .....	xix
CHAPTER 1. INTRODUCTION .....	1
1.1 Cancer .....	2
1.1.1 Definition of cancer .....	2
1.1.2 Global and Australian cancer cases .....	2
1.2 Ovarian cancer .....	3
1.2.1 Global ovarian cancer cases.....	3
1.2.2 Ovarian cancer statistics in Australia.....	4
1.2.3 Risk Factors for Ovarian Cancer.....	5
1.2.3.1 Risk of ovarian cancer increases with increasing age.....	5
1.2.3.2 Genetic factors associated with increased risk of developing ovarian cancer .....	6
1.2.3.2.1 Family history .....	6
1.2.3.2.2 Genetic factors .....	6
1.2.3.3 Lifestyle factors .....	7
1.2.3.3.1 Obesity .....	7
1.2.3.3.2 Smoking .....	7
1.2.4 Symptoms of Ovarian Cancer .....	8
1.2.5 Histopathological Subtypes of Ovarian cancer.....	8
1.2.5.1 Epithelial ovarian cancer (EOC).....	9
1.2.5.1.1 High-grade serous ovarian cancer (HGSOC) .....	9
1.2.5.1.2 Low-grade serous ovarian cancer (LGSOC).....	9
1.2.5.1.3 Endometrioid ovarian cancer (EnOC) .....	9
1.2.5.1.4 Ovarian Clear Cell Carcinoma (OCCC) .....	10
1.2.5.1.5 Mucinous ovarian cancer (MOC) .....	10
1.2.5.2 Germ cell ovarian cancer (GCOC) .....	10
1.2.5.3 Sex-cord stromal ovarian cancer (SCSOC) .....	10
1.2.6 Diagnosis of ovarian cancer.....	11

1.2.6.1 General examination .....	11
1.2.6.2 Imaging examination .....	11
1.2.6.3 Laboratory examination .....	12
1.2.7 Staging of ovarian cancer.....	13
1.2.8 Treatment options for ovarian cancer .....	14
1.2.8.1 Surgery.....	15
1.2.8.2 Chemotherapy .....	15
1.2.8.3 Other treatments.....	17
1.2.8.3.1 PARP inhibitors .....	17
1.2.8.3.2 Bevacizumab.....	18
1.2.8.3.3 Durvalumab.....	19
1.2.9 Chemoresistance and relapse .....	19
1.2.10 Molecular events in ovarian cancer .....	20
1.2.10.1 TP53.....	21
1.2.10.2 PIK3CA.....	23
1.2.10.3 BRCA1/BRCA2.....	24
1.3 Ovarian Clear Cell Carcinoma (OCCC) .....	24
1.3.1 Epidemiology of OCCC.....	25
1.3.2 Pathogenesis of OCCC .....	26
1.3.3 Treatment for OCCC.....	27
1.4 Epigenetics.....	27
1.4.1 The epigenome.....	27
1.5 Clustered Regularly Interspaced Short Palindromic Repeats (CRISPR).....	34
1.6 Drug repurposing .....	37
1.7 Thesis hypothesis and aims.....	39
CHAPTER 2. METHODS .....	40
2.1 Cell culture.....	41
2.1.1 Cell lines .....	41
2.1.2 Cell culture maintenance.....	43
2.1.3 Cryopreservation.....	44
2.1.4 Cell counting.....	45
2.1.5 Cell viability assay .....	45
2.1.6 Cell proliferation rate assay .....	46
2.2 DNA analysis.....	46

2.2.1 Genomic DNA (gDNA) extraction.....	46
2.2.2 PCR amplification of gDNA.....	47
2.2.3 PCR product clean up .....	48
2.2.4 Sanger Sequencing.....	48
2.3 Quantitative Real-Time Reverse Transcriptase PCR (qRT-PCR).....	48
2.3.1 RNA extraction from cells .....	48
2.3.2 cDNA synthesis .....	49
2.3.3 mRNA gene expression using Taqman assays .....	50
2.4 Assessment of RNA, gDNA, plasmid DNA, and PCR fragment concentration and quality using the NanoDrop spectrophotometer .....	51
2.5 Protein analyses .....	51
2.5.1 Protein extraction .....	51
2.5.2 Protein quantitation.....	52
2.5.3 Western Blot .....	53
2.6 Statistical Analysis.....	55
CHAPTER 3. Characterisation of Ovarian Clear Cell Carcinoma Cell Lines .....	56
3.1 Introduction.....	57
3.2 Methods.....	58
3.2.1 Cell line morphology .....	58
3.2.2 Cell line STR profile.....	58
3.2.3 Protein analyses and Quantitative Real-Time Reverse Transcriptase PCR (qRT-PCR) .....	61
3.2.4 Determining sensitivity of cell lines to platinum drugs .....	61
3.3 Results.....	61
3.3.1 Morphology of OCCC cells .....	61
3.3.2 STR profiling of OCCC cell lines.....	63
3.3.3 Confirming reported mutations in OCCC cell lines .....	65
3.3.4 Determining RNA and protein levels of ARID1A and ARID1B in OCCC cell lines....	67
3.3.5 Cell viability after cisplatin and carboplatin treatment.....	69
3.4 Discussion .....	71
3.5 Conclusion .....	75
CHAPTER 4. Interrogating OCCC cell lines with an epigenetic drug screening library.....	76
4.1 Introduction.....	77
4.1.1 Epigenetic therapeutic compound library screen.....	77
4.1.2 Three-dimensional (3D) bioprinting .....	77

4.2 Methods.....	79
4.2.1 Using the Tocriscreen Epigenetics Library 3.0 to screen ovarian cancer cell lines .....	79
4.2.2 Selection of drugs of interest .....	80
4.2.3 Validation of drugs of interest in 2D culture .....	82
4.2.4 Three-dimensional (3D) bioprinting and drug validation.....	82
4.2.4.1 Matrix selection for optimal 3D cell growth conditions.....	83
4.2.4.2 Generating 3D bioprinted Ovarian Cancer cell models.....	85
4.2.4.3 Drug treatments of 3D bioprinted cells.....	86
4.2.4.4 3D cell viability assays .....	87
4.2.4.4.1 CellTiter-Glo ATP-based 3D Cell Viability Assay .....	87
4.2.4.4.2 Assessing cell death in 3D bioprinted cells – the LIVE/DEAD cell viability assay	87
4.3 Results.....	87
4.3.1 Identification of drugs of interest following screening of ovarian cancer cell lines with an epigenetic compound library.....	87
4.3.2 Identification of ibrutinib as a compound of interest for further study.....	92
4.3.3 BTK, the target of ibrutinib, is expressed in ovarian cancer cell lines .....	94
4.3.4 Sensitivity of ovarian cancer cell lines cultured in 2D to ibrutinib .....	95
4.3.5 Selection of optimal matrices for 3D bioprinted OCCC cell lines .....	98
4.3.6 Sensitivity of ovarian cancer cell lines cultured in 3D to ibrutinib .....	102
4.4 Discussion .....	108
4.5 Conclusion .....	116
CHAPTER 5. KO of ARID1A and ARID1B with CRISPR-Cas9 gene editing .....	117
5.1 Introduction.....	118
5.2 Methods.....	122
5.2.1 Using CRISPR-Cas9 to KO gene expression .....	122
5.2.1.1 Generating and selecting clonal cell lines from a heterogeneous parent population to use for engineering of CRISPR isogenic cell line panels .....	122
5.2.1.2 sgRNA and primer design.....	123
5.2.1.3 Luria-Bertani (LB) broth and LB agar plates .....	125
5.2.1.4 Cloning of sgRNA into the PX-458 plasmid.....	125
5.2.1.4.1 Phosphorylation and annealing of oligomers.....	125
5.2.1.4.2 Linearization of the desired vector with BbsI and ligation of oligomers .....	125
5.2.1.4.3 Plasmid purification with PlasmidSafe exonuclease .....	126
5.2.1.4.4 Transformation of ligated plasmid into competent bacteria .....	126

5.2.1.4.5 Plasmid DNA extraction and Sanger sequencing .....	127
5.2.1.5 Plasmid transfection.....	127
5.2.1.5.1 Transfection using Lipofectamine 3000 Transfection Reagent .....	128
5.2.1.5.2 Transfection using X-tremeGENE HP DNA Transfection Reagent.....	128
5.2.1.5.3 Transfection using Lipofectamine LTX Reagent with PLUS Reagent .....	128
5.2.2 Fluorescent activated cell sorting (FACS) using a flow cytometer .....	129
5.2.3 gDNA screening to detect CRISPR induced modifications .....	130
5.2.4 Protein analyses and Quantitative Real-Time Reverse Transcriptase PCR (qRT-PCR) .....	132
5.2.5 Determining sensitivity of cell lines to cisplatin was conducted as previously described in Section 3.2.4. ....	132
5.3 Results.....	132
5.3.1 Creation of clonal cell lines from parental ovarian cancer lines.....	132
5.3.1.1 Selection of the RMG-I.b4 clonal cell line .....	133
5.3.1.2 Selection of the JHOC-5.d12 clonal cell line.....	135
5.3.2 CRISPR KO of ARID1A in ARIDA WT OCCC lines RMG-I and JHOC-5 clonal lines .....	137
5.3.2.1 Cloning ARID1A sgRNA into CRISPR-Cas9 KO vector PX458.....	137
5.3.2.2 Creation of ARID1A KO cells in RMG-I.b4 clonal cells.....	138
5.3.2.2.1 ARID1A plasmid transfection and GFP single cell sorting.....	138
5.3.2.2.2 Validation of ARID1A KO clones in RMG-I.b4 cells .....	140
5.3.2.3 Creation of ARID1A KO cells in JHOC-5.d12 clonal cells .....	145
5.3.2.3.1 ARID1A plasmid transfection and GFP single cell sorting in JHOC-5.d12 .....	145
5.3.2.3.2 Validation of ARID1A KO clones in JHOC-5.d12 cell background.....	147
5.3.3 CRISPR KO of ARID1B in ARID1B WT OCCC lines RMG-I and JHOC-5 .....	150
5.3.3.1 Cloning of ARID1B sgRNA into CRISPR-Cas9 KO vector PX458.....	150
5.3.3.2 Creation of ARID1B KO cells in RMG-I.b4 clonal cells.....	151
5.3.3.2.1 ARID1B plasmid transfection and GFP single cell sorting in RMG-I.b4 .....	151
5.3.3.2.2 CRISPR KO of ARID1B in RMG-I ARID1A KO cells.....	154
5.3.3.2.3 Validation of ARID1B KO clones in RMG-I.b4 cells and ARID1B/ARID1A KO clones in RAE1AB5 cells .....	156
5.3.3.3 Creation of ARID1B KO cells in JHOC5-D12 clonal cells .....	161
5.3.3.3.1 CRISPR KO of ARID1B in JHOC-5 clonal cells.....	161
5.3.3.3.2 Validation of ARID1B KO clones in JHOC-5.d12 cell background.....	163

5.3.4 Characterising ARID1A and ARID1B KO isogenic CRISPR-Cas9 KO clonal lines made in RMG-I.b4 and JHOC-5.d12 cell backgrounds .....	166
5.3.4.1 Determining RNA levels of ARID1A and ARID1B in the ARID1A isogenic RMG-I.b4 panel.....	166
5.3.4.2 Assessing the growth rate of RMG-I CRISPR KO clones and sensitivity to cisplatin .....	168
5.3.4.3 Assessment of RNA levels of ARID1A in JHOC-5 CRISPR-Cas9 KO clonal lines	170
5.3.4.4 Assessing the growth rate of JHOC-5 CRISPR-Cas9 KO clonal cell lines and sensitivity to cisplatin.....	170
5.3.5 STAG1 expression in the ARID1A CRISPR KO isogenic panel cells .....	172
5.4 Discussion .....	173
5.5 Conclusion .....	177
CHAPTER 6. Final discussion and future directions .....	178
6.1 Final discussion.....	179
6.1.1 Supporting evidence that the absence of both ARID1A and ARID1B is synthetic lethal .....	179
6.1.2 ARID1A in the OCCC cell line JHOC-5 .....	180
6.1.3 Effects of ARID1A and ARID1B on cell growth rate .....	181
6.1.4 OCCC and chemoresistance – effects of ARID1A KO .....	182
6.1.5 Ibrutinib as a potential therapeutic agent for OCCC .....	182
6.1.6 Potential and current status of other targeted agents in OCCC treatment .....	184
6.1.7 Retention of WT ARIDA and truncated ARID1B protein after KO .....	184
6.2 Conclusion .....	185
6.3 Limitations .....	186
6.4 Opportunities and future directions .....	187
References.....	189
Appendix.....	238
Appendix 1.....	240
Appendix 2.....	245
Appendix 3.....	251
Appendix 4.....	257
A.4.1 Manuscripts arising from thesis .....	257
A.4.2 Manuscripts in preparation from this thesis.....	257
A.4.3 Manuscripts related to this thesis.....	257

# CHAPTER 1. INTRODUCTION



## 1.1 Cancer

### 1.1.1 Definition of cancer

Cancer is characterised by uncontrolled growth of certain cells, which can proliferate and metastasise to other regions of the body. The uncontrolled proliferation of abnormal cells carries a heightened risk of tumour development. Furthermore, these aberrant cells have the potential to infiltrate adjacent tissues and can also disseminate to distant regions of the body, posing a grave threat to overall health <sup>1</sup>.

Tumours are categorised as either benign or malignant (cancerous). Benign tumours exhibit a gradual and restrained growth pattern, refraining from invading adjacent organs. On the other hand, malignant tumours demonstrate accelerated growth, possess the capability to spread, and may infiltrate neighbouring organs, thereby posing a potential life-threatening risk. In cases where malignant tumours remain localised, they are referred to as carcinoma *in situ*. If not addressed in their early stages, these tumours have the propensity to extend into surrounding tissues, evolving into aggressive forms of cancer. There are instances where cancer cells, having originated in the primary organ, break free, enter the bloodstream or lymphatic system, and subsequently migrate to distant organs. This process, known as metastasis, results in the formation of secondary tumours, adding to the complexity of cancer progression <sup>2</sup>. Cancer holds a prominent position as a leading cause of death, acting as a substantial barrier to the enhancement of life expectancy in every nation around the world <sup>3</sup>.

### 1.1.2 Global and Australian cancer cases

According to estimates from the World Health Organisation (WHO), in 2022 there were approximately 20 million new cancer cases reported, leading to about 9.7 million deaths globally. The estimated number of individuals surviving five years after a cancer diagnosis worldwide was around 53.5 million. Statistics indicate that roughly one in five people will experience a cancer diagnosis in their lifetime, with approximately 1 in 9 men and 1 in 12 women succumbing to the disease <sup>4,5</sup>.

In Australia, approximately 165,000 new cases of cancer were diagnosed in 2023, with around 91,000 male and 74,000 female patients being affected <sup>6</sup>. In the same year, an estimated 51,000 Australians died from cancer. In 2015-2019, the five-year survival rate for people diagnosed with cancer was 71% compared to that for the general Australian population <sup>6</sup>. Furthermore,

there is an escalating risk of cancer diagnosis associated with advancing age, with the highest rates reported in the age group of 85-89 years (Figure 1.1). With a rising number of Australians reaching older age, the annual count of diagnosed cancer cases sees a continual upwards trend, with the exception of those individuals 90 years or over where there is a slight decline in incidence.

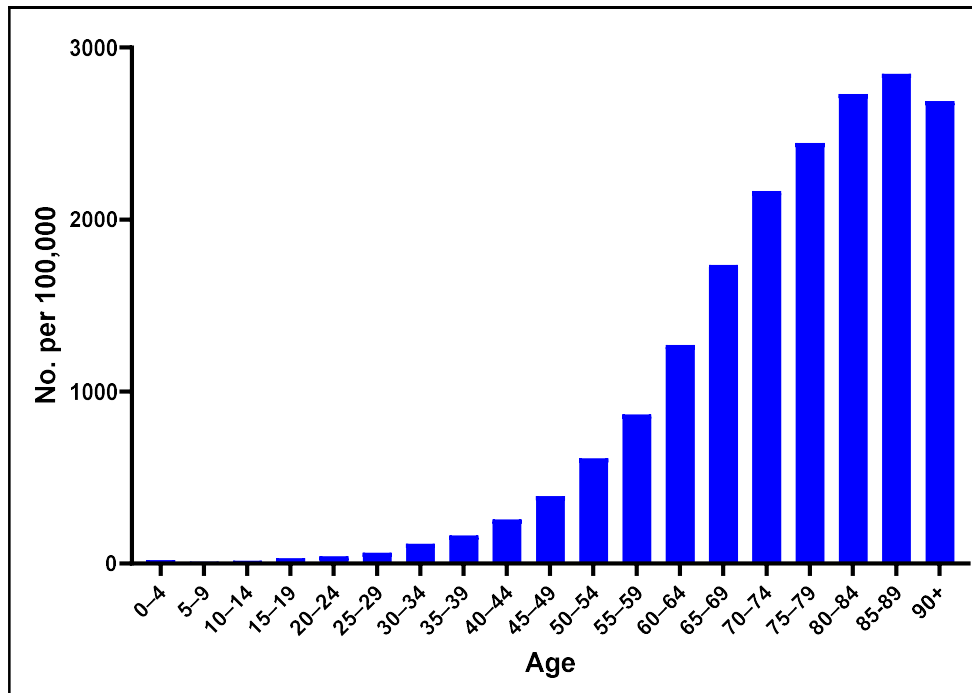


Figure 1.1 Cancer rates per 100,000 population in Australia in 2023. Adapted from the Australian Institute of Health and Welfare (AIHW) <sup>6</sup>.

## 1.2 Ovarian cancer

### 1.2.1 Global ovarian cancer cases

According to data from the WHO, in 2022, ovarian cancer ranked as the eighth most prevalent cancer in women worldwide, with 324,600 new cases diagnosed annually (Figure 1.2) <sup>7</sup>. Ovarian cancer is also the eighth most fatal cancer amongst women worldwide, resulting in approximately 207,000 deaths each year (Figure 1.2) <sup>7</sup>. Consequently, ovarian cancer is identified as the leading cause of mortality among gynaecological cancers <sup>8</sup>.

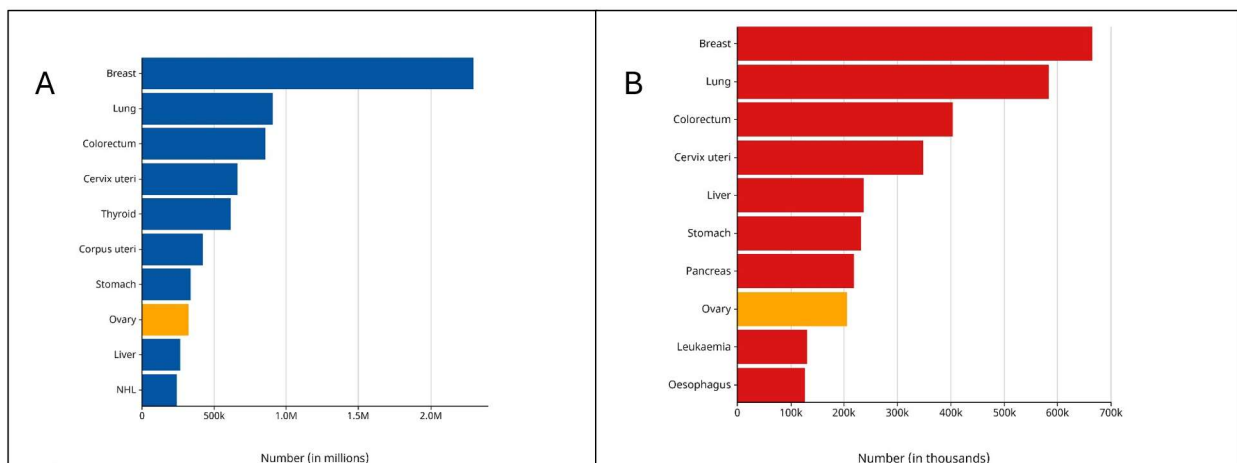


Figure 1.2 Global incidence and mortality of female cancers. Ovarian cancer ranks eighth in incidence (A) and mortality (B) in the world's top ten female cancers. This data is from the Global Cancer Observatory owned by the International Agency for Research on Cancer (IARC). Reproduced from the online database GLOBOCAN 2022 (<http://gco.iarc.fr/>) of the IARC Global Cancer Observatory.

### 1.2.2 Ovarian cancer statistics in Australia

In Australia, it was projected that approximately 1,786 new cases of ovarian cancer would be diagnosed in 2023, constituting about 2.4% of all newly diagnosed cancers during that year, making ovarian cancer the ninth most frequently diagnosed female cancer (Figure 1.3). Around 1,050 Australian women were anticipated to succumb to ovarian cancer in 2023, representing 4.6% of all female cancer-related deaths, making ovarian cancer the fifth most frequent cause of cancer deaths in women in Australia (Figure 1.3). In the same year, the five-year survival rate following a diagnosis of ovarian cancer was estimated to be 49% <sup>6</sup>.

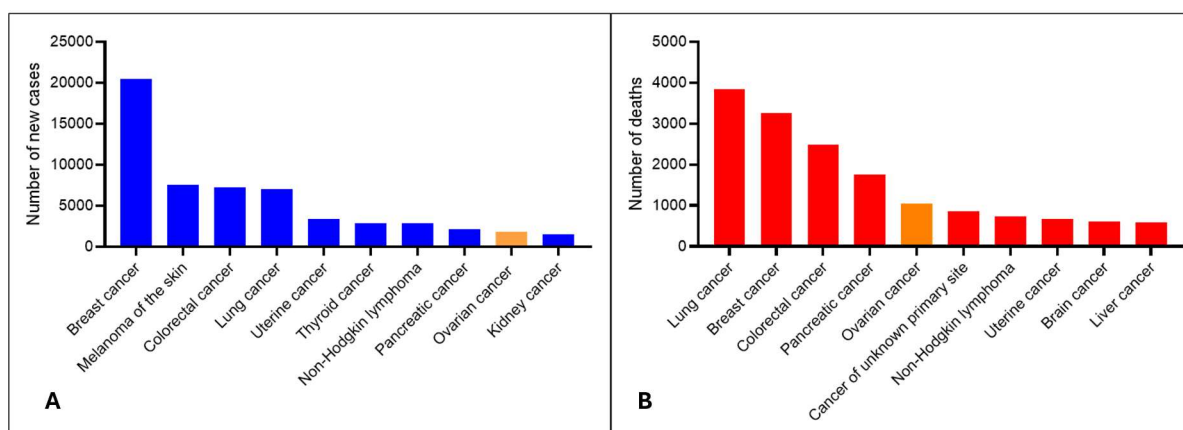


Figure 1.3 Estimated number of Australian female cancer cases and deaths in 2023. Ovarian cancer ranks ninth in incidence (A) and fifth in mortality (B) in women in Australia. Adapted from the AIHW <sup>6</sup>.

### 1.2.3 Risk Factors for Ovarian Cancer

Cancer risk factors are those that raise the likelihood of the disease occurring. There are various risk factors for different types of cancer. Lifestyle and environmental risk factors are just two examples of the many risk variables <sup>9</sup>. Risk factors associated with ovarian cancer include age, genetic and lifestyle factors.

#### 1.2.3.1 Risk of ovarian cancer increases with increasing age

Ovarian cancer is an age-related disease, with approximately 75% of women with ovarian cancer being diagnosed after menopause <sup>10-12</sup>. The median age at diagnosis is 65 years old in North America <sup>11,13</sup>. In Australia, the median age of diagnosis reported in the 45 and Up study was 68 years old calculated from 176 women presenting with ovarian cancer during 2006 - 2013 <sup>14</sup>. From the AIHW, there were 1,284 females diagnosed in 2019 with ovarian cancer, and the age of diagnosis was 64.4 years old <sup>6</sup>. Advancing age is linked to a higher prevalence of advanced stages of ovarian cancer and a diminished survival rate (Figure 1.4) <sup>11,15</sup>.

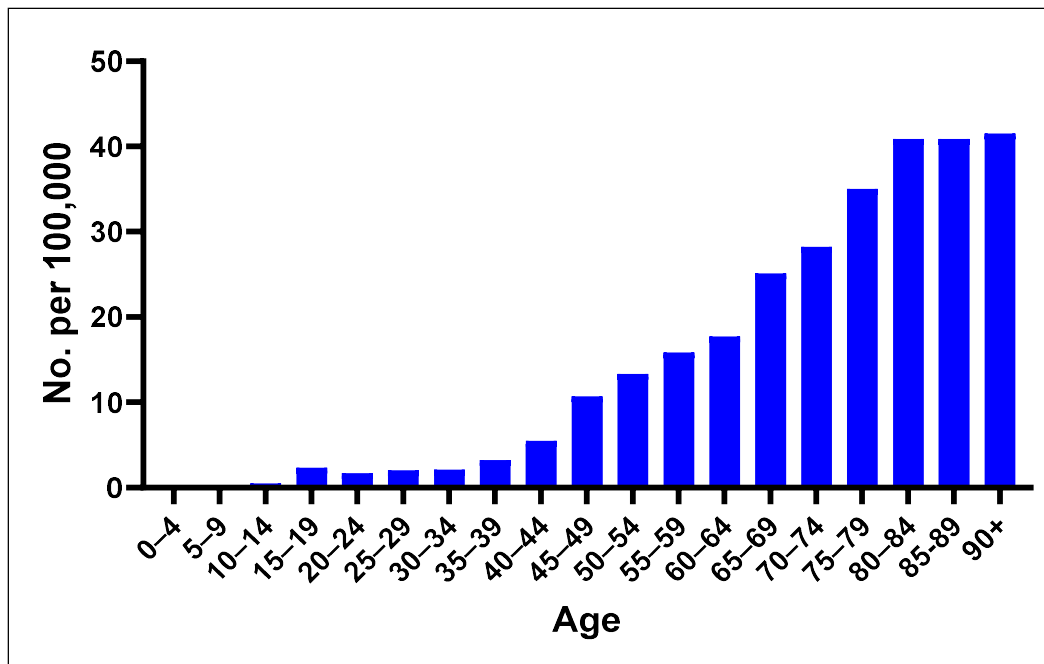


Figure 1.4 Ovarian cancer rates per 100,000 population in Australia. According to 2023 AIHW data, among Australian female patients with ovarian cancer, the incidence rate gradually increased with age. Adapted from the AIHW <sup>6</sup>.

### 1.2.3.2 Genetic factors associated with increased risk of developing ovarian cancer

#### 1.2.3.2.1 Family history

Studies have shown that women who have a first-degree relative with a history of breast, uterine, or ovarian cancer have an increased risk of developing ovarian cancer compared to women without a family history of these diseases <sup>16,17</sup>. A personal history of having had other cancers can also increase the risk of developing ovarian cancer. Research has shown that women who have had breast cancer have a 24% higher risk of developing ovarian cancer than women in the general population who have not had breast cancer <sup>18,19</sup>. Women with a first-degree relative with a history of prostate cancer have an approximately 17% increased risk of developing ovarian cancer <sup>20</sup>.

#### 1.2.3.2.2 Genetic factors

Molecular characterisation of ovarian cancer has demonstrated an association with mutations in tumour suppressor genes, where more than one-fifth of ovarian cancers are caused by

germline mutations in these genes <sup>21,22</sup>. Approximately 65-85% of hereditary ovarian cancers are caused by mutations in Breast cancer 1 (*BRCA1*) and Breast cancer 2 (*BRCA2*) <sup>23</sup>. By the age of 40, for individuals harbouring mutations in *BRCA1* or *BRCA2*, the risk of developing ovarian cancer is less than 3%. However, this risk experiences a notable increase with age, reaching 10% by age 50 <sup>24</sup>. Upon reaching the age of 80, individuals carrying *BRCA1* mutations face a cumulative lifetime risk of 49% for ovarian cancer, while those with *BRCA2* mutations have a cumulative lifetime risk of 21% <sup>25</sup>. Furthermore, *BRCA1/2* mutations not only significantly increase the risk of ovarian cancer, but also predispose individuals to breast, prostate if male, and other cancers <sup>26</sup>. Some studies have shown that all US women have a lifetime risk of 1.7% of developing ovarian cancer. However, in US, Ashkenazi Jewish women have a higher rate of hereditary ovarian cancer due to inherited mutations in *BRCA1* and *BRCA2* <sup>27,28</sup>.

### 1.2.3.3 Lifestyle factors

#### 1.2.3.3.1 Obesity

Obesity has been linked to the development of ovarian cancer. Obesity and its hormonal mechanisms are thought to increase the risk of ovarian cancer, in addition to increasing mortality in affected individuals <sup>29,30</sup>. According to one study, obesity not only reduces survival rates from ovarian cancer but increases the risk of death from this disease <sup>31</sup>. A 2007 study showed that overweight women (Body mass index (BMI) between 25 to 29.9 kg/m<sup>2</sup>) and obese women (BMI over 30 kg/m<sup>2</sup>) have a higher risk of ovarian cancer compared to women of healthy weight (BMI between 18.5 to 24.9 kg/m<sup>2</sup>) <sup>32</sup>.

#### 1.2.3.3.2 Smoking

In 2009, IARC included mucinous ovarian tumours, a subtype of ovarian cancer, in the catalogue of tobacco-related cancers <sup>33</sup>. Jordan and colleagues observed that smoking causes an almost threefold increase in the risk of benign and borderline tumours, and a twofold increase in invasive tumours in current smokers compared with never-smokers <sup>34</sup>. Studies have demonstrated a positive association between the number of cigarettes smoked daily, the duration of smoking (measured in years), intensity of smoking, and the likelihood of developing ovarian cancer <sup>35-37</sup>. Similarly, Kim and colleagues suggest that smoking

contributes to an increased risk of death from ovarian cancer<sup>30</sup>. Moreover, an Australian study suggested that smoking may have a greater detrimental effect on *BRCA* mutation carriers than on non-*BRCA* mutations carriers<sup>38</sup>.

#### 1.2.4 Symptoms of Ovarian Cancer

Identifying early symptoms of ovarian cancer has significant clinical importance, as the 5-year survival rate for early-stage disease ranges from 70 to 90%, in stark contrast to the survival rate of only 20 to 30% for late-stage disease<sup>39</sup>. However, due to the symptoms of ovarian cancer frequently being vague and non-specific, this disease has been called a "silent killer"<sup>40</sup>. Symptoms of ovarian cancer patients include bloating, pelvic and/or abdominal pain, loss of appetite, frequent urination, constipation or diarrhoea, abnormal vaginal bleeding, and weight loss<sup>41,42</sup>. A study consisting of 1,725 questionnaire responses showed that before being diagnosed with ovarian cancer, about 77% of patients had abdominal symptoms, 70% of patients had gastrointestinal symptoms, 58% of patients had pain, 50% of patients had constitutional symptoms (such as weight loss or fatigue), 34% had urinary tract symptoms, and 26% reported pelvic issues<sup>43</sup>. As some ovarian cancer patients manifest symptoms like bloating, indigestion, changes in bowel habits, and abdominal pain, it can be mistakenly conflated with more prevalent conditions such as irritable bowel syndrome<sup>40</sup>.

#### 1.2.5 Histopathological Subtypes of Ovarian cancer

Ovarian cancer originates in different areas of the ovary or in the related areas of the fallopian tubes and the peritoneum. Each ovarian cancer histopathological subtype, also known as histotype, is unique and has different morphology, biological behaviour, and even prognosis<sup>44</sup>. Ovarian cancer is broadly divided into epithelial ovarian cancer (EOC) and non-epithelial ovarian cancer. Non-epithelial ovarian cancer includes germ cell ovarian cancer and sex cord stromal ovarian cancer. EOC is the most common, accounting for 90% of ovarian cancers<sup>19,45</sup>. There are four major histotypes of EOC: serous, endometrioid, mucinous, and clear cell<sup>46,47</sup>. Serous tumours are further divided into two categories: high-grade serous and low-grade serous<sup>47</sup>.

#### 1.2.5.1 Epithelial ovarian cancer (EOC)

##### 1.2.5.1.1 High-grade serous ovarian cancer (HGSOC)

HGSOC is the most common EOC histotype, accounting for more than 70%<sup>48</sup>. Many HGSOC are now known to originate in cells at the fimbrial end of the fallopian tube and subsequently spread to the ovary or peritoneum<sup>49-51</sup>. It is the most aggressive subtype of EOC, causing approximately 70-80% of ovarian cancer deaths<sup>52</sup>. HGSOC is mostly diagnosed in postmenopausal women, and more than 85% of female patients will progress to an advanced stage, with the 10-year mortality rate being around 70%<sup>46,53</sup>. The majority of HGSOC cases exhibit a wide range of genomic instability, including copy number variants and structural rearrangements. This instability is mainly caused by defects in the homologous recombination DNA repair pathways, which accelerate the progression of the tumour, resistance to treatment and metastasis<sup>54</sup>.

##### 1.2.5.1.2 Low-grade serous ovarian cancer (LGSOC)

LGSOC originates from the ovary and is a less aggressive tumour with a relatively better prognosis than HGSOC<sup>55</sup>. The median age of female patients with LGSOC is 55 years, accounting for approximately 5% of all EOC patients<sup>56,57</sup>. LGSOC have small papillae, uniform nuclei, and variable amounts of clear stroma, and psammoma bodies may be present<sup>58</sup>. In comparison to HGSOC, LGSOC did not display the same level of extensive genomic instability or homologous recombination repair defects<sup>59</sup>.

##### 1.2.5.1.3 Endometrioid ovarian cancer (EnOC)

EnOC accounts for approximately 10% of EOC. It has been associated with endometriosis and affects women between the ages of 40 and 70 years of age<sup>60</sup>. Microscopically, EnOC appears to be cystic or predominantly solid<sup>58</sup>. Due to EnOC usually being diagnosed at an early stage, women with this histological subtype of ovarian cancer have a better prognosis. It is unclear why EnOC are often diagnosed earlier than HGSOC or LGSOC, however, a possible explanation is the occurrence of this cancer with endometriosis that is diagnosed in younger women.



#### 1.2.5.1.4 Ovarian Clear Cell Carcinoma (OCCC)

OCCC accounts for approximately 10% of patients with EOC, and has been associated with endometriosis <sup>61</sup>. Amongst all subtypes of EOC, the median age of patients first diagnosed with OCCC (55 years) is significantly lower than that of patients with HGSOC (64 years) <sup>62</sup>. Also, a higher frequency of cases occurs in East Asian countries (mainly Japan), but the cause is unknown (see Section 1.3 for further discussion on this histotype that is the subject of this thesis) <sup>62-64</sup>.

#### 1.2.5.1.5 Mucinous ovarian cancer (MOC)

MOC is a rare subtype of ovarian cancer that accounts for approximately 2-3% of EOC <sup>65</sup>. MOC is more common in women under 40 years of age and one of the risk factors is related to smoking <sup>66,67</sup>. Early stage MOC has a good prognosis, but after stage II, treatment outcomes are poor because MOC is resistant to chemotherapy <sup>61,68</sup>.

#### 1.2.5.2 Germ cell ovarian cancer (GCOC)

Germ cell ovarian cancer is a rare subtype of ovarian cancer that accounts for approximately 2-3% of all ovarian cancers <sup>69</sup>. This tumour arises in the eggs or ovum (primordial germ cells of the ovaries). Due to this disease occurring primarily in young and adolescent women, and it being highly sensitive to chemotherapy, it can be treated with surgery and chemotherapy with preservation of fertility if diagnosed early <sup>70,71</sup>. Small Cell Carcinoma of the Ovary, Hypercalcemic Type (SCCOHT), is a particularly rare and aggressive form of cancer affecting younger women that is believed to originate in the germ cells <sup>72</sup>. Studies demonstrated that the patients ranged in age from a minimum of 12 months to a maximum of 43 years, while the majority of patients were in their thirties <sup>73-75</sup>. Moreover, the tumour is unresponsive to chemotherapy, and progression-free survival (PFS) is usually short <sup>74</sup>.

#### 1.2.5.3 Sex-cord stromal ovarian cancer (SCSOC)

Sex-cord stromal ovarian cancer is also a rare subtype of ovarian cancer <sup>76</sup>. This tumour constitutes a heterogeneous group, originating from diverse cell types derived from primitive sex cords or stromal cells <sup>76,77</sup>. Included among the stromal cells are theca cells, fibroblasts,

and Leydig cells, while the gonadal primitive sex cords consist of granulosa cells and sertoli cells <sup>78</sup>. These cell types may appear individually or mixed together, exhibiting various levels of differentiation <sup>79</sup>. SCSOC usually appear in the first two to thirty years of life <sup>80,81</sup>. The most common type of sex cord-stromal tumour is the granulosa cell tumour, with the risk of developing an adult granulosa cell tumour peaking between the ages of 50 and 55 years <sup>80</sup>. In contrast to epithelial cells and germ cell tumours, there are often signs of hormone producing tumours, such as becoming more hirsute, developing other masculine features, menstrual changes, or premature sexual maturity <sup>82</sup>. For this diagnosis, a comprehensive history should be evaluated, and careful attention should be paid to whether there is precocious puberty or delay in initial menstruation <sup>80</sup>.

#### 1.2.6 Diagnosis of ovarian cancer

Since nearly 60% of EOCs are diagnosed at an advanced stage, when the five-year survival rate is only 29%, early diagnosis of ovarian cancer can also give patients a better chance of cure, thereby reducing morbidity and mortality <sup>83</sup>. At present, the diagnosis of ovarian cancer is roughly divided into three parts: general examination, imaging examination and laboratory examination.

##### 1.2.6.1 General examination

When a patient develops symptoms related to ovarian cancer, doctors first evaluate the patient's personal and family history to determine the risk level. Next, the patient will be examined, such as a vaginal exam, to evaluate for pelvic and abdominal masses. However, if the patient is obese, the accuracy of the examination will decrease, causing the mass to be missed. Some other diseases can also cause abdominal masses <sup>84</sup>.

##### 1.2.6.2 Imaging examination

If a patient is suspected of having ovarian cancer, imaging examination may be used, including transvaginal ultrasonography (TVUS) or abdominal and pelvic ultrasonography <sup>85</sup>. TVUS is the predominant imaging technique employed for ovarian cancer detection. It enables clinicians to assess ovarian tissue size and vascularity <sup>86</sup>. Moreover, TVUS images facilitate

differentiation between cystic and solid masses, as well as the detection of ascites, aiding in the assessment of the probability and stage of malignant masses<sup>87,88</sup>. However, ultrasound does not always account for the difference between ovarian cancer and other more common conditions such as ovarian cysts or endometriosis. A false positive ultrasound examination may result in more examinations. Therefore, ultrasound is not recommended as an independent screening test for ovarian cancer<sup>89</sup>.

#### 1.2.6.3 Laboratory examination

Currently, several laboratory screening methods that are useful in women at high risk for ovarian cancer include blood tests for the serum glycoprotein cancer antigen 125 (CA-125) and human epididymis protein 4 (HE4). CA-125 is an epithelial cell surface glycoprotein that has been implicated in promoting cancer cell growth and metastasis and was first described in 1981<sup>90</sup>. Approximately 80% of patients with ovarian cancer have elevated CA-125 levels (>35 U/mL), but only 50% of these elevated levels are in early-stage epithelial ovarian cancer<sup>91-93</sup>. Although CA-125 is a marker for advanced ovarian cancer, its efficacy is limited for certain ovarian cancer subtypes (such as mucinous carcinoma) due to evidence indicating that mucinous cell types may not secrete CA-125 antigen<sup>94</sup>. Studies have shown that elevated CA-125 levels are also observed in other physiological or benign pathological conditions, such as endometriosis, pregnancy, uterine fibroids, ovarian cysts and other diseases<sup>95</sup>. Furthermore, CA-125 specificity and positive predictive value were higher in postmenopausal women than in premenopausal women<sup>84,89,91</sup>. Several studies have shown an association between increased concentrations of CA-125 in the normal range and the risk of ovarian cancer recurrence. Piatek and colleagues showed that an increase in CA-125 concentration of >5 U/mL at 3 and 6 months after treatment was associated with a higher risk of recurrence. Furthermore, patients with a 5 U/mL increase in CA-125 had significantly lower 5-year survival rates at 3- and 6-months post-treatment<sup>96</sup>. James and colleagues showed that in patients with a history of ovarian cancer, the presence of three progressively higher CA-125 values at 1- to 3-month intervals was highly correlated with tumour recurrence<sup>97</sup>.

HE4 is a biomarker used in the screening of ovarian cancer<sup>98</sup>. HE4 is present in almost all serous ovarian cancers and endometrioid ovarian cancers. Furthermore, the US Food and Drug Administration (FDA) has approved the biomarker for use in monitoring patients with EOC<sup>99</sup>. However, HE4 is almost absent in OCCC and MOC<sup>100-102</sup>. Some studies have indicated that

HE4 is not elevated in benign gynaecological diseases in comparison to CA-125. Furthermore, the concentration of HE4 may be influenced by renal function, smoking status, and age. Therefore, the measurement of HE4 serum levels does not contribute to the diagnosis of ovarian cancer<sup>103-107</sup>.

#### 1.2.7 Staging of ovarian cancer

The International Federation of Gynaecology and Obstetrics (FIGO) performs surgical staging for ovarian cancer based on the extent of the cancer (Table 1.1). There are currently four main stages of ovarian cancer, and each stage is also divided into several sub-stages. Stage I means that the cancer is in one or both ovaries or fallopian tubes and has not spread to other organs or tissues. Stage II means the cancer is in one or both ovaries or fallopian tubes and has spread to other organs near the pelvis, such as the uterus, bladder, or colon. Stage III means that the cancer is in one or both ovaries or fallopian tubes and has spread outside the pelvis to other parts of the abdomen or nearby lymph nodes. Stage IV indicates that the cancer has spread beyond the pelvis and abdomen to other parts of the body, such as the lungs or liver<sup>108</sup>. Unlike many other type of cancers, the main type of metastasis in ovarian cancer is via intra-abdominal spread<sup>109</sup>. Ovarian cancer cells can metastasise to sites in the abdominal cavity such as the omentum, bowel and spleen<sup>110</sup>.

Table 1.1 FIGO staging of Ovarian cancer (2021)

Stage I: Tumour confined to ovaries
IA: Tumour limited to 1 ovary (capsule intact); no tumor on ovarian surface; no malignant cells in the ascites or peritoneal washings
IB: Tumour limited to both ovaries (capsules intact); no tumour on ovarian surface; no malignant cells in the ascites or peritoneal washings
IC: Tumour limited to 1 or both ovaries, with any of the following: IC1: Surgical spill IC2: Capsule ruptured before surgery or tumour on ovarian surface IC3: Malignant cells in the ascites or peritoneal washings
Stage II: Tumour involves 1 or both ovaries with pelvic extension (below pelvic brim) or peritoneal cancer
IIA: The tumour has extended and/or implanted into the uterus and/or the fallopian tubes
IIB: Extension to other pelvic intraperitoneal tissues
Stage III: Tumour involves 1 or both ovaries, or peritoneal cancer, with cytologically or histologically confirmed spread to the peritoneum outside the pelvis and/or metastasis to the retroperitoneal lymph nodes IIIA1: Positive retroperitoneal lymph nodes only (cytologically or histologically proven): IIIA1(i) Metastasis up to 10 mm in greatest dimension IIIA1(ii) Metastasis more than 10 mm in greatest dimension IIIA2: Microscopic extra pelvic (above the pelvic brim) peritoneal involvement with or without positive retroperitoneal lymph nodes
IIIB: Macroscopic peritoneal metastasis beyond the pelvis up to 2 cm in greatest dimension, with or without metastasis to the retroperitoneal lymph nodes
IIIC: Macroscopic peritoneal metastasis beyond the pelvis more than 2 cm in greatest dimension, with or without metastasis to the retroperitoneal lymph nodes (includes extension of tumour to capsule of liver and spleen without parenchymal involvement of either organ)
Stage IV: Distant metastasis excluding peritoneal metastases
Stage IVA: Pleural effusion with positive cytology
Stage IVB: Parenchymal metastases and metastases to extra-abdominal organs (including inguinal lymph nodes and lymph nodes outside of the abdominal cavity)

Note: Reproduced from *FIGO Cancer Report (2021)*, by Berek et al, 2021<sup>111</sup>.

### 1.2.8 Treatment options for ovarian cancer

Due to ovarian cancer being difficult to diagnose in its early stages, treatment is determined based on the stage, location, and severity of the cancer. Typically, ovarian cancer is treated with a combination of surgery and chemotherapy.

#### 1.2.8.1 Surgery

In the early stages of ovarian cancer, unilateral fallopian tube and ovary are surgically removed to preserve the uterus and contralateral ovary, thereby reducing the possibility of developing malignant tumours <sup>112,113</sup>. However, when patients have advanced ovarian cancer, debulking surgery is recommended <sup>46</sup>. If the patient's health permits, the entire uterus, both fallopian tubes, and ovaries, may be removed to achieve maximum cytoreduction <sup>114,115</sup>. Moreover, during surgical debulking, affected tissue, including sections of the intestines, liver, spleen, and bladder, will be removed <sup>47</sup>.

#### 1.2.8.2 Chemotherapy

Chemotherapy has long been used to treat ovarian cancer. Generally, chemotherapy has been used to treat any residual disease after surgery. However, when the tumour cannot be completely removed by surgery, chemotherapy will be first given to reduce the size of the tumour and then surgically removed. This is referred to as “neoadjuvant chemotherapy” <sup>116-118</sup>.

In the late 1970s, cisplatin was first proposed as a chemotherapy drug to treat advanced or recurrent ovarian cancer, with a response rate of 13-30% as a single drug <sup>119,120</sup>. In the 1980s, some studies showed that the efficacy of combined chemotherapy with cisplatin and cyclophosphamide in ovarian cancer was further improved. Compared with cisplatin only, overall survival (OS) rates were significantly increased with the combination therapy <sup>121,122</sup>. Thus, cisplatin with cyclophosphamide was a standard treatment used in the late 1980s and early 1990s.

Carboplatin, introduced in the 1990s as a derivative of cisplatin, demonstrated comparable efficacy as a single agent in terms of response and survival rates while exhibiting a markedly improved safety profile <sup>123</sup>. This advancement was particularly notable due to carboplatin's lower incidence of adverse effects such as emesis, sensory neuropathy, ototoxicity, and nephrotoxicity, making it a preferred choice over cisplatin in many clinical settings <sup>123,124</sup>. However, it is essential to note that carboplatin was associated with a higher myelosuppression incidence than cisplatin, and it is the dose-limiting toxicity of carboplatin that often necessitates careful monitoring and dosage adjustments in clinical practice <sup>125,126</sup>. Some studies have shown that using carboplatin and cyclophosphamide to treat ovarian cancer has better outcomes than cisplatin plus cyclophosphamide <sup>127</sup>. However, in the treatment of advanced ovarian cancer,

cisplatin and carboplatin have the same survival rate <sup>128</sup>. It is crucial to note that when preparing intravenous solutions of platinum drugs, it is important to select the correct excipient, as dissolution with an incorrect excipient can result in an increase in the amount of aqated drug, which in turn can lead to toxic concentrations. It is recommended that cisplatin be dissolved in saline to help slow partial aquation of the drug. Nevertheless, while the preparation of carboplatin in saline may result in an increased rate of aquation or the transformation of carboplatin to cisplatin, it remains a crucial consideration in clinical settings to avoid unintended chemical changes that could impact treatment outcomes <sup>129</sup>. Consequently, from the Australian Injectable Drugs Handbook, cisplatin is prepared in saline or glucose in saline solution, and carboplatin for clinical use is dissolved in glucose only <sup>129,130</sup>.

Since the 1990s, paclitaxel, an active chemotherapy drug, was used in the treatment of ovarian cancer, changing the standard treatment of ovarian cancer <sup>131,132</sup>. In a study of 410 patients with poor ovarian cancer reduction, the combination of paclitaxel and cisplatin improved the response rate and OS compared with the combination therapy of cisplatin and cyclophosphamide <sup>133</sup>. Piccart and colleagues also showed improved outcomes using a combination of paclitaxel and cisplatin <sup>134</sup>. Subsequently, in 2003, a study of 792 patients with stage III ovarian cancer showed that when patients were treated with cisplatin plus paclitaxel for 24 hours or carboplatin plus paclitaxel for 3 hours, the median PFS and OS were higher with carboplatin than with cisplatin <sup>135</sup>. This result indicated that carboplatin is more effective than cisplatin and easier to administer.

Currently, the standard chemotherapy for ovarian cancer is 6 cycles of carboplatin/paclitaxel combination therapy <sup>136-138</sup>. For patients with significant allergic reactions to paclitaxel or early sensory neuropathy, the less neurotoxic docetaxel can be used instead. However, docetaxel has a stronger myelosuppressive effect than paclitaxel <sup>139</sup>. Studies have indicated that some patients may also experience allergic reactions to carboplatin. Marquart and colleagues analysed a melanoma patient with carboplatin allergy and found that cisplatin could be substituted for carboplatin as a subsequent treatment <sup>140</sup>. A study by Rose and colleagues involving 281 patients showed that all patients received carboplatin treatment, and 28 of these patients experienced carboplatin hypersensitivity. Of these 28 patients, 9 were switched to oxaliplatin as a substitute for carboplatin, and all patients successfully tolerated oxaliplatin desensitisation <sup>141</sup>. Caiado and colleagues analysed the replacement of carboplatin with either cisplatin or oxaliplatin in 46 carboplatin-allergic patients, showing that oxaliplatin was better tolerated and effective for a longer period of time <sup>142</sup>. Those indicate that the use of cisplatin or oxaliplatin

in place of carboplatin may be a viable strategy to circumvent allergic reactions to carboplatin. Despite major advances in chemotherapy and drug development over the past two decades, the overall survival rate for ovarian cancer has not shown a significant improvement<sup>143</sup>. This indicates that there is a need to explore new forms of treatment.

### 1.2.8.3 Other treatments

#### 1.2.8.3.1 PARP inhibitors

Poly (ADP-ribose) polymerase (PARP) is a protein that plays a key role in the repair of DNA single-strand breaks (SSBs). When PARP is inhibited, SSBs accumulate in the cell, resulting in the generation of double-strand breaks (DSBs)<sup>144</sup>. When DNA DSBs occur, cells primarily rely on the homologous recombination repair (HRR) pathway for repair. PARP inhibitors interfere with the base excision repair (BER) pathway, thereby preventing the repair of DNA damage in cells. This results in the inability of HRR-deficient cells to repair damaged DNA via HRR or BER, resulting in synthetic lethality and cell death<sup>145,146</sup>. The proteins encoded by *BRCA1* and *BRCA2* play a role in HRR, an important process of DNA repair. Cancer cells with *BRCA1/BRCA2* mutations are particularly sensitive to PARP inhibitors, which cause unrepaired DNA fragmentation and the death of cancer cells<sup>145</sup>. Moreover, PARP inhibitors can also interfere with the NHEJ (non-homologous end joining) DNA repair pathway. When the HRR pathway is insufficient, it will force cells to rely on the error-prone NHEJ pathway, leading to increased genomic instability and cell death, particularly in cancer cells with defective HRR mechanisms<sup>144,147</sup>.

At present, three PARP inhibitors (olaparib, rucaparib, and niraparib) have been approved by the FDA for the treatment of ovarian cancer relapse after platinum therapy, and olaparib and rucaparib have also been approved for the treatment of *BRCA1/BRCA2* mutated ovarian cancer<sup>148-151</sup>. Niraparib has been approved by the Therapeutic Goods Administration (TGA) in Australia as a monotherapy for newly diagnosed women with advanced ovarian cancer who respond to platinum-based chemotherapy, regardless of whether or not they have a *BRCA* mutation<sup>152</sup>. Moreover, the TGA has granted approval for olaparib as a monotherapy for maintenance therapy in patients with platinum-sensitive relapsed HGSOC who possess a *BRCA* mutations (germline or somatic) and have demonstrated a response (complete or partial) to prior therapy<sup>153</sup>.



In addition, PARP inhibitor maintenance therapy has become the standard-of-care for recurrent EOC. In the US and the European Union (EU), three PARP inhibitors—olaparib, niraparib, and rucaparib—are employed for maintenance therapy in women with platinum-sensitive recurrent EOC <sup>154</sup>. Furthermore, olaparib has been approved in the US for the treatment of patients with advanced EOC and germline *BRCA* mutations. These patients have received three or more prior chemotherapies and are receiving PARP inhibitors without regard to sensitivity to platinum-based therapy <sup>155</sup>. Rucaparib is approved in the US and EU for patients with platinum-sensitive recurrent EOC. The patients have germline and/or somatic *BRCA* mutations and have received at least two prior chemotherapy treatments <sup>156</sup>. In addition, PARP inhibitors have been approved for the treatment of other cancers. For instance, in the US, the FDA has approved olaparib for the treatment of breast, pancreatic, and prostate cancers <sup>157,158</sup>. Rucaparib is employed to treat prostate cancer, while niraparib is utilised to treat endometrial cancer <sup>159</sup>. In Europe and the UK, olaparib is approved for the treatment of breast cancer with *BRCA* mutations or homologous recombination defects <sup>160</sup>.

#### 1.2.8.3.2 Bevacizumab

Bevacizumab is a monoclonal antibody that targets vascular endothelial growth factor (VEGF). Its introduction has revolutionised cancer treatment, as it hinders tumour angiogenesis, a key process in tumour growth and metastasis <sup>161</sup>. In the field of ovarian cancer, bevacizumab has emerged as a promising treatment strategy, particularly when combined with standard chemotherapy regimens. Ovarian cancer is characterised by its aggressiveness and a high rate of recurrence, which presents significant treatment challenges. Nevertheless, the capacity of bevacizumab to disrupt the tumour blood supply has been demonstrated to have a significant impact on patient prognosis <sup>162</sup>. The study (GOC-218) by Tewari and colleagues demonstrated that there was no significant difference in OS for ovarian cancer patients who were treated with bevacizumab compared to the control group. Nevertheless, for patients with stage IV ovarian cancer, those who received bevacizumab in combination with supportive care exhibited an improved OS relative to the control group <sup>163</sup>. Another study (ICON7) showed that among 1,528 ovarian cancer patients, there was no significant difference in 36-month PFS between the standard chemotherapy group and those who received bevacizumab. However, the 42-month PFS was 14.5 months in the standard chemotherapy group and 18.1 months with bevacizumab, thus suggesting that bevacizumab is more effective in ovarian cancer <sup>164</sup>. Despite the promise of bevacizumab therapy, it is not without its challenges, and adverse effects, such

as hypertension and proteinuria, are evident <sup>165</sup>. In 2018 the FDA approved bevacizumab as a first-line and maintenance treatment option for advanced ovarian cancer <sup>166</sup>.

#### 1.2.8.3.3 Durvalumab

Durvalumab is a targeted drug that was approved by the FDA in 2017 to treat locally advanced or metastatic urothelial carcinoma and under clinic trial for stage III unresectable non-small cell lung cancer (NSCLC) <sup>167</sup>. While this drug is not currently approved to treat ovarian cancer, it is being investigated for its potential to do so. Durvalumab is a human IgG1 monoclonal antibody against the PDL-1 (CD274) molecule <sup>168</sup>. PDL-1 is a transmembrane protein often expressed on dendritic cells and macrophages, and the PD-1 receptor is a transmembrane protein expressed on activated T cells in peripheral tissues <sup>169</sup>. In the tumour microenvironment, cancer cells can induce the up-regulation of PDL-1 because the interaction between PD-1 and PDL-1 leads to inhibition of T cell activation, thus reducing the possibility of immune attack on cancer cells and promoting tumour growth and proliferation. The combination of durvalumab and PDL-1 can prevent the interaction of PDL-1 with T cell PD-1 receptors and CD80. This will extend the lifespan of activated T cells, thereby conducting an immune attack against cancer cells, ultimately leading to the death of cancer cells <sup>170</sup>. Currently, the National University Hospital of Singapore and Box Hill Hospital in Melbourne is conducting a phase II randomised trial (ClinicalTrials.gov Identifier: NCT03405454) investigating durvalumab compared with other chemotherapy methods to treat recurrent OCCC <sup>171,172</sup>.

#### 1.2.9 Chemoresistance and relapse

Up to 75% of patients respond to surgery and chemotherapy. However, treatment with chemotherapy drugs often leads to complications and resistance. In some studies, over 70% of patients relapsed and some of them developed resistance to chemotherapy <sup>173,174</sup>. These factors result in treatment failure and over 90% of deaths, leaving little chance for a cure <sup>175</sup>. Recurrent disease occurs in approximately 25% of patients with early-stage ovarian cancer, however, for patients with advanced disease, this number is higher. More than 80% of patients diagnosed initially with advanced disease will develop a recurrence <sup>176</sup>. Hennessy and colleagues have shown that up to two-thirds of patients diagnosed with advanced ovarian cancer will experience a recurrence of the disease within 18 months of diagnosis, irrespective of the initial therapeutic intervention <sup>177</sup>. Chuang and colleagues have shown that even after complete remission with

first-line therapy, about 70-85% of patients with EOC will experience recurrent disease. The median survival for patients with recurrence is between 12 to 24 months<sup>178</sup>. While secondary cytoreductive surgery may provide clinical benefit for some patients, its success depends on the number of recurrent sites and the surgeon's skill<sup>179-181</sup>.

OCCC is more chemoresistant than HGSOC, indicating a higher resistance to chemotherapy<sup>182</sup>. Studies have shown that the relapse rates for OCCC patients are 29% and 30% at stages I and II, respectively. However, the relapse rates for patients in stages III and IV are 62% and 73%, respectively<sup>183,184</sup>. Furthermore, for OCCC patients who experience a relapse, the five-year survival rate is only 13.2%, with a median survival of 10 months. This is significantly lower than that for HGSOC patients, which is 18.2% with a median survival of 18.9 months<sup>184,185</sup>. In addition, only 30% of women with HGSOC relapsing within 5-12 months will respond to platinum drug retreatment<sup>186</sup>. In terms of OCCC, only 11-27% of patients will respond to platinum-based therapy, and when recurrent disease occurs, the response rate will drop to 1-2%<sup>187-189</sup>.

#### 1.2.10 Molecular events in ovarian cancer

Some studies have shown that there is a significant association between ovarian cancer subtypes and specific gene mutations (Figure 1.5), providing potential therapeutic opportunities for ovarian cancer<sup>190-192</sup>. *TP53*, *BRCA1/2*, *PIK3CA*, *ARID1A/B* (discussed further in Section 1.4.5) and *KRAS* are commonly reported in EOC to be mutant or have copy number differences. *SMARCA4* is mutated in SCCOHT of likely germ cell origin (GCOC), while *SMARCA2* is epigenetically silenced<sup>72</sup>.

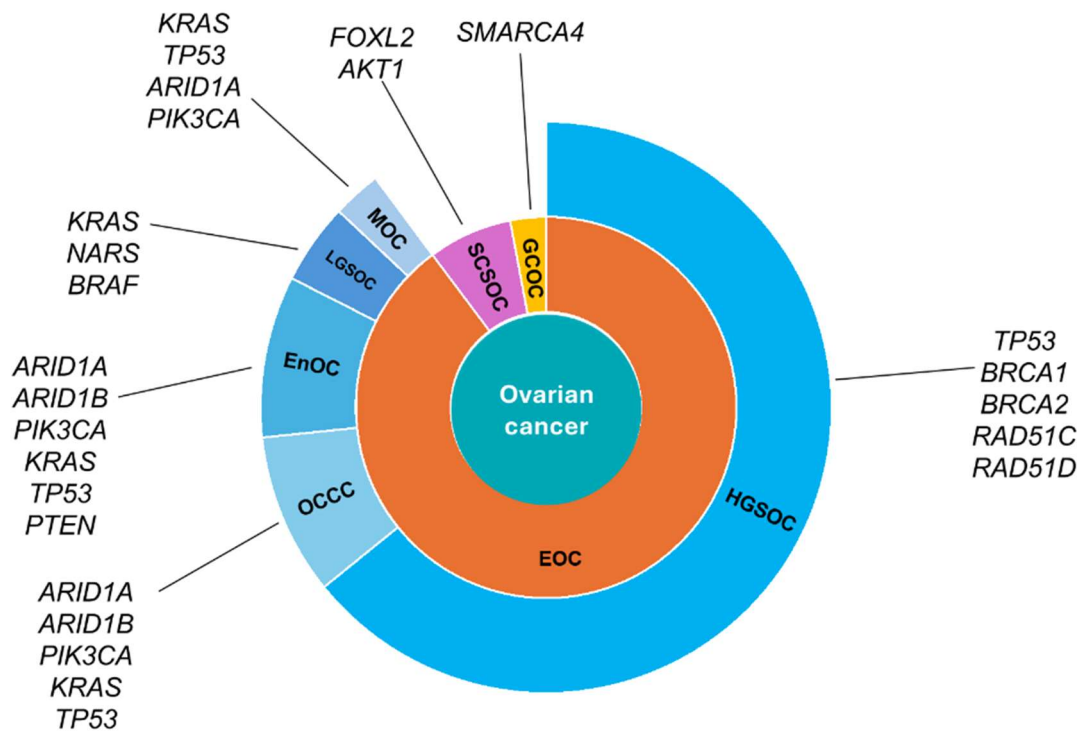


Figure 1.5 Ovarian cancer subtypes and associated mutated genes. Epithelial ovarian cancer (EOC); Germ cell ovarian cancer (GCOC); Sex cord stromal ovarian cancer (SCSOC); High-grade serous ovarian cancer (HGSOC); Endometrioid ovarian cancer (EnOC); Ovarian clear cell carcinoma (OCCC); Low-grade serous ovarian cancer (LGSOC); Mucinous ovarian cancer (MOC). AT-rich interaction domain 1A (*ARID1A/B*), Breast cancer 1/2 (*BRCA1/2*), Asparaginyl-tRNA synthetase (*NARS*), B-Raf Proto-Oncogene, Serine/Threonine Kinase (*BRAF*), Kirsten rat sarcoma virus (*KRAS*), Phosphatidylinositol-4,5-bisphosphate 3-kinase catalytic subunit alpha (*PIK3CA*), Phosphatase and tensin homolog (*PTEN*), RAD51 Recombinase C/D (*RAD51C/D*), SWI/SNF Related, Matrix Associated, Actin Dependent Regulator Of Chromatin, Subfamily A, Member 4 (*SMARCA4*), AKT Serine/Threonine Kinase 1 (*AKT1*), Forkhead box L2 (*FOXL2*), Tumour Protein P53 (*TP53*). Figure adapted from Yee, et al <sup>193</sup>.

#### 1.2.10.1 *TP53*

*TP53* is located on the short arm of chromosome 17 (17p13.1), and codes for the protein p53 that has a mass of 53 kDa <sup>194-196</sup>. Due to its critical functions in preserving cellular integrity, p53 has earned the title of "guardian of the genome" <sup>197,198</sup>. When cell DNA is damaged by chemicals, ultraviolet (UV) light, or radiation, p53 can activate DNA repair proteins that

prevent cell growth by maintaining the cell cycle at the G1/S transition, allowing DNA repair and initiating apoptosis when DNA damage becomes irreparable. This prevents damaged cells from mutating and developing tumours. In different cellular contexts, p53 prevents cancer by acting as a tumour suppressor <sup>197</sup>. It plays a role in multiple tumour suppressor pathways, including cell cycle arrest, apoptosis, senescence, differentiation, DNA repair and autophagy <sup>199,200</sup>.

p53 has a high mutation rate in cancer. *TP53* mutations are present in over 50% of all types of human cancers <sup>201</sup>. However, unlike many other tumour suppressor genes, many *TP53* mutations are missense mutations, and these missense mutations mainly occur in the region encoding the p53 DNA binding domain (DBD) <sup>202</sup>. According to a database (<https://tp53.isb-cgc.org/>) analysis by the National Cancer Institute (NCI) of the National Institutes of Health, more than 73% of the 28,866 known mutations are missense mutations (Figure 1.6) <sup>203</sup>. *TP53* missense mutations have been shown to lead to accumulation of mutant p53, numerous of these mutations being shown to gain new functions (GOF; gain-of-function), or lead to loss of wild-type (WT) p53 and, as such are unable to activate p53 target genes, thereby losing its normal tumour suppressor function (LOF; loss-of-function) <sup>204-208</sup>. Due to mutant *TP53* losing its ability to activate the classical DNA common binding motif in the promoters of p53 target genes, some mutants produce a trans-dominant inhibition of the WT protein, decreasing its ability to bind to p53 response elements and thus counteracting the tumour suppressive effect of WT p53 <sup>209,210</sup>. Some recent controversies have identified a lack of function for GOF mutant p53. Wang and colleagues demonstrated that the removal of mutant *TP53* had no effect on cell survival, proliferation, migration, metabolism, or anticancer drug treatment in 16 human cancer cell lines and 2 mouse cancer cell lines <sup>211</sup>. This goes against decades of literature that indicates that p53 GOF mutants are oncogenic and will require confirmation by additional research groups <sup>212</sup>. From the literature, more than 96% of HGSOV contain *TP53* mutations, and *TP53* is mutated in around 15% of OCCC <sup>213</sup>. Undoubtedly, mutant p53 plays a crucial role in in ovarian cancer <sup>214,215</sup>.

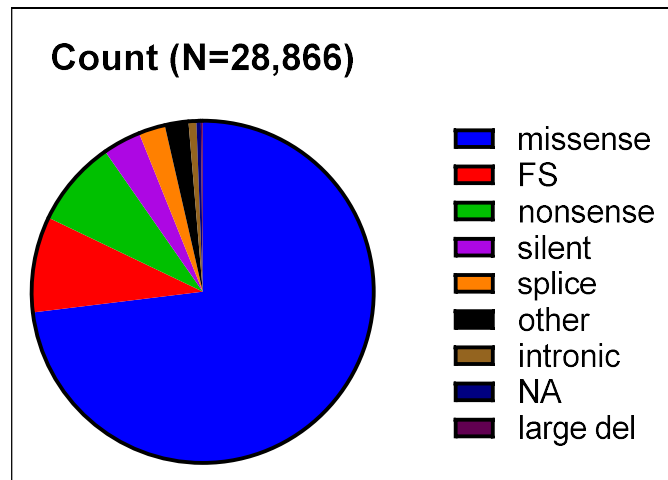


Figure 1.6 Percentage of different types of *TP53* somatic mutations found in human ovarian cancers. FS, frameshift; NA, not applicable/not available. Data from the *TP53* Database (<https://tp53.isb-cgc.org/>).

#### 1.2.10.2 *PIK3CA*

Phosphatidylinositol-3-kinase (PI3K)/AKT/mammalian target of rapamycin (mTOR) is one of the most important intracellular pathways in the body, responsible for regulating a series of life activities of cells, such as growth, survival, metabolism and movement, as well as regulating tumour formation<sup>216,217</sup>. Activation of the PI3K/AKT/mTOR pathway contributes to tumour development and resistance to anticancer therapies<sup>218</sup>. Almost all human cancers (such as breast and colorectal cancers) have disorders of the PI3K/AKT/mTOR pathway, making components of this pathway potential therapeutic targets<sup>219</sup>. Some studies found that inhibiting PI3K can reduce cell proliferation and increase cell death<sup>220-222</sup>. A study by Mabuchi and colleagues demonstrated that the frequency of strongly phosphorylated mTOR immunoreactivity was significantly higher in OCCC than in serous ovarian cancer (SOC). These findings suggested that tumour progression in OCCC may be more dependent on mTOR than in SOC. Furthermore, mTOR was activated in 86.6% of OCCC. Consequently, it is proposed that mTOR may be a potential therapeutic target for the treatment of OCCC<sup>223</sup>.

*PIK3CA* is a 34 kb gene consisting of 20 exons located on chromosome 3q26.3 and coding for a subunit of PI3K. It encodes 1068 amino acids, and the molecular weight of the protein is 124 kDa<sup>216,217,224-228</sup>. There are somatic mutations and copy number amplifications in *PIK3CA* in human cancers such as ovarian, breast, endometrial, and lung cancer<sup>227,229</sup>. *PIK3CA* mutations

are gain-of-function mutations that drive oncogenesis. Studies have shown that *PIK3CA* gene amplification is present in 24.6% of ovarian cancers <sup>230</sup>. Some studies show that the *PIK3CA* mutation rate in breast cancer is very high (40%), followed by endometrial (36%), head/neck squamous cell carcinoma (33%), colorectal (32%) and gastric cancer (25%) <sup>227,230,231</sup>. Also, some studies have shown that *PIK3CA* mutations are present in 26 of 73 (35.6%) hepatocellular carcinomas, one of 88 (1.1%) acute leukemias (12 acute lymphocytic leukemias and 76 acute myelocytic leukemias), and 6% of EOC <sup>229,231</sup>. In a study comprising 113 patients with OCCC, Stružinská and colleagues identified the *PIK3CA* as the second most frequently mutated gene, with a mutation rate of 47% among 100 eligible patients, following *ARID1A* at 51% <sup>232</sup>. Another study indicated that the incidence of *PIK3CA* mutations in EnOC and OCCC was 20% , much higher than was seen in HGSOC at 2.3% and not seen in mucinous ovarian cancer at all <sup>233</sup>. However, the number of OCCC samples included in this study was smaller than that of HGSOC (5 vs. 88), which may have an impact on the representativeness of the research results.

#### 1.2.10.3 *BRCA1/BRCA2*

Breast cancer susceptibility gene 1 (*BRCA1*) and breast cancer susceptibility gene 2 (*BRCA2*) are two tumour suppressor genes <sup>234,235</sup>. In normal cells, *BRCA1/2* participates in and triggers the cellular response to DNA damage. When cells are damaged, these genes prevent cell proliferation and promote cell apoptosis <sup>236</sup>. However, when *BRCA1/2* genes are mutated, their tumour suppressing function will be altered, causing DNA damage to accumulate in cells, and eventually the region where the mutated gene is located will be transformed into cancerous tissue <sup>237</sup>. Since 20% of EOC have *BRCA1/2* mutations, and *BRCA1/2* mutations are observed in about 6% of OCCC patients, *BRCA1/2* pathways are also of potential therapeutic interest for OCCC <sup>22</sup>. PARP inhibitors have been approved for *BRCA*-mutant ovarian cancers, see Section 1.2.8.3.1.

### 1.3 Ovarian Clear Cell Carcinoma (OCCC)

As the main topic of this thesis, OCCC will be discussed in greater detail. OCCC was originally named mesonephroma by Schiller in 1939. He believed it originated from the mesonephric gland, similar to kidney cancer <sup>238</sup>. Then, in 1973, the WHO recognised it as a distinct histological subtype of ovarian cancer and named it ovarian clear cell carcinoma. OCCC is a



rare subtype of EOC that exhibits distinctive histopathological characteristics and specific biological and clinical behaviours when compared to other types of ovarian cancer.

Pathologically, OCCC lesions usually present as large masses consisting of solid tissue protruding into the cystic cavity and often show a combination of papillary, tubular cystic and solid microscopic patterns. The tumour infiltrates the ovarian interstitium. This leads to desmoplasia, stromal destruction, hyalinisation, and fusion of the epithelial elements<sup>239</sup>. Under the microscope, OCCC has distinct morphological characteristics. It displays a combination of tubules, solid regions, and complex papillae, as well as cells with prominent nucleoli and a clear cytoplasm filled with glycogen. Most cells have apically proliferative nuclei, which are polychromatic and have distinct nucleoli. Cells come in many shapes, including cuboidal, polygonal, and flattened<sup>45,240</sup>. The histological staining indicated that the OCCC cell papillae were rounded in shape, exhibiting a clear inner core comprising one or two layers of cells with uniform but high-grade nuclei (Figure 1.7)<sup>241</sup>.

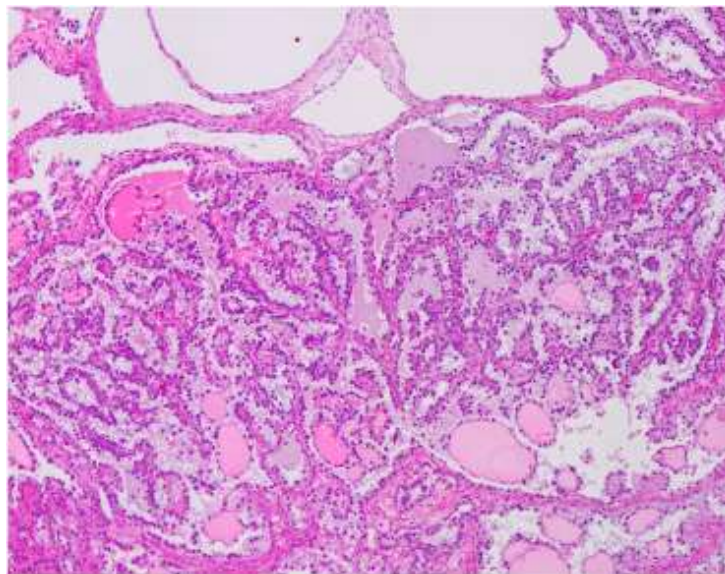


Figure 1.7. The haematoxylin and eosin (H&E) stained histology image of OCCC showing a predominantly papillary architecture. Image reproduced from Hussein et al<sup>241</sup>.

### 1.3.1 Epidemiology of OCCC

The incidence of OCCC is significantly different based on race and geography. In North America and Europe, the incidence of OCCC is about 1-12%, but in Asian countries, it is higher<sup>242</sup>. In Korea, approximately 12.5% of patients with EOC have OCCC<sup>243</sup>. A study conducted



by Qingdao University in China showed that among 697 ovarian cancer patients at a single hospital, approximately 14.2% (n=99) had OCCC <sup>244</sup>. In Taiwan, about 20% of patients with EOC had OCCC <sup>245</sup>. OCCC is particularly frequent in Japan, where it constitutes almost 27% of all EOC patients <sup>246</sup>. Ovarian Cancer Australia (<https://www.ovariancancer.net.au/booklet/resilience-kit>) reports that OCCC accounts for approximately 10% of EOC in Australia <sup>247</sup>. A Surveillance, Epidemiology, and End Results (SEER) study showed that 4.8%, 3.1%, and 11.1% of white, black, and Asian women respectively, living with EOC in the United States have the OCCC sub-type <sup>248</sup>.

### 1.3.2 Pathogenesis of OCCC

While the pathogenesis of OCCC is largely unknown, numerous studies suggest that it may arise from endometriotic lesions <sup>249</sup>. Interestingly, OCCC patients have fewer pregnancies compared with HGSOC patients <sup>67,244,250</sup>. Hermens and colleagues showed that the age-adjusted incidence rate ratio for OCCC was significantly higher in women with endometriosis, 2.29 (95% CI 1.24 to 4.20) <sup>251</sup>. Furthermore, Stamp and colleagues suggested that endometriosis was identified in the final pathology report in 51% of OCCC cases <sup>179</sup>. The study by Kvaskoff and colleagues showed that patients with endometriosis had a 3.4-fold increased risk of OCCC <sup>252</sup>.

Literature suggest that progesterone receptor and estrogen receptor mediated female steroid hormones have key influences on ovarian cancer, including effects on cancer cell proliferation and apoptosis <sup>253,254</sup>. A study by Sieh and colleagues indicated that the expression of progesterone receptor and estrogen receptor affects the prognosis of patients with HGSOC. However, their study showed that no significant correlation was identified between the expression of progesterone receptor and estrogen receptor and the prognosis of OCCC <sup>255</sup>. Moreover, a study conducted by Osaku and colleagues indicated that estrogen receptor expression was not correlated with the prognosis of CCC <sup>256</sup>.

Approximately 48.5-56.3% of OCCC patients are diagnosed at stage I, as well as approximately 9.9-11% at stage II <sup>62,187</sup>. Furthermore, most patients with OCCC present with a unilateral large ovarian mass that is diagnosed early in the progression of the disease <sup>257</sup>. In the early stages, the prognosis of OCCC is similar to, or better than, that of HGSOC. Some

studies have shown no significant difference in PFS hazard ratios between OCCC and HGSOC at stage I, as well as those at stage II <sup>258,259</sup>. However, when the cancer progresses to an advanced stage (III-IV), patients with OCCC have a significantly worse prognosis than patients with advanced HGSOC. Studies have shown that at advanced stages, OCCC patients had significantly worse 5-year OS and PFS than advanced HGSOC patients <sup>244,260</sup>.

### 1.3.3 Treatment for OCCC

The current surgical treatment options and chemotherapy for OCCC are similar to those used for other EOCs <sup>261</sup>, as previously described in sections 1.2.8.1 and 1.2.8.2. Radiation therapy to the abdomen may be beneficial for a subset of patients with OCCC following surgical treatment. In one study, 16 patients were treated with radiotherapy following surgery. The 5-year OS rate for this group was 81.8%, compared to 33.3% for patients who received platinum-based chemotherapy <sup>262</sup>. Furthermore, another study demonstrated that the administration of radiation therapy following chemotherapy in patients with early-stage OCCC (stages IC and II) resulted in a 20% increase in the five-year disease-free survival rate <sup>263</sup>. In addition, some targeted therapies have been demonstrated to exert an influence on OCCC, including bevacizumab. In a study examining the safety and efficacy of bevacizumab in conjunction with a chemotherapy combination of paclitaxel and carboplatin in newly diagnosed advanced ovarian cancer (43 patients with OCCC), Komiyama and colleagues illustrated that the PFS for OCCC cases was 12.3 months, with a response rate of 63.6% <sup>264</sup>.

## 1.4 Epigenetics

### 1.4.1 The epigenome

Epigenetics refers to changes in gene expression without altering the genetic code, meaning that epigenetic mechanisms affect the function of DNA without altering the DNA sequence <sup>265</sup>. It is important to note that, unlike genetic changes, epigenetic processes are dynamic rather than fixed. While some epigenetic changes may persist for an extended period, such as several years or even a lifetime, others may be transient <sup>266</sup>. Epigenetics can be divided into four areas of study: 1) Histone modifications, including methylation, acetylation, phosphorylation, adenylation, ubiquitination and ADP ribosylation; 2) DNA methylation; 3) MicroRNA (miRNA)-mediated and other non-coding RNA epigenetic modifications; and 4) Nucleosome positioning <sup>267</sup>. When epigenetic mechanisms are disturbed, this can lead to inappropriate

activation or inhibition of various signalling pathways, increasing the risk of diseases such as cancer <sup>268,269</sup>. Epigenetics not only plays a crucial role in cell fate determination but is increasingly recognised as playing a role in oncogenic transformation <sup>270-272</sup>. Parreno and colleagues have demonstrated that epigenetic alterations, which do not alter the DNA sequence, are sufficient to establish an oncogenic gene expression program that supports tumorigenesis and progression <sup>273</sup>.

#### 1.4.1.1 Histone

Histones are basic proteins with a mass of about 11 to 20 kDa. DNA wraps around histone proteins to form nucleosomes, which are subunits of chromatin <sup>274</sup>. Each nucleosome is surrounded by 147 base pairs of DNA, and the histone octamer consists of two dimers of H2A and H2B, and a tetramer of H3 and H4 proteins <sup>275</sup>. The structure of chromatin is regulated by two types of enzymes. The first one adds or removes covalent modifications to histones and the second is an ATP-dependent chromatin remodelling enzyme. Both enzymes relax histone-DNA contacts through the energy generated by hydrolysis of ATP, thereby facilitating changes in nucleosome positioning or chromatin structure <sup>276</sup>. SWItch/Sucrose Non-Fermentable (SWI/SNF), an ATP-dependent chromatin remodeller, plays an important role in transcription, DNA replication and repair <sup>277</sup>.

#### 1.4.1.2 Epigenetic writers

Epigenetic “writers” are enzymes responsible for making a variety of chemical modifications to DNA and histones that play a critical role in regulating gene expression. These enzymes include DNA methyltransferases (DNMTs), histone lysine methyltransferase (KMTs), protein arginine methyltransferase (PRMTs) and histone acetyltransferases (HATs). In mammals there are five members of the DNMT family, DNMT1, DNMT2, DNMT3A, DNMT3B and DNMT3L. DNMT1 is the most abundant DNMT in adult cells and functions as a maintenance methyltransferase <sup>278</sup>. In mammals, DNMT2 inhibits DNA methylation, methylating the 38th cytosine residue in the anticodon loop of aspartate transfer RNA (tRNA (Asp)) <sup>279</sup>. DNMT3A and DNMT3B are expressed at higher levels in early embryonic cells, where the rate of *de novo* methylation is high, but their expression is downregulated in adult somatic cells, making DNMT3A and DNMT3B essential for *de novo* methylation during mammalian development

<sup>280</sup>. DNMT3L is not thought to function as a DNA methyltransferase because it lacks the C-terminal structural domain residues required for methyltransferase activity. However, when DNMT3L is present *in vitro*, it can stimulate increased DNA methylation of DNMT3A and DNMT3B <sup>281,282</sup>.

The E3 ubiquitin ligase family plays a pivotal role as a group of epigenetic writers in genetic regulation and cellular homeostasis <sup>283</sup>. Among these, RING (Really Interesting New Gene) Finger Protein (RNF)20 and RNF40, as E3 ubiquitin ligases, are part of a complex responsible for the mono-ubiquitination of histone H2B lysine 120 (H2Bub1), a key epigenetic mark associated with active transcription <sup>284</sup>. These proteins play a pivotal role in transcriptional elongation, chromatin structure maintenance, and DNA damage repair. Furthermore, the inactivation of RNF20 and RNF40 has been linked to the development of several cancers, as their dysfunction may lead to dysregulated gene expression and genomic instability <sup>285</sup>. It has been demonstrated that these E3 ubiquitin ligases play a pivotal role in regulating gene expression, promoting DNA repair and maintaining normal cellular function <sup>286</sup>.

#### 1.4.1.3 Epigenetic readers

Epigenetic "readers" are proteins that recognise and interpret chemical modifications introduced by epigenetic writers on DNA and histones <sup>287</sup>. Examples of such proteins include bromodomain proteins (e.g. BRD4), chromodomain proteins (e.g. HP1), and tandem Tudor domain proteins (e.g. 53BP1). These readers play a pivotal role in translating the epigenetic code into functional outcomes by recruiting other proteins to specific genomic loci. BRD4 is a key reader of acetylated histones, which play a critical role in nucleosome stability by acetylating H3K122 as a novel histone acetyltransferase (HAT) <sup>288</sup>. HP1 can recognise methylated histones and is involved in the formation of heterochromatin and the silencing of genes <sup>289</sup>. 53BP1 is a crucial reader of histone methylation marks and is involved in DNA damage response and repair processes <sup>290</sup>. The dysregulation of epigenetic readers has been linked to a variety of diseases, including cancer, and thus they have the potential to be therapeutic targets.

#### 1.4.1.4 Epigenetic erasers

Epigenetic "eraser" is a term used to describe a group of enzymes that catalyse the removal of chemical modifications (e.g. methylation and acetylation) of DNA and histones. These

enzymes play a key role in regulating gene expression by reversing the effects of epigenetic modifications introduced by epigenetic writers <sup>287</sup>. Epigenetic erasers include DNA demethylases, histone demethylases, histone deacetylases (HDAC) and histone deubiquitinases. DNA demethylases, such as TET enzymes, are responsible for the active removal of the methyl group from cytosine residues in DNA, which results in DNA demethylation and the reactivation of silenced genes <sup>291</sup>. Histone demethylases, such as LSD1 and LSD2, are responsible for the removal of methyl groups from histones, thereby regulating chromatin structure and gene expression <sup>292</sup>. Conversely, HDAC removes acetyl groups from lysine residues of histones, resulting in chromatin condensation and transcriptional repression <sup>293</sup>. In addition, inhibitors targeting histone demethylases and HDACs have demonstrated potential as anticancer therapies in clinical studies <sup>294</sup>. Histone deubiquitinases, such as USP22, are responsible for the removal of ubiquitin from histone H2B at lysine 120, leading to changes in chromatin structure that can result in the activation or repression of gene expression. It has been demonstrated that the inhibition of *USP22* results in increased apoptosis in mouse and human embryonic fibroblasts, as well as in a range of cancer cell lines, including those derived from colorectal cancer and glioma <sup>295,296</sup>.

#### 1.4.1.5 SWItch/Sucrose Non-Fermentable (SWI/SNF) Chromatin remodelling complex

The SWI/SNF complex, identified in yeast in 1984, plays an important role in chromatin remodelling <sup>297</sup>. It is composed of over 10 subunits and is essential for regulating gene expression by modifying chromatin structure <sup>298,299</sup>. In mammals, the SWI/SNF complex is composed of at least 29 genes <sup>300</sup>. The SWI/SNF complex comprises genes that assemble into three distinct final forms: BAF (BRG1/BRM-associated factor), pBAF (polybromo-associated BAF), and the ncBAF (non-canonical BAF) <sup>301,302</sup>. Despite their diversity, all three complexes contain mutually exclusive catalytic ATPase subunits, namely SMARCA2 and SMARCA4, and share numerous associated proteins <sup>303</sup>.

The primary function of the SWI/SNF complex is to orchestrate chromatin dynamics. The complex regulates various processes in an ATP-dependent manner, including histone dimer ejection, nucleosome ejection, and nucleosome-sliding repositioning. These activities are facilitated by harnessing the energy generated through the hydrolysis of ATP, showcasing the ability of the complex to confidently remodel chromatin structure <sup>304</sup>. This complex plays a crucial and decisive role in controlling patterns of gene expression, such as gene transcription,

RNA processing, cell cycle, apoptosis, development, differentiation, and DNA replication and repair through its dynamic chromatin remodelling activities<sup>305</sup>.

#### 1.4.1.5.1 Role of SWI/SNF complexes in cancer development

Abrogation of the SWI/SNF complex is a significant factor in the development and progression of various malignancies. Research has shown that mutations in genes that code for SWI/SNF complex members, many of which are loss-of-function mutations, are present in around 20% of human cancers. This suggests that the disruption of SWI/SNF activity promotes the development or progression of cancer<sup>306-309</sup>. Loss of the subunit SMARCB1 disrupts the binding of the SWI/SNF complex to lineage-specific enhancers while preserving binding to oncogenic super-enhancers, thereby promoting the expression of oncogenes. This phenomenon is typically observed in childhood malignant rhabdomyosarcoma (MRT), epithelioid sarcoma, chordoma, and renal medullary carcinoma<sup>310-312</sup>. The SMARCA4 subunit of the catalytic ATPase is the most mutated Snf2-like ATPase in humans. Breast, lung, and colorectal cancers exhibit a loss of SMARCA4 activity<sup>313-315</sup>. Cancers with mutant *SMARCA4* are generally more aggressive and have a poorer prognosis than other highly mutated subunits, such as the PBRM1 subunit of pBAF<sup>316</sup>. Additionally, the SWI/SNF subunits ARID1A and ARID1B have also been associated with cancer progression.

#### 1.4.1.5.2 AT-rich interaction domain 1A (ARID1A) and ARID1B

##### 1.4.1.5.2.1 ARID1A

AT-rich interacting domain 1A (*ARID1A*) is located on human chromosome 1p35.3 and encodes BAF250a<sup>317</sup>. It is a component of the SWI/SNF chromatin remodelling complex. It binds DNA non-specifically through its AT-rich interacting DNA-binding domain, which regulates many cellular processes such as development, proliferation, differentiation, DNA repair and tumour suppression<sup>318</sup>. It has been demonstrated that ARID1A encodes two distinct isoforms, containing 2285 and 2086 amino acids respectively, with the latter missing a 218-amino acid segment corresponding to the region between exon 17 and exon 18. However, the relative expression and functional significance of these two isoforms remain unclear<sup>319</sup>. In cancer, *ARID1A* is the gene with the highest mutation frequency of the BAF subunits. Among cancers other than ovarian, 29% of stomach cancers, 5-10% of colorectal cancers, and 3-5% of

pancreatic cancers have *ARID1A* mutations<sup>317,320-322</sup>. Guo and colleagues have shown that *ARID1A* is effective in inhibiting the migration of cells in a variety of breast cancer cell lines. Moreover, *ARID1A* deletion may cause genomic instability in early cancer cells during carcinogenesis. In addition, loss of *ARID1A* tumour suppressor function triggers cancer development by perturbing the DNA damage response and cell cycle pathways<sup>323</sup>. Several studies have indicated that the loss of ARID1A correlates with the activation of *PIK3CA* and the simultaneous downregulation of *PTEN* expression. Both events lead to the activation of the PI3K/AKT/mTOR signalling pathway, which plays a crucial role in regulating the cell cycle (Figure 1.7)<sup>324-327</sup>.

*ARID1A* is mutated in approximately 42-67% of OCCC. A study showed that in 119 OCCC patients, 55 patients (46%) had *ARID1A* mutations, and these mutations were closely aligned with loss of the ARID1A/BAF250a protein<sup>328</sup>. Studies have shown that mutations in *ARID1A* accumulate during the transition from benign endometriosis through atypical endometriosis to OCCC. Therefore, they suggested that *ARID1A* mutations occurred at the early stage of OCCC development<sup>329,330</sup>. A study from the Johns Hopkins University School of Medicine showed that restoration of WT ARID1A in ovarian cancer cells carrying *ARID1A* mutations was sufficient to inhibit tumour cell proliferation. Moreover, when *ARID1A* was silenced, cell proliferation and tumorigenicity were enhanced. They also showed that the reduction of *ARID1A* did not affect the binding rate of p53 protein to the cyclin-dependent kinase inhibitor 1A (*CDKN1A*) gene (encoding p21) and the Sma and Mad-related gene (*SMAD3*) promoter, but the transcriptional activities of p21 and *SMAD3* were reduced by *ARID1A* knockdown. Interestingly, their results showed that there is mutual exclusion between *TP53* and *ARID1A* mutations. When *ARID1A* was mutated, all tumours contained WT *TP53*. When *TP53* was mutated, tumours contained WT *ARID1A*<sup>331</sup>.

#### 1.4.1.5.2.2 ARID1B

*ARID1B* codes for a subunit of SWI/SNF and is mutated in 5-10% of colorectal cancer and gastric cancer<sup>320,332</sup>. In the ARID domain, *ARID1A* and *ARID1B* have 50% homology overall, and their amino acid sequences show nearly 80% homology<sup>319</sup>. Although they have similar amino acid sequences, they have different functions in cell development and control of the cell cycle<sup>333</sup>. Nagl and colleagues found that during ascorbate-induced osteoblast differentiation, *ARID1A* deficiency caused a delay in cell cycle arrest of mouse MC3T3-E1 pre-osteoblasts,

but *ARID1B* deficiency had no effect on cell cycle arrest, indicating a dominant effect of *ARID1A* <sup>334</sup>. In addition, an OCCC-based study found that as the expression of *ARID1A* decreases, the transcription of RNA Polymerase II becomes dysregulated <sup>335</sup>. However, the same study found when the expression of *ARID1B* increased, the transcriptional dysregulation of RNA Polymerase II was paused and restored to normal physiological levels. Therefore, *ARID1B* seems to be able to compensate for *ARID1A*.

#### 1.4.1.5.2.3 ARID1A and synthetic lethality

Crosstalk between ARID1A and other signalling pathways enables the selective targeting of ARID1A-deficient cells by PARP, Enhancer of zeste homolog 2 (EZH2) and HDAC inhibitors. ARID1A and EZH2 act on PI3K interacting protein 1 (*PIK3IP1*), which functions as a negative regulator of PI3K/Akt signalling (Figure 1.8) <sup>336</sup>. Throughout the regulatory process, ARID1A is responsible for the activation of *PIK3IP1* expression, whereas EZH2 is responsible for the inhibition of *PIK3IP1* expression. Consequently, following loss of function of ARID1A, *PIK3IP1* is inhibited, thereby preventing the inhibition of the PI3K pathway. Consequently, the utilisation of an EZH2 inhibitor in cells exhibiting ARID1A loss of function inhibits the activity of EZH2, thereby inhibiting cell survival functions of PI3K signalling <sup>337</sup>. Studies have demonstrated that the use of EZH2 inhibitors can decrease the growth of *ARID1A* mutant cells and induce cell death <sup>336</sup>.

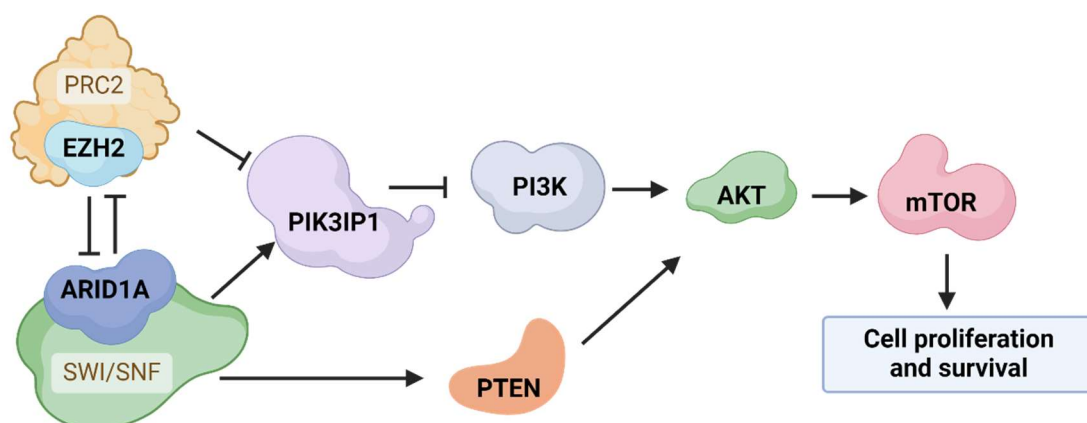


Figure 1.8 Schematic Representation of the interplay between EZH2, ARID1A, PIK3IP1, PI3K, AKT, mTOR, and PTEN in cell proliferation and survival. The figure illustrates the regulation of the PI3K/AKT/mTOR pathway by EZH2, ARID1A, PIK3IP1, and PTEN, highlighting how



EZH2 inhibits ARID1A and PIK3IP1, ARID1A promotes PTEN, and PTEN and PIK3IP1 inhibit PI3K, collectively influencing cell proliferation and survival. Polycomb repressive complex 2 (PRC2); SWItch/Sucrose Non-Fermentable (SWI/SNF); Enhancer of zeste homolog 2 (EZH2); AT-rich interaction domain 1A (ARID1A); Phosphoinositide-3-kinase-interacting protein 1 (PIK3IP1); Phosphoinositide 3-kinase (PI3K); Protein kinase B (AKT); Mammalian target of rapamycin (mTOR); Phosphatase and tensin homolog (PTEN).

It can be demonstrated that inhibition of PARP by PARP inhibitors results in a reduction in the ability of cells to repair DNA damage. Consequently, in tumours lacking *ARID1A*, PARP inhibitors can be employed to induce cell death in a selective manner, exploiting their DNA repair-reducing properties<sup>338</sup>. It has been postulated that PARP inhibitors may be employed to treat cancers with *ARID1A* mutations<sup>338</sup>. Zhao and colleagues demonstrated that treatment of a patient with pancreatic ductal adenocarcinoma with an *ARID1A* mutation using the PARP inhibitor olaparib resulted in a favourable response for more than 13 months post-treatment<sup>339</sup>.

Mutations in *ARID1A* in cancer cells render them more susceptible to treatment with HDAC inhibitors<sup>340</sup>. The loss of *ARID1A* function results in the recruitment of HDAC2 to specific target genes, which affects gene expression in *ARID1A* mutant cells<sup>337</sup>. Therefore, inhibition of HDAC2 restores the expression of certain genes in *ARID1A* deficient cells, rendering them sensitive to HDAC inhibitors. Studies by Fukumoto and colleagues have demonstrated that the use of HDAC inhibitors can inhibit the growth of oncogenic *ARID1A* mutated OCCC in a mouse model, suggesting that HDAC inhibitors could be used to treat OCCCs that have an *ARID1A* mutation<sup>340</sup>.

Interestingly, there also appears to be a synthetic lethal relationship between *ARID1A* and *ARID1B*. Helming and colleagues demonstrated that knockdown of *ARID1B* in a WT *ARID1A* cell line does not affect the expression of other SWI/SNF complexes. Nevertheless, depletion of *ARID1B* in *ARID1A* mutant cells results in the dissociation of the core catalytic ATPase subunit *SMARCA4* (*BRG1*) and a reduction in the binding of several other subunits. This can lead to the destabilisation of the SWI/SNF complex and impaired cell growth<sup>333</sup>.

## **1.5 Clustered Regularly Interspaced Short Palindromic Repeats (CRISPR)**

### **1.5.1 Definition of CRISPR**

In 1987, Ishino, a Japanese scientist, discovered a special regulatory sequence in the genome of *Escherichia coli* (*E.coli*)<sup>341</sup>. This sequence, called clustered regularly interspaced short palindromic repeats (CRISPR), consists of a small segment of DNA that repeats itself at equal intervals. CRISPR is a gene found in bacteria whose genomes contain fragments of genes from viruses that have attacked the bacteria. Bacteria use gene fragments to detect and resist viral attacks and destroy viral DNA. These sequences play a crucial role in the antiviral defence system of prokaryotes, providing a form of acquired immunity<sup>342-345</sup>. Currently, CRISPR is present in approximately 50% of sequenced bacterial genomes and almost 90% of sequenced archaeal genomes<sup>346</sup>.

The CRISPR-associated protein (CRISPR-Cas) family consists of six main types divided into two classes. Class I (types I, III, and IV) uses multiple Cas proteins, whereas class II (types II, V, and VI) uses only one Cas protein<sup>347</sup>. Class II CRISPR-Cas systems are therefore easier to use in genetic engineering applications. Among the members of the type II CRISPR-Cas system, CRISPR-Cas9, developed from *Streptococcus pyogenes*, is the most widely used system in mammals<sup>348</sup>. In 2013, Zhang and colleagues published a paper in Nature suggesting that the CRISPR-Cas9 system can be used to edit DNA and knock out specified genes<sup>349</sup>. In 2020, Jennifer Doudna and Emmanuelle Charpentier were awarded the Nobel Prize in Chemistry for their pioneering discovery and development of the CRISPR-Cas9 system, a transformative tool for genome editing<sup>350,351</sup>. Their work has significantly advanced genetic research, facilitating precise and efficient modifications of DNA.

### 1.5.2 CRISPR for gene knockout

The CRISPR-Cas9 system is composed of two main components: the Cas9 protein and single guide RNA (sgRNA) (Figure 1.9). The sgRNA is a synthetic fusion of CRISPR RNA (crRNA) and trans-activated crRNA (tracrRNA). The crRNA contains a recognition sequence of approximately 20 bases that binds specifically to the target site, while additional sequences complement the tracrRNA portion<sup>348,352</sup>. The Cas9 protein acts as a nucleic acid endonuclease and consists of an HNH domain (an endonuclease domain named for characteristic histidine and asparagine residues) and a RuvC domain (an endonuclease domain named for an *E. coli* protein involved in DNA repair). The HNH domain cleaves the DNA strand that is complementary to the sgRNA, while the RuvC domain cleaves the non-complementary DNA strand<sup>350</sup>. The 5' end of sgRNAs identifies the target site, while its 3' end binds to the Cas9

protein, guiding it to the target sequence. Once bound, the sgRNA/Cas9 complex recognises the prototypical spacer adjacent motif (PAM) and induces a DSB adjacent to the target DNA sequence <sup>353</sup>. The CRISPR-Cas system developed for *Streptococcus pyogenes* typically has a PAM consisting of NGG or NAG (N can be any nucleotide: A, T, G, or C) <sup>354</sup>. After a DSB is induced, two primary repair pathways may be activated: homology-directed repair (HDR) or NHEJ. HDR requires a template DNA for repair and is commonly used for knock-in or base pair substitution. In contrast, NHEJ is an error-prone pathway that frequently leads to the occurrence of insertion/deletion (Indel) mutations. These mutations have the potential to disrupt the open reading frame of the target gene, thereby facilitating specific gene knockouts <sup>355</sup>.

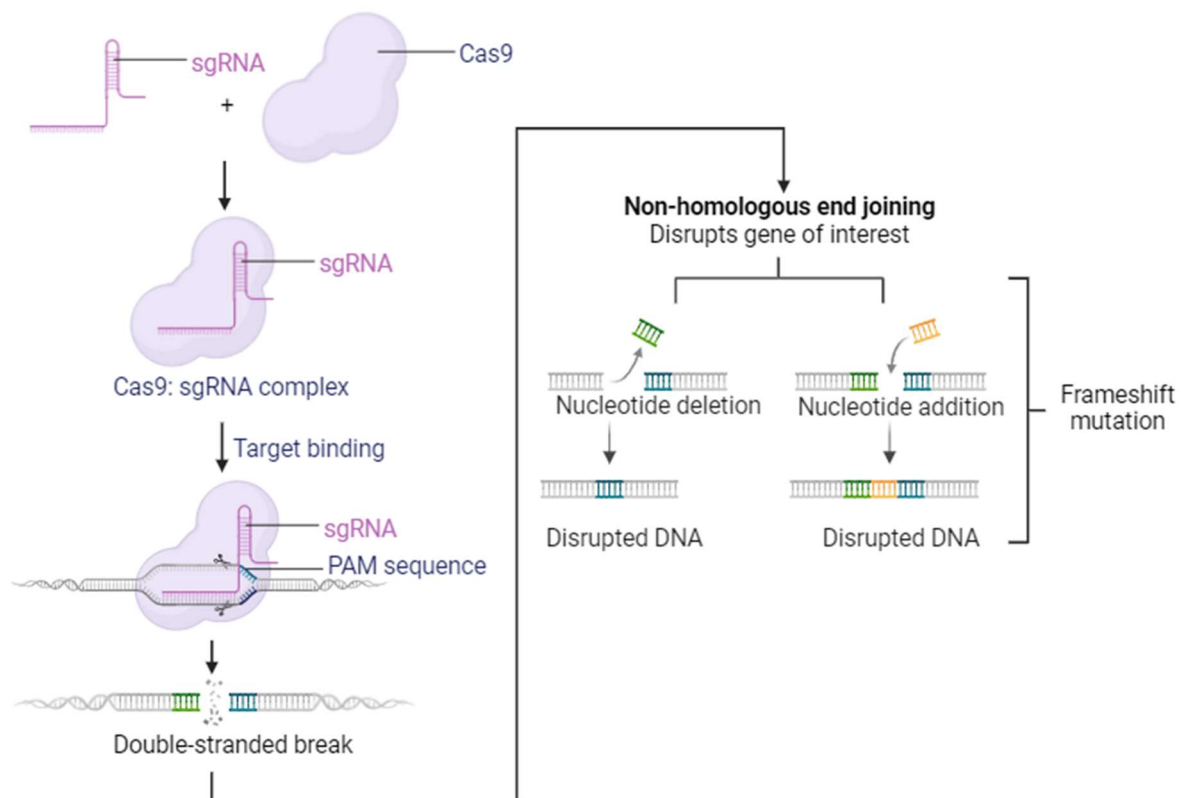


Figure 1.9 Information about CRISPR Knockout. A sgRNA binds together with a Cas9 protein to form a cas9: sgRNA complex. The Protospacer-adjacent motif (PAM) sequence acts as a binding site for sgRNA on the target DNA. Once the complex binds to the target DNA it activates the Cas9 nuclease that cleaves the target DNA resulting in a double-strand breaks (DSB). DSBs are then imperfectly repaired by NHEJ.

CRISPR technology has been widely used in basic research, gene therapy and agriculture <sup>356</sup>. It can manipulate the genome precisely and efficiently, and its application in cancer research

has the potential to target specific genetic mutations that drive tumour growth and spread <sup>357</sup>. Some researchers have used CRISPR technology to knockout or reduce the expression of the PD-1 protein on T cells, thereby improving their ability to target and kill cancer cells <sup>358,359</sup>. In addition, one study has shown that knockdown of Tripartite motif containing 11 (TRIM11) using CRISPR in colon cancer cell lines inhibits cell proliferation and induces apoptosis <sup>360</sup>. Also, studies have shown that T-cells can be genetically modified using CRISPR to form chimeric antigen receptors (CAR) on the cell surface, thereby enhancing the body's immune response to cancer <sup>361-363</sup>. Moreover, in 2023, CRISPR was approved by the FDA for the treatment of sickle cell disease (SCD) <sup>364</sup>. SCD is a genetic blood disorder caused by a mutation in the *HBB* (Haemoglobin Subunit Beta) gene that leads to the production of an abnormal haemoglobin known as haemoglobin S. This causes red blood cells to become rigid and sickle-shaped, which can obstruct blood flow and lead to severe pain, organ damage and an increased risk of infection <sup>365,366</sup>. The patient's haematopoietic stem cells are edited *in vitro* using CRISPR-Cas9 technology and then transplanted back into the patient. These edited stem cells can proliferate within the patient, leading to increased production of fetal haemoglobin (HbF). Elevated levels of HbF improve oxygen delivery and prevent the sickling of red blood cells <sup>367</sup>.

## 1.6 Drug repurposing

The process of developing a new drug is both costly and time-consuming. This process involves numerous steps, including drug design, animal testing, and clinical trials. Consequently, many drugs take a decade or more to develop <sup>368</sup>. Furthermore, although a significant proportion of drugs pass clinical trials, less than 15% of them are granted approval for routine clinical use <sup>369</sup>. This is why the repurposing of existing drugs is of such critical importance. A case in point is sildenafil, which was initially developed as an anti-angina drug but was subsequently employed for other purposes due to its side effect of lengthening penile erections <sup>370</sup>.

### 1.6.1 Drug repurposing in cancer research

Drug repurposing is important in the context of considering new cancer treatments. New therapeutic strategies are identified by utilising drugs approved for certain cancers or other indications to target other cancer types <sup>371</sup>. For example, Thalidomide, which previously caused numerous infant malformations when taken by pregnant mothers experiencing morning

sickness, is now employed as a repositioned drug in cancer treatment, where it is considered a standard therapy. The drug was approved by the FDA in 1998 for use in combination with dexamethasone in the treatment of patients with newly diagnosed multiple myeloma <sup>372</sup>. Consequently, the repurposing of drugs is regarded as an additional avenue for enhancing the value of the drug.

In the current era, the repurposing of anti-cancer drugs has shifted from the “pre-genomic era” to the “genomic era” <sup>373</sup>. Scientists can construct databases of drugs and diseases and analyse and predict that certain drugs may have new clinical potential for other purposes <sup>374-376</sup>. Alternatively, as exemplified by this project, scientists can employ drug screening alone to identify new ways to treat certain malignancies.

### 1.6.2 Drug screening

Drug screening is a technique that is now widely employed as a process of identifying and optimising potential drugs prior to the selection of candidates for clinical trials <sup>377</sup>. In the context of drug screening, the term "screening" refers to the process of identifying interactions between a chemical entity and a specific biological target. The objective is to identify compounds from the chemical library that can interact with the selected system in a specific manner. A variety of well-characterised targets are employed to elucidate the mechanism of action of the compounds under investigation. These include enzyme inhibition, receptor binding, modulation of macromolecular interactions, and interference with cell signalling <sup>378</sup>. Once compounds with the desired activity have been identified, they are subjected to parallel chemistry in an iterative process of synthesis, characterisation, and bioassay. The modification process, known as the hit-to-lead process, is designed to optimise potency and drug-like properties <sup>379</sup>.

One of the most crucial aspects of drug screening is the compound library, which typically comprises hundreds of thousands of compounds <sup>379</sup>. Drugs can be screened in compound libraries against specific biological targets or disease models to identify compounds that exhibit a desired biological activity. Such activity may include the inhibition of a specific enzyme or the blocking of cancer cell growth <sup>380</sup>. Furthermore, the library may also include known drugs or compounds that have been approved for other therapeutic uses. The compounds can then be screened against new targets or disease models to identify new potential applications.

## 1.7 Thesis hypothesis and aims

Ovarian Clear Cell Carcinoma (OCCC) is a rare and lethal subtype of ovarian cancer that often possesses mutations in *ARID1A* and, less frequently, *ARID1B* that encode subunits of the ATP-dependent SWI/SNF chromatin remodelling complex. We hypothesise that these mutations provide opportunities for novel approaches to therapeutic targeting of this difficult to treat malignancy.

Aim 1: To use an epigenetic drug compound library screen to determine whether specific compounds can decrease the viability of OCCC cell lines of known *ARID1A* and *ARID1B* status.

Aim 2: To examine the specificity and efficacy of a selected epigenomic drug in 2D and advanced 3D models of OCCC.

Aim 3: To use CRISPR-Cas9 gene editing technology to create wild-type and knockout (mutant) isogenic OCCC panels of *ARID1A* and *ARID1B*.

# CHAPTER 2. METHODS

This chapter describes general methods used throughout the thesis. Methods specific to individual chapters are detailed within those chapters where the associated data is reported.

## **2.1 Cell culture**

### **2.1.1 Cell lines**

OCCC cell lines (JHOC-5, OV207, TOV-21G, OVTOKO, OWISE, OVMANA, RMG-I) and non-OCCC cell lines (A2780.b1, OVCAR-8, and COV434) were used throughout this entire project. JHOC-5 and OVCAR-8 were a gift from Professor David Bowtell (Peter MacCallum Cancer Centre, VIC, Australia). The OV207 cell line was a gift from Drs K. Kalli and C. Conover (Mayo Clinic, Rochester, MN, USA). The TOV-21G cell line was a gift from Prof Caroline Ford (Lowy Cancer Research Group, University of NSW) who originally obtained these cells from Dr Viola Heinzlmann (University of Basel, Switzerland). OVTOKO, OWISE, OVMANA, and RMG-I cell lines were purchased from the Japanese Collection of Research Bioresources (JCRB) Cell Bank, distributed by Cellbank Australia (Westmead, NSW, Australia). The COV434 cell line was obtained from the European Collection of Authenticated Cell Cultures (ECACC; no. 0707199), distributed by Cellbank Australia. A2780.b1<sup>381</sup> is a clonal cell line derived in my laboratory from the A2780 parental EnOC cell line (gift from Ms R. Harvey (Bill Walsh Cancer Laboratory, Kolling Institute of Medical Research, Australia)). Further information on all ovarian cancer cell lines is outlined in Table 2.1. The HEK293 (human embryonic kidney 293, cat no. CRL-1573) cell line was purchased from the American Type Culture Collection (ATCC) (Manassass, VA, USA) and used as a control where indicated.



Table 2.1 Ovarian Clear Cell Carcinoma cell line specimen site of origin, *in vivo* growth in mice and commercial availability

Cell line	Specimen site	Growth in mice	Commercial availability	Catalogue numbers in JCRB	Number of References in PubMed*	References
OVISE <sup>a, b, c, d</sup>	Solid pelvic metastasis	Yes: SC; No: IP	JCRB	JCRB1043	22	Gorai et al. (1995) <sup>382^</sup> ; Yanagibashi et al. (1997) <sup>383^, #</sup>
OVMANA <sup>a, b, c, d</sup>	Primary tumour	Yes: SC; No: IP	JCRB	JCRB1045	8	Yanagibashi et al. (1997) <sup>383^, #</sup>
OVTOKO <sup>a, b, c, d</sup>	Solid splenic metastasis	Yes, SC; Yes: IP	JCRB	JCRB1048	17	Gorai et al. (1995) <sup>382^</sup> ; Yanagibashi et al. (1997) <sup>^ 383, #</sup>
JHOC-5 <sup>a, b, d</sup>	Pelvis	Yes, SC; Yes: IP	RIKEN BRC	n/a	12	Yamada et al. (1999) <sup>^ 384</sup> ; De Haven Brandon et al. (2020) <sup>385#</sup>
RMG-I <sup>a, c, d</sup>	Ascites	Yes: SC	JCRB	JCRB0172	39	Nozawa et al. (1991) <sup>386^</sup> ; Kashiyama et al. (2014) <sup>387#</sup>
TOV-21G <sup>a, b, c, d</sup>	Primary tumour	Yes: SC	ATCC	n/a	151	Provencher et al. (2000) <sup>388^</sup> ; Kashiyama et al. (2014) <sup>387^, #</sup>
OV207 <sup>b, d</sup>	Primary tumour	n/a	n/a	n/a	5	Conover et al. (1998) <sup>389^</sup> ;

ATCC (American Type Culture Collection), JCRB (Japanese Cancer Research Resources Bank); SC, subcutaneous; IP, intraperitoneal.

Molecular classification of subtypes: a. Domcke et al. (2013)<sup>390</sup>, b. Anglesio et al. (2013)<sup>391</sup>, c. Barnes et al. (2021)<sup>392</sup>, d. Papp et al. (2018)<sup>393</sup>

^primary reference, # reference reporting on *in vivo* tumour growth in mice

\* Number of publications listed in PubMed, last collated on April 7, 2024

### 2.1.2 Cell culture maintenance

Cell lines were cultured in a humidified atmosphere at 37°C with 5% CO<sub>2</sub>. OV207, OVMANA, OVISe, OVTOKO, RMG-I, JHOC-5, A2780.b1, and OVCAR-8 were grown in RPMI-1640 medium containing L-glutamine (0.3 mg/ml) (cat no. 11875-093, Invitrogen, Mt Waverly, VIC, Australia) supplemented with 10% (v/v) foetal bovine serum (FBS) (cat no. SFBS, Bovogen Biologicals, Kellor East, VIC, Australia). TOV-21G and COV434 were grown in DMEM medium containing GlutaMAX (cat no. 10565018, Invitrogen, Mt Waverly, VIC, Australia) supplemented with 10% (v/v) FBS. Cells were routinely maintained for up to 10-20 passages after thawing. Mycoplasma testing of cultured cells occurred quarterly, performed by technical staff using MycoAlert® Mycoplasma Detection Kit (cat no. LT07-318, Lonza, Sydney, NSW, Australia).

Cells were routinely passaged upon reaching 80-90% confluence in T75 flasks (cat no. 156499, Thermo Fisher Scientific, Australia). The media was removed, and flasks rinsed with 5 ml of 37°C pre-warmed PBS (phosphate buffered saline, cat no. 21600-044, Thermo Fisher Scientific, Australia). Next, 1 ml of 0.25% trypsin-EDTA (cat no. T4299, Sigma-Aldrich, Australia) was added, and flasks were incubated at 37°C for 3-5 minutes. A volume of 9.5 ml of fresh medium was added into the flask and mixed to form a cell suspension. The cells were split based on their predetermined split ratios (Table 2.2) into the appropriate flasks containing media warmed to 37°C at 5% CO<sub>2</sub>. Culture medium was changed every 96 hours.

Table 2.2 Cell culture conditions for growing cell lines

Cell line	Base medium	Weekly Split ratio	Medium for Freezing
OVMANA	RPMI 1640 + 10% (v/v) FBS	1:10	RPMI 1640 + 20% (v/v) FBS+5% (v/v) DMSO
OVTOKO	RPMI 1640 + 10% (v/v) FBS	1:20	RPMI 1640 + 10% (v/v) FBS+10% (v/v) DMSO
OVISE	RPMI 1640 + 10% (v/v) FBS	1:20	RPMI 1640 + 20% (v/v) FBS+10% (v/v) DMSO
OV207	RPMI 1640 + 10% (v/v) FBS	1:10	RPMI 1640 + 10% (v/v) FBS+10% (v/v) DMSO
TOV-21G	DMEM + 10% (v/v) FBS	1:20	DMEM + 10% (v/v) FBS+10% (v/v) DMSO
RMG-I	RPMI 1640 + 10% (v/v) FBS	1:10	RPMI 1640 + 20% (v/v) FBS+10% (v/v) DMSO
JHOC-5	RPMI 1640 + 10% (v/v) FBS	1:20	RPMI 1640 + 10% (v/v) FBS+10% (v/v) DMSO
A2780.b1	RPMI 1640 + 10% (v/v) FBS	1:10	RPMI 1640 + 10% (v/v) FBS+10% (v/v) DMSO
OVCAR-8	RPMI 1640 + 10% (v/v) FBS	1:20	RPMI 1640 + 10% (v/v) FBS+10% (v/v) DMSO
COV434	DMEM + 10% (v/v) FBS	900,000 cells in a T25 cm <sup>2</sup> flask	DMEM + 10% (v/v) FBS+10% (v/v) DMSO
HEK293	DMEM + 10% (v/v) FBS	1:20	DMEM + 10% (v/v) FBS+10% (v/v) DMSO

DMEM: Dulbecco's Modified Eagle's Medium; RPMI: Roswell Park Memorial Institute Medium; DMSO: Dimethyl sulfoxide; FBS: Fetal bovine serum; v/v: Volume/Volume.

### 2.1.3 Cryopreservation

Cells were harvested at the confluency of 70 - 90% as described above. The cell suspension was then transferred into a 15 ml tube and centrifuged for 5 minutes at  $350 \times g$ . The supernatant was removed, and the cell pellet resuspended in 1 ml of appropriate media (with 10-20% FBS) containing 5-10% (v/v) DMSO (Dimethyl Sulfoxide, cat no. D2650, Sigma-Aldrich, Australia) for each cell stock and transferred to a 2 ml cryovial (cat no. 430487, Sigma-Aldrich, Sydney, NSW, Australia). The vials were placed in a CoolCell LX freezer container (cat no. 432138, Sigma-Aldrich, Sydney, NSW, Australia) and stored at  $-80^{\circ}\text{C}$  overnight. The cryovials were then transferred to a vapour phase liquid nitrogen tank (cat no. 800-190, MVE biological solutions, Ball Ground, GA, USA) for long term storage to maintain cell stocks. To resuscitate

cells, frozen stocks were placed in a 37°C water bath until just thawed, then resuspended in 5 ml pre-warmed culture media and plated into a T25 culture flask (cat no. 156367, Thermo Fisher Scientific, Australia). The culture medium was replaced 24 hours after thawed cells were plated to remove DMSO.

#### 2.1.4 Cell counting

Cells were counted after trypsinisation using the Moxi Z mini automated cell counter (Orflo Technologies, Ketchum, ID, USA). Seventy-five µl of cell suspension was loaded into type S cell count cassettes (cat no. MXC002, Orflo Technologies, Ketchum, ID, USA). The cells flow in single file through a small hole in these cassettes into a thin-filmed membrane, then an electric current passes through causing a momentary increase in the measured voltage that is directly proportional to cell or particle volume. The output measurement is cell count reported as cell number per ml.

We also used the DeNovix CellDrop FL (DeNovix Inc, Wilmington, DE, USA) instrument to determine cell counts. In the Brightfield mode (version: v2.1.6), 10 µl of cell suspension was loaded into the sample chamber. Cells were counted based on size and shape, and the output measurement provided as cell number per ml.

#### 2.1.5 Cell viability assay

Cells were seeded at a specific density (Table 2.3) in 100 µl medium in 96-well plates. Then, the cells were incubated at 37°C for 18 hours before being treated with compound (compounds are different in each chapter). After treatment was added, cells were incubated for another 72 hours. A volume of 100 µl media was removed and 20 µl of MTS solution added (cat no. G3581, Promega, Wisconsin, United States) into each well. Cells were incubated at 37°C for 90 minutes, and the absorbance recorded using the SPARK 200 microplate reader (Tecan, Männedorf, Switzerland) at 490nm. All the data was analysed in Microsoft Excel and then analysed and graphed in GraphPad PRISM to obtain half-maximal inhibitory concentration (IC<sub>50</sub>) of drugs, HillSlope and R-squared values. The IC<sub>50</sub> is the concentration of an inhibitor where the response (or binding) is reduced by half. The hillslope refers to the slope factor that the steepness is quantified by, and the R-squared value represents the proportion of the variance for a dependent variable, explained by an independent variable.

Table 2.3 Cell seeding density for cell viability assay

Cell line name	Cell subtype	Seed density (cells/96 well)
JHOC-5	OCCC	2,500
RMG-I		6,000
OV207		2000
OVTOKO		2,500
OVMANA		4,500
OVISE		4,500
TOV-21G		5,000
A2780.b1	EnOC	5,000
OVCAR-8	HGSOC	2,500
COV434	SCCOHT	25,000

### 2.1.6 Cell proliferation rate assay

Cells were seeded at a specific density (Table 2.3) in 200 µl of medium in 96-well plates. Cell images were captured every 3 or 6 hours, depending on the experiment, using an IncuCyte Live Cell Imager S3 (Sartorius, Goettingen, Germany) with a 10X objective lens. Cell confluence was assessed over time using Incucyte software (version 2023A). The data were then plotted into GraphPad PRISM to generate growth curves and represented as % confluence or confluence (relative to time 0h) over time.

## 2.2 DNA analysis

### 2.2.1 Genomic DNA (gDNA) extraction

Cells were seeded at 200,000 cells per well in 6-well plates for 24 hours before extraction. Trypsinised cells were pelleted, washed with PBS and the pellet stored at -80°C, or gDNA extracted immediately using the ISOLATE II Genomic DNA kit (cat no. BIO-52067, Meridian Bioscience, Cincinnati, OH, USA). Cells were resuspended in 200 µl Lysis Buffer GL followed by the addition of 25 µl Proteinase K and 200 µl Lysis Buffer G3. The lysate was incubated at 70°C for 10 minutes. After incubation, 210 µl of 100% ethanol was added and the mixture vortexed vigorously. The solution was transferred into an ISOLATE II Genomic DNA Spin

Column in a collection tube and centrifuged for 1 minute at  $11,000 \times g$ . The sample was washed with 500  $\mu\text{l}$  Wash Buffer GW1, followed by 600  $\mu\text{l}$  Wash Buffer GW2. The gDNA was eluted with 100  $\mu\text{l}$  Elution Buffer G prewarmed to  $70^{\circ}\text{C}$ , quantitated using the Nanodrop spectrophotometer (see Section 2.4) and stored at  $4^{\circ}\text{C}$ .

### 2.2.2 PCR amplification of gDNA

Polymerase Chain Reaction (PCR) primers were reconstituted to 100  $\mu\text{M}$  using TE buffer (10mM Tris, 0.1mM EDTA pH 7.5). gDNA was diluted to 100 ng/ $\mu\text{l}$  and the target sequence amplified by PCR. PCR was conducted using the Phusion Green Hot Start II High-Fidelity PCR Master Mix (cat no. F-566L, ThermoFisher Scientific, Australia) and reaction components listed in Table 2.4. PCR cycling conditions are shown in Table 2.5.

Table 2.4 Components of the PCR reaction.

<b>Components</b>	<b>amount per reaction tube (<math>\mu\text{l}</math>)</b>	<b>Final amount or concentration</b>
Distilled water (dH <sub>2</sub> O)	9.5	
2 $\times$ Phusion Green HS II HF Master Mix	12.5	1 $\times$
gDNA template (100ng/ $\mu\text{l}$ )	0.5	50ng
Forward primer (10 $\mu\text{M}$ )	1.25	0.5 $\mu\text{M}$
Reverse primer (10 $\mu\text{M}$ )	1.25	0.5 $\mu\text{M}$
Total reaction volume	25	

Table 2.5 Thermocycling conditions for PCR

Cycle step	Temp.	Time	Cycles
Initial Denaturation	98°C	30s	1
Denaturation	98°C	10s	30
Annealing	X°C	30s	
Extension	72°C	15s	
Final extension	72°C	10 minutes	1
Hold	4°C	∞	1

### 2.2.3 PCR product clean up

PCR products were purified using the Wizard® SV Gel and PCR Clean-Up System (cat no. A9281, Promega, Australia). A volume of 20 µl of Membrane Binding Solution was added to 20 µl PCR reaction, mixed, and transferred into an SV Minicolumn, followed by incubation for 1 minute. The column was centrifuged at  $16,000 \times g$  for 1 minute and washed with 700 µl, then 500 µl membrane wash solution. Purified PCR fragments were eluted in 30 µl of DNase-free water and quantitated using the Nanodrop spectrophotometer (see Section 2.4). Fragments were stored at  $-20^{\circ}\text{C}$ .

### 2.2.4 Sanger Sequencing

Seventy-five ng of PCR fragment (from Section 2.2.3) and 1 µl of forward or reverse primer were mixed and made up to a total volume of 12 µl using deionised water in a 1.5 ml tube. The mixture was sent to the Australian Genome Research Facility (AGRF) for Sanger sequencing on a fee-for-service basis. The results were analysed using Benchling (<https://www.benchling.com/>).

## 2.3 Quantitative Real-Time Reverse Transcriptase PCR (qRT-PCR)

### 2.3.1 RNA extraction from cells

RNA was extracted using the RNeasy Mini Kit (cat no. 74106, Qiagen, Doncaster, VIC, Australia). Briefly, cells were seeded into a 6-well plate at 200,000 cell/well density for 24 hours. Cells were then washed with cold PBS, lysed in 350 µl of RLT buffer, scraped from the

well plate and the lysate transferred to a 1.5 ml microcentrifuge tube. A volume of 350  $\mu$ l of 70% ethanol was added to the lysate, mixed by pipetting and transferred to a RNeasy Mini spin column placed in a 2 ml collection tube. The column was centrifuged at 13,200rpm for 30 seconds. The flow through was discarded and the RNA bound to the column was washed with 700  $\mu$ l of Buffer RW1 and then washed twice with 500  $\mu$ l of RPE buffer. The RNA was eluted using 30  $\mu$ l of MilliQ water and stored at -80°C.

### 2.3.2 cDNA synthesis

After RNA had been extracted, the concentration was determined using the NanoDrop spectrophotometer (see Section 2.4). RNA was converted to cDNA using the SuperScript™ IV First-Strand Synthesis System (SSIV, cat no. 18091200, Thermo Fisher Scientific). Briefly, a volume of 500ng RNA was manually diluted in MilliQ water to a final volume of 5.5  $\mu$ l. Random hexamers and dNTPs were added, and the reaction heated to 65°C for 5 minutes, followed by immediate incubation on ice. SSIV buffer, Dithiothreitol (DTT), RNase inhibitor and SSIV reverse transcriptase enzyme (Table 2.6) were added to the reaction, mixed, centrifuged and placed in an MJ Research PTC-200 Thermal Cycler (MJ Research Inc, QC, Canada) using the conditions listed in Table 2.7. The cDNA was stored at 4°C and diluted 1:10 in RNase-Free water before being used in real-time PCR (see Section 2.3.3).

Table 2.6 SuperScript reagents

	<b>Component</b>	<b>Final concentration</b>	<b>Amount of 10 <math>\mu</math>l reaction</b>
Step 1	DEPC-treated water	To 5.5 $\mu$ l	To 5.5 $\mu$ l
	10mM dNTP mix	0.5 mM each	0.5 $\mu$ l
	50 ng/ $\mu$ l random hexamers	2.5 ng/ $\mu$ l	0.5 $\mu$ l
	RNA	500 ng	500 ng
Step 2	5x SSIV Buffer	1X	2 $\mu$ l
	100mM DTT	5 mM	0.5 $\mu$ l
	RNase Inhibitor	2.0 U/ $\mu$ l	0.5 $\mu$ l
	SuperScript™ IV Reverse Transcriptase (200U/ $\mu$ l)	100U	0.5 $\mu$ l



Table 2. 7 PCR cycling conditions for cDNA synthesis

Step	Temperature	Minutes: Seconds
1. Activation	23°C	10:00
2. Incubation	55°C	10:00
3. Inactivation	80°C	10:00
4. Store	4°C	∞

### 2.3.3 mRNA gene expression using Taqman assays

qRT-PCR was performed in triplicate using the TaqMan Fast Advanced Master Mix (cat no. n4444557, Thermo Fisher Scientific, Australia). The Taqman reaction mixes were constituted as described in Table 2.8, comprising of the specific Taqman gene assay (Table 2.9), mastermix and H<sub>2</sub>O, and 7 µl dispensed into 384-well PCR plates (cat no. 4309849, Thermo Fisher Scientific), followed by 3 µl of 1:10 diluted cDNA using an epMotion 5075 robot (Eppendorf South Pacific Pty Ltd., North Ryde, NSW, Australia). The 384-well plate was sealed using MicroAmp optical adhesive film (cat no. 4311971, Thermo Fisher Scientific, Australia), vortexed for 1 minute using a LP Vortex Mixer (Thermo Fisher Scientific), spun in an ArdyBio Mini-Plate Centrifuge (Major Science Co., Ltd, Taoyuan, Taiwan) and PCR amplification conducted on the QuantStudio 12K Flex Real-Time PCR System (Thermo Fisher Scientific, Australia) using standard cycling conditions recommended for Taqman assays (Table 2.10).

Table 2.8 Real-Time PCR reaction using TaqMan assays

Component	Volume (µl)
20 x Taqman gene assay	0.5
2 x TaqMan Fast Advanced Master Mix Kit	5
DNase free H <sub>2</sub> O	1.5
cDNA (diluted 1:10)	3
Final volume	10

Table 2.9 Taqman assay probe

Taqman probe	Assay number	Manufacturer
<i>ARID1A</i>	Hs00195664_m1	ThermoFisher Scientific, Australia
<i>ARID1B</i>	Hs00368175_m1	
<i>BTK</i>	Hs00975865_m1	
<i>HMBS</i>	97639748	Integrated DNA Technologies, Australia

AT-Rich Interaction Domain 1A/B (ARID1A/B); Bruton's tyrosine kinase (BTK); hydroxymethylbilane synthase (HMBS) used as a reference gene.

Table 2.10 TaqMan assay PCR cycling conditions

Step	Temperature	Time
Initial denaturation	95°C	20 seconds
Denaturation	95°C	1 seconds
Anneal/Extension	60°C	20 seconds
Denaturation and Anneal/Extension steps were repeated for 40 cycles.		

## 2.4 Assessment of RNA, gDNA, plasmid DNA, and PCR fragment concentration and quality using the NanoDrop spectrophotometer

To measure the quality and quantity of RNA, gDNA, plasmid DNA (see Section 5.2.1.4.5), and PCR fragments, the NanoDrop One/OneC UV-Vis Spectrophotometer (Thermo Fisher Scientific, Australia) was used. A volume of 2 µl of sample was added to the NanoDrop and the absorbance measured at wavelengths of 260nm and 280nm. A ratio of >1.8 of A260/A280 (pure DNA) or >2.0 of A260/A280 (pure RNA) was deemed acceptable for downstream analyses.

## 2.5 Protein analyses

### 2.5.1 Protein extraction

All protein extractions were performed on cells grown in a 6-well plate with 200,000 cells per well for 24 hours, unless specifically stated otherwise. Culture medium was removed, and cells rinsed with 1 ml of cold PBS and 200 µl of urea lysis buffer (20 mM NaH<sub>2</sub>PO<sub>4</sub>, 0.5 M NaCl, 20 mM imidazole, 8 M urea, 0.5% triton, 20 mM Tris, pH 8, 0.5 mM DTT, 0.5 mM

iodoacetamide) containing 1% Halt Protease & Phosphatase Inhibitor (cat no. 1861284, Thermo Fisher Scientific, Australia) added directly to the well. Cells were scraped from well plates and the lysates transferred to a microcentrifuge tube, placed on ice and sonicated (Qsonica Pty. Ltd., Newtown, CT, USA) with 30% amplitude for 15 seconds. Protein lysates were stored at  $-80^{\circ}\text{C}$  for up to one month.

### 2.5.2 Protein quantitation

The Pierce Bicinchoninic Acid (BCA) Protein Assay Kit (cat no. 23225, Thermo Fisher Scientific) was used to determine the protein concentration of extracted cell lysates. Protein lysates were diluted 1:5 with MilliQ water (20  $\mu\text{l}$  protein lysate + 80  $\mu\text{l}$  water). A standard curve was produced by serial dilution of a 2 mg/ml BSA (bovine serum albumin) stock solution as shown in Table 2.11. Twenty-five  $\mu\text{l}$  of each standard or diluted sample was added to a 96-well microplate in triplicate and 200  $\mu\text{l}$  of working reagent (made by mixing BCA Reagent A with BCA Reagent B at a 50:1 ratio) was added. The plate was incubated at  $37^{\circ}\text{C}$  for 30 minutes before the absorbance was measured at 562nm on a Tecan Spark microplate reader (Tecan Australia Pty Ltd., Port Melbourne, Vic, Australia). A standard curve was produced using these serially diluted samples, and a line of best fit (linear regression) was fitted to the data to determine the relationship between protein concentration and absorbance. The equation was then used to interpolate the protein concentration of samples from absorbance values.

Table 2.11 Serial dilutions used to create BCA assay standard curves with Bovine serum albumin (BSA) stock

Vial label	Volume of Diluent (μl)	Volume and source of BSA (μl)	Final BSA Concentration (μg/ml)
A	0	300 of Stock	2,000
B	125	375 of Stock	1,500
C	325	325 of Stock	1,000
D	175	175 of vial B dilution	750
E	325	325 of vial C dilution	500
F	325	325 of vial E dilution	250
G	325	325 of vial F dilution	125
H	400	100 of vial G dilution	25
I	400	0	0 = Blank

### 2.5.3 Western Blot

Protein lysate 7.5-15 μg was diluted in 4 x NuPAGE loading buffer (cat no. 928-40004, LI-COR Bioscience) and heated for 5 minutes at 95°C. Protein samples (15 μl) and Chameleon Duo Pre-stained Protein Ladder (1 μl) (cat no. 928-60000, LI-COR Bioscience) were loaded into precast NuPAGE 4-12% Bis- Tris gels, 15 wells and 1.5mm thickness (cat no. NP0336BOX, ThermoFisher Scientific, Australia). Samples were electrophoresed at 180 volts for 1 hour using MOPS (3-(N-morpholino) propanesulfonic acid) running buffer (50 mM MOPS, 50 mM Tris, 0.1% Sodium Dodecyl Sulfate (SDS), 1 mM Ethylenediaminetetraacetic acid (EDTA)), followed by transfer to a nitrocellulose membrane (cat no. 10600016 Amersham Protran Nitrocellulose Blotting Membrane, GE Healthcare, Sigma-Aldrich Corporation) or Odyssey Nitrocellulose Membrane (cat no. 926-31092, LI-COR Bioscience) using a wet transfer system (Bio-Rad Laboratories, Gladesville, NSW, Australia). Transfer occurred in transfer buffer (25mM TRIS, 152mM glycine and 20% (v/v) methanol) at 100 volts for 1.5 hours at room temperature. For very large proteins (>200kDa) transfer was extended to 3 hours and carried out at 4°C.

Table 2.12 Primary and secondary antibody details and dilutions used for western blotting

<b>Primary antibody</b>	<b>Primary antibody manufacturer</b>	<b>Primary antibody catalogue number</b>	<b>Primary antibody dilution ratio</b>	<b>Secondary antibody</b>	<b>Size (kDa)</b>	<b>Secondary antibody dilution ratio</b>
Anti-rabbit ARID1A	Sigma-Aldrich, Sydney, NSW, Australia	HPA005456	1:750	IRDye 800CW Donkey anti-Rabbit IgG (LICOR, cat no. LCR-926-32213)	270	1:15,000
Anti-rabbit ARID1B	Cell Signalling Arundel, QLD, Australia	92964	1:750		250, 280	1:15,000
Anti-rabbit GAPDH	Cell Signalling Arundel, QLD, Australia	2118	1:10,000		37	1:30,000

After transfer, the membrane was dried at room temperature for 5 minutes to maximise protein retention, then blocked in 5 ml diluted blocking buffer (Intercept Blocking Buffer (TBS) (cat no. 927-60001, LI-COR Bioscience) diluted 1:1 (v/v) in Tris-Buffered Saline (TBS)) for 1 hour at room temperature on a Ratek rocking platform (Ratek Instruments, Boronia, Victoria, Australia). The membrane was probed with primary antibodies (Table 2.12) diluted in blocking buffer containing 0.2% Tween 20 overnight on a rocker at 4°C. The next day the membrane was washed 3 times for 5 minutes with western washing buffer (10X TBS, 0.1% Tween-20) and probed with near infrared (NIR) fluorescent secondary antibodies (LI-COR) in diluted blocking buffer with 0.2% Tween 20 at indicated dilution ratios in Table 2.12 for 1 hour at room temperature protected from light. The washing procedure was repeated, and membranes were dried in a 37°C incubator for 10 minutes. Fluorescence was detected and visualised using the Odyssey CLx imaging system (LI-COR Bioscience). Quantitation of fluorescent bands was undertaken using ImageStudio Lite version 5.2 using the western blot analysis module (LI-COR Bioscience).

## **2.6 Statistical Analysis**

GraphPad Prism version 9.0.0 (GraphPad Software, Boston, MA, USA) was used for all statistical analyses. All experiments were completed from 3 independent replicates (n=3), with data expressed as mean  $\pm$  standard error mean (SEM) unless otherwise stated. Tukey *post hoc* analysis was performed for all ANOVAs. For all analyses,  $P < 0.05$  was considered to be statistically significant.

# CHAPTER 3. Characterisation of Ovarian Clear Cell Carcinoma Cell Lines

This chapter reports on investigations of the characteristics of OCCC cell lines used in this project. It includes morphological analysis, mutational analysis of *ARID1A* and *ARID1B*, gene and protein expression profiling, and assessment of sensitivity to cisplatin and carboplatin.

### 3.1 Introduction

There are three clear morphologies visible microscopically for OCCC, specifically papillary, tubulo-cystic and solid, often being mixed <sup>239</sup>. The most common is papillary (approximately 70%), which is characterised by small, round, unbranched papillae with a hyaline or oedematous stromal core, including 1 - 2 layers of cuboidal or flattened cells <sup>394</sup>. Tubulo-cystic is the second most common (approximately 65%) variant, characterised by the presence of small tubules and cysts of varying sizes, with or without intraluminal dense eosinophilic secretions and outpouchings. The least common is solid morphology (about 62% of cases), which consists of diffuse sheets or nested clusters of polyhedral cells <sup>395-398</sup>.

Studies have shown that the most frequently mutated gene in OCCC is *ARID1A*, which regulates many cellular processes including development, proliferation, differentiation, DNA repair and tumour suppression <sup>318</sup>. In the ARID domain, ARID1A and ARID1B have 50% sequence homology overall, and their amino acid sequences show nearly 80% homology <sup>319</sup>. Depletion of ARID1A inhibits RNA polymerase II (RNAPII) transcription. Trizzino and colleagues showed that when ARID1A was depleted in OCCC cells, ARID1B expression was increased, allowing the inhibited RNAPII to return to its original level <sup>335</sup>. Therefore, both *ARID1A* and *ARID1B* play an important role in tumour suppression. The mutations identified in *ARID1A* are typically LOF (Loss of Function) mutations, resulting in loss of the ARID1A protein and so loss of its tumour suppressive function <sup>319</sup>.

Moreover, based on some studies, it has been shown that when ARID1A levels are reduced or absent, OCCC cells display elevated resistance to platinum-based chemotherapy <sup>399,400</sup>. This might be related to the insensitivity of ARID1A mutant OCCC to platinum compounds <sup>401</sup>. In this chapter, I report the characterisation of seven OCCC cell lines in the laboratory, including *ARID1A* and *ARID1B* mutation analyses, as well as short tandem repeat (STR) profiling. This important work underpins the remainder of my thesis.



## 3.2 Methods

### 3.2.1 Cell line morphology

Cells were seeded at a specific density (Table 2.2.1) into 200 µl medium in 96-well plates. Cell images were captured in an IncuCyte Live Cell imager S3 using the 10X objective lens after 24 hours.

Table 3.1 Cell seeding density

Cell line name	Seed density (cells/96 well)	Base medium
JHOC-5	2,500	RPMI 1640 + 10% (v/v) FBS
RMG-I	6,000	
OV207	2000	
OVTOKO	2,500	
OVMANA	4,500	
OVISE	4,500	
TOV-21G	5,000	DMEM + 10% (v/v) FBS

### 3.2.2 Cell line STR profile

To avoid cross-contamination or misidentification of cell lines, and to ensure that the cells we used were human OCCC cells, we performed STR analyses on all OCCC cell lines. Cells were seeded into 6-well plates with 200,000 cells per well and incubated at 37°C in an incubator. Once cells were 80% confluent, gDNA was extracted from all cell lines using the ISOLATE II Genomic DNA Kit (see Section 2.2.1). PCR primers (Table 3.2) were reconstituted to 100 µM using TE buffer (10 mM Tris, 0.1 mM EDTA pH 7.5). gDNA was diluted to 100 ng/µl, then PCR was used to amplify the target sequence. PCR was conducted using the Phusion Green Hot Start II High-Fidelity PCR Master Mix (cat no. F-566L, ThermoFisher Scientific, Australia) and reaction components listed in Table 2.3. The cycling conditions are shown in Tables 2.4. The resulting PCR fragments were cleaned up using Wizard® SV Gel and PCR Clean-Up System (see Section 2.2.3) and quantitated using the Nanodrop spectrophotometer (see Section 2.4). The following were mixed – 75 ng of PCR fragment and 1 µl of forward or reverse primer, made up to a total volume to 12 µl using deionised water in a 1.5 ml tube. Cell line authentication was outsourced to the AGRF for genetic identification using the Promega GenePrint 10 kit on a fee-for-service basis. According to the ASN-0002 standard published by

the American Tissue Culture Collection (ATCC) Standards Development Organization (SDO) Workgroup, a minimum of 8 STR loci (TH01, TPOX, vWA, CSF1PO, D16S539, D7S820, D13S317, and D5S818) are recommended to be used for authentication of human cell lines, plus Amelogenin for sex determination. Samples were analysed by STR for TH01, TPOX, vWA, CSF1PO, D16S539, D7S820, D13S317, D21S11, D5S818 alleles and Amelogenin. The STR result was a report summarising all the loci for samples, as well as GeneMapper data plots. STR data were entered into the DSMZ CellDive database (Liebniz Institute) (<https://celldive.dsmz.de/str/search>) for comparison <sup>402</sup>. The DSMZ database is a collection of over 4,500 datasets from cell lines of various origins. Data from a single cell line with more than 80% similarity to the cell line of interest recorded in the database are considered correct for cell line authentication.

Table 3.2 Primer sequences used for cell line mutation verification.

Gene	Exon	Annealing Temp.	Size (bp)	Cell line	Mutation	Primer	Primer sequence, 5'-3'	Reference
<i>ARID1A</i>	1	63.9	563	OVISe	p.H203fs*197 (c.607_608insA)	Forward	GAACAATAACCTCACGGAGCC	Mamo et al. <sup>403</sup>
						Reverse	ACGTGAGCAGTTGGTTGAGG	
	3	65.1	495	OVISe	p.Q543E (c.1627C>G)	Forward	ACAACCAGCAAAGTCCTCACC	
				TOV-21G	p.Q542fs*80(c.1621_1622delAC)	Reverse	TGCACGTTAGAGAACCACTCTG	
	7	63.3	349	TOV-21G	p.Q758fs*75 (c.2268delC)	Forward	TCCCAGGATAAGGATGGAGAG	
						Reverse	GGACAGCCCTTCTCTCACAAG	
	16	63.7	350	OVMANA	p.Q1332* (c.3994 C>T)	Forward	CAGAGTGAGGTAAGCATGACCC	
						Reverse	CCTTGGGTGGAGAACTGATTG	
	18	62.7	582	OV207	p.W1545* (c.4635G>A)	Forward	ATGTACAGCGTGCCATACAGC	
						Reverse	GTGATTCTGCATGCTTGGTG	
<i>ARID1B</i>				OVTOKO	p.Q2209fs*22 (c.6624delC)	Forward	GCAGTGCAGAAGGGCAGTATC	Sim et al. <sup>404</sup>
				OVMANA	p.S2264* (c. 6791 C>G)	Reverse	TGCATAAATAAAGGGCAACAGTC	
	8	62.2	555	OVISe	p.Y840* (c.2481 C>A)	Forward	TCGGTCACTGTTGCTTTTGT	
						Reverse	TCTACAACCTGCTGCCATGC	
	20	66.7	388	TOV-21G	p.L1975fs*21(c.5925insG)	Forward	CAAGCCAAAAGTCACCGGAACA	
						Reverse	ACAAGTCTAGCTGCCCCGGAAT	Designed in-house using Benchling

### 3.2.3 Protein analyses and Quantitative Real-Time Reverse Transcriptase PCR (qRT-PCR)

Protein analyses was conducted as previously described in Section 2.5. qRT-PCR was conducted as previously described in Section 2.3.

### 3.2.4 Determining sensitivity of cell lines to platinum drugs

Cells were seeded at a specific density (see Table 3.1) in 100  $\mu$ l medium in 96-well plates. Then, the cells were incubated at 37°C for 18 hours before being treated with either cisplatin or carboplatin, with the concentration ranges shown in Table 3.3. After drug was added, cells were incubated for a further 72 hours. Cell viability was assessed using an MTS assay described in Section 2.1.5.

Table 3.3 Concentration ranges of platinum drugs used to assess chemosensitivity in OCCC cell lines

Cell line	Cisplatin		Carboplatin	
	Concentration range	Dilution factor	concentration range	Dilution factor
RMG-I	0.19- 100 $\mu$ M	2-fold dilution	2.6-100 $\mu$ M	1.5-fold dilution
OVTOKO	0.078- 40 $\mu$ M			
OVISE	0.078- 40 $\mu$ M			
OVMANA	0.078- 40 $\mu$ M			
TOV-21G	0.097- 50 $\mu$ M			
JHOC-5	0.19- 100 $\mu$ M			
OV207*	0.2- 25 $\mu$ M			

\*This experiment was performed by Kristie Dickson in our research laboratory

## 3.3 Results

### 3.3.1 Morphology of OCCC cells

We used seven OCCC cell lines in this project, so firstly these cell lines needed to be characterised to confirm that they were the same as those published in the literature. We first

studied the morphology of all cell lines. Images were captured using the IncuCyte S3 Live-Cell Imaging System with the 10X objective (Figure 3.1). All seven OCCC cells showed the characteristics of epithelial-like cells. RMG-I cells are polygonal in shape and exhibit a relatively small cell size. The cells exhibit well-defined boundaries between them, and the monolayer is relatively homogeneous. The nuclei of the cells were clearly discernible, and many exhibited distinct nucleoli. Additionally, some cells exhibited cytoplasmic extensions or protrusions. JHOC-5 cells are elongated and spindle-shaped. The nuclei were typically rounded and situated in the centre of the cells, with some exhibiting visible nucleoli. OV207 cells are elongated and spindle-shaped too, exhibiting a multitude of cellular extensions. The nuclei are prominent and oval or elongated in shape. The cells display a degree of translucency. OVTOKO cells are also elongated and spindle-shaped with tapering ends. The nuclei of the cells are visible and oval or elongated. The cells are distributed throughout the cytoplasm and are typically located in the centre of the cell body. OVMANA cells are predominantly round or oval in shape, with some giant cells present. They form clusters or groups. The nucleus is clearly visible and is located in the centre of the cell. OVISE cells exhibit a polygonal or cobblestone appearance, and they form dense clusters. The nuclei are conspicuous and situated in the centre of each cell, exhibiting a uniform distribution. TOV-21G cells exhibit a heterogeneous morphology, with some cells exhibiting elongated and spindle-shaped characteristics, while others exhibit more polygonal or rounded morphologies. Some cells form small clusters or groups, while others are more isolated. Some cells exhibit elongated cytoplasmic extensions. The nuclei are readily discernible in the majority of cells, manifesting as dark, rounded structures.

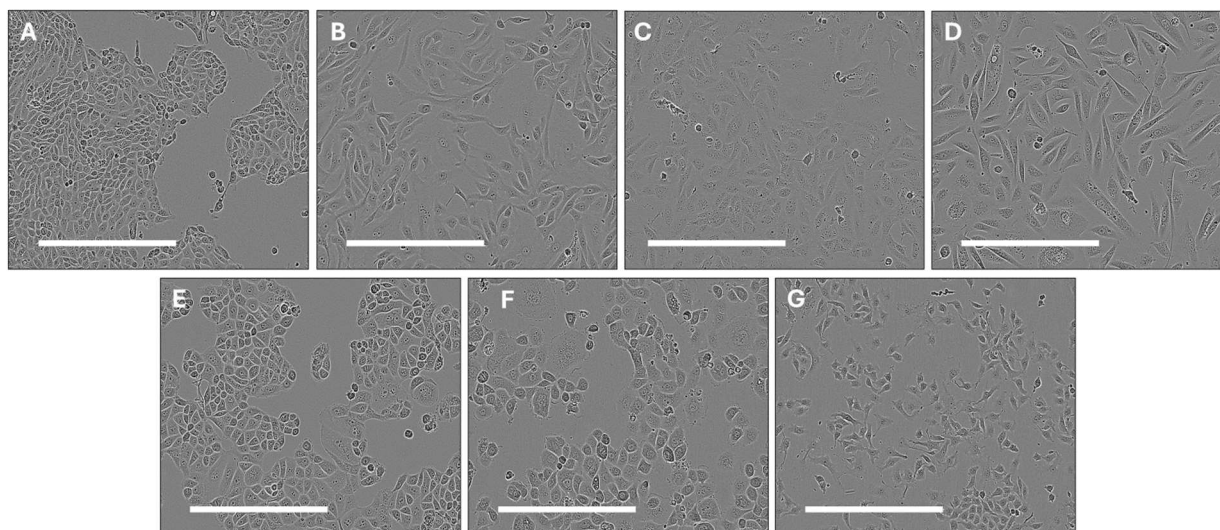


Figure 3.1 Representative images of OCCC cell lines growing in 96-well plates captured with the IncuCyte S3 Live-Cell Imaging System with 10X objective. A: RMG-I, B: JHOC-5, C: OV207, D: OVTOKO, E: OVMANA, F: OWISE, G: TOV-21G. Scale bar = 400  $\mu$ m.

### 3.3.2 STR profiling of OCCC cell lines

Once we had determined the morphology of each cell line, we then used STR profiling to authenticate the cells to avoid cross-contamination or misidentification, which could lead to erroneous conclusions in subsequent studies.

STR profiling was performed on nine allele markers as well as Amelogenin for sex determination. The percentage similarity of markers to cell lines recorded in the DMSZ database is reported in Table 3.4. STR profiling results are reported in their entirety in Appendix 1. All cell lines displayed greater than 80% similarity which is the cut-off used for authentication. In fact, only one cell line, RMG-1, showed a similarity of 94.4%, with the other cell lines all displaying 100% similarity.

Only a repeat length of 12 was present at the D13S317 marker in RMG-I cells, however, the two alleles published in the DMSZ database for this cell line were 8 and 12 nucleotides long (Figure 3.2). This would indicate either homozygosity of repeat length 12 at this marker site, or loss of a single allele. This type of small discrepancy is acceptable, as long as overall similarity across the markers tested is >80%, and likely the result of clonal expansion of a variant.

Table 3.4 STR profiling results for the OCCC cell lines used this study

Cell line	Similarity (%)
RMG-I	94.4%
JHOC-5	100%
OV207	100%
OVTOKO	100%
OVMANA	100%
OVISE	100%
TOV-21G	100%

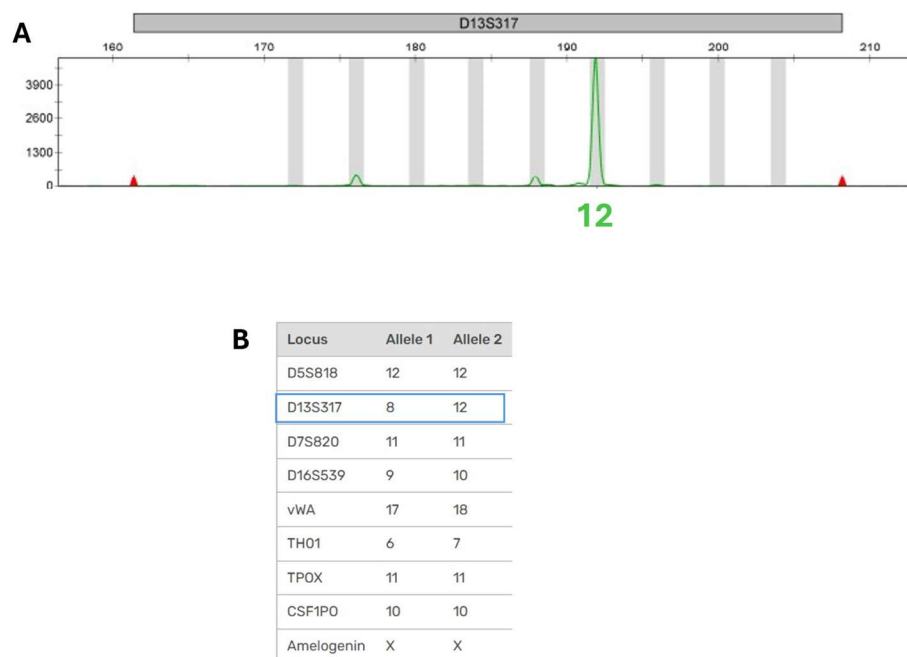


Figure 3.2 Allelic differences observed for the microsatellite marker D13S317 in our RMG-I cells compared to data held in the DMSZ database. A. D13S317 marker in RMG-I STR profiling shows a single allele at size 12 B. All microsatellite markers in RMG-I cells STR profiling from the DMSZ database. Discrepant alleles for D13S317 are shown in the blue box (8,12), indicating either loss of allele 1 or homozygosity of allele 2 in our RMG-1 cell line. All other microsatellite markers were identical.

### 3.3.3 Confirming reported mutations in OCCC cell lines

It has been reported in the literature that *ARID1A* and *TP53* mutation are mutually exclusive<sup>331</sup>. Furthermore, the OV207 cells had been shown to contain *TP53* mutations<sup>215</sup>. Consequently, OV207 was considered to be an *ARID1A* WT cell line. However, a study and a patent indicate the presence of *ARID1A* mutations in OV207 cells<sup>405,406</sup>. So, in order to further verify the *ARID1A* and *ARID1B* mutations reported in the literature, gDNA of five cell lines OV207, OVTOKO, OVISe, OVMANA and TOV-21G was extracted, PCR amplified and sequenced. RMG-I and JHOC-5 cells are reported as *ARID1A* and *ARID1B* wild-type in the literature<sup>335,391</sup>. Fragments containing *ARID1A* and *ARID1B* mutations reported in the literature were amplified by PCR using specific screening primers (Table 3.2). PCR results showed all the cell lines had bands of the expected size (Figure 3.3).

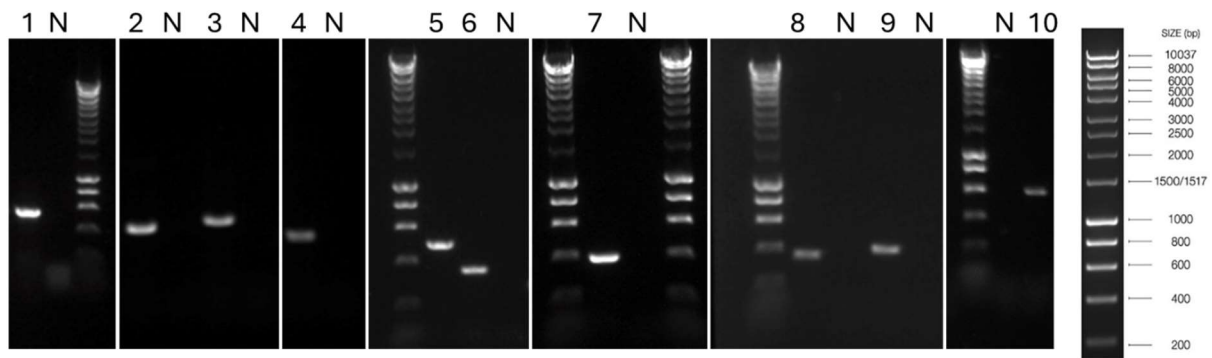


Figure 3.3 DNA gel electrophoresis image of PCR amplified fragments containing mutation sites in different cell lines. 1. OVISe (*ARID1A*, p.H203fs) 2. OVISe (*ARID1A*, p.Q543fs) 3. OVISe (*ARID1B*, p.Y840\*) 4. OVTOKO (*ARID1A*, p.F1991fs) 5. TOV21G (*ARID1A*, p.N549fs) 6. TOV-21G (*ARID1A*, p.N756fs) 7. TOV-21G (*ARID1B*, p.L1974fs) 8. OVMANA (*ARID1A*, p.Q1332\*) 9. OVMANA (*ARID1A*, p.S2047\*), 10. OV207 (p.W1545\*), and N indicates no-template control. The size of the fragments is shown in Table 3.2. DNA ladder is HyperLadder 1kb (cat no. BIO-33053, Meridian Bioscience, London, UK).

PCR fragments were purified (see Section 2.2.3) and underwent commercial Sanger sequencing (see Section 2.2.4). Sequencing results were analysed using Benchling by aligning to the control, wild-type sequence. Results confirmed that all mutations described in the literature were present in the cell lines in our laboratory (Figure 3.4 and 3.5). The results indicate that the *ARID1A* mutations observed in the cell lines employed in this project are distributed throughout *ARID1A*. Also, exon 3 exhibits the highest number of mutations.



Interestingly, some mutations are homozygous, but the OVISe, OV207, and OVMANA cells exhibited heterozygous *ARID1A* mutations, which means both the mutant and WT alleles are present in these cell lines. In particular, the OVMANA cell line exhibits heterozygous mutations in two mutation sites. A similar pattern is observed for *ARID1B*, with heterozygous mutations present in the OVISe and TOV-21G cell lines.

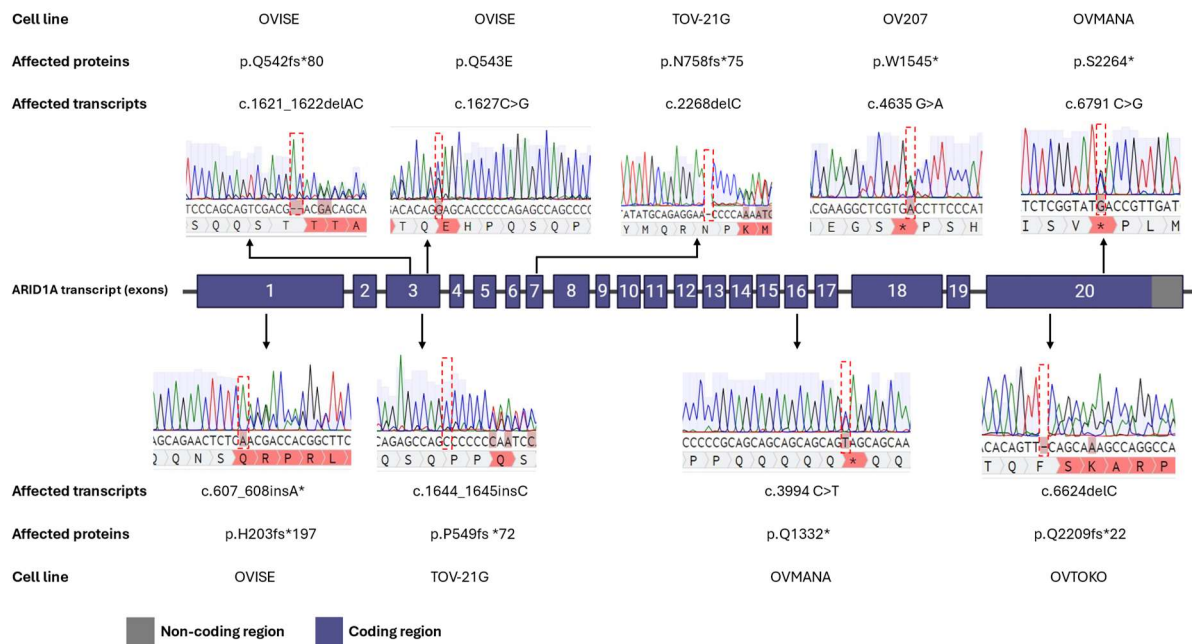


Figure 3.4 Sanger sequencing of the four OCCC cell lines OVISe, OV207, OVMANA and TOV-21G for *ARID1A* mutations. Cell lines were sequenced using screening primers to appropriate regions (Table 3.2). All the results were aligned to control wild-type sequence (accession number: NC\_000001) in Benchling. Gray indicates a non-coding region and coding regions are indicated by blue. Mutated nucleotides are indicated by red dashed line boxes and shading. Affected codons are indicated by red shading.

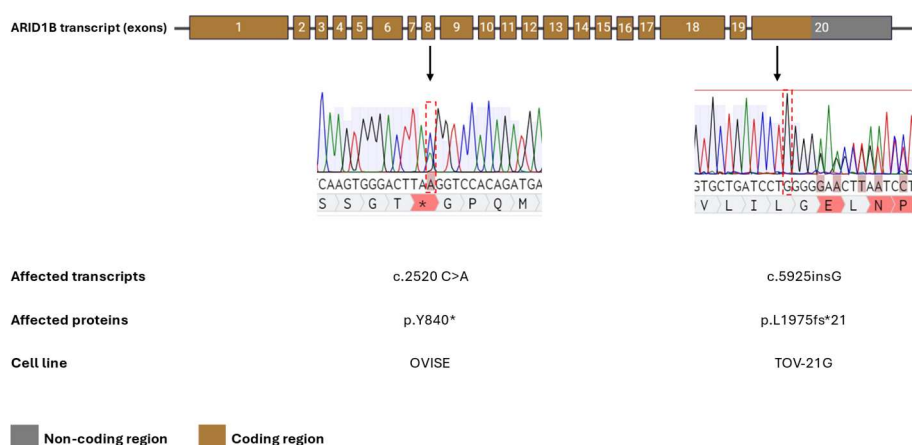


Figure 3.5 Sanger sequencing of two OCCC cell lines, OVISE and TOV-21G, for *ARID1B* mutations. Cell lines were sequenced using screening primers (Table 3.2). All the results were aligned to the control sequence (accession number: NC\_000006) in Benchling. Gray indicates a non-coding region and coding regions are indicated by brown. Mutated nucleotides are indicated by red dashed line boxes and shading. Affected codons are indicated by red shading.

### 3.3.4 Determining RNA and protein levels of ARID1A and ARID1B in OCCC cell lines

qRT-PCR was employed to analyse the RNA extracted from seven cell lines and the control cell line, HEK293, which is WT for *ARID1A* and *ARID1B* (Figure 3.6). The results showed that all the OCCC cell lines expressed *ARID1A* and *ARID1B* mRNA, however no statistically significant difference was observed between any of the cell lines tested. In terms of *ARID1A*, RMG-I and OV207 (both *ARID1A* WT) exhibited a trend towards a higher level of mRNA expression than the other cell lines, while three *ARID1A* mutant cell lines, OVMANA, OVISE, and TOV-21G, exhibited a trend towards a lower level of *ARID1A* mRNA expression. However, the *ARID1A* WT line JHOC-5 exhibited a trend towards a lower level of *ARID1A* mRNA compared to the *ARID1A* mutant cell lines OVMANA and OVTOKO, which expressed the highest levels of *ARID1A* mRNA. It is of interest to note that the OVTOKO cell line exhibited a trend of higher mRNA levels for *ARID1B*, while the JHOC-5 cell line exhibited a trend of the second lowest mRNA level, approaching that of the OVMANA cell line.

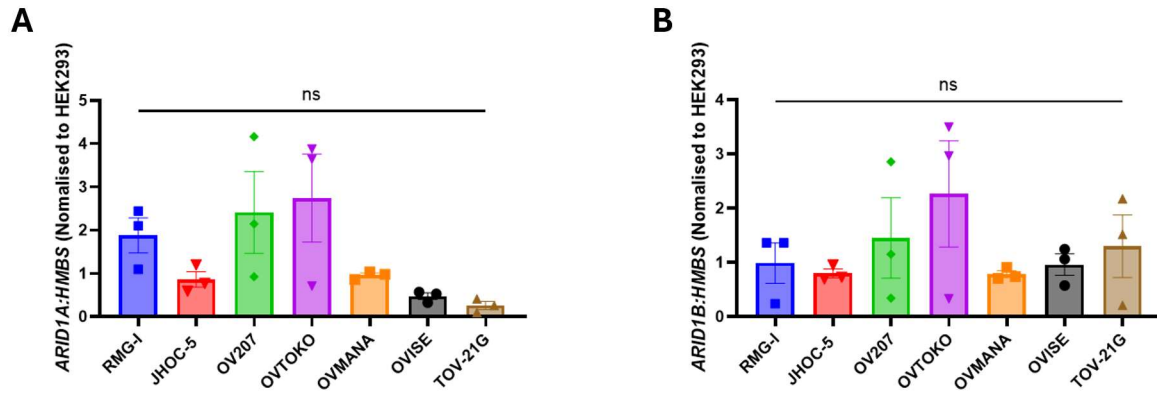


Figure 3.6 *ARID1A* and *ARID1B* mRNA expression levels for all OCCC cells. A. Graphs of mRNA levels of *ARID1A* in OCCC relative to *HMBS* and normalised to HEK293. B. Graphs of mRNA levels of *ARID1B* in OCCC relative to *HMBS* and normalised to HEK293. A one-way ANOVA and *post-hoc* Tukey test was performed to determine statistical significance. Data is shown as the mean  $\pm$  SEM, N=3. ns, not significant.

After determining the mRNA levels of ARID1A and ARID1B in OCCC cell lines, protein levels were assessed. Western Blot was used to analyse the proteins extracted from 7 cell lines and the control cell line HEK293 (Figure 3.7). The results of protein blotting images demonstrated that ARID1A was displayed in RMG-I, JHOC-5, and OV207. Two distinct bands observed in JHOC-5, and one strong band as well as one faint band observed in RMG-I and OV207. OVTOKO and OVISE had a faint band in ARID1A. The bands were barely observed in OVMANA and TOV-21G. All cells had ARID1B protein, with all samples exhibiting two distinct bands. Quantitative analysis revealed that in OCCC, RMG-I exhibited the highest level of ARID1A protein, with the exception of JHOC-5. The ARID1A protein was found to be similar in all remaining cell lines. Similarly, the ARID1B protein was present in all OCCC cell lines, with no statistically significant difference observed.

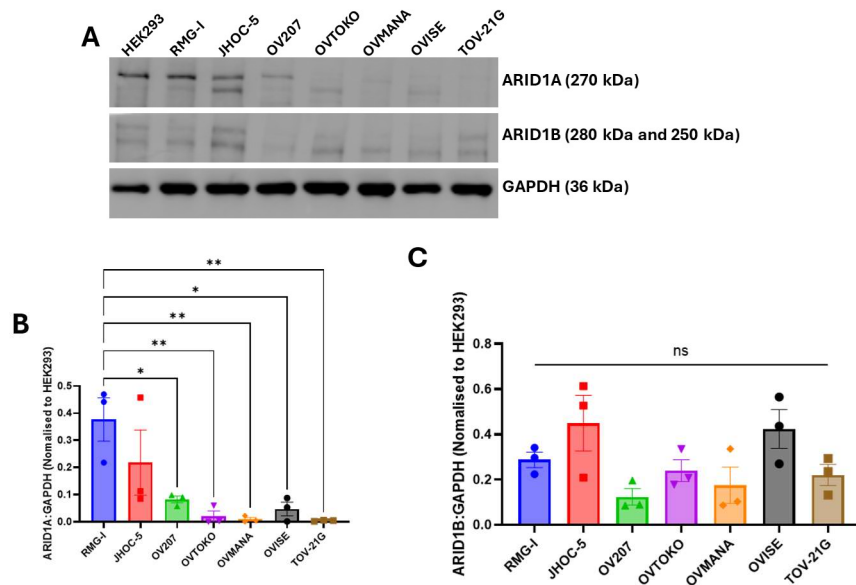


Figure 3.7 Protein expression levels of all OCCC cell lines. A. Representative western blots comparing basal levels of ARID1A and ARID1B in seven OCCC cell lines compared to a control cell line with wild-type expression of proteins of interest (HEK293). B. Graphical representation of protein levels of ARID1A in OCCC normalised to HEK293. There is no statistical significance between JHOC-5 and TOV-21G (N=3, \*P<0.05, \*\*P<0.01) C. Graphical representation of protein levels of ARID1B in OCCC cell lines normalised to HEK293 (N=3). Data is presented as the mean  $\pm$  SEM, N=3. The protein loading control is GAPDH (37 kDa). The full western blot image is present in Appendix 1.

### 3.3.5 Cell viability after cisplatin and carboplatin treatment

To investigate the sensitivity of OCCC to platinum compounds and the effect of mutant ARID1A and ARID1B on platinum compounds in OCCC, we treated seven OCCC cell lines with cisplatin and carboplatin. To facilitate comparison and consistency between the data, we determined the half maximal inhibitory concentration (IC<sub>50</sub>) of each compound for each cell line.

The cell lines were treated with ten concentrations of cisplatin and carboplatin for 72h and the IC<sub>50</sub> values were calculated (Figure 3.8). In terms of cisplatin, two *ARID1A* mutant only cell lines, OVTOKO and OVMANA, were more sensitive to cisplatin with IC<sub>50</sub> values of 2.14  $\mu$ M and 1.986  $\mu$ M, respectively. This was followed by two cell lines with both *ARID1A* and

*ARID1B* mutations, OVISe and TOV-21G, with IC<sub>50</sub> values of 2.579  $\mu$ M and 2.783  $\mu$ M, respectively. Then, JHOC-5 and OV207 were more resistant to cisplatin, with IC<sub>50</sub> values of 2.875  $\mu$ M and 3.075  $\mu$ M, respectively. Interestingly, RMG-I that is WT for *ARID1A* and *ARID1B* was the most resistant to cisplatin (IC<sub>50</sub> = 4.969  $\mu$ M). With regards to carboplatin, OV207 cells were the most sensitive (IC<sub>50</sub> 23.23  $\mu$ M), followed by OVTOKO (IC<sub>50</sub> = 24.21  $\mu$ M), JHOC-5 (IC<sub>50</sub> = 32.13  $\mu$ M), OVISe (IC<sub>50</sub> = 40.71  $\mu$ M), and TOV-21G (IC<sub>50</sub> = 54.68  $\mu$ M). OVMANA and RMG-I were most resistant to carboplatin, with IC<sub>50</sub> values of 55.86  $\mu$ M and 55.23  $\mu$ M, respectively. Dose curves are presented in Appendix 1 (Figure 1A.1 and Figure 1A.2).

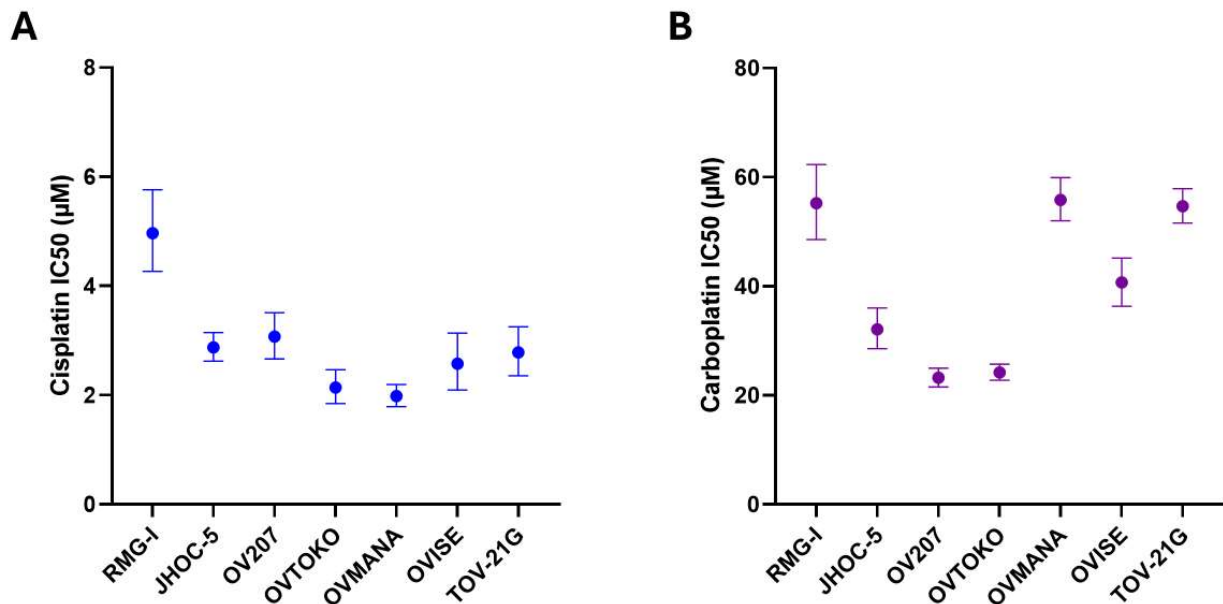


Figure 3.8 IC<sub>50</sub> of cisplatin and carboplatin in OCCC cell lines. Seven OCCC were treated with 10 concentrations of cisplatin and carboplatin (Table 3.4) for 72h, and an MTS assay performed to determine how many live cells remained (% viable cells). These experiments were repeated at least 3 times to generate dose curves and IC<sub>50</sub> was calculated from the dose curve. Error bars depict 95% confidence intervals (CI).

The seven OCCCs were ranked according to the IC<sub>50</sub> of cisplatin or carboplatin, with the highest value at the top and the lowest at the bottom. It was observed that the sensitivity of the cells to cisplatin or carboplatin was not associated with the expression of *ARID1A* or *ARID1B* in the cells or the presence of mutations in these genes. The *ARID1A* WT cell line RMG-I

demonstrated the highest resistance to cisplatin. Furthermore, both *ARID1A* WT cell lines, RMG-I and JHOC-5, exhibited a slight increase in resistance to platinum compounds compared to some *ARID1A* mutated cells (Figure 3.9).

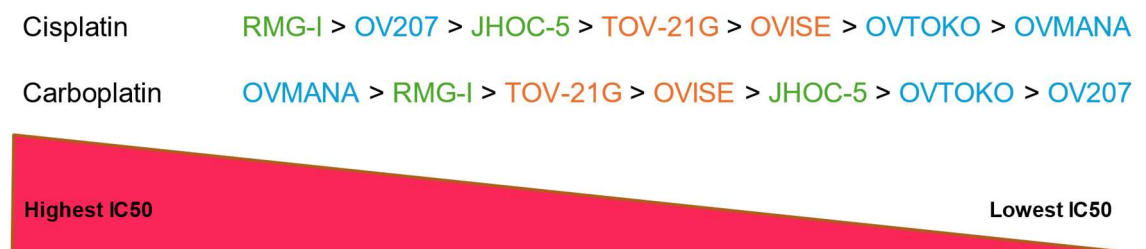


Figure 3.9 Comparison of IC50 of cisplatin and carboplatin in seven OCCC cells. Seven OCCC cells were ranked in order of increasing IC50 for cisplatin and carboplatin. The order from left to right indicates IC50 from highest to lowest. The upper section of the chart indicates cisplatin, while the lower section indicates carboplatin. Green: *ARID1A* and *ARID1B* WT. Blue: Only *ARID1A* mutation. Orange: Both *ARID1A* and *ARID1B* mutations.

### 3.4 Discussion

I commenced this thesis by undertaking several experiments to determine that I was working with the same OCCC cell lines as reported in the literature and to extend knowledge of these cell lines. This included morphological analyses, mutation analysis of *ARID1A* and *ARID1B*, gene and protein expression and sensitivity to both cisplatin and carboplatin.

The OCCC cell lines used in this project exhibited epithelial-like characteristics with distinct cell shapes and nuclei. RMG-I cells are polygonal with well-defined boundaries, JHOC-5, OV207, OVTOKO, and OVISE cells are elongated and spindle-shaped with prominent nuclei, while OVMANA cells are round or oval and form clusters. TOV-21G cells display a heterogeneous mix of elongated, spindle-shaped, polygonal, or rounded morphologies, often with noticeable cytoplasmic extensions and discernible nuclei.

In addition, the cell line authentication results using STR analyses showed that all cell lines were authenticated, and most cell lines had a similarity rate of 100%, but RMG-I had a similarity rate of 94%. Cell line authentication plays an important role in medical and biological research and is used to avoid potentially disastrous outcomes such as wrong conclusions and results that are not reproducible due to the use of cross-contaminated or misidentified cells, as

well as to avoid wasting a lot of time, effort, and money <sup>407</sup>. A widely used cell authentication method is Short Tandem Repeat (STR) analysis, which is the cell authentication method we used in this project. In 2012, the American Type Culture Collection (ATCC) Standards Development Organization (SDO) Workgroup ASN-0002 developed a standard to establish criteria for the authentication of human cell lines by STR analysis, which was eventually published by the American National Standards Institute (ANSI). The standard has been continuously updated to improve the accuracy of cell authentication. However, STR analysis still has many shortcomings and limitations <sup>408</sup>. Microsatellite instability and loss of heterozygosity in cancer cells can interfere with the results of STR authentication <sup>409</sup>. Current alternatives to STR include Single nucleotide polymorphisms (SNP), which involve identifying and comparing specific genetic variants at single nucleotide positions in the DNA sequence of a cell line. By analysing these variants, it is possible to confirm the identity of the cell line, detect cross-contamination and ensure the purity of the sample. However, due to cost and other factors, STR analysis remains the method of choice for cell line authentication in most studies <sup>410</sup>.

We also used Sanger sequencing to confirm that the *ARID1A* and *ARID1B* mutations described in the literature are present in the cell lines used in this project. Furthermore, examination of protein levels showed that all wild-type ARID1A cells had ARID1A protein expression and there was no detectable ARID1A protein in the ARID1A mutant cells, except OV207. This is also consistent with the literature that most *ARID1A* mutations are nonsense or out-of-frame mutations resulting in truncation of the protein product <sup>411</sup>. Our results indicate that the *ARID1A* mutation in OVISe, OV207, and OVMANA, as well as the *ARID1B* mutation in OVISe and TOV-21G, are heterozygous, this suggests that WT sequence is present. Moreover, the results of ARID1A and ARID1B protein levels demonstrated that ARID1A was still present in OV207 cell despite these cell lines having reported mutations, while ARID1B was detected in both OVISe and TOV-21G, in comparison to the other OCCC cell lines that did not possess *ARID1B* mutations.

It has been reported that *ARID1A* and *TP53* mutations do not occur concurrently <sup>331</sup>. This is not the case for OV207 cells, however, we were able to show that there was retention of some *ARID1A* WT sequence in OV207 cells, as well as mutated *ARID1A* sequence. Our group had previously reported that the *TP53* mutation found in OV207 (c.818G>A; R273H) is present in virtually 100% of cells <sup>202</sup>. We suggest that some retained *ARID1A* WT sequence supports the

co-existence of *ARID1A* and *TP53* mutations in OV207 cells. In a similar vein, it has been reported that mutation of *ARID1B* in *ARID1A* mutant cells is a synthetic lethal combination<sup>333</sup>. *ARID1A* and *ARID1B* mutations co-exist in both OVISE and TOV-21G cells. We were able to show that WT sequence was present in both *ARID1A* and *ARID1B* in TOV-21G cells, likely supporting the co-existence of these two mutations. In OVISE cells, both *ARID1B* WT and mutant sequence was observed, however, due to the presence of three mutations in *ARID1A*, one in exon 1 and two in exon 3, we could not be entirely sure whether any truly WT *ARID1A* transcript remained.

Upon examination of protein levels in OCCC cells, a doublet was observed in ARID1A in JHOC-5 cells. Since *ARID1A* has two isoforms encoding different numbers of amino acids (2285 and 2086 amino acid), and our protein bands were around 270 kDa and 250 kDa which close to the size of the two isoforms (around 270 kDa and 240 kDa), so this may lead to the observed the doublet<sup>319</sup>. Although two different isoforms of *ARID1A* have been identified (described in Section 1.4.5.2.1), none of the mutations detected are located in the missing portion of the shorter isoform. Thus, protein and mRNA analyses are not affected. Also, a doublet was observed for ARID1B in all OCCC cell lines. Company datasheets for these antibodies report that two bands of molecular weights of 280 and 250 kDa should be detected and our result confirmed that. The reason why a doublets been observed may undergo various post-translational modifications, such as phosphorylation, ubiquitination or glycosylation, which can change their molecular weight<sup>412</sup>.

However, the mRNA results show that even in cells with *ARID1A* and/or *ARID1B* mutations, mRNA expression is still present, and some mutant cell lines even express higher levels of mRNA. For example, OVTOKO, has high levels of *ARID1A* mRNA but almost no detectable ARID1A protein. There are several mechanisms that could contribute to the apparent discrepancies in gene and protein expression caused by the mutation. One possibility is that the mutation affects translation efficiency, leading to changes in protein levels that are not reflected in mRNA levels<sup>413</sup>. There are also effects of post-transcriptional modification on protein expression or activity, for example regulatory factors such as RNA binding proteins (RBP) can affect mRNA stability and translation<sup>414</sup>.

Chemotherapy, the most widely used adjuvant treatment for cancer, has a wide range of drugs used in clinical practice, including the platinum compounds cisplatin and carboplatin. They inhibit tumour cell growth by inhibiting DNA replication and transcription through internal



and interstrand cross-links formed by binding to DNA and then inducing double-stranded DNA damage, which ultimately prevents tumour cells from replicating<sup>415</sup>. We generated the dose curves of cisplatin and carboplatin and calculated the corresponding IC50s by performing platinum sensitivity experiments on all OCCC cell lines and found that the IC50 levels of carboplatin were extremely high compared to those of cisplatin, almost ten times higher. Research findings indicate that carboplatin exhibits lower potency than cisplatin, primarily attributed to its slower hydrolysis process. Consequently, in certain cancer types, the efficacy of carboplatin is inferior to that of cisplatin<sup>415</sup>. *In vitro*, in some cases, carboplatin is only 1/8 to 1/45 as effective as cisplatin, so up to 10 times the dose of carboplatin is required to achieve a similar cytotoxic effect as cisplatin<sup>416,417</sup>. In the clinic, four times the dose of carboplatin is used to achieve the same effect as cisplatin, and the maximum plasma concentration ( $C_{\max}$ ) of carboplatin ( $C_{\max} = 135 \mu\text{M}$ ) is almost ten times that of cisplatin ( $C_{\max} = 14.4 \mu\text{M}$ )<sup>417-420</sup>. Carboplatin has replaced cisplatin as the most clinically used platinum compound due to its lower toxicity compared to cisplatin<sup>124</sup>. Moreover, the carboplatin/paclitaxel doublet remains the primary chemotherapy regimen for ovarian cancer. The combination of carboplatin, which causes DNA damage and thus inhibits cancer cell division, and paclitaxel, which stabilises microtubules, prevents cell division and promotes cell death, improves the overall efficacy of treatment<sup>135,421</sup>.

The literature indicates that OCCC has a low response rate to chemotherapeutic agents compared to other ovarian cancers. A study of 101 patients with OCCC and 235 patients with serous ovarian cancer (SOC) showed that the response rate to platinum-based chemotherapy was significantly lower in patients with OCCC than in patients with SOC<sup>187</sup>. Recio and colleagues evaluated 111 patients with OCCC who underwent primary surgery and postoperative treatment, of whom 71 patients (64%) did not receive platinum-based chemotherapy and 40 patients (36%) did receive platinum-based chemotherapy. It was found that the estimated 5-year survival of patients who received platinum-based chemotherapy was not significantly different from the estimated 5-year survival of patients who received non-platinum-based chemotherapy (36% vs. 32%;  $P = 0.23$ )<sup>422</sup>. Interestingly, the results of the platinum sensitivity experiments showed that the cisplatin IC50 was greater than  $1.986 \mu\text{M}$  for seven OCCC cell lines (range from  $4.969 \mu\text{M}$  to  $1.986 \mu\text{M}$ , average  $2.915 \mu\text{M}$ ), but the literature and data from our research laboratory showed that the cisplatin IC50 for several other non-OCCC were lower than the OCCC, including A2780 (IC50 =  $1.4 \mu\text{M}$ , EnOC, data obtained from literature<sup>423</sup>), TYK-nu (IC50 =  $0.6905 \mu\text{M}$ , HGSOC, data generated in our research

laboratory), Caov-3 ( $IC_{50} = 1.086 \mu M$ , HGSOC, data generated in our research laboratory), and PEO1 ( $IC_{50} = 0.5333 \mu M$ , ovarian cystadenocarcinoma, data generated in our research laboratory). Therefore, our results align with the reports in the literature that OCCC is more resistant to platinum-based chemotherapy compared to non-OCCC.

### 3.5 Conclusion

In this chapter, we first confirmed the morphology of seven OCCC cells and authenticated all OCCC cell lines by cell line authentication (STR profiling). We then confirmed the mutations of *ARID1A* and *ARID1B* in OCCC cells reported in the literature. We also showed that *ARID1A* and *ARID1B* mRNA and protein are expressed at different levels in OCCC cell lines, however, in the case of protein, this was not statistically significant. Although the mutation of *ARID1B* in *ARID1A* mutant cells is a synthetic lethal combination, we confirmed the presence of *ARID1B* heterozygous mutations in *ARID1A* mutant cells. In addition, while *ARID1A* mutations and *TP53* mutations are mutually exclusive, *ARID1A* heterozygous mutations are found in *TP53* mutant cells. Finally, we performed sensitivity experiments with platinum compounds against OCCC, determined the dose curves of OCCC to cisplatin and carboplatin, and calculated  $IC_{50}$  levels for each cell line. Data presented in this chapter confirmed that the OCCC cell lines in our laboratory were appropriate to use for the remainder of the studies reported in this thesis.

# CHAPTER 4. Interrogating OCCC cell lines with an epigenetic drug screening library

There is a paucity of therapeutic options for patients with OCCC. As previously discussed in this thesis, OCCC are a chemoresistant malignancy<sup>187,422</sup>. This chapter describes the screening of ovarian cancer cell lines using the Tocris Epigenetics Library and investigates efficacy of a selected drug that inhibit OCCC in both 2D and 3D models.

## 4.1 Introduction

### 4.1.1 Epigenetic therapeutic compound library screen

In order to identify compounds that target OCCC, the Tocris Epigenetics Library 3.0 (Tocris Bioscience, Bristol, UK) was employed to screen seven OCCC cell lines (JHOC-5, RMG-I, OVTOKO, OVMANA, OVISE, OV207 and TOV-21G) and three non-OCCC cell lines (A2780.b1, COV434, and OVCAR-8). This library is designed for high-throughput screening (HTS), high-content screening (HCS), target validation and assay development. It contains compounds that target more than 40 epigenetic targets, including epigenetic readers (16%), writers (43%), erasers (19%), and transcriptional modulators (23%) such as methyltransferases (e.g., Euchromatic histone-lysine N-methyltransferase 2 (EHMT2) and protein arginine N-methyltransferase (PRMT)), demethylases (e.g., Lysine-specific histone demethylase (LSD)) and deubiquitinating enzymes (e.g., ubiquitin-specific proteases (USPs) including USP7, USP10 and USP13)<sup>424</sup>. The rationale for targeting the epigenome is that SWI/SNF functions as an epigenomic complex, interacting with other epigenomic factors that may impact on cell survival.

### 4.1.2 Three-dimensional (3D) bioprinting

Two-dimensional (2D) HTS assays have been widely used to test the therapeutic potential of compounds against cancer. 2D cultured cells grow as a monolayer on a flat rigid plastic surface. While well established for traditional cell culture applications, this model is limited when it comes to mimicking aspects of the *in vivo* tumour microenvironment such as cell-to-cell and cell-to-matrix interaction and communication. Moreover, since 2D cultured cells are stretched out, cytoskeleton rearrangement occurs, that can lead to abnormal gene and protein expression<sup>425-428</sup>. However, due to their simplicity and affordability, these cell culture models are widely used in most cancer studies, including HTS<sup>429</sup>. In contrast to 2D cell culture models, 3D cultured cells have a different spatial conformation. The cell-to-cell and cell-to-matrix interactions more closely mimic the natural environment *in vivo*, so the cell morphology is very similar to what is observed in the human body<sup>430</sup>. One example of this is reported by Simão

and colleagues who used neural stem cells grown in 3D to simulate brain function. These cells exhibited complex electrophysiological activity and synaptic function, thus allowing a better understanding of crosstalk between human nerve cells <sup>431</sup>.

In this project, we employed 3D bioprinting of mammalian cells encapsulated in specific hydrogels using the RASTRUM that is a 3D bioprinter platform designed by the Australian company Inventia Life Science. Through 3D bioprinting, we gain enhanced control over the distribution of cells within the 3D space compared to conventional techniques. Advanced 3D culture also provides excellent flexibility and the ability to mimic the complex cancer microenvironment in an *in vitro* manner. This allows for more reproducible cell patterning and a controlled tumour microenvironment <sup>432</sup>. In the bioprinting process using the RASTRUM, cells are encapsulated using a drop-on-demand system, which carefully dispenses cells and hydrogel from independent nozzles within the printhead. Poly(ethylene glycol) (PEG)-based hydrogels are formed when bioink and activator are printed in a 1:1 ratio, and instantly gelate to form a matrix with cells encapsulated (Figure 4.1) <sup>433</sup>. In addition, compared to other 3D bioprinting platforms, there are several advantages to using the RASTRUM platform, such as limited variation between print batches, printing can be done at room temperature, the 3D model is transparent and does not display autofluorescence, and the gels can be dissolved to allow the extraction of protein, RNA, and DNA <sup>434</sup>. Additionally, this platform is highly automated, utilising commercially available hydrogels with varying stiffness and supporting optimisation of print conditions.

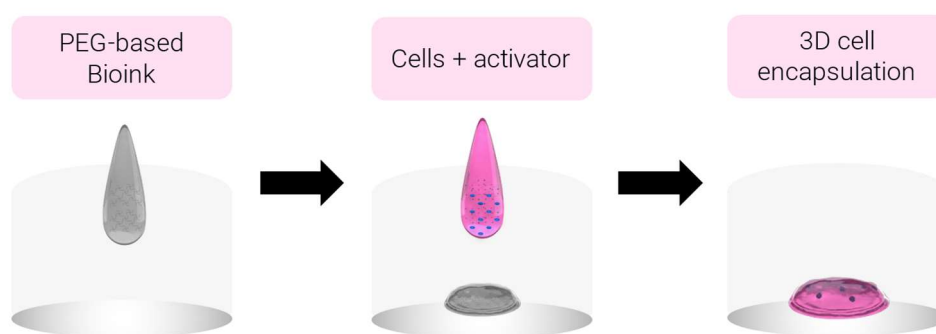


Figure 4.1 Schematic diagram of the bioprinting process using the RASTRUM bioprinter. Cancer cells are encapsulated in a hydrogel through a two-droplet system. First droplets containing PEG-based bioink is injected into the well plate, followed by the addition of droplets containing cells and activator. When the bioink and activator meet, they instantly gelate,

allowing for the rapid production of 3D cell models at room temperature. PEG: Polyethylene glycol; 3D: three dimensional. Adapted from Jung et al. 2022 <sup>435</sup>.

## **4.2 Methods**

### **4.2.1 Using the Tocriscreen Epigenetics Library 3.0 to screen ovarian cancer cell lines**

The Tocriscreen Epigenetics Library 3.0 (cat no.7578, Tocris Bioscience, Avonmouth, Bristol, UK) contains 160 epigenetic compounds (dissolved in DMSO, stock concentration of 10 mM) for HTS (full compound list in Appendix 2). Due to cell line availability in the laboratory, seven OCCC cell lines (JHOC-5, RMG-I, OVTOKO, OVMANA, OVISe, OV207 and TOV-21G) and three non-OCCC cell lines (A2780.b1, COV434, and OVCAR-8) were used for screening. All cell lines are described in Chapter 2, Section 2.1.2. Due to the growth rate (doubling time) and size of the cells, cell seeding densities were based on the controls reaching 70-95% confluence 72 hours post addition of drug. Cells were seeded into 96-well plates in 100  $\mu$ l media at specific seeding densities (Table 4.1). The next day, based on a previous publication <sup>436</sup>, cells were treated with drugs in the library diluted to a final concentration of 5  $\mu$ M and 0.5  $\mu$ M. This was achieved by adding 100  $\mu$ l of 10  $\mu$ M and 1  $\mu$ M drug stocks per well in triplicate to 100  $\mu$ L of seeded cells, resulting in a final volume of 200  $\mu$ l. In each plate, a blank (media only), an untreated control (cells only), and a vehicle control (DMSO at a final concentration of 0.1%) were included. After 72 hours of drug treatment, cell viability was assessed using the MTS assay as described in Chapter 2, Section 2.1.5. After obtaining the absorbance value, the absorbance of the media only value was subtracted and normalised to the DMSO vehicle treated sample to calculate cell viability expressed as % DMSO vehicle control. The workflow is outlined in Figure 4.2.

Table 4.1 Cell seeding density for use of the drug screening library

Cell line name	Cell subtype	Seeding density (cells/96 well)
JHOC-5	OCCC	2,500
RMG-I		6,000
OV207		2000
OVTOKO		2,500
OVMANA		4,500
OVISE		4,500
TOV-21G		5,000
A2780.b1	EnOC	5,000
OVCAR-8	HGSOC	2,500
COV434	SCCOHT	25,000

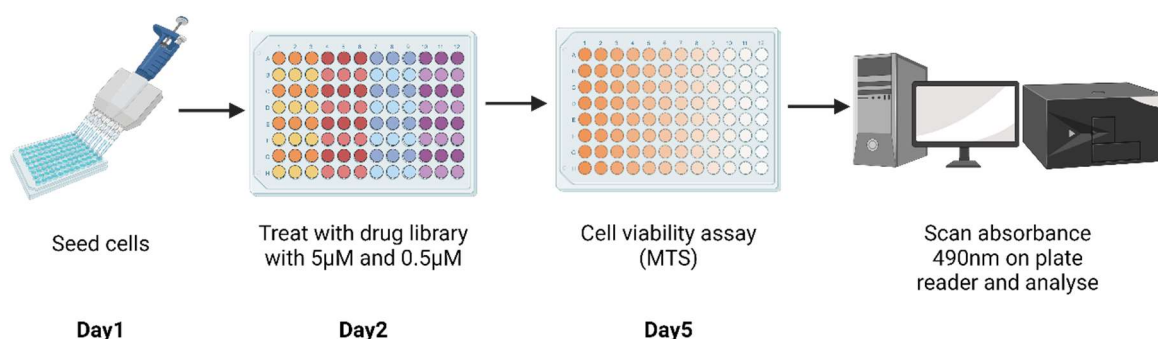


Figure 4.2 Workflow of treating ovarian cancer cell lines with the Tocris drug screening library.

#### 4.2.2 Selection of drugs of interest

Resulting cell viabilities at both concentrations (of 5 µM and 0.5 µM) were analysed using the filtration approach outlined in Figure 4.3 to select compounds of interest. In step 1, compounds were screened for their ability to inhibit OCCC relative to non-OCCC cells. If the average cell viability across all cell lines was lower for OCCC than non-OCCC, the drug was further considered. In step 2, amongst the remaining compounds, compounds that inhibited OCCC to

a greater extent than non-OCCC (difference greater than 10%) were selected to next step. The 10% threshold was chosen to balance the risks of misinterpreting small differences as noise and overlooking potential drugs due to an overly stringent cutoff. Step 3 required that the compounds had an inhibitory effect on cell viability in OCCC or non-OCCC. Cell viability above 100% suggests that a compound may promote proliferation rather than inhibition, so a threshold below 100% ensures selected compounds do not promote cancer cell growth. Therefore, compounds that appeared to promote cell viability or had no effect on average cell viability ( $\geq 100\%$  viability) were excluded. Lastly, if the compound(s) displayed the same trend at both concentrations of drug tested, this warranted selection for further analyses.

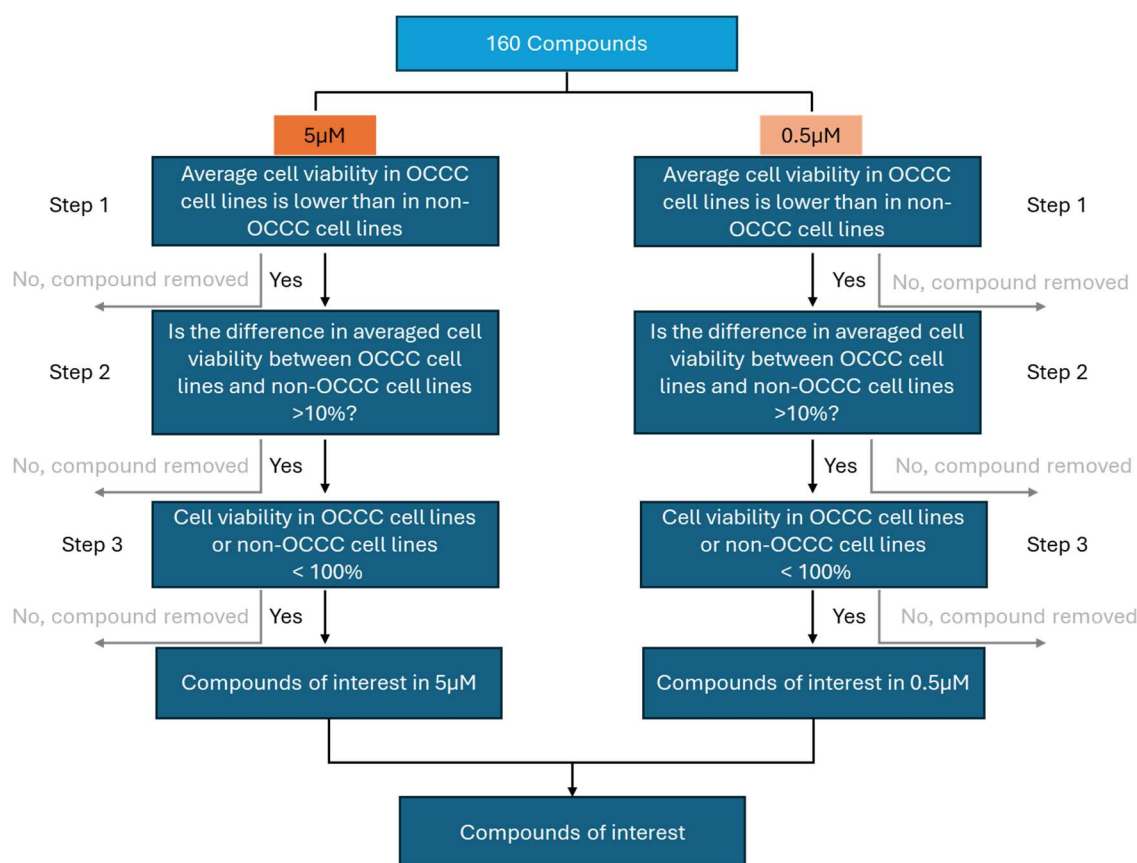


Figure 4.3 Flow diagram summarising inclusion and exclusion criteria for drug compounds in the Tocriscreen Epigenetics Library 3.0 screened against ovarian cancer cell lines. Cell viability data from seven OCCC and three non-OCCC samples were analysed to identify compounds of interest that may selectively inhibit OCCC over non-OCCC cells. Grey arrows indicate compounds excluded from further analysis.



#### 4.2.3 Validation of drugs of interest in 2D culture

To determine the IC<sub>50</sub> levels of the candidate drug of interest for validation of drug screening results, cells were challenged with a concentration range of compounds and cell viability determined using an MTS assay. Cells were seeded at a specific density depending on cell line (Chapter 2, Table 2.3) in 100 µl medium into 96-well plates and incubated at 37°C for 18 hours before being treated with a dose range of the drug of interest diluted from a stock concentration of 10 µM into ten different concentrations (Table 4.2). Next, 100 µl of the drug of interest was added into each well and cells were incubated for a further 72 hours. Following this, cell viability was determined using an MTS assay described in Chapter 2, Section 2.1.5.

Table 4.2 Dilutions of the drug of interest<sup>^</sup> to determine IC<sub>50</sub> levels

Ovarian cancer cell lines <sup>^^</sup>		COV434	
Final concentration (µM)	Dilution factor	Final concentration (µM)	Dilution factor
0.003617	4-fold dilution	9.690335	1.2-fold dilution
0.014468		11.6284	
0.05787		13.95408	
0.231481		16.7449	
0.925926		20.09388	
3.703704		24.11265	
14.81481	1.5-fold dilution	28.93519	
22.22222		34.72222	
33.33333		41.66667	
50		50	

<sup>^</sup>ibrutinib sourced from MedChemExpress (cat no. HY-10997); <sup>^^</sup>All ovarian cancer cell lines analysed with the exception of COV434.

#### 4.2.4 Three-dimensional (3D) bioprinting and drug validation

OSCC models were cultured under 3D cell culture conditions using PEG-based 3D biofunctionalised hydrogels created with the RASTRUM 3D bioprinter (Inventia Life Science, Alexandria, NSW, Australia).

#### 4.2.4.1 Matrix selection for optimal 3D cell growth conditions

To choose the optimal cell growth matrix for growth of RMG-I and JHOC-5 cell lines in 3D, I performed matrix selection using hydrogels containing different peptides. The RASTRUM imaging plug was chosen for matrix selection over the large plug model as it prints a smaller plug of cells in the centre of the well, optimising the focal plane for image analysis. Four separate biofunctionalised hydrogels were tested for cell growth in 3D, specifically arginine–glycine–aspartic acid (RGD), peptide set (RGD, Ile-Lys-Val-Ala-Val (IKVAV), Tyr-Ile-Gly-Ser-Arg (YIGSR)), Fibronectin, and Laminin-511 (full-length proteins) (Table 4.3). RGD is the principal integrin-binding domain present in extracellular matrix (ECM) proteins. Thus, RGD is employed as a supporting scaffold for some ECMs <sup>437</sup>. In a similar manner, ECM hydrogels synthesised from IKVAV and YIGSR as short cell adhesion peptides have also been demonstrated to enhance cell viability and facilitate cell growth <sup>438-440</sup>. The amino acid sequence IKVAV has been demonstrated to promote a number of cellular processes, including cell adhesion, neurite growth, angiogenesis, collagenase IV production and tumour growth. A study demonstrated that IKVAV-containing laminin  $\alpha$ 1 chain peptides are capable of forming amyloid-like fibrils and exert a pivotal influence on biological activity <sup>441</sup>. YIGSR is a short peptide derived from laminin and fibronectin. Studies have demonstrated that it can be employed to enhance the survival, maintenance of stemness, adhesion, and paracrine functions of mesenchymal stem cells (MSCs) <sup>442</sup>. Fibronectin is a highly abundant component of the ovarian tumour-associated microenvironment and has been demonstrated to play a role in ovarian cancer migration, invasion, and metastasis <sup>443,444</sup>. Laminin is a structural component of the basement membrane and is also a key ECM regulator for cell adhesion, migration, differentiation and proliferation <sup>445</sup>. It has been demonstrated that a matrix with 3 kPa stiffness enhanced EOC cell adhesion and migration <sup>446</sup>. Therefore, 3kPa was selected as the optimal stiffness for the printing matrix.

3D cultures bioprinted using the RASTRUM 3D bioprinter used two components, specifically bioink and activator. For a typical print run using the RASTRUM 3D bio-printer, 40mL of sterile filtered water, 16mL of sterile ethanol, and bioinks and activators (Table 4.3) were placed into the RASTRUM cartridge (Figure 4.4) according to the manufacturer's manual. The cartridge and a new sterile 96-well plate (cat no. 3595, Corning Incorporated, Australia) were then placed into the RASTRUM printer, and the inert base printed into the 96-well plate preventing cell attachment to the well bottom and formation of a 2D monolayer culture instead of 3D growth. While printing the inert base, cells were harvested (See Section 2.1.2) and

counted (See Section 2.1.4). Next, 1,250,000 cells in suspension were transferred into a 15 ml tube and centrifuged at 350g for 5 minutes at room temperature. The supernatant was removed, and the cell pellet resuspended in 200 µl of activator. After the inert base was printed, the cartridge was removed from the printer and 200 µl of the cells in activator mixture were transferred into the cartridge. The cartridge was then re-inserted into the printer in order to bioprint the cells in activator and bioink on the inert base to form a 3D hydrogel structure. Finally, 18,000 cells were printed into each well, and 150 µl appropriate growth medium (Chapter 2, Table 2.2) was gently dispensed per 96 well and brightfield images scanned in an IncuCyte live cell imager using the organoid assay mode with 4X objective (Sartorius, Australia). CellTiter-Glo ATP-based 3D Cell Viability Assay (See Section 4.2.4.4.1) and *in situ* staining with the LIVE/DEAD Cell Imaging Kit (See Section 4.2.4.4.2) were performed at day 7 post print. Among all the matrices tested, those where cells showed increased growth over time were selected for further bioprinting experiments.

Table 4.3 List of bioinks and activators for matrix selection using the RASTRUM 3D bioprinter<sup>^</sup>

Matrix	Peptide/Protein	ECM component representation	Matrix #	RASTRUM bioinks and activators
Inert base	-	-	-	Activator F3 and Bioink F32
RGD	Peptide	Fibronectin, Collagen	Px03.31P	Activator F178 and Bioink F243
RGD, IKVAV, YIGSR	Peptide	Fibronectin, Collagen, Laminins	Px03.01p	Activator F178 and Bioink F182
Fibronectin	Full-length protein	Fibronectin	Px03.30F	Activator F206 and Bioink F97
Laminin-511	Full length protein	Laminin	Px03.32	Bioink F97 and Activator F287

RGD: Arginylglycylaspartic acid; IKVAV: Ile-Lys-Val-Ala-Val; YIGSR: Tyr-Ile-Gly-Ser-Arg.

<sup>^</sup>All bioinks and activators are purchased from Inventia Life Science.

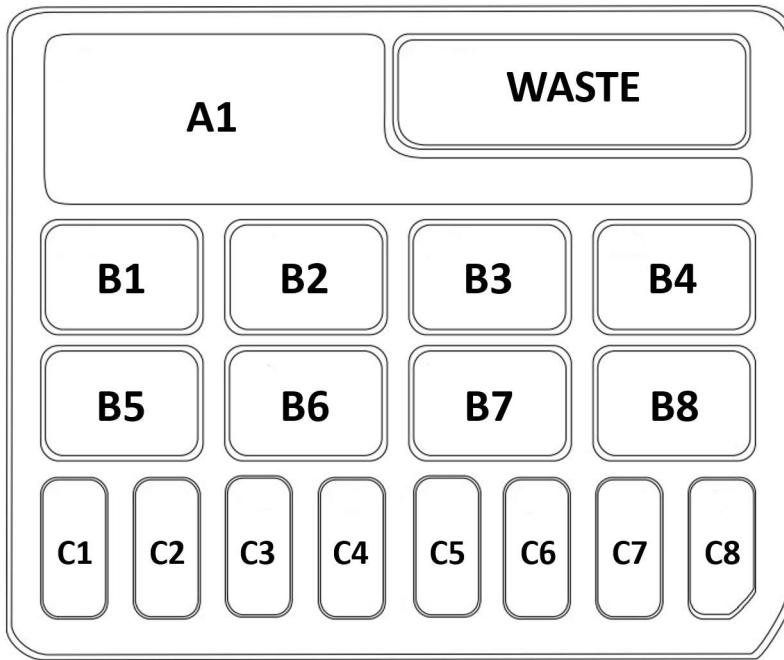


Figure 4.4 Layout of the RASTRUM 3D bioprinter cartridge. The cartridge can be divided into 4 parts, specifically A1 is for sterile Milli-Q water to rinse the system between each step, B1 to B8 are for filtered 70% methanol to keep the system sterile, C1 to C8 are for bioinks and activators, and the WASTE well collects all the waste after rinse and sterilisation steps.

#### 4.2.4.2 Generating 3D bioprinted Ovarian Cancer cell models

Based on matrix selection (See Section 4.2.3.1 above), we chose a matrix containing RGD with 3 kPa stiffness, which is intended to mimic the extracellular matrix in contact with ovarian cancer cells (Px03.31P) and printed cells using a large plug model. The large plug cell model is optimal for intercellular analysis, as it maximises the volume of cell-containing gel in each well. Also, it can be utilised for fluorescent staining and high-magnification imaging.

A volume of 40mL of sterile filtered water, 16 ml of sterile ethanol, and 1.3 ml Activator F3, 1.3 ml Bioink F32, and 600 µl Bioink F243 were placed into the RASTRUM cartridge following the manufacturer's protocol. The inert base was printed, cells harvested and counted as described above in Section 4.2.3.1 Next, 3,750,000 OCCC cells, with the exception of OVMANA that was 3,060,000 cells, were pelleted by centrifugation at 350g for 5 minutes. The supernatant was removed, and the cell pellet resuspended in 600 µl of Activator F178 before it was transferred into the cartridge and placed into the printer. Cells were printed on the inert base (18,000 OCCC cells per well, excluding OVMANA which was 16,000 cells per well) and

150  $\mu$ L of normal growth medium was gently added per well, and cells incubated at 37°C and 5% CO<sub>2</sub> for up to 4 days to allow formation of 3D structures. CTG Cell Viability Assay (See Section 4.2.4.4.1) was assessed at days 1, 4 and 7 post print. *In situ* staining with the LIVE/DEAD Cell Imaging Kit (See Section 4.2.4.4.2) was performed at day 7 post print. Figure 4.4 shows an overview of the process of 3D drug screen validation.

#### 4.2.4.3 Drug treatments of 3D bioprinted cells

After printing the large plug, cells were cultured for 4 days before the culture medium was removed from the 96-well plate. Serial dilutions of drugs of interest (See Table 4.2) were added into 200  $\mu$ L culture media, along with a vehicle control (DMSO) and media alone, and incubated for 72 hours. Cell viability was assessed using the CTG Cell Viability Assay (See Section 4.2.3.4.1) at day 7 post-printing in all of the treated cell lines (See Figure 4.5).

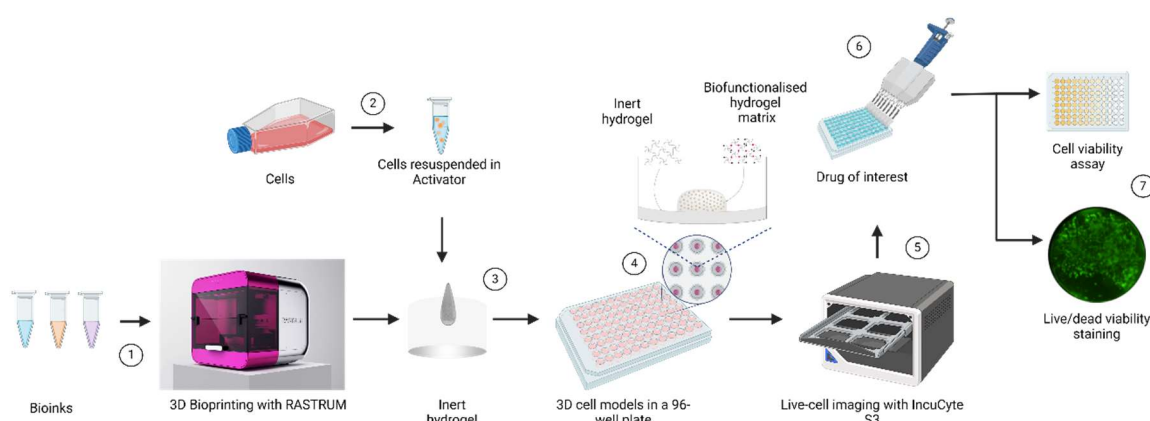


Figure 4.5 Workflow of 3D bioprinting with the RASTRUM platform to test cell viability after drug treatment. Cells were harvested and resuspended in activator solutions that on addition to the biofunctionalised hydrogel (bioink) formed an instant gel printed on top of an inert base. 3D cell structures were allowed to form over 4 days, after which cells were treated with the drug of interest within the dose range 0.004 – 50  $\mu$ M, as well as a DMSO vehicle control. Cell viability was measured at day 7 post-printing using the CellTiter-Glo ATP-based 3D Cell Viability Assay (Promega) and visualised by *in situ* staining with the LIVE/DEAD Cell Imaging Kit (ThermoFisher Scientific).

#### 4.2.4.4 3D cell viability assays

##### 4.2.4.4.1 CellTiter-Glo ATP-based 3D Cell Viability Assay

The CellTiter-Glo<sup>®</sup> 3D Cell Viability Assay has been designed for the determination of cell viability in 3D spheroid cultures. Briefly, after drug incubation a volume of 100µl media was removed from bioprinted cultures and 100µL of CellTiter-Glo 3D Viability Assay (cat no. G9681, Promega, Madison, Wisconsin, United State) (CTG) solution was added into each well. Cells were incubated at room temperature for 30 minutes. Next, 100 µl of the supernatant was transferred to a white 96-well Opti Plate (cat. no. 6005290, PerkinElmer, Incorporated, UK), and luminescence was measured as relative light units (RLU) using the Tecan200 plate reader.

##### 4.2.4.4.2 Assessing cell death in 3D bioprinted cells – the LIVE/DEAD cell viability assay

LIVE/DEAD cell viability assay can determine the viability of cells in a population based on plasma membrane integrity and esterase activity. Cells were stained with the LIVE/DEAD<sup>™</sup> Viability/Cytotoxicity Kit (cat no. L3224, ThermoFisher Scientific, Australia). The kit contains two dyes: calcein-AM (Green), which indicates intracellular esterase activity only seen in live/viable cells, and ethidium homodimer-1 (Red), which fluoresces when bound to free DNA and indicates loss of plasma membrane integrity. Culture medium was removed, and cells were washed with 100 µl of PBS. Calcein-AM and ethidium homodimer-1 were diluted in PBS (at 1:4,000 and 1:1,000 ratio respectively) and 100 µl of the diluted mixture was added into each well and incubated at 37°C for 30 minutes. Next, dye mixture was removed, and the cells washed with 100 µl PBS. Finally, 100 µl PBS was added into each well and visualised using IncuCyte live cell imager with 4X and 10X objectives and the whole well scan mode in RED, GREEN, and phase channels.

## 4.3 Results

### 4.3.1 Identification of drugs of interest following screening of ovarian cancer cell lines with an epigenetic compound library

Ten ovarian cancer cell lines, seven OCCC cell lines (JHOC-5, RMG-I, OVTOKO, OVMANA, OVISE, OV207 and TOV-21G) and three non-OCCC cell lines (A2780.b1, COV434, and OVCAR-8), were screened using the Tocriscreen Epigenetics Library 3.0 and cell viability data

obtained for each cell line at two different drug compound concentrations (5  $\mu$ M and 0.5  $\mu$ M). A summary of cell viability, represented as a percentage of the DMSO control, for all 160 compounds screened in all ovarian cancer lines at both concentrations is presented in Figure 4.6. Most of the drugs tested did not affect cell viability at both concentrations (cell viability more than 80%). Moreover, more drugs appeared to inhibit most of the non-OCCC cell lines (less than 25% cell viability) compared to OCCC cells, especially at 5  $\mu$ M. Subsequently, heatmaps were generated for drug treatments of all cell lines at both drug concentrations (Figure 4.7). The results indicated that at 5  $\mu$ M, some of the drugs exhibited a clear inhibition of cell activity, for example Drugs 129, 130, 147, 153, and 160, while some drugs inhibited nearly all cell lines, such as Drugs 147, 153, and 160. However, at 0.5  $\mu$ M, although there were some drugs that exhibited a similar effect, the number of drugs was considerably fewer in comparison to 5  $\mu$ M. Consequently, we have divided cell viability post drug treatment into three groups; specifically, viability lower than 50%, viability between 50% to 100%, and viability greater than 100% indicating that the drug had a proliferative effect on these cells. The results of this analysis are presented in Tables 4.4 and 4.5.

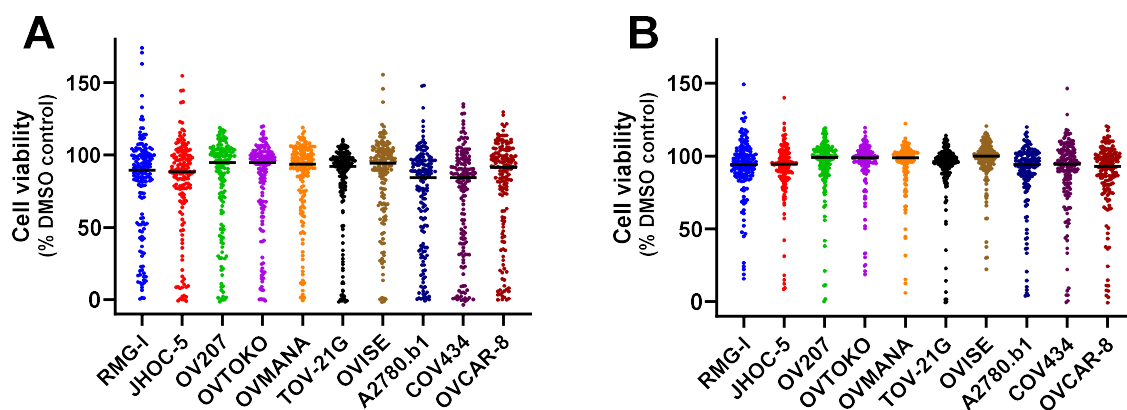


Figure 4.6 Scatter plot of cell viability in 10 ovarian cancer cell lines after treatment with the 160 drug compound screening library. (A) Cells treated with a 5  $\mu$ M concentration of each drug. (B) Cells treated with a 0.5  $\mu$ M concentration of each drug. Cell viability was normalised to DMSO vehicle control, and the figure generated using GraphPad software. The black bar indicates median value. Data was generated from a single biological replicate.

At 5  $\mu$ M, approximately 26.25% (range, 21.25%-30%) of the drugs led to less than 50% cell viability of each non-OCCC, compared to 16.87% (range, 13.12%-20.62%) in the OCCC.

Conversely, 27.41% (range, 18.12%-35.62%) of the drugs demonstrated a growth promoting effect on OCCC, but this was only 20.21% (range, 15%-26.25%) in non-OCCC. Interestingly, 55.71% (range, 43.75%-64.38%) drugs in OCCC and 53.54% (range, 50.62%-57.50%) drugs in non-OCCC demonstrated cell viability within the 50%-100% range. In terms of 0.5  $\mu$ M, the results indicated that 4.38% (range, 5%-3.12%) of the drugs exhibited less than 50% effect on cell viability in OCCC, in comparison to 8.54% (range, 7.50%-9.38%) in non-OCCC. In non-OCCC, 29.38% (range, 27.50%-32.50%) of the drugs exhibited a promotion of cell growth, with this number increased to 37.14% (range, 25%-48.12%) in OCCC. It is also noteworthy that, like for 5  $\mu$ M drug concentrations, 58.48% (range, 48.75%-68.12%) of the drugs at 0.5  $\mu$ M concentration exhibited an effect on the cell viability in OCCC and 62.08% (range, 60%-63.75%) in non-OCCC, with the range between 50% to 100%. Interestingly, the results showed that only Drug-110 (A 196) produced a strong proliferative effect (cell viability more than 110%) at both drug concentrations in more than three OCCC cell lines.



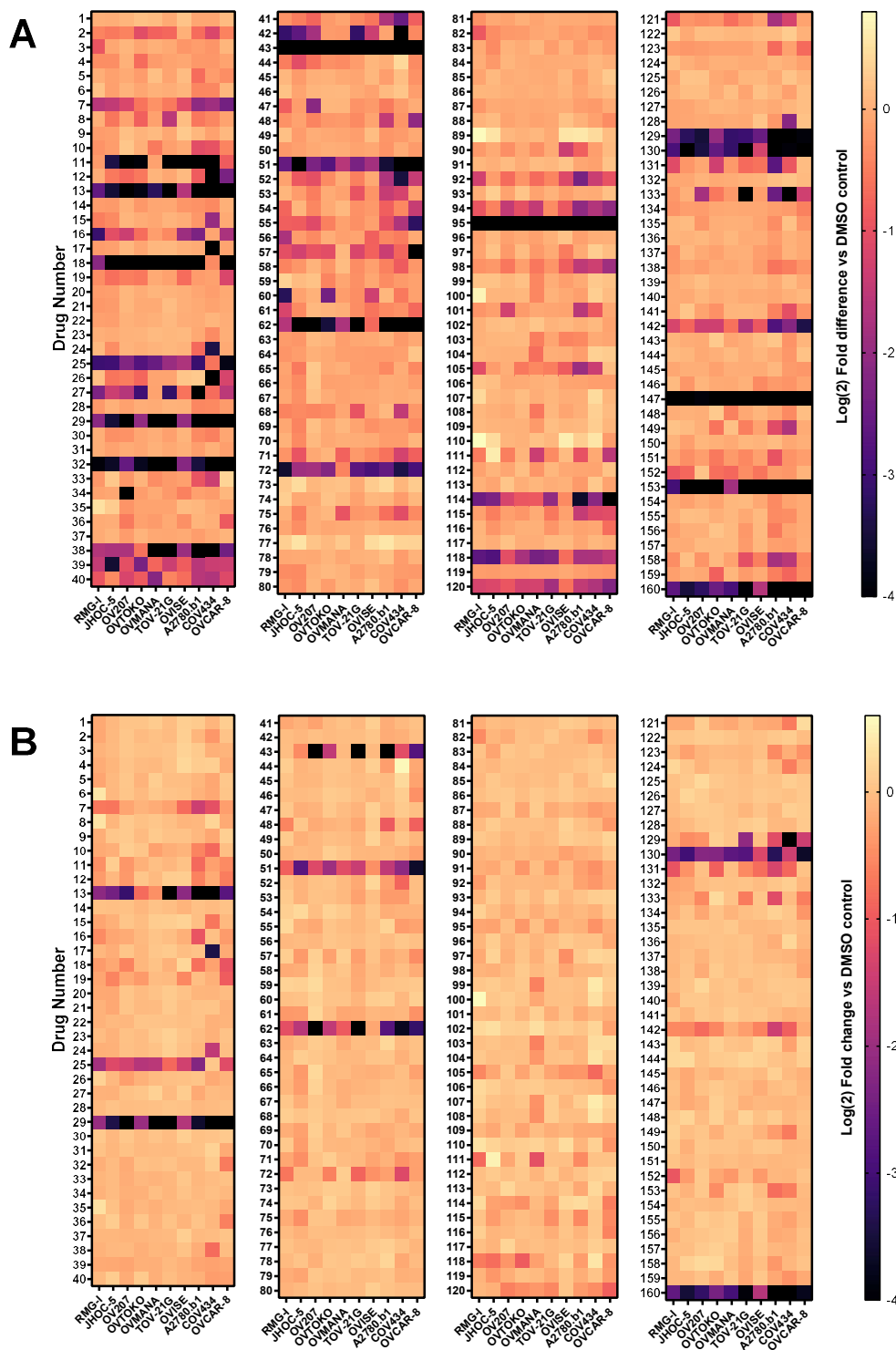


Figure 4.7 Heatmap of cell viability in 10 ovarian cancer cell lines after treatment with the drug screening library (N=1). (A) Cells treated with a 5  $\mu$ M concentration of each drug. (B) Cells treated with a 0.5  $\mu$ M concentration of each drug. Cell viability was normalised to DMSO vehicle control, and heatmaps generated using GraphPad software. All the values between -4 to -14 were visualised at -4.

Table 4.4 Cell viability in OCCC cell lines post drug treatment with 160 compounds from the epigenetic screening library

Cell line	RMG-I		JHOC-5		OV207		OVTOKO		OVMANA		OVISe		TOV-21G	
Subtype	OCCC													
Concentration (μM)	5	0.5	5	0.5	5	0.5	5	0.5	5	0.5	5	0.5	5	0.5
<50% viability	32 (20%)	8 (5%)	27 (16.87)	7 (4.37%)	33 (20.62%)	7 (4.37%)	26 (16.25%)	7 (4.37%)	21 (13.12%)	7 (4.37%)	28 (17.50%)	8 (5%)	22 (13.75%)	5 (3.12%)
Between 50 - 100% viability	87 (54.38%)	104 (65%)	94 (58.75%)	109 (68.13%)	70 (43.75%)	82 (51.25%)	92 (57.50%)	87 (53.13%)	91 (56.88%)	85 (53.13%)	103 (64.38%)	112 (70%)	87 (54.38%)	78 (48.75%)
> 100% viability	41 (25.62%)	48 (30%)	39 (24.38%)	44 (27.5%)	57 (35.63%)	71 (44.38%)	42 (26.25%)	66 (42.50%)	48 (30%)	68 (42.50%)	29 (18.12%)	40 (25%)	51 (31.87%)	77 (48.13%)
Total	160	160	160	160	160	160	160	160	160	160	160	160	160	160

OCCC: Ovarian clear cell carcinoma

Table 4.5 Cell viability in non-OCCC cell lines post drug treatment with 160 compounds from the epigenetic screening library

Cell line	A2780.b1		COV434		OVCAR-8	
Subtypes	EnOC		SCCOHT		HGSOC	
Concentration(μM)	5	0.5	5	0.5	5	0.5
<50% viability	44 (27.50%)	15 (9.38%)	48 (30%)	12 (7.50%)	34 (21.25%)	14 (8.75%)
Between 50 -100% viability	92 (57.50%)	100 (62.50%)	81 (50.62%)	96 (60%)	84 (52.50%)	102 (63.75%)
> 100% viability	24 (15%)	45 (28.12%)	31 (19.38%)	52 (32.50%)	42 (26.25%)	44 (27.50%)
Total	160	160	160	160	160	160

EnOC: Endometrioid ovarian carcinoma, SCCOHT: Small cell carcinoma of the ovary, hypercalcemic type, HGSOC: High-grade serous ovarian cancer.

### 4.3.2 Identification of ibrutinib as a compound of interest for further study

Subsequently, a classification system was employed to filter cell viability data obtained from the drug screen library (Section 4.3.1), thereby identifying compounds with enhanced inhibitory properties against OCCC. It was found that only one compound met the criteria at both concentrations described in Section 4.2.2 (Figure 4.8). This compound was D152, ibrutinib.

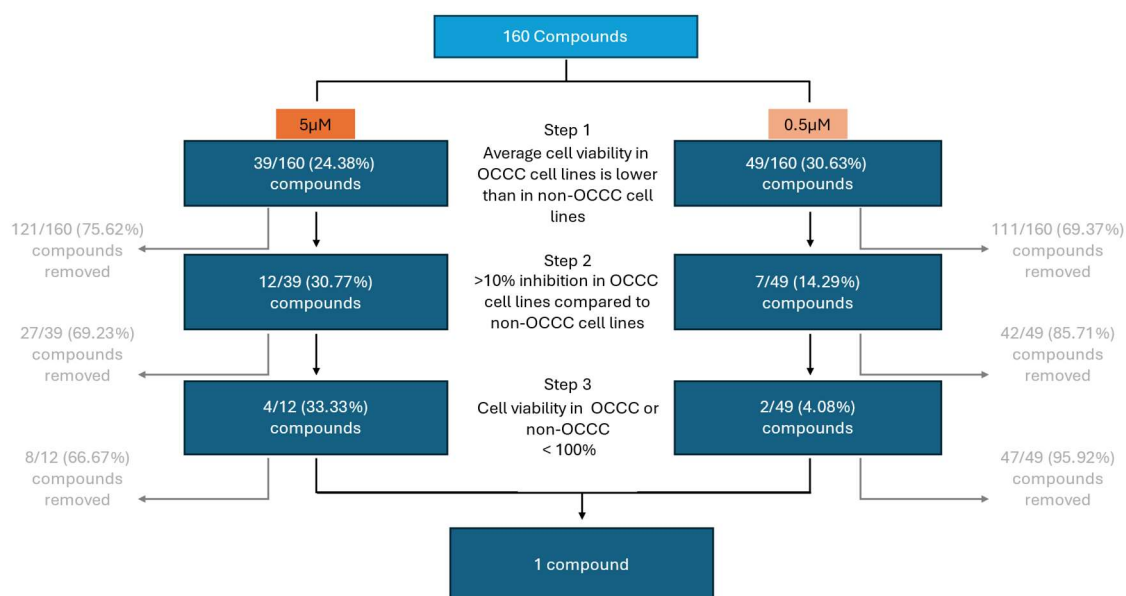


Figure 4.8 Result of selecting compounds of interest from the Tocriscreen epigenetics 3.0 library screening. A 3-step triage system was used to identify 5 compounds (Ibrutinib overlapped in both concentrations) of interest that show selective inhibition in the OCCC cell lines compared to non-OCCC cell lines.

Upon analysing the heatmaps of Drug 152, ibrutinib, at both drug concentrations tested, there is a strong inhibitory effect, especially at 5  $\mu$ M on all OCCCs compared to non-OCCCs with the exception of OV207 where a growth promoting effect was observed (Figure 4.9). Drug 152 also promoted grow of OVCAR-8 cells compared to DMSO control.

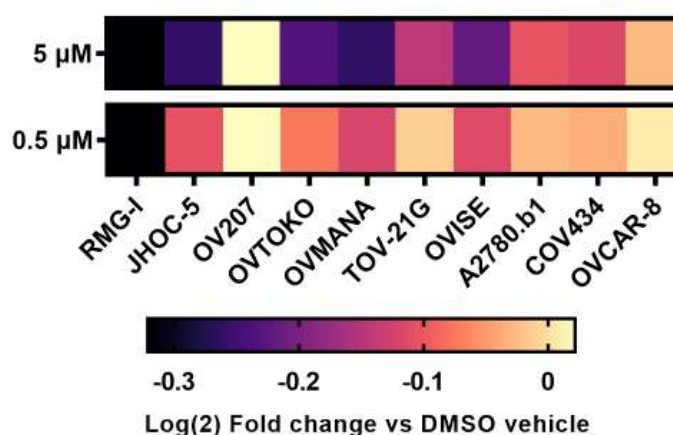


Figure 4.9 Heatmap of Log (2) fold change in cell viability after treatment with ibrutinib (Drug 152) at 5 and 0.5  $\mu$ M concentrations in seven OCCC and three non-OCCC ovarian cancer cell lines (n=1). Cell viability was normalised to DMSO vehicle control.

As the screening library experiments were conducted only once, we repeated drug treatments twice more with Drug 152 at both concentrations. Data from this triplicate experiment is shown in Figure 4.10. The results indicate that, apart from OV207 and OVCAR-8, Drug 152 had an inhibitory effect on ovarian cancer cells at both concentrations. At 5  $\mu$ M, in OCCC, RMG-I and OVMANA were strongly inhibited, followed by OVTOKO, JHOC-5, OVISE, and TOV-21G. In contrast, non-OCCC demonstrated only minimal inhibition and exhibited higher cell viability. At 0.5  $\mu$ M, RMG-I and OVMANA remained strongly inhibited in OCCC, followed by OVISE, and JHOC-5, OVTOKO, while TOV-21G exhibited minimal differences in inhibition. In non-OCCC, COV434 showed similar inhibition as JHOC-5, OVTOKO and TOV-21G, but A2780.b1 was hardly inhibited. A one-way ANOVA with Tukey's *post hoc* statistical analysis was performed, and the results shown in Appendix 2.

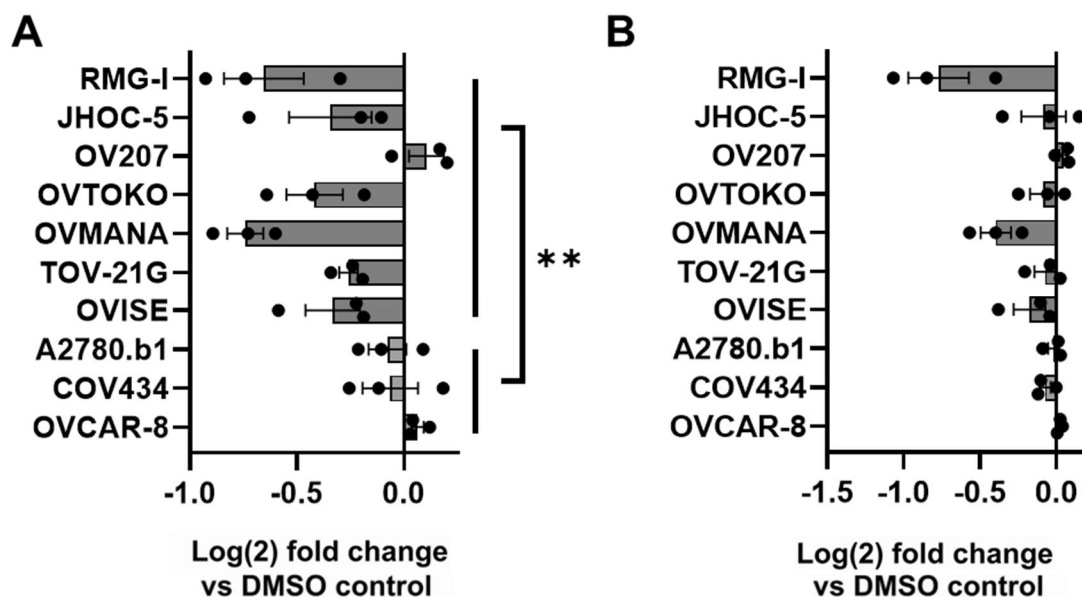


Figure 4.10 Bar chart of cell viability in seven OCCC and three non-OCCC ovarian cancer cell lines after treatment with the Drug 152 (ibrutinib) at (A) 5  $\mu$ M and (B) 0.5  $\mu$ M concentrations. Cell viability was normalised to DMSO vehicle control, and heatmaps generated using GraphPad software. Two-tailed t test showed that there was a significant difference in cell viability between OCCC and non-OCCC at 5  $\mu$ M ( $P=0.0045$ ). Data is presented as the mean  $\pm$  SEM,  $N=3$ . Data analysed using a One-Way ANOVA with Tukey's *post hoc* test in shown in Appendix 2.

#### 4.3.3 BTK, the target of ibrutinib, is expressed in ovarian cancer cell lines

Drug 152 is ibrutinib, a small molecule inhibitor of Bruton's tyrosine kinase (BTK), a tyrosine kinase encoded by the human *BTK* gene. While BTK is the primary target of ibrutinib, other tyrosine kinases including B lymphocyte kinases (BLK) and Tec can be inhibited<sup>447</sup>. BTK plays a crucial role in B-cell development and is also seen as a potential target for cancer therapy. We sought to determine whether BTK was expressed in ovarian cancer cell lines, and if so whether its inhibition may directly lead to a therapeutic effect. RNA was extracted from seven OCCC cell lines and the control cell line HEK293, then qRT-PCR was employed to analyse the expression of *BTK* mRNA. The results demonstrated that all OCCC cell lines expressed *BTK* mRNA, with OVISE displaying the highest mRNA expression levels, followed by RMG-I, and OVTOKO, then JHOC-5 and OVMANA. The mRNA expression levels of TOV-21G and OV207 were found to be extremely low, with the mRNA of OV207 exhibiting negligible expression (Figure 4.11).

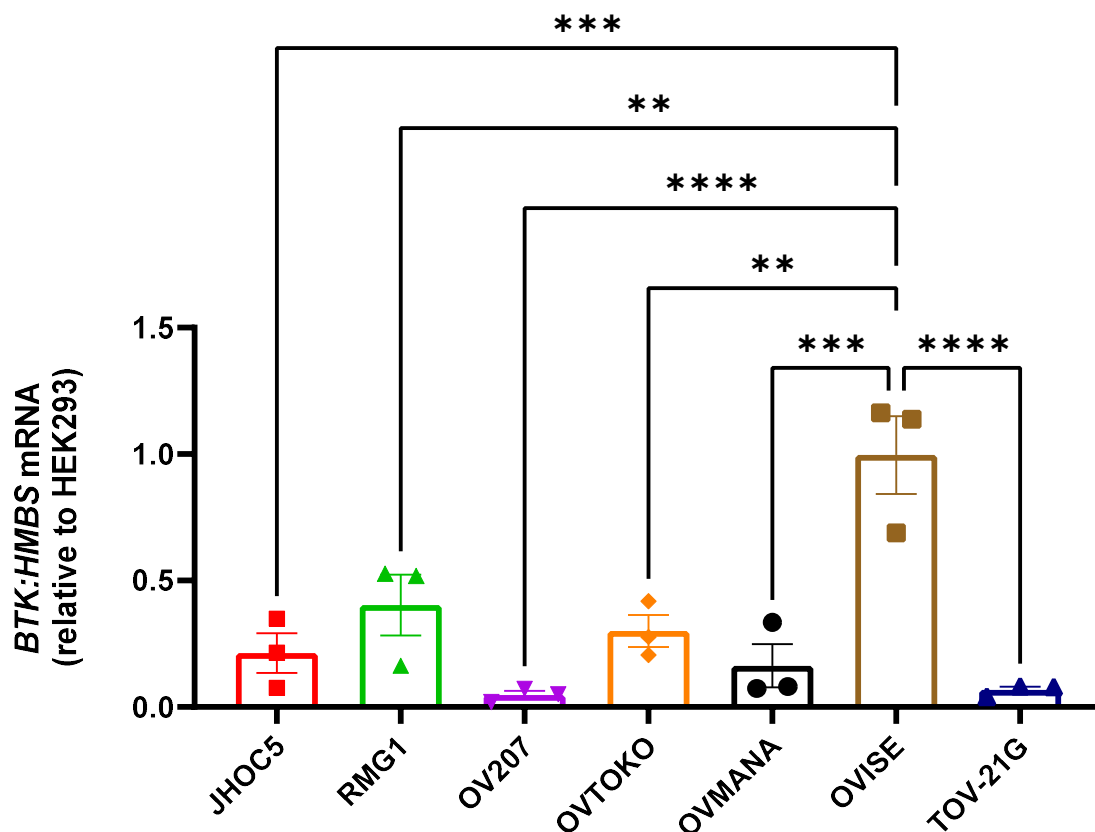


Figure 4.11 mRNA expression level of *BTK* in all OCCC cells normalised to HEK293 cells. Experiments were repeated three times and data presented as the mean  $\pm$  SEM, N=3. *HMBS* was used as the reference gene. A one-way ANOVA with Tukey's *post-hoc* test was performed to determine statistical significance between OCCC cell lines (\*\*P<0.01, \*\*\*P<0.001, \*\*\*\*P<0.0001).

#### 4.3.4 Sensitivity of ovarian cancer cell lines cultured in 2D to ibrutinib

To further determine the sensitivity of ovarian cancer cells to ibrutinib, OCCC and non-OCCC cell lines were treated with ibrutinib at 11 different concentrations between 0.003617 to 50  $\mu$ M, with the exception of COV434 where concentrations tested were between 9.690335 to 50  $\mu$ M. Ibrutinib dose curves for these cell lines were used to calculate the IC<sub>50</sub> of each cell line to ibrutinib (Figure 4.12 and 4.13).

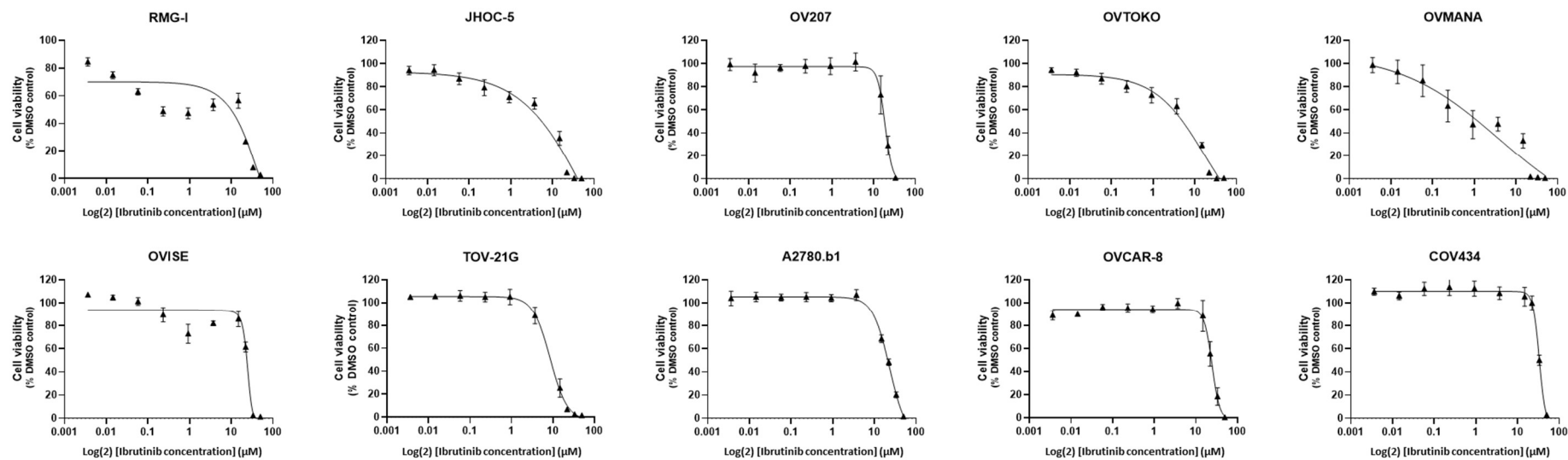


Figure 4.12 Ibrutinib dose curves of 10 ovarian cancer cell lines. The 10 cell lines were treated with 11 concentrations of ibrutinib (Table 4.2) for 72h, and an MTS assay performed to determine how many live cells remained (% viable cells). These experiments were repeated at least 3 times before dose curves were generated.

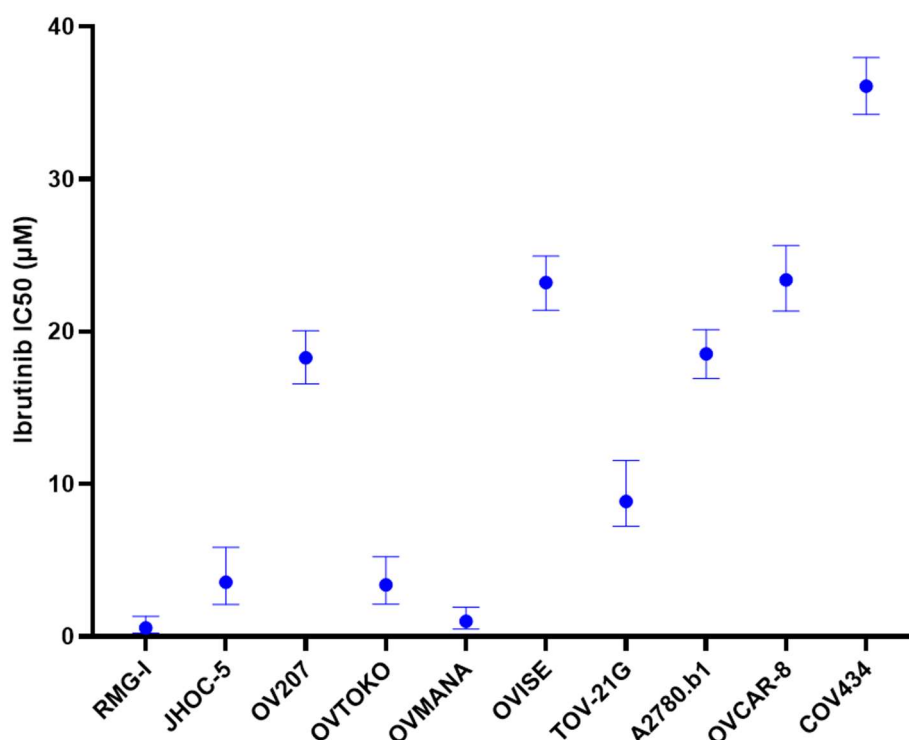


Figure 4.13 IC<sub>50</sub> of ibrutinib in 10 ovarian cancer cell lines. Cells were treated with 11 concentrations of ibrutinib (Table 4.2) for 72h, and an MTS assay performed to determine how many live cells remained (% viable cells). These experiments were repeated at least 3 times to generate dose curves and IC<sub>50</sub> was calculated from the dose curve (see Section 2.1.5). 95% CIs are shown.

The IC<sub>50</sub> values indicate that almost all OCCC cell lines demonstrated lower sensitivities to ibrutinib, compared with non-OCCC cell lines. Among the OCCC cell lines, RMG-I (IC<sub>50</sub> 0.5544 µM) and OVMANA (IC<sub>50</sub> 0.9955 µM) exhibited the highest sensitivities to ibrutinib, while JHOC-5 (IC<sub>50</sub> 3.563 µM) and OVTOKO (IC<sub>50</sub> 3.385 µM) demonstrated slightly lower sensitivities, followed by TOV-21G (IC<sub>50</sub> 8.855 µM) and OV207 (IC<sub>50</sub> 18.27 µM). OVISE (IC<sub>50</sub> 23.22 µM) had the lowest sensitivity to ibrutinib among the OCCC cell lines. Although non-OCCC cell lines showed low sensitivities to ibrutinib, the IC<sub>50</sub> for one of the non-OCCC cell lines, A2780.b1 (IC<sub>50</sub> 20.35 µM), was slightly lower than that of OVISE. The OVCAR-8 (IC<sub>50</sub> 23.39 µM) and OVISE cell lines had comparable sensitivities to ibrutinib. COV434 (IC<sub>50</sub> 36.09 µM) had the lowest sensitivity of the ovarian cancers, almost seventy times that of the most sensitive cell line RMG-I (Table 4.6 and Figure 4.14).



Table 4.6 IC50 comparisons (cell viability: MTS) for ibrutinib in 10 ovarian cancer cell lines grown in 2D

Cell line	Cell subtype	IC50 (μM)	95% CI (μM)
RMG-I	OCCC	0.5544	0.2138 - 1.327
JHOC-5		3.563	2.102 - 5.838
OV207		18.27	16.57 - 20.06
OVTOKO		3.385	2.118 - 5.227
OVMANA		0.9955	0.5010 - 1.920
OVISE		23.22	21.39 - 24.95
TOV-21G		8.855	7.227 - 11.54
A2780.b1	EnOC	20.35	18.72 - 22.01
OVCAR-8	HGSOC	23.39	21.34 - 25.63
COV434	SCCOHT	36.09	34.24 - 37.97

OCCC: Ovarian clear cell carcinoma; EnOC: Endometrioid ovarian carcinoma; SCCOHT: Small cell carcinoma of the ovary, hypercalcemic type; HGSOC: High-grade serous ovarian cancer.

OVISE > OV207 > TOV-21G > JHOC-5 > OVTOKO > OVMANA > RMG-I



Figure 4.14 Comparison of IC50 of ibrutinib in seven OCCC cells in 2D. Seven OCCC cells were ranked in order of increasing IC50 for ibrutinib. The order from left to right indicates IC50 from highest to lowest. Green: *ARID1A* and *ARID1B* WT. Blue: Only *ARID1A* mutation. Orange: Both *ARID1A* and *ARID1B* mutations.

#### 4.3.5 Selection of optimal matrices for 3D bioprinted OCCC cell lines

Previous experiments with ibrutinib were conducted under 2D culture conditions. Next, we sought to analyse ovarian cancer cell line response to ibrutinib when cultured in 3D. This required initial optimisation of 3D culture conditions. Consequently, RMG-I and JHOC-5 were employed for matrix selection. Each matrix selection combination comprised two matrices

containing different peptides and a matrix with no peptides. The number of cells printed in each matrix was identical, and cell viability was quantified using the CTG assay on the seventh day.

Matrix selection in RMG-I cells showed the best cell growth in both RGD and the combination of RGD, IKVAV and YIGSR matrixes compared to a matrix that did not contain peptides. RMG-I cell line viability demonstrated a 2-fold increase in RGD, IKVAV, and YIGSR matrixes compared with no peptides/proteins (Figure 4.15). Further, cells proliferated at a higher rate in fibronectin and laminin-511 matrix compared to peptide-free matrix. Cells grown in fibronectin exhibited a higher proliferation rate than those grown in laminin-511. In addition, the cell proliferation rate was found to be higher in RGD compared to peptide-free matrices. However, the cell proliferation rate was found to be lower in the case of laminin-511 than in a matrix that did not contain peptides. In JHOC-5 cells, the cell proliferation rate in fibronectin and laminin-511 was found to be higher than in a matrix that did not contain peptides. Unlike RMG-I cells, JHOC-5 cells grown in laminin-511 exhibited a higher proliferation rate than those grown in fibronectin. Then, the cell proliferation rate was found to be higher in RGD compared to peptide-free matrices. Nevertheless, the cell proliferation rate was found to be lower in the laminin-511 than in the peptide-free matrix. Thus, RGD was selected as the matrix for 3D bioprinting for following experiments.

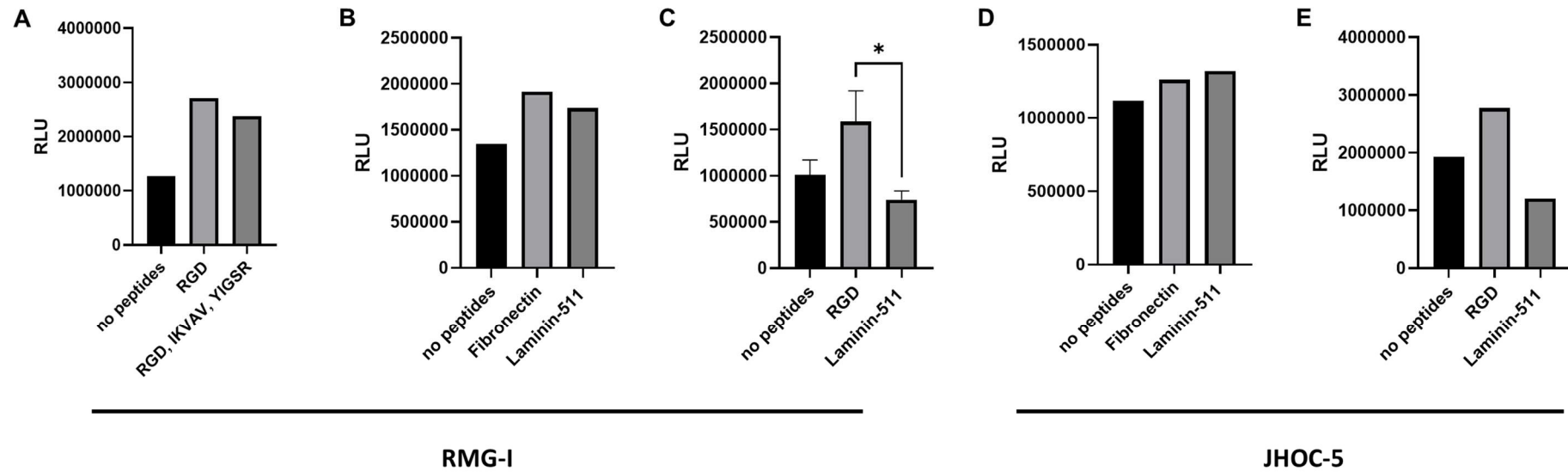


Figure 4.15 Bar chart of growth trends for matrix selection in 3D bioprinted OCCC cell lines RMG-I and JHOC-5. RMG-I (A, B, and C) and JHOC-5 (D and E) were bioprinted in a matrix set with 18,000 cells per well printed. After 7 days, CTG assays were performed to determine Relative Light Unit (RLU) in each condition. With the exception of data presented in panel C that was performed in triplicate, all other experiments were performed in singleton. A one-way ANOVA and Tukey's *post hoc* test was performed to determine statistical significance for experiments conducted in triplicate (\* $P < 0.05$ ). Error bars depict mean  $\pm$  SEM.

Given the matrix selection that preceded it, it was determined that RGD would be the matrix used for 3D bioprinting. Initial assessment of the 3D bioprinted cultures was conducted on days 1, 4, and 7 post cells seeding. As a result, it can be observed that almost all the OCCC cells, with the exception of OVMANA and TOV-21G, exhibited higher proliferation between days 4 to 7 inclusive after cell seeding. Furthermore, JHOC-5 and RMG-I demonstrated a notable increase in proliferation measured at day 7 after bioprinting compared to day 1. However, OV207 and OVTOKO demonstrated minimal differences in their growth patterns on days 1, 4, and 7 after bioprinting. Although the growth trend of OVMANA exhibited a decline on day 4 after bioprinting, its growth trend at day 7 remained higher than that on day one (Figure 4.16).

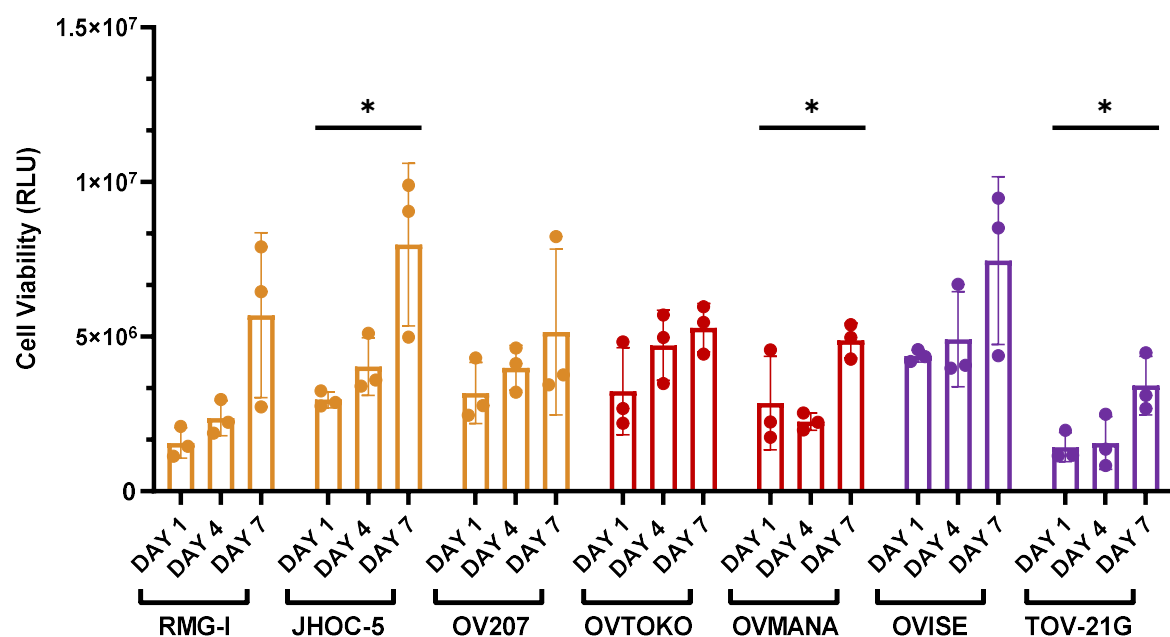


Figure 4.16 Bar chart of cell culture growth trends of seven 3D bioprinted OCCC models. OCCC cell lines were bioprinted in the RGD matrix with 18,000 cells per well, excluding OVMANA which was 16,000 cells per well, and CTG assays were performed to determine RLU on days 1, 4 and 7. There is a trend of increased cell viability measured on days 4 and 7 post bioprinting observed for each of the cell lines. A one-way ANOVA and Tukey's *post hoc* test was performed to determine statistical significance (\*P<0.05). Data is presented as the mean  $\pm$  SEM, N=3.

#### 4.3.6 Sensitivity of ovarian cancer cell lines cultured in 3D to ibrutinib

Seven OCCC cell lines were 3D bioprinted and treated with ten different concentrations of ibrutinib for 72 hours on the fourth day after printing to ensure that cells were in a growth phase (Table 4.2). The outcomes of this experiment were used to generate a dose curve for ibrutinib and to calculate the IC<sub>50</sub> of ibrutinib in OCCC cell lines cultured in 3D (Figure 4.17 and 4.18). The results indicated that TOV-21G (IC<sub>50</sub> of 10.14  $\mu$ M), JHOC-5 (IC<sub>50</sub> of 13.92  $\mu$ M), and OVTOKO (IC<sub>50</sub> of 15.46  $\mu$ M) exhibited greater sensitivity to ibrutinib in 3D culture compared to the other cell lines bioprinted. In contrast, OVMANA (IC<sub>50</sub> of 23.06  $\mu$ M), OV207 (IC<sub>50</sub> of 23.63  $\mu$ M), and RMG-I (IC<sub>50</sub> of 23.59  $\mu$ M) were found to be more resistant to ibrutinib. OWISE (IC<sub>50</sub> of 28.16  $\mu$ M) was the least sensitive to ibrutinib among all OCCC cell lines (Table 4.7 and Figure 4.19).

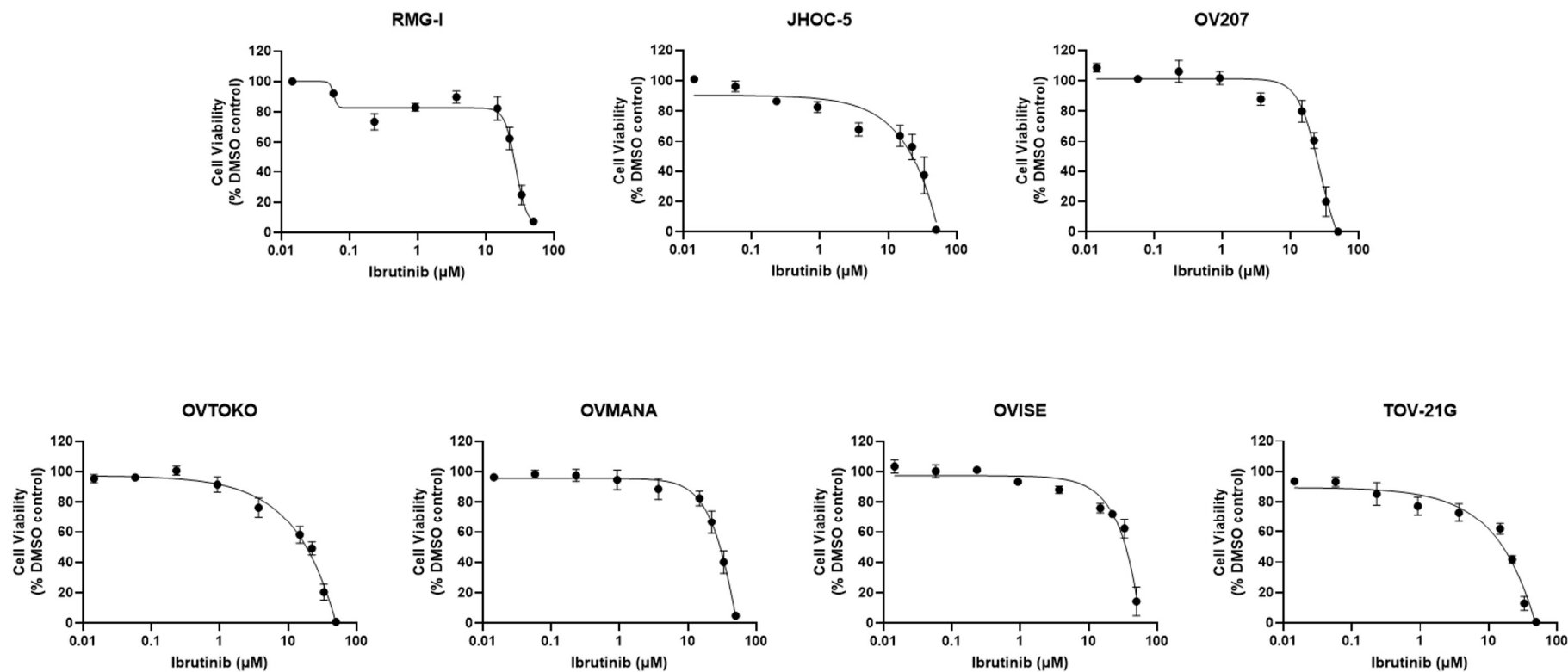


Figure 4.17 Ibrutinib dose curves of 7 bioprinted OCCC cell lines. Cell lines were with 10 concentrations of ibrutinib (Table 4.2) for 72h, and a CTG assay performed to determine how many live cells remained (% viable cells). These experiments were repeated at least 3 times before dose curves were generated. Data is shown as the mean  $\pm$  SEM.

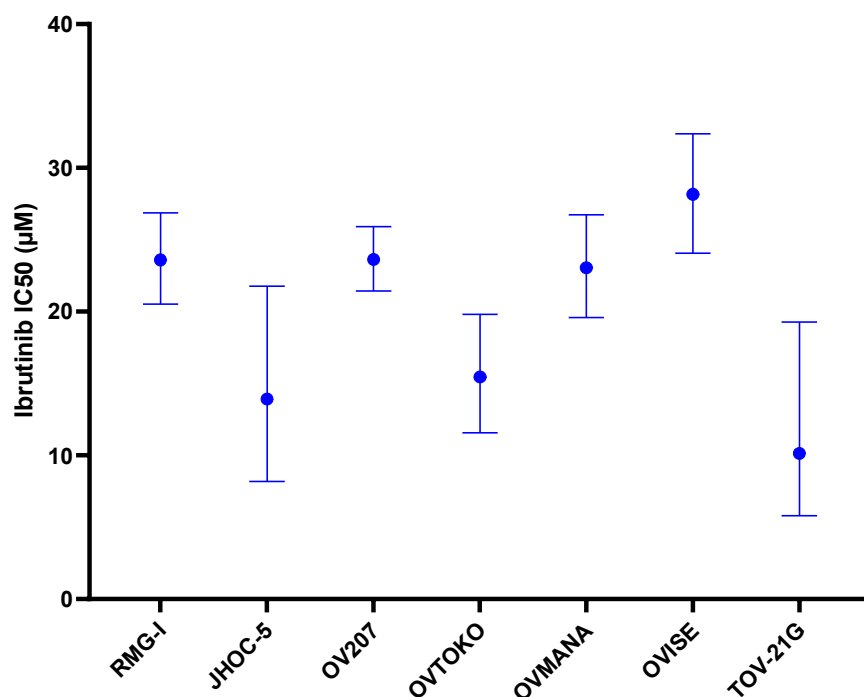


Figure 4.18 IC<sub>50</sub> of ibrutinib in 7 bioprinted OCCC cell lines. Cells were treated with 10 concentrations of ibrutinib (Table 4.2) for 72h, and a CTG assay performed to determine how many live cells remained (% viable cells). These experiments were repeated at least 3 times to generate dose curves and IC<sub>50</sub> was calculated from the dose curve. 95% CIs are shown. IC<sub>50</sub> calculations were performed using GraphPad.

Table 4.7 IC<sub>50</sub> comparisons (cell viability: CTG) for Ibrutinib in 10 ovarian cancer cell lines grown in 3D

Cell line	IC <sub>50</sub> (µM)	95% CI (µM)
RMG-I	23.59	20.53 - 26.86
JHOC-5	13.92	8.185 - 21.78
OV207	23.63	21.43 - 25.91
OVTOKO	15.46	11.58 - 19.81
OVMANA	23.06	19.57 - 26.72
OVISe	28.16	24.06 - 32.37
TOV-21G	10.14	5.800 - 19.26

OCCC: Ovarian clear cell carcinoma; EnOC: Endometrioid ovarian carcinoma; SCCOHT: Small cell carcinoma of the ovary, hypercalcemic type; HGSOC: High-grade serous ovarian cancer.

OVISE > OV207 > RMG1 > OVMANA > OVTOKO > JHOC5 > TOV21G



Figure 4.19 Comparison of IC<sub>50</sub> of ibrutinib in seven OCCC cells in 3D. Seven OCCC cells were ranked in order of increasing IC<sub>50</sub> for ibrutinib. The order from left to right indicates IC<sub>50</sub> from highest to lowest. Green: *ARID1A* and *ARID1B* WT. Blue: Only *ARID1A* mutation. Orange: Both *ARID1A* and *ARID1B* mutations.

Upon comparing the IC<sub>50</sub> of ibrutinib in 2D and 3D, there was little difference between IC<sub>50</sub>s in 2D and 3D in the TOV-21G, OVISE, and OV207 cell lines. The ibrutinib IC<sub>50</sub> concentrations in bioprinted JHOC-5 and OVTOKO cells were more than 5-fold higher than those cultured in 2D. The biggest differences were observed between OVMANA and RMG-I, with the IC<sub>50</sub> of ibrutinib in bioprinted cells being approximately 20 times higher than that in 2D (Figure 4.20).

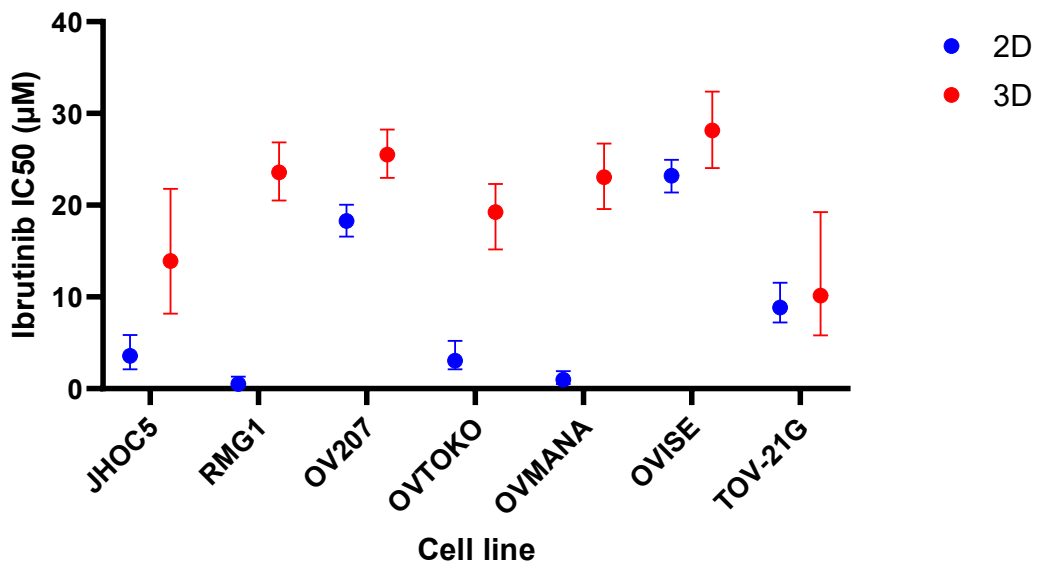


Figure 4.20 Summary of IC<sub>50</sub> of ibrutinib in 7 OCCC cell lines in 2D and 3D bioprinted models. Blue indicates data from cell lines cultured in 2D and red indicates data from bioprinted cells. 95% CI are shown.



The viability of 3D bioprinted RMG-I and JHOC-5 cells treated with ten different concentrations of ibrutinib was also assessed using the LIVE/DEAD viability assay. The results demonstrated that at the highest concentration of ibrutinib, most of the cells stained red, indicating that these cells were dead. However, there was a paucity of red colour at the second highest concentration. Nevertheless, at the highest concentration of ibrutinib, there were fewer live cells (green), while the rest of the concentrations exhibited lots of green cells (Figure 4.21). The data indicates that in both cell lines, the majority of cells died at the highest concentration, while a minority survived. At the second highest concentration, a similar pattern was observed, with some cells dying but the majority surviving. In the subsequent concentrations, the majority of cells survived.

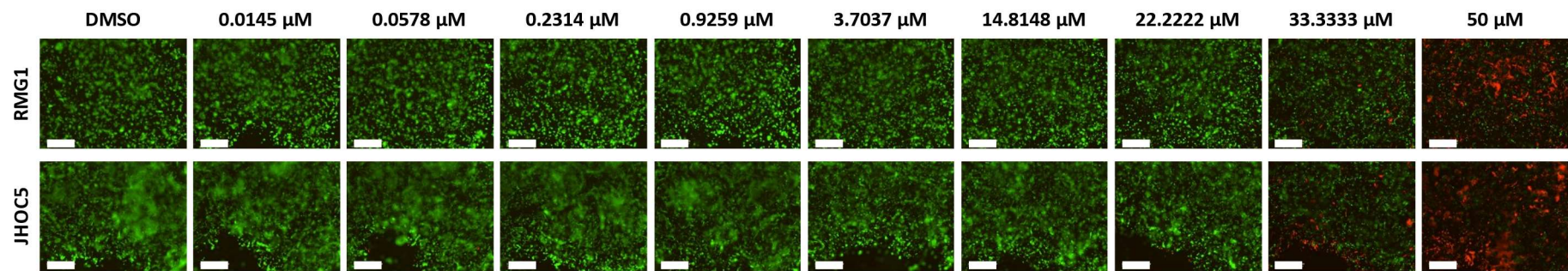


Figure 4.21 Images of RMG-I and JHOC-5 3D bioprinted cell lines treated with ibrutinib or DMSO control and stained using the LIVE/DEAD viability assay. Cells were treated with 10 different concentrations of ibrutinib indicated in the figure. Images were acquired with the IncuCyte S3 analysis software with 4X objective. Scale bar = 800  $\mu$ M.

## 4.4 Discussion

This chapter reports use of an epigenetic drug screening library comprising 160 compounds to screen against ten ovarian cancer cell lines. The most effective compound against OCCC was selected and employed to target different cell culture models, including an investigation into drug sensitivity under 2D and 3D cell culture conditions. Ten ovarian cancer cells (seven OCCC cell lines (JHOC-5, RMG-I, OVTOKO, OVMANA, OVISe, OV207 and TOV-21G) and three non-OCCC cell lines (A2780.b1, COV434, and OVCAR-8) were treated with 160 epigenetic drugs. Our findings indicate that at 5  $\mu$ M, only 16.875% (range, 13.125%-20.625%) of the drugs were able to reduce the cell viability of OCCC to below 50%, while nearly 26.25% (range, 21.25%-30%) of the drugs could reduce the cell viability of non-OCCC to below 50%. At 0.5  $\mu$ M, this number was 4.375% (range, 5%-3.125%) in OCCC, and 8.54% (range, 7.5%-9.375%) in non-OCCC. Conversely, at 5  $\mu$ M, 27.41% (range, 18.125%-35.625%) of the drugs demonstrated a growth promoting effect on OCCC, whereas this number was 20.21% (range, 15%-26.25%) for non-OCCC. At 0.5  $\mu$ M, this number was 37.14% (range, 25%-48.125%) in OCCC, and 29.375% (range, 27.5%-32.5%) in non-OCCC. These findings indicate that, in general, the OCCC cell line models screened were more resistant to the drug compounds compared with the non-OCCC cell lines.

It is generally accepted that OCCC is more chemoresistant than HGSOc<sup>257,448</sup>, which leads to a poorer prognosis. The mechanism of chemoresistance in OCCC is complex, and as a result, some studies have suggested that resistance in OCCC may be related to factors such as low proliferation rate of the tumours, increased damage to DNA repair activity, and up-regulation of growth factor signalling pathways<sup>449</sup>. A study by Hiroaki and colleagues, comprising 41 patients with OCCC and 90 patients with SOC between 1988 and 1997, demonstrated a markedly low response rate to chemotherapy in patients with OCCC, at only 14.6%. Conversely, the response rate to chemotherapy in SOC patients was 72.2%. Upon examination of the proliferative activity of the tumours, it was found that OCCC exhibited lower proliferative activity than SOC. Consequently, the researchers concluded that rapidly proliferating cells are the most sensitive to cytotoxic agents, while slowly proliferating cells are usually less sensitive to cytotoxic agents<sup>449</sup>. Another study demonstrated that in a comparison of 11 OCCC cell lines and 5 SOC lines, the IC<sub>50</sub> for cisplatin in OCCC cells ranged from 1.3 to 18.0  $\mu$ M, whereas in SOC cells it ranged from 2.2 to 13.0  $\mu$ M. In contrast, the doubling time for OCCC cells was approximately 61.4 hours (the doubling time for our

OCCC cells was 54.3 hours, with the exception of OV207), which was significantly longer than the 29.8 hours for SOC <sup>450</sup>. These findings thus indicate that drug resistance of OCCC may be associated with a lower rate of OCCC cell proliferation.

Protein kinases are enzymes that catalyse the phosphorylation of proteins, a process that modifies their activity or ability to interact with other proteins. This phosphorylation event can have profound effects on cellular processes such as growth, differentiation, survival, and proliferation. Additionally, protein kinases are integral components of signal transduction cascades, transmitting signals from the cell membrane to the cytoplasm and nucleus. Dysregulation of protein kinase activity has been implicated in the pathogenesis of a variety of diseases, including cardiovascular diseases, neurological disorders, autoimmune diseases, and various cancers <sup>451-453</sup>.

Bruton tyrosine kinase (BTK) is a kinase that plays a key role in several cell signalling pathways, particularly in the immune system. BTK is classified as a non-receptor tyrosine kinase (NRTK) and is a member of the Tec kinase family (TFK). The molecular structure of BTK consists of five distinct structural domains, which are an amino terminal pleckstrin homology (PH) domain, a proline-rich TEC homology domain (TH), the SRC homology domain 2 (SH2), the SRC homology domain 3 (SH3) and the tyrosine kinase structural domain (Figure 4.22) <sup>454-456</sup>. These structural components enable BTK to participate in complex protein-protein interactions and signalling cascades within the cell.

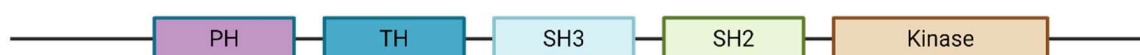


Figure 4.22 Schematic overview of the structure of Bruton's tyrosine kinase (BTK). BTK consists of five distinct structural domains: pleckstrin homology (PH) domain, Tec homology (TH), SRC homology (SH) 2 and 3 domains, and the tyrosine kinase structural domain.

One of the major functions of BTK is to participate in B cell receptor (BCR) signalling <sup>457</sup>. BTK is essential for the transduction of BCR signals, which are critical for B cell activation, proliferation, and differentiation <sup>458</sup>. In addition, BTK has been shown to play a role in other receptor-triggered signalling pathways, such as the Toll-like receptor (TLR) in B cells or the

Fc- $\gamma$  receptor (FC $\gamma$ R) in macrophages<sup>455,459,460</sup>. In addition, BTK is involved in the synthesis of pro-inflammatory cytokines such as tumour necrosis factor  $\alpha$  (TNF $\alpha$ ) and interleukin 1 $\beta$  (IL-1 $\beta$ ), as well as degranulation and histamine release<sup>461-463</sup>. Several studies have shown that BTK is responsible for regulating nucleotide-binding domain, leucine-rich-containing family, pyrin domain-containing-3 (NLRP3) vesicles by altering subcellular localisation and inflammatory vesicle assembly. This is a cytoplasmic multi-protein signalling complex that activates inflammatory factors such as interleukin-1 (IL-1) or interleukin-18 (IL-18) to trigger an inflammatory response. Therefore, inhibition of BTK may inhibit the activation of inflammatory vesicles, thereby reducing the secretion of inflammatory factors to protect cells<sup>461,464,465</sup>.

BTK is a potential target for the treatment of leukaemia and lymphoma because it plays a key role in B cell survival and proliferation and is overexpressed in several B cell malignancies<sup>466</sup>. In addition, BTK has long been thought to be expressed exclusively in haematopoietic cells and is critical for B cell maturation and proliferation as well as monocyte/macrophage activation<sup>467</sup>. Interestingly, isoforms of BTK are expressed in tissues and malignancies unrelated to B cells (Figure 4.23). BTK-A is the most extensively researched variant and is involved in the function, maturation and trafficking of myeloid cells. It plays a pivotal role in the regulation of myeloid cell signalling. BTK-A is highly expressed, primarily in cells of the haematopoietic lineage, including myeloid cells, lymphocytes, mature B-lymphocytes, mast cells, monocytes and macrophages<sup>468-470</sup>. Zucha and colleagues found that the BTK protein was present in ovarian cancer cells and was 77 kDa in size, which consistent with BTK-A, so this isoform is expected to occur in OCCC cells. BTK-C is found in breast and prostate cancer cells<sup>453</sup>. This isoform has a 34 amino acid stretch and is the predominant form in breast tumour cells. Also, it has been demonstrated that BTK-C is a survival factor in prostate cancer cells<sup>471,472</sup>. p65BTK, an isoform of BTK, is overexpressed in colon, lung, and ovarian cancers. Grassilli and colleagues found that p65BTK levels correlated with early recurrence and shorter progression-free survival in ovarian cancer patients, both of which are indicators of resistance to therapy<sup>473</sup>. Lavitrano and colleagues found that p65BTK expression correlated with histotype and cancer progression by analysing three different groups of patients. They used drug-resistant *TP53*-null colon cancer cells as a model, and showed that colon cancer cells were less resistant to 5-FU when p65BTK was inhibited<sup>474</sup>. Giordano and colleagues used a p65BTK inhibitor, ibrutinib, on lung cancer cells and showed that inhibition of p65BTK affected the proliferation and clonogenicity of the cell line<sup>475</sup>. BTK-D is a splice variant isoform of BTK

that lacks the kinase structural domain, has 483 amino acids, and has a total molecular weight of 52 kDa. This isoform can act as a dominant-negative BTK because it inhibits BTK-dependent differentiation and pre-B-cell receptor responses in leukaemia cells <sup>476</sup>. These studies suggest that BTK may be a potential target for the treatment of solid tumours.

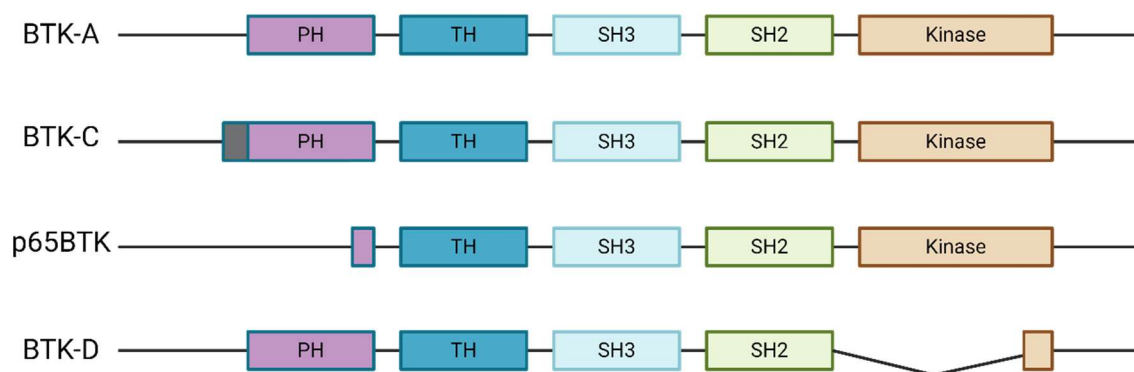


Figure 4.23 Structures of BTK isoforms. BTK-C has a 34-amino acid extension of PH domain. p65BTK has a partial PH domain. BTK-D has a partially deleted kinase domain.

The results of our drug screening experiments and the treatment of ten ovarian cancer cell lines with ibrutinib demonstrated that ibrutinib inhibited cell viability of the majority of ovarian cancer cells. Furthermore, ibrutinib demonstrated a more pronounced inhibitory effect on OCCC compared to non-OCCC cell lines. However, the results of our ibrutinib sensitivity experiments indicated that the response of OCCC cells to ibrutinib was inconsistent in both 2D and 3D environments. We propose that this inconsistency may be attributed to the differences in the 2D and 3D structures. Ibrutinib is an oral irreversible BTK inhibitor that covalently binds to the cysteine at position 481 of the kinase structural domain (Cys-481), thereby blocking kinase activity <sup>477</sup>. It effectively disrupts BCR signalling and downregulates NF- $\kappa$ B signalling, leading to a reduction in tumour growth and an increase in apoptosis <sup>478</sup>. Ibrutinib was approved by the FDA in 2013 for clinical use in the treatment of haematological malignancies <sup>479</sup>. Its efficacy has been shown in a variety of diseases, including chronic lymphocytic leukaemia (CLL), Wahl's macroglobulinemia, and mantle cell lymphoma <sup>480</sup>. A 2013 study showed that ibrutinib was well tolerated and extended progression free survival in patients with B-cell non-Hodgkin lymphoma (NHL) or CLL. Also, no significant myelosuppression, or renal or hepatic toxicity was observed, suggesting a good clinical safety profile <sup>481</sup>. Byrd and colleagues conducted a study to evaluate the safety, efficacy, pharmacokinetics, and pharmacodynamics of ibrutinib in 85 patients with relapsed or refractory CLL or small lymphoblastic lymphoma,

which showed that in the early stages of disease, ibrutinib can increase lymphocyte levels and reduce lymph node and spleen size. However, after long-term use, lymphocyte counts returned to normal or below baseline, and patients experienced an overall response rate of 71% <sup>482</sup>. Ibrutinib also inhibits the activation of EGFR, human epidermal growth factor receptor 2 (HER2), Erb-B2 receptor tyrosine kinase 3 (ErbB3) and Erb-B2 receptor tyrosine kinase 4 (ErbB4), which inhibits breast cancer cell growth and leads to apoptosis <sup>483,484</sup>. Its ability to disrupt key signalling pathways and inhibit tumour growth makes ibrutinib an attractive drug to consider as a potential treatment for cancer. Additionally, ibrutinib has been, or is being, investigated in clinical trials to treat other solid tumours, including Epidermal Growth Factor Receptor (EGFR) mutant non-small cell lung cancer, c-MYC and HER2 amplified oesophagogastric carcinoma, advanced carcinoid and pancreatic neuroendocrine tumors, metastatic kidney cancer and others (Table 4.8) <sup>485-488</sup>.

Table 4.8 Clinical trials of ibrutinib in solid tumours

Identifier	Disease	Status
NCT02950038	Non-small cell lung cancer (NSCLC)	Withdrawn
NCT02643667	Prostate cancer	Completed
NCT03332498	Colorectal cancers	Completed
NCT03379428	Breast cancer	Active
NCT02884453	Amplified oesophagogastric carcinoma	Unknow status
NCT02899078	Metastatic kidney cancer	Completed
NCT03646461	head and neck squamous cell carcinoma	Active
NCT02562898	Pancreatic cancer	Completed
NCT02321540	Epidermal Growth Factor Receptor (EGFR) mutant non-small cell lung cancer	Completed
NCT02436668	Metastatic pancreatic adenocarcinoma	Completed

It is noteworthy that two cases have been identified in the literature where ibrutinib was employed for the treatment of LGSOC. The first case involved a 52-year-old patient who had undergone two surgeries following the diagnosis of ovarian cancer, in addition to ineffective chemotherapy <sup>489</sup>. Following the second surgical resection, drug sensitivity testing was conducted on a tumoroid of the removed cancer. The results demonstrated that ibrutinib

exhibited promising activity among 42 small molecule drugs. Following treatment with ibrutinib, the patient's CA-125 levels decreased, and stable disease was observed over a period exceeding 65 weeks. Another patient was a 61-year-old female with chronic lymphocytic leukaemia <sup>490</sup>. Following examination, the patient was diagnosed with LGSOC, FIGO stage IIIb. The patient was treated with ibrutinib following the recurrence of ovarian cancer, exhibiting a continuous decrease in CA-125 levels, which returned to normal after 12 months of treatment. Furthermore, the patient did not exhibit any symptoms indicative of recurrent ovarian cancer during the period of continued treatment. These two cases indicate that ibrutinib can be employed as a treatment for ovarian cancer, albeit a distinct histotype to OCCC.

Upon examination of the mRNA levels of BTK in OCCC cells, it was observed that the mRNA content in OV207 cells was almost negligible. This was accompanied by proliferation when OV207 cells were treated with 5  $\mu$ M and 0.5  $\mu$ M ibrutinib. Also, under 2D conditions, the cell viability of RMG-I cells first declined to between 50% and 60% as the concentration of ibrutinib increased. Then as the concentration increased, the cell viability rebounded and declined after rebounding to a certain point and eventually reached the lowest value. This also occurred in 3D conditions, but the decrease was not significant, with cell activity only reaching 80%. We postulate that this may be due to the off-target activity of ibrutinib and non-specific interactions with other kinases, given the low BTK content <sup>491</sup>. Consequently, ibrutinib facilitated the proliferation of this cell line, which leads to the growth of cell number.

It was interesting to note that OVISE cells exhibited greater resistance to ibrutinib when cultured in both 2D and 3D conditions compared with other OCCC cell lines. Additionally, the mRNA level of *BTK* was found to be comparatively more highly expressed in OVISE cells. Consequently, we thought that the elevated expression of *BTK* might be associated with OCCC resistance. In a study comprising 50 patients with ovarian cancer, Zucha and colleagues observed elevated *BTK* expression in malignant cells <sup>492</sup>. Then, immunohistochemical staining revealed that BTK levels were higher in metastatic and advanced disease. From the same study, the subsequent experiments demonstrated that elevated expression of cancer stem cell (CSC) markers was associated with cellular resistance to platinum-based drugs. Additionally, *BTK* overexpression was observed by these authors to promote ovarian cancer cells survival and cisplatin resistance, suggesting that *BTK* signalling is crucial for regulating ovarian CSC. Finally, the combination of cisplatin and ibrutinib was found to enhance the efficacy of cisplatin *in vitro* in ovarian cancer cell line models. It is noteworthy that Lohse and colleagues tested six patient-derived ovarian cancer cell lines with 30 different drugs and demonstrated



that ibrutinib exhibited only weak inhibition in papillary-serous cell lines (P5X and P9A1) and EnOC cell lines (E1P and E3X), with no effect observed in OCCC cell lines<sup>493</sup>. Notably, none of the cell lines used in their study overlapped with those in my research. The potential benefits of ibrutinib as a treatment for OCCC should be further investigated.

These results demonstrated that the *ARID1A* WT cell lines (RMG-I and JHOC-5) exhibited slightly higher sensitivity to drugs in the drug library compared to *ARID1A* mutated cell lines (OV207, OVTOKO, OVMANA, OWISE and TOV-21G). This suggests that the *ARID1A* mutation may contribute to elevated drug resistance in OCCC cell lines. In a study of 60 OCCC samples, the *ARID1A* deletion was identified in 9 cases (15%)<sup>494</sup>. However, none of the 15 HGSOC samples had *ARID1A* loss. Further studies demonstrated that patients with loss of ARID1A expression exhibited higher levels of chemoresistance in OCCC and had shorter overall survival times compared to patients with positive ARID1A expression<sup>494</sup>. Another study by Yokoyama and colleagues demonstrated that in patients with advanced (stage III and IV) ovarian cancer, from immunohistochemistry (IHC) results, ARID1A expression levels were significantly lower in patients who did not achieve a complete clinical remission (CR) compared with those who did<sup>399</sup>. Their study also demonstrated that patients who experienced a relapse following a complete CR exhibited relatively low expression levels of ARID1A compared to those who did not relapse. Moreover, at advanced stages of cancer, there was a significant difference in progression-free survival between ARID1A-positive and ARID1A-negative patients. Therefore, they concluded that reduced ARID1A expression is associated with chemotherapy resistance<sup>399</sup>.

The treatment of ten ovarian cancer cells with 5  $\mu$ M and 0.5  $\mu$ M ibrutinib demonstrated that both OV207 and OVCAR8 exhibited enhanced proliferation. Notably, both OV207 (p.Arg273His (c.818 G > A)) and OVCAR8 (c.376-1 G>A) have a *TP53* mutation, suggesting that *TP53* mutations may increase resistance to ibrutinib. Cell lines with mutations in *TP53* are typically more resistant to chemotherapies than WT *TP53* cell lines<sup>495</sup>. Furthermore, restoration of WT p53 in mutant *TP53* cell lines has been shown to restore sensitivity to chemotherapy<sup>496</sup>. Interestingly, some studies have demonstrated that ibrutinib can be therapeutically effective in treating aggressive CLL with *TP53* mutations<sup>497,498</sup>. It is possible that the response to ibrutinib will be different in haematological malignancies versus solid tumours. Since we have only shown increased proliferation in OV207 and OVCAR-8 cells, we would need to use additional cell lines, and/or investigate *TP53* isogenic cell line panels, to

verify whether *TP53* mutations affect the sensitivity of OCCC cells to ibrutinib, or indeed in *TP53* mutant ovarian cancer in general, regardless of histotype.

Compared to 2D cell culture systems, 3D bioprinted systems can more accurately reflect the microenvironment of the tumour where the cells are located <sup>499</sup>. Our results demonstrate that OCCC cells can proliferate in 3D when bioprinted with biofunctionalised hydrogels. All ovarian cancer cell lines exhibited reduced sensitivity to ibrutinib in 3D compared to 2D. For instance, in OVMANA cells, the IC<sub>50</sub> of ibrutinib in 3D is more than 20 times higher than that in 2D. Some studies have indicated that cells exhibit greater resistance to anti-cancer drugs when cultured in 3D. Loessner and colleagues treated 2D monolayers and 3D spheroids with paclitaxel. Their findings indicated that cell survival was higher in 3D spheroids (40-60%) compared to 2D monolayers (20%) <sup>500</sup>. Another study demonstrated that four anticancer drugs with distinct mechanisms of action (melphalan, fluorouracil (5-FU), oxaliplatin, and irinotecan) and two promising investigational cancer drugs (acriflavine and VLX50) exhibited high activity in 2D monolayer cultures but showed progressively diminished efficacy in 3D spheroids <sup>501</sup>. This study suggests that genetic and phenotypic changes induced by the formation of 3D spheroids are associated with increased drug resistance. There are a number of reasons for the observed differences. One study found that endometrial cell proliferation in the spheroids remained unchanged when the spheroids were treated with drugs <sup>502</sup>. They proposed that drug-treated spheroids may have altered cell-cell interactions at the edges, thereby increasing nutrient penetration into the inner regions of the spheroids. This, in turn, initiated cell proliferation in quiescent cells, leading to the development of drug resistance <sup>502</sup>. Swietach and colleagues demonstrated that lower pH decreased drug uptake, which resulted in the development of resistance in the colon cancer cells <sup>503</sup>. Luca and colleagues demonstrated that the structural and spatial arrangement of the colorectal cancer cells differed in 2D and 3D cultures. This, in turn, caused differences in the binding efficiency of the receptors on the cell surface. Nevertheless, numerous compound agents bind to specific receptors on the cell surface, which can also result in augmented cellular resistance <sup>504</sup>.

It should be noted that this study is not without limitations. Firstly, the sample size of non-OCCC cell lines was low. Also, many matrix selection experiments for optimisation could only be performed once because of the high cost of using the RASTRUM bioprinter (more than \$400 per 96-well plate). Thirdly, the compound library utilised for drug screening encompassed 160 drug compounds that is a relatively small number compared with commercial screens of thousands of compounds. Due to logistical constraints, only two concentrations of each

compound were employed to treat the cells for the discovery arm of this work, however, it should be noted that screening using this library has previously been performed in this manner<sup>436</sup>. The utilisation of compound libraries containing a greater number of drugs could be employed in future experiments, thereby facilitating the identification of additional promising compounds for the treatment of OCCC.

## **4.5 Conclusion**

In this chapter, 7 OCCC and 3 non-OCCC were screened with an epigenetic drug screening library, and Drug 152 (Ibrutinib) showed a greater efficacy in OCCC cell lines. Two studies have demonstrated that ibrutinib has been used to treat LGSOC, with encouraging outcomes<sup>489,490</sup>. This study has the potential to pave the way for future clinical trials of ibrutinib for patients with OCCC.

# CHAPTER 5. KO of ARID1A and ARID1B with CRISPR- Cas9 gene editing

The absence of *ARID1A* or *ARID1B* in cells is of significance due to their role as DNA binding subunits of the SWI/SNF chromatin remodelling complex. This chapter describes the creation of ARID1A and ARID1B null cells in ARID WT cells using CRISPR-Cas9 gene editing and examines the characterisation of these cells, including gene and protein expression profiles and an assessment of sensitivity to cisplatin.

## 5.1 Introduction

CRISPR-Cas9 (described in Section 1.5) is a gene editing tool used widely in various scientific research fields. Prior to the advent of CRISPR-based KOs, depletion of specific RNA was commonly performed using small interfering RNAs (siRNA) and microRNAs (miRNA) <sup>505</sup>. SiRNAs are known for their specificity in targeting individual mRNAs to induce gene silencing, whereas miRNAs have the capability to regulate the expression of multiple mRNAs concurrently. Both siRNAs and miRNAs are integral components of the RNA interference (RNAi) pathway <sup>506</sup>. RNAi depletes gene expression, achieving protein knockdown but not complete KO of protein expression <sup>507,508</sup>. CRISPR, however, has the capacity to completely and permanently silence genes (knockout) by editing DNA (insertions and deletions) to create premature truncation of proteins <sup>509</sup>. Consequently, CRISPR can prevent the expression of WT proteins, thus eliminating any confounding effects of residual protein expression following knockdown by RNAi methodologies. Furthermore, RNAi silencing methods have been observed to have a high off-target effect. Smith and colleagues have demonstrated that off-target effects of CRISPR were considerably lower than those of RNAi, which has led to the replacement of RNAi in the many research applications <sup>510</sup>. In this project, CRISPR technology was employed as a tool to KO ARID1A and/or ARID1B genes in ARID1A/B WT OCCC cells. The workflow for generating CRISPR KO cell lines is outlined in Figure 5.1.

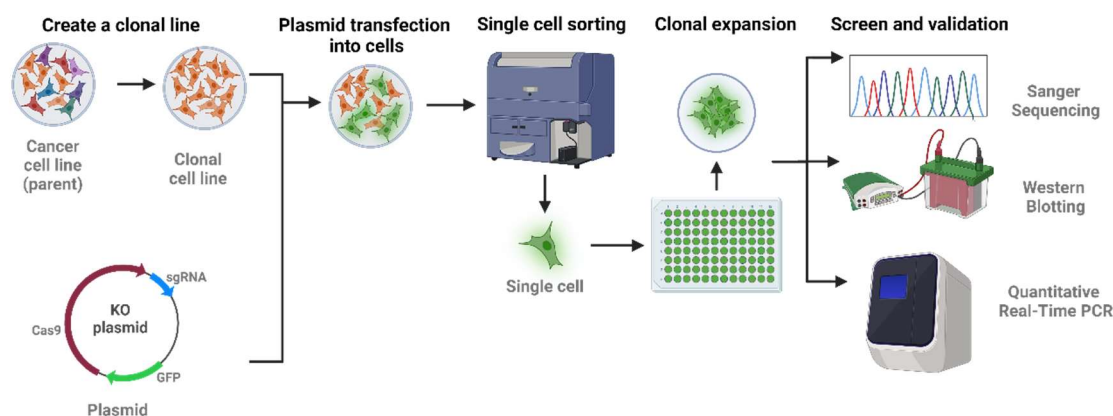


Figure 5.1 Workflow for generating CRISPR KO cancer cell lines. A clonal cell line was produced from a parental cell line. A CRISPR KO plasmid containing a target sgRNA (single-guide RNA) was transfected into the clonal line. After transfection, single cell sorting was performed to sort single GFP positive cells into a 96-well plate. The potential KO clones were expanded, screened, and validated by Sanger sequencing, Western blot, and Quantitative Real-Time PCR.

The absence of ARID1A or ARID1B in cells is of significance due to their role in the SWI/SNF chromatin remodelling complex. The Cancer Dependency Map Project at Broad Institute (DepMap; <https://depmap.org/portal/interactive/>) was employed to investigate the effects of ARID1A or ARID1B KO in cells, with a particular focus on OCCC (Figure 5.2). The data indicated that the majority of ovarian cancer cells exhibited sensitivity to ARID1A KO. In OCCC, RMG-I was the most sensitive to KO of ARID1A, while OVMANA and OVTOKO that have multiple *ARID1A* mutations were not sensitive to KO of ARID1A. A similar pattern was observed with *ARID1B*, with the majority of ovarian cancer cells demonstrating sensitivity to KO of ARID1B. Also, almost all OCCC were sensitive to KO of ARID1B, except for OVTOKO.

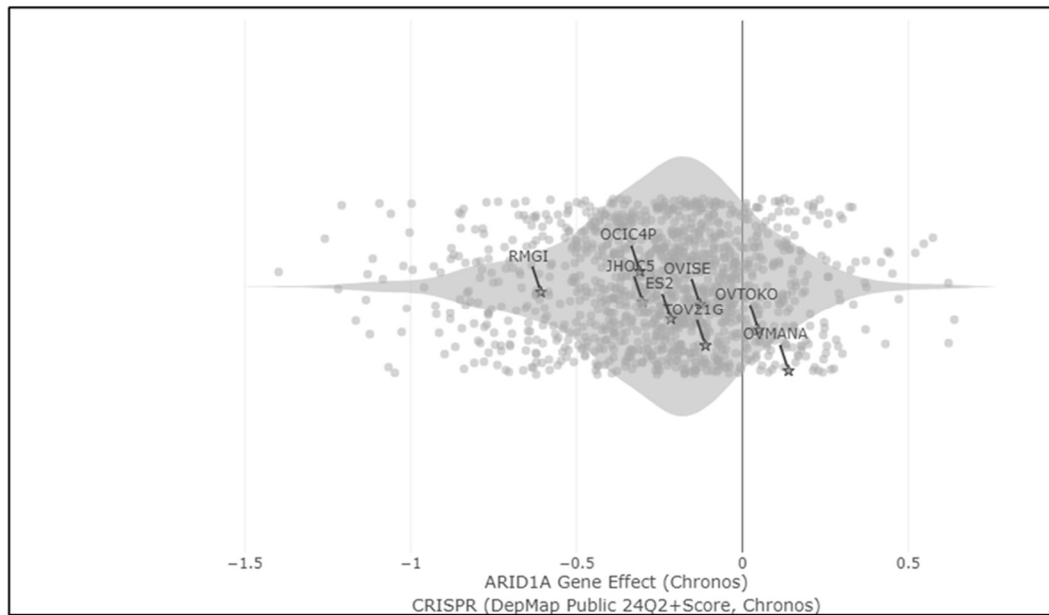
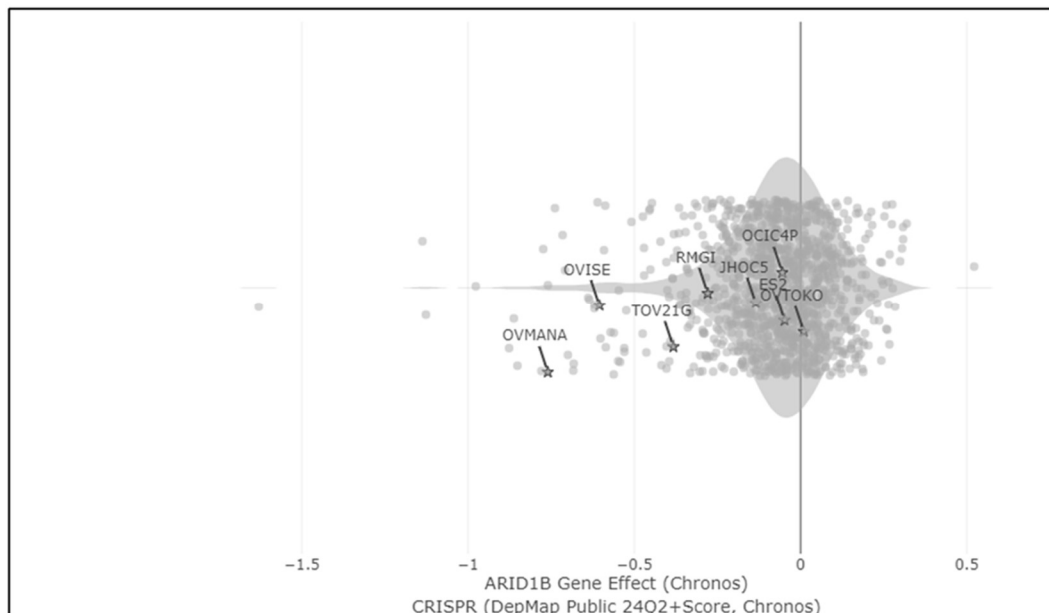
**A****B**

Figure 5.2 Effect of ARID1A and ARID1B KO on cell lines. The effect of A) *ARID1A* and B) *ARID1B* gene KO on various cell lines using the chronos score from DepMap Data Explorer (<https://depmap.org/portal/interactive/>), with the x-axis representing the gene effect. Negative values indicate a greater dependency on ARID1A/ARID1B for cell survival with significant sensitivity to ARID1A or ARID1B KO. Gray indicated all cancer cell lines and the highlighted cell lines are OCCC. To create this plot, first select "Gene" as the X-axis in DepMap Data Explorer. Subsequently, select either "ARID1A" or "ARID1B" in the next drop-down box, "CRISPR" in the dataset box, finally, "Clear cell" in the Find cell lines box.

In this chapter, we report on assembling the guide RNA into the PX458 vector (also known as pSpCas9(BB)-2A-GFP). The PX458 vector was first described in 2013 by the Zhang lab <sup>349</sup>. Furthermore, it is employed in a multitude of CRISPR gene editing applications. The PX458 plasmid contains the Cas9 nuclease gene and GFP (green fluorescent protein) reporter gene driven by a CMV (cytomegalovirus) promoter and an sgRNA scaffold driven by a U6 promoter to allow cloning and expression of specific sgRNA expression (Figure 5.3). Upon transfection of the plasmid into cells, the Cas9 endonuclease acts as a form of “molecular scissors” to produce DSBs at specific DNA sequences, which are then repaired by the cell's natural repair mechanisms (non-homologous end joining (NHEJ)), resulting in genetic modification. Once the cells have been successfully transfected with this vector, they fluoresce green, which allows for the identification and screening of the edited cells.

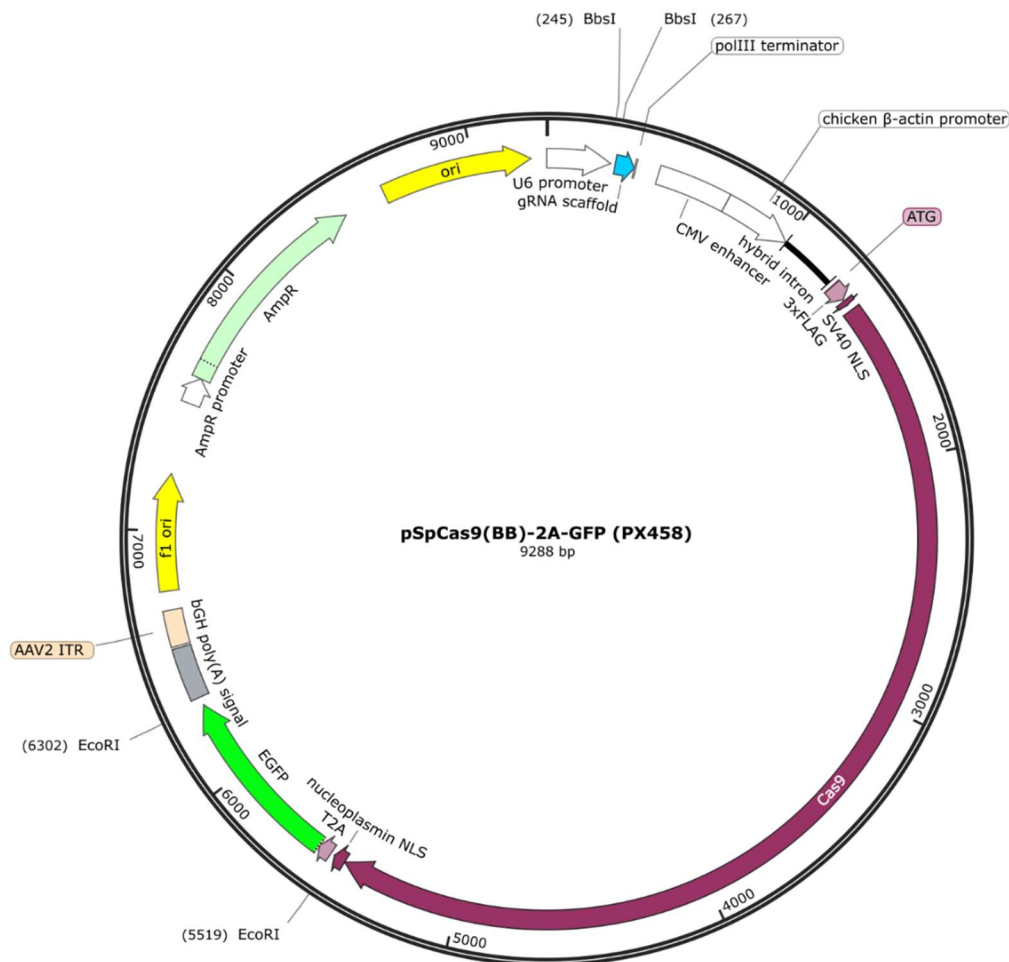


Figure 5.3 PX458 vector map. PX458 vector contains the Cas9 nuclease gene, a sgRNA scaffold, a GFP reporter gene for visualisation, a CMV promoter to drive Cas9 and GFP expression and a U6 promoter for sgRNA expression. BbsI (BpiI) sites in the sgRNA scaffold allow cloning of a sgRNA into the vector. Image created with SnapGene



([www.snapgene.com/resources](http://www.snapgene.com/resources)). Cas9: CRISPR-associated protein 9; EGFP: Enhanced green fluorescent protein; sgRNA: single guide RNA; ori: Origin of replication; AmpR: Ampicillin resistance gene; U6 promoter: U6 small nuclear RNA promoter; CMV enhancer: Cytomegalovirus enhancer; SV40 : Simian Virus 40; 3xFLAG: Three copies of the FLAG epitope tag; NLS: Nuclear localization signal; 2A: 2A self-cleaving peptide; bGH poly(A) signal: Bovine growth hormone polyadenylation signal; AAV2 ITR: Adeno-associated virus 2 inverted terminal repeat; polIII terminator: RNA polymerase III terminator; BbsI: Type IIS restriction enzyme site; EcoRI: Restriction enzyme site EcoRI.

ARID1A depletion has been shown to result in either up- or down-regulation of certain genes at the transcript level, including Cyclin-dependent kinase inhibitor 1A (*CDKN1A*), Dual Specificity Phosphatase 4 (*DUSP4*), Aldehyde Dehydrogenase 1 Family Member A1 (*ALDH1A1*), Mothers Against Decapentaplegic Homolog 3 (*SMAD3*), and STAG1 Cohesin Complex Component (*STAG1*). Guan and colleagues have demonstrated that ARID1A KO resulted in the downregulation of *CDKN1A* and *SMAD3* expression in ovarian surface epithelial cells <sup>331</sup>. Yoshino and colleagues have shown that *ALDH1A1* was the most significantly elevated gene in ARID1A KO human cholangiocarcinoma cell lines <sup>511</sup>. A study by Mandal and colleagues demonstrated that *DUSP4* was downregulated in ARID1A-deficient human endometrial epithelial cells <sup>512</sup>. Consequently, expression of these genes can be employed to investigate the functional role of ARID1A in downstream studies. Zhao and colleagues have demonstrated that in OCCC ARID1A inactivation leads to the downregulation of *STAG1* <sup>513</sup>. In this project, we chose to assess *STAG1* mRNA levels in ARID1A KO cells to determine whether this gene was down-regulated in OCCC cells relative to WT ARID1A.

## 5.2 Methods

All methods specific to the experiments performed in this chapter are outlined in the following sections.

### 5.2.1 Using CRISPR-Cas9 to KO gene expression

5.2.1.1 Generating and selecting clonal cell lines from a heterogeneous parent population to use for engineering of CRISPR isogenic cell line panels

RMG-I and JHOC-5 parental cell lines were seeded into 96-well plates at a density of 0.5 cells/well and clonal growth was monitored using the IncuCyte S3 Live-Cell imager. Nomenclature was based on their location in the 96-well plate e.g., RMG-I.b4. When clones were established in a 96-well, cells were transferred to a 12-well plate, then to a 6-well plate. Once confluent in a 6-well plate, cells were transferred into a T25 flask, grown and two frozen stocks generated (see Section 2.1.3). The clones were assessed using growth rate (see Section 2.1.6) and cell morphology and response to cisplatin (see Sections 2.1.5) in order to select a clonal cell line representative of the original parental line.

#### 5.2.1.2 sgRNA and primer design

sgRNA (described in Section 1.5.2) were either identified from published papers or designed using Benchling (<https://www.benchling.com/>). In order to maximise on-target efficiency and minimise any off-target effects, multiple exons were selected for the same gene to design sgRNA. Also, the sgRNA were designed to target exons in the first half of the gene in order to reduce the likelihood of a semi-functional truncated protein being produced. In data reported in Chapter 3, *ARID1A* gene mutations in OCCC could be observed throughout almost the entire gene (see Section 3.3.3), thus exons 1 and 2 were selected for the creation of the *ARID1A* KO model as they are at the 5'- end of the gene. *ARID1B* gene mutations in our OCCC cell lines are located in exons 8 and 20 (see Section 3.3.3). Consequently, the neighbouring exons 6 and exon 10 in the middle of the gene were selected to create the *ARID1B* KO model. Designed sgRNA were selected according to maximum values of On Target score (Efficiency) and Off Target score (Specificity). Research indicates that an on-target score of greater than 50 is optimal for achieving the highest efficiency targeting of DNA <sup>354,514</sup>. Moreover, a high off-target score suggests that the sgRNA is more unlikely to exhibit a significant off-target effect. The combination of a high on-target score and a high off-target score should result in high on-target potency with reduced off-target activity. Subsequently, all sgRNAs with on-target scores exceeding 50 were initially identified and selected. As there were no predicted guides with an off-target score exceeding 50. Then, among those sgRNA, the one with the highest off-target score had been selected for each exon. It has been shown that if the target sgRNA does not start with a guanine, this base was added to the 5'- end of the sgRNA target sequence before cloning to increase the expression of the sgRNA from the human U6 promoter <sup>515</sup>. All primers were ordered from Integrated DNA Technologies (IDT, Iowa, United States). All sgRNA are shown in Table 5.1.

Table 5.1 sgRNA target sequences used for CRISPR KO of *ARID1A* or *ARID1B*

Gene	Exon	PAM Sequence (NGG)	sgRNA Target sequence, 5' - 3'	SgRNA targeting DNA strand	Efficiency Score (On-Target Score)	Specificity Score (Off-Target Score)	Primer	Oligomers sequence, 5'-3'^	Reference
<i>ARID1A</i>	1	CGG	GAAGAACTCGAACGGGAACG	Top	67.1	48.5	Forward	CACCGAAGAAGCTCGAACGGGAACG	Xu et al. <sup>516</sup>
							Reverse	AAACCGTTCCCGTTCGAGTTCTTC	
<i>ARID1A</i>	2	GGG	GGTCATCGGGTACCGCTGCG	Bottom	66.1	48.3	Forward	CACCGGTCATCGGGTACCGCTGCG	
							Reverse	AAACCGCAGCGGTACCCGATGACC	
<i>ARID1B</i>	6	TGG	GGAAGCAACCAGTCTCGATC	Top	57.2	48.0	Forward	CACCGGAAGCAACCAGTCTCGATC	Designed in-house using Benchling
							Reverse	AAACGATCGAGACTGGTTGCTTCC	
<i>ARID1B</i>	10	AGG	CTCTAGCCTGATGAACACGC	Top	69.8	47.3	Forward	CACCGCTCTAGCCTGATGAACACGC	
							Reverse	AAACGCGTGTTTCATCAGGCTAGAGC	

^The sgRNA target sequence is highlighted in blue, and the restriction enzyme BbsI overhangs are noted in red. Purple G and C represent addition of a guanine to the 5'- end of the sgRNA target sequence before cloning to increase the expression of the sgRNA from the human U6 promoter.

#### 5.2.1.3 Luria-Bertani (LB) broth and LB agar plates

Briefly, 25g of LB powder (cat no. 244620, BD Biosciences, Australia) dissolved in 1L of MilliQ water, mixed thoroughly, and aliquoted into four 250 ml Schott bottles. Five grams of Bacto Agar (cat no. 214010, BD Biosciences, Australia) was added to each of the two bottles, and the four bottles autoclaved in an Autoclave Steam Steriliser for 1 hour at 120°C. After autoclaving, 250 µl of 100 mg/ml ampicillin (final concentration 100 µg/ml) was added to one of the bottles. A 10 ml serological pipette was used to transfer 10ml of agar into each petri dish to solidify. LB broth was stored at room temperature and LB agar plates at 4°C until required.

#### 5.2.1.4 Cloning of sgRNA into the PX-458 plasmid

##### 5.2.1.4.1 Phosphorylation and annealing of oligomers

Oligomers listed in Table 5.1 were annealed to form the sgRNA. All sgRNA oligomers were reconstituted in DNase-free water to a final concentration of 100 µM. Next, 1 µl of each forward and reverse oligomer were mixed with 1 µl of 10X T4 ligation Buffer (final concentration 1x, cat no. B0202s, New England Biolabs, Notting Hill, Victoria, Australia), 6.5 µl of DNase-free water and 0.5 µl 10,000 U/ml T4 Polynucleotide Kinase (PNK) (final concentration 500 U/ml, cat no. M0201S, New England Biolabs, Notting Hill, Victoria, Australia) into a PCR tube followed by incubation at 37°C for 30 minutes, 95°C for 5 minutes and then ramped down to 25°C decreasing by 5°C/minute using the Proflex PCR system (ThermoFisher Scientific, Massachusetts, United States).

##### 5.2.1.4.2 Linearization of the desired vector with BbsI and ligation of oligomers

The annealed oligomer (see 5.2.4.1 above) was diluted using a 1:250 ratio with DNase-free water. Next, 100 ng of the plasmid pSpCas9-2A-EGP (PX458) (cat no. 48138, Watertown, MA, USA) was mixed with 2 µl diluted annealed oligo, 2µl 10X FastDigest buffer (final concentration 1x, cat no. FD1014, New England Biolabs, Notting Hill, Victoria, Australia), 2 µl 10 mM Dithiothreitol (DTT) (final concentration 1 mM, cat no. R0861, ThermoFisher Scientific, Australia), 0.8 µl 25 mM Adenosine triphosphate (ATP) (final concentration 1 mM, cat no. E3101K, New England Biolabs, Notting Hill, Victoria, Australia), 1 µl 10X FastDigest

BbsI (Bpil) (final concentration 1x, cat no. FD1014, New England Biolabs, Notting Hill, Victoria, Australia), 0.5 µl 3x10<sup>6</sup> U/ml T7 DNA ligase (final concentration 75,000 U/ml, cat no. M0318s, New England Biolabs, Notting Hill, Victoria, Australia), and RNase-free water to a final volume of 20 µl. The reactions were then incubated at 37°C for 5 minutes, followed by 23°C for 5 minutes for 6 cycles in the Proflex PCR system to ligate sgRNA into the PX458 CRISPR KO plasmid.

#### 5.2.1.4.3 Plasmid purification with PlasmidSafe exonuclease

Since plasmids are susceptible to contamination by fragments of bacterial genomic DNA generated during alkaline lysis in these preparations, it is necessary to treat the ligation reaction with PlasmidSafe exonuclease to prevent unwanted recombination products. Following the ligation, 11 µl of the resulting reaction, 1.5 µl 10X PlasmidSafe Buffer (final concentration 1x, cat no. E3101K, New England Biolabs, Notting Hill, Victoria, Australia), 0.6 µl 25 mM ATP (final concentration 1mM), and 1 µl 10 U/µl PlasmidSafe exonuclease (final concentration 1 U/µl, cat no. E3101K, New England Biolabs, Notting Hill, Victoria, Australia) and RNase-free water to a final volume of 15 µl were mixed and incubated at 37°C for 30 minutes in the Proflex PCR system.

#### 5.2.1.4.4 Transformation of ligated plasmid into competent bacteria

During the ligation incubation, NEB 5-alpha competent *E. coli* (DH5α) (cat no. C2988J, New England Biolabs, Notting Hill, Victoria, Australia) cells were thawed on ice for at least 10 minutes. A volume of 2 µl of plasmid DNA from Section 5.2.1.4.3 was added to 25 µl DH5α, followed by gently flicking the tube 4 to 5 times to mix. The bacteria and plasmid DNA mixture were then incubated on ice for 30 minutes, then heat shocked at 42°C for 30 seconds in a water bath, followed by recovery on ice for 5 mins. After recovery, 125 µl of Super Optimal broth with Catabolite resuspension medium (cat no. B9035, New England Biolabs, Notting Hill, Victoria, Australia) was added and incubated at 37°C at 230 rpm for 1 hour in a shaking incubator (Infors-HT, Noble Park North VIC, Australia). Fifty µl of the mixture was spread onto ampicillin-positive LB agar plates and the plates were incubated at 37°C overnight in an oven. The PX458 plasmid carries an ampicillin resistance gene that allows for the selection of *E. coli* bacteria that contain the plasmid of interest with ligated sgRNA when selected with

ampicillin. Consequently, these plasmid containing bacteria exhibiting antibiotic resistance are able to proliferate and form colonies on agar plates.

#### 5.2.1.4.5 Plasmid DNA extraction and Sanger sequencing

For extraction of plasmid DNA from the bacteria, a volume of 10 ml of LB broth and 10 µl of a 100 mg/ml ampicillin stock (final concentration 100 µg/ml) solution was aliquoted into a 50 ml tube. One colony corresponding to each exon was picked from the ampicillin-positive plate and added to the tube of LB broth. The tube was incubated at 37°C at 230rpm overnight in a shaking incubator.

On the following day, a glycerol stock of the bacterial culture containing the plasmid was made by adding 850 µl of the overnight culture to 150 µl of 100% sterile glycerol (cat no. AJA242-500ML, Ajax-Finechem, NSW, Australia) in a 1.5 ml tube followed by mixing by slow vortexing. The bacterial stock was stored in a -80°C freezer until required.

The remaining bacterial culture was centrifuged for 3 minutes at maximum speed, and the supernatant discarded. The cell pellet was resuspended in 600 µl of MilliQ water and the PureYield™ Plasmid Miniprep System (cat no. A1223, Promega, Australia) was used to extract plasmid DNA as per the manufacturers' instructions. Plasmid DNA was eluted in 30 µl MilliQ water and quantitated using the nanodrop (see Section 2.4).

One hundred ng of plasmid DNA samples were sent to AGRF for Sanger sequencing (see Section 2.2.4) using the U6 sequencing primer (5'-GACTATCATATATGCTTACCGT-3'). The target sequences were then aligned to the corresponding sgRNA sequences using Benchling.

#### 5.2.1.5 Plasmid transfection

RMG-I and JHOC-5 cells were seeded into 12-well plates at densities of 1,400,000 cells/well or 300,000 cells/well, respectively. The next day, cells were transiently transfected with plasmid DNA (PX458 containing *ARID1A* or *ARID1B* sgRNA) using different transfection reagents as described below.

#### 5.2.1.5.1 Transfection using Lipofectamine 3000 Transfection Reagent

For transfection using Lipofectamine 3000 Transfection Reagent (cat no. L300-015, ThermoFisher Scientific, Australia), 3 µl of Lipofectamine 3000 Reagent was first added to 50 µl of OPTI-MEM serum free media (cat no. 31985062, ThermoFisher Scientific, Australia) in a 1.5 µl microcentrifuge tube. Then, 2 µl of P3000<sup>TM</sup> Enhancer Reagent and 1 µg of plasmid DNA were added to 50 µl of OPTI-MEM serum free media in another 1.5 µl microcentrifuge tube. Both tubes were mixed together and incubated for 15 minutes at room temperature. After incubation, culture media was removed from the 12-well plate and the DNA: transfection agent complex was added dropwise to each well of seeded cells. Cells were then incubated for 3 hours at 37°C in an incubator with 5% CO<sub>2</sub>. The transfection medium was replaced with 1ml growth medium.

#### 5.2.1.5.2 Transfection using X-tremeGENE HP DNA Transfection Reagent

For transfection using X-tremeGENE HP DNA Transfection Reagent (cat no. 06366236001, Merck, Australia), 1 µg of plasmid DNA was added to 100 µl OPTI-MEM serum free media in a 1.5 µl microcentrifuge tube. Then, 3 µl of X-tremeGENE HP transfection reagent was added to the plasmid DNA: media solution, mixed and incubated for 15 minutes at room temperature. Finally, the pDNA:X-tremeGENE HP complex was added dropwise to each of the 12 wells containing media and cells.

#### 5.2.1.5.3 Transfection using Lipofectamine LTX Reagent with PLUS Reagent

For transfection using Lipofectamine LTX Reagent with PLUS Reagent (cat no. 15338100, ThermoFisher Scientific, Australia), 1 µg of plasmid DNA was added in 200 µl OPTI-MEM Medium in a 1.5 µl microcentrifuge tube. Next, 1 µl Plus Reagent was added into the same tube, mixed and incubated for 5 minutes at room temperature before 3 µl of Lipofectamine LTX Reagent was added, mixed then incubated for 30 minutes at room temperature. Next, the complex was added dropwise to each of the 12 wells containing media and cells.

In all experiments, a reagent control that contained transfection reagent without plasmid DNA was included to ensure that the transfection agent was not toxic to the cells. A cell alone control was also included. To measure plasmid transfection using Green fluorescent protein (GFP)

expression, cells were imaged using the IncuCyte Live Cell imager (4X objective) with phase and green (Acquisition Time: 300ms) channels, every 3 hours for 48 hours. Cells were then sorted for GFP expression using flow cytometry as described in Section 5.22.

### 5.2.2 Fluorescent activated cell sorting (FACS) using a flow cytometer

After cells were transfected with plasmid DNA (Section 5.2.1.5), media was removed from the well, and cells gently washed with 1ml PBS. Next, cells were trypsinised with 300 µl trypsin, resuspended in 2 ml of media, transferred to a 15ml tube, and centrifuged at 1500 rpm for 5 minutes (Eppendorf, Macquarie Park NSW, Australia). The media was then removed, and the pellet resuspended in 1 ml PBS which contained 10% FBS and 100 U/ml Penicillin-Streptomycin (PEN/STREP) (Stock concentration 10,000 U/ml, cat no.15140122, ThermoFisher Scientific, Australia).

Fluorescent activated cell sorting (FACS) was undertaken using the BD FACSMelody cell sorter (BD Biosciences, Australia). To facilitate the sorting process, all live cells were initially gated and classified among all cell events, and single cells were subsequently captured from this population. Then, single cells were gated based on GFP expression ensuring that no untransfected cells were captured in this gate. All cells aligning with the reagent control were gated as GFP-negative, while cells located inside the GFP gate were GFP-positive. Single GFP positive cells were sorted into a 96-well plate with 200 µl growth medium containing 100 U/ml PEN/STREP and 0.1% Gentamicin/Amphotericin Solution (cat no. R01510, ThermoFisher Scientific, Australia) in each well. Media was refreshed weekly. Plates were imaged with the IncuCyte Live-cell imager once per week using whole well scan mode, and the growth of single clones in individual wells were followed. When clones were established in a 96-well, cells were transferred to a 12-well plate, then to a 6-well plate. Once confluent in a 6-well plate, cells were split into 3 aliquots. The first aliquot was transferred into a T25 flask, grown and two frozen stocks generated (see Section 2.1.3). The second aliquot was transferred into a new 6-well plate, and after cells reached 80% confluency, gDNA was extracted (see Section 2.2.1). The final aliquot was transferred into a new 6-well plate, and after cells were 80% confluent, protein was extracted (see Section 2.5.1).



### 5.2.3 gDNA screening to detect CRISPR induced modifications

To determine if CRISPR was successful, the gDNA region around the sgRNA target sequence was amplified utilising either published primers or primers designed in-house to the gene and exon of interest (Table 5.2).

Table 5.2 Primers used for CRISPR KO screening

Gene	Exon	Annealing Temp.	Size (bp)	DMSO and touchdown need	Primer	Primer sequence, 5'-3'^	Reference
<i>ARID1A</i>	1	65.7	387	3% DMSO+ Touchdown	Forward	AAAGCCGAGCAGCAGCAG	Xu et al. <sup>516</sup>
					Reverse	GTAGGGTTGCCCCAAGCC	
<i>ARID1A</i>	2	61.3	442	n/a	Forward	AGGTTGGTCTCATTGCTCTTTC	
					Reverse	TTGGAAGCCAAGGATACATTC	
<i>ARID1B</i>	6	63.1	470	n/a	Forward	TGGGTGTTACCCAGAAAACC	Designed in-house using Benchling
					Reverse	TCTCGTATGCCTTGGTGAGA	
<i>ARID1B</i>	10	61.5	523	n/a	Forward	GGGCAAACCACTGCTAATGT	
					Reverse	CGAAATGTTTGTCTCCACCA	

^ The sequencing primer is highlighted in blue.

The issue of high GC content (>65%) in some gDNA regions hindering specific binding of primers and PCR amplification was ameliorated by the inclusion of 3% DMSO in PCR reactions <sup>517,518</sup>. In some studies, touchdown PCR had also been shown to reduce the effect of GC-rich sequence <sup>517,519</sup>. It is a technique that gradually lowers the annealing temperature in successive cycles to enhance the specificity and yield of the desired DNA product by initially favouring stringent binding conditions. Therefore, in this project, for GC-rich gDNA regions, we added 3% DMSO and used a touchdown PCR protocol. PCR was conducted using the Phusion Green Hot Start II High-Fidelity PCR Master Mix, described in Section 2.2.2. All the cycling conditions are shown in Tables 5.3 and 5.4.

Table 5.3 Thermocycling conditions for PCR

Cycle step	Temp.	Time	Cycles
Initial Denaturation	98°C	30s	1
Denaturation	98°C	10s	30
Annealing <sup>#</sup>	X°C	30s	
Extension	72°C	15s	
Final extension	72°C	10m	1
Hold	4°C	∞	1

# Annealing temperature shown in Table 5.2.

Table 5.4 Thermocycling conditions for touchdown PCR

Cycle step	Temp.	Time	Cycles
Initial denaturation	98°C	30s	1
Denaturation	98°C	10s	10
Annealing <sup>^</sup>	72°C	20s	
Extend	72°C	15s	
Denaturation	98°C	10s	30
Annealing <sup>#</sup>	X°C	20s	
Extend	72°C	15s	
Final extension	72°C	10m	1
Hold	4°C	∞	1

<sup>^</sup> Annealing temperature decreased 0.6°C per cycle from 72°C to the annealing temperature shown in Table 5.2 over 10 cycles. # Annealing temperature shown in Table 5.2.

PCR products were purified using the Wizard® SV Gel and PCR Clean-Up System (see Section 2.2.3) and the DNA concentration measured using the Nanodrop spectrophotometer (see Section 2.4). DNA fragments were sent to AGRF, Sydney for Sanger sequencing, specifically 120 ng purified DNA fragment, 1 µl of 10mM sequencing primer (Table 5.2), and DNase-Free water to a total volume of 12 µl.

Sanger sequencing traces were analysed using Benchling and the ICE CRISPR Analysis Tool (<https://www.synthego.com/products/bioinformatics/crispr-analysis>). Benchling was used to analyse sequencing chromatograms to determine whether CRISPR KO had been successful. WT and potential KO sequences were aligned in the region nearby the sgRNA and the presence of variants determined. ICE is an algorithm designed to analyse CRISPR-induced edits using Sanger sequencing data by comparing chromatogram trace files from edited and unedited populations. The process starts by aligning these sequences to a guide sequence and generating possible genotypes based on the known activity of the Cas9 nuclease. A regression analysis then determines the best-fitting combination of these genotypes to explain the observed data, inferring their CRISPR score. This method provides precise details on each modification by identifying the percentage of the genome altered by indels (insertions or deletions).

#### 5.2.4 Protein analyses and Quantitative Real-Time Reverse Transcriptase PCR (qRT-PCR)

Protein analyses and qRT-PCR were conducted as previously described in Sections 2.3 and 2.5, respectively.

5.2.5 Determining sensitivity of cell lines to cisplatin was conducted as previously described in Section 3.2.4.

### 5.3 Results

#### 5.3.1 Creation of clonal cell lines from parental ovarian cancer lines

Since cancer cell lines are not entirely homogenous, it is necessary to prepare clonal lines, where all cells in the population have the same genetic background for the creation of a CRISPR isogenic panel. Both RMG-I and JHOC-5 cells have been reported as WT for *ARID1A*, so clonal lines were created from these parental cell lines to use for genetic engineering with CRISPR-Cas9.

### 5.3.1.1 Selection of the RMG-I.b4 clonal cell line

Initially, we started with the ARID1A WT RMG-I cell line. First, we seeded a 96-well plate with RMG-I cells at 0.5 cells per well. After 13 days of cell growth, we observed 25 clones of the 96 wells that were seeded (26%). Next, we isolated three clonal lines from the RMG-I parental lines: RMG-I.b4, RMG-I.c9, and RMG-I.b10. Then, RMG-I clones b4, c9, and b10 were characterised to determine which one had the most similar morphology, growth rate, and sensitivity to the DNA damaging agent cisplatin compared with the heterogeneous parental RMG-I cell line.

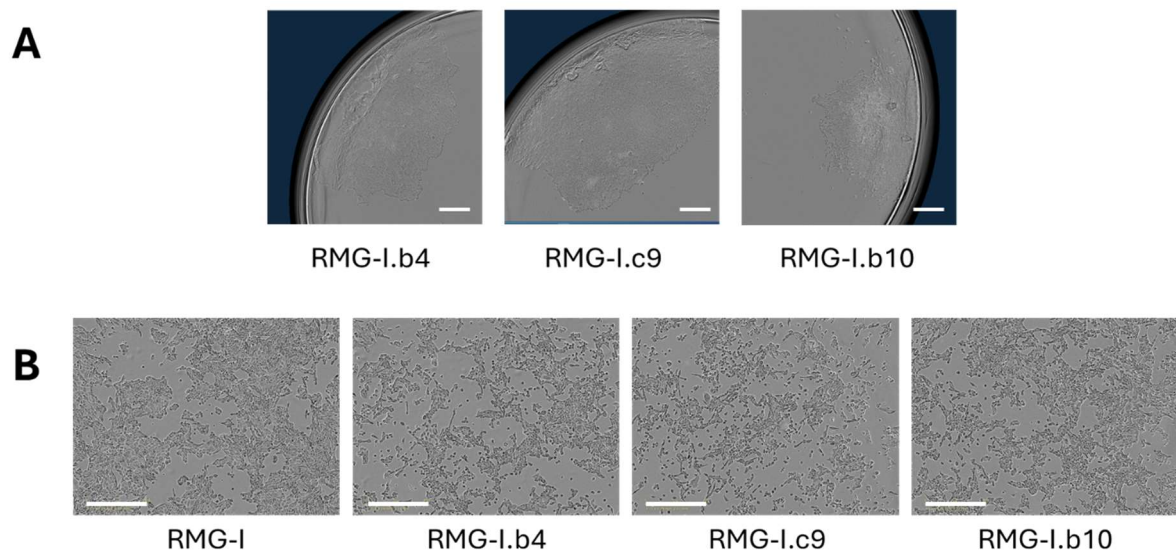


Figure 5.4 Representative images of three RMG-I clonal lines. A) RMG-I clonal cell lines b4, c9, and b10 growing in a 96-well plate from a single cell after 13 days post seeding captured on the IncuCyte S3 instrument using a whole well scan type with a 4X objective. Scale bar=500  $\mu$ m. B) RMG-I and clonal cell lines b4, c9, and b10 seeded 4,500 cells per well into a 96-well plate 2 days post seeding captured on the IncuCyte S3 instrument with a 10X objective. Scale bar=400  $\mu$ m.

To investigate whether RMG-I clones have a similar morphology to parental lines, all the cells were seeded into 96-well plates and imaged using the IncuCyte. The results showed that RMG-I cells had an epithelial appearance. In addition, there were no obvious morphological difference between the three clones and the parental cell lines (Figure 5.4). Moreover, the IncuCyte results showed that the b4, c9 and b10 cells grew more slowly than the parental line, however, this difference was not statistically significant (Figure 5.5).

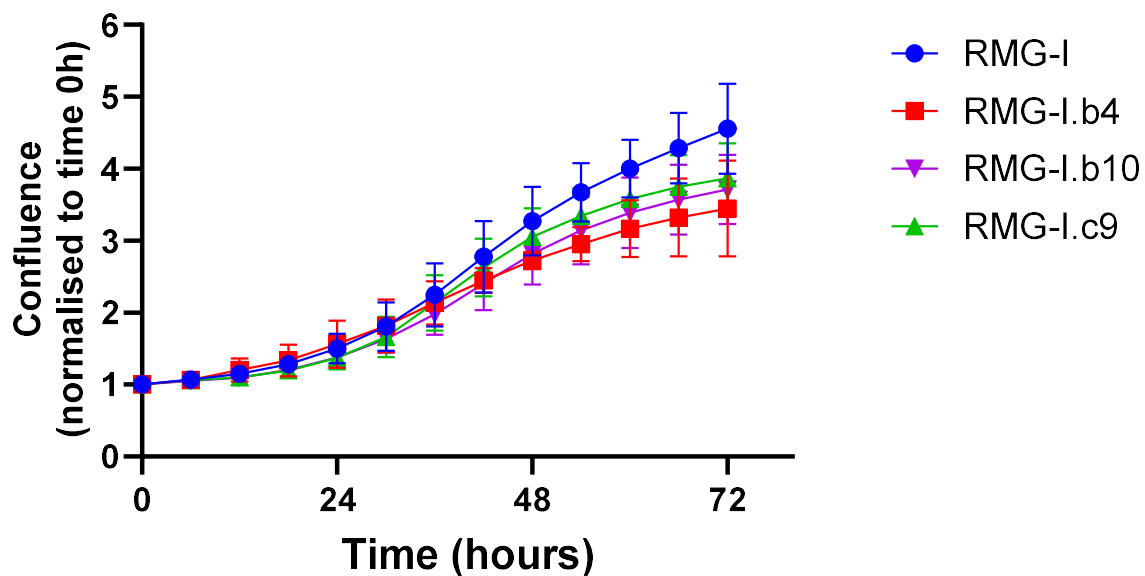


Figure 5.5 Growth rate of RMG-I parental and clonal lines over 72h. All cells were seeded into 96-well plates at 4,000 cells/well density. Images were captured by the IncuCyte at 6 hourly intervals over 72h and the percentage confluence recorded. Data is shown for a representative experiment (N=3). There was no significant difference in growth patterns between the RMG-I parental line and clonal cell lines.

MTS assays were used to determine cell viability after treatment with cisplatin for 72 hours. The results showed that the b4 clone has a similar response to cisplatin compared to the parental line, followed by c9 and b10. The cisplatin IC<sub>50</sub> of clone b4 was 5.846  $\mu$ M, similar to the parental line which was 5.788  $\mu$ M (Figure 5.6) (analyses conducted using GraphPad, see Section 2.1.5). Thus, the RMG-I.b4 clone was selected as a homogeneous line for future CRISPR KO experiments. Dose curves are presented in Appendix 3.

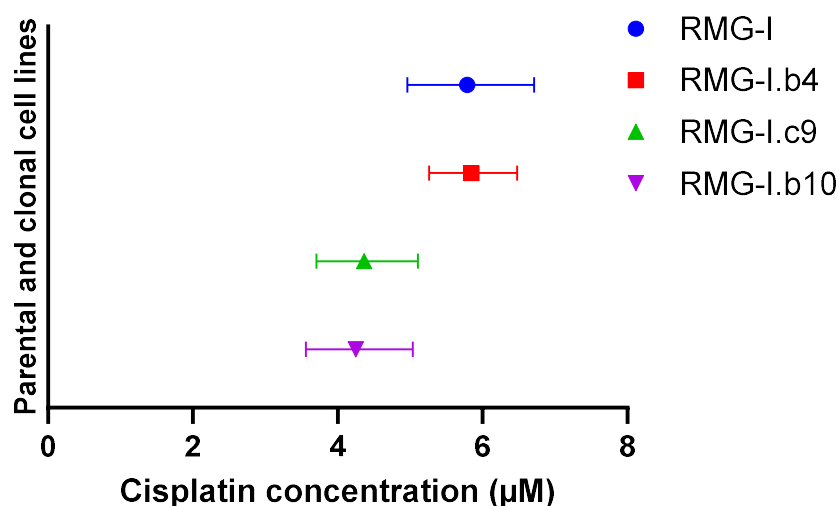


Figure 5.6 IC<sub>50</sub> cisplatin concentration of RMG-I parental and clonal lines b4, c9 and b10 determined by MTS assay 72 hours post treatment. Clonal line b4 (5.846 µM) had a similar response to cisplatin as the parental line (5.788 µM). These experiments were repeated 3 times to generate dose curves and IC<sub>50</sub> was calculated. Confidence intervals are indicated (95% CI).

### 5.3.1.2 Selection of the JHOC-5.d12 clonal cell line

The JHOC-5 cell line is reported to be WT for both *ARID1A* and *ARID1B*. In order to create a clonal cell line, we seeded a 96-well plate with JHOC-5 cells at 0.5 cells per well, resulting in 14 out of 96 wells developing growth of a clone (14.5%). We created three clonal lines from the JHOC-5 parental line: JHOC-5.c7, JHOC-5.d12, and JHOC-5.h7. These clonal lines were characterised in order to determine which one had the most similar morphology, growth rate, and sensitivity to the DNA damaging agent cisplatin compared to the heterogeneous parental JHOC-5 cell line. The results demonstrated that there were no discernible morphological differences between the JHOC-5 parental cells and three clonal cell lines (c7, d12 and h7) (Figure 5.7).

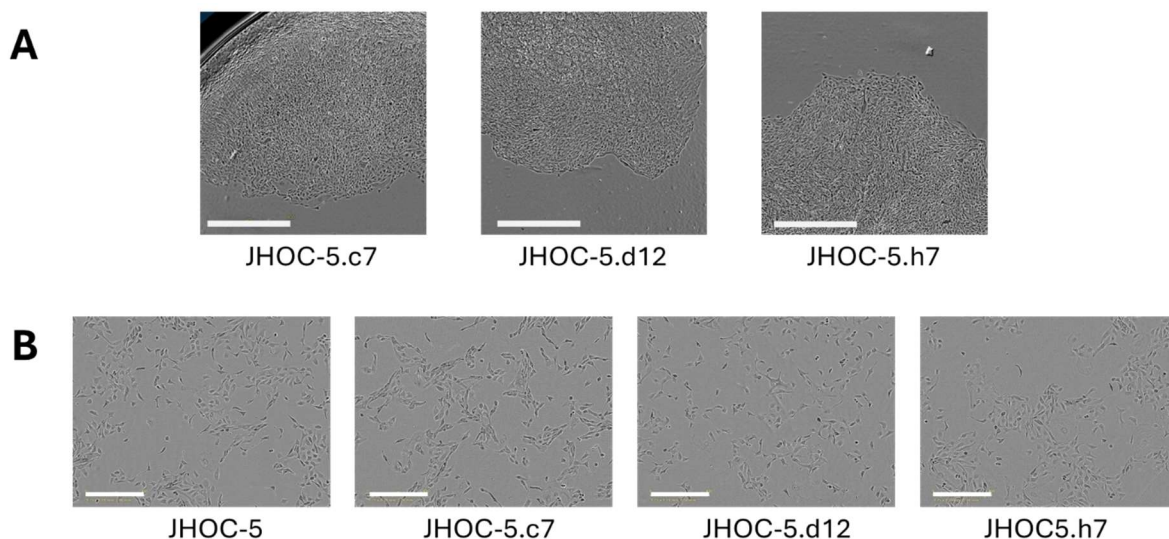


Figure 5.7 Representative images of JHOC-5 parental and three JHOC-5 clonal lines. A) JHOC-5 clones c7, d12, and h7 growing in a 96-well plate from a single cell 12 days post seeding captured on the IncuCyte S3 instrument in whole well scan type with a 4X objective. Scale bar=800  $\mu$ m. B) JHOC-5 and clones c7, d12, and h7 seeded 2,500 cells per well into a 96-well plate after 2 days post seeding captured on the IncuCyte S3 instrument with a 10X objective. Scale bar=400  $\mu$ m.

Furthermore, results demonstrated that growth rate of the c7 clonal cell line was comparable to that of the JHOC-5 heterogeneous parental line, whereas the growth rates of the d12 and h7 cell lines were slightly slower than that of the parental line. The MTS results indicated that the IC<sub>50</sub> of cisplatin for the d12 clone was 3.047  $\mu$ M, which was very similar to that of the parental line at 2.875  $\mu$ M. The cisplatin IC<sub>50</sub> values of clones c7 and d7 were 3.944  $\mu$ M and 4.328  $\mu$ M, respectively. Because the IC<sub>50</sub> of clone d12 had a cisplatin IC<sub>50</sub> close to that of the JHOC-5 parental line and the growth rates of the three clones were not very different from that of the parental line (Figure 5.8), this suggested that clone d12 retained a similar level of cisplatin sensitivity and proliferative capacity as the JHOC-5 parental line. The JHOC-5.d12 clone was selected for future CRISPR KO experiments. Dose curves are presented in Appendix 3.

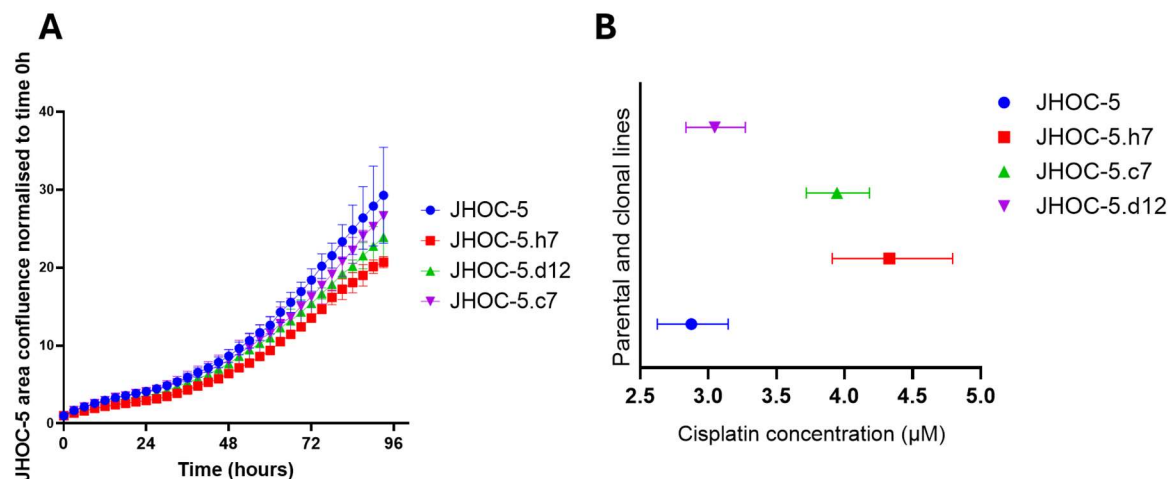


Figure 5.8 Growth rate and cell viability of the JHOC-5 parental line and clonal cell lines. A) All cells were seeded into 96-well plates with 2500 cells/well density. Cells were imaged in the IncuCyte for 93h. Images were captured every 3 hours and the percentage confluence recorded (N=2). B) IC50 values of JHOC-5 parental and clonal lines were measured by MTS assay 72 hours post treatment with cisplatin (N=3). Confidence intervals are indicated (95% CI).

### 5.3.2 CRISPR KO of ARID1A in ARIDA WT OCCC lines RMG-I and JHOC-5 clonal lines

#### 5.3.2.1 Cloning ARID1A sgRNA into CRISPR-Cas9 KO vector PX458

The *ARID1A* sgRNAs (Table 5.1) targeting exons 1 and 2 were successfully cloned into the PX458 vector (Figure 5.9).



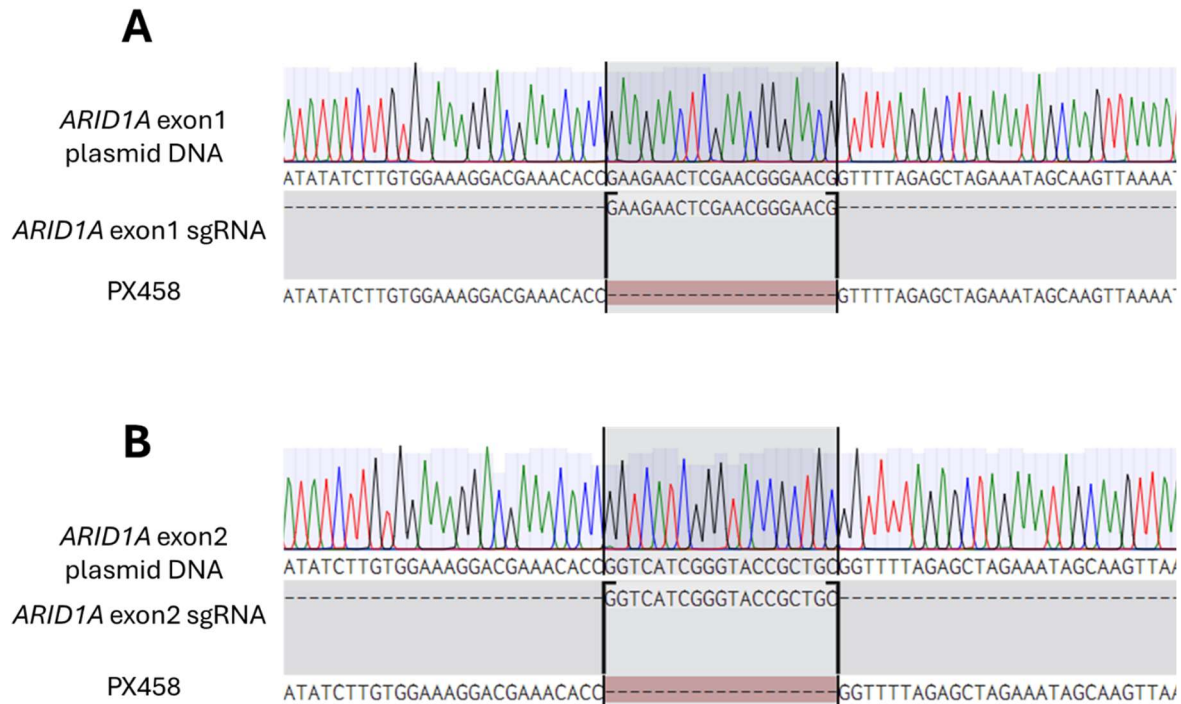


Figure 5.9 Sequence confirmation of *ARID1A* sgRNA cloned into the CRISPR-Cas9 vector PX458. Sequence confirmation of sgRNA designed to A) exon 1 of *ARID1A* and B) exon 2 of *ARID1A* cloned into PX458. Two colonies (plasmid DNA 1 and 2) were sequenced for each cloned plasmid vector (analysed in Benchling).

### 5.3.2.2 Creation of *ARID1A* KO cells in RMG-I.b4 clonal cells

#### 5.3.2.2.1 *ARID1A* plasmid transfection and GFP single cell sorting

Both *ARID1A* sgRNA plasmids targeting exons 1 and 2, were independently transfected into the RMG-I.b4 clonal cell line according to the ratio of 1:3 of plasmid DNA ( $\mu$ g): Lipofectamine 3000 ( $\mu$ l). The results showed that GFP was expressed in both cases suggesting successful plasmid transfection, while no GFP expression was found for the transfection reagent controls (Figure 5.10).

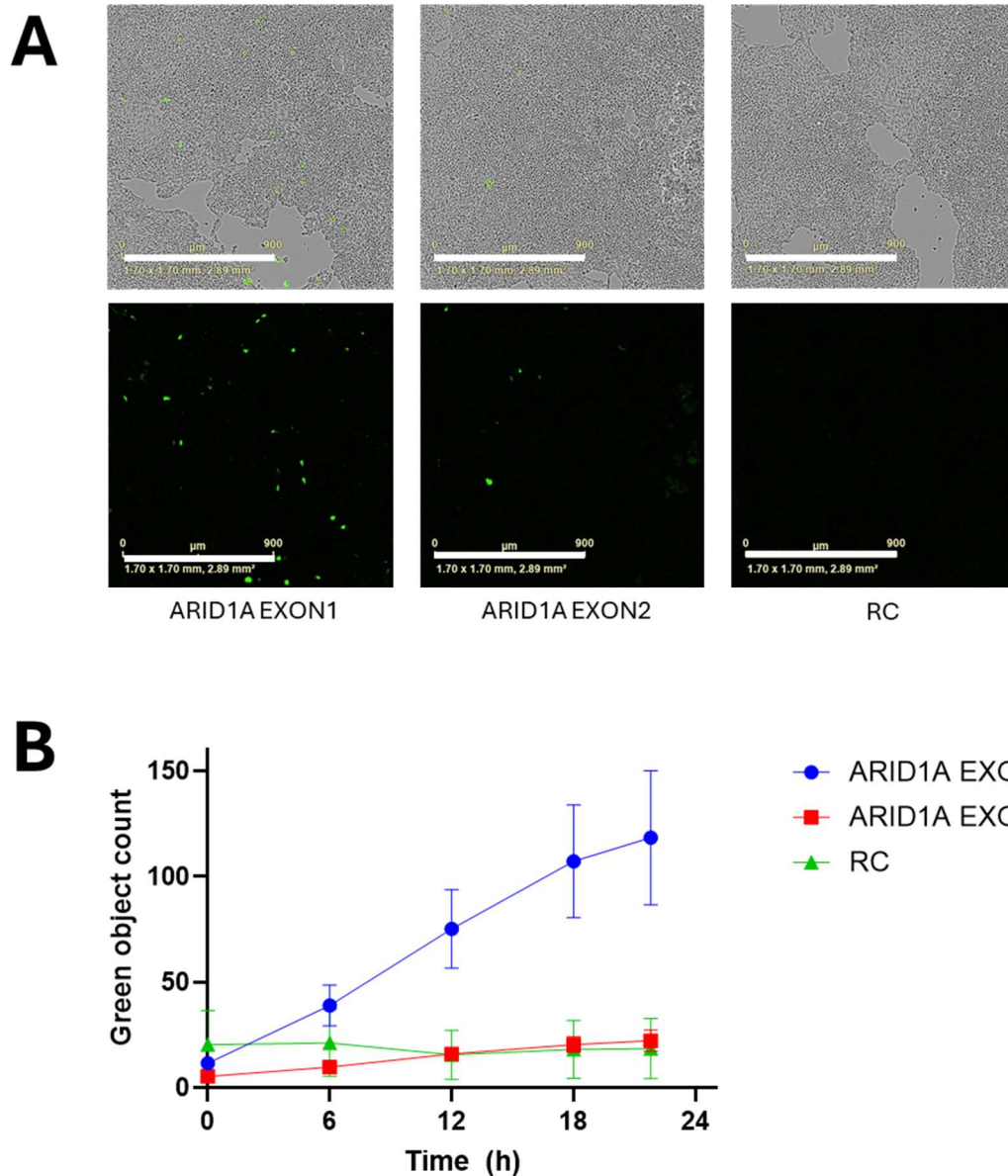


Figure 5.10 Transfection of RMG-I.b4 clonal cells with *ARID1A* plasmid DNA using lipofectamine 3000 transfection reagent for 24 hours. A) Phase contrast and GFP cell images of Lipofectamine 3000 Reagent control (RC) and both *ARID1A* plasmid DNAs transfected using the reagent Lipofectamine 3000 at a ratio of 1:3. Scale bar=1  $\mu$ m. B) Green objective count as analysed by the IncuCyte S3 analysis software. N=1, graphs represent the mean  $\pm$  SEM for 9 technical replicates.

After 24 hours transfection, single cell sorting was used to sort RMG-I cells into single cells based on GFP expression. For each exon, GFP signal positive cells were sorted into two 96-well plates. Cells were compared with the reagent control to ensure that cells were selected that

fluoresced above endogenous baseline levels. Flow cytometry results showed that for the exon 1 plasmid vector, 0.57% of the cell population was successfully transfected, while for the exon 2 plasmid vector, 0.17% of the cell population was transfected (Figure 5.11). Despite successful cell sorting of 190 transfected cells, the overall transfection efficiencies were very low and warranted further optimisation for future experiments.

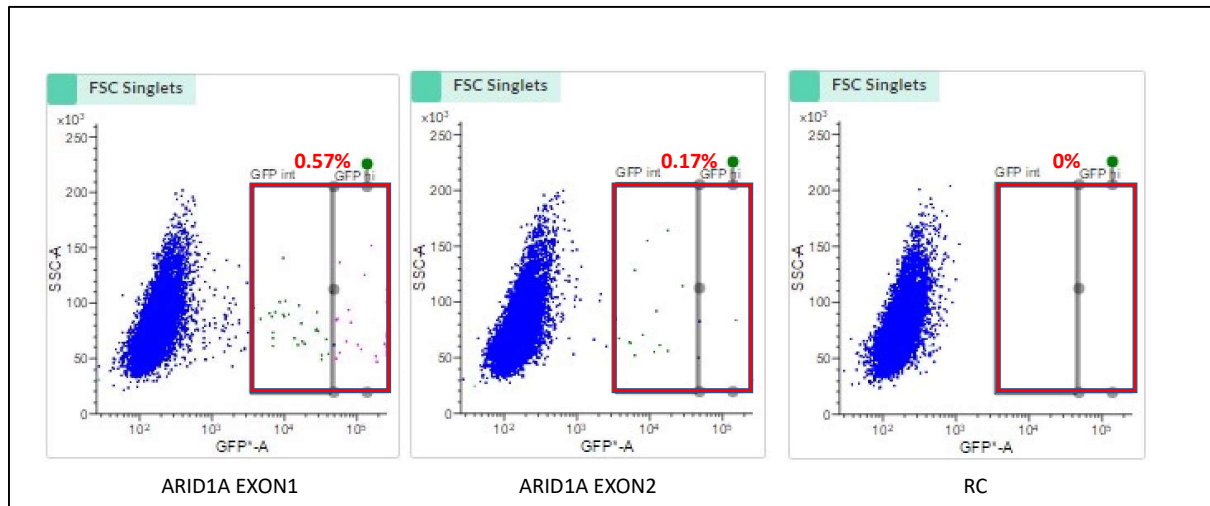


Figure 5.11 Flow cytometry analysis of RMG-I.b4 clonal cells transfected with reagent control and *ARID1A* exon 1 or exon 2 targeting plasmid vectors. Single cells were gated based on GFP intensity and side scatter (blue population). Percentage of cells with GFP expression are illustrated in the red box. RC: reagent control.

#### 5.3.2.2.2 Validation of *ARID1A* KO clones in RMG-I.b4 cells

To screen for RMG-I CRISPR KO clonal cells grown from single cells, the well plates were imaged using the IncuCyte. Of the 380 wells that were seeded with a single cell post transfection, 50 clones (13.1%) grew. For the RC, 37 clones (39%) were observed from 95 wells seeded for single cells post transfection. To name the CRISPR KO cells from each clonal parental cell line, we designed a nomenclature rule. The whole name had 5 parts. The first part was the abbreviation of the cell line name, such as the RMG-I cell line was “R”. The second part was the abbreviation of the gene name, such as *ARID1A* was “A”. The third part was the plasmid DNA exon number, such as exon 1, noted as “E1”. The fourth part was the 96-well plate number, noting that if the cell was from the first plate it was “A”. The last part was the

well location in the 96-well plate, such as “A1”. The nomenclature for all cell lines is summarised in Table 5.5.

Table 5.5 Nomenclature for cell sorted CRISPR KO clones

Name	Abbreviation
RMG-I	R
JHOC-5	J
ARID1A	A
ARID1B	B
Double KO	DK
Exon	E
Plate 1	A
Plate 2	B

For all 50 *ARID1A* clones originating from the RMG-I.b4 cell line, gDNA was extracted and the regions proposed to be edited amplified by PCR. PCR products were sequenced by Sanger sequencing and the results were analysed using Benchling. Analysis showed that the *ARID1A* target sequence was mutated in 4 of the 23 exon 1 clones and for exon 2, 14 of the 27 clones were altered. All clones with detected sequence aberrations were analysed using the ICE CRISPR Analysis Tool to identify the exact genetic mutation (Figure 5.12).

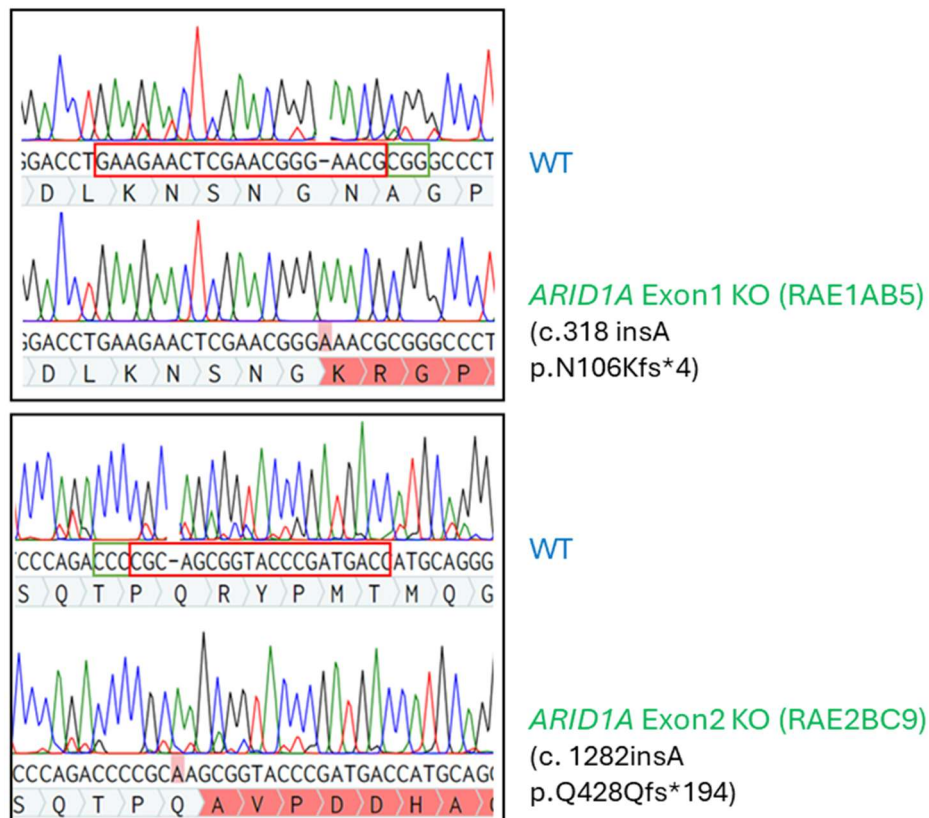


Figure 5.12 Representative alignment of Sanger sequencing of RMG-I CRISPR KO *ARID1A* Exon1 (RAE1AB5; upper panel) and Exon2 (RAE2BC9; lower panel) clones in Benchling. The sgRNA target sequence is highlighted in red box, and the PAM are noted in green box.

After ICE analysis, we grouped the clones with identical sequence and selected a clone from each unique group as a representative (Table 5.6). RAE1BF1 could not be analysed by ICE, possibly due to the presence of a large deletion as the result of CRISPR engineering, so for this clone, ARID1A protein levels only were assessed.

Table 5.6 Summary of all RMG-I ARID1A CRISPR KO cells and mutation types

RMG-I ARID1A KO clone	sgRNA target	<i>ARID1A</i> mutation	cDNA change	ICE KO Score
RAE1AB5	EXON1	p.N106Kfs*4	c.318insA	97
RAE1AF8		p.N106Tfs*7	c.318delA	78
RAE1BE5		p.N106Tfs*4 p.G105Tfs*7	c.317insC c.313delGGGA	96
RAE1BF1		N/A	N/A	N/A
RAE2AB6	EXON2	p.Q428Hfs*1859 p.Q428Qfs*194	c.1282insACA c.1282insA	46
RAE2AB12; RAE2AE7		p.Q428Qfs*194 p.Q428Pfs*193	c.1282insA c.1282delAG	94 93
RAE2AD2		p.Q428Hfs*168	c.1282del 85bp	29
RAE2AB9		p.Q428Qfs*3 p.Q428fs	c.1283delGCGG c.1282insN^	74
RAE2AG1; RAE2AG6; RAE2AF7; RAE2BG5 <sup>#</sup> ; RAE2BC9		p.Q428Qfs*194	c.1282insA	97 to 98
RAE2BE7		p.Q428Rfs*1857 p.Q428Qfs*194	c.1282delAGC c.1282insA	45
RAE2BD8		p.Q428Hfs*1856 p.Q428Qfs*194	c.1282delAGCGGT c.1282insA	45
RAE2AC9; RAE2AH9		Heterozygous p.Q428Qfs*194	c.1282insA	48

N/A: sequencing data could not be obtained for this clone. ^N= base unable to be determined

# RAE2BG5 has ICE KO Score 79

To further validate that detected mutations in *ARID1A* resulted in total loss of protein Western blotting was used. Thirteen samples, including one reagent control cell line and 12 KO plasmid transfected cell lines, 4 from exon 1 and 8 from exon 2, were analysed. ARID1A protein was

absent in 3 out of 4 exon 1 clones and 3 out of 8 of the exon 2 clones analysed by Western blot (Figure 5.13).

The summary of screening and validation for KO ARID1A lines in the clonal RMG-I.b4 cell line is shown in the flow diagram outlined in Figure 5.14. Analysis revealed three KO clones with unique mutations using exon 1 sgRNA, and for exon 2 sgRNA we engineered clones with three unique mutations, with five clones having the identical mutation c.1284insA (p.Q428Q).

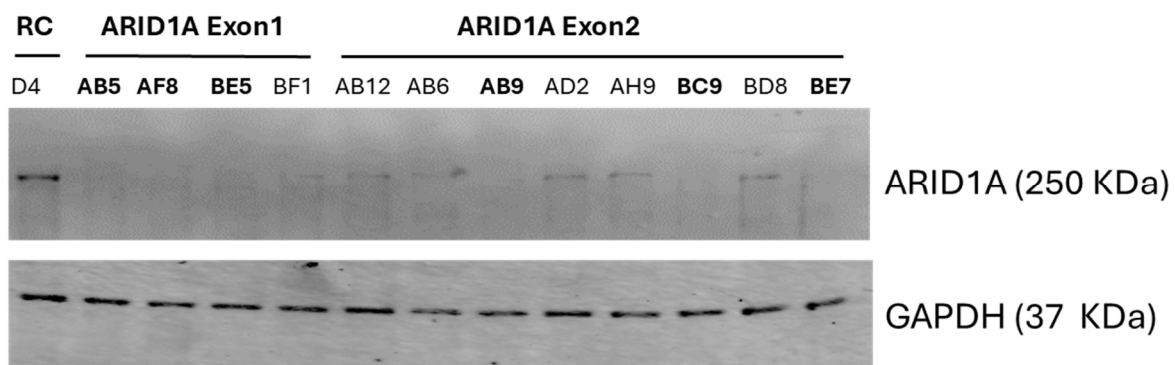


Figure 5.13 Protein levels of ARID1A in ARID1A CRISPR KO cells. Whole cell protein lysate was quantitated and analysed via Western blotting. The protein loading control is GAPDH. The reagent control (RC) sample based on the clonal RMG-I.b4 and had ARID1A protein expression. For each of the ARID1A targeted exons (exons 1 and 2), there were 3 clonal lines that had no ARID1A protein expression that are highlighted in Bold. Other cell lines had depleted, but not entirely absent, ARID1A.



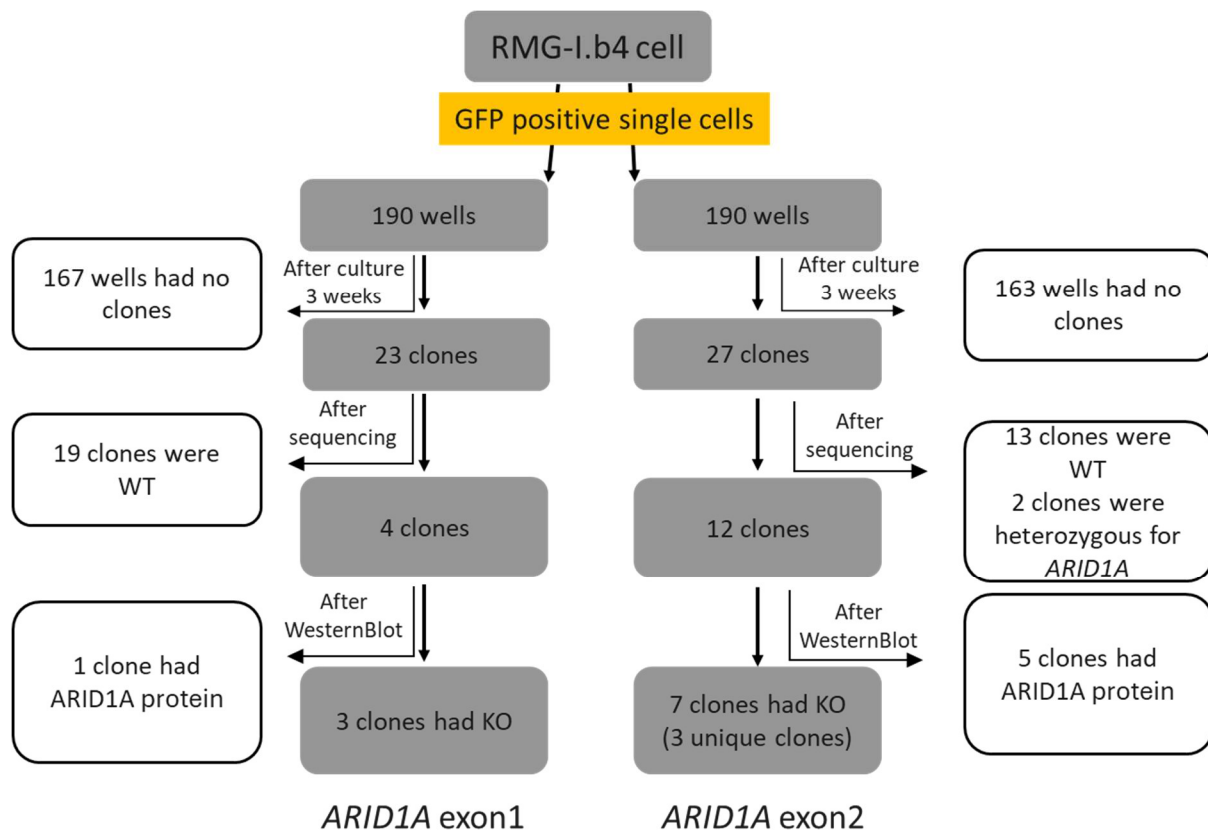


Figure 5.14 Flow diagram summarising inclusion and exclusion criteria for the RMG-I.b4 CRISPR KO cell cohort. Single cells were flow sorted into 190 wells for each exon. Cells were cultured for 3 weeks and underwent sequencing for *ARID1A*. After the removal of cells from the pipeline with WT sequence for *ARID1A*, mutant *ARID1A* variants were validated with Western blotting looking for absence of ARID1A protein levels. Due to the in-frame deletions, some expression of mutant ARID1A protein remained. The final outcome of this CRISPR KO experiment yielded 3 unique exon 1 clones and 3 unique exon 2 clones with clear ARID1A KO.

### 5.3.2.3 Creation of ARID1A KO cells in JHOC-5.d12 clonal cells

#### 5.3.2.3.1 ARID1A plasmid transfection and GFP single cell sorting in JHOC-5.d12

For optimising of transfection into JHOC-5.d12 cells, previously used transfection reagents, Lipofectamine 3000 and X-tremeGENE HP, were employed. In addition, a third transfection reagent, Lipofectamine LTX, was available and also tested in JHOC-5. The result showed lipofectamine LTX was the most effective transfection reagent (Appendix 3). Thus, Lipofectamine LTX reagent was selected for JHOC-5 CRISPR KO experiments. Two different



*ARID1A* CRISPR KO plasmid DNAs targeting different exons were transfected into JHOC-5.d12 clonal cells using Lipofectamine LTX reagent. The results showed that GFP was expressed in cells containing plasmid DNA and no expression was observed in cells without plasmid DNA. Also, from the flow cytometry results, it showed that for the CRISPR KO plasmid targeting *ARID1A* exon 1, only 0.88% of the cell populations were successfully transfected with the plasmid, and the number for the CRISPR KO plasmid targeting *ARID1A* exon 2 was 1.16% (Figure 5.15 and Figure 5.16).

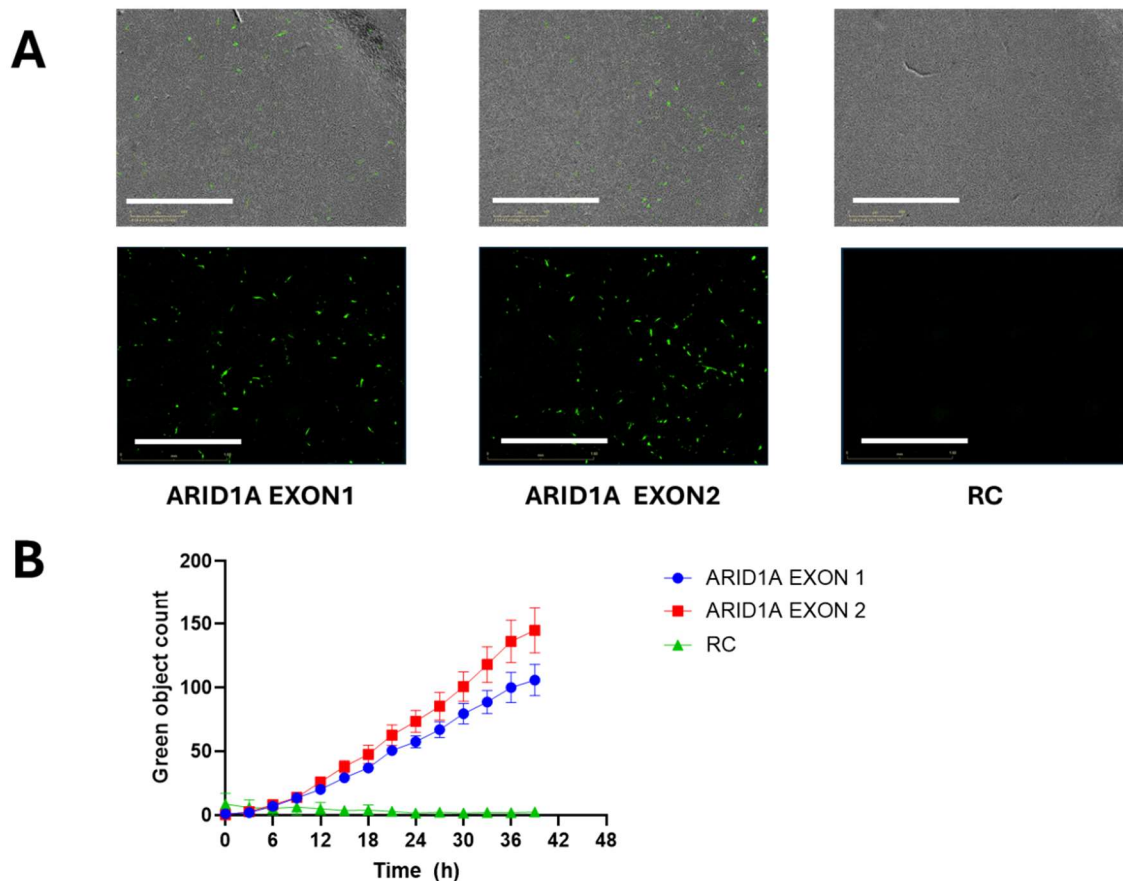


Figure 5.15 Transfection of JHOC-5.d12 cells with *ARID1A* CRISPR KO plasmid DNA using lipofectamine LTX reagent for 39 hours and flow cytometry analysis of JHOC-5.d12 transfected with reagent control (RC) and *ARID1A* CRISPR KO plasmid DNAs. A) Phase contrast and GFP cell images of Lipofectamine LTX RC and both *ARID1A* plasmid DNAs transfected using the reagent Lipofectamine LTX at a ratio of 1:3. Scale bar = 1.6mm. B) Green objective count as analysed by the IncuCyte S3 analysis software. N=1, graphs represent mean  $\pm$  SEM for 9 technical replicates.

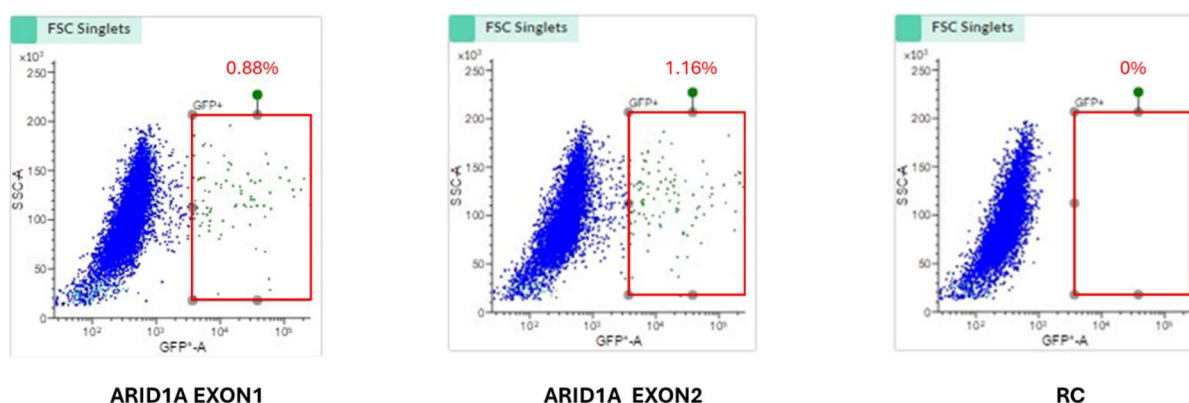


Figure 5.16 Flow cytometry analysis of JHOC-5.d12 clonal cells transfected with reagent control and *ARID1A* exon 1 or exon 2 targeting plasmid vectors. Single cells were gated based on GFP intensity and side scatter (blue population). Percentage of cells with GFP expression are illustrated in the red box. RC: reagent control.

#### 5.3.2.3.2 Validation of ARID1A KO clones in JHOC-5.d12 cell background

When we performed CRISPR KO in RMG-I cells, the target protein was still detected in some samples, despite Sanger sequencing indicating the presence of mutations. This suggests the possibility of incomplete knockout or the presence of alternative splicing or protein isoforms that retain the target protein function. Therefore, when we performed CRISPR KO in the JHOC-5 clonal cell line, we first used Western blot to detect whether there was any target protein expression, and then subjected the samples that did not express the target protein to Sanger sequencing to confirm the altered sites.

Due to human error, one of the 96-well plates of ARID1A CRISPR KO exon 1 of JHOC-5 fell to the ground, resulting in exon 1 having only a single 96-well plate for analysis. Of the total 285 wells seeded with a single GFP exon 1 or exon 2 CRISPR KO cell, 42 (14%) of cells grew into clones, specifically 11/95 (11.6%) for exon 1 sgRNA and 31/190 (16.3%) for exon 2 sgRNA. Following the detection of ARID1A protein via Western blot analysis, it was observed that 9 clones out of 11 for putative exon 1 KO clones exhibited no ARID1A protein, while 20 clones out of 31 putative exon 2 KO clones exhibited no ARID1A protein (representative blot shown in Figure 5.17). We note that unlike for RMG-I, in some JHOC-5 KO clones and JHOC-5.d12, ARID1A displayed a doublet band, both bands disappearing upon ARID1A KO.

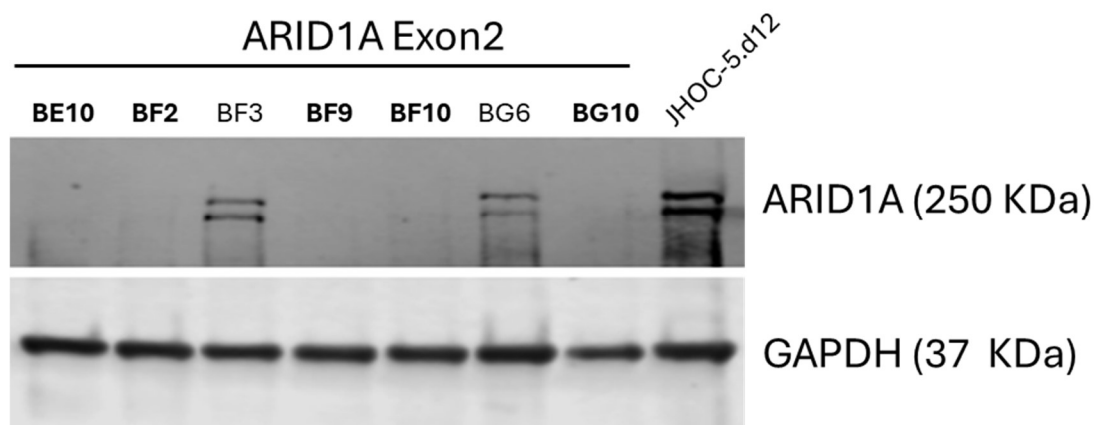


Figure 5.17 Representative protein levels of ARID1A in ARID1A CRISPR JHOC-5 KO clones. Whole cell protein lysate was quantitated and analysed by Western blotting. The protein loading control is GAPDH. JHOC-5.d12 cells displayed ARID1A protein. In seven cell lines where exon 2 was targeted, 5 samples had no ARID1A protein (highlighted in bold).

Sanger sequencing results indicated that of the 20 CRISPR KO clones targeting exon 2, 17 clones exhibited mutations in *ARID1A* and 3 were heterozygous for *ARID1A* with WT *ARID1A* remaining (Figure 5.18, Table 5.7). However, the sequencing of all exon 1 clones showed messy sequencing peaks and background interference, rendering the data unable to be analysed. This issue is currently being investigated by other members of our research group. A summary is presented in the accompanying flowchart (Figure 5.19).

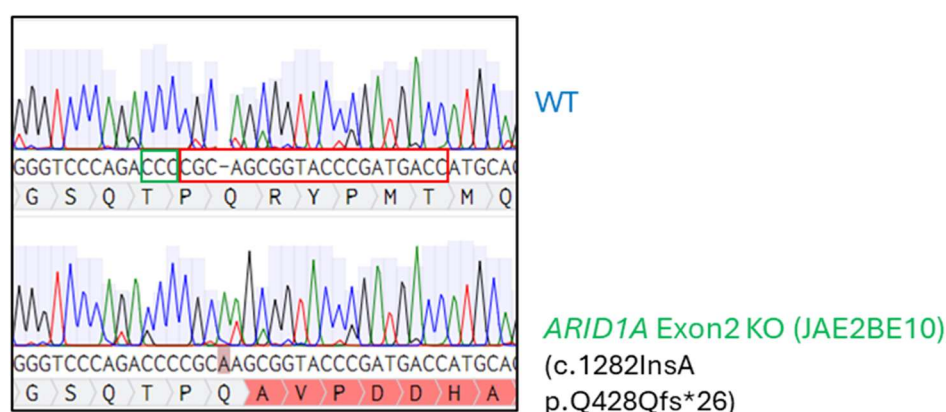


Figure 5.18 Representative alignment of Sanger sequencing of JHOC-5 CRISPR KO *ARID1A* Exon2 (RAE2BE10) clones in Benchling. *ARID1A* Exon2 KO was aligned with WT sequence. The sgRNA target sequence is highlighted in red box, and the PAM are noted in green box.

Table 5.7 Summary of all JHOC-5 ARID1A CRISPR knockout cells and mutation types

<b>JHOC-5 ARID1A KO clone</b>	<b>sgRNA target</b>	<b>ARID1A mutation</b>	<b>cDNA change</b>	<b>ICE KO Score</b>
JAE1AC6; JAE1AC9; JAE1AD10; JAE1AE4; JAE1AE2; JAE1AF6; JAE1AF7; JAE1AG10; JAE1AF3	EXON1	N/A	N/A	N/A
JAE2AC4; JAE2AD8; JAE2AE2; JAE2AE7; JAE2AF10; JAE2BB11; JAE2BC6; JAE2BD2; JAE2BD11; JAE2BE5; JAE2BE10; JAE2BF2; JAE2BF9; JAE2BF10	EXON2	p.Q428Qfs*194	c.1282insA	96 to 98
JAE2AC9		p.Q428Qfs*194 p.P427P fs*1858	c.1282insA c.1280delGCA	77
JAE2AF7		p.Q428Qfs*194 p.P427Pfs*1858	c.1282insA c.1280delGCA	95
JAE2BG10		p.Q428Qfs*194 p.Q428Pfs*193	c.1282insA c.1282delAG	95
JAE2BB4		Heterozygous	Heterozygous	88
JAE2BE7		Heterozygous	Heterozygous	52
JAE2AD10		Heterozygous	Heterozygous	9

N/A: sequencing data could not be determined for this clone.

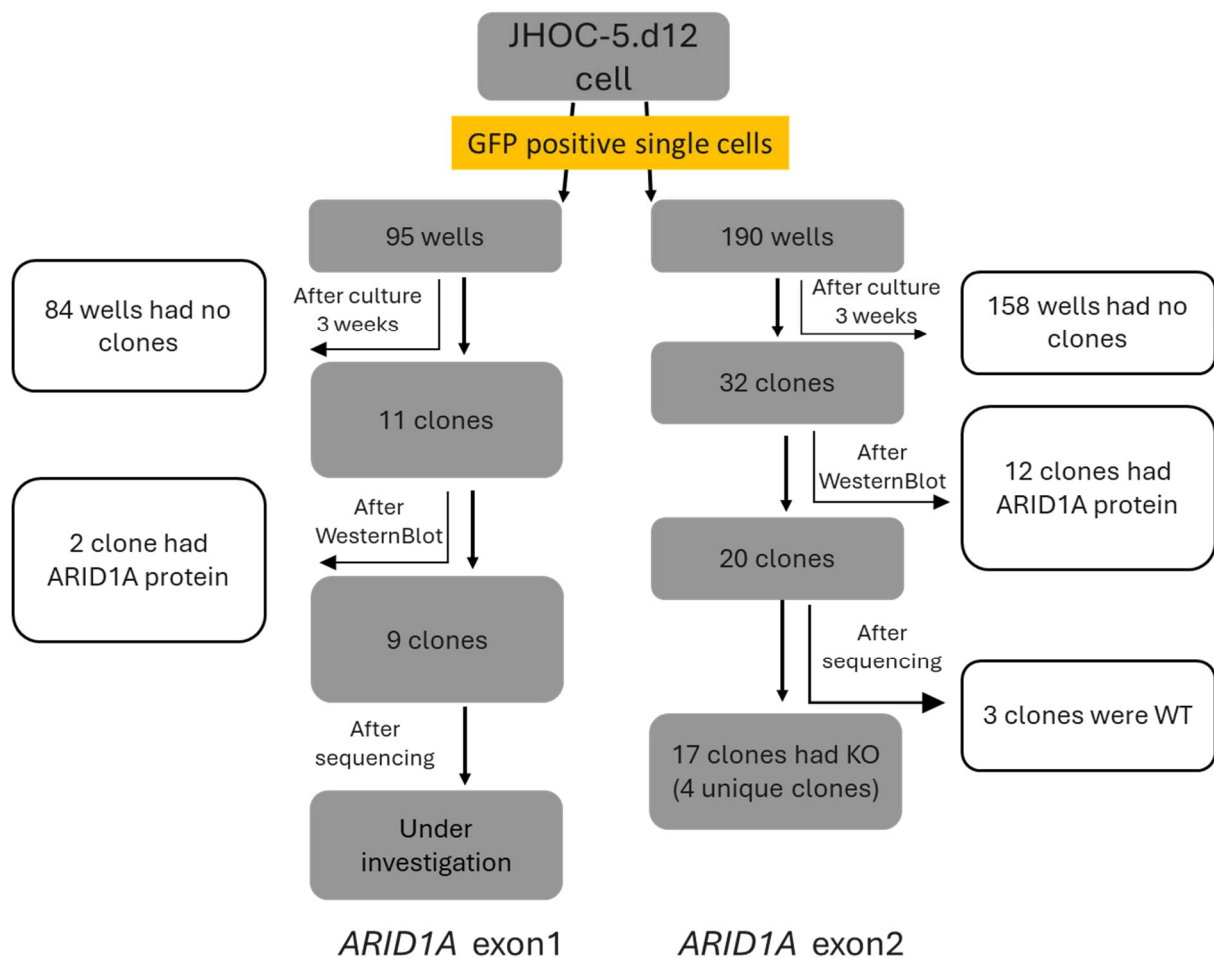


Figure 5.19 Flow diagram summarising inclusion and exclusion criteria for CRISPR-Cas9 KO of ARID1A in the JHOC-5.d12 cell cohort. Single cells were flow sorted into 95 wells for exon 1 and 190 wells for exon 2. Cells were cultured for 3 weeks and ARID1A protein levels were assessed by Western blot, clones with ARID1A protein were removed from the pipeline. After Sanger sequencing, some engineered changes were identical, and some clonal lines were WT for *ARID1A*. The final outcome of this CRISPR KO experiment yielded 4 unique clones with clear *ARID1A* KO in exon 2. *ARID1A* exon 1 KOs remain under investigation.

### 5.3.3 CRISPR KO of ARID1B in ARID1B WT OCCC lines RMG-I and JHOC-5

#### 5.3.3.1 Cloning of ARID1B sgRNA into CRISPR-Cas9 KO vector PX458

*ARID1A* and *ARID1B* have an overall 50% sequence homology, and amino acid sequence homology is close to 80%. Both ARID1A and ARID1B have roles in regulating the cell cycle and both are known to be mutated in OCCC. For these reasons, we decided to KO the *ARID1B*

gene in RMG-I cells for future experiments. To use CRISPR to KO the *ARID1B* gene, PX458 has again been used as the vector into which *ARID1B* sgRNA was cloned. The results show that sgRNA of *ARID1B* was successfully cloned into PX458 as the sgRNA region aligned perfectly with the sequencing results (Figure 5.20).

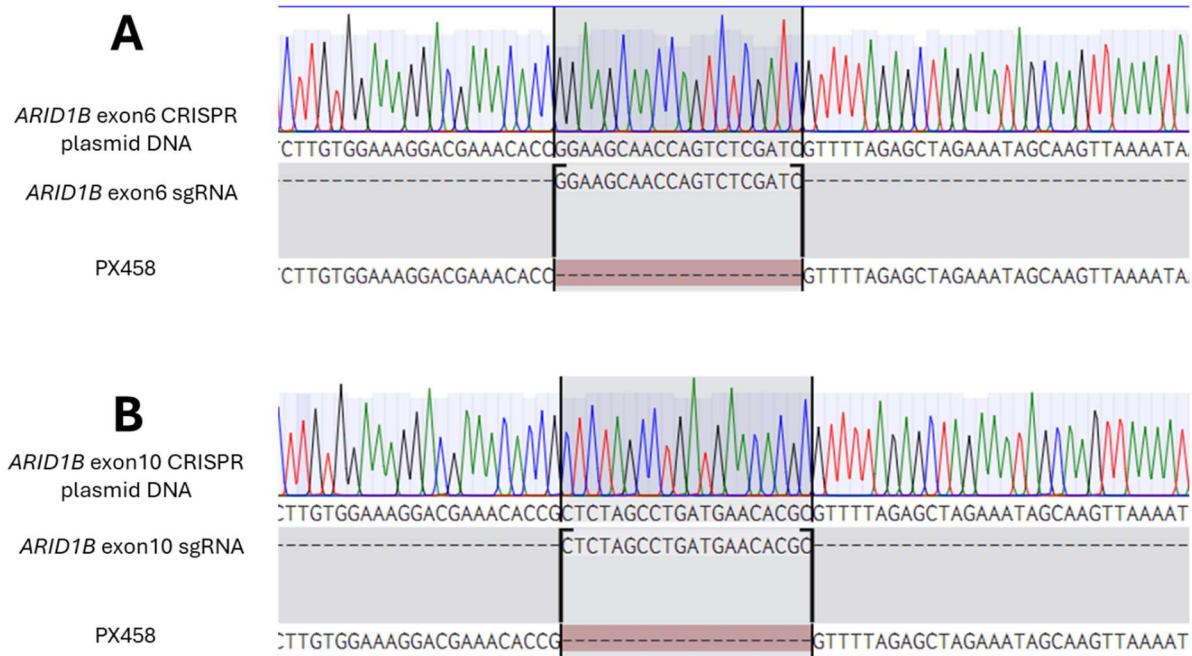


Figure 5.20 Sanger sequencing validated that sgRNA targeting A) *ARID1B* exon 6, and B) *ARID1B* exon 10, were successfully cloned into PX458. Sequences were analysed using Benchling.

### 5.3.3.2 Creation of ARID1B KO cells in RMG-I.b4 clonal cells

#### 5.3.3.2.1 ARID1B plasmid transfection and GFP single cell sorting in RMG-I.b4

Previous transfection efficiency in RMG-I.b4 cells with lipofectamine 3000 transfection reagent and ARID1A KO PX458 plasmid was very low, at less than 1% of cells expressing GFP (Figure 5.11), so it was preferable to optimise the transfection efficiency of plasmid DNA transfected into RMG-I cells for CRISPR studies. Therefore, we used another transfection reagent, X-tremeGENE HP with a ratio of 1:3 (DNA: transfection reagent) and *ARID1B* exon 6 CRISPR KO plasmid DNA to compare the transfection efficiency of Lipofectamine 3000. After 48 hours, the results showed that the number of GFP positive cells increased steadily over time for X-tremeGENE HP, with only a very low number of GFP positive cells resulting from transfection with Lipofectamine3000. X-tremeGENE HP not only showed a higher



transfection efficiency than lipofectamine 3000 but was also much less cytotoxic to the cells (Figure 5.21). Due to X-tremeGENE HP having a higher transfection efficiency in RMG-I cells, we used this transfection reagent for future RMG-I CRISPR experiments.

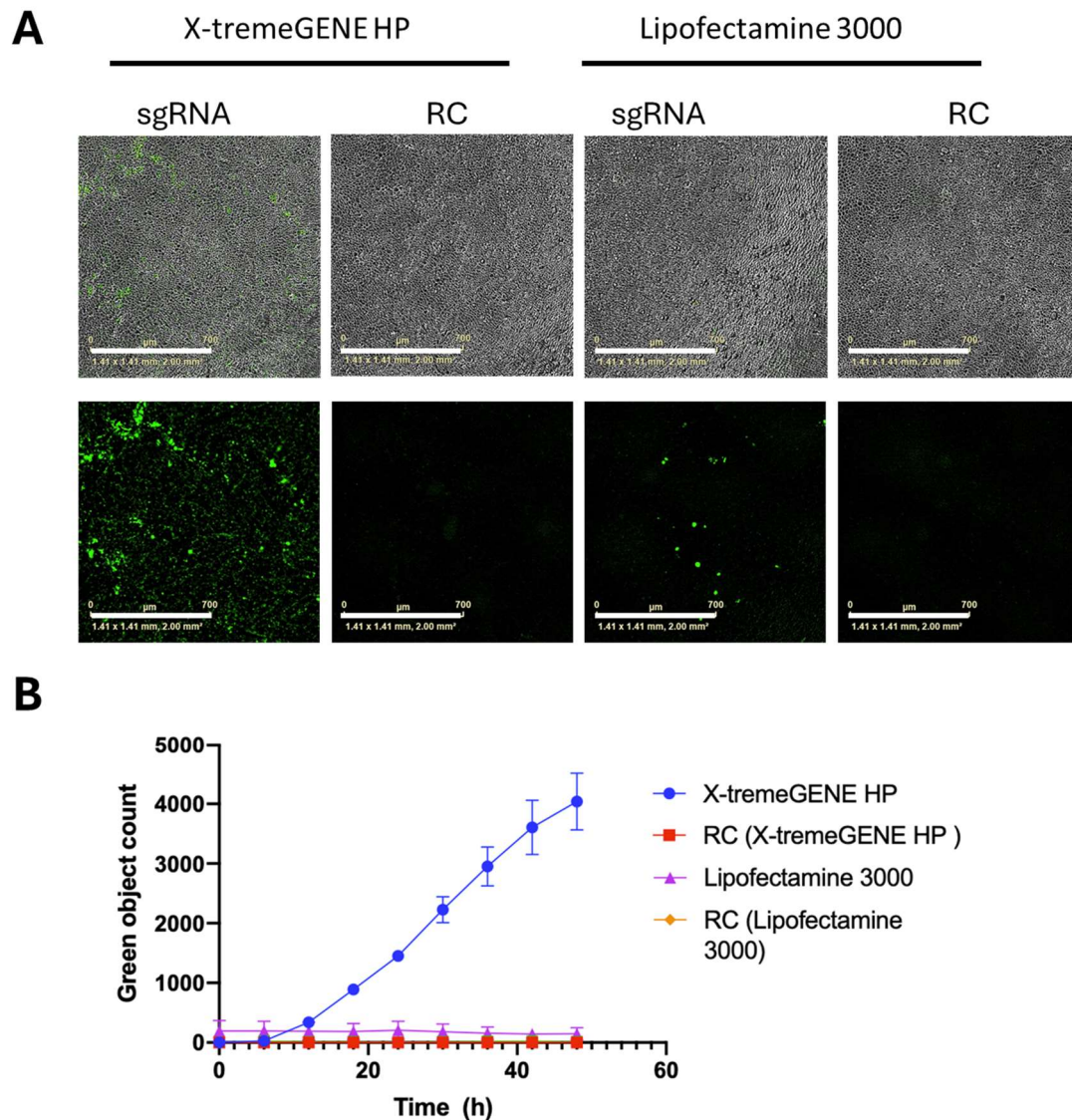


Figure 5.21 Transfection comparison between lipofectamine 3000 and X-tremeGENE HP in RMG-I.b4 cells transfected with the CRISPR-Cas9 KO plasmid targeting *ARID1B* exon 6. A) Phase contrast/GFP (upper panel) and GFP only cell images (lower panel) of Lipofectamine 3000 and X-tremeGENE HP and RC 48 hours after transfection. Scale bar=1mm. B) Green objective count analysed by the IncuCyte S3 analysis software. N=1, graphs represent mean  $\pm$  SEM for 9 technical replicates. RC: Reagent control.

The *ARID1B* CRISPR-Cas9 KO plasmids containing *ARID1B* sgRNA targeting exon 6 or exon 10 were transfected into RMG-I.b4 cells using X-tremeGENE HP. The results showed that GFP was expressed in cells containing plasmid DNA and no expression was observed in cells without plasmid DNA (Figure 5.22).

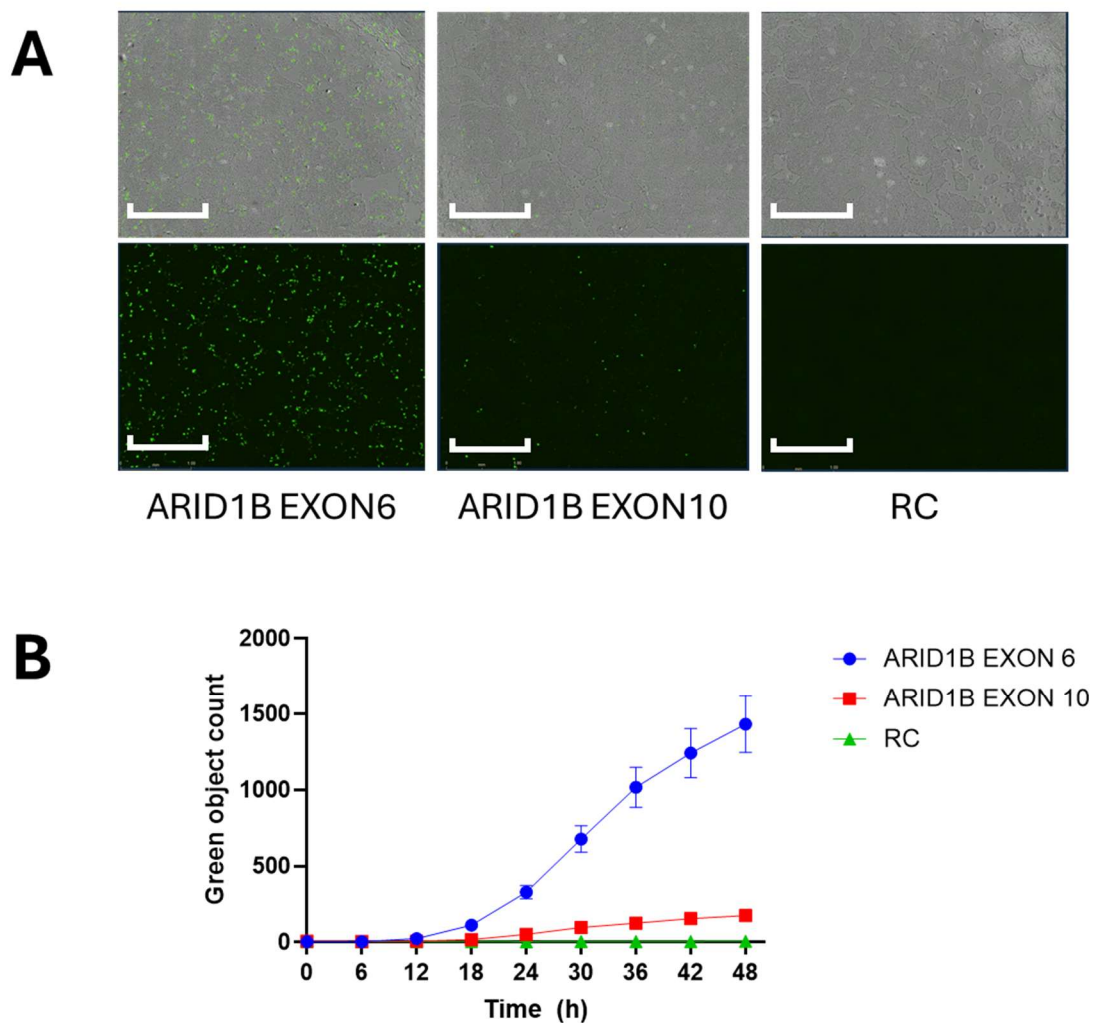


Figure 5.22 Transfection of RMG-I.b4 clonal cells with CRISPR-Cas9 KO vectors targeting *ARID1B* using X-tremeGENE HP reagent for 48 hours. A) Phase contrast/GFP (upper panel) and GFP only cell images (lower panel) of X-tremeGENE HP transfected cells. Reagent Control (RC) and both CRISPR-Cas9 vectors targeting *ARID1B* were transfected with X-tremeGENE HP at a ratio of 1:3 (mg DNA to ml transfection reagent). Scale bar = 1mm. B) Green objective count as analysed by the IncuCyte S3 analysis software. N=1, graphs represent mean  $\pm$  SEM for 9 technical replicates.



After 48 hours transfection, single cell sorting was used to sort RMG-I.b4 transfected with the ARID1B CRISPR KO plasmid based on GFP expression. As with *ARID1A*, GFP-positive cells transfected from both exon targets were sorted into two 96-well plates each. The flow cytometry results showed that 2.07% of the cell population were successfully transfected with the ARID1B exon 6 KO plasmid, while efficiency for the ARID1B exon 10 KO plasmid was only 0.48% (Figure 5.23).

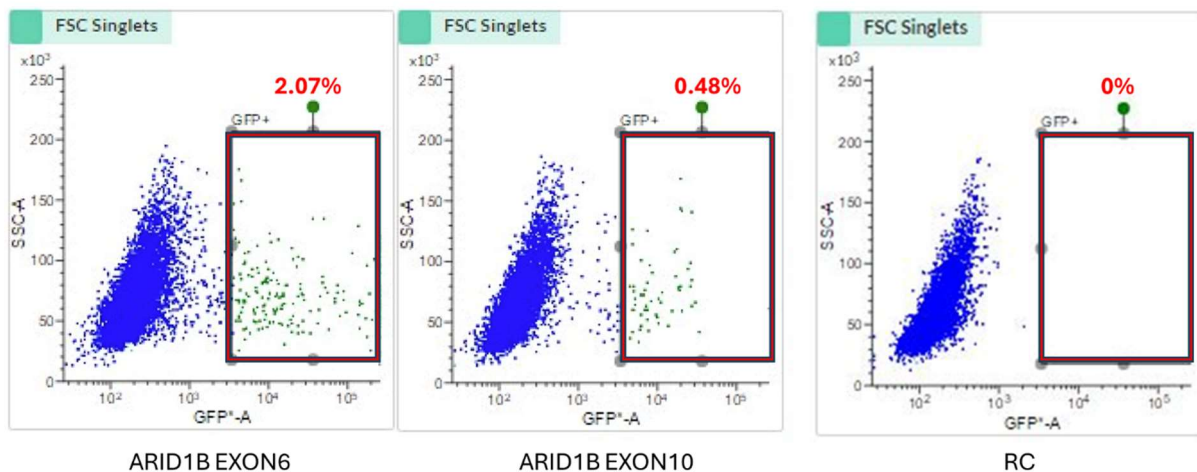


Figure 5.23 Flow cytometry analysis of RMG-I.b4 clonal cells transfected with *ARID1B* CRISPR-Cas9 KO plasmid DNA (targeting exon 6 or exon 10) or reagent control (RC). Single cells were gated based on GFP intensity and side scatter (blue population). The percentage of cells with GFP expression are illustrated in the red box.

#### 5.3.3.2.2 CRISPR KO of ARID1B in RMG-I ARID1A KO cells

*ARID1B* and *ARID1A* show 50% sequence homology overall and have been reported to have opposing functions in cell cycle arrest<sup>319</sup>. Also, they are mutually exclusive because a single SWI/SNF chromatin remodelling complex can contain either ARID1A or ARID1B<sup>333</sup>. Therefore, the loss of ARID1A and ARID1B affects assembly of the SWI/SNF complex, thus affecting cell stability and cell proliferation. In fact, complete loss of both ARID1A and ARID1B has been reported to be synthetic lethal<sup>333</sup>. To explore this likelihood of synthetic lethality, we attempted to transfect a CRISPR-Cas9 KO vector targeting ARID1B into the RMG-I *ARID1A* KO cell line RAE1AB5 using the transfection agent X-tremeGENE HP. The

results showed that GFP was expressed in cells containing plasmid DNA and no expression was observed in cells without plasmid DNA (Figure 5.24 and 5.25).

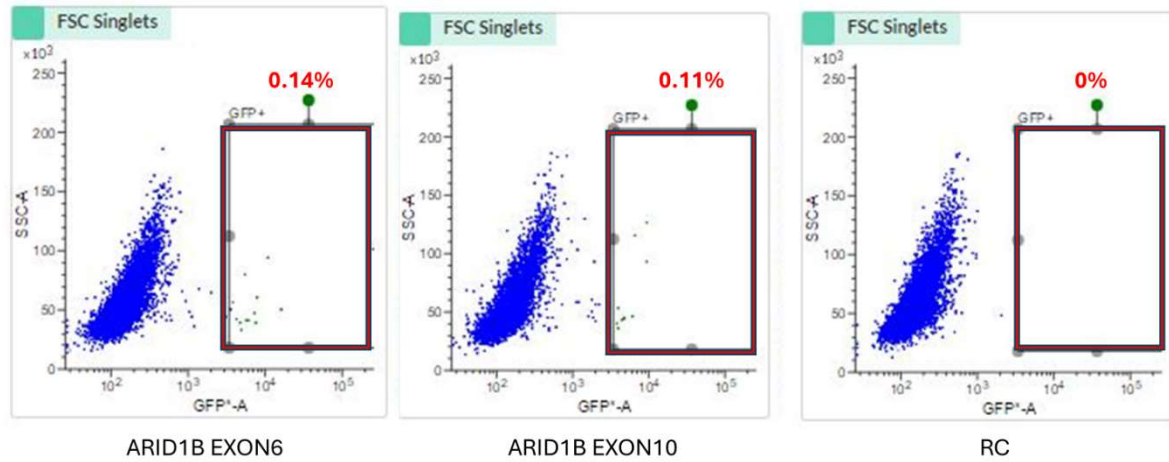


Figure 5.24 Flow cytometry analysis of the RMG-I *ARID1A* KO cell line RAE1AB5 transfected with RC and a CRISPR-Cas9 vector targeting *ARID1B*. Single cells were gated based on GFP intensity and side scatter (blue population). Percentage of cells with GFP expression are illustrated in the red box. RC: Reagent control.

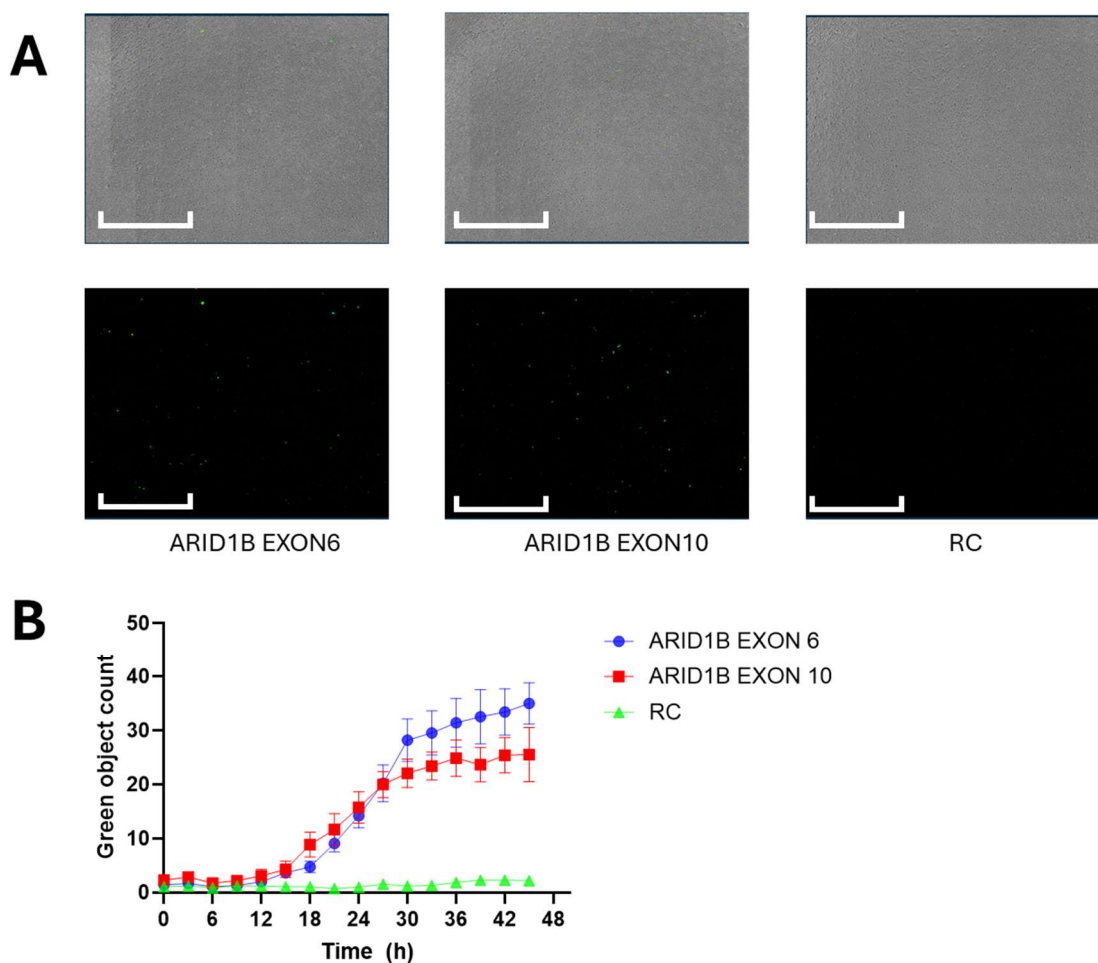


Figure 5.25 Transfection of the RMG-I *ARID1A* KO cell line RAE1AB5 with a CRISPR-Cas9 vector targeting *ARID1B* using X-tremeGENE HP reagent for 24 hours. A) Phase contrast/GFP (upper panel) and GFP only cell images (lower panel) are shown. The ratio of plasmid DNA (mg) to transfection reagent (ml) was 1:3. Scale bar = 1.3mm. B) Green objective count as analysed by the IncuCyte S3 analysis software. N=1, graphs represent mean  $\pm$  SEM for 9 technical replicates. RC: Reagent control.

### 5.3.3.2.3 Validation of ARID1B KO clones in RMG-I.b4 cells and ARID1B/ARID1A KO clones in RAE1AB5 cells

Of the 380 wells seeded for single cells post transfection, only 12 clones (3.16%) grew. In the RC, 34 clones (36%) were observed in 95 wells sorted as single cells. For all 12 putative ARID1B KO clones, gDNA was extracted and the edited regions amplified by PCR. PCR products were sequenced by Sanger sequencing and the results analysed using Benchling. Analysis showed that the *ARID1B* target sequence was altered in 3 of the 8 clones where

*ARID1B* exon 6 was targeted for KO. Of the 4 exon 2 engineered clones, 3 were altered (Figure 5.26).

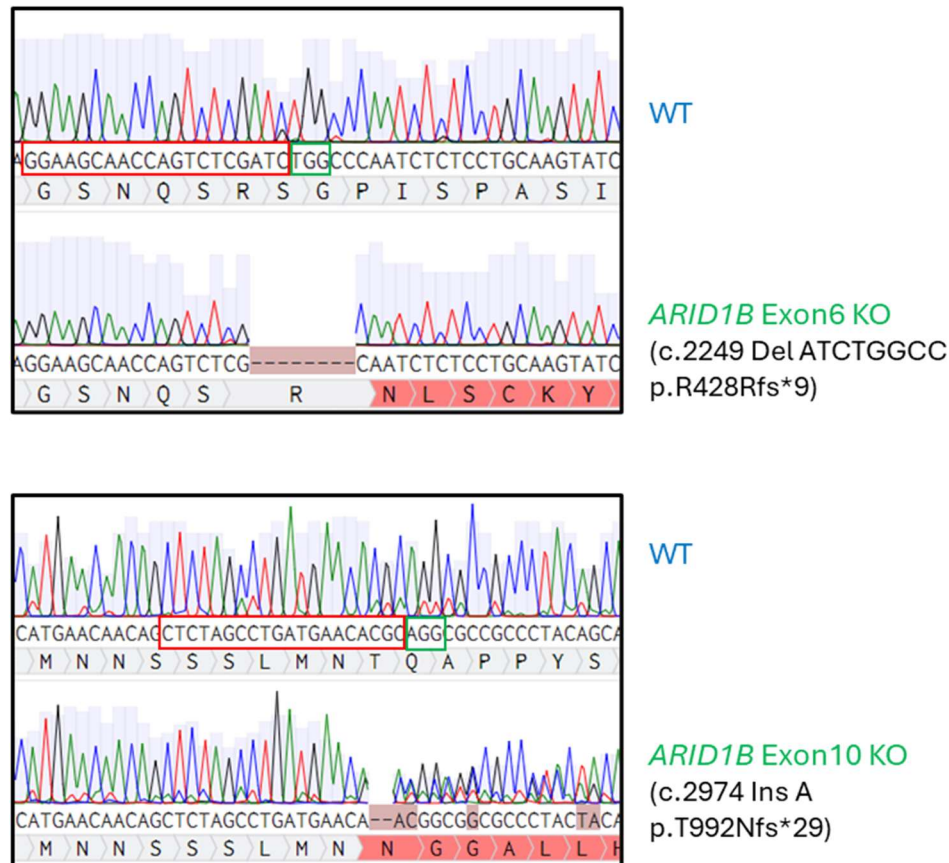


Figure 5.26 Alignment of Sanger sequencing of RMG-I CRISPR KO *ARID1B* Exon6 (RBE6AB6) and Exon10 (RBE10BF3) clones in Benchling. *ARID1B* Exon6 KO (upper panel) and *ARID1B* Exon10 KO (lower panel) were aligned with WT sequence. The sgRNA target sequence is highlighted in red box, and the PAM are noted in green box.

An attempt to KO *ARID1B* in RMG-I *ARID1A* KO (RAE1AB5) cells showed that of the 380 wells seeded for single cells post transfection, only 5 clones (1.31%) grew. However, in the RC, 30 clones (32%) were observed in 95-wells seeded for single cells post transfection. For all 5 putative *ARID1A* and *ARID1B* double KOs (DKs), gDNA was extracted and underwent Sanger sequencing after amplifying the edited regions using PCR. The results showed that only one clone in exon 6 was partially altered (heterozygous) for *ARID1B*, and all of the exon 10 clones were WT (Figure 5.27). The heterozygous clone was used for further studies.

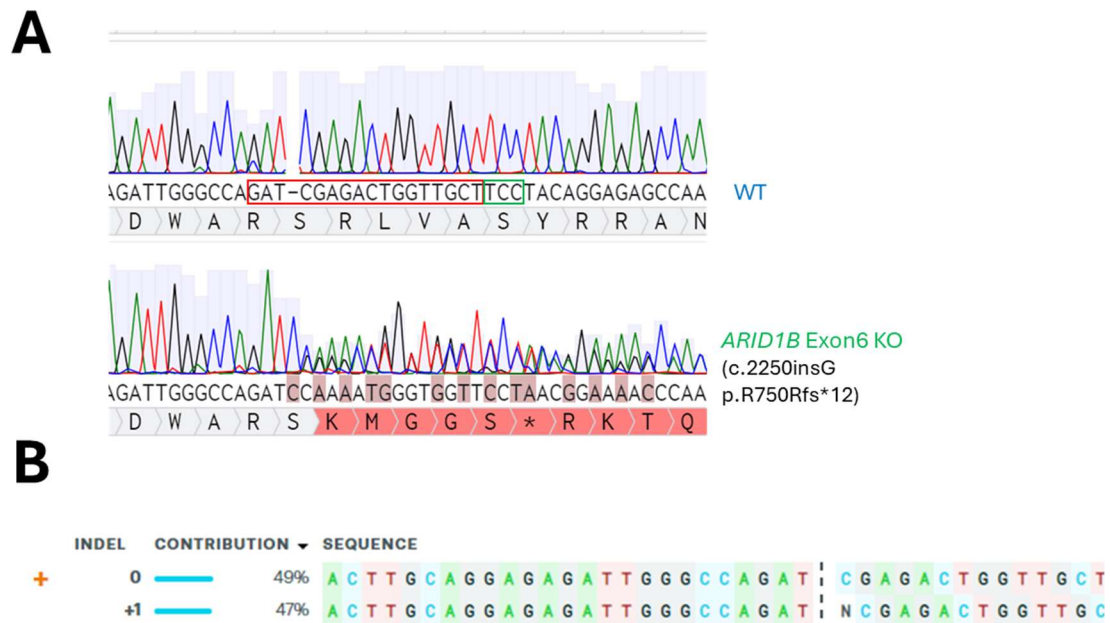


Figure 5.27 Analysis of Sanger sequencing of *ARID1B* in ARID1A KO cells (RDKBE6AB5). A) Alignment of Sanger sequencing of *ARID1B* in ARID1A KO cells in Benchling. The sgRNA target sequence is highlighted in red box, and the PAM are noted in green box. B) Partial editing of *ARID1B* in ARID1A KO cells, resulting in 49% WT sequence and 47% with a 1 bp insertion (p.R750Rfs\*12, c.2250insG).

Following Sanger sequencing, ARID1B protein expression was detected using Western blotting. The results demonstrated that in experiments designed to KO ARID1B in ARID1A WT RMG-I cells, 2 of the 6 KO clonal lines had no ARID1B protein. In experiments designed to KO ARID1B in ARID1A mutant RMG-I cells, the single clone with a mutation in *ARID1B* still had ARID1B protein (Figure 5.28). We noted that ARID1B in RMG-I, RMG-I.b4, and some KO clones displayed a doublet band, and that the exon6 AG8 clone exhibited a smaller truncated band. A summary of the attempt to KO ARID1B in the RMG-I cell line, as well as in RMG-I *ARID1A* KO cells is presented (Figures 5.29 and 5.30).

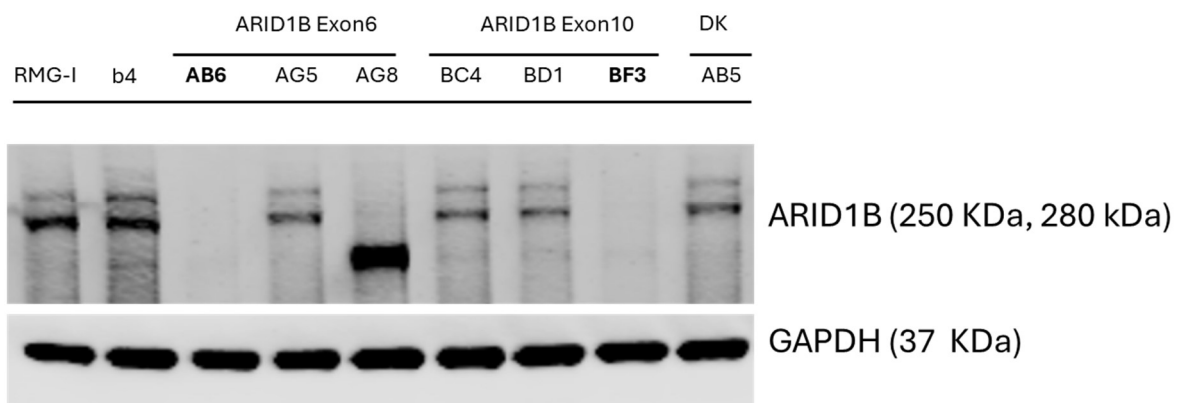


Figure 5.28 Protein expression of ARID1B in cells that had undergone attempts to KO this protein. Whole cell protein lysate was quantitated and analysed via Western blotting. The protein loading control is GAPDH. ARID1B protein was detected in both RMG-I and the clonal line RMG-I.b4 . For each *ARID1B* exon targeted, there was one sample that had no ARID1B protein. These ARID1B KO clonal lines are highlighted in bold. ARID1B protein was present in the ARID1A complete KO cells where the attempt was made to knockout ARID1B (DK).

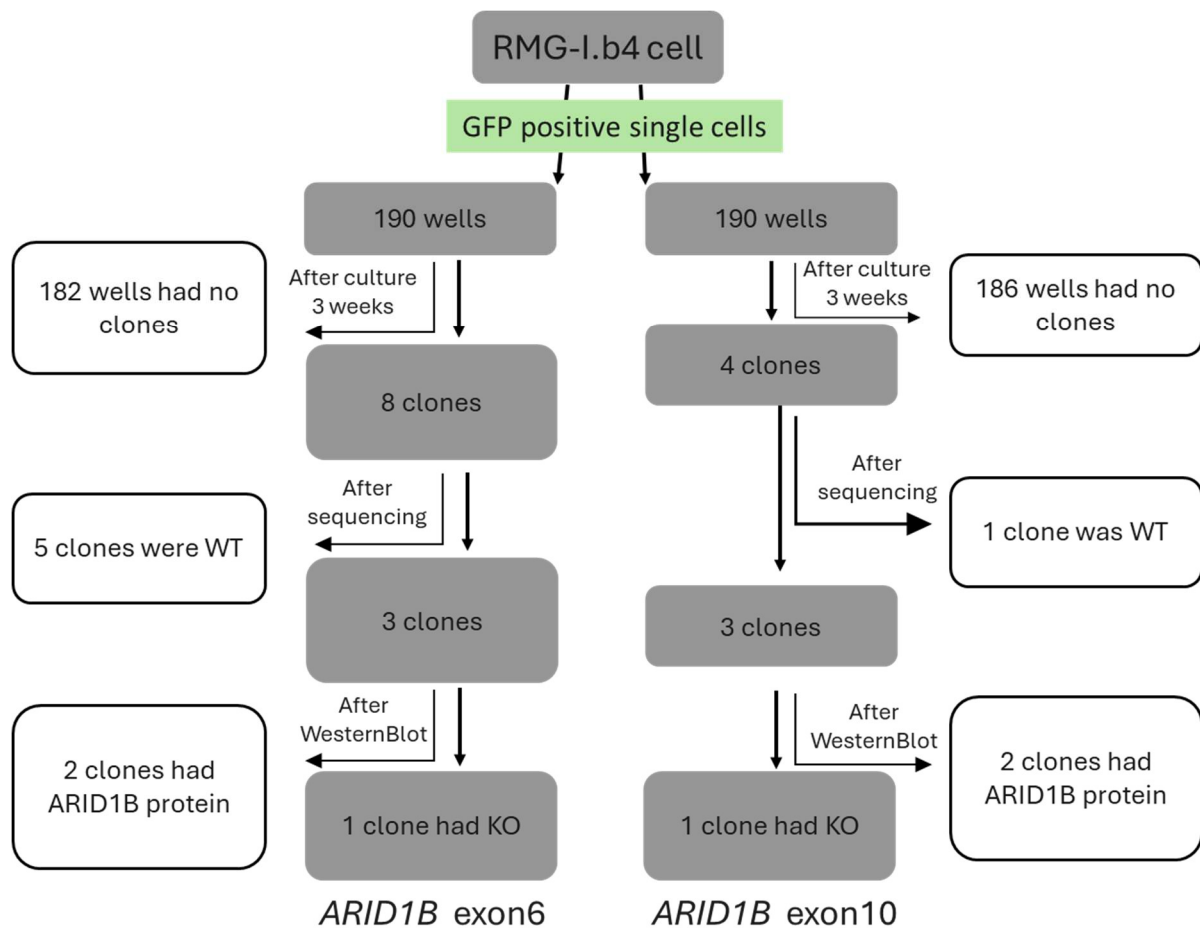


Figure 5.29 Flow diagram summarising inclusion and exclusion criteria for the RMG-I.b4 ARID1B CRISPR KO cell cohort. Single cells were flow sorted into 190 wells for each targeted exon. Cells were cultured for 3 weeks and underwent sequencing for *ARID1B*. Clones with an aberration in *ARID1B* were investigated for ARID1B protein levels. In some clones with mutations detected, ARID1B protein was present, due to in-frame deletions. The outcome of this CRISPR KO experiment yielded two ARID1B KO clonal lines, one targeting exon 6 and one targeting exon 10.



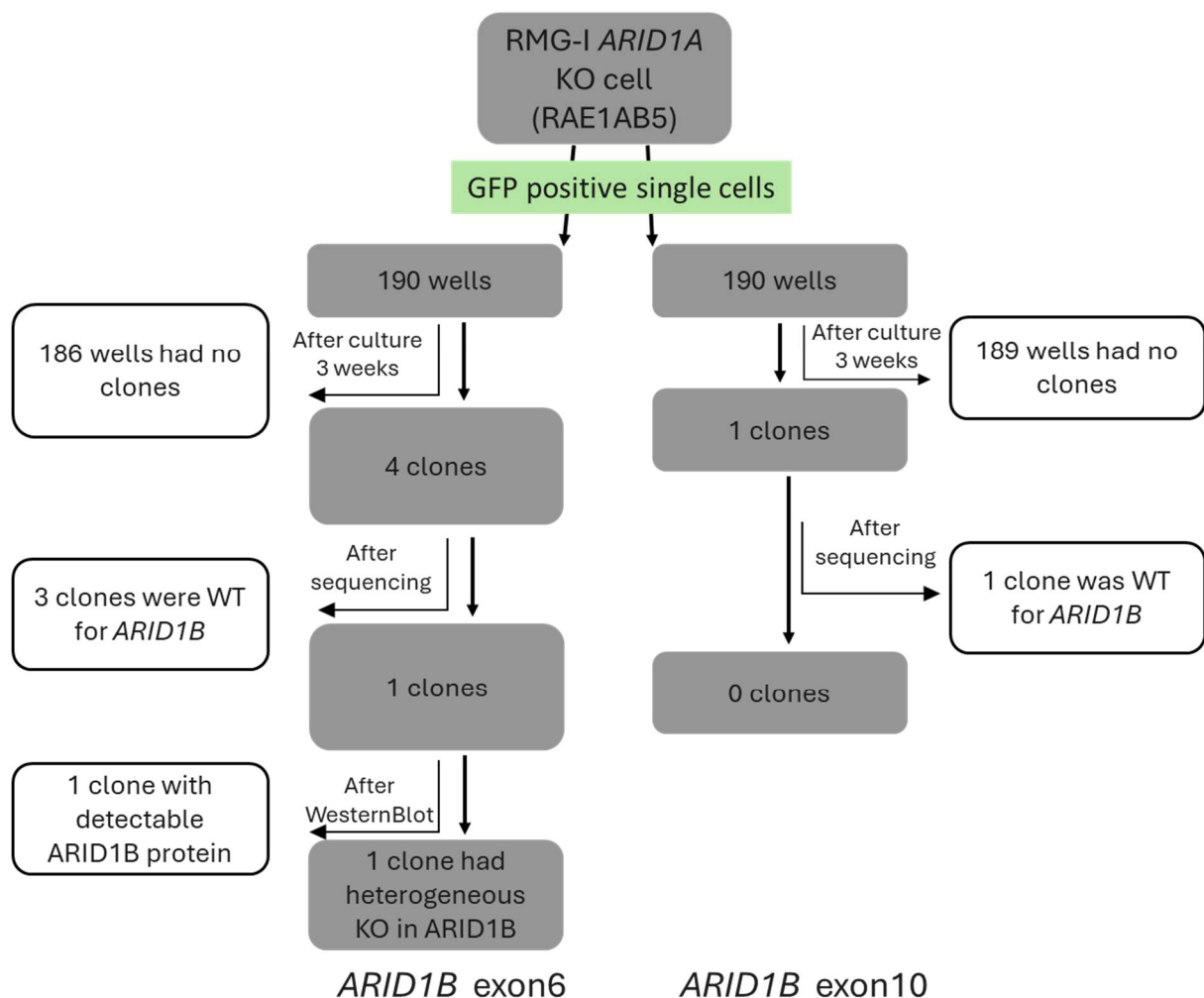


Figure 5.30 Flow diagram summarising inclusion and exclusion criteria for identifying *ARID1B* CRISPR KO in a previously validated *ARID1A* KO RMG-I.b4 clone RAE1AB5 to attempt to isolate a double KO (DK) of both *ARID1A* and *ARID1B* in a single cell line. Single cells were flow sorted into 190 wells for each targeted exon. Cells were cultured for 3 weeks and underwent sequencing for *ARID1B*. After removal of cells that were WT for *ARID1B* from the pipeline, a single clonal cell line was identified that had complete *ARID1A* KO and a heterozygous KO of *ARID1B*.

### 5.3.3.3 Creation of *ARID1B* KO cells in JHOC5-D12 clonal cells

#### 5.3.3.3.1 CRISPR KO of *ARID1B* in JHOC-5 clonal cells

Following the KO of *ARID1A* in JHOC-5 cells, CRISPR was employed to KO *ARID1B* in JHOC-5. Two different *ARID1B* exons were targeted for CRISPR KO. Plasmid DNA was transfected into JHOC-5.d12 cells using the Lipofectamine LTX reagent. The IncuCyte images



demonstrated that cells containing plasmid DNA expressed GFP, while cells without plasmid DNA did not. Furthermore, flow cytometry results demonstrated that 1.08% of the cell population expressed GFP post transfection in cell lines where exon 6 was targeted, while 1.27% of cells expressed GFP in cell lines where exon 10 was targeted (Figure 5.31 and Figure 5.32).

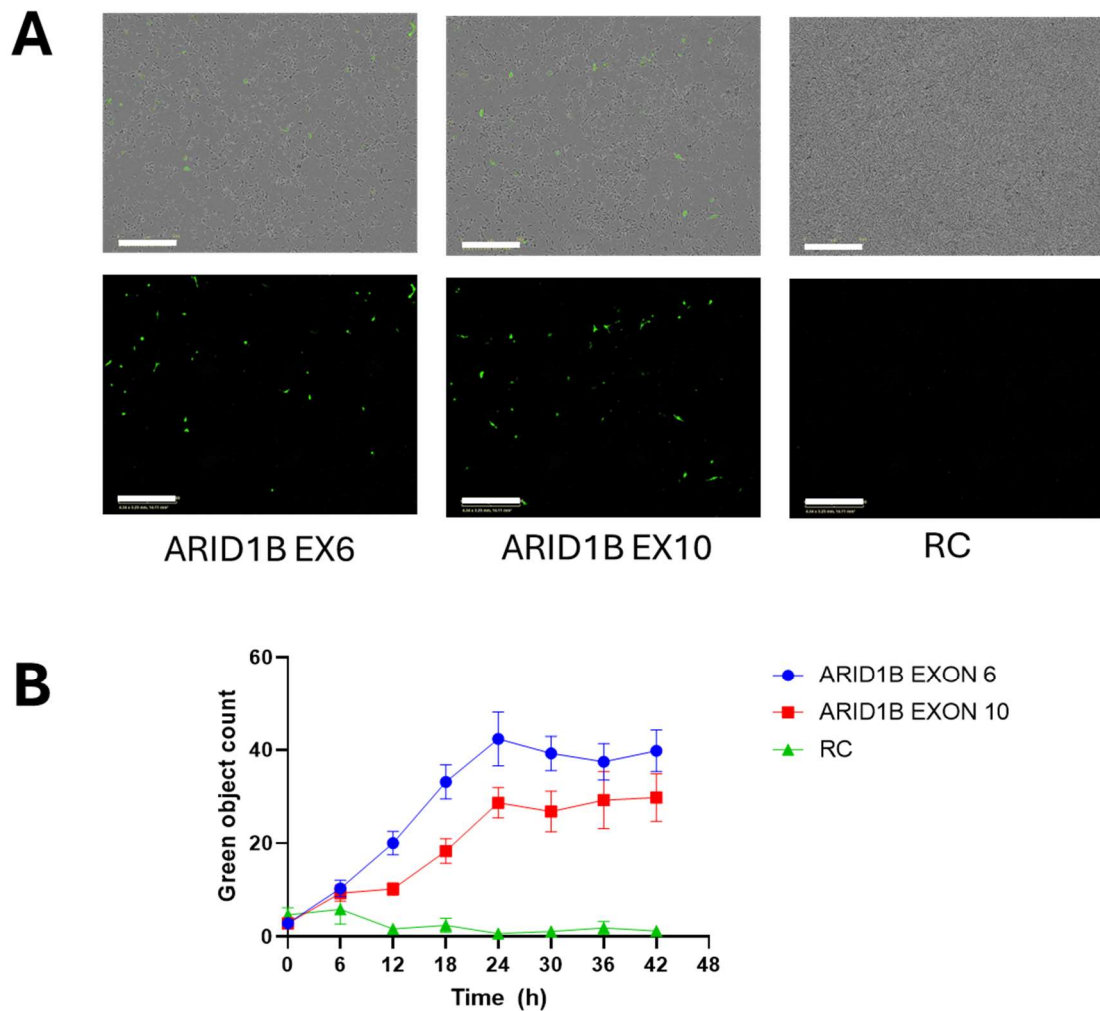


Figure 5.31 Transfection of the JHOC-5.d12 clonal cell line with CRISPR KO plasmids targeting *ARID1B* exons 6 and 10. Plasmid DNA was transfected using lipofectamine LTX reagent for 48 hours and flow cytometry analysis was performed. A) Phase contrast/GFP (upper panel) and GFP only cell images (lower panel) are shown. The ratio of plasmid DNA (mg) to transfection reagent (ml) was 1:3. Scale bar=800μm. B) Single cells were gated based on GFP intensity and side scatter (blue population). Percentage of cells with GFP expression are illustrated in the red box. RC: Reagent control.

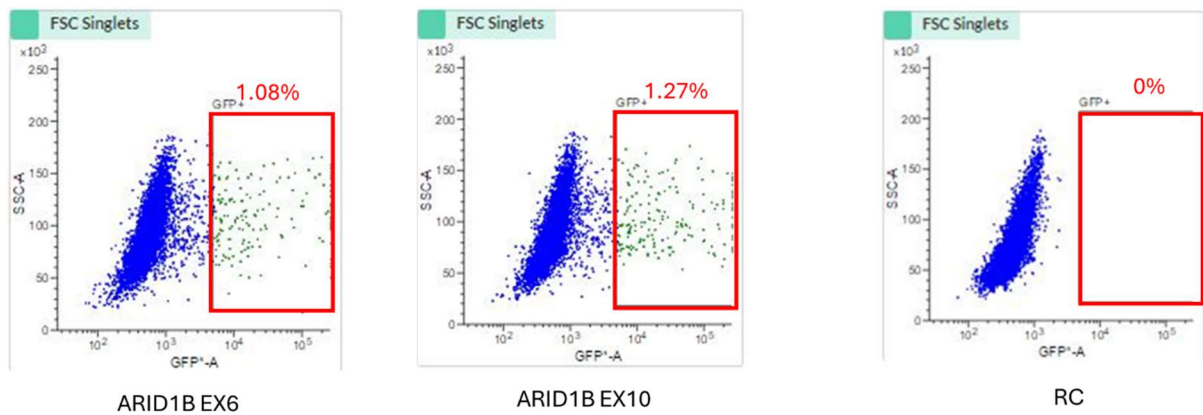


Figure 5.32 Flow cytometry analysis of the JHOC-5.d12 transfected with RC and a CRISPR-Cas9 vector targeting *ARID1B*. Single cells were gated based on GFP intensity and side scatter (blue population). Percentage of cells with GFP expression are illustrated in the red box. RC: Reagent control.

#### 5.3.3.3.2 Validation of ARID1B KO clones in JHOC-5.d12 cell background

After a three-week period of screening and culturing, cell growth was observed in a total of 37 (9.8%) out of 380 wells. Following the examination of target protein levels using Western blotting, the results indicated that 5 (29%) out of seventeen clonal lines where exon 6 was targeted displayed no ARID1B protein, while 9 (45%) out of twenty clonal cell lines where exon 10 was targeted exhibited no ARID1B protein (Figure 5.33).

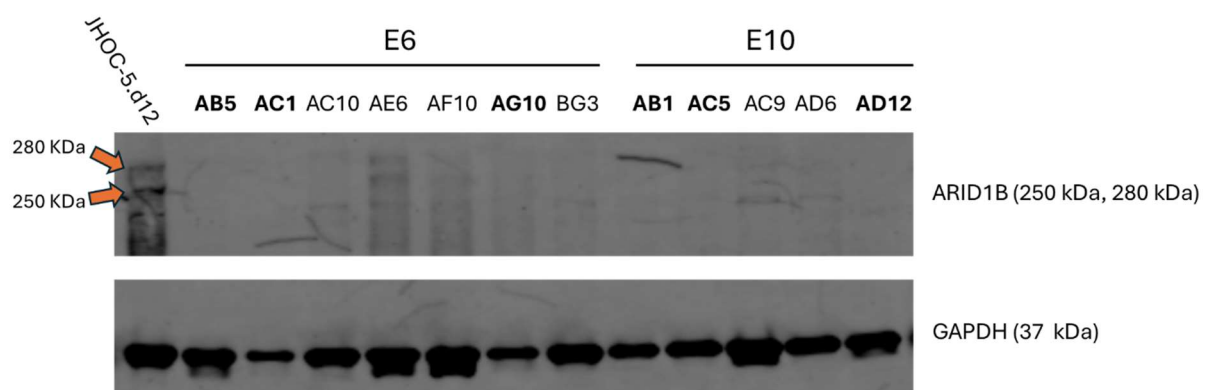


Figure 5.33 Representative protein levels of ARID1B CRISPR KO cells. Whole cell protein lysate was quantitated and analysed via Western blotting. The protein loading control is GAPDH. JHOC-5.d12 cells displayed ARID1B protein. In seven cell lines where exon 6 was targeted and five cell lines where exon 10 was targeted, 6 samples had no ARID1B protein (highlighted in bold).

Sanger sequencing was performed on five clones where exon 6 was targeted and nine clones where exon 10 was targeted. Three exon 6 clones and all exon 10 clones exhibited complete KO with multiple changes. It was not feasible to present the results of Sanger sequencing using Benchling, as there was an excess of types of change. Consequently, only the results analysed by the ICE program are displayed (Figure 5.34 and Table 5.8). A summary is presented in the accompanying flowchart (Figure 5.35).

**A**



**B**

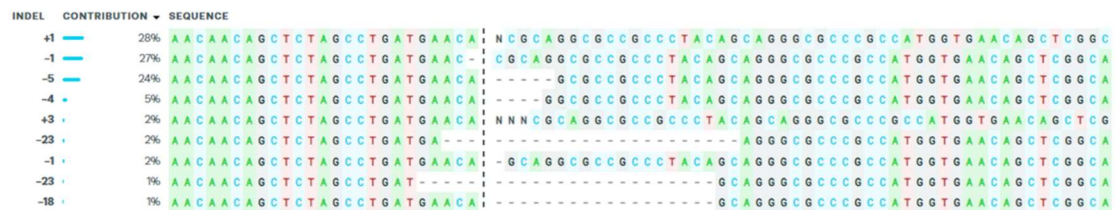


Figure 5.34 Representative analysis of Sanger sequencing of JHOC-5 CRISPR KO cell lines targeting *ARID1B* Exon6 and Exon10, visualised using the ICE CRISPR Analysis Tool. A) *ARID1B* Exon6 KO (JBE6BB8) and B) *ARID1B* Exon10 KO (JBE10AH3).

Table 5.8 Summary of all JHOC-5 ARID1B CRISPR KO cells and mutation types

<b>JHOC-5 ARID1B KO clone</b>	<b>sgRNA target</b>	<b>Main ARID1B mutations in sgRNA target site ^</b>	<b>ICE KO Score</b>
JBE6BB8	EXON1	Ins1, Del 2	68
JBE6BB9		Del 8, Ins 2, Del 22	73
JBE6AC1		Del 1, Ins 1	71
JBE10AG6	EXON2	Not determined	50
JBE10AH3		Ins 1, Del 1, Del 5	89
JBE10AC5		Ins 1, Del 28	90
JBE10BG11		Ins 1	87
JBE10AD12		Ins 1	82
JBE10AE4		Ins 1	87
JBE10BF2		Ins 1	87
JBE10AB1		Ins 1	88
JBE10AE9		Del 7, Ins 1	84

^ Multiple changes were observed in each clone, so only reported the main ARID1B mutations in sgRNA target site.

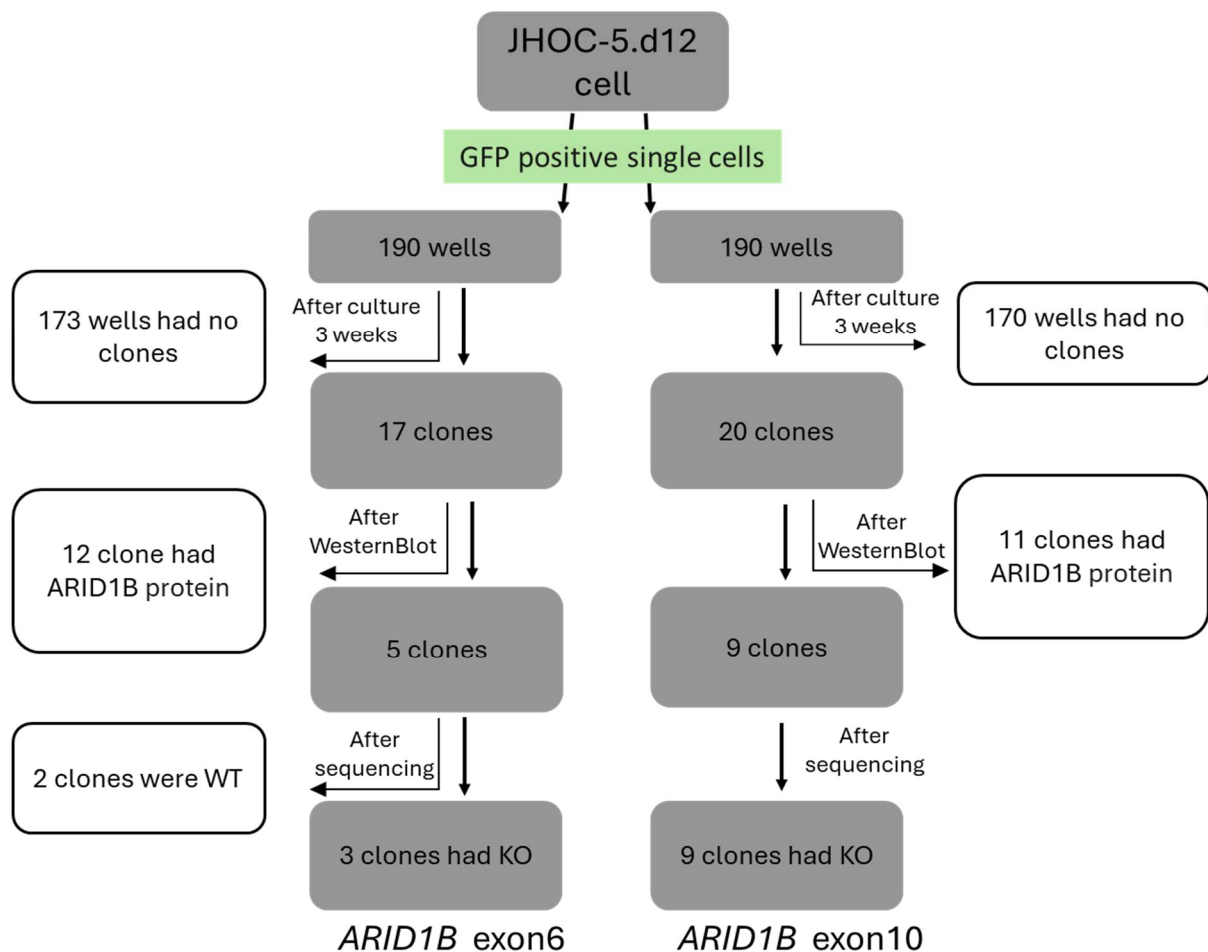


Figure 5.35 Flow diagram summarising inclusion and exclusion criteria for CRISPR-Cas9 KO of ARID1B in the JHOC-5.d12 clonal cell line. Single cells were flow sorted into 190 wells for each exon. Cells were cultured for 3 weeks and ARID1B protein levels were assessed using Western blot. In both exons 6 and 10, 14 engineered variants showed no ARID1B protein, and the remaining 23 samples retained ARID1B protein. After Sanger sequencing, some changes were identical, and some still expressed WT *ARID1B*. The outcome of this CRISPR KO experiment yielded 3 clones with clear ARID1B KO resulting from engineered sequence changes in exon 6, and 9 clones with clear ARID1B KO resulting from engineered sequence changes in exon 10.

#### 5.3.4 Characterising ARID1A and ARID1B KO isogenic CRISPR-Cas9 KO clonal lines made in RMG-I.b4 and JHOC-5.d12 cell backgrounds

##### 5.3.4.1 Determining RNA levels of ARID1A and ARID1B in the ARID1A isogenic RMG-I.b4 panel

Firstly, in order to ascertain the mRNA expression level of *ARID1A* in the RMG-I CRISPR clonal line, we conducted an analysis of the RNA extracted from the RMG-I.b4 clone and the 6 representative RMG-I *ARID1A* CRISPR KO clones using qRT-PCR. The results demonstrated that, with the exception of RAE1AF8, the mRNA expression level of *ARID1A* in the majority of clones was lower than in the RMG-I.b4 clone, although this was not statistically significant (Figure 5.36).

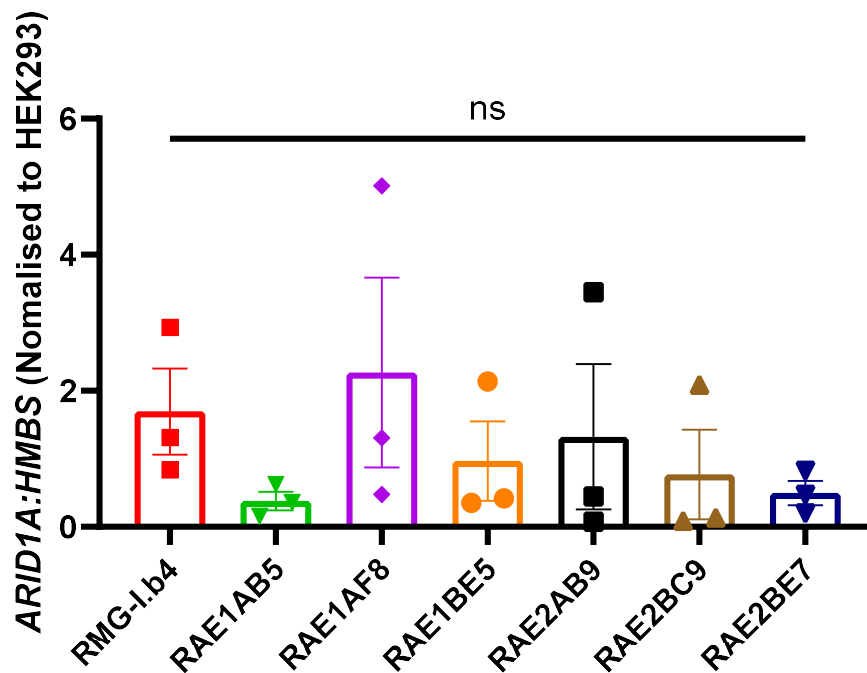


Figure 5.36 *ARID1A* mRNA expression levels for RMG-I CRISPR KO cell lines. Graph of mRNA levels of *ARID1A* in RMG-I CRISPR KO cell lines relative to *HMBS* and normalised to HEK293. A one-way ANOVA and *post-hoc* Tukey's test was performed to determine statistical significance. Data is shown as the mean  $\pm$  SEM, N=3. ns, not significant.

Then, the *ARID1B* mRNA expression levels of the RMG-I.b4 clone, two RMG-I *ARID1B* CRISPR KO clones (RBE6AB6 and RBE10BF3), and the RMG-I double KO clone (*ARID1A* KO/*ARID1B* heterozygous KO) RBDKE6AB5 were analysed using qRT-PCR. The results demonstrated that the *ARID1B* mRNA expression levels of the two RMG-I *ARID1B* CRISPR KO clones were reduced in comparison to the RMG-I.b4 clone. However, the mRNA expression level of *ARID1B* in the RMG-I double KO was higher (Figure 5.37).

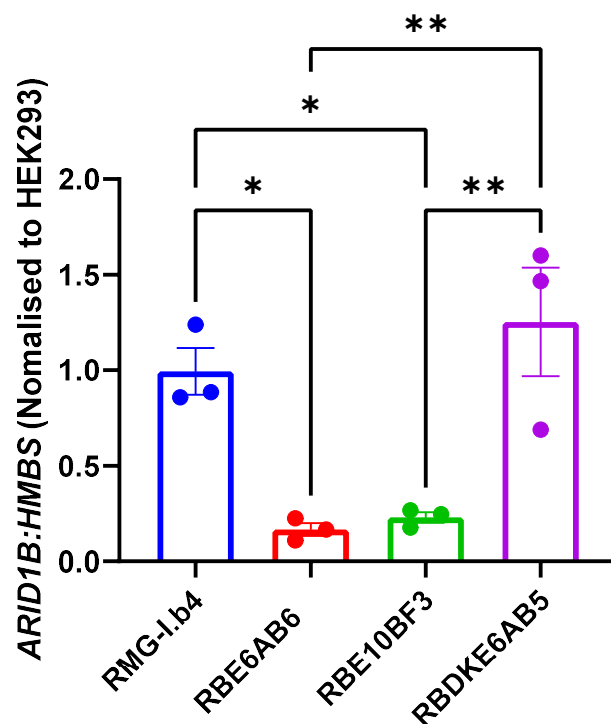


Figure 5.37 *ARID1B* mRNA expression levels for the RMG-I isogenic panel of cell lines. Graph of mRNA levels of *ARID1B* in RMG-I CRISPR engineered cells relative to *HMBS* and normalised to HEK293. A one-way ANOVA and *post-hoc* Tukey's test was performed to determine statistical significance. Data is shown as the mean  $\pm$  SEM, N=3. \*P<0.05, \*\*P<0.01.

#### 5.3.4.2 Assessing the growth rate of RMG-I CRISPR KO clones and sensitivity to cisplatin

To verify the *in vitro* growth rate of the RMG-I CRISPR clones, the RMG-I parental line, the RMG-I.b4 clonal line, 7 representative CRISPR KO clones (5 RMG-I *ARID1A* CRISPR KO clones, and 2 *ARID1B* CRISPR KO clones) were seeded at 6,000 cells per well into 96-well plates and imaged using the IncuCyte. The results demonstrated that the RMG-I, RMG-I.b4 clone, and the RAE1AF8, RAE1BE5, and RAE1AG1 cell lines maintained a comparable growth rate. In comparison, RAE1AB5 and RAE2BC9 cell line demonstrated a slight acceleration in growth to these cell lines. Conversely, RBE6AB6 and RBE10BF3 cell lines exhibited a slightly slower growth pattern over time compared to RMG-I and RMG-I.b4 clone (Figure 5.38).

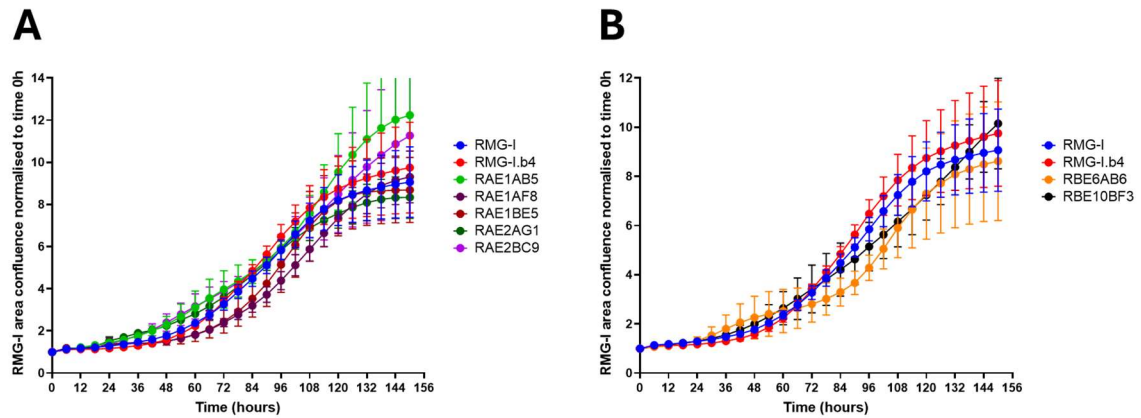


Figure 5.38 Growth rate of RMG-I parental line and CRISPR KO clonal lines. All cells were seeded into 96-well plates at 6,000 cells/well density. Cells were imaged in the IncuCyte for 150 hours. Images were captured every 6 hours and the percentage confluence recorded. There was no significant difference between RMG-I, RMG-I.b4 and CRISPR KO cell lines. Data is shown as the mean  $\pm$  SEM, N=3.

MTS assay was used to determine the IC<sub>50</sub> of cisplatin of 9 cell lines. The results demonstrated that, in comparison to RMG-I and the RMG-I.b4 clonal line, CRISPR KO clones RAE1AB5 and RBE6AB6 exhibited cisplatin resistance, whereas RBE10BF3, RAE2BC9, RAE1AF8, and RAE1BE5 demonstrated cisplatin sensitivity. Conversely, RAE1AG1 exhibited a similar IC<sub>50</sub> as the RMG-I parental cell line (Figure 5.39). Dose curves are presented in Appendix 3.

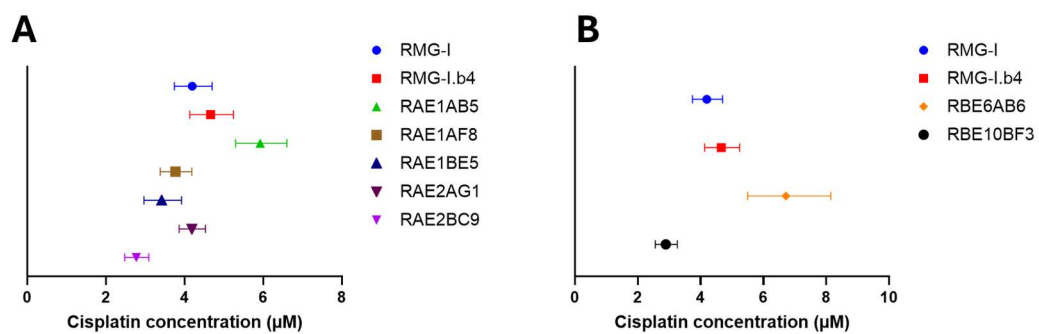


Figure 5.39 IC<sub>50</sub> cisplatin concentration of RMG-I CRISPR KO cell lines. A) RMG-I CRISPR KO ARID1A and B) RMG-I CRISPR KO ARID1B cells were seeded into 96-well plates at 6,000 cells/well density. MTS assay was performed after 72 hours treatment with cisplatin. RAE1AB5 and RBE6AB6 were resistant to cisplatin. These experiments were repeated at least 3 times to generate dose curves and IC<sub>50</sub> was calculated from the dose curve. Confidence intervals are indicated (95% CI).



#### 5.3.4.3 Assessment of RNA levels of ARID1A in JHOC-5 CRISPR-Cas9 KO clonal lines

Firstly, in order to ascertain the *ARID1A* mRNA expression level of *ARID1A* in the JHOC-5 CRISPR-Cas9 KO clonal line, we conducted an analysis of the RNA extracted from the JHOC-5 parental cell line, the JHOC-5.d12 clonal cell line and 2 representative *ARID1A* CRISPR-Cas9 KO cell lines. The results demonstrated that the mRNA expression level of *ARID1A* in 2 CRISPR-Cas9 KO clones was lower than in the parental JHOC-5 cell line and the JHOC-5.d12 clonal cell line (Figure 5.40).

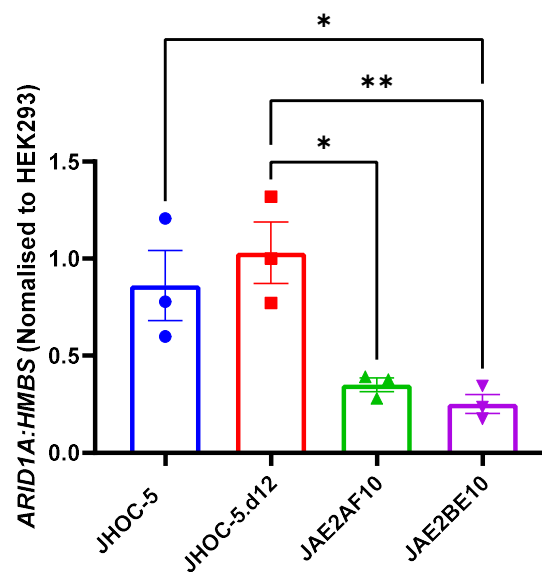


Figure 5.40 *ARID1A* mRNA expression levels for JHOC5 CRISPR-Cas9 KO cells. Graphs of mRNA levels of *ARID1A* in JHOC5 CRISPR-Cas9 parental and KO cells relative to *HMBS* and normalised to HEK293. A one-way ANOVA and *post-hoc* Tukey's test was performed to determine statistical significance. Data is shown as the mean  $\pm$  SEM, N=3. \*P<0.05, \*\*P<0.01.

#### 5.3.4.4 Assessing the growth rate of JHOC-5 CRISPR-Cas9 KO clonal cell lines and sensitivity to cisplatin

To verify the growth rate of the JHOC-5 CRISPR-Cas9 KO clonal cell lines, we seeded the JHOC-5 parental cell line and JHOC-5.d12 clonal cell line, as well as 7 representative CRISPR-Cas9 KO clonal cell lines (3 JHOC-5 *ARID1A* CRISPR-Cas9 KO clones, and 4 *ARID1B* CRISPR-Cas9 KO clones) at 2,500 cells per well into 96-well plates and imaged them using

an IncuCyte. The results demonstrated that all CRISPR clones exhibited a slower growth rate than the JHOC-5 and JHOC-5.d12 clones. The growth rates of JAE2AC9, JBE10AC5, and JBE10AH3 were notably slower. Interestingly, the growth rates of JBE10AC5 and JBE10AH3 were nearly identical (Figure 5.41).

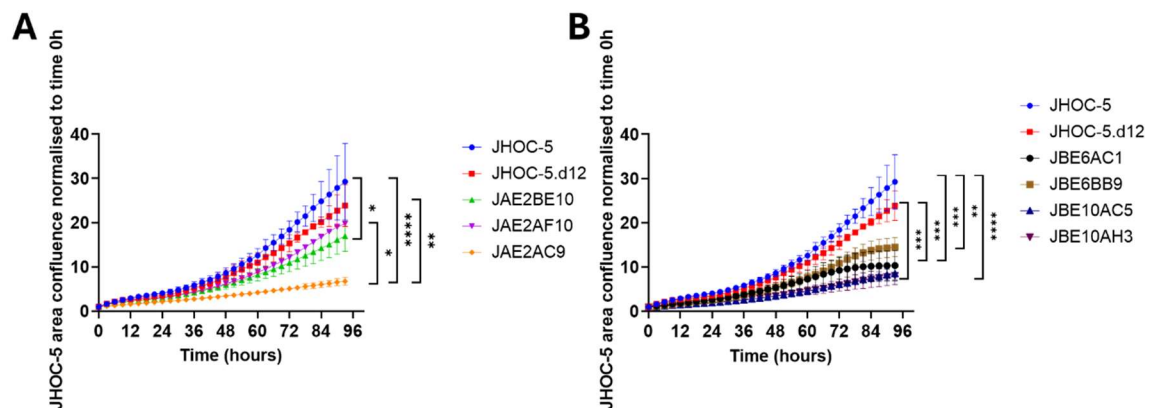


Figure 5.41 Growth rate of JHOC-5 parental line and CRISPR clonal lines. A) JHOC-5 CRISPR KO ARID1A and B) JHOC-5 CRISPR KO ARID1B cells were seeded into 96-well plates at 2,500 cells/well density. Cells were imaged in the IncuCyte for 93 hours. Images were captured every 3 hours and the percentage confluence recorded. Data is shown as the mean  $\pm$  SEM, N=3. (one-way ANOVA and *post-hoc* Tukey's test, \* $P < 0.05$ , \*\* $P < 0.01$ , \*\*\* $P < 0.001$ , \*\*\*\* $P < 0.0001$ ).

MTS assay was used to determine the cisplatin IC<sub>50</sub> of 9 cell lines (JHOC-5 parental cell line and JHOC-5.d12 clonal cell line, as well as 7 representative CRISPR-Cas9 KO clonal cell lines). The results demonstrated that, in comparison to the JHOC-5 and JHOC-5.d12 clones, all CRISPR clones exhibited cisplatin resistance, with the JBE6AC1 clone exhibiting the most pronounced resistance. The IC<sub>50</sub> of the JAE2AC9 clone was found to be comparable to that of the JHOC-5.d12 clone (Figure 5.42). Dose curves are presented in Appendix 3.

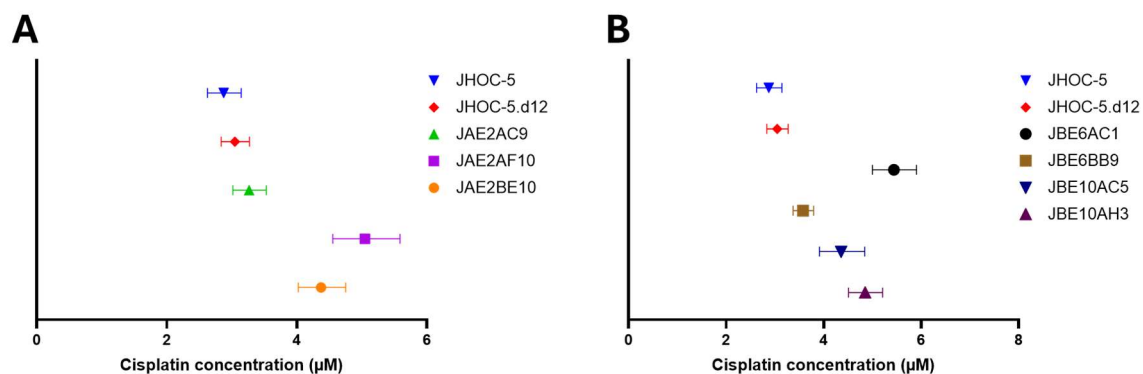


Figure 5.42 IC<sub>50</sub> cisplatin concentration of JHOC-5 CRISPR KO cell lines. A) JHOC-5 CRISPR KO ARID1A and B) JHOC-5 CRISPR KO ARID1B cells were seeded into 96-well plates at 2,500 cells/well density. MTS assay was performed after 72 hours treatment with cisplatin. These experiments were repeated at least 3 times to generate dose curves and IC<sub>50</sub> was calculated from the dose curve. Confidence intervals are indicated (95% CI).

### 5.3.5 *STAG1* expression in the ARID1A CRISPR KO isogenic panel cells

A study has demonstrated that inactivation of *ARID1A* is associated with loss of *STAG1* expression in OCCC<sup>513</sup>. This marker was selected to determine whether there were changes seen in ARID1A KO cells. To ascertain the impact of CRISPR KO of ARID1A on downstream biomarker genes, the level of *STAG1* mRNA expression was validated in CRISPR-Cas9 KO cells and compared with parental cell lines. RNA was extracted from the JHOC-5.d12 clonal cell line, two JHOC-5 CRISPR-Cas9 KO cell lines, RMG-I.b4 clonal cell line, four RMG-I CRISPR-Cas9 KO cell lines, and the RDKBE6AB5, as well as the control cell line HEK293, and analyses conducted using qRT-PCR. The results demonstrated that in comparison to the JHOC-5.d12 clonal cell line, the JHOC-5 CRISPR-Cas9 KO cells exhibited a modest decrease in *STAG1* mRNA expression. In comparison to the RMG-I.b4 clonal cell line, the expression level of *STAG1* mRNA was decreased in the majority of RMG-I CRISPR-Cas9 KO cell lines, including in RDKBE6AB5. However, the *STAG1* mRNA expression level in RAE1BE5 was higher than that of the RMG-I.b4 clone (Figure 5.43).

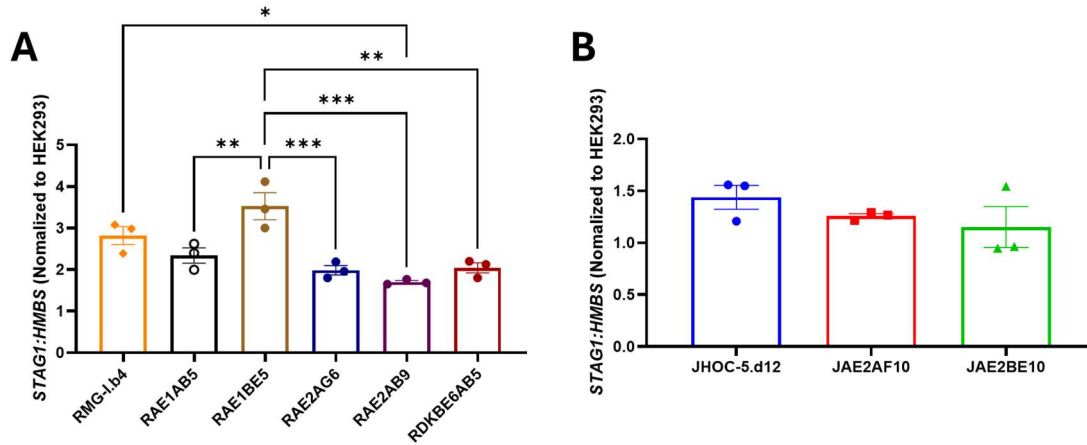


Figure 5.43 *STAG1* mRNA expression levels for RMG-I and JHOC-5 CRISPR-Cas9 KO cells. Graph of mRNA levels of *ARID1A* in A) RMG-I and B) JHOC5 CRISPR engineered cells relative to *HMBS* and normalised to HEK293. A one-way ANOVA and *post-hoc* Tukey's test was performed to determine statistical significance. Data is shown as the mean  $\pm$  SEM, N=3. ns, not significant, \*P<0.05, \*\*P<0.01, \*\*\*P<0.001. Data presented in panel A was generated by Dr Amani Alghalayini in my research group and Panel B was generated by me.

## 5.4 Discussion

In this project, we employed the CRISPR system to induce KO of *ARID1A* and *ARID1B* in RMG-I and JHOC-5 OCCC cell lines. Both RMG-I and JHOC-5 are reported in the literature as WT for *ARID1A* and *ARID1B*. We firstly selected WT *ARID1A* and *ARID1B* RMG-I.b4 and JHOC-5.d12 cells as homogenous clonal cell lines that represented parental cell lines for CRISPR-Cas9 KO. After transfection with *ARID1A* and *ARID1B* PX458 CRISPR-Cas9 KO plasmids, and single cell growth, validated clones with complete KO of *ARID1A* or *ARID1B* were obtained in RMG-I.b4 and JHOC-5.d12 cells. Furthermore, we created a heterozygous KO only of *ARID1B* in RMG-I *ARID1A* KO cell line.

The greater the number of copies of a gene, the more challenging CRISPR editing becomes. This is because gene copies can be dispersed throughout the genome or exist in tandem repeats, making it difficult to ensure that all copies are edited simultaneously and consistently. The presence of multiple copies increases the likelihood of incomplete edits, which may result in the formation of chimeric cells within the edited population<sup>520-522</sup>. Studies have indicated that an increase in the number of copies of the genome within a cell can prevent the complete KO

of a gene <sup>523</sup>. Consequently, the number of copies of the genome can affect the efficiency of CRISPR. During CRISPR experimentation, we observed that genome copy number influences the efficacy of gene KO. The Cell Model Passports database (<https://cellmodelpassports.sanger.ac.uk/>), revealed that JHOC-5 has four copies of both *ARID1A* and *ARID1B* and RMG-I has only one copy of *ARID1A* and three copies of *ARID1B*. This may be the reason why the *ARID1A* exon1 KO could not be validated by Sanger sequencing in JHOC-5. Multiple gene copy number may have affected our editing to interpret Sanger sequencing data for *ARID1A* and *ARID1B* if these genes were mutated in more than 1-2 copies.

When we attempted to KO *ARID1B* in RMG-I cells with an engineered KO of *ARID1A*, we only generated one clone with complete KO of *ARID1A* and a partial KO of *ARID1B*. While anecdotal, this supports the synthetic lethality of *ARID1A* and *ARID1B* that has been reported in the literature <sup>333</sup>. When *ARID1A* is mutated in cancer, cells are more dependent on the *ARID1B*-related SWI/SNF complex for functions including DNA repair, replication and transcriptional regulation. Loss of both subunits therefore disrupts these critical functions, leading to synthetic lethality <sup>524</sup>. It has been demonstrated that the knockdown of *ARID1B* in *ARID1A*-mutated colorectal cancer cells results in the destabilisation of the SWI/SNF complex and the inhibition of colorectal cancer proliferation <sup>525</sup>. A study by Sato and colleagues found that siRNA-mediated knockdown of *ARID1B* significantly reduced cell growth in *ARID1A* mutant OCCC <sup>526</sup>. Furthermore, Helming and colleagues have shown that the knockdown of *ARID1B* in *ARID1A*-mutated OCCC cells impairs cell growth <sup>333</sup>. This synthetic lethality of *ARID1A* and *ARID1B* may contribute to the reason why only one of our RMG-I DK clones could be obtained and this clone was heterozygous for *ARID1B*.

In order to amplify the gDNA region surrounding the *ARID1A* exon 1 CRISPR sgRNA target site, the touchdown PCR technique was employed, given the high GC content of the sequence. This is a modified PCR technique, designed to increase the specificity and yield of amplified DNA. DNA sequences with a GC content of more than 60% may prevent successful PCR. This is due to the formation of secondary structures, such as self- and cross-primer dimers within the DNA template, hairpin structures. These structures can block the DNA polymerase and prevent primers from annealing to the template, thus terminating the synthesis of new DNA strands during PCR. Furthermore, elevated levels of GC result in the formation of additional hydrogen bonds between cytosine (C) and guanine (G) base pairs, necessitating a greater

expenditure of energy to break these bonds, which consequently leads to an increase in melting temperatures ( $T_m$ )<sup>527</sup>. The initial PCR cycle begins with a higher annealing temperature, which gradually reduces as the cycle progresses. This allows the initial high temperature to break the extra hydrogen bonds between the GCs. Furthermore, the high temperature reduces non-specific binding and facilitates the hybridisation of the primers to the exact complementary sequences<sup>517,528</sup>. At a subsequent stage, as the temperature declines, it permits the remaining reactions to proceed in an orderly manner<sup>517</sup>. Currently, touchdown PCR is a commonly employed technique in PCR experiments involving high GC content.

The results of growth rate analyses indicated that 2 out of 5 of the RMG-I clones exhibited an increase in growth rate when *ARID1A* was knocked out compared to WT ARID1A control cells. *ARID1A* is a tumour suppressor that inhibits the biological behaviours of malignant tumours and exerts an anticancer effect by promoting apoptosis through the regulation of the cell cycle. A number of studies have demonstrated that when *ARID1A* is mutated in cells, it loses its inhibitory effect on cancerous growth, resulting in uncontrolled cell proliferation<sup>529</sup>. A study by He and colleagues demonstrated that when *ARID1A* was knocked down in hepatocellular carcinoma cells, it significantly promoted cell migration and invasion. Additionally, their study found that overexpression of *ARID1A* inhibited the invasive and migratory abilities of cells<sup>530</sup>. Peerapen and colleagues found that knockdown of *ARID1A* in colorectal cancer cells resulted in a significant increase in the secretion of the angiogenic factor VEGF<sup>531</sup>. Some other studies have demonstrated that *ARID1A* deletion can result in alterations to the cell cycle that inhibit apoptosis. Zhang and colleagues observed that knockdown of *ARID1A* using siRNA promoted cell proliferation and inhibited paclitaxel-induced apoptosis<sup>532</sup>. Xie and colleagues demonstrated that depletion of *ARID1A* promoted proliferation and inhibited 5-fluorouracil-induced apoptosis in colorectal cancer cell lines<sup>533</sup>. Nagl and colleagues suggested that when cells were depleted of ARID1A, they had an accelerated cell cycle compared to normal cells, resulting in enhanced proliferation. Their study also revealed that the depletion of ARID1B led to slower cell proliferation. Thus they concluded that the SWI/SNF complex containing ARID1A has an anti-proliferative function, while the SWI/SNF complex containing ARID1B has a pro-proliferative function<sup>534</sup>. This partially correlated with our results, in that when ARID1B was knocked out in RMG-I and JHOC-5 clonal lines, cell proliferation slowed down. When ARID1A was knocked out, RMG-I KO clones had an increase in growth rate. However, all JHOC-5 KO clones exhibited a decrease in growth rate when ARID1A was knocked out. Studies have shown that off-target effects of CRISPR-Cas9 may lead to genomic instability

and disruption of normal gene function, resulting in, for example, adverse DNA damage, immune responses and cytotoxicity <sup>515,535</sup>. This may therefore be responsible for the slow growth rate of the JHOC-5 KO clones.

Three different transfection reagents, X-tremeGene, Lipofectamine LTX and Lipofectamine 3000, were employed to facilitate the transfection of plasmids into cells. Each of the three transfection reagents exhibited disparate transfection efficiencies across distinct cell types. The ratio of DNA to transfection reagents has been demonstrated to influence transfection efficiency. Arnold and colleagues demonstrated that the ratio of DNA to transfection reagents at a specific point resulted in the highest transfection efficiency, and that neither an excess nor a deficiency of this ratio improved transfection efficiency <sup>536</sup>. Additionally, different types of transfection reagents can also affect transfection efficiency. It has been demonstrated that liposomal reagents, such as Lipofectamine LTX and Lipofectamine 3000, are more effective at transfecting certain plasmid DNA into cells <sup>537</sup>. A study showed that Lipofectamine LTX and Lipofectamine 2000 liposomal reagents were able to transfect plasmid DNA into cells with transfection efficiencies of 38% and 23%, respectively, at 48 hours, which were higher than the 20% of non-liposomal reagents <sup>538</sup>. Nevertheless, for cells that are challenging to transfect with liposomal reagents, non-liposomal reagents may offer superior transfection efficiencies. A comparative study by Sandbichler and colleagues demonstrated that X-tremeGENE exhibited superior transfection efficiencies compared to Lipofectamine LTX for the transfection of DNA into the zebrafish cell line Z3 <sup>539</sup>.

It should be noted that CRISPR is not the only technology for gene editing. Another gene editing technology, Transcription Activator-Like Effector Nucleases (TALENs), was first reported in 2009 and is now widely used for precise and efficient gene editing in live cells <sup>540-542</sup>. While both CRISPR and TALEN are revolutionary tools for genome editing, they differ significantly in terms of mechanism, efficiency, and specificity. In terms of its mechanism, CRISPR is derived from the bacterial immune system and uses a guide RNA to direct the enzyme Cas9 to a specific DNA sequence, where Cas9 induces a DSB <sup>543</sup>. In contrast, TALENs are engineered proteins consisting of a customisable array of TAL effector repeats that bind to specific DNA sequences and bind to the FokI nuclease structural domain to produce DSBs upon dimerization <sup>544</sup>. In terms of efficiency, CRISPR appears to have an advantage over TALENs. It has been shown that CRISPR-Cas9 can efficiently generate mutations in 5 genes simultaneously in mouse embryonic stem cells. Furthermore, the co-injection of Cas9 mRNA

and sgRNA targeting two genes into zygotes has been demonstrated to produce mice with biallelic mutations in both genes with an 80% efficiency <sup>545</sup>. In terms of specificity, the off-target effect is reduced due to the longer DNA recognition sequence of TALENs <sup>546,547</sup>. In CRISPR, the presence of a PAM sequence near the target site is a prerequisite; however, TALENs do not require a PAM sequence, which allows it to target any desired sequence within the genome, independent of the PAM site <sup>546,548</sup>. The choice between CRISPR and TALENs depends on the specific requirements of the genome editing task, and each tool has unique advantages that can be exploited to achieve precise gene modification.

## **5.5 Conclusion**

In this chapter, we engineered KO of ARID1A or ARID1B into the RMG-I.b4 and JHOC-5.d12 clonal cell lines. Additionally, a heterozygous KO of ARID1B in the validated RMG-I ARID1A KO cell line was created. These isogenic panels will provide resources for future studies of ARID1A/1B in OCCC.



# CHAPTER 6. Final discussion and future directions

## 6.1 Final discussion

OCCC is a subtype of ovarian cancer that is resistant to standard platinum-taxane therapy, warranting investigation to identify drugs with therapeutic potential. The morphology of the cell lines used as preclinical models of OCCC was determined, and all cell lines were verified by STR cell line identification. The OCCC dose curves for cisplatin and carboplatin were established and the IC<sub>50</sub> levels for these drugs calculated for each cell line. Using an epigenetic drug screening library, it was established that the BTK inhibitor ibrutinib showed enhanced efficacy in OCCC cell lines, which achieved aim 1 and 2. Also, as primary OCCC is characterised by mutation of gene encoding the SWI/SNF subunit *ARID1A*, and less frequently *ARID1B*, we sought to engineer small isogenic panels of CRISPR KO cells that could be used for the purpose of drug discovery and increasing our knowledge of the biology of these tumours. We have successfully used CRISPR KO technology to generate *ARID1A* and *ARID1B* null cells in the RMG-I and JHOC-5 OCCC cell lines that are both reported to be *ARID1A/ARID1B* WT.

### 6.1.1 Supporting evidence that the absence of both *ARID1A* and *ARID1B* is synthetic lethal

Both *ARID1A* and *ARID1B* have been observed to exhibit high mutation frequency in OCCC cells. It has been reported that mutations in *ARID1B* are frequently accompanied by mutations in *ARID1A* in ovarian cancer<sup>333</sup>. Moreover, *ARID1A* and *ARID1B* are essential in order for the SWI/SNF complex to function normally to support multiple cellular processes. Dual loss of these subunits disrupts these critical functions, leading to synthetic lethality<sup>333,524</sup>. In Chapter 3 of this thesis, we report that *ARID1A* and *ARID1B* mutations were detected in both OVISE and TOV-21G, but *ARID1B* protein of the correct size detected by Western blot was present in these cell lines suggesting retention of WT function. Also, we observed a faint *ARID1A* band upon Western blotting in OVISE, suggesting that some WT *ARID1A* was retained. Moreover, our sequence analysis demonstrated the retention of WT *ARID1A* and *ARID1B* in these cell lines. Furthermore, we report in Chapter 5 that *ARID1B* could not undergo complete KO in RMG-I CRISPR KO *ARID1A* cells. These findings support that in order for cancer cells to survive, they require at least some WT function of at least one of either *ARID1A* or *ARID1B*. It has been demonstrated that the knockdown of *ARID1B* in *ARID1A*-mutated ovarian cancer cells resulted in destabilisation of the SWI/SNF complex and the inhibition of cancer cell proliferation<sup>526</sup>. A study by Helming and colleagues has also shown

that knockdown of ARID1B in *ARID1A*-mutated OCCC cells impairs cell growth, which is also consistent with our results. Additionally, they discovered that in cell lines where both *ARID1A* and *ARID1B* were mutated, all lines retained at least one allele of either *ARID1A* or *ARID1B*, indicating that at least one *ARID1* allele is essential for survival of cancer cells <sup>333</sup>.

#### 6.1.2 ARID1A in the OCCC cell line JHOC-5

Previous literature reported the presence of WT *ARID1A* in JHOC-5 cells, and our results also showed the presence of ARID1A protein and mRNA expression in JHOC-5 cells, reported in Chapter 3. However, it is interesting to note that when Western blotting was employed to examine ARID1A protein levels in 7 OCCC cells, four out of five *ARID1A* mutant cell lines (OVTOKO, OVMANA, OVISE, and TOV-21G) had no ARID1A protein bands displayed, however, a band was observed in OV207 cells. In two cell lines that were reported to be ARID1A wild-type (RMG-I and JHOC-5), a doublet band for ARID1A was present in JHOC-5 cells, whereas only one band was present in RMG-I cells. Western blot analyses reported in Chapter 5 also showed the presence of doublets for ARID1A in some JHOC-5 CRISPR engineered cell lines where ARID1A was unable to be completely knocked out. More interestingly, when ARID1A was successfully knocked out in JHOC-5 cells, this doublet band disappeared entirely, indicating that both bands represent the ARID1A protein. Wu and colleagues demonstrated that there are two distinct ARID1A isoforms, encoding 2285 and 2086 amino acids, respectively. However, they were unable to elucidate whether these two isoforms had different functions <sup>549</sup>. Selvanathan and colleagues proceeded to investigate these two isoforms further and discovered that the short ARID1A (ARID1A-S) isoform was encoded by sequence that lacked 651 nucleotides at the 5' end of exon 18 compared to the long ARID1A (ARID1A-L) isoform. They also demonstrated that ARID1A-L expression enhanced cell proliferation, whereas ARID1A-S expression reduced cell viability and inhibited cell growth <sup>550</sup>. Interestingly, in another study, Kurz and colleagues identified nine distinct *ARID1A* transcript variants, four of which exhibited differential expression in germ cell tumours (GCTs). However, only one variant encoded the full-length ARID1A protein <sup>551</sup>. *ARID1A* has two isoforms encoding different numbers of amino acids, so the protein size should be around 270 kDa and 240 kDa. In this project, both sgRNAs of ARID1A were located at the 5' end of the gene (exons 1 and 2), therefore CRISPR modification would affect all isoforms. Also, JHOC-5 cells have been reported to have 4 copies of *ARID1A* and the two protein bands were around

270 kDa and 250 kDa which is close to the size of the two isoforms. Moreover, we observed introduction of a partial ARID1A KO in these cell lines, likely due to the presence of multiple copies of *ARID1A* that increases the difficulty of achieving a total KO. The fact that sequence analysis proved to be very difficult, may support this latter suggestion.

### 6.1.3 Effects of ARID1A and ARID1B on cell growth rate

SWI/SNF subunits ARID1A and ARID1B can regulate cell growth and proliferation <sup>552</sup>. Reported in Chapter 5, when we CRISPR engineered ARID1A KOs in RMG-I and JHOC-5 cells, the growth rate of engineered cells was faster than for the parental cell lines. In contrast, the growth rate of cells slowed down when cells underwent KO of ARID1B. Interestingly, previous studies have indicated that *ARID1A*-mutated cells exhibit a slightly shorter doubling time (average of 56 hours) compared to *ARID1A* and *ARID1B* WT cell lines (average of 68.5 hours) <sup>553-555</sup>. It has been demonstrated that ARID1A plays a role in cell division and proliferation by regulating cell cycle entry and progression. Guan and colleagues have suggested that cell proliferation is enhanced by shRNA inhibition of *ARID1A* <sup>331</sup>. Nagl and colleagues have shown that the ARID family subunits exert opposing effects on cell cycle regulation. They used siRNA to construct ARID1A or ARID1B knockdown cells in mouse MC3T3-E1 pre-osteoblasts. When ARID1A was present but ARID1B was absent, the proliferation rate of these cells was increased. However, when ARID1A was absent and ARID1B was present, cell proliferation was decreased <sup>534</sup>. Our findings, in conjunction with those of the referenced studies, illustrate the impact of ARID family subunits on cell proliferation, thereby suggesting a proliferative function for ARID1A and a proliferative inhibitory function for ARID1B. Future studies could provide insight into cell cycle alterations following gene editing through the application of techniques such as Incucyte live cell imaging. This approach offers a more comprehensive temporal perspective by tracking cell proliferation and morphological changes in a continuous, real-time manner <sup>556</sup>. Additionally, Flow cytometry could be employed to profile alterations in cell cycle progression by quantifying DNA content and identifying phase-specific disruptions, such as G1 stalls or G2/M checkpoint delays <sup>557</sup>.

#### 6.1.4 OCCC and chemoresistance – effects of ARID1A KO

Debulking surgery and platinum-based chemotherapy have constituted the primary treatment modality for ovarian cancer patients, including those with OCCC. However, this treatment approach also encounters the challenge of drug resistance. In Chapter 3, we report the sensitivity of different OCCC cell lines to platinum drugs. It was found that cell lines containing endogenous *ARID1A* mutation were more sensitive to platinum drugs compared to the *ARID1A* WT cell lines, for example *ARID1A* mutated cell lines OVTOKO and OVMANA were more sensitive to cisplatin compared to the RMG-I and JHOC-5 cell lines. Further, *ARID1A* mutated OVTOKO and OV207 were more sensitive to carboplatin compared to JHOC-5. These discoveries contrast with some previously reported findings. A study suggested that the high mutation frequency of *ARID1A* may be responsible for its resistance to platinum-based chemotherapy<sup>399</sup>. Lyu and colleagues demonstrated that the cisplatin IC<sub>50</sub> was markedly elevated following siRNA-mediated reduction of *ARID1A* expression in WT *ARID1A* OCCC cells. Furthermore, following the administration of the same concentration of cisplatin, the survival of cells in the *ARID1A* siRNA group was found to be significantly higher than that of the negative control group<sup>558</sup>.

Although we have not studied any additional factors that may be contributing to platinum resistance in our cell lines, many studies have indicated that other factors can also impact OCCC platinum resistance. Niimi and colleagues demonstrated that *REV7*, which is involved in a multitude of biological processes, including DNA repair and mutagenesis, cell cycle regulation, gene transcription, and oncogenesis, is expressed in the majority of EOC. Furthermore, they observed that high levels of *REV7* expression are frequently detected in OCCC and mucinous ovarian cancers. Knockdown of the *REV7* gene results in an increase in the sensitivity of tumour cells to cisplatin, leading to apoptosis<sup>559</sup>. Another study demonstrated that VEGF expression was significantly higher in cisplatin resistant OCCC cell lines compared to non-resistant OCCC<sup>560</sup>. These factors can be investigated in future studies to better understand their roles in platinum resistance and potentially identify new therapeutic targets.

#### 6.1.5 Ibrutinib as a potential therapeutic agent for OCCC

In Chapter 4 of this thesis, we report the identification of ibrutinib that was part of an epigenetic drug screening library, as a potential therapeutic agent for OCCC which achieved aim 1.

Ibrutinib is an irreversible BTK inhibitor that covalently binds to the cysteine-481 residue at the BTK active site, thereby blocking its kinase activity <sup>477</sup>. It effectively disrupts BCR signalling and down-regulates NF- $\kappa$ B signalling, ultimately leading to a reduction in tumour growth and an increase in apoptosis <sup>478</sup>. While ibrutinib has not yet been clinically approved for ovarian cancer, two case studies of patients with LGSOC have recently been reported with encouraging results <sup>489,490</sup>. In the first case, following two surgeries and unsuccessful chemotherapy a 52-year-old patient showed stable disease and decreased CA-125 levels after ibrutinib treatment. The second case involved a 61-year-old female with chronic lymphocytic leukemia who, after being diagnosed with FIGO stage IIb LGSOC, also experienced normalized CA-125 levels and no recurrent symptoms after 12 months of ibrutinib treatment. Even though the cases reported to date are LGSOCs, these studies suggest that ibrutinib may be effective for treating other subtypes of ovarian cancer.

BTK has multiple isoforms and plays a crucial role in cancer biology. Among these isoforms, BTK-A is the most widely studied variant and is involved in myeloid cell function, maturation and trafficking. It plays an important role in the regulation of myeloid cell signalling <sup>468</sup>. BTK-A is abundantly expressed mainly in cells of the haematopoietic lineage, including myeloid cells, lymphocytes, mature B-lymphocytes, mast cells, monocytes and macrophages <sup>469,470</sup>. BTK-C, which is found in breast and prostate cancer cells, represents a new isoform transcribed from an alternative promoter. In contrast to BTK-A, this isoform has a 34 amino acid stretch and is the predominant form in breast tumour cells, thus highlighting its potential importance in epithelial cancers <sup>471,472</sup>. Furthermore, it has been demonstrated that BTK-C is a survival factor in prostate cancer cells. Inhibition of BTK-C in prostate cancer using ibrutinib has been shown to result in the upregulation of apoptosis-related genes <sup>472</sup>. Additionally, p65BTK, a truncated isoform lacking most of the N-terminal PH structural domain, is widely expressed in colon cancer cell lines and tissues. Inhibition of p65BTK with ibrutinib has been shown to affect the growth and survival of colon cancer cells <sup>561</sup>. BTK-D is a splice variant isoform of BTK that lacks the kinase structural domain, has 483 amino acids, and a total molecular weight of 52 kDa. This isoform can act as a dominant-negative BTK because it inhibits BTK-dependent differentiation and pre-B-cell receptor responses in leukaemia cells <sup>476</sup>. These findings indicate that BTK isoforms exhibit distinct expression patterns in different cancer types. To date, no study has investigated the predominant isoforms in ovarian cancer. To fully comprehend the role(s) of different BTK isoforms in cancer progression and to develop

targeted therapies that leverage the unique properties of each BTK variant, further investigation of the signalling pathways and regulatory mechanisms involved in these isoforms is essential.

#### 6.1.6 Potential and current status of other targeted agents in OCCC treatment

It seems reasonable to posit that the use of ibrutinib as a treatment for OCCC may only be a matter of time. A number of clinical trials have been conducted to explore alternative treatments for OCCC. A trial (GOG-254, NCT00979992) conducted by Chan and colleagues demonstrated that sunitinib, a potent and selective protein tyrosine kinase inhibitor, exhibited minimal activity in the second- and third-line treatment of persistent or recurrent OCCC <sup>562</sup>. Although the outcome of the results was unsatisfactory, this indicates that investigation of additional targeted agents in conjunction with conventional platinum-based therapies is an active space for the treatment of OCCC. A study by Ackroyd and colleagues demonstrated that the tumour mutational burden (TMB) was higher in OCCC compared to both endometrial clear cell carcinoma (ECCC) and clear cell renal cell carcinoma (ccRCC) <sup>563</sup>. This molecular profile suggests that OCCC may be more responsive to immunotherapy. One completed clinical trial (NCT03602586) with unpublished results employed a combination of two immunotherapeutic drugs (pembrolizumab (a monoclonal antibody directed against programmed cell death protein 1 (PD-1) and epacadostat (a novel inhibitor of indoleamine-2,3-dioxygenase-1)) to treat OCCC, with suggestions that immunotherapy may be a promising avenue for the treatment of OCCC. Also, a clinical trial using durvalumab, an immune checkpoint inhibitor of PD-L1, has been conducted in patients with OCCC, the outcome of which is currently unknown (MOCCA, NCT03405454).

#### 6.1.7 Retention of WT ARIDA and truncated ARID1B protein after KO

This project not only underscores the utility of CRISPR-Cas9 gene editing technology in modelling genetic mutations and studying their effects but also highlights the potential for translating these findings into clinical applications. In this project, we utilized CRISPR technology (reported in Chapter 5) to KO ARID1A protein in two cell lines reported to be *ARID1A* WT, specifically RMG-I and JHOC-5.

CRISPR-Cas9 gene editing technology offers an affordable and simple way to KO nearly any protein of interest. CRISPR KO cell lines are designed to primarily mimic deletions and/or

premature termination of translation due to nonsense mutations or frameshift insertions or deletions<sup>564</sup>. These mechanisms effectively disrupt the gene and prevent the production of functional protein. Interestingly, Feng and colleagues conducted experiments using CRISPR to KO the ARID1A protein. Despite successfully inducing base pair deletions, subsequent Western blot revealed that the ARID1A protein was still detected and expressed new bands with lower molecular weights in the cells. This finding led them to propose several hypotheses to explain the persistence of mutant ARID1A protein expression. One possibility is that editing and/or frameshift mutations in early exons might lead to the expression of other isoforms from downstream alternative translation initiation sites, which could partially restore ARID1A's expression and function<sup>565</sup>. However, this case does not occur in our cells.

## 6.2 Conclusion

Ovarian cancer remains a significant gynaecological disease with global impact on women's health. Accordingly, the pursuit of novel therapeutic modalities remains a prevailing area of scientific inquiry. In Chapter 3, we discussed the morphology of OCCC cell lines, validated their *ARID1A* and *ARID1B* mutations, as well as explored their sensitivity to platinum compounds. In Chapter 4, we reported use of an epigenetic drug compound library to screen OCCC cell lines and discovered the BTK inhibitor ibrutinib as a drug with preferential effects against OCCC. The effects of ibrutinib were also explored in 3D bio-printed OCCC cells, displaying potential as a possible therapeutic to be used clinically for this malignancy. In Chapter 5, we reported the use of CRISPR-Cas9 gene editing to KO ARID1A or ARID1B in cells, thereby demonstrating that cellular activity is altered after ARID1A or ARID1B KO. Data presented in this thesis has helped to establish CRISPR-Cas9 engineering techniques in my laboratory that will have sustained impact on multiple projects. The discovery of ibrutinib as a drug with potential for the treatment of OCCC may, after additional confirmatory experiments, be progressed to a clinical trial (Figure 6.1).



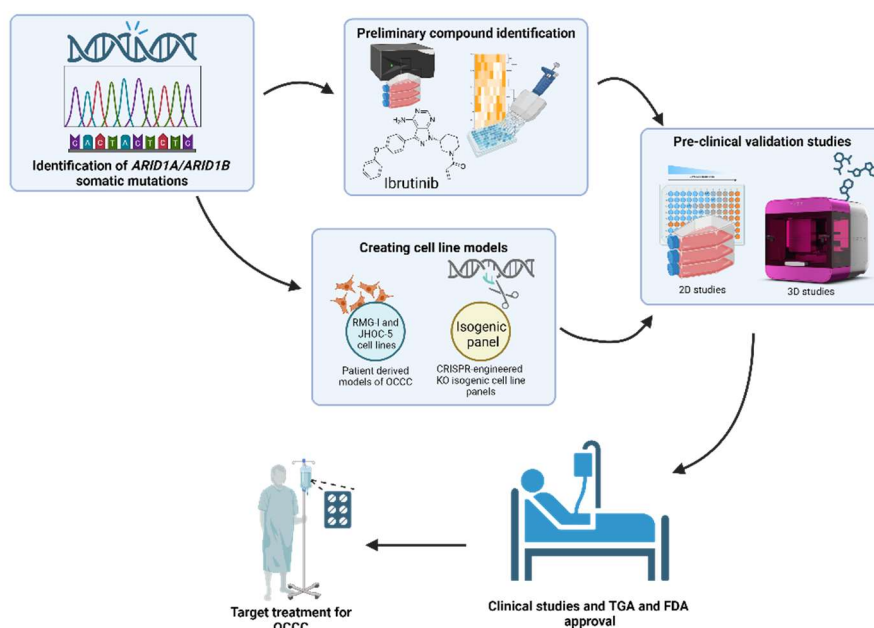


Figure 6.1 Schematic outlining the process of identifying a molecular target therapy for *ARID1A* and/or *ARID1B* mutated OCCC. OCCC cell lines with *ARID1A* and /or *ARID1B* mutations were screened with a drug compound library. CRISPR-engineered isogenic panels were constructed and can be used for screening and/or validation of molecular target drugs. Both cell lines with endogenous mutations and engineered mutations can be challenged with drugs of interest such as ibrutinib in 2D and 3D settings. In the future, following the establishment of further preclinical evidence, clinical trials may be employed to evaluate the safety and efficacy of these compounds, with the ultimate objective of developing new therapies for OCCC patients. TGA: Therapeutic Goods Administration. FDA: Food and Drug Administration. OCCC: Ovarian Clear Cell Carcinoma. KO: knockout.

### 6.3 Limitations

It should be noted that this study is not without limitations. Firstly, the cohort of non-OCCC cell lines was small. Although seven different OCCC cell lines were used, only three non-OCCC cell lines were included for discovery, and not every subtype of ovarian cancer was represented. Secondly, many matrix selection experiments for optimisation could only be performed once because of the high cost of using the RASTRUM bio-printer (more than \$400 per 96-well plate). Thirdly, the compound library utilized for drug screening encompassed 160 drug compounds that is a relatively small number compared with commercial screens of thousands of compounds. Also, due to logistical constraints, only two concentrations of each

compound were employed to treat the cells for the discovery arm of this work, however, it should be noted that screening using this library has previously been performed in this manner<sup>436</sup>. Moreover, due to time constraints, we only demonstrated that ibrutinib has significant effects in OCCC. To further investigate, we could use the CRISPR isogenic panel we developed to test ibrutinib's effects and determine if this compound shows greater efficacy in ARID1A KO OCCC cells compared to ARID1A WT OCCC. Despite these perceived limitations, the compound ibrutinib was identified and shows promise for development as a potential therapeutic for OCCC.

## **6.4 Opportunities and future directions**

In Chapter 1 of this thesis, we described the TGA and FDA approvals of PARP inhibitors (olaparib, rucaparib, and niraparib) to treat patients with some subtypes of ovarian cancer, like HGSOC. Reported in Chapter 4 of this thesis, we discovered that ibrutinib had a pronounced effect on the viability of OCCC cells compared to non-OCCC cells. This finding is particularly intriguing given that ibrutinib is not traditionally associated with ovarian cancer treatment. In a study by Curtis and colleagues on mantle cell lymphoma (MCL), it was demonstrated that the combination of olaparib and ibrutinib had a greater inhibitory effect on MCL cell growth than either drug alone. Furthermore, the combination of a PARP inhibitor with ibrutinib therapy was demonstrated to delay the emergence of ibrutinib resistance<sup>566</sup>. Currently, there are no studies exploring the combined use of ibrutinib and PARP inhibitors for ovarian cancer treatment. This combination therapy represents a novel approach with the potential to enhance treatment efficacy. By leveraging the unique mechanisms of action of both drugs, specifically PARP inhibitors targeting DNA repair pathways and ibrutinib inhibiting BTK signalling, this strategy could provide a synergistic effect that improves therapeutic outcomes for patients with OCCC. Future research will focus on testing the efficacy of this combination in OCCC models. Preclinical studies could evaluate the impact of ibrutinib and PARP inhibitors on cell viability, apoptosis, and other markers of cancer cell survival and proliferation. Additionally, exploring the molecular mechanisms underlying the interaction between these drugs may reveal insights into how they can be used most effectively together.

In this project, we employed a drug screening approach to rapidly identify potential new treatments. This method allows for the swift assay of various compounds, expediting the drug discovery process. High Throughput Screening (HTS), which is commonly defined as the

ability to screen 10,000 to 100,000 compounds per day, exemplifies this approach. Screening exceeding this threshold of compounds is referred to as ultra-high throughput screening (uHTS)<sup>567</sup>. However, for this project, we utilized a more modest drug library containing 160 drugs. Compared to traditional screening methods, *in silico* predictions based on modelling have also been widely used, which is increasingly prevalent in drug discovery. Shi and colleagues have pioneered a drug-target interaction prediction system that analyses drug–target interaction to forecast whether a new drug will interact with existing targets. This innovative approach can significantly enhance the efficiency and effectiveness of drug screening<sup>568</sup>. The initial results from our drug library screen provided valuable insights, but the small size of the library suggests that expanding the number of screened compounds could yield even more promising candidates. In future studies, we plan to increase the size of the drug libraries and integrate advanced computational analyses. This combined approach will leverage the strengths of both empirical screening and predictive modelling, facilitating the identification of optimal treatments for OCCC.

This project examined the potential efficacy of ibrutinib as a treatment for OCCC. However, the mechanism of decreased OCCC cell viability following treatment with ibrutinib remains incompletely understood. Consequently, future studies may explore this mechanism, for example, through experiments to determine apoptosis. For instance, an evaluation of NF- $\kappa$ B transcriptional activation following BTK inhibition could provide insights into the downstream effects of ibrutinib, thus facilitating a deeper understanding of its role in cellular regulation. BTK represents an important component of the BCR signalling pathway, which is closely related to NF- $\kappa$ B activation<sup>457</sup>. Ibrutinib disrupts this pathway, potentially altering NF- $\kappa$ B-mediated transcriptional activity, which controls key cellular processes such as proliferation, survival and immune response. By assessing NF- $\kappa$ B transcriptional activation, researchers can elucidate how ibrutinib affects the expression of target genes associated with cell death or survival pathways. Apoptosis-regulated genes should also be studied in ibrutinib treated OCCC cell lines.

## References

- 1 National Cancer Institute. *What Is Cancer?*, <<https://www.cancer.gov/about-cancer/understanding/what-is-cancer>> (Accessed 29, February, 2024)
- 2 AIHW & AACR. Cancer in Australia: an overview 2012. (AIHW, Canberra, 2012).
- 3 Bray, F., Laversanne, M., Weiderpass, E. & Soerjomataram, I. The ever-increasing importance of cancer as a leading cause of premature death worldwide. *Cancer* **127**, 3029-3030 (2021). <https://doi.org/10.1002/cncr.33587>
- 4 Global cancer burden growing, amidst mounting need for services. *Saudi Med J* **45**, 326-327 (2024).
- 5 Bray, F. *et al.* Global cancer statistics 2022: GLOBOCAN estimates of incidence and mortality worldwide for 36 cancers in 185 countries. *CA Cancer J Clin* **74**, 229-263 (2024). <https://doi.org/10.3322/caac.21834>
- 6 Australian Institute of Health Welfare. Cancer data in Australia. Cancer data in Australia. (AIHW, Canberra, 2023).
- 7 World Health Organization/International Agency for Research on Cancer (IARC). *Cancer Today*, <<https://gco.iarc.fr/today/en>> (2024).
- 8 Xi, Y. *et al.* Trends in gynaecologic cancer mortality and the impact of the COVID-19 pandemic in the United States. *Infect Agent Cancer* **19**, 4 (2024). <https://doi.org/10.1186/s13027-024-00567-6>
- 9 Anand, P. *et al.* Cancer is a preventable disease that requires major lifestyle changes. *Pharm Res* **25**, 2097-2116 (2008). <https://doi.org/10.1007/s11095-008-9661-9>
- 10 Chornokur, G., Amankwah, E. K., Schildkraut, J. M. & Phelan, C. M. Global ovarian cancer health disparities. *Gynecol Oncol* **129**, 258-264 (2013). <https://doi.org/10.1016/j.ygyno.2012.12.016>
- 11 Chan, J. K. *et al.* Ovarian cancer in younger vs older women: a population-based analysis. *Br J Cancer* **95**, 1314-1320 (2006). <https://doi.org/10.1038/sj.bjc.6603457>
- 12 Bandera, E. V., Lee, V. S., Rodriguez-Rodriguez, L., Powell, C. B. & Kushi, L. H. Racial/Ethnic Disparities in Ovarian Cancer Treatment and Survival. *Clin Cancer Res* **22**, 5909-5914 (2016). <https://doi.org/10.1158/1078-0432.Ccr-16-1119>
- 13 Arora, N., Talhouk, A., McAlpine, J. N., Law, M. R. & Hanley, G. E. Long-term mortality among women with epithelial ovarian cancer: a population-based study in

- British Columbia, Canada. *BMC Cancer* **18**, 1039 (2018).  
<https://doi.org/10.1186/s12885-018-4970-9>
- 14 Goldsbury, D. E. *et al.* Health services costs for ovarian cancer in Australia: Estimates from the 45 and Up Study. *PLoS One* **18**, e0282851 (2023).  
<https://doi.org/10.1371/journal.pone.0282851>
  - 15 Poole, E. M. *et al.* Hormonal and reproductive risk factors for epithelial ovarian cancer by tumor aggressiveness. *Cancer Epidemiol Biomarkers Prev* **22**, 429-437 (2013).  
<https://doi.org/10.1158/1055-9965.Epi-12-1183-t>
  - 16 Mori, M. *et al.* Reproductive, genetic, and dietary risk factors for ovarian cancer. *Am J Epidemiol* **128**, 771-777 (1988). <https://doi.org/10.1093/oxfordjournals.aje.a115030>
  - 17 Gayther, S. A. & Pharoah, P. D. The inherited genetics of ovarian and endometrial cancer. *Curr Opin Genet Dev* **20**, 231-238 (2010).  
<https://doi.org/10.1016/j.gde.2010.03.001>
  - 18 Schonfeld, S. J., Berrington de Gonzalez, A., Visvanathan, K., Pfeiffer, R. M. & Anderson, W. F. Declining second primary ovarian cancer after first primary breast cancer. *J Clin Oncol* **31**, 738-743 (2013). <https://doi.org/10.1200/jco.2012.43.2757>
  - 19 Torre, L. A. *et al.* Ovarian cancer statistics, 2018. *CA Cancer J Clin* **68**, 284-296 (2018).  
<https://doi.org/10.3322/caac.21456>
  - 20 Zheng, Q. *et al.* First-degree family history of prostate cancer is associated the risk of breast cancer and ovarian cancer. *Medicine (Baltimore)* **100**, e23816 (2021).  
<https://doi.org/10.1097/md.00000000000023816>
  - 21 Walsh, T. *et al.* Mutations in 12 genes for inherited ovarian, fallopian tube, and peritoneal carcinoma identified by massively parallel sequencing. *Proc Natl Acad Sci U S A* **108**, 18032-18037 (2011). <https://doi.org/10.1073/pnas.1115052108>
  - 22 Alsop, K. *et al.* BRCA mutation frequency and patterns of treatment response in BRCA mutation-positive women with ovarian cancer: a report from the Australian Ovarian Cancer Study Group. *J Clin Oncol* **30**, 2654-2663 (2012).  
<https://doi.org/10.1200/jco.2011.39.8545>
  - 23 Toss, A. *et al.* Hereditary ovarian cancer: not only BRCA 1 and 2 genes. *Biomed Res Int* **2015**, 341723 (2015). <https://doi.org/10.1155/2015/341723>
  - 24 Andrews, L. & Mutch, D. G. Hereditary Ovarian Cancer and Risk Reduction. *Best Pract Res Clin Obstet Gynaecol* **41**, 31-48 (2017).  
<https://doi.org/10.1016/j.bpobgyn.2016.10.017>

- 25 Kotsopoulos, J. *et al.* Age-specific ovarian cancer risks among women with a BRCA1 or BRCA2 mutation. *Gynecol Oncol* **150**, 85-91 (2018). <https://doi.org/10.1016/j.ygyno.2018.05.011>
- 26 Graff, R. E. *et al.* Cross-cancer evaluation of polygenic risk scores for 16 cancer types in two large cohorts. *Nat Commun* **12**, 970 (2021). <https://doi.org/10.1038/s41467-021-21288-z>
- 27 Robles-Díaz, L., Goldfrank, D. J., Kauff, N. D., Robson, M. & Offit, K. Hereditary ovarian cancer in Ashkenazi Jews. *Fam Cancer* **3**, 259-264 (2004). <https://doi.org/10.1007/s10689-004-9552-0>
- 28 Moslehi, R. *et al.* BRCA1 and BRCA2 mutation analysis of 208 Ashkenazi Jewish women with ovarian cancer. *Am J Hum Genet* **66**, 1259-1272 (2000). <https://doi.org/10.1086/302853>
- 29 Leitzmann, M. F. *et al.* Body mass index and risk of ovarian cancer. *Cancer* **115**, 812-822 (2009). <https://doi.org/10.1002/cncr.24086>
- 30 Kim, S. J. *et al.* Epidemiologic factors that predict long-term survival following a diagnosis of epithelial ovarian cancer. *Br J Cancer* **116**, 964-971 (2017). <https://doi.org/10.1038/bjc.2017.35>
- 31 Bandera, E. V. *et al.* Impact of body mass index on ovarian cancer survival varies by stage. *Br J Cancer* **117**, 282-289 (2017). <https://doi.org/10.1038/bjc.2017.162>
- 32 Olsen, C. M. *et al.* Obesity and the risk of epithelial ovarian cancer: a systematic review and meta-analysis. *Eur J Cancer* **43**, 690-709 (2007). <https://doi.org/10.1016/j.ejca.2006.11.010>
- 33 Secretan, B. *et al.* A review of human carcinogens--Part E: tobacco, areca nut, alcohol, coal smoke, and salted fish. *Lancet Oncol* **10**, 1033-1034 (2009). [https://doi.org/10.1016/s1470-2045\(09\)70326-2](https://doi.org/10.1016/s1470-2045(09)70326-2)
- 34 Jordan, S. J., Green, A. C., Whiteman, D. C. & Webb, P. M. Risk factors for benign, borderline and invasive mucinous ovarian tumors: epidemiological evidence of a neoplastic continuum? *Gynecol Oncol* **107**, 223-230 (2007). <https://doi.org/10.1016/j.ygyno.2007.06.006>
- 35 Gram, I. T. *et al.* Cigarette smoking and risk of histological subtypes of epithelial ovarian cancer in the EPIC cohort study. *Inter J of Can* **130**, 2204-2210 (2012). <https://doi.org/https://doi.org/10.1002/ijc.26235>

- 36 Licaj, I. *et al.* Epithelial ovarian cancer subtypes attributable to smoking in the Norwegian Women and Cancer Study, 2012. *Cancer Medicine* **5**, 720-727 (2016). <https://doi.org/https://doi.org/10.1002/cam4.590>
- 37 Gram, I. T., Braaten, T., Adami, H.-O., Lund, E. & Weiderpass, E. Cigarette smoking and risk of borderline and invasive epithelial ovarian cancer. *Inter J of Can* **122**, 647-652 (2008). <https://doi.org/https://doi.org/10.1002/ijc.23108>
- 38 Gersekowski, K. *et al.* Germline BRCA variants, lifestyle and ovarian cancer survival. *Gynecol Oncol* **165**, 437-445 (2022). <https://doi.org/10.1016/j.ygyno.2022.03.020>
- 39 Boring, C. C., Squires, T. S., Tong, T. & Montgomery, S. Cancer statistics, 1994. *CA: a can j for clinicians* **44**, 7-26 (1994).
- 40 Fitch, M., Deane, K., Howell, D. & Gray, R. E. Women's experiences with ovarian cancer: reflections on being diagnosed. *Can Oncol Nurs J* **12**, 152-168 (2002). <https://doi.org/10.5737/1181912x123152159>
- 41 Rufford, B. D., Jacobs, I. J. & Menon, U. Feasibility of screening for ovarian cancer using symptoms as selection criteria. *Bjog* **114**, 59-64 (2007). <https://doi.org/10.1111/j.1471-0528.2006.01153.x>
- 42 Bankhead, C. R., Kehoe, S. T. & Austoker, J. Symptoms associated with diagnosis of ovarian cancer: a systematic review. *Bjog* **112**, 857-865 (2005). <https://doi.org/10.1111/j.1471-0528.2005.00572.x>
- 43 Goff, B. A., Mandel, L., Muntz, H. G. & Melancon, C. H. Ovarian carcinoma diagnosis. *Cancer* **89**, 2068-2075 (2000). [https://doi.org/https://doi.org/10.1002/1097-0142\(20001115\)89:10<2068::AID-CNCR6>3.0.CO;2-Z](https://doi.org/https://doi.org/10.1002/1097-0142(20001115)89:10<2068::AID-CNCR6>3.0.CO;2-Z)
- 44 Febina, R. & Bibha, C. *Ovarian Cancer: Molecular Classification and Targeted Therapy*. (IntechOpen, 2021).
- 45 Prat, J. Ovarian carcinomas: five distinct diseases with different origins, genetic alterations, and clinicopathological features. *Virchows Arch* **460**, 237-249 (2012). <https://doi.org/10.1007/s00428-012-1203-5>
- 46 Stewart, C., Ralyea, C. & Lockwood, S. Ovarian cancer: an integrated review. *Seminars in oncology nursing* **35**, 151-156 (2019).
- 47 Jayson, G. C., Kohn, E. C., Kitchener, H. C. & Ledermann, J. A. Ovarian cancer. *Lancet* **384**, 1376-1388 (2014). [https://doi.org/https://doi.org/10.1016/S0140-6736\(13\)62146-7](https://doi.org/https://doi.org/10.1016/S0140-6736(13)62146-7)
- 48 Lheureux, S., Gourley, C., Vergote, I. & Oza, A. M. Epithelial ovarian cancer. *Lancet* **393**, 1240-1253 (2019). [https://doi.org/10.1016/s0140-6736\(18\)32552-2](https://doi.org/10.1016/s0140-6736(18)32552-2)

- 49 Labidi-Galy, S. I. *et al.* High grade serous ovarian carcinomas originate in the fallopian tube. *Nat Commun* **8**, 1093 (2017). <https://doi.org/10.1038/s41467-017-00962-1>
- 50 Zhang, S. *et al.* Both fallopian tube and ovarian surface epithelium are cells-of-origin for high-grade serous ovarian carcinoma. *Nature Commu* **10**, 5367 (2019). <https://doi.org/10.1038/s41467-019-13116-2>
- 51 Crum, C. P. *et al.* Lessons from BRCA: the tubal fimbria emerges as an origin for pelvic serous cancer. *Clin Med Res* **5**, 35-44 (2007). <https://doi.org/10.3121/cmr.2007.702>
- 52 Karst, A. M., Levanon, K. & Drapkin, R. Modeling high-grade serous ovarian carcinogenesis from the fallopian tube. *Proc Natl Acad Sci U S A* **108**, 7547-7552 (2011). <https://doi.org/10.1073/pnas.1017300108>
- 53 George, S. H., Garcia, R. & Slomovitz, B. M. Ovarian Cancer: The Fallopian Tube as the Site of Origin and Opportunities for Prevention. *Front Oncol* **6**, 108 (2016). <https://doi.org/10.3389/fonc.2016.00108>
- 54 Integrated genomic analyses of ovarian carcinoma. *Nature* **474**, 609-615 (2011). <https://doi.org/10.1038/nature10166>
- 55 Bergamini, A. *et al.* Different patterns of disease spread between advanced-stage type I and II epithelial ovarian cancer. *Gynecol and obste investigation* **81**, 10-14 (2016).
- 56 Gadducci, A. & Cosio, S. Therapeutic Approach to Low-Grade Serous Ovarian Carcinoma: State of Art and Perspectives of Clinical Research. *Cancers (Basel)* **12** (2020). <https://doi.org/10.3390/cancers12051336>
- 57 Kaldawy, A. *et al.* Low-grade serous ovarian cancer: A review. *Gynecol Oncol* **143**, 433-438 (2016). <https://doi.org/10.1016/j.ygyno.2016.08.320>
- 58 Prat, J. New insights into ovarian cancer pathology. *Annals of oncol* **23**, x111-x117 (2012).
- 59 Thomson, J. P. *et al.* Whole exome sequencing of low grade serous ovarian carcinoma identifies genomic events associated with clinical outcome. *Gynecol Oncol* **174**, 157-166 (2023). <https://doi.org/https://doi.org/10.1016/j.ygyno.2023.04.011>
- 60 Nasioudis, D. *et al.* Adjuvant chemotherapy for early stage endometrioid ovarian carcinoma: An analysis of the National Cancer Data Base. *Gynecol Oncol* **156**, 315-319 (2020). <https://doi.org/10.1016/j.ygyno.2019.11.125>
- 61 Rendi, M. H., Garcia, R. L. & Dizon, D. S. Epithelial carcinoma of the ovary, fallopian tube, and peritoneum: histopathology. Available via [www.uptodate.com](http://www.uptodate.com). Published (2016).



- 62 Chan, J. K. *et al.* Do clear cell ovarian carcinomas have poorer prognosis compared to other epithelial cell types? A study of 1411 clear cell ovarian cancers. *Gynecol Oncol* **109**, 370-376 (2008). <https://doi.org/10.1016/j.ygyno.2008.02.006>
- 63 Fujiwara, K., Shintani, D. & Nishikawa, T. Clear-cell carcinoma of the ovary. *Ann Oncol* **27 Suppl 1**, i50-i52 (2016). <https://doi.org/10.1093/annonc/mdw086>
- 64 Iida, Y., Okamoto, A., Hollis, R. L., Gourley, C. & Herrington, C. S. Clear cell carcinoma of the ovary: a clinical and molecular perspective. *Int J of Gynecol Cancer* **31**, 605-616 (2021). <https://doi.org/10.1136/ijgc-2020-001656>
- 65 Seidman, J. D., Kurman, R. J. & Ronnett, B. M. Primary and metastatic mucinous adenocarcinomas in the ovaries: incidence in routine practice with a new approach to improve intraoperative diagnosis. *The Ame j of surgical pathol* **27**, 985-993 (2003).
- 66 Babaier, A. & Ghatage, P. Mucinous Cancer of the Ovary: Overview and Current Status. *Diagnostics (Basel)* **10** (2020). <https://doi.org/10.3390/diagnostics10010052>
- 67 Wentzensen, N. *et al.* Ovarian Cancer Risk Factors by Histologic Subtype: An Analysis From the Ovarian Cancer Cohort Consortium. *J Clin Oncol* **34**, 2888-2898 (2016). <https://doi.org/10.1200/jco.2016.66.8178>
- 68 Vargas, A. N. Natural history of ovarian cancer. *ecancermedicalscience* **8** (2014).
- 69 Brown, J. *et al.* Gynecologic Cancer Intergroup (GCIG) consensus review for ovarian germ cell tumors. *Int J Gynecol Cancer* **24**, S48-S54 (2014). <https://doi.org/10.1097/igc.0000000000000223>
- 70 Smith, H. O. *et al.* Incidence and survival rates for female malignant germ cell tumors. *Obstet Gynecol* **107**, 1075-1085 (2006). <https://doi.org/10.1097/01.AOG.0000216004.22588.ce>
- 71 Iavazzo, C., Vorgias, G., Iavazzo, P. E. & Gkegkes, I. D. Is fertility sparing surgery a treatment option for premenopausal patients with dysgerminoma? *Bratisl Lek Listy* **117**, 738-740 (2016). [https://doi.org/10.4149/bl\\_2016\\_131](https://doi.org/10.4149/bl_2016_131)
- 72 Auguste, A. *et al.* Small Cell Carcinoma of the Ovary, Hypercalcemic Type (SCCOHT) beyond SMARCA4 Mutations: A Comprehensive Genomic Analysis. *Cells* **9** (2020). <https://doi.org/10.3390/cells9061496>
- 73 Young, R. H., Oliva, E. & Scully, R. E. Small cell carcinoma of the ovary, hypercalcemic type. A clinicopathological analysis of 150 cases. *Am J Surg Pathol* **18**, 1102-1116 (1994). <https://doi.org/10.1097/00000478-199411000-00004>

- 74 Harrison, M. L. *et al.* Small cell of the ovary, hypercalcemic type -- analysis of combined experience and recommendation for management. A GCIG study. *Gynecol Oncol* **100**, 233-238 (2006). <https://doi.org/10.1016/j.ygyno.2005.10.024>
- 75 Atwi, D. *et al.* Small Cell Carcinoma of the Ovary, Hypercalcemic Type, in a 12-Month-Old Girl. *Pediatr Dev Pathol* **24**, 493-497 (2021). <https://doi.org/10.1177/10935266211021213>
- 76 Haroon, S. *et al.* Clinicopathological spectrum of ovarian sex cord-stromal tumors; 20 years' retrospective study in a developing country. *J Ovarian Res* **6**, 87 (2013). <https://doi.org/10.1186/1757-2215-6-87>
- 77 Shim, S. H. *et al.* Laparoscopic management of early-stage malignant nonepithelial ovarian tumors: surgical and survival outcomes. *Int J Gynecol Cancer* **23**, 249-255 (2013). <https://doi.org/10.1097/IGC.0b013e318272e754>
- 78 Jung, S. E. *et al.* CT and MRI findings of sex cord-stromal tumor of the ovary. *AJR Am J Roentgenol* **185**, 207-215 (2005). <https://doi.org/10.2214/ajr.185.1.01850207>
- 79 Prat, J. Pathology of the ovary. (*No Title*), 47 (2004).
- 80 Schultz, K. A. *et al.* Ovarian Sex Cord-Stromal Tumors. *J Oncol Pract* **12**, 940-946 (2016). <https://doi.org/10.1200/jop.2016.016261>
- 81 Abu-Rustum, N. R. *et al.* Retroperitoneal nodal metastasis in primary and recurrent granulosa cell tumors of the ovary. *Gynecol Oncol* **103**, 31-34 (2006). <https://doi.org/10.1016/j.ygyno.2006.01.050>
- 82 Schneider, D. T. *et al.* Ovarian sex cord-stromal tumors in children and adolescents. *J Clin Oncol* **21**, 2357-2363 (2003). <https://doi.org/10.1200/jco.2003.05.038>
- 83 Howlander N, Noone AM, Krapcho M, Miller D, Brest A, Yu M, Ruhl J, Tatalovich Z, Mariotto A, Lewis DR, Chen HS, Feuer EJ, Cronin KA (eds). SEER Cancer Statistics Review, 1975-2017, National Cancer Institute. Bethesda, MD, [https://seer.cancer.gov/csr/1975\\_2017/](https://seer.cancer.gov/csr/1975_2017/), based on November 2019 SEER data submission, posted to the SEER web site, April 2020.
- 84 Liu, J. H. & Zanotti, K. M. Management of the adnexal mass. *Obstet Gynecol* **117**, 1413-1428 (2011). <https://doi.org/10.1097/AOG.0b013e31821c62b6>
- 85 van Nagell, J. R., Jr. & Hoff, J. T. Transvaginal ultrasonography in ovarian cancer screening: current perspectives. *Int J Womens Health* **6**, 25-33 (2013). <https://doi.org/10.2147/ijwh.S38347>
- 86 Pavlik, E. J. *et al.* Ovarian volume related to age. *Gynecol Oncol* **77**, 410-412 (2000). <https://doi.org/10.1006/gyno.2000.5783>

- 87 Ameye, L. *et al.* Clinically oriented three-step strategy for assessment of adnexal pathology. *Ultrasound Obstet Gynecol* **40**, 582-591 (2012). <https://doi.org/10.1002/uog.11177>
- 88 Timmerman, D. *et al.* Simple ultrasound rules to distinguish between benign and malignant adnexal masses before surgery: prospective validation by IOTA group. *Bmj* **341**, c6839 (2010). <https://doi.org/10.1136/bmj.c6839>
- 89 Clarke-Pearson, D. L. Clinical practice. Screening for ovarian cancer. *N Engl J Med* **361**, 170-177 (2009). <https://doi.org/10.1056/NEJMcp0901926>
- 90 Bast, R. C., Jr. *et al.* Reactivity of a monoclonal antibody with human ovarian carcinoma. *J Clin Invest* **68**, 1331-1337 (1981). <https://doi.org/10.1172/jci110380>
- 91 Cannistra, S. A. Cancer of the ovary. *N Engl J Med* **351**, 2519-2529 (2004). <https://doi.org/10.1056/NEJMra041842>
- 92 Zurawski, V. R., Jr., Orjaseter, H., Andersen, A. & Jellum, E. Elevated serum CA 125 levels prior to diagnosis of ovarian neoplasia: relevance for early detection of ovarian cancer. *Int J Cancer* **42**, 677-680 (1988). <https://doi.org/10.1002/ijc.2910420507>
- 93 Bast, R. C., Jr. *et al.* A radioimmunoassay using a monoclonal antibody to monitor the course of epithelial ovarian cancer. *N Engl J Med* **309**, 883-887 (1983). <https://doi.org/10.1056/nejm198310133091503>
- 94 Høgdall, E. V. *et al.* CA125 expression pattern, prognosis and correlation with serum CA125 in ovarian tumor patients. From The Danish "MALOVA" Ovarian Cancer Study. *Gynecol Oncol* **104**, 508-515 (2007). <https://doi.org/10.1016/j.ygyno.2006.09.028>
- 95 ROSENTHAL, A. N., MENON, U. & JACOBS, I. J. Screening for Ovarian Cancer. *Clinical Obstetrics and Gynecology* **49**, 433-447 (2006).
- 96 Piatek, S. *et al.* Rising serum CA-125 levels within the normal range is strongly associated recurrence risk and survival of ovarian cancer. *J of Ovar Res* **13**, 102 (2020). <https://doi.org/10.1186/s13048-020-00681-0>
- 97 Wilder, J. L. *et al.* Clinical implications of a rising serum CA-125 within the normal range in patients with epithelial ovarian cancer: a preliminary investigation. *Gynecol Oncol* **89**, 233-235 (2003). [https://doi.org/10.1016/s0090-8258\(03\)00051-9](https://doi.org/10.1016/s0090-8258(03)00051-9)
- 98 Andersen, M. R. *et al.* Use of a Symptom Index, CA125, and HE4 to predict ovarian cancer. *Gynecol Oncol* **116**, 378-383 (2010). <https://doi.org/10.1016/j.ygyno.2009.10.087>

- 99 Montagnana, M. *et al.* HE4 in ovarian cancer: from discovery to clinical application. *Adv Clin Chem* **55**, 1-20 (2011).
- 100 Dochez, V. *et al.* Biomarkers and algorithms for diagnosis of ovarian cancer: CA125, HE4, RMI and ROMA, a review. *J Ovarian Res* **12**, 28 (2019). <https://doi.org/10.1186/s13048-019-0503-7>
- 101 Ruggeri, G. *et al.* HE4 and epithelial ovarian cancer: comparison and clinical evaluation of two immunoassays and a combination algorithm. *Clin Chim Acta* **412**, 1447-1453 (2011). <https://doi.org/10.1016/j.cca.2011.04.028>
- 102 Drapkin, R. *et al.* Human epididymis protein 4 (HE4) is a secreted glycoprotein that is overexpressed by serous and endometrioid ovarian carcinomas. *Cancer Res* **65**, 2162-2169 (2005). <https://doi.org/10.1158/0008-5472.Can-04-3924>
- 103 Van Gorp, T. *et al.* HE4 and CA125 as a diagnostic test in ovarian cancer: prospective validation of the Risk of Ovarian Malignancy Algorithm. *British Journal of Cancer* **104**, 863-870 (2011). <https://doi.org/10.1038/sj.bjc.6606092>
- 104 Ferraro, S., Schiumarini, D. & Panteghini, M. Human epididymis protein 4: factors of variation. *Clin Chim Acta* **438**, 171-177 (2015). <https://doi.org/10.1016/j.cca.2014.08.020>
- 105 Karlsen, N. S., Karlsen, M. A., Høgdall, C. K. & Høgdall, E. V. HE4 tissue expression and serum HE4 levels in healthy individuals and patients with benign or malignant tumors: a systematic review. *Cancer Epidemiol Biomarkers Prev* **23**, 2285-2295 (2014). <https://doi.org/10.1158/1055-9965.Epi-14-0447>
- 106 Bolstad, N., Øijordsbakken, M., Nustad, K. & Bjerner, J. Human epididymis protein 4 reference limits and natural variation in a Nordic reference population. *Tumour Biol* **33**, 141-148 (2012). <https://doi.org/10.1007/s13277-011-0256-4>
- 107 Nagy, B. *et al.* Elevated human epididymis protein 4 concentrations in chronic kidney disease. *Annals of Clinical Biochemistry* **49**, 377-380 (2012). <https://doi.org/10.1258/acb.2011.011258>
- 108 Prat, J. Staging classification for cancer of the ovary, fallopian tube, and peritoneum. *Int J Gynaecol Obstet* **124**, 1-5 (2014). <https://doi.org/10.1016/j.ijgo.2013.10.001>
- 109 Caruso, G. *et al.* Ovarian Cancer Metastasis to the Breast: A Case Report and Review of the Literature. *Case Rep Oncol* **13**, 1317-1324 (2020). <https://doi.org/10.1159/000509770>
- 110 Thomakos, N. *et al.* Rare Distant Metastatic Disease of Ovarian and Peritoneal Carcinomatosis: A Review of the Literature. *Cancers* **11**, 1044 (2019).

- 111 Berek, J. S., Renz, M., Kehoe, S., Kumar, L. & Friedlander, M. Cancer of the ovary, fallopian tube, and peritoneum: 2021 update. *Int J of Gynecol & Obste* **155**, 61-85 (2021). <https://doi.org/https://doi.org/10.1002/ijgo.13878>
- 112 Mallen, A. *et al.* Surgical prevention strategies in ovarian cancer. *Gynecol oncol* **151**, 166-175 (2018).
- 113 Walker, J. L. *et al.* Society of Gynecologic Oncology recommendations for the prevention of ovarian cancer. *Cancer* **121**, 2108-2120 (2015). <https://doi.org/https://doi.org/10.1002/cncr.29321>
- 114 Berek, J. S. & Hacker, N. F. *Berek and Hacker's gynecol oncol.* (Lippincott Williams & Wilkins, 2010).
- 115 Hacker, N. F., Berek, J. S., Lagasse, L. D., Nieberg, R. K. & Elashoff, R. M. Primary cytoreductive surgery for epithelial ovarian cancer. *Obstet Gynecol* **61**, 413-420 (1983).
- 116 van der Burg, M. E. *et al.* The effect of debulking surgery after induction chemotherapy on the prognosis in advanced epithelial ovarian cancer. Gynecological Cancer Cooperative Group of the European Organization for Research and Treatment of Cancer. *N Engl J Med* **332**, 629-634 (1995). <https://doi.org/10.1056/nejm199503093321002>
- 117 Rose, P. G. *et al.* Secondary surgical cytoreduction for advanced ovarian carcinoma. *N Engl J Med* **351**, 2489-2497 (2004). <https://doi.org/10.1056/NEJMoa041125>
- 118 Vergote, I. *et al.* Neoadjuvant chemotherapy or primary surgery in stage IIIC or IV ovarian cancer. *N Engl J Med* **363**, 943-953 (2010). <https://doi.org/10.1056/NEJMoa0908806>
- 119 Rossof, A. H. *et al.* Phase II evaluation of cis-dichlorodiammineplatinum(II) in advanced malignancies of the genitourinary and gynecologic organs: a Southwest Oncology Group Study. *Cancer Treat Rep* **63**, 1557-1564 (1979).
- 120 Thigpen, T., Shingleton, H., Homesley, H., LaGasse, L. & Blessing, J. cis-Dichlorodiammineplatinum(II) in the treatment of gynecologic malignancies: phase II trials by the Gynecologic Oncology Group. *Cancer Treat Rep* **63**, 1549-1555 (1979).
- 121 Decker, D. G. *et al.* Cyclophosphamide plus cis-platinum in combination: treatment program for stage III or IV ovarian carcinoma. *Obstet Gynecol* **60**, 481-487 (1982).
- 122 Omura, G. A. *et al.* Randomized trial of cyclophosphamide plus cisplatin with or without doxorubicin in ovarian carcinoma: a Gynecologic Oncology Group Study. *J Clin Oncol* **7**, 457-465 (1989). <https://doi.org/10.1200/jco.1989.7.4.457>

- 123 Lokich, J. & Anderson, N. Carboplatin versus cisplatin in solid tumors: an analysis of the literature. *Ann Oncol* **9**, 13-21 (1998). <https://doi.org/10.1023/a:1008215213739>
- 124 Ho, G. Y., Woodward, N. & Coward, J. I. G. Cisplatin versus carboplatin: comparative review of therapeutic management in solid malignancies. *Critical Reviews in Oncol/Hematol* **102**, 37-46 (2016). <https://doi.org/https://doi.org/10.1016/j.critrevonc.2016.03.014>
- 125 de Castria, T. B., da Silva, E. M., Gois, A. F. & Riera, R. Cisplatin versus carboplatin in combination with third-generation drugs for advanced non-small cell lung cancer. *Cochrane Database Syst Rev*, Cd009256 (2013). <https://doi.org/10.1002/14651858.CD009256.pub2>
- 126 Oun, R., Moussa, Y. E. & Wheate, N. J. The side effects of platinum-based chemotherapy drugs: a review for chemists. *Dalton Trans* **47**, 6645-6653 (2018). <https://doi.org/10.1039/c8dt00838h>
- 127 Alberts, D. S. *et al.* Improved therapeutic index of carboplatin plus cyclophosphamide versus cisplatin plus cyclophosphamide: final report by the Southwest Oncology Group of a phase III randomized trial in stages III and IV ovarian cancer. *J Clin Oncol* **10**, 706-717 (1992). <https://doi.org/10.1200/jco.1992.10.5.706>
- 128 Chemotherapy in advanced ovarian cancer: an overview of randomised clinical trials. Advanced Ovarian Cancer Trialists Group. *Bmj* **303**, 884-893 (1991). <https://doi.org/10.1136/bmj.303.6807.884>
- 129 Alassadi, S., Pisani, M. J. & Wheate, N. J. A chemical perspective on the clinical use of platinum-based anticancer drugs. *Dalton Transactions* **51**, 10835-10846 (2022). <https://doi.org/10.1039/D2DT01875F>
- 130 Symons, K. & Ermer, J. *Australian injectable drugs handbook (AIDH) ninth edition*. Ninth edition. edn, (Society of Hospital Pharmacists of Australia, 2023).
- 131 Cragg, G. M. Paclitaxel (Taxol): a success story with valuable lessons for natural product drug discovery and development. *Med Res Rev* **18**, 315-331 (1998). [https://doi.org/10.1002/\(sici\)1098-1128\(199809\)18:5<315::aid-med3>3.0.co;2-w](https://doi.org/10.1002/(sici)1098-1128(199809)18:5<315::aid-med3>3.0.co;2-w)
- 132 Uziely, B. *et al.* Paclitaxel (Taxol) in heavily pretreated ovarian cancer: antitumor activity and complications. *Ann Oncol* **5**, 827-833 (1994). <https://doi.org/10.1093/oxfordjournals.annonc.a059012>
- 133 McGuire, W. P. *et al.* Cyclophosphamide and cisplatin compared with paclitaxel and cisplatin in patients with stage III and stage IV ovarian cancer. *N Engl J Med* **334**, 1-6 (1996). <https://doi.org/10.1056/nejm199601043340101>



- 134 Piccart, M. J. *et al.* Randomized intergroup trial of cisplatin-paclitaxel versus cisplatin-cyclophosphamide in women with advanced epithelial ovarian cancer: three-year results. *J Natl Cancer Inst* **92**, 699-708 (2000). <https://doi.org/10.1093/jnci/92.9.699>
- 135 Ozols, R. F. *et al.* Phase III trial of carboplatin and paclitaxel compared with cisplatin and paclitaxel in patients with optimally resected stage III ovarian cancer: a Gynecologic Oncology Group study. *J Clin Oncol* **21**, 3194-3200 (2003). <https://doi.org/10.1200/jco.2003.02.153>
- 136 McGuire, W. P. *et al.* Cyclophosphamide and cisplatin versus paclitaxel and cisplatin: a phase III randomized trial in patients with suboptimal stage III/IV ovarian cancer (from the Gynecologic Oncology Group). *Semin Oncol* **23**, 40-47 (1996).
- 137 Gemignani, M. L. *et al.* Paclitaxel-based chemotherapy in carcinoma of the fallopian tube. *Gynecol Oncol* **80**, 16-20 (2001). <https://doi.org/10.1006/gyno.2000.6012>
- 138 Bookman, M. A. *et al.* Evaluation of new platinum-based treatment regimens in advanced-stage ovarian cancer: a Phase III Trial of the Gynecologic Cancer Intergroup. *J Clin Oncol* **27**, 1419-1425 (2009). <https://doi.org/10.1200/jco.2008.19.1684>
- 139 Vasey, P. A. *et al.* Docetaxel and cisplatin in combination as first-line chemotherapy for advanced epithelial ovarian cancer. Scottish Gynaecological Cancer Trials Group. *J Clin Oncol* **17**, 2069-2080 (1999). <https://doi.org/10.1200/jco.1999.17.7.2069>
- 140 Marquart, E., Jalili, A., Mothes-Luksch, N., Wagner, S. N. & Kinaciyan, T. Anaphylactic reaction to carboplatin diagnosed by skin testing-a reliable tool in platinum-based immediate-type hypersensitivity reactions. *Wien Med Wochenschr* **173**, 256-259 (2023). <https://doi.org/10.1007/s10354-022-00938-x>
- 141 Rose, P. G., Metz, C. & Link, N. Desensitization with oxaliplatin in patients intolerant of carboplatin desensitization. *International Journal of Gynecologic Cancer* **24** (2014).
- 142 Kolomeyevskaya, N. V. *et al.* Oxaliplatin Is a Safe Alternative Option for Patients With Recurrent Gynecologic Cancers After Hypersensitivity Reaction to Carboplatin. *Int J of Gynecol Can* **25**, 42-48 (2015). <https://doi.org/10.1097/igc.0000000000000307>
- 143 Lee, J.-Y. *et al.* Changes in ovarian cancer survival during the 20 years before the era of targeted therapy. *BMC Cancer* **18**, 601 (2018). <https://doi.org/10.1186/s12885-018-4498-z>
- 144 Helleday, T., Petermann, E., Lundin, C., Hodgson, B. & Sharma, R. A. DNA repair pathways as targets for cancer therapy. *Nat Rev Cancer* **8**, 193-204 (2008).
- 145 Farmer, H. *et al.* Targeting the DNA repair defect in BRCA mutant cells as a therapeutic strategy. *Nature* **434**, 917-921 (2005).

- 146 Xie, T. *et al.* Targeting Homologous Recombination Deficiency in Ovarian Cancer with PARP Inhibitors: Synthetic Lethal Strategies That Impact Overall Survival. *Cancers (Basel)* **14** (2022). <https://doi.org/10.3390/cancers14194621>
- 147 Murai, J. *et al.* Trapping of PARP1 and PARP2 by clinical PARP inhibitors. *Cancer research* **72**, 5588-5599 (2012).
- 148 Pujade-Lauraine, E. *et al.* Olaparib tablets as maintenance therapy in patients with platinum-sensitive, relapsed ovarian cancer and a BRCA1/2 mutation (SOLO2/ENGOT-Ov21): a double-blind, randomised, placebo-controlled, phase 3 trial. *The lancet oncol* **18**, 1274-1284 (2017).
- 149 Ledermann, J. *et al.* Olaparib maintenance therapy in platinum-sensitive relapsed ovarian cancer. *New Eng J of Med* **366**, 1382-1392 (2012).
- 150 Mirza, M. R. *et al.* Niraparib maintenance therapy in platinum-sensitive, recurrent ovarian cancer. *New Eng J of Med* **375**, 2154-2164 (2016).
- 151 Coleman, R. L. *et al.* Rucaparib maintenance treatment for recurrent ovarian carcinoma after response to platinum therapy (ARIEL3): a randomised, double-blind, placebo-controlled, phase 3 trial. *Lancet* **390**, 1949-1961 (2017).
- 152 GSK. TGA approves Zejula for ovarian cancer providing another option for newly diagnosed women with this deadly disease, <<https://au.gsk.com/en-au/media/press-releases/tga-approves-zejula-for-ovarian-cancer-providing-another-option-for-newly-diagnosed-women-with-this-deadly-disease/>> (
- 153 The Department of Health and Aged Care. *Australian Public Assessment Report for Olaparib*, <<https://www.tga.gov.au/resources/auspar/auspar-olaparib-1>> (2021).
- 154 DiSilvestro, P. *et al.* Maintenance Treatment of Newly Diagnosed Advanced Ovarian Cancer: Time for a Paradigm Shift? *Cancers (Basel)* **13** (2021). <https://doi.org/10.3390/cancers13225756>
- 155 Lorusso, D. *et al.* Spotlight on olaparib in the treatment of BRCA-mutated ovarian cancer: design, development and place in therapy. *Drug Des Devel Ther* **12**, 1501-1509 (2018). <https://doi.org/10.2147/dddt.S124447>
- 156 Ledermann, J. A. *et al.* Rucaparib for patients with platinum-sensitive, recurrent ovarian carcinoma (ARIEL3): post-progression outcomes and updated safety results from a randomised, placebo-controlled, phase 3 trial. *Lancet Oncol* **21**, 710-722 (2020). [https://doi.org/10.1016/s1470-2045\(20\)30061-9](https://doi.org/10.1016/s1470-2045(20)30061-9)



- 157 Robson, M. *et al.* Olaparib for Metastatic Breast Cancer in Patients with a Germline BRCA Mutation. *N Engl J Med* **377**, 523-533 (2017). <https://doi.org/10.1056/NEJMoa1706450>
- 158 Golan, T. *et al.* Maintenance Olaparib for Germline BRCA-Mutated Metastatic Pancreatic Cancer. *N Engl J Med* **381**, 317-327 (2019). <https://doi.org/10.1056/NEJMoa1903387>
- 159 Wu, M. S. & Goldberg, H. Role of Rucaparib in the Treatment of Prostate Cancer: Clinical Perspectives and Considerations. *Cancer Manag Res* **14**, 3159-3174 (2022). <https://doi.org/10.2147/cmar.S353411>
- 160 The Institute of Cancer Research. *EMA recommends olaparib for treatment of high-risk, early breast cancer*, <<https://www.icr.ac.uk/news-archive/ema-recommends-olaparib-for-treatment-of-high-risk-early-breast-cancer>> (
- 161 Culy, C. Bevacizumab: antiangiogenic cancer therapy. *Drugs Today (Barc)* **41**, 23-36 (2005). <https://doi.org/10.1358/dot.2005.41.1.875776>
- 162 Žak, K. *et al.* The Potential Influence of Residual or Recurrent Disease on Bevacizumab Treatment Efficacy in Ovarian Cancer: Current Evidence and Future Perspectives. *Cancers* **16**, 1063 (2024).
- 163 Tewari, K. S. *et al.* Final Overall Survival of a Randomized Trial of Bevacizumab for Primary Treatment of Ovarian Cancer. *J Clin Oncol* **37**, 2317-2328 (2019). <https://doi.org/10.1200/jco.19.01009>
- 164 Perren, T. J. *et al.* A phase 3 trial of bevacizumab in ovarian cancer. *N Engl J Med* **365**, 2484-2496 (2011). <https://doi.org/10.1056/NEJMoa1103799>
- 165 Zhao, T., Wang, X., Xu, T., Xu, X. & Liu, Z. Bevacizumab significantly increases the risks of hypertension and proteinuria in cancer patients: A systematic review and comprehensive meta-analysis. *Oncotarget* **8**, 51492-51506 (2017). <https://doi.org/10.18632/oncotarget.18190>
- 166 Colombari, O. *et al.* Bevacizumab for Newly Diagnosed Ovarian Cancers: Best Candidates Among High-Risk Disease Patients (ICON-7). *JNCI Cancer Spectr* **4**, pkaa026 (2020). <https://doi.org/10.1093/jncics/pkaa026>
- 167 US Food & Drug Administration. Highlights of prescribing information. Opdivo (nivolumab) injection, for intravenous use (2017).

- 168 Alvarez-Argote, J. & Dasanu, C. A. Durvalumab in cancer medicine: a comprehensive review. *Expert Opinion on Biological Therapy* **19**, 927-935 (2019).  
<https://doi.org/10.1080/14712598.2019.1635115>
- 169 Stewart, R. *et al.* Identification and characterization of MEDI4736, an antagonistic anti-PD-L1 monoclonal antibody. *Cancer immunology research* **3**, 1052-1062 (2015).
- 170 Lee, H. T. *et al.* Molecular mechanism of PD-1/PD-L1 blockade via anti-PD-L1 antibodies atezolizumab and durvalumab. *Sci Rep* **7**, 5532 (2017).  
<https://doi.org/10.1038/s41598-017-06002-8>
- 171 *A Multicentre Phase II Trial of Durvalumab Versus Physician's Choice Chemotherapy in Recurrent Ovarian Clear Cell Adenocarcinomas*,  
<<https://clinicaltrials.gov/ct2/show/NCT03405454?cond=Ovarian+Clear+Cell+Carcinoma&draw=2&rank=3>> (
- 172 *MOCCA : A Multicentre Phase II Randomised Trial of Durvalumab (MEDI4736) Versus Physician's Choice Chemotherapy in Recurrent Ovarian Clear Cell Adenocarcinomas*,  
<[https://trials.cancervic.org.au/details.aspx?ID=vctl\\_nct03405454#](https://trials.cancervic.org.au/details.aspx?ID=vctl_nct03405454#)> (
- 173 Partridge, E. *et al.* Results from four rounds of ovarian cancer screening in a randomized trial. *Obstet Gynecol* **113**, 775-782 (2009).  
<https://doi.org/10.1097/AOG.0b013e31819cda77>
- 174 Bast, R. C., Jr. *et al.* Prevention and early detection of ovarian cancer: mission impossible? *Recent Results Cancer Res* **174**, 91-100 (2007).  
[https://doi.org/10.1007/978-3-540-37696-5\\_9](https://doi.org/10.1007/978-3-540-37696-5_9)
- 175 Agarwal, R. & Kaye, S. B. Ovarian cancer: strategies for overcoming resistance to chemotherapy. *Nat Rev Cancer* **3**, 502-516 (2003). <https://doi.org/10.1038/nrc1123>
- 176 Schwab, M. *Encyclopedia of cancer*. (Springer Science & Business Media, 2008).
- 177 Hennessy, B. T., Coleman, R. L. & Markman, M. Ovarian cancer. *Lancet* **374**, 1371-1382 (2009). [https://doi.org/10.1016/s0140-6736\(09\)61338-6](https://doi.org/10.1016/s0140-6736(09)61338-6)
- 178 Chuang, Y. T. & Chang, C. L. Extending platinum-free interval in partially platinum-sensitive recurrent ovarian cancer by a non-platinum regimen: its possible clinical significance. *Taiwan J Obstet Gynecol* **51**, 336-341 (2012).  
<https://doi.org/10.1016/j.tjog.2012.07.003>
- 179 Tay, E. H., Grant, P. T., Gebiski, V. & Hacker, N. F. Secondary cytoreductive surgery for recurrent epithelial ovarian cancer. *Obstet Gynecol* **99**, 1008-1013 (2002).  
[https://doi.org/10.1016/s0029-7844\(02\)01977-4](https://doi.org/10.1016/s0029-7844(02)01977-4)

- 180 Eisenkop, S. M., Friedman, R. L. & Spirtos, N. M. The role of secondary cytoreductive surgery in the treatment of patients with recurrent epithelial ovarian carcinoma. *Cancer* **88**, 144-153 (2000). [https://doi.org/10.1002/\(sici\)1097-0142\(20000101\)88:1<144::aid-cncr20>3.3.co;2-o](https://doi.org/10.1002/(sici)1097-0142(20000101)88:1<144::aid-cncr20>3.3.co;2-o)
- 181 Gadducci, A. *et al.* Complete salvage surgical cytoreduction improves further survival of patients with late recurrent ovarian cancer. *Gynecol Oncol* **79**, 344-349 (2000). <https://doi.org/10.1006/gyno.2000.5992>
- 182 du Bois, A. *et al.* A randomized clinical trial of cisplatin/paclitaxel versus carboplatin/paclitaxel as first-line treatment of ovarian cancer. *J Natl Cancer Inst* **95**, 1320-1329 (2003). <https://doi.org/10.1093/jnci/djg036>
- 183 Okamoto, A. *et al.* Gynecologic Cancer InterGroup (GCIg) consensus review for clear cell carcinoma of the ovary. *Int J Gynecol Cancer* **24**, S20-25 (2014). <https://doi.org/10.1097/igc.0000000000000289>
- 184 Kajiyama, H. *et al.* Postrecurrent oncologic outcome of patients with ovarian clear cell carcinoma. *Int J Gynecol Cancer* **22**, 801-806 (2012). <https://doi.org/10.1097/IGC.0b013e3182540145>
- 185 Kajiyama, H. *et al.* Oncologic outcomes after secondary surgery in recurrent clear-cell carcinoma of the ovary. *Int J Gynecol Cancer* **29**, 910-915 (2019). <https://doi.org/10.1136/ijgc-2018-000142>
- 186 Markman, M. *et al.* Second-line platinum therapy in patients with ovarian cancer previously treated with cisplatin. *J Clin Oncol* **9**, 389-393 (1991). <https://doi.org/10.1200/jco.1991.9.3.389>
- 187 Sugiyama, T. *et al.* Clinical characteristics of clear cell carcinoma of the ovary: a distinct histologic type with poor prognosis and resistance to platinum-based chemotherapy. *Cancer* **88**, 2584-2589 (2000).
- 188 Mabuchi, S., Sugiyama, T. & Kimura, T. Clear cell carcinoma of the ovary: molecular insights and future therapeutic perspectives. *J Gynecol Oncol* **27**, e31 (2016). <https://doi.org/10.3802/jgo.2016.27.e31>
- 189 Tan, T. Z. *et al.* Analysis of gene expression signatures identifies prognostic and functionally distinct ovarian clear cell carcinoma subtypes. *EBioMedicine* **50**, 203-210 (2019). <https://doi.org/10.1016/j.ebiom.2019.11.017>
- 190 Wang, Z. & Sun, Y. Targeting p53 for Novel Anticancer Therapy. *Transl Oncol* **3**, 1-12 (2010). <https://doi.org/10.1593/tlo.09250>

- 191 Della Pepa, C. *et al.* Low Grade Serous Ovarian Carcinoma: from the molecular characterization to the best therapeutic strategy. *Cancer Treat Rev* **41**, 136-143 (2015). <https://doi.org/10.1016/j.ctrv.2014.12.003>
- 192 Sadlecki, P., Antosik, P., Grzanka, D., Grabiec, M. & Walentowicz-Sadlecka, M. KRAS mutation testing in borderline ovarian tumors and low-grade ovarian carcinomas with a rapid, fully integrated molecular diagnostic system. *Tumour Biol* **39**, 1010428317733984 (2017). <https://doi.org/10.1177/1010428317733984>
- 193 Yee, C., Dickson, K.-A., Muntasir, M. N., Ma, Y. & Marsh, D. J. Three-Dimensional Modelling of Ovarian Cancer: From Cell Lines to Organoids for Discovery and Personalized Medicine. *Front in Bioengi and Biotech* **10** (2022). <https://doi.org/10.3389/fbioe.2022.836984>
- 194 Matlashewski, G. *et al.* Isolation and characterization of a human p53 cDNA clone: expression of the human p53 gene. *Embo j* **3**, 3257-3262 (1984).
- 195 Isobe, M., Emanuel, B. S., Givol, D., Oren, M. & Croce, C. M. Localization of gene for human p53 tumour antigen to band 17p13. *Nature* **320**, 84-85 (1986). <https://doi.org/10.1038/320084a0>
- 196 Kern, S. E. *et al.* Identification of p53 as a sequence-specific DNA-binding protein. *Science* **252**, 1708-1711 (1991). <https://doi.org/10.1126/science.2047879>
- 197 Lane, D. P. Cancer. p53, guardian of the genome. *Nature* **358**, 15-16 (1992). <https://doi.org/10.1038/358015a0>
- 198 Sigal, A. & Rotter, V. Oncogenic mutations of the p53 tumor suppressor: the demons of the guardian of the genome. *Cancer Res* **60**, 6788-6793 (2000).
- 199 Jiang, L. *et al.* Ferroptosis as a p53-mediated activity during tumour suppression. *Nature* **520**, 57-62 (2015). <https://doi.org/10.1038/nature14344>
- 200 Rufini, A., Tucci, P., Celardo, I. & Melino, G. Senescence and aging: the critical roles of p53. *Oncogene* **32**, 5129-5143 (2013). <https://doi.org/10.1038/onc.2012.640>
- 201 Baugh, E. H., Ke, H., Levine, A. J., Bonneau, R. A. & Chan, C. S. Why are there hotspot mutations in the TP53 gene in human cancers? *Cell Death Differ* **25**, 154-160 (2018). <https://doi.org/10.1038/cdd.2017.180>
- 202 Cole, A. J. *et al.* Assessing mutant p53 in primary high-grade serous ovarian cancer using immunohistochemistry and massively parallel sequencing. *Sci Rep* **6**, 26191 (2016). <https://doi.org/10.1038/srep26191>
- 203 National Institutes of Health, U.S. Department of Health and Human Services. *The TP53 Database*, <<https://tp53.isb-cgc.org/>> (

- 204 Haupt, Y., Maya, R., Kazaz, A. & Oren, M. Mdm2 promotes the rapid degradation of p53. *Nature* **387**, 296-299 (1997). <https://doi.org/10.1038/387296a0>
- 205 Kubbutat, M. H., Jones, S. N. & Vousden, K. H. Regulation of p53 stability by Mdm2. *Nature* **387**, 299-303 (1997). <https://doi.org/10.1038/387299a0>
- 206 Honda, R., Tanaka, H. & Yasuda, H. Oncoprotein MDM2 is a ubiquitin ligase E3 for tumor suppressor p53. *FEBS Lett* **420**, 25-27 (1997). [https://doi.org/10.1016/s0014-5793\(97\)01480-4](https://doi.org/10.1016/s0014-5793(97)01480-4)
- 207 Bo, H., Heuvel, A. P. J. v. d., Varun, V. P., Shengliang, Z. & Wafik, S. E.-D. Targeting Tumor Suppressor p53 for Cancer Therapy: Strategies, Challenges and Opportunities. *Current Drug Targets* **15**, 80-89 (2014). <https://doi.org/http://dx.doi.org/10.2174/1389450114666140106101412>
- 208 Parrales, A. & Iwakuma, T. Targeting Oncogenic Mutant p53 for Cancer Therapy. *Front Oncol* **5**, 288 (2015). <https://doi.org/10.3389/fonc.2015.00288>
- 209 Mantovani, F., Walerych, D. & Sal, G. D. Targeting mutant p53 in cancer: a long road to precision therapy. *Febs j* **284**, 837-850 (2017). <https://doi.org/10.1111/febs.13948>
- 210 Kim, M. P. & Lozano, G. Mutant p53 partners in crime. *Cell Death Differ* **25**, 161-168 (2018). <https://doi.org/10.1038/cdd.2017.185>
- 211 Wang, Z. *et al.* Loss-of-Function but Not Gain-of-Function Properties of Mutant TP53 Are Critical for the Proliferation, Survival, and Metastasis of a Broad Range of Cancer Cells. *Cancer Discov* **14**, 362-379 (2024). <https://doi.org/10.1158/2159-8290.Cd-23-0402>
- 212 Liu, Y., Su, Z., Tavana, O. & Gu, W. Understanding the complexity of p53 in a new era of tumor suppression. *Cancer Cell* **42**, 946-967 (2024). <https://doi.org/10.1016/j.ccell.2024.04.009>
- 213 Shih-Chu Ho, E. *et al.* p53 Mutation Is Infrequent in Clear Cell Carcinoma of the Ovary. *Gynecol Oncol* **80**, 189-193 (2001). <https://doi.org/https://doi.org/10.1006/gyno.2000.6025>
- 214 Cancer Genome Atlas Research, N. Integrated genomic analyses of ovarian carcinoma. *Nature* **474**, 609-615 (2011). <https://doi.org/10.1038/nature10166>
- 215 Cole, A. J. *et al.* Assessing mutant p53 in primary high-grade serous ovarian cancer using immunohistochemistry and massively parallel sequencing. *Sci rep* **6**, 26191-26191 (2016). <https://doi.org/10.1038/srep26191>
- 216 Engelman, J. A., Luo, J. & Cantley, L. C. The evolution of phosphatidylinositol 3-kinases as regulators of growth and metabolism. *Nat Rev Gene* **7**, 606-619 (2006).

- 217 Katso, R. *et al.* Cellular function of phosphoinositide 3-kinases: implications for development, immunity, homeostasis, and cancer. *Annual review of cell and developmental biology* **17**, 615-675 (2001).
- 218 Martini, M., De Santis, M. C., Braccini, L., Gulluni, F. & Hirsch, E. PI3K/AKT signaling pathway and cancer: an updated review. *Annals of medicine* **46**, 372-383 (2014).
- 219 Asati, V., Mahapatra, D. K. & Bharti, S. K. PI3K/Akt/mTOR and Ras/Raf/MEK/ERK signaling pathways inhibitors as anticancer agents: Structural and pharmacological perspectives. *Euro j of med chem* **109**, 314-341 (2016).
- 220 Hennessy, B. T., Smith, D. L., Ram, P. T., Lu, Y. & Mills, G. B. Exploiting the PI3K/AKT pathway for cancer drug discovery. *Nat rev Drug dis* **4**, 988-1004 (2005).
- 221 Lonetti, A. *et al.* PI3K pan-inhibition impairs more efficiently proliferation and survival of T-cell acute lymphoblastic leukemia cell lines when compared to isoform-selective PI3K inhibitors. *Oncotarget* **6**, 10399-10414 (2015).  
<https://doi.org/10.18632/oncotarget.3295>
- 222 Zwang, Y. *et al.* Synergistic interactions with PI3K inhibition that induce apoptosis. *Elife* **6** (2017). <https://doi.org/10.7554/eLife.24523>
- 223 Mabuchi, S. *et al.* mTOR is a promising therapeutic target both in cisplatin-sensitive and cisplatin-resistant clear cell carcinoma of the ovary. *Clin Cancer Res* **15**, 5404-5413 (2009). <https://doi.org/10.1158/1078-0432.Ccr-09-0365>
- 224 Donahue, T. R. *et al.* Integrative survival-based molecular profiling of human pancreatic cancer. *Clin Cancer Res* **18**, 1352-1363 (2012).
- 225 Yuan, T. & Cantley, L. PI3K pathway alterations in cancer: variations on a theme. *Oncogene* **27**, 5497-5510 (2008).
- 226 Pacold, M. E. *et al.* Crystal structure and functional analysis of Ras binding to its effector phosphoinositide 3-kinase  $\gamma$ . *Cell* **103**, 931-944 (2000).
- 227 Ligresti, G. *et al.* PIK3CA mutations in human solid tumors: role in sensitivity to various therapeutic approaches. *Cell Cycle* **8**, 1352-1358 (2009).  
<https://doi.org/10.4161/cc.8.9.8255>
- 228 Shayesteh, L. *et al.* PIK3CA is implicated as an oncogene in ovarian cancer. *Nat genetics* **21**, 99-102 (1999).
- 229 Samuels, Y. *et al.* High frequency of mutations of the PIK3CA gene in human cancers. *Science* **304**, 554 (2004). <https://doi.org/10.1126/science.1096502>



- 230 Campbell, I. G. *et al.* Mutation of the PIK3CA gene in ovarian and breast cancer. *Cancer Res* **64**, 7678-7681 (2004). <https://doi.org/10.1158/0008-5472.Can-04-2933>
- 231 Lee, J. W. *et al.* PIK3CA gene is frequently mutated in breast carcinomas and hepatocellular carcinomas. *Oncogene* **24**, 1477-1480 (2005). <https://doi.org/10.1038/sj.onc.1208304>
- 232 Stružinská, I. *et al.* A comprehensive molecular analysis of 113 primary ovarian clear cell carcinomas reveals common therapeutically significant aberrations. *Diagnostic Pathol* **18**, 72 (2023). <https://doi.org/10.1186/s13000-023-01358-0>
- 233 Campbell, I. G. *et al.* Mutation of the PIK3CA gene in ovarian and breast cancer. *Cancer research* **64**, 7678-7681 (2004).
- 234 Yoshida, K. & Miki, Y. Role of BRCA1 and BRCA2 as regulators of DNA repair, transcription, and cell cycle in response to DNA damage. *Cancer science* **95**, 866-871 (2004).
- 235 Gudmundsdottir, K. & Ashworth, A. The roles of BRCA1 and BRCA2 and associated proteins in the maintenance of genomic stability. *Oncogene* **25**, 5864-5874 (2006).
- 236 Deng, C.-X. BRCA1: cell cycle checkpoint, genetic instability, DNA damage response and cancer evolution. *Nucleic acids research* **34**, 1416-1426 (2006).
- 237 E., B. *New finding may unlock secrets of BRCA mutations.*, 2010).
- 238 Saavedra, J. A. & Sandow, J. [Clear cell adenocarcinoma of the ovary (Saphir and Lackner) and so-called mesonephroma ovarii (Schiller) as combined tumors. Review of the literature and case report]. *Arch Gynakol* **206**, 131-153 (1968). <https://doi.org/10.1007/bf00666920>
- 239 Pozzati, F. *et al.* Imaging in gynecological disease (14): clinical and ultrasound characteristics of ovarian clear cell carcinoma. *Ultrasound Obstet Gynecol* **52**, 792-800 (2018). <https://doi.org/10.1002/uog.19171>
- 240 Kurman, R. J., Carcangiu, M. L., Herrington, C. S. & Carcangiu, M. L. *WHO Classification of Tumours of Female Reproductive Organs*. (International Agency for Research on Cancer (I A R C) (UN), 2014).
- 241 Hussein, Y. R. & Soslow, R. A. Molecular insights into the classification of high-grade endometrial carcinoma. *Pathology* **50**, 151-161 (2018). <https://doi.org/https://doi.org/10.1016/j.pathol.2017.09.010>
- 242 del Carmen, M. G., Birrer, M. & Schorge, J. O. Carcinosarcoma of the ovary: a review of the literature. *Gynecol Oncol* **125**, 271-277 (2012). <https://doi.org/10.1016/j.ygyno.2011.12.418>

- 243 Kim, S. I. *et al.* Trends in the Incidence and Survival Rates of Primary Ovarian Clear Cell Carcinoma Compared to Ovarian Serous Carcinoma in Korea. *Front Oncol* **12**, 874037 (2022). <https://doi.org/10.3389/fonc.2022.874037>
- 244 Dong, S. *et al.* Comparison of the clinical characteristics and prognosis between clear cell carcinomas and high-grade serous ovarian carcinomas. *Ginekol Pol* **94**, 792-798 (2023). <https://doi.org/10.5603/GP.a2022.0123>
- 245 Ku, F. C. *et al.* Clear cell carcinomas of the ovary have poorer outcomes compared with serous carcinomas: Results from a single-center Taiwanese study. *J Formos Med Assoc* **117**, 117-125 (2018). <https://doi.org/10.1016/j.jfma.2017.03.007>
- 246 Machida, H. *et al.* Trends and characteristics of epithelial ovarian cancer in Japan between 2002 and 2015: A JSGO-JSOG joint study. *Gynecol Oncol* **153**, 589-596 (2019). <https://doi.org/10.1016/j.ygyno.2019.03.243>
- 247 Ovarian Cancer Australia. *Resilience Kit*, <<https://www.ovariancancer.net.au/booklet/resilience-kit>> (Assessed 22, March, 2024)
- 248 Chan, J. K. *et al.* Do clear cell ovarian carcinomas have poorer prognosis compared to other epithelial cell types? A study of 1411 clear cell ovarian cancers. *Gynecologic oncology* **109**, 370-376 (2008).
- 249 Atiya, H. I. *et al.* Endometriosis-Associated Mesenchymal Stem Cells Support Ovarian Clear Cell Carcinoma through Iron Regulation. *Cancer Res* **82**, 4680-4693 (2022). <https://doi.org/10.1158/0008-5472.Can-22-1294>
- 250 Pearce, C. L. *et al.* Association between endometriosis and risk of histological subtypes of ovarian cancer: a pooled analysis of case-control studies. *The lancet oncology* **13**, 385-394 (2012).
- 251 Hermens, M. *et al.* Incidence of endometrioid and clear-cell ovarian cancer in histological proven endometriosis: the ENOCA population-based cohort study. *American journal of obstetrics and gynecology* **223**, 107. e101-107. e111 (2020).
- 252 Kvaskoff, M. *et al.* Endometriosis and cancer: a systematic review and meta-analysis. *Hum Reprod Update* **27**, 393-420 (2021). <https://doi.org/10.1093/humupd/dmaa045>
- 253 Kolkova, Z. *et al.* The G protein-coupled estrogen receptor 1 (GPER/GPR30) does not predict survival in patients with ovarian cancer. *J Ovarian Res* **5**, 9 (2012). <https://doi.org/10.1186/1757-2215-5-9>
- 254 Modugno, F. *et al.* Hormone response in ovarian cancer: time to reconsider as a clinical target? *Endocr Relat Cancer* **19**, R255-279 (2012). <https://doi.org/10.1530/erc-12-0175>



- 255 Sieh, W. *et al.* Hormone-receptor expression and ovarian cancer survival: an Ovarian Tumor Tissue Analysis consortium study. *The Lancet Oncology* **14**, 853-862 (2013).  
[https://doi.org/10.1016/S1470-2045\(13\)70253-5](https://doi.org/10.1016/S1470-2045(13)70253-5)
- 256 Osaku, D. *et al.* Differential expression of estrogen receptor subtypes in ovarian high-grade serous carcinoma and clear cell carcinoma. *Reprod Med Biol* **20**, 467-476 (2021).  
<https://doi.org/10.1002/rmb2.12402>
- 257 Anglesio, M. S., Carey, M. S., Köbel, M., Mackay, H. & Huntsman, D. G. Clear cell carcinoma of the ovary: a report from the first Ovarian Clear Cell Symposium, June 24th, 2010. *Gynecol Oncol* **121**, 407-415 (2011).  
<https://doi.org/10.1016/j.ygyno.2011.01.005>
- 258 Oliver, K. E. *et al.* An evaluation of progression free survival and overall survival of ovarian cancer patients with clear cell carcinoma versus serous carcinoma treated with platinum therapy: an NRG oncology/gynecologic oncology group experience. *Gynecologic oncology* **147**, 243-249 (2017).
- 259 Lee, Y. Y. *et al.* Prognosis of ovarian clear cell carcinoma compared to other histological subtypes: a meta-analysis. *Gynecol Oncol* **122**, 541-547 (2011).  
<https://doi.org/10.1016/j.ygyno.2011.05.009>
- 260 Liu, H. *et al.* Prognosis of ovarian clear cell cancer compared with other epithelial cancer types: A population-based analysis. *Oncol letters* **19**, 1947-1957 (2020).
- 261 Ogasawara, A., Sato, S. & Hasegawa, K. Current and future strategies for treatment of ovarian clear cell carcinoma. *J of Obstet and Gynaecol Res* **46**, 1678-1689 (2020).  
<https://doi.org/https://doi.org/10.1111/jog.14350>
- 262 Nagai, Y. *et al.* Postoperative whole abdominal radiotherapy in clear cell adenocarcinoma of the ovary. *Gynecol Oncol* **107**, 469-473 (2007).  
<https://doi.org/10.1016/j.ygyno.2007.07.079>
- 263 Hoskins, P. J. *et al.* Low-stage ovarian clear cell carcinoma: population-based outcomes in British Columbia, Canada, with evidence for a survival benefit as a result of irradiation. *J Clin Oncol* **30**, 1656-1662 (2012).  
<https://doi.org/10.1200/jco.2011.40.1646>
- 264 Komiyama, S. *et al.* Bevacizumab combined with platinum-taxane chemotherapy as first-line treatment for advanced ovarian cancer: a prospective observational study of safety and efficacy in Japanese patients (JGOG3022 trial). *Int J Clin Oncol* **24**, 103-114 (2019). <https://doi.org/10.1007/s10147-018-1319-y>

- 265 Wang, W. *et al.* Biological function of long non-coding RNA (LncRNA) Xist. *Frontiers in cell and developmental biology* **9**, 645647 (2021).
- 266 Mansuy, I. M. & Mohanna, S. Epigenetics and the human brain: where nurture meets nature. *Cerebrum* **2011**, 8 (2011).
- 267 Samanta, S., Rajasingh, S., Cao, T., Dawn, B. & Rajasingh, J. Epigenetic dysfunctional diseases and therapy for infection and inflammation. *Biochim Biophys Acta Mol Basis Dis* **1863**, 518-528 (2017). <https://doi.org/10.1016/j.bbadis.2016.11.030>
- 268 Chahwan, R., Wontakal, S. N. & Roa, S. The multidimensional nature of epigenetic information and its role in disease. *Discov Med* **11**, 233-243 (2011).
- 269 Novak, K. Epigenetics changes in cancer cells. *MedGenMed* **6**, 17 (2004).
- 270 Jones, P. A. & Baylin, S. B. The epigenomics of cancer. *Cell* **128**, 683-692 (2007). <https://doi.org/10.1016/j.cell.2007.01.029>
- 271 McKenna, E. S. & Roberts, C. W. Epigenetics and cancer without genomic instability. *Cell Cycle* **8**, 23-26 (2009). <https://doi.org/10.4161/cc.8.1.7290>
- 272 Sparmann, A. & van Lohuizen, M. Polycomb silencers control cell fate, development and cancer. *Nat Rev Cancer* **6**, 846-856 (2006). <https://doi.org/10.1038/nrc1991>
- 273 Parreno, V. *et al.* Transient loss of Polycomb components induces an epigenetic cancer fate. *bioRxiv*, 2023.2001.2004.522799 (2023). <https://doi.org/10.1101/2023.01.04.522799>
- 274 Youngson, R. M. *Collins Dictionary of Human Biology*. (Collins, 2006).
- 275 Bhasin, M., Reinherz, E. L. & Reche, P. A. Recognition and classification of histones using support vector machine. *J Comput Biol* **13**, 102-112 (2006). <https://doi.org/10.1089/cmb.2006.13.102>
- 276 Li, B., Carey, M. & Workman, J. L. The role of chromatin during transcription. *Cell* **128**, 707-719 (2007). <https://doi.org/10.1016/j.cell.2007.01.015>
- 277 Winston, F. & Carlson, M. Yeast SNF/SWI transcriptional activators and the SPT/SIN chromatin connection. *Trends Genet* **8**, 387-391 (1992). [https://doi.org/10.1016/0168-9525\(92\)90300-s](https://doi.org/10.1016/0168-9525(92)90300-s)
- 278 Robertson, K. D. *et al.* The human DNA methyltransferases (DNMTs) 1, 3a and 3b: coordinate mRNA expression in normal tissues and overexpression in tumors. *Nucleic acids research* **27**, 2291-2298 (1999).
- 279 Kaiser, S. *et al.* The RNA methyltransferase Dnmt2 methylates DNA in the structural context of a tRNA. *RNA Biol* **14**, 1241-1251 (2017). <https://doi.org/10.1080/15476286.2016.1236170>

- 280 Okano, M., Bell, D. W., Haber, D. A. & Li, E. DNA methyltransferases Dnmt3a and Dnmt3b are essential for de novo methylation and mammalian development. *Cell* **99**, 247-257 (1999).
- 281 Gowher, H., Liebert, K., Hermann, A., Xu, G. & Jeltsch, A. Mechanism of Stimulation of Catalytic Activity of Dnmt3A and Dnmt3B DNA-(cytosine-C5)-methyltransferases by Dnmt3L\*. *Journal of Biological Chemistry* **280**, 13341-13348 (2005). <https://doi.org/https://doi.org/10.1074/jbc.M413412200>
- 282 Suetake, I., Shinozaki, F., Miyagawa, J., Takeshima, H. & Tajima, S. DNMT3L stimulates the DNA methylation activity of Dnmt3a and Dnmt3b through a direct interaction. *Journal of Biological Chemistry* **279**, 27816-27823 (2004).
- 283 Deshaies, R. J. & Joazeiro, C. A. RING domain E3 ubiquitin ligases. *Annu Rev Biochem* **78**, 399-434 (2009). <https://doi.org/10.1146/annurev.biochem.78.101807.093809>
- 284 So, C. C., Ramachandran, S. & Martin, A. E3 Ubiquitin Ligases RNF20 and RNF40 Are Required for Double-Stranded Break (DSB) Repair: Evidence for Monoubiquitination of Histone H2B Lysine 120 as a Novel Axis of DSB Signaling and Repair. *Mol Cell Biol* **39** (2019). <https://doi.org/10.1128/mcb.00488-18>
- 285 Sethi, G., Shanmugam, M. K., Arfuso, F. & Kumar, A. P. Role of RNF20 in cancer development and progression - a comprehensive review. *Biosci Rep* **38** (2018). <https://doi.org/10.1042/bsr20171287>
- 286 Yang, Q., Zhao, J., Chen, D. & Wang, Y. E3 ubiquitin ligases: styles, structures and functions. *Mol Biomed* **2**, 23 (2021). <https://doi.org/10.1186/s43556-021-00043-2>
- 287 Biswas, S. & Rao, C. M. Epigenetic tools (The Writers, The Readers and The Erasers) and their implications in cancer therapy. *Euro J of Pharm* **837**, 8-24 (2018). <https://doi.org/https://doi.org/10.1016/j.ejphar.2018.08.021>
- 288 Devaiah, B. N. *et al.* BRD4 is a histone acetyltransferase that evicts nucleosomes from chromatin. *Nature structural & molecular biology* **23**, 540-548 (2016).
- 289 Ren, C. *et al.* Small-molecule modulators of methyl-lysine binding for the CBX7 chromodomain. *Chem & bio* **22**, 161-168 (2015).
- 290 Roy, S. *et al.* Structural insight into p53 recognition by the 53BP1 tandem Tudor domain. *J of mole bio* **398**, 489-496 (2010).
- 291 Lorsbach, R. *et al.* TET1, a member of a novel protein family, is fused to MLL in acute myeloid leukemia containing the t (10; 11)(q22; q23). *Leukemia* **17**, 637-641 (2003).
- 292 Maiques-Diaz, A. & Somervaille, T. C. LSD1: biologic roles and therapeutic targeting. *Epigenomics* **8**, 1103-1116 (2016).

- 293 Tang, J., Yan, H. & Zhuang, S. Histone deacetylases as targets for treatment of multiple diseases. *Clin Sci (Lond)* **124**, 651-662 (2013). <https://doi.org/10.1042/cs20120504>
- 294 Ruzic, D. *et al.* Targeting Histone Deacetylases: Opportunities for Cancer Treatment and Chemoprevention. *Pharmaceutics* **14** (2022). <https://doi.org/10.3390/pharmaceutics14010209>
- 295 Xu, H., Liu, Y. L., Yang, Y. M. & Dong, X. S. Knock-down of ubiquitin-specific protease 22 by micro-RNA interference inhibits colorectal cancer growth. *Int J Colorectal Dis* **27**, 21-30 (2012). <https://doi.org/10.1007/s00384-011-1275-8>
- 296 Lin, Z. *et al.* USP22 antagonizes p53 transcriptional activation by deubiquitinating Sirt1 to suppress cell apoptosis and is required for mouse embryonic development. *Mol Cell* **46**, 484-494 (2012). <https://doi.org/10.1016/j.molcel.2012.03.024>
- 297 Stern, M., Jensen, R. & Herskowitz, I. Five SWI genes are required for expression of the HO gene in yeast. *J Mol Biol* **178**, 853-868 (1984). [https://doi.org/10.1016/0022-2836\(84\)90315-2](https://doi.org/10.1016/0022-2836(84)90315-2)
- 298 Alpsy, A. & Dykhuizen, E. C. Glioma tumor suppressor candidate region gene 1 (GLTSCR1) and its paralog GLTSCR1-like form SWI/SNF chromatin remodeling subcomplexes. *J Biol Chem* **293**, 3892-3903 (2018). <https://doi.org/10.1074/jbc.RA117.001065>
- 299 Alpsy, A. *et al.* BRD9 is a critical regulator of androgen receptor signaling and prostate cancer progression. *Cancer research* **81**, 820-833 (2021).
- 300 Andrades, A. *et al.* SWI/SNF complexes in hematological malignancies: biological implications and therapeutic opportunities. *Mol Cancer* **22**, 39 (2023). <https://doi.org/10.1186/s12943-023-01736-8>
- 301 Mashtalir, N. *et al.* Modular Organization and Assembly of SWI/SNF Family Chromatin Remodeling Complexes. *Cell* **175**, 1272-1288.e1220 (2018). <https://doi.org/10.1016/j.cell.2018.09.032>
- 302 Innis, S. M. & Cabot, B. GBAF, a small BAF sub-complex with big implications: a systematic review. *Epigenetics Chromatin* **13**, 48 (2020). <https://doi.org/10.1186/s13072-020-00370-8>
- 303 Reisman, D. N., Sciarrotta, J., Bouldin, T. W., Weissman, B. E. & Funkhouser, W. K. The expression of the SWI/SNF ATPase subunits BRG1 and BRM in normal human tissues. *Appl Immunohistochem Mol Morphol* **13**, 66-74 (2005). <https://doi.org/10.1097/00129039-200503000-00011>

- 304 Krishnamurthy, N., Kato, S., Lippman, S. & Kurzrock, R. Chromatin remodeling (SWI/SNF) complexes, cancer, and response to immunotherapy. *J for ImmunoTherapy of Cancer* **10**, e004669 (2022). <https://doi.org/10.1136/jitc-2022-004669>
- 305 Savas, S. & Skardasi, G. The SWI/SNF complex subunit genes: Their functions, variations, and links to risk and survival outcomes in human cancers. *Crit Rev Oncol Hematol* **123**, 114-131 (2018). <https://doi.org/10.1016/j.critrevonc.2018.01.009>
- 306 Sima, X. *et al.* The genetic alteration spectrum of the SWI/SNF complex: The oncogenic roles of BRD9 and ACTL6A. *PLoS One* **14**, e0222305 (2019). <https://doi.org/10.1371/journal.pone.0222305>
- 307 Centore, R. C., Sandoval, G. J., Soares, L. M. M., Kadoch, C. & Chan, H. M. Mammalian SWI/SNF Chromatin Remodeling Complexes: Emerging Mechanisms and Therapeutic Strategies. *Trends in Genetics* **36**, 936-950 (2020). <https://doi.org/10.1016/j.tig.2020.07.011>
- 308 Shain, A. H. & Pollack, J. R. The spectrum of SWI/SNF mutations, ubiquitous in human cancers. *PLoS One* **8**, e55119 (2013). <https://doi.org/10.1371/journal.pone.0055119>
- 309 Kadoch, C. *et al.* Proteomic and bioinformatic analysis of mammalian SWI/SNF complexes identifies extensive roles in human malignancy. *Nat Genet* **45**, 592-601 (2013). <https://doi.org/10.1038/ng.2628>
- 310 Versteeg, I. *et al.* Truncating mutations of hSNF5/INI1 in aggressive paediatric cancer. *Nature* **394**, 203-206 (1998). <https://doi.org/10.1038/28212>
- 311 Margol, A. S. & Judkins, A. R. Pathology and diagnosis of SMARCB1-deficient tumors. *Cancer Genet* **207**, 358-364 (2014). <https://doi.org/10.1016/j.cancergen.2014.07.004>
- 312 Cooper, G. W. & Hong, A. L. SMARCB1-Deficient Cancers: Novel Molecular Insights and Therapeutic Vulnerabilities. *Cancers (Basel)* **14** (2022). <https://doi.org/10.3390/cancers14153645>
- 313 Medina, P. P. *et al.* Frequent BRG1/SMARCA4-inactivating mutations in human lung cancer cell lines. *Hum Mutat* **29**, 617-622 (2008). <https://doi.org/10.1002/humu.20730>
- 314 Bai, J. *et al.* BRG1 is a prognostic marker and potential therapeutic target in human breast cancer. *PLoS One* **8**, e59772 (2013). <https://doi.org/10.1371/journal.pone.0059772>
- 315 Pyo, J. S., Son, B. K., Oh, D. & Kim, E. K. BRG1 is correlated with poor prognosis in colorectal cancer. *Hum Pathol* **73**, 66-73 (2018). <https://doi.org/10.1016/j.humpath.2017.12.013>

- 316 Hodges, C., Kirkland, J. G. & Crabtree, G. R. The Many Roles of BAF (mSWI/SNF) and PBAF Complexes in Cancer. *Cold Spring Harb Perspect Med* **6** (2016). <https://doi.org/10.1101/cshperspect.a026930>
- 317 Guan, B. *et al.* Mutation and loss of expression of ARID1A in uterine low-grade endometrioid carcinoma. *Am J Surg Pathol* **35**, 625-632 (2011). <https://doi.org/10.1097/PAS.0b013e318212782a>
- 318 Reisman, D., Glaros, S. & Thompson, E. A. The SWI/SNF complex and cancer. *Oncogene* **28**, 1653-1668 (2009). <https://doi.org/10.1038/onc.2009.4>
- 319 Wu, J. N. & Roberts, C. W. ARID1A mutations in cancer: another epigenetic tumor suppressor? *Cancer Discov* **3**, 35-43 (2013). <https://doi.org/10.1158/2159-8290.Cd-12-0361>
- 320 Kadoch, C. *et al.* Proteomic and bioinformatic analysis of mammalian SWI/SNF complexes identifies extensive roles in human malignancy. *Nat gen* **45**, 592-601 (2013).
- 321 McConechy, M. K. *et al.* Use of mutation profiles to refine the classification of endometrial carcinomas. *The J of pathol* **228**, 20-30 (2012).
- 322 Wang, K. *et al.* Exome sequencing identifies frequent mutation of ARID1A in molecular subtypes of gastric cancer. *Nat gen* **43**, 1219 (2011).
- 323 Guo, X. *et al.* ARID1A and CEBP $\alpha$  cooperatively inhibit UCA1 transcription in breast cancer. *Oncogene* **37**, 5939-5951 (2018). <https://doi.org/10.1038/s41388-018-0371-4>
- 324 Bosse, T. *et al.* Loss of ARID1A expression and its relationship with PI3K-Akt pathway alterations, TP53 and microsatellite instability in endometrial cancer. *Mod Pathol* **26**, 1525-1535 (2013). <https://doi.org/10.1038/modpathol.2013.96>
- 325 Lee, D., Yu, E. J., Ham, I. H., Hur, H. & Kim, Y. S. AKT inhibition is an effective treatment strategy in ARID1A-deficient gastric cancer cells. *Onco Targets Ther* **10**, 4153-4159 (2017). <https://doi.org/10.2147/ott.S139664>
- 326 Samartzis, E. P. *et al.* Loss of ARID1A expression sensitizes cancer cells to PI3K- and AKT-inhibition. *Oncotarget* **5**, 5295-5303 (2014). <https://doi.org/10.18632/oncotarget.2092>
- 327 Chandler, R. L. *et al.* Coexistent ARID1A–PIK3CA mutations promote ovarian clear-cell tumorigenesis through pro-tumorigenic inflammatory cytokine signalling. *Nature communications* **6**, 6118 (2015).
- 328 Wiegand, K. C. *et al.* ARID1A mutations in endometriosis-associated ovarian carcinomas. *N Engl J Med* **363**, 1532-1543 (2010). <https://doi.org/10.1056/NEJMoa1008433>



- 329 Yamamoto, S., Tsuda, H., Takano, M., Tamai, S. & Matsubara, O. Loss of ARID1A protein expression occurs as an early event in ovarian clear-cell carcinoma development and frequently coexists with PIK3CA mutations. *Mod Pathol* **25**, 615-624 (2012). <https://doi.org/10.1038/modpathol.2011.189>
- 330 Xiao, W., Awadallah, A. & Xin, W. Loss of ARID1A/BAF250a expression in ovarian endometriosis and clear cell carcinoma. *Int J Clin Exp Pathol* **5**, 642-650 (2012).
- 331 Guan, B., Wang, T. L. & Shih Ie, M. ARID1A, a factor that promotes formation of SWI/SNF-mediated chromatin remodeling, is a tumor suppressor in gynecologic cancers. *Cancer Res* **71**, 6718-6727 (2011). <https://doi.org/10.1158/0008-5472.Can-11-1562>
- 332 Itamochi, H. *et al.* Whole-genome sequencing revealed novel prognostic biomarkers and promising targets for therapy of ovarian clear cell carcinoma. *British j of cancer* **117**, 717-724 (2017).
- 333 Helming, K. C. *et al.* ARID1B is a specific vulnerability in ARID1A-mutant cancers. *Nat Med* **20**, 251-254 (2014). <https://doi.org/10.1038/nm.3480>
- 334 Nagl, N. G., Jr. *et al.* The p270 (ARID1A/SMARCF1) subunit of mammalian SWI/SNF-related complexes is essential for normal cell cycle arrest. *Cancer Res* **65**, 9236-9244 (2005). <https://doi.org/10.1158/0008-5472.Can-05-1225>
- 335 Trizzino, M. *et al.* The Tumor Suppressor ARID1A Controls Global Transcription via Pausing of RNA Polymerase II. *Cell Rep* **23**, 3933-3945 (2018). <https://doi.org/10.1016/j.celrep.2018.05.097>
- 336 Bitler, B. G. *et al.* Synthetic lethality by targeting EZH2 methyltransferase activity in ARID1A-mutated cancers. *Nat Med* **21**, 231-238 (2015). <https://doi.org/10.1038/nm.3799>
- 337 Hein, K. Z., Stephen, B. & Fu, S. Therapeutic Role of Synthetic Lethality in ARID1A-Deficient Malignancies. *J Immunother Precis Oncol* **7**, 41-52 (2024). <https://doi.org/10.36401/jipo-22-37>
- 338 Park, Y. *et al.* Loss of ARID1A in Tumor Cells Renders Selective Vulnerability to Combined Ionizing Radiation and PARP Inhibitor Therapy. *Clin Cancer Res* **25**, 5584-5594 (2019). <https://doi.org/10.1158/1078-0432.Ccr-18-4222>
- 339 Zhao, X. S., Zhou, J., Dong, L., Zhang, H. & Ye, Y. J. Durable response to olaparib in pancreatic duct adenocarcinoma with deleterious ARID1A mutation. *Chin Med J (Engl)* **132**, 3012-3014 (2019). <https://doi.org/10.1097/cm9.0000000000000550>

- 340 Fukumoto, T. *et al.* Repurposing Pan-HDAC Inhibitors for ARID1A-Mutated Ovarian  
Cancer. *Cell Rep* **22**, 3393-3400 (2018). <https://doi.org/10.1016/j.celrep.2018.03.019>
- 341 Ishino, Y., Shinagawa, H., Makino, K., Amemura, M. & Nakata, A. Nucleotide  
sequence of the iap gene, responsible for alkaline phosphatase isozyme conversion in  
Escherichia coli, and identification of the gene product. *J Bacteriol* **169**, 5429-5433  
(1987). <https://doi.org/10.1128/jb.169.12.5429-5433.1987>
- 342 Barrangou, R. The roles of CRISPR-Cas systems in adaptive immunity and beyond.  
*Curr Opin Immunol* **32**, 36-41 (2015). <https://doi.org/10.1016/j.coi.2014.12.008>
- 343 Redman, M., King, A., Watson, C. & King, D. What is CRISPR/Cas9? *Arch Dis Child*  
*Educ Pract Ed* **101**, 213-215 (2016). <https://doi.org/10.1136/archdischild-2016-310459>
- 344 Barrangou, R. *et al.* CRISPR provides acquired resistance against viruses in  
prokaryotes. *Science* **315**, 1709-1712 (2007). <https://doi.org/10.1126/science.1138140>
- 345 Marraffini, L. A. & Sontheimer, E. J. CRISPR interference limits horizontal gene  
transfer in staphylococci by targeting DNA. *Science* **322**, 1843-1845 (2008).  
<https://doi.org/10.1126/science.1165771>
- 346 Hille, F. *et al.* The Biology of CRISPR-Cas: Backward and Forward. *Cell* **172**, 1239-  
1259 (2018). <https://doi.org/10.1016/j.cell.2017.11.032>
- 347 Makarova, K. S. *et al.* An updated evolutionary classification of CRISPR-Cas systems.  
*Nat Rev Microbiol* **13**, 722-736 (2015). <https://doi.org/10.1038/nrmicro3569>
- 348 Cong, L. *et al.* Multiplex genome engineering using CRISPR/Cas systems. *Science* **339**,  
819-823 (2013). <https://doi.org/10.1126/science.1231143>
- 349 Ran, F. A. *et al.* Genome engineering using the CRISPR-Cas9 system. *Nat Prot* **8**,  
2281-2308 (2013). <https://doi.org/10.1038/nprot.2013.143>
- 350 Jinek, M. *et al.* A programmable dual-RNA-guided DNA endonuclease in adaptive  
bacterial immunity. *Science* **337**, 816-821 (2012).  
<https://doi.org/10.1126/science.1225829>
- 351 Westermann, L., Neubauer, B. & Köttgen, M. Nobel Prize 2020 in Chemistry honors  
CRISPR: a tool for rewriting the code of life. *Pflugers Arch* **473**, 1-2 (2021).  
<https://doi.org/10.1007/s00424-020-02497-9>
- 352 Mali, P. *et al.* RNA-guided human genome engineering via Cas9. *Science* **339**, 823-826  
(2013). <https://doi.org/10.1126/science.1232033>
- 353 Bolotin, A., Quinquis, B., Sorokin, A. & Ehrlich, S. D. Clustered regularly interspaced  
short palindrome repeats (CRISPRs) have spacers of extrachromosomal origin. *Microb*  
**151**, 2551-2561 (2005).



- 354 Hsu, P. D. *et al.* DNA targeting specificity of RNA-guided Cas9 nucleases. *Nat Biotechnol* **31**, 827-832 (2013). <https://doi.org/10.1038/nbt.2647>
- 355 Liu, C., Zhang, L., Liu, H. & Cheng, K. Delivery strategies of the CRISPR-Cas9 gene-editing system for therapeutic applications. *J Control Release* **266**, 17-26 (2017). <https://doi.org/10.1016/j.jconrel.2017.09.012>
- 356 De, A. & Biswas, A. R. Nanotechnology and Computational tool based study of CRISPR/Cas-9 research in Biomedical Engineering. *J Nano Res Adv Mater Polym Sci.* **2020; 1 1** (2020).
- 357 Hale, C. R. *et al.* Essential features and rational design of CRISPR RNAs that function with the Cas RAMP module complex to cleave RNAs. *Mol Cell* **45**, 292-302 (2012). <https://doi.org/10.1016/j.molcel.2011.10.023>
- 358 Su, S. *et al.* CRISPR-Cas9 mediated efficient PD-1 disruption on human primary T cells from cancer patients. *Scientific Reports* **6**, 20070 (2016). <https://doi.org/10.1038/srep20070>
- 359 Schumann, K. *et al.* Generation of knock-in primary human T cells using Cas9 ribonucleoproteins. *Proc Natl Acad Sci U S A* **112**, 10437-10442 (2015). <https://doi.org/10.1073/pnas.1512503112>
- 360 Yin, Y. *et al.* TRIM11, a direct target of miR-24-3p, promotes cell proliferation and inhibits apoptosis in colon cancer. *Oncotarget* **7**, 86755 (2016).
- 361 Eyquem, J. *et al.* Targeting a CAR to the TRAC locus with CRISPR/Cas9 enhances tumour rejection. *Nature* **543**, 113-117 (2017). <https://doi.org/10.1038/nature21405>
- 362 Andrea, A. E., Chiron, A., Bessoles, S. & Hacein-Bey-Abina, S. Engineering Next-Generation CAR-T Cells for Better Toxicity Management. *Int J Mol Sci* **21** (2020). <https://doi.org/10.3390/ijms21228620>
- 363 Ren, J. *et al.* Multiplex Genome Editing to Generate Universal CAR T Cells Resistant to PD1 Inhibition. *Clinical Cancer Research* **23**, 2255-2266 (2017). <https://doi.org/10.1158/1078-0432.Ccr-16-1300>
- 364 Parums, D. V. Editorial: First Regulatory Approvals for CRISPR-Cas9 Therapeutic Gene Editing for Sickle Cell Disease and Transfusion-Dependent  $\beta$ -Thalassemia. *Med Sci Monit* **30**, e944204 (2024). <https://doi.org/10.12659/msm.944204>
- 365 Platt, O. S. *et al.* Pain in sickle cell disease. Rates and risk factors. *N Engl J Med* **325**, 11-16 (1991). <https://doi.org/10.1056/nejm199107043250103>
- 366 Steinberg, M. H. & Sebastiani, P. Genetic modifiers of sickle cell disease. *Am J Hematol* **87**, 795-803 (2012). <https://doi.org/10.1002/ajh.23232>

- 367 Casgevy and Lyfgenia: Two gene therapies for sickle cell disease. *Med Lett Drugs Ther* **66**, 9-10 (2024). <https://doi.org/10.58347/tml.2024.1694a>
- 368 Nosengo, N. Can you teach old drugs new tricks? *Nature* **534**, 314-316 (2016). <https://doi.org/10.1038/534314a>
- 369 Hay, M., Thomas, D. W., Craighead, J. L., Economides, C. & Rosenthal, J. Clinical development success rates for investigational drugs. *Nat Biotechnol* **32**, 40-51 (2014). <https://doi.org/10.1038/nbt.2786>
- 370 Langtry, H. D. & Markham, A. Sildenafil: a review of its use in erectile dysfunction. *Drugs* **57**, 967-989 (1999).
- 371 Gonzalez-Fierro, A. & Dueñas-González, A. Drug repurposing for cancer therapy, easier said than done. *Semin Cancer Biol* **68**, 123-131 (2021). <https://doi.org/10.1016/j.semcancer.2019.12.012>
- 372 Tremblay, G. *et al.* Quality of life analyses in patients with multiple myeloma: results from the Selinexor (KPT-330) Treatment of Refractory Myeloma (STORM) phase 2b study. *BMC cancer* **21**, 1-10 (2021).
- 373 Mao, Y. *et al.* Drug repurposing screening and mechanism analysis based on human colorectal cancer organoids. *Protein & Cell* **15**, 285-304 (2023). <https://doi.org/10.1093/procel/pwad038>
- 374 Yang, W. *et al.* Genomics of Drug Sensitivity in Cancer (GDSC): a resource for therapeutic biomarker discovery in cancer cells. *Nucleic Acids Res* **41**, D955-961 (2013). <https://doi.org/10.1093/nar/gks1111>
- 375 Basu, A. *et al.* An interactive resource to identify cancer genetic and lineage dependencies targeted by small molecules. *Cell* **154**, 1151-1161 (2013). <https://doi.org/10.1016/j.cell.2013.08.003>
- 376 Seashore-Ludlow, B. *et al.* Harnessing Connectivity in a Large-Scale Small-Molecule Sensitivity Dataset. *Cancer Discov* **5**, 1210-1223 (2015). <https://doi.org/10.1158/2159-8290.Cd-15-0235>
- 377 Gao, G., Ahn, M., Cho, W. W., Kim, B. S. & Cho, D. W. 3D Printing of Pharmaceutical Application: Drug Screening and Drug Delivery. *Pharma* **13** (2021). <https://doi.org/10.3390/pharmaceutics13091373>
- 378 Williams, M. & Raddatz, R. Receptors as drug targets. *Curr Protoc Pharmacol* **Chapter 1**, Unit 1.1 (2006). <https://doi.org/10.1002/0471141755.ph0101s32>

- 379 Entzeroth, M., Flotow, H. & Condrón, P. Overview of High-Throughput Screening. *Current Protocols in Pharmacology* **44**, 9.4.1-9.4.27 (2009). <https://doi.org/10.1002/0471141755.ph0904s44>
- 380 Harris, C. J., Hill, R. D., Sheppard, D. W., Slater, M. J. & Stouten, P. F. The design and application of target-focused compound libraries. *Comb Chem High Throughput Screen* **14**, 521-531 (2011). <https://doi.org/10.2174/138620711795767802>
- 381 Dickson, K. A. *et al.* CRISPR single base-editing: in silico predictions to variant clonal cell lines. *Hum Mol Genet* **32**, 2704-2716 (2023). <https://doi.org/10.1093/hmg/ddad105>
- 382 Gorai, I. *et al.* Establishment and characterization of two human ovarian clear cell adenocarcinoma lines from metastatic lesions with different properties. *Gynecol Oncol* **57**, 33-46 (1995). <https://doi.org/10.1006/gyno.1995.1097>
- 383 Yanagibashi, T. *et al.* Complexity of expression of the intermediate filaments of six new human ovarian carcinoma cell lines: new expression of cytokeratin 20. *British Journal of Cancer* **76**, 829-835 (1997). <https://doi.org/10.1038/bjc.1997.471>
- 384 Yamada, K. *et al.* Establishment and characterization of cell lines derived from serous adenocarcinoma (JHOS-2) and clear cell adenocarcinoma (JHOC-5, JHOC-6) of human ovary. *Hum Cell* **12**, 131-138 (1999).
- 385 De Haven Brandon, A. *et al.* Identification of ovarian high-grade serous carcinoma cell lines that show estrogen-sensitive growth as xenografts in immunocompromised mice. *Scientific Reports* **10** (2020). <https://doi.org/10.1038/s41598-020-67533-1>
- 386 Nozawa, S. *et al.* A new CA125-like antigen (CA602) recognized by two monoclonal antibodies against a newly established ovarian clear cell carcinoma cell line (RMG-II). *Jpn J Cancer Res* **82**, 854-861 (1991). <https://doi.org/10.1111/j.1349-7006.1991.tb02713.x>
- 387 Kashiya, T. *et al.* Antitumor activity and induction of TP53-dependent apoptosis toward ovarian clear cell adenocarcinoma by the dual PI3K/mTOR inhibitor DS-7423. *PLoS One* **9**, e87220-e87220 (2014). <https://doi.org/10.1371/journal.pone.0087220>
- 388 Provencher, D. M. *et al.* Characterization of four novel epithelial ovarian cancer cell lines. *In Vitro Cell Dev Biol Anim* **36**, 357-361 (2000). [https://doi.org/10.1290/1071-2690\(2000\)036<0357:Cofneo>2.0.Co;2](https://doi.org/10.1290/1071-2690(2000)036<0357:Cofneo>2.0.Co;2)
- 389 Conover, C. A. *et al.* Biological characterization of human epithelial ovarian carcinoma cells in primary culture: the insulin-like growth factor system. *Exp Cell Res* **238**, 439-449 (1998). <https://doi.org/10.1006/excr.1997.3861>

- 390 Domcke, S., Sinha, R., Levine, D. A., Sander, C. & Schultz, N. Evaluating cell lines as tumour models by comparison of genomic profiles. *Nat Commun* **4**, 2126 (2013). <https://doi.org/10.1038/ncomms3126>
- 391 Anglesio, M. S. *et al.* Type-Specific Cell Line Models for Type-Specific Ovarian Cancer Research. *PLOS ONE* **8**, e72162 (2013). <https://doi.org/10.1371/journal.pone.0072162>
- 392 Barnes, B. M. *et al.* Distinct transcriptional programs stratify ovarian cancer cell lines into the five major histological subtypes. *Genome Med* **13**, 140 (2021). <https://doi.org/10.1186/s13073-021-00952-5>
- 393 Papp, E. *et al.* Integrated Genomic, Epigenomic, and Expression Analyses of Ovarian Cancer Cell Lines. *Cell Rep* **25**, 2617-2633 (2018). <https://doi.org/10.1016/j.celrep.2018.10.096>
- 394 Sangoi, A. R., Soslow, R. A., Teng, N. N. & Longacre, T. A. Ovarian clear cell carcinoma with papillary features: a potential mimic of serous tumor of low malignant potential. *Am J Surg Pathol* **32**, 269-274 (2008). <https://doi.org/10.1097/PAS.0b013e31814fa9b0>
- 395 DeLair, D. *et al.* Morphologic spectrum of immunohistochemically characterized clear cell carcinoma of the ovary: a study of 155 cases. *Am J Surg Pathol* **35**, 36-44 (2011). <https://doi.org/10.1097/PAS.0b013e3181ff400e>
- 396 Offman, S. L. & Longacre, T. A. Clear cell carcinoma of the female genital tract (not everything is as clear as it seems). *Adv Anat Pathol* **19**, 296-312 (2012). <https://doi.org/10.1097/PAP.0b013e31826663b1>
- 397 Bennett, J. A., Morales-Oyarvide, V., Campbell, S., Longacre, T. A. & Oliva, E. Mismatch Repair Protein Expression in Clear Cell Carcinoma of the Ovary: Incidence and Morphologic Associations in 109 Cases. *Am J Surg Pathol* **40**, 656-663 (2016). <https://doi.org/10.1097/pas.0000000000000602>
- 398 Bennett, J. A., Dong, F., Young, R. H. & Oliva, E. Clear cell carcinoma of the ovary: evaluation of prognostic parameters based on a clinicopathological analysis of 100 cases. *Histopathology* **66**, 808-815 (2015). <https://doi.org/10.1111/his.12514>
- 399 Yokoyama, Y., Matsushita, Y., Shigeto, T., Futagami, M. & Mizunuma, H. Decreased ARID1A expression is correlated with chemoresistance in epithelial ovarian cancer. *J Gynecol Oncol* **25**, 58-63 (2014).

- 400 Katagiri, A. *et al.* Loss of ARID1A expression is related to shorter progression-free survival and chemoresistance in ovarian clear cell carcinoma. *Mod Pathol* **25**, 282-288 (2012). <https://doi.org/10.1038/modpathol.2011.161>
- 401 Fadare, O. & Parkash, V. Pathology of endometrioid and clear cell carcinoma of the ovary. *Surgical pathology clinics* **12**, 529-564 (2019).
- 402 Dirks, W. G. *et al.* Cell line cross-contamination initiative: An interactive reference database of STR profiles covering common cancer cell lines. *International Journal of Cancer* **126**, 303-304 (2010). <https://doi.org/https://doi.org/10.1002/ijc.24999>
- 403 Mamo, A. *et al.* An integrated genomic approach identifies ARID1A as a candidate tumor-suppressor gene in breast cancer. *Oncogene* **31**, 2090-2100 (2012). <https://doi.org/10.1038/onc.2011.386>
- 404 Sim, J. C. *et al.* Expanding the phenotypic spectrum of ARID1B-mediated disorders and identification of altered cell-cycle dynamics due to ARID1B haploinsufficiency. *Orphanet J Rare Dis* **9**, 43 (2014). <https://doi.org/10.1186/1750-1172-9-43>
- 405 Vogelstein, B., Kinzler, K. W., Velculescu, V., Papadopoulos, N. & Jones, S. ARID1A and PPP2R1A Mutations in Cancer. US patent US 2013/0210900 A1 (2011).
- 406 Jones, S. *et al.* Frequent mutations of chromatin remodeling gene ARID1A in ovarian clear cell carcinoma. *Science* **330**, 228-231 (2010). <https://doi.org/10.1126/science.1196333>
- 407 Souren, N. Y. *et al.* Cell line authentication: a necessity for reproducible biomedical research. *Embo j* **41**, e111307 (2022). <https://doi.org/10.15252/embj.2022111307>
- 408 American Type Culture Collection Standards Development Organization Workgroup ASN-0002. *Authentication Of Human Cell Lines: Standardization Of Short Tandem Repeat (STR) Profiling - Revised 2022*, <<https://webstore.ansi.org/standards/atcc/ansiatccasn00022022>> (Accessed 22, April, 2024).
- 409 Almeida, J. L. & Korch, C. T. in *Assay Guidance Manual* (eds S. Markossian *et al.*) (Eli Lilly & Company and the National Center for Advancing Translational Sciences, 2004).
- 410 Demichelis, F. *et al.* SNP panel identification assay (SPIA): a genetic-based assay for the identification of cell lines. *Nucleic Acids Res* **36**, 2446-2456 (2008). <https://doi.org/10.1093/nar/gkn089>
- 411 Guan, B., Gao, M., Wu, C. H., Wang, T. L. & Shih Ie, M. Functional analysis of in-frame indel ARID1A mutations reveals new regulatory mechanisms of its tumor

- suppressor functions. *Neoplasia* **14**, 986-993 (2012).  
<https://doi.org/10.1593/neo.121218>
- 412 Bass, J. J. *et al.* An overview of technical considerations for Western blotting applications to physiological research. *Scandinavian Journal of Medicine & Science in Sports* **27**, 4-25 (2017). <https://doi.org/10.1111/sms.12702>
- 413 Karousis, E. D. & Mühlemann, O. Nonsense-Mediated mRNA Decay Begins Where Translation Ends. *Cold Spring Harb Perspect Biol* **11** (2019).  
<https://doi.org/10.1101/cshperspect.a032862>
- 414 Yakhnin, H. *et al.* Complex regulation of the global regulatory gene *csrA*: CsrA-mediated translational repression, transcription from five promoters by E $\sigma^{70}$  and E $\sigma(S)$ , and indirect transcriptional activation by CsrA. *Mol Microbiol* **81**, 689-704 (2011).  
<https://doi.org/10.1111/j.1365-2958.2011.07723.x>
- 415 Dasari, S. & Bernard Tchounwou, P. Cisplatin in cancer therapy: Molecular mechanisms of action. *Euro J of Pharm* **740**, 364-378 (2014).  
<https://doi.org/10.1016/j.ejphar.2014.07.025>
- 416 Kanat, O., Ertas, H. & Caner, B. Platinum-induced neurotoxicity: A review of possible mechanisms. *World J Clin Oncol* **8**, 329-335 (2017).  
<https://doi.org/10.5306/wjco.v8.i4.329>
- 417 Fong, C. W. (2015). Molecular mechanisms of cytotoxic side effects of platinum anticancer drugs – a molecular orbital study.
- 418 Rantanen, V., Grénman, S., Kulmala, J. & Grénman, R. Comparative evaluation of cisplatin and carboplatin sensitivity in endometrial adenocarcinoma cell lines. *Br J Cancer* **69**, 482-486 (1994). <https://doi.org/10.1038/bjc.1994.87>
- 419 Terheggen, P. M. *et al.* Formation of interaction products of carboplatin with DNA in vitro and in cancer patients. *Br J Cancer* **63**, 195-200 (1991).  
<https://doi.org/10.1038/bjc.1991.48>
- 420 Liston, D. R. & Davis, M. Clinically Relevant Concentrations of Anticancer Drugs: A Guide for Nonclinical Studies. *Clin Cancer Res* **23**, 3489-3498 (2017).  
<https://doi.org/10.1158/1078-0432.Ccr-16-3083>
- 421 Boyd, L. R. & Muggia, F. M. Carboplatin/Paclitaxel Induction in Ovarian Cancer: The Finer Points. *Oncology (Williston Park)* **32**, 418-420, 422-414 (2018).
- 422 Recio, F. O., Piver, M. S., Hempling, R. E. & Driscoll, D. L. Lack of improved survival plus increase in thromboembolic complications in patients with clear cell carcinoma of the ovary treated with platinum versus nonplatinum-based chemotherapy. *Cancer* **78**,



- 2157-2163 (1996). [https://doi.org/10.1002/\(sici\)1097-0142\(19961115\)78:10<2157::aid-cncl17>3.0.co;2-y](https://doi.org/10.1002/(sici)1097-0142(19961115)78:10<2157::aid-cncl17>3.0.co;2-y)
- 423 Sarwar, S. *et al.* Enhanced Accumulation of Cisplatin in Ovarian Cancer Cells from Combination with Wedelolactone and Resulting Inhibition of Multiple Epigenetic Drivers. *Drug Des Devel Ther* **15**, 2211-2227 (2021). <https://doi.org/10.2147/dddt.S288707>
- 424 Tocris Bioscience. *Tocriscreen Epigenetics* 3.0, <[https://www.tocris.com/products/tocriscreen-epigenetics-3-0\\_7578#product-details](https://www.tocris.com/products/tocriscreen-epigenetics-3-0_7578#product-details)> (Accessed 27, April, 2024)
- 425 Cukierman, E., Pankov, R., Stevens, D. R. & Yamada, K. M. Taking cell-matrix adhesions to the third dimension. *Science* **294**, 1708-1712 (2001). <https://doi.org/10.1126/science.1064829>
- 426 Kelm, J. M., Timmins, N. E., Brown, C. J., Fussenegger, M. & Nielsen, L. K. Method for generation of homogeneous multicellular tumor spheroids applicable to a wide variety of cell types. *Biotechnol Bioeng* **83**, 173-180 (2003). <https://doi.org/10.1002/bit.10655>
- 427 Delarue, M. *et al.* Compressive stress inhibits proliferation in tumor spheroids through a volume limitation. *Biophys J* **107**, 1821-1828 (2014). <https://doi.org/10.1016/j.bpj.2014.08.031>
- 428 Nickerson, C. A. *et al.* Three-dimensional tissue assemblies: novel models for the study of Salmonella enterica serovar Typhimurium pathogenesis. *Infect Immun* **69**, 7106-7120 (2001). <https://doi.org/10.1128/iai.69.11.7106-7120.2001>
- 429 Antoni, D., Burckel, H., Josset, E. & Noel, G. Three-dimensional cell culture: a breakthrough in vivo. *Int j of mol sci* **16**, 5517-5527 (2015).
- 430 Baal, N., Widmer-Teske, R., McKinnon, T., Preissner, K. T. & Zygmunt, M. T. In vitro spheroid model of placental vasculogenesis: does it work? *Lab Invest* **89**, 152-163 (2009). <https://doi.org/10.1038/labinvest.2008.126>
- 431 Simão, D. *et al.* Functional metabolic interactions of human neuron-astrocyte 3D in vitro networks. *Scientific Reports* **6**, 33285 (2016). <https://doi.org/10.1038/srep33285>
- 432 Zhang, Y. S. *et al.* Bioprinting the Cancer Microenvironment. *ACS Biomater Sci Eng* **2**, 1710-1721 (2016). <https://doi.org/10.1021/acsbiomaterials.6b00246>
- 433 Science, I. L. *Not your average approach to 3D bioprinting*, <<https://inventia.life/drop-on-demand-technology>> (

- 434 Science, I. L. *Create a relevant microenvironment with predictable matrix and model performance that gives you better data.*, <<https://inventia.life/rastrum-matrix>> (
- 435 Jung, M. *et al.* A high-throughput 3D bioprinted cancer cell migration and invasion model with versatile and broad biological applicability. *Biomater Sci* **10**, 5876-5887 (2022). <https://doi.org/10.1039/d2bm00651k>
- 436 Andricovich, J. *et al.* Loss of KDM6A Activates Super-Enhancers to Induce Gender-Specific Squamous-like Pancreatic Cancer and Confers Sensitivity to BET Inhibitors. *Cancer Cell* **33**, 512-526.e518 (2018). <https://doi.org/10.1016/j.ccell.2018.02.003>
- 437 Arnaout, M. A., Mahalingam, B. & Xiong, J. P. Integrin structure, allostery, and bidirectional signaling. *Annu Rev Cell Dev Biol* **21**, 381-410 (2005). <https://doi.org/10.1146/annurev.cellbio.21.090704.151217>
- 438 Farrukh, A. *et al.* Bifunctional Hydrogels Containing the Laminin Motif IKVAV Promote Neurogenesis. *Stem Cell Reports* **9**, 1432-1440 (2017). <https://doi.org/10.1016/j.stemcr.2017.09.002>
- 439 Sarwat, M. *et al.* Going beyond RGD: screening of a cell-adhesion peptide library in 3D cell culture. *Biomed Mater* **15**, 055033 (2020). <https://doi.org/10.1088/1748-605X/ab9d6e>
- 440 Frith, J. E., Mills, R. J., Hudson, J. E. & Cooper-White, J. J. Tailored integrin-extracellular matrix interactions to direct human mesenchymal stem cell differentiation. *Stem Cells Dev* **21**, 2442-2456 (2012). <https://doi.org/10.1089/scd.2011.0615>
- 441 Yamada, M. *et al.* Ile-Lys-Val-Ala-Val (IKVAV)-containing laminin  $\alpha$ 1 chain peptides form amyloid-like fibrils. *FEBS Letters* **530**, 48-52 (2002). [https://doi.org/https://doi.org/10.1016/S0014-5793\(02\)03393-8](https://doi.org/https://doi.org/10.1016/S0014-5793(02)03393-8)
- 442 Han, Q. *et al.* A supramolecular hydrogel based on the combination of YIGSR and RGD enhances mesenchymal stem cells paracrine function via integrin  $\alpha$ 2 $\beta$ 1 and PI3K/AKT signaling pathway for acute kidney injury therapy. *Chemical Engineering Journal* **436**, 135088 (2022). <https://doi.org/https://doi.org/10.1016/j.cej.2022.135088>
- 443 Ricciardelli, C. & Rodgers, R. J. Extracellular matrix of ovarian tumors. *Semin Reprod Med* **24**, 270-282 (2006). <https://doi.org/10.1055/s-2006-948556>
- 444 Kenny, H. A. *et al.* Mesothelial cells promote early ovarian cancer metastasis through fibronectin secretion. *J Clin Invest* **124**, 4614-4628 (2014). <https://doi.org/10.1172/jci74778>



- 445 Hamill, K. J., Kligys, K., Hopkinson, S. B. & Jones, J. C. Laminin deposition in the extracellular matrix: a complex picture emerges. *J Cell Sci* **122**, 4409-4417 (2009). <https://doi.org/10.1242/jcs.041095>
- 446 McGrail, D. J., Kieu, Q. M. & Dawson, M. R. The malignancy of metastatic ovarian cancer cells is increased on soft matrices through a mechanosensitive Rho-ROCK pathway. *J Cell Sci* **127**, 2621-2626 (2014). <https://doi.org/10.1242/jcs.144378>
- 447 Nicolson, P. L. R. *et al.* Inhibition of Btk by Btk-specific concentrations of ibrutinib and acalabrutinib delays but does not block platelet aggregation mediated by glycoprotein VI. *Haematologica* **103**, 2097-2108 (2018). <https://doi.org/10.3324/haematol.2018.193391>
- 448 Yoshida, K. *et al.* Expression of the chrXq27.3 miRNA cluster in recurrent ovarian clear cell carcinoma and its impact on cisplatin resistance. *Oncogene* **40**, 1255-1268 (2021). <https://doi.org/10.1038/s41388-020-01595-3>
- 449 Itamochi, H. *et al.* Low proliferation activity may be associated with chemoresistance in clear cell carcinoma of the ovary. *Obst & Gynecol* **100**, 281-287 (2002). [https://doi.org/https://doi.org/10.1016/S0029-7844\(02\)02040-9](https://doi.org/https://doi.org/10.1016/S0029-7844(02)02040-9)
- 450 Itamochi, H. *et al.* Mechanisms of cisplatin resistance in clear cell carcinoma of the ovary. *Oncol* **62**, 349-353 (2002). <https://doi.org/10.1159/000065067>
- 451 Das, D. & Hong, J. Irreversible Kinase Inhibitors Targeting Cysteine Residues and their Applications in Cancer Therapy. *Mini Rev Med Chem* **20**, 1732-1753 (2020). <https://doi.org/10.2174/1389557520666200513121524>
- 452 Gross, S., Rahal, R., Stransky, N., Lengauer, C. & Hoeflich, K. P. Targeting cancer with kinase inhibitors. *J Clin Invest* **125**, 1780-1789 (2015). <https://doi.org/10.1172/jci76094>
- 453 Hanahan, D. & Weinberg, R. A. Hallmarks of cancer: the next generation. *Cell* **144**, 646-674 (2011). <https://doi.org/10.1016/j.cell.2011.02.013>
- 454 Szklener, K., Michalski, A., Żak, K., Piwoński, M. & Mańdziuk, S. Ibrutinib in the Treatment of Solid Tumors: Current State of Knowledge and Future Directions. *Cells* **11** (2022). <https://doi.org/10.3390/cells11081338>
- 455 Zain, R. & Vihinen, M. Structure-Function Relationships of Covalent and Non-Covalent BTK Inhibitors. *Front Immunol* **12**, 694853 (2021). <https://doi.org/10.3389/fimmu.2021.694853>

- 456 Ran, F. *et al.* Recent development of BTK-based dual inhibitors in the treatment of  
cancers. *Eur J Med Chem* **233**, 114232 (2022).  
<https://doi.org/10.1016/j.ejmech.2022.114232>
- 457 Garg, N., Padron, E. J., Rammohan, K. W. & Goodman, C. F. Bruton's Tyrosine Kinase  
Inhibitors: The Next Frontier of B-Cell-Targeted Therapies for Cancer, Autoimmune  
Disorders, and Multiple Sclerosis. *J Clin Med* **11** (2022).  
<https://doi.org/10.3390/jcm11206139>
- 458 Zhang, H. & Qiu, L. in *Protein Kinase Inhibitors as Sensitizing Agents for  
Chemotherapy* Vol. 4 (eds Zhe-Sheng Chen & Dong-Hua Yang) 109-124 (Academic  
Press, 2019).
- 459 Liu, J., Chen, C., Wang, D., Zhang, J. & Zhang, T. Emerging small-molecule inhibitors  
of the Bruton's tyrosine kinase (BTK): Current development. *Eur J Med Chem* **217**,  
113329 (2021). <https://doi.org/10.1016/j.ejmech.2021.113329>
- 460 Caldwell, R. D. *et al.* Discovery of Evobrutinib: An Oral, Potent, and Highly Selective,  
Covalent Bruton's Tyrosine Kinase (BTK) Inhibitor for the Treatment of  
Immunological Diseases. *J Med Chem* **62**, 7643-7655 (2019).  
<https://doi.org/10.1021/acs.jmedchem.9b00794>
- 461 Ito, M. *et al.* Bruton's tyrosine kinase is essential for NLRP3 inflammasome activation  
and contributes to ischaemic brain injury. *Nat Commun* **6**, 7360 (2015).  
<https://doi.org/10.1038/ncomms8360>
- 462 Liu, X. *et al.* Human NACHT, LRR, and PYD domain-containing protein 3 (NLRP3)  
inflammasome activity is regulated by and potentially targetable through Bruton  
tyrosine kinase. *J Allergy Clin Immunol* **140**, 1054-1067.e1010 (2017).  
<https://doi.org/10.1016/j.jaci.2017.01.017>
- 463 Bittner, Z. A. *et al.* BTK operates a phospho-tyrosine switch to regulate NLRP3  
inflammasome activity. *J Exp Med* **218** (2021). <https://doi.org/10.1084/jem.20201656>
- 464 Franke, M. *et al.* The NLRP3 inflammasome drives inflammation in  
ischemia/reperfusion injury after transient middle cerebral artery occlusion in mice.  
*Brain Behav Immun* **92**, 223-233 (2021). <https://doi.org/10.1016/j.bbi.2020.12.009>
- 465 Zhao, J., Chen, J., Li, Y. Y., Xia, L. L. & Wu, Y. G. Bruton's tyrosine kinase regulates  
macrophage-induced inflammation in the diabetic kidney via NLRP3 inflammasome  
activation. *Int J Mol Med* **48** (2021). <https://doi.org/10.3892/ijmm.2021.5010>

- 466 Pal Singh, S., Dammeijer, F. & Hendriks, R. W. Role of Bruton's tyrosine kinase in B cells and malignancies. *Mol Cancer* **17**, 57 (2018). <https://doi.org/10.1186/s12943-018-0779-z>
- 467 Mohamed, A. J. *et al.* Bruton's tyrosine kinase (Btk): function, regulation, and transformation with special emphasis on the PH domain. *Immunol Rev* **228**, 58-73 (2009). <https://doi.org/10.1111/j.1600-065X.2008.00741.x>
- 468 Horwood, N. J. *et al.* Bruton's tyrosine kinase is required for lipopolysaccharide-induced tumor necrosis factor alpha production. *J Exp Med* **197**, 1603-1611 (2003). <https://doi.org/10.1084/jem.20021845>
- 469 Smith, C. I. *et al.* Expression of Bruton's agammaglobulinemia tyrosine kinase gene, BTK, is selectively down-regulated in T lymphocytes and plasma cells. *J Immunol* **152**, 557-565 (1994).
- 470 Neys, S. F. H., Rip, J., Hendriks, R. W. & Corneth, O. B. J. Bruton's Tyrosine Kinase Inhibition as an Emerging Therapy in Systemic Autoimmune Disease. *Drugs* **81**, 1605-1626 (2021). <https://doi.org/10.1007/s40265-021-01592-0>
- 471 Eifert, C. *et al.* A novel isoform of the B cell tyrosine kinase BTK protects breast cancer cells from apoptosis. *Genes Chromosomes Cancer* **52**, 961-975 (2013). <https://doi.org/10.1002/gcc.22091>
- 472 Kokabee, L. *et al.* Bruton's tyrosine kinase is a potential therapeutic target in prostate cancer. *Cancer Biol Ther* **16**, 1604-1615 (2015). <https://doi.org/10.1080/15384047.2015.1078023>
- 473 Grassilli, E. *et al.* p65BTK Is a Novel Biomarker and Therapeutic Target in Solid Tumors. *Front Cell Dev Biol* **9**, 690365 (2021). <https://doi.org/10.3389/fcell.2021.690365>
- 474 Lavitrano, M. *et al.* BTK inhibitors synergise with 5-FU to treat drug-resistant TP53-null colon cancers. *J of Pathol* **250**, 134-147 (2020). <https://doi.org/https://doi.org/10.1002/path.5347>
- 475 Giordano, F. *et al.* p65BTK is a novel potential actionable target in KRAS-mutated/EGFR-wild type lung adenocarcinoma. *J Exp Clin Cancer Res* **38**, 260 (2019). <https://doi.org/10.1186/s13046-019-1199-7>
- 476 Feldhahn, N. *et al.* Deficiency of Bruton's tyrosine kinase in B cell precursor leukemia cells. *Proc Natl Acad Sci U S A* **102**, 13266-13271 (2005). <https://doi.org/10.1073/pnas.0505196102>

- 477 Pan, Z. *et al.* Discovery of selective irreversible inhibitors for Bruton's tyrosine kinase. *ChemMedChem* **2**, 58-61 (2007). <https://doi.org/10.1002/cmdc.200600221>
- 478 Saleh, L. M. *et al.* Ibrutinib downregulates a subset of miRNA leading to upregulation of tumor suppressors and inhibition of cell proliferation in chronic lymphocytic leukemia. *Leukemia* **31**, 340-349 (2017). <https://doi.org/10.1038/leu.2016.181>
- 479 O'Brien, S. *et al.* Ibrutinib as initial therapy for elderly patients with chronic lymphocytic leukaemia or small lymphocytic lymphoma: an open-label, multicentre, phase 1b/2 trial. *Lancet Oncol* **15**, 48-58 (2014). [https://doi.org/10.1016/s1470-2045\(13\)70513-8](https://doi.org/10.1016/s1470-2045(13)70513-8)
- 480 Varughese, T. *et al.* Serious Infections in Patients Receiving Ibrutinib for Treatment of Lymphoid Cancer. *Clin Infect Dis* **67**, 687-692 (2018). <https://doi.org/10.1093/cid/ciy175>
- 481 Advani, R. H. *et al.* Bruton tyrosine kinase inhibitor ibrutinib (PCI-32765) has significant activity in patients with relapsed/refractory B-cell malignancies. *J Clin Oncol* **31**, 88-94 (2013). <https://doi.org/10.1200/jco.2012.42.7906>
- 482 Byrd, J. C. *et al.* Targeting BTK with ibrutinib in relapsed chronic lymphocytic leukemia. *N Engl J Med* **369**, 32-42 (2013). <https://doi.org/10.1056/NEJMoa1215637>
- 483 Chen, J., Kinoshita, T., Sukbuntherng, J., Chang, B. Y. & Elias, L. Ibrutinib Inhibits ERBB Receptor Tyrosine Kinases and HER2-Amplified Breast Cancer Cell Growth. *Mol Cancer Ther* **15**, 2835-2844 (2016). <https://doi.org/10.1158/1535-7163.Mct-15-0923>
- 484 Wang, X. *et al.* Bruton's Tyrosine Kinase Inhibitors Prevent Therapeutic Escape in Breast Cancer Cells. *Mol Cancer Ther* **15**, 2198-2208 (2016). <https://doi.org/10.1158/1535-7163.Mct-15-0813>
- 485 Gao, W. *et al.* Selective antitumor activity of ibrutinib in EGFR-mutant non-small cell lung cancer cells. *J Natl Cancer Inst* **106** (2014). <https://doi.org/10.1093/jnci/dju204>
- 486 Turkes, F. *et al.* Ibrutinib in c-MYC and HER2 Amplified Oesophagogastric Carcinoma: Results of the Proof-of-Concept iMYC Study. *Curr Oncol* **29**, 2174-2184 (2022). <https://doi.org/10.3390/curroncol29040176>
- 487 Al-Toubah, T. *et al.* A Phase II Study of Ibrutinib in Advanced Neuroendocrine Neoplasms. *Neuroendocrinology* **110**, 377-383 (2020). <https://doi.org/10.1159/000502383>

- 488 Lara, P. *et al.* Pilot trial of ibrutinib plus nivolumab in patients with metastatic renal cell cancer (mRCC): results from a dose-finding cohort. *J of Clin Oncol* **36**, 4580-4580 (2018). [https://doi.org/10.1200/JCO.2018.36.15\\_suppl.4580](https://doi.org/10.1200/JCO.2018.36.15_suppl.4580)
- 489 Gray, H. J. *et al.* Extraordinary clinical response to ibrutinib in low-grade ovarian cancer guided by organoid drug testing. *npj Precision Oncol* **7**, 45 (2023). <https://doi.org/10.1038/s41698-023-00379-8>
- 490 Metzler, J. M., Fink, D. & Imesch, P. Ibrutinib Could Suppress CA-125 in Ovarian Cancer: A Hypothesis. *Applied Sciences* **11**, 222 (2021).
- 491 George, B. *et al.* Ibrutinib Resistance Mechanisms and Treatment Strategies for B-Cell lymphomas. *Cancers (Basel)* **12** (2020). <https://doi.org/10.3390/cancers12051328>
- 492 Zucha, M. A. *et al.* Bruton's tyrosine kinase (Btk) inhibitor ibrutinib suppresses stem-like traits in ovarian cancer. *Oncotarget* **6**, 13255-13268 (2015). <https://doi.org/10.18632/oncotarget.3658>
- 493 Lohse, I. *et al.* Ovarian Cancer Treatment Stratification Using Ex Vivo Drug Sensitivity Testing. *Anticancer Res* **39**, 4023-4030 (2019). <https://doi.org/10.21873/anticancer.13558>
- 494 Katagiri, A. *et al.* Loss of ARID1A expression is related to shorter progression-free survival and chemoresistance in ovarian clear cell carcinoma. *Modern Pathol* **25**, 282-288 (2012). <https://doi.org/10.1038/modpathol.2011.161>
- 495 Iwadate, Y. *et al.* Mutation of the p53 gene in human astrocytic tumours correlates with increased resistance to DNA-damaging agents but not to anti-microtubule anti-cancer agents. *Br J Cancer* **77**, 547-551 (1998). <https://doi.org/10.1038/bjc.1998.88>
- 496 Wallace-Brodeur, R. R. & Lowe, S. W. Clinical implications of p53 mutations. *Cell Mol Life Sci* **55**, 64-75 (1999). <https://doi.org/10.1007/s000180050270>
- 497 Lee, H. J. *et al.* p53-independent ibrutinib responses in an Eμ-TCL1 mouse model demonstrates efficacy in high-risk CLL. *Blood Cancer J* **6**, e434-e434 (2016). <https://doi.org/10.1038/bcj.2016.41>
- 498 Cafforio, L. *et al.* Treatment with ibrutinib does not induce a TP53 clonal evolution in chronic lymphocytic leukemia. *Haematologica* **107**, 334-337 (2022). <https://doi.org/10.3324/haematol.2020.263715>
- 499 Shield, K., Ackland, M. L., Ahmed, N. & Rice, G. E. Multicellular spheroids in ovarian cancer metastases: Biology and pathology. *Gynecol Oncol* **113**, 143-148 (2009). <https://doi.org/10.1016/j.ygyno.2008.11.032>

- 500 Loessner, D. *et al.* Bioengineered 3D platform to explore cell-ECM interactions and drug resistance of epithelial ovarian cancer cells. *Biomaterials* **31**, 8494-8506 (2010). <https://doi.org/10.1016/j.biomaterials.2010.07.064>
- 501 Karlsson, H., Fryknäs, M., Larsson, R. & Nygren, P. Loss of cancer drug activity in colon cancer HCT-116 cells during spheroid formation in a new 3-D spheroid cell culture system. *Exp Cell Res* **318**, 1577-1585 (2012). <https://doi.org/10.1016/j.yexcr.2012.03.026>
- 502 Chitcholtan, K., Sykes, P. H. & Evans, J. J. The resistance of intracellular mediators to doxorubicin and cisplatin are distinct in 3D and 2D endometrial cancer. *J Transl Med* **10**, 38 (2012). <https://doi.org/10.1186/1479-5876-10-38>
- 503 Swietach, P., Hulikova, A., Patiar, S., Vaughan-Jones, R. D. & Harris, A. L. Importance of intracellular pH in determining the uptake and efficacy of the weakly basic chemotherapeutic drug, doxorubicin. *PLoS One* **7**, e35949 (2012). <https://doi.org/10.1371/journal.pone.0035949>
- 504 Luca, A. C. *et al.* Impact of the 3D microenvironment on phenotype, gene expression, and EGFR inhibition of colorectal cancer cell lines. *PLoS One* **8**, e59689 (2013). <https://doi.org/10.1371/journal.pone.0059689>
- 505 Agrawal, N. *et al.* RNA interference: biology, mechanism, and applications. *Microbiol Mol Biol Rev* **67**, 657-685 (2003). <https://doi.org/10.1128/mmb.67.4.657-685.2003>
- 506 Lam, J. K., Chow, M. Y., Zhang, Y. & Leung, S. W. siRNA Versus miRNA as Therapeutics for Gene Silencing. *Mol Ther Nucleic Acids* **4**, e252 (2015). <https://doi.org/10.1038/mtna.2015.23>
- 507 Fire, A. *et al.* Potent and specific genetic interference by double-stranded RNA in *Caenorhabditis elegans*. *Nature* **391**, 806-811 (1998). <https://doi.org/10.1038/35888>
- 508 Endoh, T. & Ohtsuki, T. Cellular siRNA delivery using cell-penetrating peptides modified for endosomal escape. *Adv Drug Deliv Rev* **61**, 704-709 (2009). <https://doi.org/10.1016/j.addr.2009.04.005>
- 509 Giuliano, C. J., Lin, A., Girish, V. & Sheltzer, J. M. Generating Single Cell-Derived Knockout Clones in Mammalian Cells with CRISPR/Cas9. *Current Protocols in Molecular Biology* **128**, e100 (2019). <https://doi.org/https://doi.org/10.1002/cpmb.100>
- 510 Smith, I. *et al.* Evaluation of RNAi and CRISPR technologies by large-scale gene expression profiling in the Connectivity Map. *PLoS Biol* **15**, e2003213 (2017). <https://doi.org/10.1371/journal.pbio.2003213>



- 511 Yoshino, J. *et al.* Loss of ARID1A induces a stemness gene ALDH1A1 expression with histone acetylation in the malignant subtype of cholangiocarcinoma. *Carcinogenesis* **41**, 734-742 (2020). <https://doi.org/10.1093/carcin/bgz179>
- 512 Mandal, J., Yu, Z. C., Shih, I. M. & Wang, T. L. ARID1A loss activates MAPK signaling via DUSP4 downregulation. *J Biomed Sci* **30**, 94 (2023). <https://doi.org/10.1186/s12929-023-00985-5>
- 513 Zhao, B. *et al.* ARID1A promotes genomic stability through protecting telomere cohesion. *Nature Communications* **10**, 4067 (2019). <https://doi.org/10.1038/s41467-019-12037-4>
- 514 Doench, J. G. *et al.* Optimized sgRNA design to maximize activity and minimize off-target effects of CRISPR-Cas9. *Nat Biotech* **34**, 184-191 (2016). <https://doi.org/10.1038/nbt.3437>
- 515 Zhang, X. H., Tee, L. Y., Wang, X. G., Huang, Q. S. & Yang, S. H. Off-target Effects in CRISPR/Cas9-mediated Genome Engineering. *Mol Ther Nucleic Acids* **4**, e264 (2015). <https://doi.org/10.1038/mtna.2015.37>
- 516 Xu, G. *et al.* ARID1A determines luminal identity and therapeutic response in estrogen-receptor-positive breast cancer. *Nat Genet* **52**, 198-207 (2020). <https://doi.org/10.1038/s41588-019-0554-0>
- 517 Frey, U. H., Bachmann, H. S., Peters, J. & Siffert, W. PCR-amplification of GC-rich regions: 'slowdown PCR'. *Nat Prot* **3**, 1312-1317 (2008). <https://doi.org/10.1038/nprot.2008.112>
- 518 Winship, P. R. An improved method for directly sequencing PCR amplified material using dimethyl sulphoxide. *Nucleic Acids Res* **17**, 1266 (1989). <https://doi.org/10.1093/nar/17.3.1266>
- 519 Don, R. H., Cox, P. T., Wainwright, B. J., Baker, K. & Mattick, J. S. 'Touchdown' PCR to circumvent spurious priming during gene amplification. *Nucleic Acids Res* **19**, 4008 (1991). <https://doi.org/10.1093/nar/19.14.4008>
- 520 Fan, H. & Chu, J. Y. A brief review of short tandem repeat mutation. *Genomics Proteomics Bioinformatics* **5**, 7-14 (2007). [https://doi.org/10.1016/s1672-0229\(07\)60009-6](https://doi.org/10.1016/s1672-0229(07)60009-6)
- 521 Tørresen, O. K. *et al.* Tandem repeats lead to sequence assembly errors and impose multi-level challenges for genome and protein databases. *Nucleic Acids Res* **47**, 10994-11006 (2019). <https://doi.org/10.1093/nar/gkz841>

- 522 MOLNAR, M. *Why Are Some Genes Difficult to CRISPR Edit?*,  
 <<https://www.synthego.com/blog/genes-difficult-crispr-edit>> (
- 523 Aguirre, A. J. *et al.* Genomic Copy Number Dictates a Gene-Independent Cell  
 Response to CRISPR/Cas9 Targeting. *Cancer Discov* **6**, 914-929 (2016).  
<https://doi.org/10.1158/2159-8290.Cd-16-0154>
- 524 Wang, Z. *et al.* Dual ARID1A/ARID1B loss leads to rapid carcinogenesis and  
 disruptive redistribution of BAF complexes. *Nat Cancer* **1**, 909-922 (2020).  
<https://doi.org/10.1038/s43018-020-00109-0>
- 525 Niedermaier, B. *et al.* Targeting ARID1A-mutant colorectal cancer: depletion of  
 ARID1B increases radiosensitivity and modulates DNA damage response. *Sci Rep* **9**,  
 18207 (2019). <https://doi.org/10.1038/s41598-019-54757-z>
- 526 Sato, E. *et al.* ARID1B as a Potential Therapeutic Target for ARID1A-Mutant Ovarian  
 Clear Cell Carcinoma. *Int J Mol Sci* **19** (2018). <https://doi.org/10.3390/ijms19061710>
- 527 Borah, P. Primer designing for PCR. *Science Vision* **11**, 134-136 (2011).
- 528 Hecker, K. H. & Roux, K. H. High and low annealing temperatures increase both  
 specificity and yield in touchdown and stepdown PCR. *Biotechniques* **20**, 478-485  
 (1996). <https://doi.org/10.2144/19962003478>
- 529 Wang, L. *et al.* Inhibition of Arid1a increases stem/progenitor cell-like properties of  
 liver cancer. *Cancer Letters* **546**, 215869 (2022).  
<https://doi.org/https://doi.org/10.1016/j.canlet.2022.215869>
- 530 He, F. *et al.* Decreased expression of ARID1A associates with poor prognosis and  
 promotes metastases of hepatocellular carcinoma. *J Exp Clin Cancer Res* **34**, 47 (2015).  
<https://doi.org/10.1186/s13046-015-0164-3>
- 531 Peerapen, P., Sueksakit, K., Boonmark, W., Yoodee, S. & Thongboonkerd, V. ARID1A  
 knockdown enhances carcinogenesis features and aggressiveness of Caco-2 colon  
 cancer cells: An in vitro cellular mechanism study. *J Cancer* **13**, 373-384 (2022).  
<https://doi.org/10.7150/jca.65511>
- 532 Zhang, Y. *et al.* ARID1A is downregulated in non-small cell lung cancer and regulates  
 cell proliferation and apoptosis. *Tumour Biol* **35**, 5701-5707 (2014).  
<https://doi.org/10.1007/s13277-014-1755-x>
- 533 Xie, C., Fu, L., Han, Y., Li, Q. & Wang, E. Decreased ARID1A expression facilitates  
 cell proliferation and inhibits 5-fluorouracil-induced apoptosis in colorectal carcinoma.  
*Tumour Biol* **35**, 7921-7927 (2014). <https://doi.org/10.1007/s13277-014-2074-y>



- 534 Nagl, N. G., Wang, X., Patsialou, A., Van Scoy, M. & Moran, E. Distinct mammalian SWI/SNF chromatin remodeling complexes with opposing roles in cell-cycle control. *The EMBO Journal* **26**, 752-763 (2007). <https://doi.org/https://doi.org/10.1038/sj.emboj.7601541>
- 535 Asmamaw Mengstie, M. *et al.* Recent Advancements in Reducing the Off-Target Effect of CRISPR-Cas9 Genome Editing. *Biologics* **18**, 21-28 (2024). <https://doi.org/10.2147/btt.S429411>
- 536 Arnold, A. S. *et al.* Comparing reagents for efficient transfection of human primary myoblasts: FuGENE 6, Effectene and ExGen 500. *Fundam Clin Pharmacol* **20**, 81-89 (2006). <https://doi.org/10.1111/j.1472-8206.2005.00344.x>
- 537 Young, A. T., Lakey, J. R., Murray, A. G. & Moore, R. B. Gene therapy: a lipofection approach for gene transfer into primary endothelial cells. *Cell Trans* **11**, 573-582 (2002).
- 538 Hunt, M. A., Currie, M. J., Robinson, B. A. & Dachs, G. U. Optimizing transfection of primary human umbilical vein endothelial cells using commercially available chemical transfection reagents. *J Biomol Tech* **21**, 66-72 (2010).
- 539 Sandbichler, A. M., Aschberger, T. & Pelster, B. A method to evaluate the efficiency of transfection reagents in an adherent zebrafish cell line. *Biores Open Access* **2**, 20-27 (2013). <https://doi.org/10.1089/biores.2012.0287>
- 540 Boch, J. *et al.* Breaking the code of DNA binding specificity of TAL-type III effectors. *Science* **326**, 1509-1512 (2009). <https://doi.org/10.1126/science.1178811>
- 541 Thakore, P. I. & Gersbach, C. A. Design, Assembly, and Characterization of TALE-Based Transcriptional Activators and Repressors. *Methods Mol Biol* **1338**, 71-88 (2016). [https://doi.org/10.1007/978-1-4939-2932-0\\_7](https://doi.org/10.1007/978-1-4939-2932-0_7)
- 542 Method of the Year 2011. *Nat Methods* **9**, 1 (2012). <https://doi.org/10.1038/nmeth.1852>
- 543 Asmamaw, M. & Zawdie, B. Mechanism and Applications of CRISPR/Cas-9-Mediated Genome Editing. *Biologics* **15**, 353-361 (2021). <https://doi.org/10.2147/btt.S326422>
- 544 Nemudryi, A. A., Valetdinova, K. R., Medvedev, S. P. & Zakian, S. M. TALEN and CRISPR/Cas Genome Editing Systems: Tools of Discovery. *Acta Naturae* **6**, 19-40 (2014).
- 545 Wang, H. *et al.* One-step generation of mice carrying mutations in multiple genes by CRISPR/Cas-mediated genome engineering. *Cell* **153**, 910-918 (2013). <https://doi.org/10.1016/j.cell.2013.04.025>

- 546 Bhardwaj, A. & Nain, V. TALENs-an indispensable tool in the era of CRISPR: a mini review. *J Genet Eng Biotechnol* **19**, 125 (2021). <https://doi.org/10.1186/s43141-021-00225-z>
- 547 Mussolino, C. *et al.* TALENs facilitate targeted genome editing in human cells with high specificity and low cytotoxicity. *Nucleic Acids Res* **42**, 6762-6773 (2014). <https://doi.org/10.1093/nar/gku305>
- 548 Zhang, D., Zhang, Z., Unver, T. & Zhang, B. CRISPR/Cas: A powerful tool for gene function study and crop improvement. *J Adv Res* **29**, 207-221 (2021). <https://doi.org/10.1016/j.jare.2020.10.003>
- 549 Wu, J. N. & Roberts, C. W. M. ARID1A Mutations in Cancer: Another Epigenetic Tumor Suppressor? *Cancer Discovery* **3**, 35-43 (2013). <https://doi.org/10.1158/2159-8290.Cd-12-0361>
- 550 Selvanathan, S. P. *et al.* EWS-FLI1 modulated alternative splicing of ARID1A reveals novel oncogenic function through the BAF complex. *Nucleic Acids Res* **47**, 9619-9636 (2019). <https://doi.org/10.1093/nar/gkz699>
- 551 Kurz, L. *et al.* ARID1A Regulates Transcription and the Epigenetic Landscape via POLE and DMAP1 while ARID1A Deficiency or Pharmacological Inhibition Sensitizes Germ Cell Tumor Cells to ATR Inhibition. *Cancers (Basel)* **12** (2020). <https://doi.org/10.3390/cancers12040905>
- 552 Pagliaroli, L. & Trizzino, M. The Evolutionary Conserved SWI/SNF Subunits ARID1A and ARID1B Are Key Modulators of Pluripotency and Cell-Fate Determination. *Front Cell Dev Biol* **9**, 643361 (2021). <https://doi.org/10.3389/fcell.2021.643361>
- 553 Nozawa, S., Tsukazaki, K., Sakayori, M., Jeng, C. H. & Iizuka, R. Establishment of a human ovarian clear cell carcinoma cell line (RMG-I) and its single cell cloning--with special reference to the stem cell of the tumor. *Hum Cell* **1**, 426-435 (1988).
- 554 Yanagibashi, T. *et al.* Complexity of expression of the intermediate filaments of six new human ovarian carcinoma cell lines: new expression of cytokeratin 20. *Br J Cancer* **76**, 829-835 (1997). <https://doi.org/10.1038/bjc.1997.471>
- 555 Yamada, T. *et al.* Establishment and characterization of a cell line (HCH-1) originating from a human clear cell carcinoma of the ovary. *Journal of Ovarian Research* **9**, 32 (2016). <https://doi.org/10.1186/s13048-016-0242-y>
- 556 Lanigan, T. M. *et al.* Real time visualization of cancer cell death, survival and proliferation using fluorochrome-transfected cells in an IncuCyte(®) imaging system. *J Biol Methods* **7**, e133 (2020). <https://doi.org/10.14440/jbm.2020.323>

- 557 Kim, K. H. & Sederstrom, J. M. Assaying Cell Cycle Status Using Flow Cytometry. *Curr Protoc Mol Biol* **111**, 28.26.21-28.26.11 (2015). <https://doi.org/10.1002/0471142727.mb2806s111>
- 558 Lyu, C., Zhang, Y., Zhou, X. & Lang, J. ARID1A gene silencing reduces the sensitivity of ovarian clear cell carcinoma to cisplatin. *Exp Ther Med* **12**, 4067-4071 (2016). <https://doi.org/10.3892/etm.2016.3863>
- 559 Niimi, K. *et al.* Suppression of REV7 enhances cisplatin sensitivity in ovarian clear cell carcinoma cells. *Cancer Sci* **105**, 545-552 (2014). <https://doi.org/10.1111/cas.12390>
- 560 Mabuchi, S. *et al.* Vascular endothelial growth factor is a promising therapeutic target for the treatment of clear cell carcinoma of the ovary. *Mol Cancer Ther* **9**, 2411-2422 (2010). <https://doi.org/10.1158/1535-7163.Mct-10-0169>
- 561 Grassilli, E. *et al.* A novel oncogenic BTK isoform is overexpressed in colon cancers and required for RAS-mediated transformation. *Oncogene* **35**, 4368-4378 (2016). <https://doi.org/10.1038/onc.2015.504>
- 562 Chan, J. K. *et al.* A phase II evaluation of sunitinib in the treatment of persistent or recurrent clear cell ovarian carcinoma: An NRG Oncology/Gynecologic Oncology Group Study (GOG-254). *Gynecol Oncol* **150**, 247-252 (2018). <https://doi.org/10.1016/j.ygyno.2018.05.029>
- 563 Ackroyd, S. A. *et al.* Molecular portraits of clear cell ovarian and endometrial carcinoma with comparison to clear cell renal cell carcinoma. *Gynecol Oncol* **169**, 164-171 (2023). <https://doi.org/https://doi.org/10.1016/j.ygyno.2022.10.020>
- 564 Reber, S. *et al.* CRISPR-Trap: a clean approach for the generation of gene knockouts and gene replacements in human cells. *Mol Biol Cell* **29**, 75-83 (2018). <https://doi.org/10.1091/mbc.E17-05-0288>
- 565 Feng, X. *et al.* Genome-wide CRISPR screens using isogenic cells reveal vulnerabilities conferred by loss of tumor suppressors. *Sci Adv* **8**, eabm6638 (2022). <https://doi.org/10.1126/sciadv.abm6638>
- 566 Curtis, A., Rueter, J., Rajan, S., Zhang, R. & Shopland, L. Additive and synergistic inhibition of mantle cell lymphoma cell growth by combining olaparib with ibrutinib. *J Cell Biochem* **119**, 5843-5851 (2018). <https://doi.org/10.1002/jcb.26773>
- 567 Hüser, J. *et al.* High-throughput screening for targeted lead discovery. *High-Throughput Screening in Drug Discovery* **35**, 15-36 (2006).
- 568 Shi, J.-Y., Yiu, S.-M., Li, Y., Leung, H. C. M. & Chin, F. Y. L. Predicting drug–target interaction for new drugs using enhanced similarity measures and super-target

clustering. *Methods* **83**, 98-104 (2015).  
<https://doi.org/https://doi.org/10.1016/j.ymeth.2015.04.036>

# Appendix

The additional data, figures and tables presented in this chapter expands the main body of the thesis to give clarity to certain areas. The appendixes are divided into 4 sections.

Appendix 1 extends the cell line authentication results using STR analyses and includes the dose-response curves of OCCC cells treated with the platinum-based drugs cisplatin and carboplatin and full western blot image of ARID1A and ARID1B in seven OCCC cell lines compared to a control cell line with wild-type expression of proteins of interest (HEK293) , as presented in Chapter 3. Appendix 2 corresponds to Chapter 4 and contains the complete list of compounds from the Tocriscreen Epigenetics Library 3.0, along with the statistical analysis results of cell viability in seven OCCC and three non-OCCC ovarian cancer cell lines following treatment with ibrutinib at concentrations of 5  $\mu$ M and 0.5  $\mu$ M. Appendix 3 expands on Chapter 5 by displaying the dose-response curves for clonal and CRISPR-engineered cell lines in the RMG-I and JHOC-5 cell lines treated with cisplatin, as well as the optimisation results for three different transfection reagents used in JHOC-5 cells. Appendix 4 presents publications related to this thesis.

# List of Appendix

Appendix 1.....	240
Appendix 2.....	245
Appendix 3.....	251
Appendix 4.....	257
A.4.1 Manuscripts arising from thesis .....	257
A.4.2 Manuscripts in preparation from this thesis.....	257
A.4.3 Manuscripts related to this thesis .....	257

## Appendix 1

Table A.1 The cell line authentication results using STR analyses

Sample Name	Marker	Allele 1	Allele 2	Size 1	Size 2
RMG-I	AMEL	X	X	104.01	104.01
RMG-I	CSF1PO	10	10	333.53	333.53
RMG-I	D13S317	12	12	191.74	191.74
RMG-I	D16S539	9	10	278.86	282.88
RMG-I	D21S11	29	30	219.33	223.37
RMG-I	D5S818	12	12	134.72	134.72
RMG-I	D7S820	11	11	232.31	232.31
RMG-I	TH01	6	7	161.94	165.89
RMG-I	TPOX	11	11	280.96	280.96
RMG-I	vWA	17	18	150.18	154.21
JHOC-5	AMEL	X	X	104.15	104.15
JHOC-5	CSF1PO	10	12	333.44	341.55
JHOC-5	D13S317	9	12	180	191.88
JHOC-5	D16S539	11	13	287.09	294.98
JHOC-5	D21S11	29	30	219.49	223.52
JHOC-5	D5S818	10	10	126.88	126.88
JHOC-5	D7S820	12	12	236.49	236.49
JHOC-5	TH01	7	7	166.07	166.07
JHOC-5	TPOX	11	11	280.85	280.85
JHOC-5	vWA	14	16	138.45	146.17
OV207	AMEL	X	X	104.05	104.05
OV207	CSF1PO	11	11	337.54	337.54
OV207	D13S317	12	12	191.85	191.85
OV207	D16S539	13	13	294.88	294.88
OV207	D21S11	31.2	31.2	229.42	229.42
OV207	D5S818	11	12	130.56	134.76
OV207	D7S820	8	8	220.33	220.33
OV207	TH01	9.3	9.3	176.84	176.84
OV207	TPOX	8	8	268.88	268.88

OV207	vWA	15	16	142.5	146.24
OVTOKO	AMEL	X	X	104.07	104.07
OVTOKO	CSF1PO	12	12	341.55	341.55
OVTOKO	D13S317	8	12	175.89	191.73
OVTOKO	D16S539	11	12	286.9	290.89
OVTOKO	D21S11	29	31	219.39	227.38
OVTOKO	D5S818	11	12	130.75	134.86
OVTOKO	D7S820	9	10	224.24	228.24
OVTOKO	TH01	6	9.3	161.91	176.75
OVTOKO	TPOX	8	12	268.86	284.83
OVTOKO	vWA	14	17	138.41	150.23
OVMANA	AMEL	X	X	104.09	104.09
OVMANA	CSF1PO	12	13	341.55	345.61
OVMANA	D13S317	8	9	175.95	179.91
OVMANA	D16S539	10	10	282.8	282.8
OVMANA	D21S11	28	31	215.39	227.4
OVMANA	D5S818	13	13	138.84	138.84
OVMANA	D7S820	10	11	228.26	232.29
OVMANA	TH01	7	9	165.95	173.87
OVMANA	TPOX	8	8	268.88	268.88
OVMANA	vWA	15	16	142.17	146.23
OVISE	AMEL	X	X	103.99	103.99
OVISE	CSF1PO	9	11	329.46	337.54
OVISE	D13S317	11	12	187.74	191.78
OVISE	D16S539	9	9	278.83	278.83
OVISE	D21S11	28	30	215.37	223.38
OVISE	D5S818	10	10	126.46	126.46
OVISE	D7S820	11	12	232.18	236.27
OVISE	TH01	9	9.3	173.81	176.82
OVISE	TPOX	8	8	268.84	268.84
OVISE	vWA	18	18	154.24	154.24
TOV-21G	AMEL	X	X	103.97	103.97



TOV-21G	CSF1PO	13	15	345.61	353.65
TOV-21G	D13S317	11	12	187.89	191.87
TOV-21G	D16S539	10	12	282.78	290.8
TOV-21G	D21S11	28	34.2	215.32	241.43
TOV-21G	D5S818	12	13	134.68	138.9
TOV-21G	D7S820	12	12	236.22	236.22
TOV-21G	TH01	7	9.3	165.93	176.81
TOV-21G	TPOX	8	11	268.95	280.96
TOV-21G	vWA	17	17	150.27	150.27

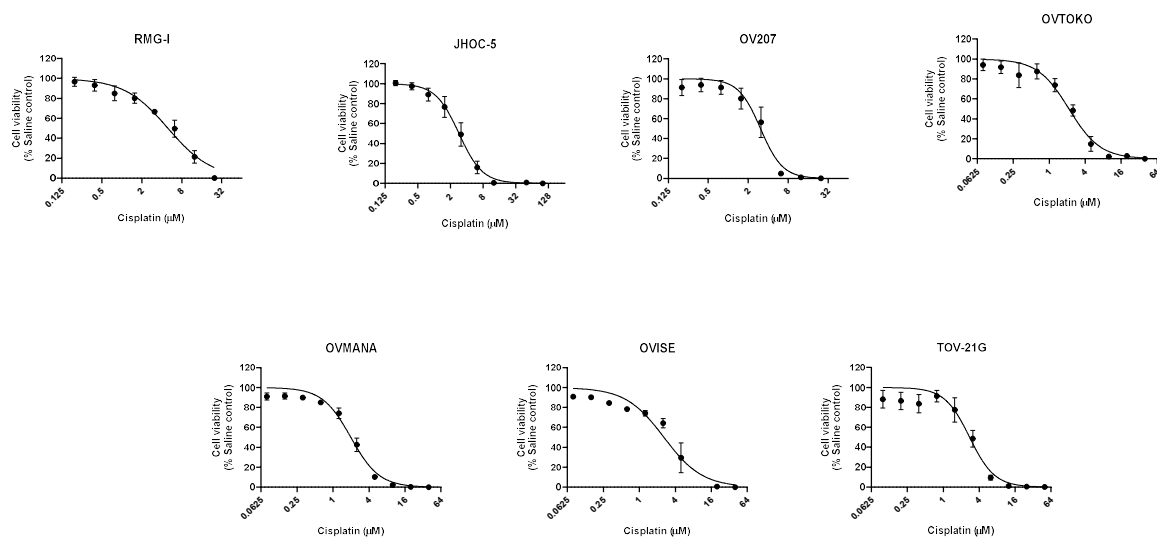


Figure A.1 Cisplatin dose curves of 7 OCCC cell lines. Cell lines were with 11 concentrations of cisplatin for 72h, and a MTS assay performed to determine how many live cells remained (% viable cells). These experiments were repeated at least 3 times before dose curves were generated. Data is shown as the mean  $\pm$  SEM.

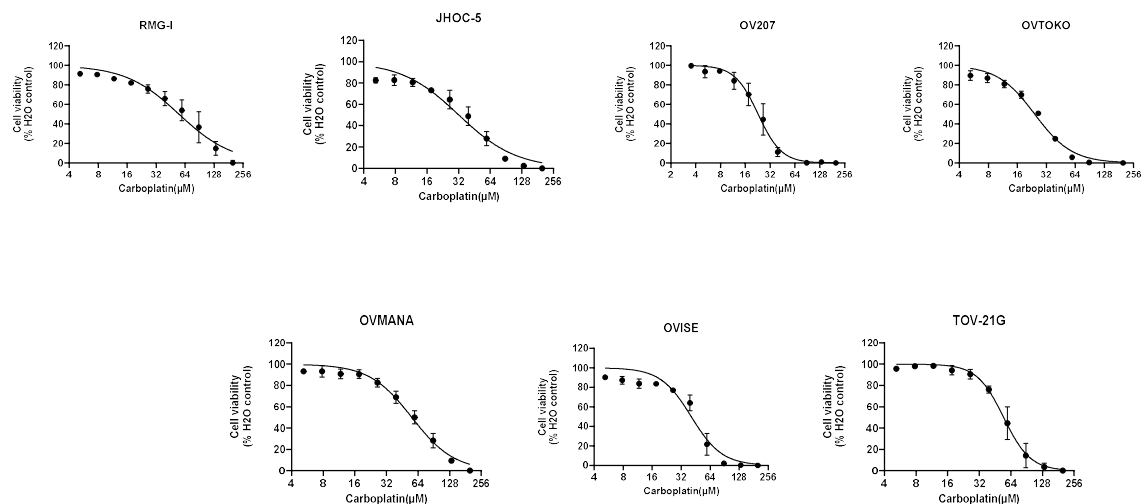


Figure A.2 Carboplatin dose curves of 7 OCCC cell lines. Cell lines were with 11 concentrations of carboplatin for 72h, and a MTS assay performed to determine how many live cells remained (% viable cells). These experiments were repeated at least 3 times before dose curves were generated. Data is shown as the mean  $\pm$  SEM.

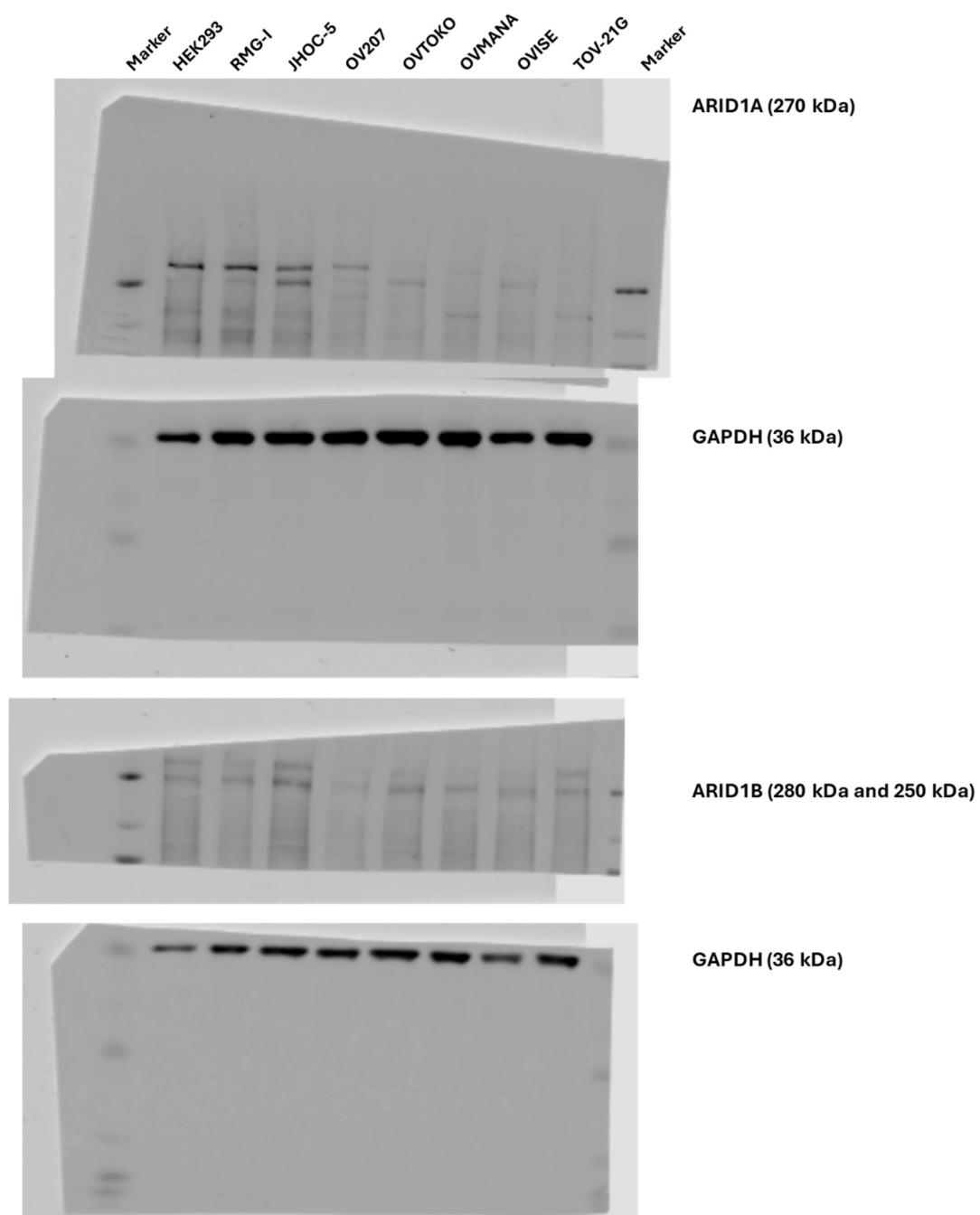


Figure A.3 Full western blot image of ARID1A and ARID1B in seven OCCC cell lines compared to a control cell line with wild-type expression of proteins of interest (HEK293). The marker is Chameleon Duo Pre-stained Protein Ladder (cat no. 928-60000, LI-COR Bioscience).

## Appendix 2

Table A.2 Full compound list of the Tocriscreen Epigenetics Library 3.0

Drug number	Product name	Primary Target
1	Fasudil hydrochloride	Rho-Kinases
2	GF 109203X	Protein Kinase C
3	Ceramide	Protein Ser/Thr Phosphatases
4	Cyclosporin A	Protein Ser/Thr Phosphatases
5	8-Bromo-cAMP, sodium salt	cAMP
6	PD 98059	MEK
7	Etoposide	DNA Topoisomerases
8	Kenpaullone	Glycogen Synthase Kinase 3
9	Resveratrol	Cyclooxygenases
10	Arctigenin	MEK
11	NSC 663284	Cdc25 Phosphatase
12	BVT 948	Protein Tyrosine Phosphatases
13	Doxorubicin hydrochloride	DNA Topoisomerases
14	Salubrinal	Protein Ser/Thr Phosphatases
15	CGP 53353	Protein Kinase C
16	ZM 447439	Aurora Kinases
17	Acyclovir	RNA/DNA Polymerase
18	Ryuvidine	Other Lysine Methyltransferases
19	Decitabine	DNA Methyltransferases
20	Sodium 4-Phenylbutyrate	Non-selective HDACs
21	Valproic acid, sodium salt	Non-selective HDACs
22	AICAR	AMPK
23	Metformin hydrochloride	AMPK
24	H 89 dihydrochloride	Protein Kinase A
25	PI 103 hydrochloride	PI 3-kinase
26	CI 994	Class I HDACs
27	Dorsomorphin dihydrochloride	AMPK
28	Mirin	ATM and ATR Kinases
29	Triptolide	RNA/DNA Polymerase

<b>30</b>	PJ 34 hydrochloride	Poly(ADP-ribose) Polymerase
<b>31</b>	RG 108	DNA Methyltransferases
<b>32</b>	BIX 01294	G9a/GLP
<b>33</b>	Sal 003	Protein Ser/Thr Phosphatases
<b>34</b>	PRIMA-1MET	p53
<b>35</b>	XAV 939	Tankyrase
<b>36</b>	AR-A 014418	Glycogen Synthase Kinase 3
<b>37</b>	3-Methyladenine	PI 3-kinase
<b>38</b>	Alexidine dihydrochloride	Protein Tyrosine Phosphatases
<b>39</b>	Nicotinamide	Poly(ADP-ribose) Polymerase
<b>40</b>	Bisindolylmaleimide II	Protein Kinase C
<b>41</b>	Ro 3306	Cyclin-Dependent Protein Kinases
<b>42</b>	UNC 0638	G9a/GLP
<b>43</b>	SMER 3	Ubiquitin E3 Ligases
<b>44</b>	CHIR 99021	Glycogen Synthase Kinase 3
<b>45</b>	IOX 2	Hydroxylases
<b>46</b>	IOX 1	Histone Demethylases
<b>47</b>	P 22077	Deubiquitinating Enzymes
<b>48</b>	(+)-JQ1	Bromodomains
<b>49</b>	SGC 0946	Other Lysine Methyltransferases
<b>50</b>	CP 690550 citrate	JAK Kinase
<b>51</b>	ML 228	Hypoxia Inducible Factors (HIF)
<b>52</b>	GSK J4	Histone Demethylases
<b>53</b>	SB 747651A dihydrochloride	Other Kinases
<b>54</b>	I-BET 151 dihydrochloride	Bromodomains
<b>55</b>	SAHA	Non-selective HDACs
<b>56</b>	AK 7	Class III HDACs (Sirtuins)
<b>57</b>	Bromosporine	Bromodomains
<b>58</b>	BIX 02189	MEK
<b>59</b>	SGC-CBP30	Bromodomains
<b>60</b>	UNC 1999	EZH2
<b>61</b>	UNC 2400	EZH2
<b>62</b>	JIB 04	Histone Demethylases

63	RN 1 dihydrochloride	Histone Demethylases
64	PRT 4165	Ubiquitin E3 Ligases
65	UNC 2327	Protein Arginine Methyltransferases
66	PFI 3	Bromodomains
67	TC-E 5002	Histone Demethylases
68	UNC 0642	G9a/GLP
69	GSK 2830371	Protein Ser/Thr Phosphatases
70	A 366	G9a/GLP
71	Spautin 1	Deubiquitinating Enzymes
72	AZ 20	ATM and ATR Kinases
73	Furamide dihydrochloride	Protein Arginine Methyltransferases
74	TC-S 7009	Hypoxia Inducible Factors (HIF)
75	OF 1	Bromodomains
76	MM 102	WDR5
77	WDR5 0103	WDR5
78	GSK LSD 1 dihydrochloride	Histone Demethylases
79	SGC 707	Protein Arginine Methyltransferases
80	Heclin	Ubiquitin E3 Ligases
81	XY1	Protein Arginine Methyltransferases
82	CW 008	Protein Kinase A
83	LP 99	Bromodomains
84	ent-LP 99	Bromodomains
85	Sephin 1	Protein Ser/Thr Phosphatases
86	EPZ 004777	Other Lysine Methyltransferases
87	PFI 4	Bromodomains
88	BI 9564	Bromodomains
89	I-BRD9	Bromodomains
90	A66	PI 3-kinase
91	(-)-JQ1	Bromodomains
92	AZD 1480	JAK Kinase
93	GS 143	Ubiquitin E3 Ligases
94	GN 44028	Hypoxia Inducible Factors (HIF)
95	NVS-CECR2-1	Bromodomains

<b>96</b>	TGX 221	PI 3-kinase
<b>97</b>	PDD 00017273	Poly(ADP-ribose) Glycohydrolase
<b>98</b>	BAY 299	Bromodomains
<b>99</b>	BAY 598	Other Lysine Methyltransferases
<b>100</b>	TP 472N	Bromodomains
<b>101</b>	TP 472	Bromodomains
<b>102</b>	TP 064	Protein Arginine Methyltransferases
<b>103</b>	AZD 2461	Poly(ADP-ribose) Polymerase
<b>104</b>	Lin28 1632	DNA, RNA and Protein Synthesis
<b>105</b>	Nutlin 3a	Ubiquitin E3 Ligases
<b>106</b>	PF 06409577	AMPK
<b>107</b>	TC JL 37	JAK Kinase
<b>108</b>	VH 298	Ubiquitin E3 Ligases
<b>109</b>	cis VH 298	Ubiquitin E3 Ligases
<b>110</b>	A 196	Other Lysine Methyltransferases
<b>111</b>	OTX 015	Bromodomains
<b>112</b>	GSK 6853	Bromodomains
<b>113</b>	GSK 9311 hydrochloride	Bromodomains
<b>114</b>	MS 275	Class I HDACs
<b>115</b>	Rucaparib camsylate	Poly(ADP-ribose) Polymerase
<b>116</b>	Entecavir	RNA/DNA Polymerase
<b>117</b>	L Moses dihydrochloride	Bromodomains
<b>118</b>	Autophinib	PI 3-kinase
<b>119</b>	AZ 5704	ATM and ATR Kinases
<b>120</b>	Ciclopirox	Histone Demethylases
<b>121</b>	A 485	Histone Acetyltransferases
<b>122</b>	PF 06551600 malonate	JAK Kinase
<b>123</b>	EPZ 015666	Protein Arginine Methyltransferases
<b>124</b>	BAY 6035	Other Lysine Methyltransferases
<b>125</b>	FM19G11	Hypoxia Inducible Factors (HIF)
<b>126</b>	TP 238	Bromodomains
<b>127</b>	WM 1119	Histone Acetyltransferases
<b>128</b>	Raphin 1	Protein Ser/Thr Phosphatases

<b>129</b>	K 03861	Cyclin-dependent Kinase
<b>130</b>	Omipalisib	PI 3-kinase
<b>131</b>	Idasanutlin	Ubiquitin E3 Ligases
<b>132</b>	GSK J5 HCl	Histone Demethylases
<b>133</b>	AT 7867	Akt (Protein Kinase B)
<b>134</b>	Veliparib dihydrochloride	Poly(ADP-ribose) Polymerase
<b>135</b>	Tasquinimod	Class II HDACs
<b>136</b>	CeMMEC1	Bromodomains
<b>137</b>	SGC 6870	Protein Arginine Methyltransferases
<b>138</b>	SGC 6870N	Protein Arginine Methyltransferases
<b>139</b>	Santacruzamate A	Class I HDACs
<b>140</b>	SMIP 004	Ubiquitin E3 Ligases
<b>141</b>	EIDD 1931	RNA Polymerase
<b>142</b>	iHAP1	Protein Ser/Thr Phosphatases
<b>143</b>	WM 3835	Histone Acetyltransferases
<b>144</b>	iBET-BD2	Bromodomains
<b>145</b>	SGC SMARCA-BRDVIII	Bromodomains
<b>146</b>	NI 57	Bromodomains
<b>147</b>	CRT 0066854 hydrochloride	Protein Kinase C
<b>148</b>	LW 6	Other Dehydrogenases
<b>149</b>	Pyridone 6	JAK Kinase
<b>150</b>	WM 8014	Histone Acetyltransferases
<b>151</b>	RGFP 966	Class I HDACs
<b>152</b>	Ibrutinib	Bruton's Tyrosine Kinase
<b>153</b>	WS 383	Ubiquitin E3 Ligases
<b>154</b>	Ruxolitinib	JAK Kinase
<b>155</b>	AGI 5198	Isocitrate dehydrogenase 1 (IDH1)
<b>156</b>	Baricitinib	JAK Kinase
<b>157</b>	Favipiravir	RNA Polymerase
<b>158</b>	Remdesivir	RNA Polymerase
<b>159</b>	GS 441524	RNA Polymerase
<b>160</b>	Dinaciclib	CDK1 Subfamily



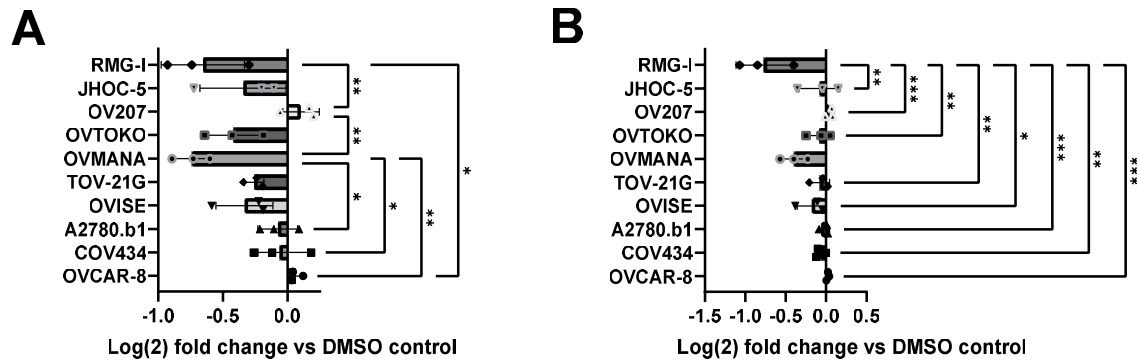


Figure A.4 Bar chart of cell viability in seven OCCC and three non-OCCC ovarian cancer cell lines after treatment with the Drug 152 (ibrutinib) at (A) 5  $\mu$ M and (B) 0.5  $\mu$ M concentrations. Cell viability was normalised to DMSO vehicle control, and heatmaps generated using GraphPad software. Data is presented as the mean  $\pm$  SEM, N=3. (\*\*P<0.01, \*\*\*P<0.001, \*\*\*\*P<0.0001).

## Appendix 3

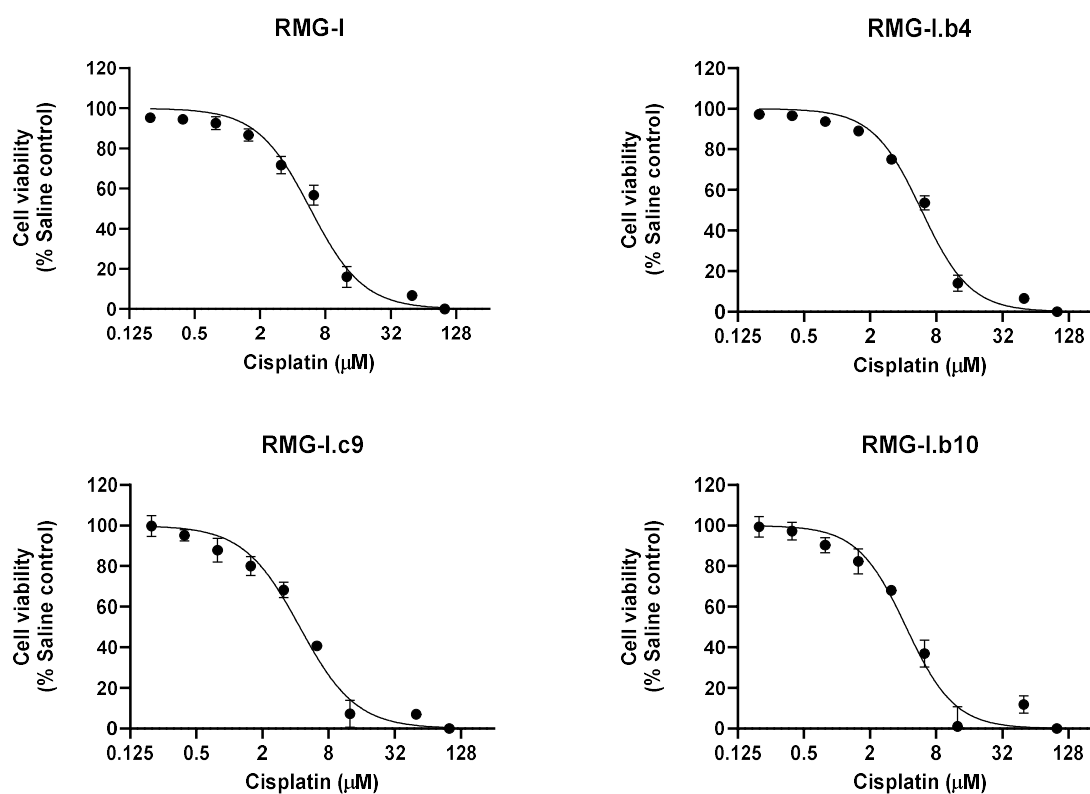


Figure A.5 Dose curves of RMG-I parental and clonal lines b4, c9 and b10 measured by MTS assay 72 hours post treatment with cisplatin. MTS assay performed to determine how many live cells remained (% viable cells). These experiments were repeated at least 3 times before dose curves were generated. Data is shown as the mean  $\pm$  SEM.

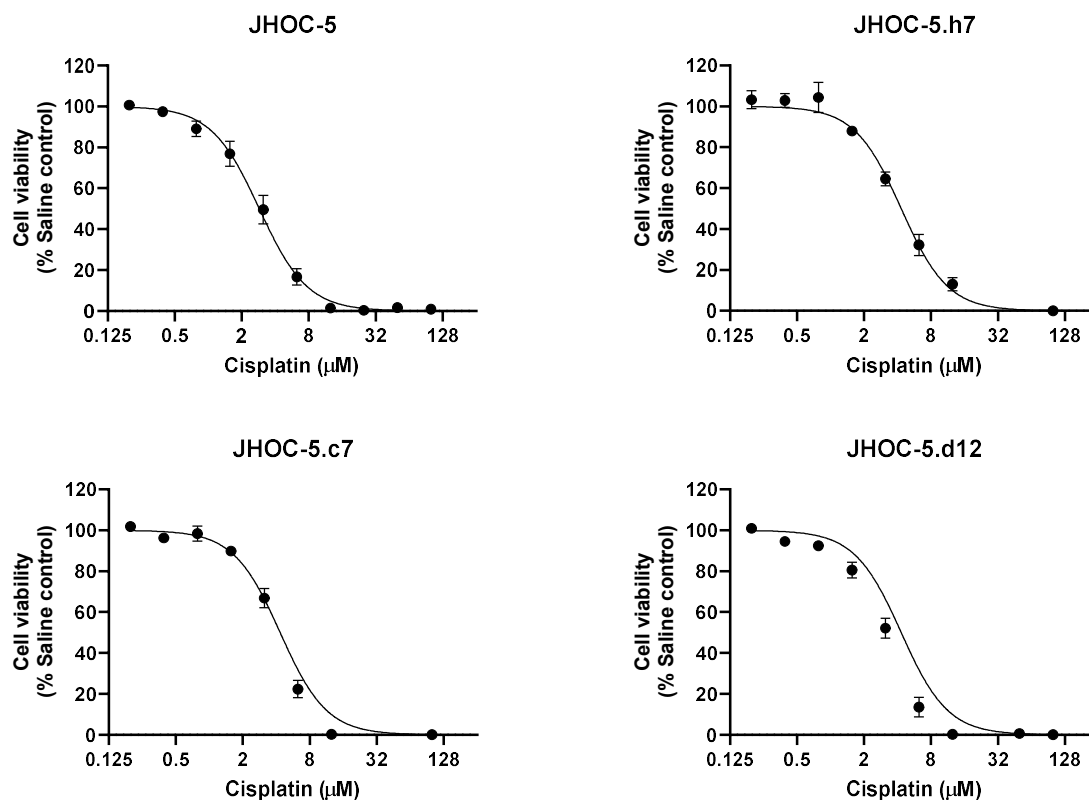


Figure A.6 Dose curves of JHOC-5 parental and clonal lines h7, c7, and d12 measured by MTS assay 72 hours post treatment with cisplatin. MTS assay performed to determine how many live cells remained (% viable cells). These experiments were repeated at least 3 times before dose curves were generated. Data is shown as the mean  $\pm$  SEM.

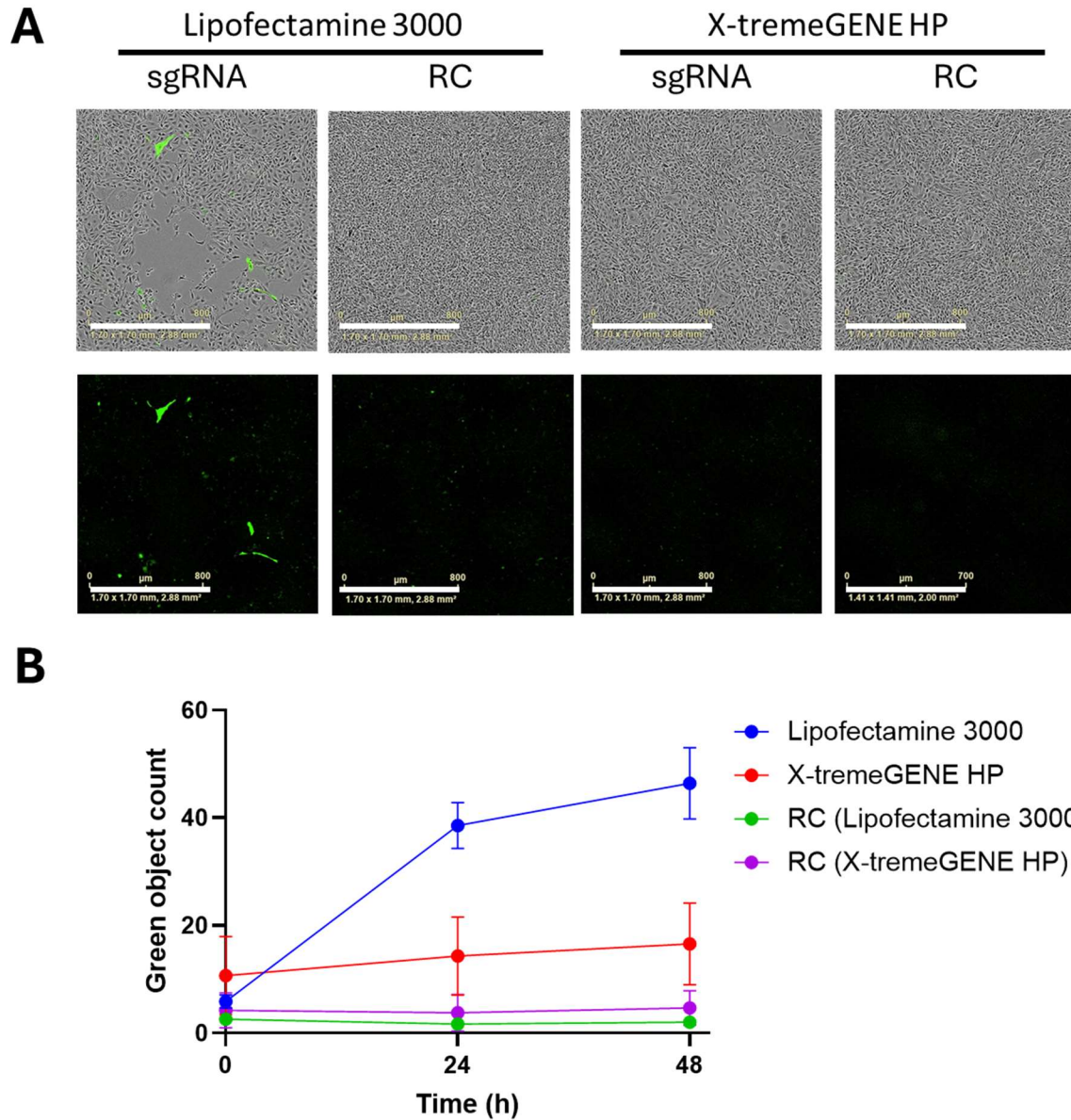


Figure A.7 Transfection comparison between lipofectamine 3000 and X-tremeGENE HP in JHOC-5.d12 cells using the *ARID1B* CRISPR KO plasmid DNA that targets exon 6. A) GFP cell images of Lipofectamine 3000 and X-tremeGENE HP and RC 48 hours after transfection. Scale bar= 800μm. B) Green objective count as analysed by the IncuCyte S3 analysis software. Graphs represent mean ± SEM for 9 technical replicates (N=1 biological experiment).

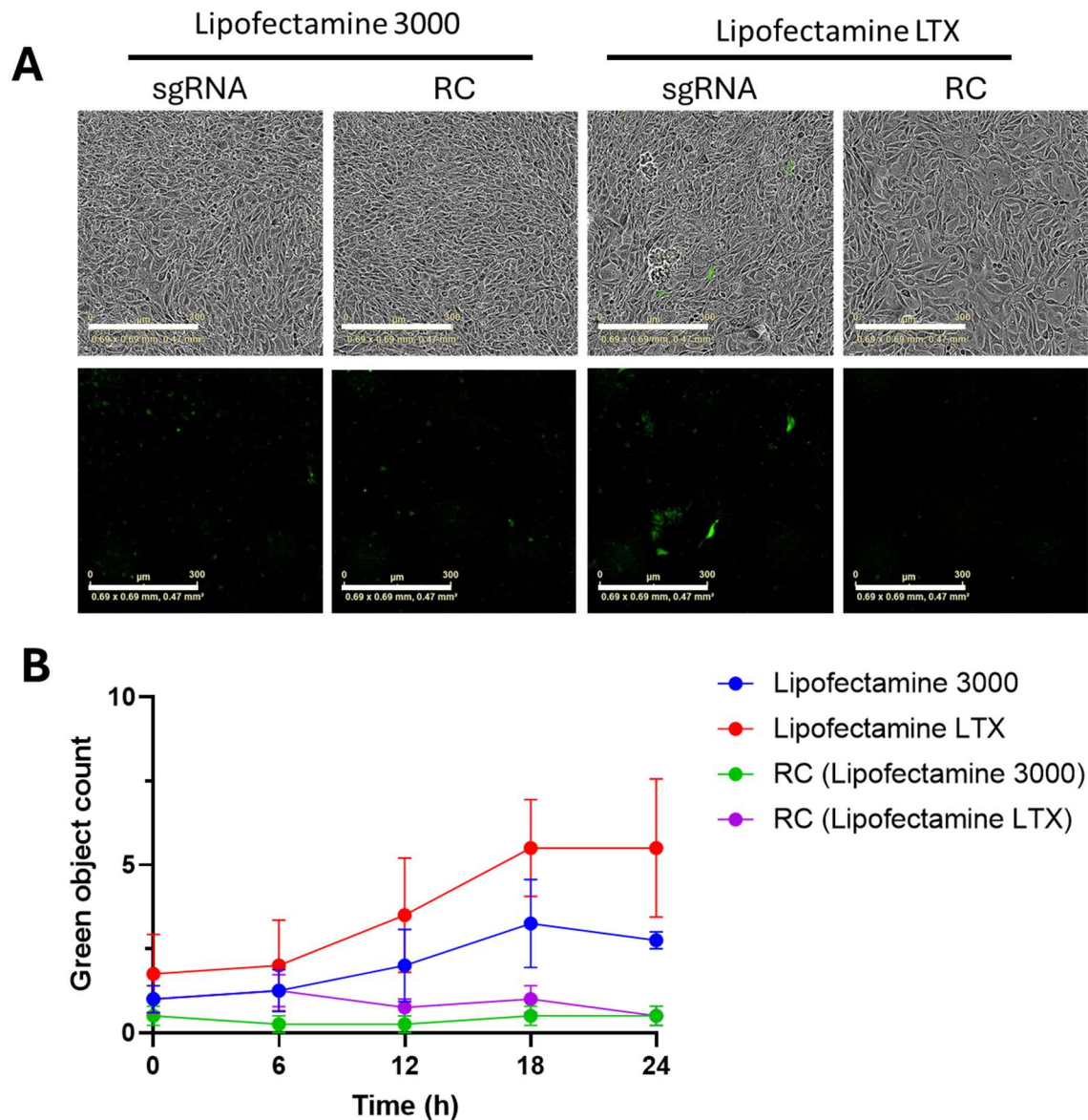


Figure A.8 Transfection comparison between lipofectamine 3000 and lipofectamine LTX reagents in JHOC-5.d12 clonal cells using *ARID1A* CRISPR KO plasmid DNA that targets exon 1. A) GFP cell images of Lipofectamine 3000 and lipofectamine LTX and RC 48 hours after transfection. Scale bar= 400μm. B) Green objective count as analysed by the IncuCyte S3 analysis software. N=1, graphs represent SEM for 4 technical replicates.

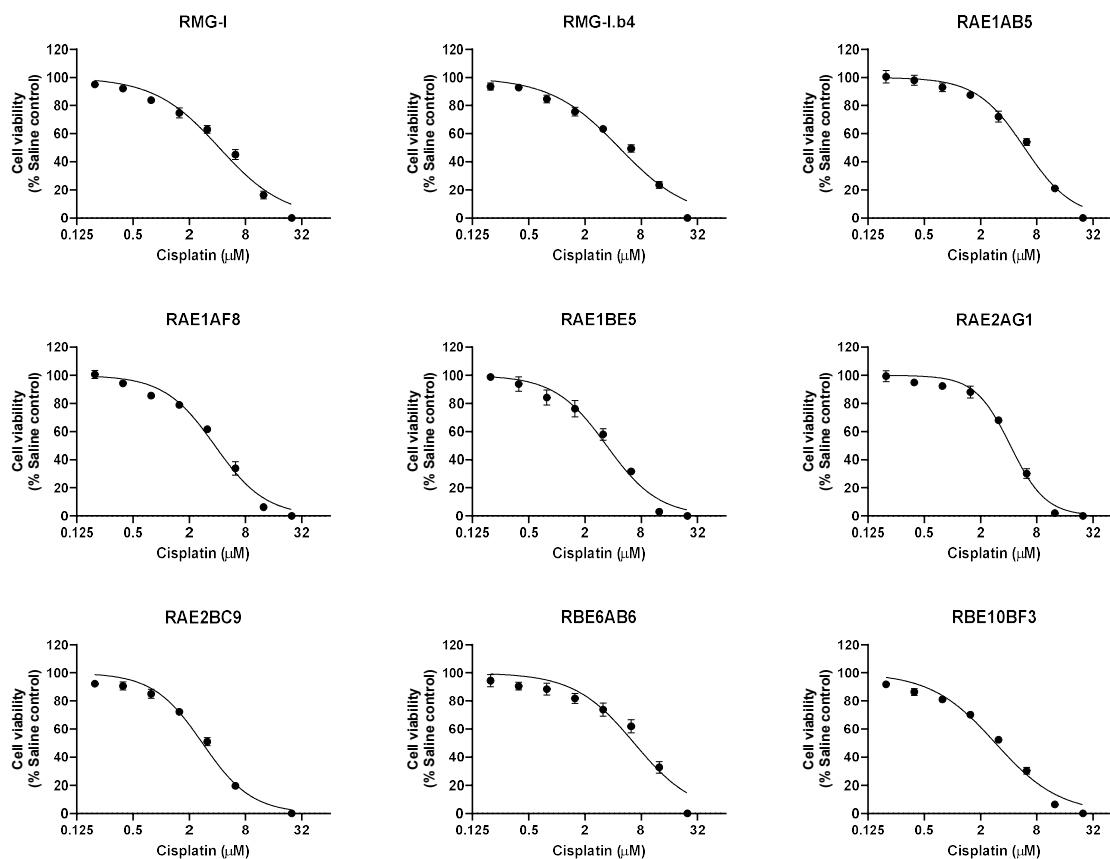


Figure A.9 Dose curves of RMG-I parental line and CRISPR clonal lines measured by MTS assay 72 hours post treatment with cisplatin. MTS assay performed to determine how many live cells remained (% viable cells). These experiments were repeated at least 3 times before dose curves were generated. Data is shown as the mean  $\pm$  SEM.

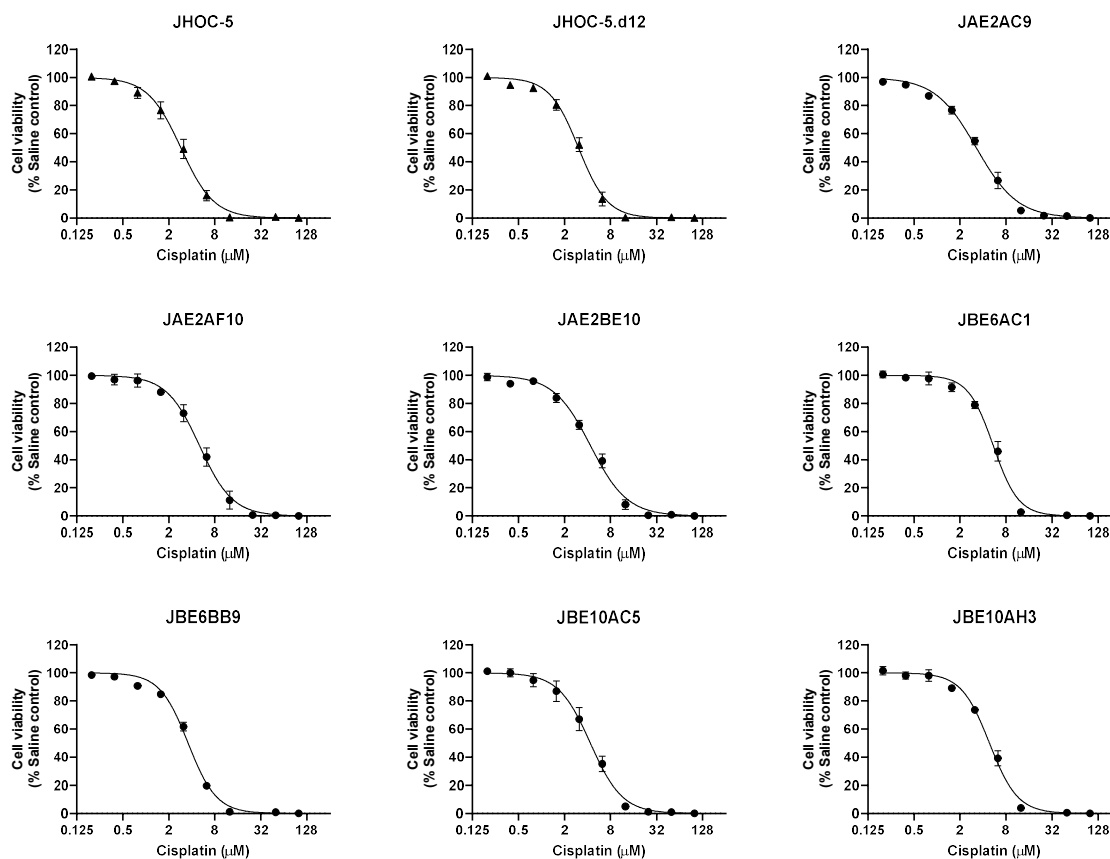


Figure A.10 Dose curves of JHOC-5 parental line and CRISPR clonal lines measured by MTS assay 72 hours post treatment with cisplatin. MTS assay performed to determine how many live cells remained (% viable cells). These experiments were repeated at least 3 times before dose curves were generated. Data is shown as the mean  $\pm$  SEM.

## Appendix 4

Appendix 4 contains 5 published papers, 1 submitted paper, and 1 paper in preparation which have arisen or related to this thesis.

### A.4.1 Manuscripts arising from thesis

1. **Ma Y**, Field NR, Xie T, Briscas S, Kokinogoulis EG, Skipper TS, Alghalayini A, Sarker FA, Tran N, Bowden NA, Dickson K-A, and Marsh DJ. Aberrant SWI/SNF complex members are predominant in rare ovarian malignancies – therapeutic vulnerabilities in treatment resistant subtypes. *Cancers*. (Submitted, 9/8/2024).
2. Yee C, Dickson KA, Muntasir MN, **Ma Y**, Marsh DJ (2022). Three-Dimensional Modelling of Ovarian Cancer: From Cell Lines to Organoids for Discovery and Personalized Medicine. *Front Bioeng Biotechnol* 10:836984. PMID: 35223797.

### A.4.2 Manuscripts in preparation from this thesis

1. **Ma Y**, Dickson K-A, *et al.*, and Marsh DJ. Epigenetic compound library screen identifies ibrutinib as an inhibitor of ovarian clear cell carcinoma viability. (In preparation).

### A.4.3 Manuscripts related to this thesis

1. Dickson KA, Field N, Blackman T, **Ma Y**, Xie T, Kurangil E, Idrees S, Rathnayake SNH, Mahbub RM, Faiz A, Marsh DJ (2023). CRISPR single base-editing: in silico predictions to variant clonal cell lines. *Hum Mol Genet* 32(17):2704-2716. PMID: 37369005.
2. Xie T, Dickson KA, Yee C, **Ma Y**, Ford CE, Bowden NA, Marsh DJ (2022). Targeting homologous recombination deficiency in ovarian cancer with PARP inhibitors: synthetic lethal strategies that Impact overall survival. *Cancers (Basel)* 14(19):4621. PMID: 36230543.
3. Dickson KA, Xie T, Evenhuis C, **Ma Y**, Marsh DJ (2021). PARP inhibitors display differential efficacy in models of BRCA mutant high-grade serous ovarian cancer. *Int J Mol Sci* 22(16):8506. PMID: 34445211.
4. Marsh DJ, **Ma Y**, Dickson KA (2020). Histone monoubiquitination in chromatin remodelling: focus on the histone H2B interactome and cancer. *Cancers (Basel)* 12(11):3462. PMID: 33233707.





# Three-Dimensional Modelling of Ovarian Cancer: From Cell Lines to Organoids for Discovery and Personalized Medicine

Christine Yee<sup>1\*</sup>, Kristie-Ann Dickson<sup>1</sup>, Mohammed N. Muntasir<sup>1</sup>, Yue Ma<sup>1</sup> and Deborah J. Marsh<sup>1,2</sup>

<sup>1</sup>Translational Oncology Group, School of Life Sciences, Faculty of Science, University of Technology Sydney, Ultimo, NSW, Australia, <sup>2</sup>Northern Clinical School, Faculty of Medicine and Health, University of Sydney, Camperdown, NSW, Australia

## OPEN ACCESS

### Edited by:

Dunja Aksentijevic,  
Queen Mary University of London,  
United Kingdom

### Reviewed by:

Ting-Yuan Tu,  
National Cheng Kung University,  
Taiwan  
Hermann Frieboes,  
University of Louisville, United States

### \*Correspondence:

Christine Yee  
Christine.Yee@uts.edu.au

### Specialty section:

This article was submitted to  
Preclinical Cell and Gene Therapy,  
a section of the journal  
Frontiers in Bioengineering and  
Biotechnology

**Received:** 16 December 2021

**Accepted:** 19 January 2022

**Published:** 10 February 2022

### Citation:

Yee C, Dickson K-A, Muntasir MN,  
Ma Y and Marsh DJ (2022) Three-  
Dimensional Modelling of Ovarian  
Cancer: From Cell Lines to Organoids  
for Discovery and  
Personalized Medicine.  
Front. Bioeng. Biotechnol. 10:836984.  
doi: 10.3389/fbioe.2022.836984

Ovarian cancer has the highest mortality of all of the gynecological malignancies. There are several distinct histotypes of this malignancy characterized by specific molecular events and clinical behavior. These histotypes have differing responses to platinum-based drugs that have been the mainstay of therapy for ovarian cancer for decades. For histotypes that initially respond to a chemotherapeutic regime of carboplatin and paclitaxel such as high-grade serous ovarian cancer, the development of chemoresistance is common and underpins incurable disease. Recent discoveries have led to the clinical use of PARP (poly ADP ribose polymerase) inhibitors for ovarian cancers defective in homologous recombination repair, as well as the anti-angiogenic bevacizumab. While predictive molecular testing involving identification of a genomic scar and/or the presence of germline or somatic *BRCA1* or *BRCA2* mutation are in clinical use to inform the likely success of a PARP inhibitor, no similar tests are available to identify women likely to respond to bevacizumab. Functional tests to predict patient response to any drug are, in fact, essentially absent from clinical care. New drugs are needed to treat ovarian cancer. In this review, we discuss applications to address the currently unmet need of developing physiologically relevant *in vitro* and *ex vivo* models of ovarian cancer for fundamental discovery science, and personalized medicine approaches. Traditional two-dimensional (2D) *in vitro* cell culture of ovarian cancer lacks critical cell-to-cell interactions afforded by culture in three-dimensions. Additionally, modelling interactions with the tumor microenvironment, including the surface of organs in the peritoneal cavity that support metastatic growth of ovarian cancer, will improve the power of these models. Being able to reliably grow primary tumoroid cultures of ovarian cancer will improve the ability to recapitulate tumor heterogeneity. Three-dimensional (3D) modelling systems, from cell lines to organoid or tumoroid cultures, represent enhanced starting points from which improved translational outcomes for women with ovarian cancer will emerge.

**Keywords:** ovarian cancer, 3D cell culture, 3D bio-printing, organoids, tumoroid, drug screening, personalized medicine

# 1 INTRODUCTION

Globally, ovarian cancer is the eighth most frequently diagnosed malignancy and cause of cancer-related death in women (Sung et al., 2021). The classification of ovarian cancer includes distinct histological subtypes with varied sites of origin underpinned by defining molecular events affecting tumor suppressors and oncogenes. These events drive specific patterns of clinical behavior characteristic of histotypes, including response to chemotherapeutic agents and molecular target drugs. Malignant histological subtypes arising from epithelial cells include high-grade serous ovarian cancer (HGSOC), ovarian clear cell carcinoma (OCCC), endometrioid ovarian cancer (EnOC), mucinous ovarian cancer (MOC), low-grade serous ovarian cancer (LGSOC) and malignant Brenner cell tumors (Shih Ie and Kurman, 2004; Kurman and Shih Ie, 2010). Ovarian carcinosarcomas (OCS), also known as malignant mixed mullerian tumors (MMMT), have epithelial and mesenchymal components (Harris et al., 2003). Ovarian sex-cord stromal tumors (SCST), the most common of which are granulosa cell tumors (GCT) along with the rarer Sertoli–Leydig cell tumors, are of stromal cell origin (Fuller et al., 2017). An extremely rare subtype of ovarian cancer primarily affecting women under 40 years of age is small cell carcinoma of the ovary, hypercalcemic type (SCCOHT), an ovarian rhabdoid tumor (Auguste et al., 2020).

Almost all HGSOC have a somatic *TP53* mutation and p53 immunohistochemistry is a surrogate marker for *TP53* mutation in these tumors (Bell, 2011; Cole et al., 2016; Köbel and Kang, 2021). *TP53* mutations are also observed in MOC (Köbel and Kang, 2021), ovarian carcinosarcomas (Trento et al., 2020) and less frequently in OCCC (Parra-Herran et al., 2019). *BRCA1* and *BRCA2* mutations occur in HGSOC, including in the germline of affected patients (Alsop et al., 2012), and rarely in patients with OCCC (De Pauw et al., 2021). *ARID1A* and *ARID1B* encode members of the SWI/SNF (SWItch/Sucose Non-Fermentable) ATP-dependent chromatin remodeling complex important for interaction of this complex with DNA, both genes being mutated in OCCC and endometrioid ovarian cancers (McCluggage and Stewart, 2021). The SWI/SNF complex is also disrupted in the very rare SCCOHT with mutation of *SMARCA4* and epigenetic silencing of *SMARCA2* that encode catalytic subunits important for nucleosome sliding and eviction (Jelinic et al., 2016; Xue et al., 2021). OCCC and endometrioid carcinomas also have in common a disrupted PTEN-PI3K pathway with mutations observed in *PTEN* and *PIK3CA*, as well as mutations in *CTNNB1* (Kuo et al., 2009; Hollis et al., 2020). The RAS/MAPK pathway has been implicated in LGSOC, with mutations identified in *KRAS*, *NRAS*, and *BRAF* (Moujaber et al., 2021). Mutations in the RAS/MAPK pathway are also observed in EnOC (Hollis et al., 2020), OCCC (Kim et al., 2018), and MOC (Cheasley et al., 2021). Adult ovarian GCTs are characterized predominantly by mutation of *FOXL2*, and Sertoli–Leydig Cell Tumors (SLCTs) harbor mutations in *DICER1* (Fuller et al., 2017; De Paolis et al., 2021). Epithelial and stromal cell ovarian cancer histotypes and associated genes known to be mutated are summarized in **Figure 1**.

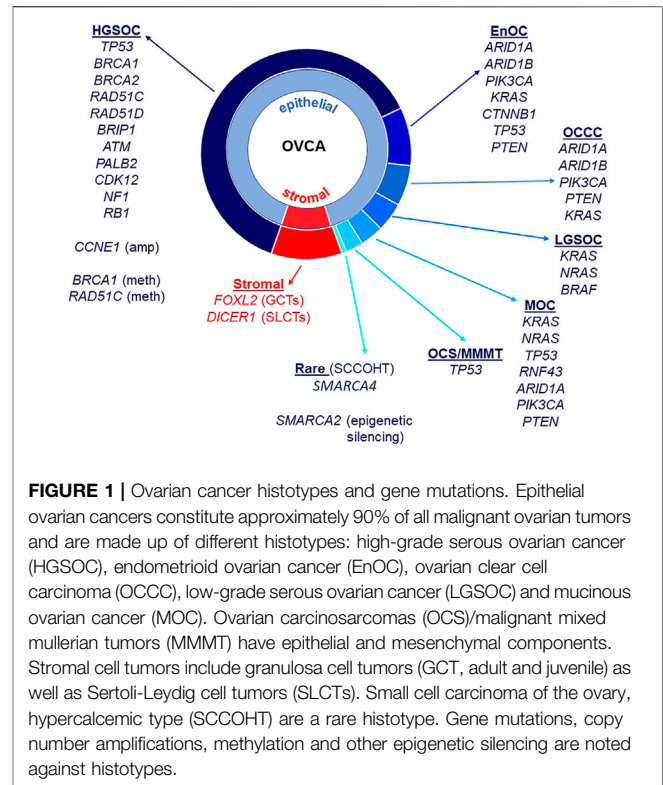


**FIGURE 1 |** Ovarian cancer histotypes and gene mutations. Epithelial ovarian cancers constitute approximately 90% of all malignant ovarian tumors and are made up of different histotypes: high-grade serous ovarian cancer (HGSOC), endometrioid ovarian cancer (EnOC), ovarian clear cell carcinoma (OCCC), low-grade serous ovarian cancer (LGSOC) and mucinous ovarian cancer (MOC). Ovarian carcinosarcomas (OCS)/malignant mixed mullerian tumors (MMMT) have epithelial and mesenchymal components. Stromal cell tumors include granulosa cell tumors (GCT, adult and juvenile) as well as Sertoli–Leydig cell tumors (SLCTs). Small cell carcinoma of the ovary, hypercalcemic type (SCCOHT), are a rare histotype. Gene mutations, copy number amplifications, methylation and other epigenetic silencing are noted against histotypes.

In addition to mutations, methylation of *BRCA1* is also observed in HGSOC, as is amplification of *CCNE1* (Bell, 2011; Patch et al., 2015). Along with defects in *BRCA1* and *BRCA2*, other genes that function in homologous recombination repair (HRR) are mutated in ovarian cancer, albeit at lower frequencies, including *RAD51C*, *RAD51D*, *BRIP1*, *PALB2*, and *ATM* (Pennington et al., 2014). Defects in HRR can lead to the presence of “genomic scars” caused by the cancer cell’s inability to accurately repair sites of double strand breaks (DSBs). These include extensive loss of heterozygosity (LOH), large scale transitions (LST) and telomeric allelic imbalance (TAI) (Watkins et al., 2014; Chao et al., 2018; Nguyen et al., 2020). Tumors with defects in HRR are responsive to poly adenosine diphosphate-ribose polymerase inhibitors (PARPis), functioning in a synthetic lethal manner to inhibit repair of single strand breaks *via* the base excision repair pathway (Dedes et al., 2011). As a predictive DNA marker of defective HRR, genomic scars are helpful, but not all tumors with a genomic scar will respond to a PARPi. Reasons for this include reversion of a *BRCA* mutation, occurrence of a secondary mutation that restores wild-type function or changes in methylation patterns of an HRR gene that in effect functionally restores HRR but the genomic scar remains (Patch et al., 2015). Functional analyses, alongside molecular assays, are required to confirm the predicted response of women with ovarian cancer to PARPis such as the FDA-approved drugs olaparib, niraparib and rucaparib (Dickson et al., 2021; Lee et al., 2021; Valabrega et al., 2021).

Predicting which women will respond to a PARPi is particularly important given the unprecedented improvement

seen in Progression Free Survival (PFS) and Overall Survival (OS) for subsets of women administered these drugs, including as maintenance therapy (Audeh et al., 2010; Ledermann et al., 2012; Ledermann J. et al., 2014; Moore et al., 2018). Ovarian cancers with germline or somatic mutation of *BRCA1* or *BRCA2*, mutation of *RAD51C* or *RAD51D*, methylation of *BRCA1*, or high LOH have all been reported to respond to PARP inhibition (Audeh et al., 2010; Wang et al., 2012; Ledermann J. et al., 2014; Kondrashova et al., 2017; Swisher et al., 2017; Moore et al., 2018). Furthermore, loss of *RAD51C* methylation has recently been implicated as a mechanism of PARPi resistance (Nesic et al., 2021). The combination of molecular testing and functional analyses conducted in robust tumor or ascites models has the power to strongly predict whether a woman is likely to respond to a PARPi at each stage of her disease progression.

Unlike for PARPis, there are no clinically approved biomarkers to predict responses of women with ovarian cancer to the anti-angiogenic bevacizumab, although numerous studies have focused on this area (Buechel et al., 2021; Gao et al., 2021; Hsu et al., 2021). Given the advances seen in PFS and OS of some women receiving this monoclonal antibody that targets vascular endothelial growth factor (VEGF), development of functional assays to predict the likelihood that a woman will respond to bevacizumab would represent a major advance (Burger et al., 2011; Perren et al., 2011; Oza et al., 2015).

The majority of women with HGSOC will respond initially to carboplatin, although some tumors display innate platinum resistance (Davis et al., 2014). There are no robust markers to predict response to platinum drugs, including through the development of acquired chemoresistance, although defects in HRR in primary tumors have been associated with a more favorable response (Konstantinopoulos et al., 2010; Muggia and Safra, 2014). The use of platinum drugs in histotypes other than HGSOC must be questioned given frequent low response rates. Only 11–27% of OCCC respond initially to platinum therapy, dropping to only 1–2% response rates in recurrent disease (Sugiyama et al., 2000; Mabuchi et al., 2016; Tan et al., 2019). LGSOC also display a poor response to platinum drugs; however, the presence of activating mutations in mitogen-activated protein kinase (MAPK) pathway genes *KRAS*, *BRAF*, and *NRAS* has seen favorable responses in LGSOC with the MEK inhibitor trametinib (reviewed in Moujaber et al. (2021)).

The mutations and genomic variations described above offer opportunities to develop new molecular-based therapeutic strategies to treat ovarian cancer subtypes. Some molecular events, such as those described in the HRR pathway, are already being targeted clinically by FDA-approved PARPis. For both discovery science and translational approaches to predicting which women are likely to benefit from which therapies, robust models are needed that expand upon traditional 2D cell culture and pre-clinical models, and include both molecular profiling and functional analyses. In this review, we discuss methods of 3D modelling that are either currently being employed in ovarian cancer cell lines, primary or metastatic tumor tissue and ascites, or have the potential to be used into the future for these purposes.

## 2 THE MICROENVIRONMENT—CONSIDERATIONS WHEN MODELLING OVARIAN CANCER

### 2.1 Sites of Origin of Ovarian Cancer

There are numerous factors to examine when considering the microenvironment that supports the initiation, development and metastasis of ovarian cancer, not least being the very first microenvironment of these malignancies and that is the site of origin of the initial lesion. Many, perhaps most, HGSOC originate in the fallopian tube as Serous Tubal Intraepithelial Carcinomas (STICs), shedding onto the surface of the ovary and establishing a tumor (Crum et al., 2007; Karst et al., 2011; Perets and Drapkin, 2016; Zhang et al., 2019). This discovery has led to the generation of important models of non-cancerous fallopian tube epithelial cells transformed with c-Myc, H-Ras<sup>V12</sup> or SV40 large T antigen (SV40 Tag) (Karst et al., 2011; Perets and Drapkin, 2016). These models complement those of normal ovarian surface epithelial (OSE) cells immortalized with factors including SV40 Tag, human telomerase (hTERT) and HPV-E6/E7 (Tsao et al., 1995; Davies et al., 2003; Kalli et al., 2004; Shin et al., 2018). OCCC and EnOC have been associated with endometriosis (Samartzis et al., 2020). While MOC has previously been reported as originating from metastatic deposits of primary tumors of the colon, stomach, pancreas and uterus, evidence now shows that these tumors do in fact arise in the ovary following a progression model commencing with benign and borderline precursor lesions (Ledermann J. A. et al., 2014; Cheasley et al., 2019). While constituting ~10% of all ovarian cancers, tumors arising in ovarian stromal cells have different considerations. In contrast to epithelial cell tumors, the sex cord stromal tumor GCT arise in granulosa cells that produce estrogen (Jamieson and Fuller, 2012). Knowledge of the sites of origin of ovarian tumors is imperative to ensure selection of models that best address both research questions and translational approaches.

### 2.2 The Ovarian Cancer Microenvironment and Metastatic Spread

The microenvironment of an ovarian cancer consists of both tumor and non-tumor cells, including immune cells. Patient-derived organoids or tumoroids retain cellular heterogeneity and immune cells, thus are able to more strongly recapitulate a three-dimensional (3D) tumor microenvironment *ex vivo* compared to homogeneous cell lines (Hill et al., 2018; Kopper et al., 2019). Ovarian tumoroid cultures have been established from both ascitic fluid and primary tumors, to date primarily from the more common HGSOC but also from LGSOC, MOC, OCCC, and EnOC (Hill et al., 2018; De Witte et al., 2020; Nanki et al., 2020). These models show great promise for conducting *ex vivo* drug assays to predict therapeutic response in the women from which they were established (De Witte et al., 2020; Maenhoudt et al., 2020; Nanki et al., 2020; Gorski et al., 2021).

Given the location of ovaries, there are no anatomical barriers preventing metastasis to organs in the pelvic cavity including the

**TABLE 1** | Ovarian cancer cell line origin, *in vivo* growth and classifications.

Cell line	OvCa Histotype	Specimen site	Growth <i>in vivo</i> in mice	Commercial availability	References
CaOV-3	HGSOC <sup>a,b,d</sup>	Ovary tumor	Yes: IP; No: SC, IB	ATCC	Buick et al. (1985) <sup>f</sup> ; Hernandez et al. (2016) <sup>g</sup> Hernandez et al. (2016) <sup>g</sup>
CaOV-4	HGSOC <sup>a,c,d</sup>	Fallopian tube metastasis	Yes: SC, IP, IB	ATCC	
COV318	HGSOC <sup>a,d,e</sup>	Ascites	No: SC, IP	ECACC	van den Berg-Bakker et al. (1993) <sup>f</sup> ; De Haven Brandon et al. (2020) <sup>g</sup>
COV362**	HGSOC <sup>a,d</sup>	Pleural effusion	Yes: IP, forms ascites and IB; No: SC	ECACC	van den Berg-Bakker et al. (1993) <sup>f</sup> ; De Haven Brandon et al. (2020) <sup>g</sup>
KURAMOCHI	HGSOC <sup>a,b,d</sup>	Ascites	Yes: SC; No: IP, IB	JCRB	Motoyama (1981) <sup>f</sup> ; De Haven Brandon et al. (2020) <sup>g</sup>
OW28	HGSOC <sup>a,d</sup>	Ascites	Unknown	ECACC	Wilson et al. (1996)
OV202	HGSOC	Primary tumor	Unknown	No	Conover et al. (1998) <sup>f</sup>
OVCA-3	HGSOC <sup>a,b,d,e</sup>	Ascites	Yes: SC, IP	ATCC	Hamilton et al. (1983) <sup>f</sup> ; Hernandez et al. (2016) <sup>g</sup> ; De Haven Brandon et al. (2020) <sup>g</sup>
OVCA-4	HGSOC <sup>a,d</sup>	Ascites	Yes: SC, IP; No: IB	MERCK Millipore	Pirker et al. (1985) <sup>f</sup> ; Hernandez et al. (2016) <sup>g</sup> ; De Haven Brandon et al. (2020) <sup>g</sup>
OVKATE	HGSOC <sup>a,d,e</sup>	Solid metastasis	Yes: SC, IP	JCRB	Yanagibashi et al. (1997) <sup>f,g</sup> ; Mitra et al. (2015b) <sup>g</sup>
OVSAHO	HGSOC <sup>a,d,e</sup>	Solid metastasis	Yes: SC; Yes: IP, forms ascites	JCRB	Yanagibashi et al. (1997) <sup>f,g</sup> ; De Haven Brandon et al. (2020) <sup>g</sup>
PEO1	HGSOC <sup>c</sup>	Ascites	No	ECACC	Langdon et al. (1988) <sup>f</sup> ; Hernandez et al. (2016) <sup>g</sup>
PEO4	HGSOC <sup>c</sup>	Ascites	No	ECACC	Langdon et al. (1988) <sup>f</sup> ; Hernandez et al. (2016) <sup>g</sup>
UWB1.289	HGSOC <sup>c</sup>	Ovary tumor	No: SC, IP	ATCC	DelloRusso et al. (2007) <sup>f</sup> ; Mitra et al. (2015b) <sup>g</sup>
UWB1.289 + BRCA1 A2780*	HGSOC <sup>c</sup>	Ovary tumor	Unknown	ATCC	DelloRusso et al. (2007) <sup>f</sup>
TOV-112D	EnOC <sup>a,b,c,d</sup>	Tumor tissue	Yes: SC and IP, forms ascites	ECACC	Behrens et al. (1987) <sup>f</sup> ; Hernandez et al. (2016) <sup>g</sup>
OVISE	EnOC <sup>b,d,e</sup>	Ovary tumor	Yes: IP; No: SC	ATCC	Provencher et al. (2000) <sup>f</sup> ; Hernandez et al. (2016) <sup>g</sup>
	OCCC <sup>a,b,d,e</sup>	Solid pelvic metastasis	Yes: SC; No: IP	JCRB	Gorai et al. (1995) <sup>f</sup> ; Yanagibashi et al. (1997) <sup>f,g</sup>
OVMANA	OCCC <sup>a,b,d,e</sup>	Primary tumor	Yes: SC; No: IP	JCRB	Yanagibashi et al. (1997) <sup>f,g</sup>
OVTKO	OCCC <sup>a,b,d,e</sup>	Solid splenic metastasis	Yes: SC; Yes: IP	JCRB	Gorai et al. (1995) <sup>f</sup> ; Yanagibashi et al. (1997) <sup>f,g</sup>
RMG-I	OCCC <sup>a,d,e</sup>	Ascites	Yes: SC	JCRB	Nozawa et al. (1991) <sup>f</sup> ; Kashiya et al. (2014) <sup>g</sup>
TOV-21G	OCCC <sup>a,b,d,e</sup>	Ovary tumor	Yes: SC	ATCC	Provencher et al. (2000) <sup>f</sup> ; Kashiya et al. (2014) <sup>g</sup>
MCAS	MOC <sup>b,e</sup>	NS	Yes: SC	JCRB	Kidera et al. (1985) <sup>f</sup> ; Sato et al. (2012) <sup>g</sup>
RMUG-S	MOC <sup>d,e</sup>	Ascites	Yes: SC, IP	JCRB	Sakayori et al. (1990) <sup>f</sup> ; Sato et al. (2012) <sup>g</sup> ; Matsuo et al. (2011) <sup>g</sup>
KGN	GCT	Tumor tissue	Unknown	RIKEN BRC	Nishi et al. (2001) <sup>f</sup>
COV434***	SCCOHT	Primary tumor	Unknown	No	van den Berg-Bakker et al. (1993) <sup>f</sup> ; Karnezis et al. (2021)

Note: Cell lines identified with >50 publications via PUBMED, on 10/12/2021.

OvCa, Ovarian Cancer; NS, Not specified; ATCC, American Type Culture Collection; JCRB, Japanese Cancer Research Resources Bank; ECACC, European Collection of Authenticated Cell Cultures; RIKEN BRC, RIKEN, BioResource Center Cell Bank; SC, subcutaneous; IP, intraperitoneal; IB, intrabursal.

\*Originally classified HGSOC,

\*\*Originally classified EnOC,

\*\*\*Originally classified as a GCT (Granulosa Cell Tumor),

Recent classification of histotypes.

<sup>a</sup>Domcke et al. (2013),

<sup>b</sup>Anglesio et al. (2013),

<sup>c</sup>Beauford et al. (2014),

<sup>d</sup>Barnes et al. (2021),

<sup>e</sup>Papp et al. (2018).

<sup>f</sup>Original histotype reference,

<sup>g</sup>*in vivo* tumour growth in mice reference.

EnOC, Endometrioid Ovarian Cancer; OCCC, Ovarian Clear Cell Carcinoma; MOC, Mucinous Ovarian Cancer; HGSOC, High Grade Serous Ovarian Cancer; SCCOHT, Small Cell Carcinoma of the Ovary, Hypercalcemic Type.

uterus, bladder, rectum, and small intestine, as well as beyond the peritoneal cavity to organs such as the liver and lung (Motohara et al., 2019). Ovarian cancer cells detach from the primary tumor and are attracted to adipose-rich omental tissue. They disseminate by forming aggregates of multicellular spheroids that float in malignant ascitic fluid alongside fibroblasts, adipocytes, mesothelial, endothelial and inflammatory cells, as

well as cell-free DNA, before “seeding” onto new microenvironments and establishing metastatic deposits (Ford et al., 2020). Given that many commercially available ovarian cancer cell lines are in fact established from ascites rather than primary tumors (Table 1, Supplementary Tables S1,S2) consideration should be given to including these cell types when establishing three dimensional models of ovarian cancer.



This is especially relevant for the study of ovarian cancer cell metastasis. An example of this is the organotypic model used by Ford and colleagues to determine the ability of ovarian cancer cell lines undergoing depletion of genes of interest to metastasize and adhere to omental-type tissue (Henry et al., 2017).

### 3 OVARIAN CANCER CELL LINE MODELS

To date, the majority of *in vitro* studies in ovarian cancer have relied on the use of 2D cell culture of immortalized cell lines derived from primary ovarian cancers, pleural effusion, ascitic fluid from the peritoneal cavity or a distant metastatic site. Many cell lines have been well characterized morphologically and molecularly and, when able to be tested, maintain unique features of their derivative sample. Several studies have attempted to determine “the best” ovarian cancer cell line models for investigators to use for both fundamental discovery science and translational projects (Anglesio et al., 2013; Domcke et al., 2013; Beaufort et al., 2014; Papp et al., 2018; Barnes et al., 2021). Comparison of the molecular profiles of ovarian cancer cell lines with that of primary tumors has led to the histotype reclassification of a number of frequently used ovarian cancer cell lines, including SK-OV-3 and A2780. Still, there remains conflicting reports in the field as to the accuracy of some ovarian cancer cell lines. We have summarized the current state of knowledge of site and histotype origin of a group of ovarian cancer cell line models, as well as models of normal cells representing sites of origin (Table 1, Supplementary Tables S1–S3).

With the exception of the PEO series of HGSOC, few ovarian cancer cell line models allow insight into the development and progression of ovarian cancer (Langdon et al., 1988). The PEO1 drug sensitive cell line has the pathogenic *BRCA2* mutation, c.5193C > G, derived after initial treatment with cisplatin, 5-Fluorouracil (5-FU) and chlorambucil. The PEO4 cell line represents malignant cells after the patient developed chemoresistance, having a secondary *BRCA2* reversion mutation which restores wild-type *BRCA2* function. The PEO6 cell line was collected from the same patient before death (Langdon et al., 1988). Other ovarian cancer cell lines have been made resistant to cisplatin *in vitro*, including A2870/A2780CisR (Behrens et al., 1987), TYK-nu/TYK-nu.CP-r (Yoshiya et al., 1989) and CaOV3/CaOV3CisR (Joshi et al., 2021). The A2780/A2780VeliR lines were made resistant *in vitro* to the PARPi veliparib (Dickson et al., 2021). Still, often phenotypes such as drug response observed *in vitro* have been unable to mirror *in vivo* models, likely due to factors missing in the tumor microenvironment that are absent from homogeneous cell lines cultures such as stromal and immune cells (Beaufort et al., 2014).

Ovarian cancer cell lines show variable ability to grow in nude mice when implanted either subcutaneously (SC), intraperitoneally (IP) or intrabursally (Hernandez et al., 2016). Further, while some cell lines grow well in both SC and IP locations, others show a strong propensity to grow in one location only, suggesting a preference for a particular

microenvironment. Ovarian cancer cell lines demonstrated to grow in mice are noted in Table 1 and Supplementary Tables S1,S2.

## 4 MOUSE MODELS OF OVARIAN CANCER

Animal models continue to be the most physiologically relevant pre-clinical models to study disease pathogenesis and drug response, encompassing a whole-body system, including immune system, tumor microenvironment and vascularization. A number of non-mammalian models including fruit flies, the African clawed frog (*Xenopus*) and the laying hen, have been utilized for the study of ovarian cancer development (reviewed by (Johnson and Giles, 2013; Rosales-Nieves and González-Reyes, 2014; Bernardo et al., 2015; Tudrej et al., 2019)). The most widely used mammalian model is the mouse (*Mus musculus*), sharing 85 percent protein-encoding gene homology with humans (Makałowski et al., 1996), although concerns with translatability of disease mechanisms and drug responses between species remain. Further, the natural occurrence of ovarian cancer is low in the aging mouse, with rapid progression times contrasting with the development of human ovarian cancer (Sale and Orsulic, 2006). Nevertheless, genetically engineered mouse (GEM) models, syngeneic and patient-derived xenograft (PDX) models have enabled a greater understanding of ovarian cancer development and treatment responses.

### 4.1 GEM and Syngeneic Models

GEM models have enabled specific gene knockout to be modelled in a whole-body system, contributing to the understanding of individual and combinations of genes commonly mutated in ovarian cancer. Conditional knockout mice, using the Cre-lox system for cell type specificity, have been used to reproduce oncogenic mutations and HR defects to study ovarian cancer development and responses to clinically relevant treatments such as platin-based drugs and PARPi (Szabova et al., 2012; Perets et al., 2013; Szabova et al., 2014; Zhai et al., 2017). Extensive overviews of GEM models of ovarian cancer have been published in recent years, highlighting comparisons and translatability to the human condition (Stuckelberger and Drapkin, 2018; Maniati et al., 2020; Zakarya et al., 2020). Syngeneic mouse models transplant mouse cell lines into a recipient from the same genetic background, enabling the study of immune response, immunotherapies and tumor vascularization (Zhang et al., 2002; Yu et al., 2018). The murine ID8 ovarian cancer cell line (C57Bl/6 background) (Roby et al., 2000), has been used for a number of syngeneic mouse models, achieving primary ovarian tumors and ascites within 90 days (Greenaway et al., 2008). This model has also been used to study metastasis and immune infiltrates at the trocar site, where an incision is made into the abdomen for laparoscopic surgery (Wilkinson-Ryan et al., 2019). Injection with M0505 cells (derived from spontaneously transformed OSE of FVB/N mice) resulted in Pax8+ tumors with similar histology to human HGSOC (McCloskey et al., 2014). Generation of multiple fallopian tube epithelial cell lines with combinations of common mutations in HGSOC (*Tp53*, *Brca1*, *Brca2*, *Ccne1*,

*Akt2*, *Brd4*, *Smarca4*, *Kras*, *Myc*, *Nf1*, and *Pten*) using CRISPR/Cas9 recapitulated histopathological and clinical features observed in HGSOC patients, such as ascites and peritoneal metastases (Iyer et al., 2021). Overall, GEM and syngeneic models have proven their value for discovery studies and research into the origin of ovarian cancer.

## 4.2 Patient-Derived Xenograft Models

PDX models are the most useful *in vivo* model for testing response to targeted therapies of primary tumors attributed to their unique molecular profiles, to enable a precision medicine approach. The major advantage of using PDX models is the ability to reproduce histology of the human tumor (Colombo et al., 2015), although alterations in steroid hormone receptors and immune response genes have been reported, irrespective of the maintained mutational profile (Dong et al., 2016). Another advantage of PDX models is that they bypass the *in vitro* culture of tumor cells that may inadvertently drive phenotype divergence from the original tumor (Siolas and Hannon, 2013).

Limitations of primary tumor tissue implanted heterotypically into immunodeficient mice include the inability to recapitulate immune responses, site-specific tumor microenvironment interactions and lastly, that the tumor may not metastasize (Jin et al., 2010). The general methodology of producing PDX models requires multiple *in vivo* passages, leading to extended model creation times (Morton and Houghton, 2007). The reported engraftment rate can be variable and heavily influenced by ovarian cancer histotype; treatment history; stage and site of malignancy, with higher engraftment rates observed in non-epithelial histotypes (Wu et al., 2019). Platinum resistance has also been found to predict PDX engraftment success, with successful engraftment correlating with shorter PFS and OS of the derivative patient (Heo et al., 2017).

An extensive review of ovarian cancer PDX models by Scott et al. (2013), highlighted a number of gaps in the field related to variations in methodologies, genetic stability over multiple generations, representation of few ovarian cancer histotypes and the limitation of using immunocompromised mice as hosts. More recent developments have addressed some of these concerns, with higher rates of successful engraftment and propagation of rarer ovarian cancer histotypes such as LGSOC (De Thaye et al., 2020) and MOC (Ricci et al., 2020) as well as evaluation of drug responses for homologous recombination deficient (HRD) mutated ovarian cancers (George et al., 2017) and enabling the evaluation of immunotherapies through the use of humanized mouse models (Odunsi et al., 2020). Furthermore, the ability to label tumor cells with luciferin prior to transplantation has enabled tumor growth tracking *via* bioluminescence imaging (Liu et al., 2017).

## 5 3D IN VITRO OVARIAN CANCER MODELS

Two-dimensional (2D) growth of cancer cells as monolayers may fail to recapitulate aspects of the derivative cell behavior and

morphology. Differential drug responses in 2D *versus* 3D cultures have been observed in many *in vitro* models of cancer, including ovarian cancers. Previously, high costs of materials, significant manual labor and low levels of reproducibility and matrix tunability rendered 3D culture models less favorable to 2D, irrespective of their higher physiological relevance (Jensen and Teng, 2020). Recent technological advances have enabled higher degrees of control over the creation of 3D cell cultures in areas including matrix stiffness and composition, spatial orientation and creation in an automated and high-throughput manner.

A number of different methodologies and techniques are being used in order to more efficiently create 3D cell culture models of cancer, including ovarian cancers. While there is still no “perfect” 3D *in vitro* model that can replace *in vivo* preclinical models, methodological advances are moving the field towards more accurate representations of human tumors, including in regards to drug response. Further, efforts towards creation of high-throughput *in vitro* and *ex vivo* models for drug screening have been a focus in recent years, and will eventually replace 2D cultures. An overview of techniques used to create 3D *in vitro* ovarian cancer models and their considerations is summarized in Table 2.

## 5.1 Scaffold-Free Models

### 5.1.1 Liquid Overlay Techniques

Liquid overlay techniques, such as the use of ultra-low attachment (ULA) plates or low-attachment coatings enable spheroid formation attributed to the hydrophilic properties of the neutrally charged polystyrene plastic or polymer coating, causing cells to adhere to each other rather than on a 2D surface. By preventing attachment to a surface, use of low attachment plates and coatings present a cost-effective and timely method for spheroid formation or maintenance of existing spheroid structures. Two methods have been used extensively for ovarian cancer spheroid culture to identify mechanisms of progression and various stages of disease, from primary tumor modelling to the generation of spheroids of metastatic ascites. The attachment and disaggregation of these spheroids on top of an ECM or in an immunodeficient mouse also allows assessment of the metastatic potential of the cancer.

#### 5.1.1.1 Flat-Bottomed Ultra-Low Attachment Plates and Low Attachment Coatings

The use of flat-bottomed ULA plates (Figure 2) enables heterogenous multicellular aggregate formation from cell suspensions of adherent cells and can be used for short-term maintenance of primary ascites-derived spheroids. This method is often combined with secondary metastatic invasion assays involving the transfer of spheroids to regular tissue culture plastic plates or onto an extracellular matrix (ECM).

Culture of ovarian cancer cell lines in ULA plates as “ascitic” spheroids has been used as a model to investigate the efficacy of an oncolytic virus-based therapeutic on ovarian cancer metastasis (Tong et al., 2015). Patient-derived ovarian cancer ascites cells, when maintained on ULA plates, demonstrated epithelial-mesenchymal transition (EMT) during spheroid formation (Rafehi et al., 2016). Patient-derived solid-tumor and ascites-

**TABLE 2 |** Advantages and disadvantages of common 3D *in vitro* models of ovarian cancer.

Model type	Technique	Advantages	Disadvantages
Scaffold-free	Liquid overlay—Flat-bottom plates	Fast spheroid generation	Heterogenous spheroids No cell-ECM interactions
	Liquid overlay—Round-bottom plates	Fast spheroid generation May replicate necrotic core	May require Matrigel for cell-cell adhesion No cell-ECM interactions
	Hanging drop	High homogeneity Fast spheroid generation	Difficulties with media change, drug addition No cell-ECM interactions
Scaffold-based—Natural hydrogels	Matrigel	High biocompatibility Integrin interactions Commercially available Mimics basement membrane ECM Enables organoid propagation	Not human derived Limited control of mechanical properties Temperature dependent stability Batch-to-batch variation
	Collagen-I	High biocompatibility Enhances mesenchymal traits Variety of sources (animal, marine)	Not human derived Limited control of mechanical properties
	Alginate	High biocompatibility  Low immunogenicity Can be combined with other biomaterials	Stiffness modulated by multivalent cations (possible cytotoxicity) No cell-ECM interaction
	Agarose and Agar	High biocompatibility	Innately inert for cell adhesion studies
Scaffold-based—Synthetic hydrogels	Polyethylene glycol (PEG)	Tunable stiffness Low batch-to-batch variation Able to be used as bioink for bioprinting	Requires biofunctionalization
	Gelatin methacryloyl (GelMA)	High biocompatibility Innate RGD and MMP cleavability	UV photocrosslinking may cause DNA damage
	Peptide-based e.g. RADA16-I	Defined nanofibers Highly engineerable Self-assembling	Low mechanical strength
Decellularized ECM		High biocompatibility Retention of native ECM and growth factors	Limited control of mechanical properties Donor heterogeneity
Organotypic omental mesothelial model Organoids		Modelling metastasis to omentum Organotypic co-culture Maintenance of patient mutational profile and tumor histology Can be biobanked  Can predict patient responses CRISPR-editable	Reliance on primary cells (when used) No vasculature No vasculature  Loss of stromal and immune cells in longer-term culture Varied success rates
3D Bioprinting	Droplet	High-throughput High precision	High equipment cost Limited compatible bioinks
	Extrusion	Compatible with multiple ECM types	Low-throughput Potential for cell stress during extrusion process Low precision
Bioreactors	Rotating wall vessel	Mimic microgravity and transcoelomic metastases	Only spheroid culture
	Orbital shakers	Spheroid formation studies Maintenance of patient-derived explants	Only spheroid culture
	Compressive stress	Hydrostatic compression stress	Not commercially available
	Tumor-on-a-chip	Model shear stress on EMT Able to control drug or nutrient gradients	Short-term culture Potential variation between in-house fabricated devices

Note: ECM, extracellular matrix; MMP, matrix metalloproteinase; UV, ultraviolet; EMT, epithelial-mesenchymal transition.

derived ovarian cancer cell lines both form spheroids similar to those found in patient ascites when grown on ULA plates, and were shown to be self-renewing through serial passaging over a 6-month period (Yamawaki et al., 2021). Patient-derived spheroids

were also more tumorigenic in immunodeficient mice, more stem-like and more invasive than their parental cell line (Liao et al., 2014). A direct comparison of cisplatin and paclitaxel sensitive and resistant A2780 cells grown as 2D monolayers

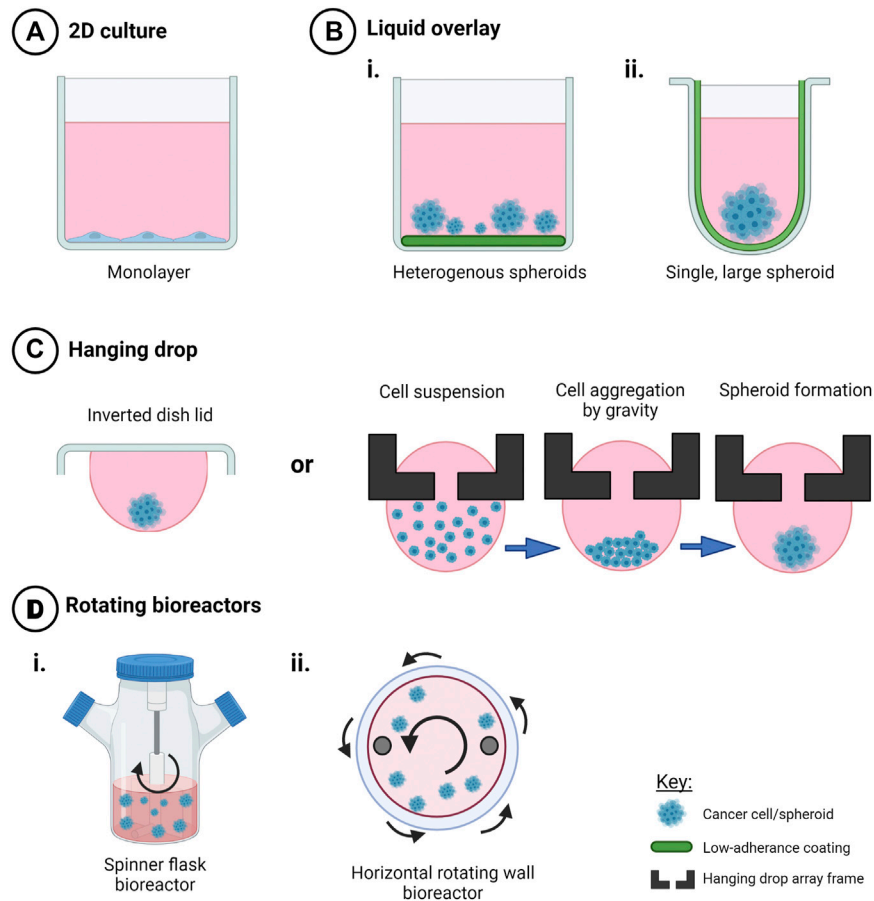


**FIGURE 2 |** Techniques to create scaffold-free 3D *in vitro* cancer models. Creation of 3D cell models in the absence of scaffolds promotes cell-cell interactions in three dimensions that mediate cell behavior and drug response when compared to (A) 2D monolayers. Use of (B) liquid overlay techniques with i) flat or ii) round-bottomed ULA plates (C), hanging drop techniques and (D) rotating bioreactors such as i) spinner flasks and ii) horizontal rotating vessels have been used as time and cost-effective spheroid creation methods or to investigate drug response and other factors that may influence ovarian cancer progression, such as fluid shear stress and hypoxia. Created with Biorender.com.

versus 3D aggregates formed in ULA plates, identified gene expression changes attributed to conformation that may lead to drug resistance (Nowacka et al., 2021).

Poly(2-hydroxyethyl methacrylate), known as poly-HEMA, is a non-ionic polymer coating that discourages the formation of ECM and creates a low-adhesion environment that favors spheroid formation (Ivascu and Kubbies, 2006). A poly-HEMA coating in culture flasks has been used for the production of 3D heterotypic models of normal ovary and to study early ovarian cancer development (Lawrenson et al., 2012). Ovarian cancer cell lines grown under poly-HEMA conditions in the presence of activated platelet releasate, formed spheroids faster and were more resistant to the chemotherapeutic agents cisplatin, carboplatin and paclitaxel (Casagrande et al., 2021).

While flat-bottomed, ULA plates and non-adherent coatings present a cost-effective method for production and maintenance of ovarian cancer spheroids, these methods result in heterogeneous spheroid morphologies which may impact on downstream analysis, reproducibility and drug response. As such, we

suggest that this method is best suited for investigations into drivers of spontaneous spheroid formation.

#### 5.1.1.2 Round-Bottomed ULA Plates

The use of round-bottomed ULA plates (Figure 2) facilitates single spheroid formation by gravity, and is often supplemented with ~2% Matrigel to fast track cell aggregations over periods of time less than 72 h. This method allows high consistency between replicates from a cell line or patient sample, as well as facilitating the ability to section and morphologically analyze biologically-relevant structures. Formation of single large spheroids (>500  $\mu$ m diameter) enables the formation of a hypoxic core, and drug, oxygen and metabolite gradients that mimic solid tumor physiology (Vinci et al., 2012; Heredia-Soto et al., 2018).

The use of round-bottomed, ULA plates have assisted in the identification of Nectin-4 as essential for adhesion events in early spheroid formation of HGSOV cell lines, and as potential targets to improve chemotherapeutic sensitivity (Boylan et al., 2020). Pre-formed OVCAR-8 spheroids grown in round-bottomed ULA plates and further embedded as single spheroids in Matrigel,



developed vascularization after subcutaneous transplantation into athymic nude mice, enabling the evaluation of therapeutics such as the anti-angiogenic bevacizumab and the nano-drug Doxil® (Singh et al., 2020).

This method of spheroid formation has been utilized for speed, reproducibility and commercial availability, although spheroid morphology and overall size may differ due to intrinsic cell line-related characteristics. In a comparison of hanging drop arrays, liquid overlay on ULA plates and liquid overlay on ULA plates with a nutator device to produce three dimensional agitation, both the hanging drop and ULA plates with agitation demonstrated higher cellular compaction, higher ECM content and increased resistance to cisplatin compared with cultures on liquid overlaid ULA plates only (Raghavan et al., 2016). Addition of agitation may improve the comparability to other scaffold-free spheroid formation techniques, although this is yet to be tested on primary ovarian cancer cells.

### 5.1.2 Hanging Drop Techniques

Hanging drop cultures rely on surface tension and gravity to form homogenous, multicellular spheroid/aggregate cultures without the need for specialized equipment (Figure 2). Suspended cells in media are seeded either on the lid of a culture dish or in hang drop vessels, gather at the base of the droplet by gravity, aggregate by cell-cell integrin bridges and further mature by cell-mediated contraction to form compact spheroids within days (Sodek et al., 2009).

The hanging drop technique has been used in numerous studies investigating ovarian cancer morphology and phenotypes. The simplicity of the model has enabled it to act as a “low-stiffness” model as compared to traditional polystyrene plastic culture dishes (Mieulet et al., 2021). An advantage of this technique, particularly for low-volume primary tumor samples, is the formation of spheroids within days with high viability. Further, cell numbers as low as 10 cells per droplet will form spheroids that are uniform in both volume and circularity, amenable to many downstream analyses including high throughput analysis of drug responses (Raghavan et al., 2015).

The use of the hanging drop technique has led to the identification of mechanisms that promote ovarian cancer progression, chemoresistance and recurrence. A study of six ovarian cancer cell lines found a positive relationship between EMT status, spindle-like morphology and compactness of the formed spheroid, with more mesenchymal ovarian cancer cells exhibiting greater invasive and chemoresistant phenotypes (Sodek et al., 2009). Serial passaging of OVCAR-3 and ascites-derived spheroids in the hang drop system showed increasing stemness, proliferation, resistance to cisplatin and tumorigenicity *in vivo* with passage age (Ward Rashidi et al., 2019). Using a high-throughput 384-well hang drop array culture, increasing spheroid size and cell count was associated with resistance to cisplatin in A2780 and OVCAR-3 cells, which has impact particularly in ascitic spheroids escaping chemotherapeutic treatment (Raghavan et al., 2015). The stem-like changes and chemoresistance observed in this simple, multicellular spheroid model that would not be observed in traditional 2D cultures, emphasizes the importance of three-dimensional cell-cell

interactions when modelling drug response. 3D heterotypic multicellular tumor spheroids generated by the hanging-drop technique using the cell lines HEY or SK-OV-3 in co-culture with the mouse fibroblast line NIH3T3, were used to identify off-target effects of drugs targeting cancer cells relative to neighboring stromal cells (Weydert et al., 2020).

While simple in design, using the hanging drop technique for spheroid creation has logistical issues with media replacements, drug addition, evaporation and downstream analysis of individual spheroids per hanging drop (Kunz-Schughart et al., 2004; Mehta et al., 2012). These models are therefore limited to short-term culture and require frequent attention. Improvements to the efficiency and reproducibility of this method include development of hanging drop arrays for use with liquid handling robotics and single cell seeding in nanoliter-sized wells in a microchip format (Raghavan et al., 2015; Ganguli et al., 2021). Creation of an open-source, 3D printable multi-purpose hanging drop “dripper” for use with standard tissue culture plates enables metastasis and migration assays as well as co-cultures of cells within the same plate (Zhao L. et al., 2019).

## 5.2 Scaffold-Based Hydrogel Models

Inclusion of scaffolds in 3D multicellular *in vitro* models of ovarian cancer adds another level of model complexity, allowing for the recreation of the physical and mechanical tumor microenvironment that can influence ovarian cancer cell behavior. Several methodologies pertaining to the use of scaffolds relevant to ovarian cancer are described here and in Figure 3.

### 5.2.1 Natural Scaffolds

Naturally derived ECM hydrogels such as Matrigel, collagens, alginate, and agarose have been favored in 3D cell culture models due to their history of high biocompatibility with various cell types, including ovarian cancer cell lines and tumor organoids, although they are limited in their mechanical tunability and composition consistency.

#### 5.2.1.1 Matrigel

Matrigel, derived from the murine Engelbreth-Holm-Swarm (EHS) sarcoma, has been used for over 40 years as a mimic for the basement membrane and a structural support for many cell types (Orkin et al., 1977). The major constituents of this ECM are laminins, collagen IV, entactin, and the heparin sulfate proteoglycan perlecan (Hughes et al., 2010), though ratios often differ by batch, raising the need for caution when interpreting results of cells cultured in Matrigel (Vukicevic et al., 1992). Matrigel or EHS matrix may also contain collagens I, XVIII, VI, and III, alongside growth factors and enzymes such as TGF- $\beta$ , FGF, and matrix metalloproteinases (MMPs) (Hughes et al., 2010).

Matrigel has been widely used for *in vitro* ovarian cancer models as the ECM components overlap with those found *in vivo*. As a matrix, Matrigel has been utilized for the assessment of *in vitro* ovarian cancer cell invasion by cell penetration through Matrigel-coated transwell inserts (Woo et al., 2007; Fujisawa et al., 2012; Hallas-Potts et al., 2019). Metastatic outgrowth of

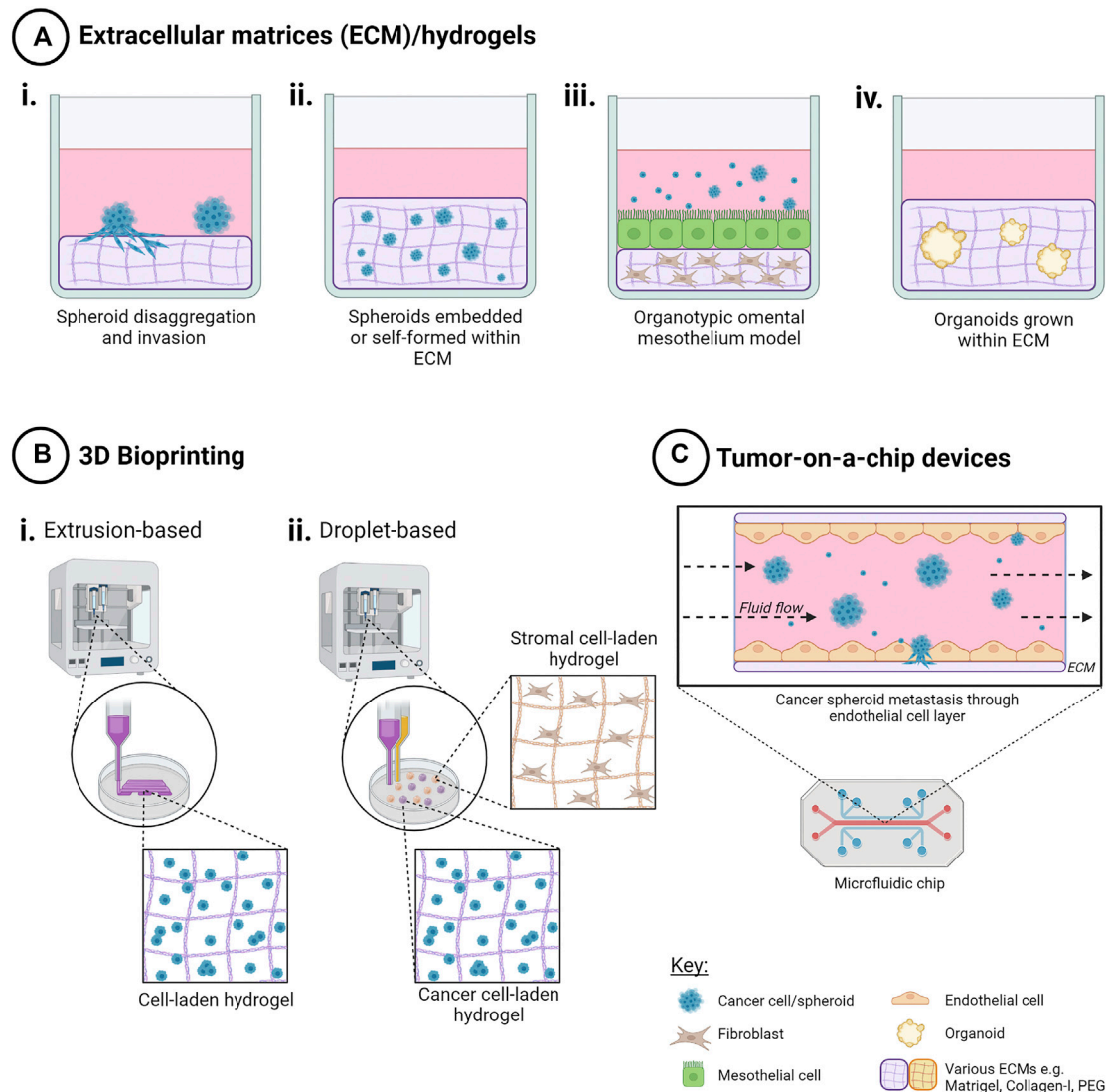
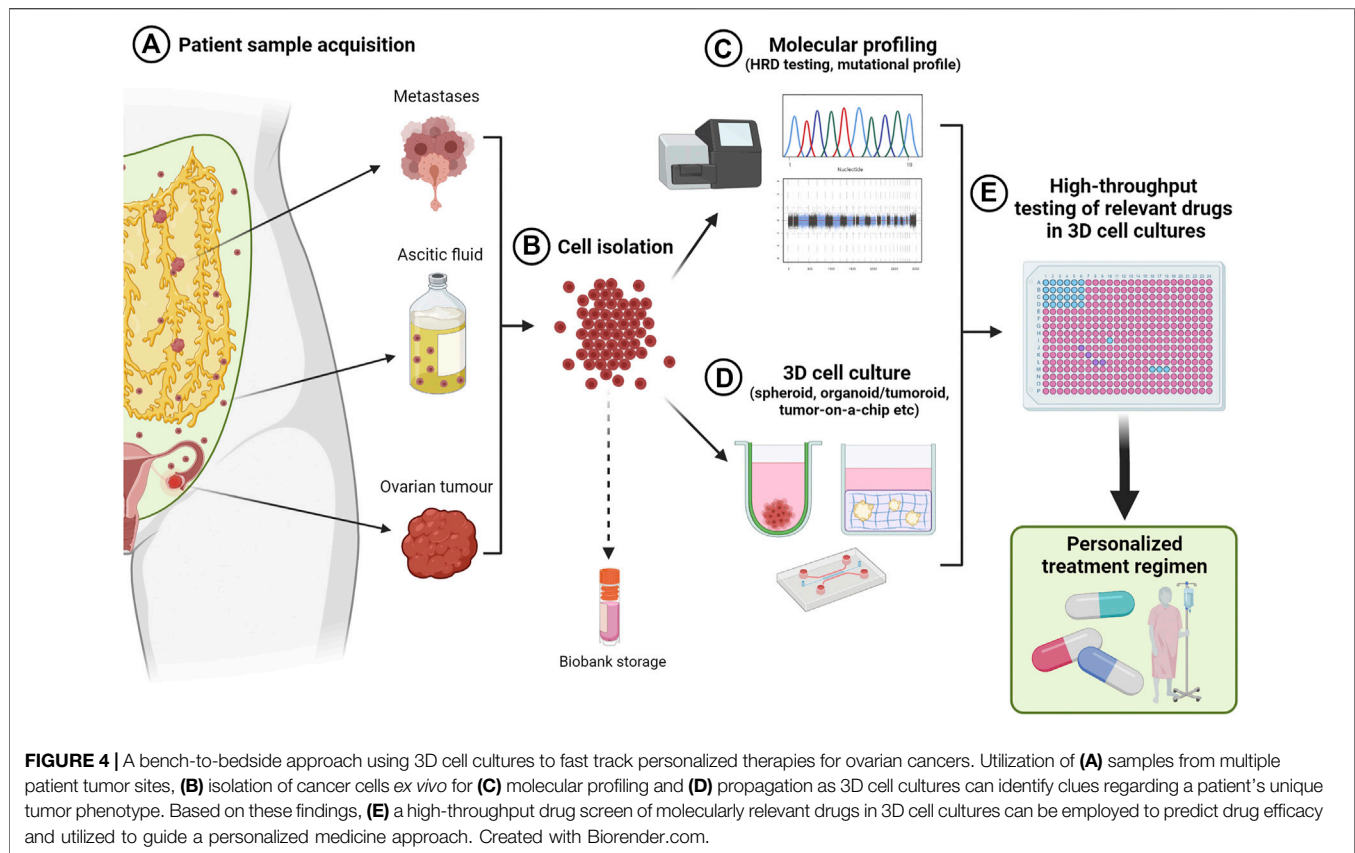


**FIGURE 3** | Techniques to create 3D *in vitro* cancer models using scaffolds. Addition of extracellular matrix (ECM) as scaffolds for 3D cell cultures enables both cell-cell and cell-ECM interactions for a more physiologically relevant 3D cancer cell model. Methods include **(A)** ECM/hydrogels with cancer cells i) on top of, or ii) encapsulated within an ECM, iii) organotypic omental co-culture model and iv) organoid propagation. **(B)** 3D bioprinting techniques such as i) extrusion-based bioprinting enables creation of 3D cell-laden models in hydrogels in a layer-by-layer manner, and ii) droplet-based bioprinting enabling high-throughput creation of 3D cell models in hydrogels with higher spatial control for more complex co-culture. **(C)** Tumor-on-a-chip microfluidic devices have been used to model the effects of fluid shear stress, as well as simulating nutrient, gas and drug gradients, for ascites metastasis modelling. Created with Biorender.com.

ovarian cancer spheroids embedded within Matrigel has also been assessed (Sodek et al., 2008). Numerous ovarian cancer cell lines have been reported to require encapsulation within Matrigel or prior growth in Matrigel for successful seeding as *in vivo* tumors into athymic nude mice (Mullen et al., 1996). Growth of ovarian cancer cells on top of a Matrigel bed has been used to model seeding of metastatic ovarian cancer onto the peritoneum, resulting in ovarian cancer nodules in the absence of vascularization, and modelling chemoresistant metastases in the presence of a hypoxic core (Evans et al., 2011). At a 2–2.5% concentration in culture media, Matrigel has been utilized to promote efficient formation of dense, single spheroids of a

number of cancer cell types, including ovarian, over 24 h in poly-HEMA treated, non-adherent, round-bottom plates for high-throughput toxicity studies (Ivascu and Kubbies, 2006). Further, Matrigel has been used as a scaffold to propagate primary cell types associated with ovarian cancer such as mesothelial cells and fibroblasts (Kenny et al., 2007), as well as to establish ovarian cancer tumoroids from patient biopsies that maintain key characteristics of the primary tumor (Maenhoudt and Vankelecom, 2021).

Aside from commercial availability and high biocompatibility with a wide range of cell types, there continues to be concerns regarding the use of Matrigel in a



number of areas, including: batch-to-batch variation, potential for xenogeneic contaminants derived from mouse on human cells, inefficient cell retrieval requiring temperature reversal to 4°C, potential DNA/RNA contamination from the matrix, and matrix autofluorescence that reduces signal-to-noise ratio when imaging fluorescently stained cells *in situ* (Graf and Boppart, 2010; Hughes et al., 2010). The reported average modulus value of Matrigel was found to be approximately 450 Pa (Soofi et al., 2009), which remains below the average stiffness of human or mouse ovary or omentum (Alkhouli et al., 2013; McKenzie et al., 2018; Hopkins et al., 2021). Further, the polymerization temperature for Matrigel of 22–37°C, mediated by entactin interaction with laminins and collagen IV, also limits its bioprintability in the absence of temperature-controlled environments or as a hybrid bioink (Fan et al., 2016).

Overall, Matrigel continues to be one of the most versatile ECMs for *in vitro* modelling of ovarian cancer cells. Synthetic alternatives are becoming more prominent but have yet to meet the standards of enabling the propagation of patient-derived spheroids and organoids as well as having mechanical properties to enable bio-printing for highly reproducible and high-throughput ovarian cancer model development. Until this time, Matrigel's major advantages lie with its rich ECM

composition for biocompatibility with a wide range of cell types, including for ovarian cancers.

#### 5.2.1.2 Collagens

Collagens are the most abundant ECM proteins in the body and are also the most widely used ECM for *in vitro* cell cultures due to high biocompatibility and commercial availability. Collagens provide structural support and facilitate cell adhesion, proliferation, differentiation and migration both *in vivo* and *in vitro*. Made up of 28 identified collagen types, the low antigenicity of collagen has enabled cross-species compatibility and in turn, availability from a variety of biological sources, including rat, bovine, porcine, and recombinant human (Lynn et al., 2004; Yang et al., 2004). Excessive microfibrillar collagen-I produced by resident fibroblasts has been implicated in the promotion of cancer progression, metastatic and chemoresistant tumor microenvironments (Gurler et al., 2015). Crosslinking of collagen that increases stromal stiffness has also been implicated in chemoresistance (Sterzyńska et al., 2018). While there have been anti-cancer therapeutic strategies developed to enhance the efficiency of chemotherapy (Zhao Y. et al., 2019), collagen is abundant in both pathophysiological and normophysiological states and therefore, anti-collagen therapies require a targeted method of delivery (Xu et al., 2019).

Collagens, particularly collagen-I, have been used extensively in 3D ovarian cancer spheroid and organotypic cultures. OVCAR-5 spheroids plated on a collagen-I coating, were observed to readily disaggregate with increasing collagen concentration, compared to laminin or collagen-IV coatings, thus highlighting its properties as a promoter of cancer cell adhesion and invasion (Burlinson et al., 2004). Rat-tail collagen-I has been used as the ECM to support primary mesothelial and fibroblast cells in an omental model of ovarian cancer metastasis (Kenny et al., 2007). Encapsulation of human ovarian cancer cell lines derived from primary tumors in collagen-I hydrogels showed enhanced mesenchymal traits, invasiveness and drug resistance (Liu et al., 2018). Microfibrillar collagen-VI, in addition to collagen-I, has also been reported to promote platinum resistance, cancer cell survival and HGSOc relapse both *in vivo* and *ex vivo* in collagen hydrogels (Pietilä et al., 2021). Collagen-XI has been implicated in tumor aggressiveness and poor clinical outcome of patients with ovarian cancer (Wu et al., 2014), although it has not been used as a scaffold for 3D ovarian cancer cultures. Marine collagen sources, such as from jellyfish species, have been found to have high amino acid similarity to collagen-I from mammals, showing similar *in vitro* cell behavior responses to traditional collagen-I matrices, and as such, are being investigated as a more sustainable collagen source (Paradiso et al., 2019).

### 5.2.1.3 Alginate

Alginate is a natural polysaccharide derived from the brown algae *Phaeophycota*. Features such as high biocompatibility, biodegradability, low immunogenicity, and low cost have been the drivers behind its use in tissue engineering and drug delivery studies (Gombotz and Wee, 1998). Control of the degree of gelation, and in turn stiffness, can be modulated by multivalent cations including  $\text{Ca}^{2+}$ ,  $\text{Fe}^{3+}$ , or  $\text{Sr}^{2+}$  for crosslinking. These cations can also mediate individual biofunctional properties such as cell attachment or absorption of serum proteins (Machida-Sano et al., 2009). However, proteins are unable to interact with the matrix, and as such ECM-cell signaling is lacking in alginate models and is considered a more synthetic ECM that can be biofunctionalized by the addition of peptides (Rowley et al., 1999). Further, certain cations may also induce cytotoxicity and may differ in stability.

While more studies have used alginate as a drug delivery system, alginate and alginate mixes, such as chitosan-alginate, have also been used as 3D hydrogel scaffolds for the enrichment of a cancer stem cell (CSC) phenotype in prostate, breast and hepatocellular carcinomas (Florczyk et al., 2016). Alginate encapsulation has been used as a method for *ex vivo* culture of murine ovary slices for the investigation of ovarian surface epithelial changes that may drive cancer development (King et al., 2011). Many reports have also combined alginate with other ECMs, both natural and synthetic, to create more biofunctionalized scaffolds to support a variety of ovarian cell types. Shin and colleagues combined alginate, for its biocompatible properties, with marine collagen and agarose to create a hydrogel that supported the growth of A2780 endometrioid ovarian cancer cells (Shin et al., 2016). A double

network of alginate and polyethylene glycol (PEG)-based hydrogels was shown to increase doxorubicin resistance and CSC markers in SK-OV-3 cells compared to 2D cultures (Zhou et al., 2020). SK-OV-3 cells grown in these scaffolds were also reported to be more tumorigenic in a triple immunodeficient mouse model NCG (NOD-*Prkdc<sup>em26Cd52</sup>Il2rg<sup>em26Cd22</sup>/NjuCrl*) (Zhou et al., 2020).

### 5.2.1.4 Agarose and Agar

Agarose is a natural linear polysaccharide derived from the marine red algae *Rhodophyceae*, made from repeating monomeric units of agarobiose (Zarrintaj et al., 2018). In comparison, agar, famously used for microbiological growth purposes, is comprised of a heterogeneous mixture of agarobiose and agaropectin. Their features of high biocompatibility, commercial availability, ability to adjust stiffness with concentration and reversible polymerization enabled the use of agar and agarose as *in vitro* and *in vivo* cell scaffolds that mimic soft tissue stiffness (Varoni et al., 2012). Whilst normally inert to cell interaction, agarose can be bioengineered to integrate biofunctional peptides that supports cell adhesion and cell viability (Yamada et al., 2020).

The use of soft agar to determine tumorigenicity and invasiveness of cancer cell lines has been employed for more than 50 years (Shin et al., 1975). Early work utilized soft agar assays where clusters of cancer cells from malignant effusions from ovarian cancer patients were propagated as clones on an agar base and responded to the anti-cancer drugs cisplatin and 5-FU in a similar manner to their derivative patient (Ozols et al., 1980). Agarose, as a hydrogel for ovarian cancer cells, has been used to show physiological cancer characteristics such as elevated expression of HIF-1 $\alpha$ , VEGF-A, profibrogenic MMP-2 and -9 when compared to 2D SK-OV-3 monolayers (Xu et al., 2014). In contrast, an agarose coating was used as a non-adherent surface on which the liquid overlay technique of spheroid formation was used. HEY and OVHS1 ovarian cancer cells grown by liquid overlay technique with an agarose low-attachment base, formed spheroids more readily than the normal ovarian cell line IOSE29, and further, showed metastatic features such as disaggregation and MMP activation when transferred onto an ECM (Shield et al., 2007).

## 5.2.2 Synthetic ECM Hydrogel Scaffolds

Synthetic ECMs are becoming a more popular *in vitro* ECM option compared to gold standard EHS-derived ECMs, due to a higher degree of control over properties such as stiffness, pore size and biofunctionalization.

### 5.2.2.1 PEG-Based Hydrogels

Hydrogels based on bioinert polyethylene glycol (PEG) have been widely utilized for *in vitro* 3D models for their ability to customize biofunctionalization by peptides and hydrogel stiffness control. The inclusion of MMP-degradable crosslinkers also enables more physiological proteolytic ECM remodeling by cancer cells (Lutolf et al., 2003). A 4-arm PEG-maleimide based hydrogel was designed to recreate the omentum ECM with GFOGER (collagen-I), PHSRN-RGD (fibronectin), RGD (fibronectin,



vitronectin, collagen-VI), and DGEA (collagen-IV) biofunctionalization peptide motifs, adjusting stiffness to a physiological level of ~2.9 kPa for omental tissue and incorporating MMP-degradable crosslinkers (Brooks et al., 2019). This hydrogel supported cell growth and viability of SK-OV-3 multicellular spheroids that were pre-made in non-adherent polydimethylsiloxane (PDMS)-coated grids and spheroids from patient-derived ascites, with paclitaxel and doxorubicin treatments mimicking the drug responses seen in patients. PEG-crosslinked poly(methyl vinyl ether-*alt*-maleic acid) or PEMM/alginate network hydrogels induced EMT, a CSC-like phenotype and chemoresistance in encapsulated SK-OV-3 spheroids, driven by hydrogel stiffness, porosity and cation of choice for crosslinking (Zhou et al., 2020). This pro-metastatic phenotype was confirmed when hydrogels were implanted into immunodeficient mice. An extension of this work by the same authors showed higher RGD (arginine-glycine-aspartic acid) concentrations encouraged spheroid cell dispersion and drug sensitivity, whereas hydrogels with lower RGD concentrations had preserved cell aggregations with CSC-like changes and drug resistance when grown on PEMM hydrogel discs with varying RGD concentrations (Zhou et al., 2021). When taken together to account for mechanical properties, lower stiffness hydrogels with low RGD levels promoted a CSC-like phenotype with drug resistance. While this study highlighted the importance of cell-ECM interactions in drug resistance, the hydrogels studied were of a stiffness much higher than *in vivo* physiological conditions ranging from 60–240 kPa.

#### 5.2.2.2 Gelatin Methacryloyl

GelMA is a semi-synthetic bioengineered, biocompatible material with high batch-to-batch consistency, control of mechanophysical properties, innate RGD responsive peptide motifs and ability to be cleaved by MMPs, having been designed as an alternative to Matrigel (Zhu et al., 2019). GelMA requires modification with a photocrosslinker (typically UV or visible light responsive) for efficient polymerization and to prevent degradation. Visible light, as expected, promotes higher cell viability and lower free radical damage compared to UV light when using GelMA (Noshadi et al., 2017). Addition of Laminin-411 and hyaluronic acid to GelMA hydrogels of 3.4 kPa stiffness enabled ovarian cancer spheroid formation, proliferation and chemoresistance to paclitaxel (Kaemmerer et al., 2014). GelMA hydrogel models also showed similar tumorigenic responses when transplanted into NOD/SCID mice. Interestingly, peripheral blood mononuclear cells or PBMCs grown on GelMA hydrogels showed suppressed pro-inflammatory responses to stimulation with lipopolysaccharide (LPS), particularly in the presence of tumor necrosis factor (TNF), whereby cellular TNF mRNA levels were elevated, but soluble TNF was bound to the hydrogel (Donaldson et al., 2018). This study highlighted the need to consider the immunogenic properties of biomaterials to match hydrogel models for their appropriate application, and may have implications on future 3D *in vitro* immunotherapy models. In the 3D bioprinting field, ovarian cancer cell lines have to date only been used to test printability of GelMA with extrusion based

bioprinting, prior to testing its biocompatibility with murine oocytes (Wu et al., 2021).

#### 5.2.2.3 Peptide-Based Hydrogels

Self-assembling peptide-based hydrogels are increasingly being used as a biomimetic material for 3D *in vitro* culture for their engineerability, ability to form well-defined nanofibers with natural amino acid constituents and absence of animal-derived contaminants (Yang et al., 2020). RADA16-I peptide-based hydrogels performed as well as Matrigel and Collagen-I based hydrogels in terms of cell viability, adhesion, migration and drug resistance of encapsulated A2780 and SK-OV-3 ovarian cancer cells (Yang and Zhao, 2011). A disadvantage of some peptide-based hydrogels is their low mechanical strength, where hydrogels with encapsulated cells are able to be disrupted easily by mechanical forces such as pipetting (Song et al., 2020). A study by Hedegaard and colleagues utilized peptide amphiphile-based hydrogels with elastin mimetics, fibronectin, keratin, RGDS (arginine-glycine-aspartic acid-serine) motif for cell adhesion and GHK (glycine-histidine-lysine) motif for pro-angiogenic signaling with encapsulated OVCAR-4 cells in monoculture as well as in co-culture with HUVECs and human mesenchymal stem cells (Hedegaard et al., 2020). Tumor spheroids grown in this hydrogel were comparable in morphology, viability and drug response compared to those grown in GelMA and Matrigel. Importantly, this model is one of the first to incorporate peptides to promote angiogenesis, addressing one of the major missing components of 3D *in vitro* cell culture models.

#### 5.2.3 Decellularized Ovary ECM

Decellularized extracellular matrices (dECM) are the natural matrices from an organ that have been void of all native cellular components, preserving the biological and mechanical properties of the original ECM. These ECMs can be used to seed new cells in an organ's native conformation in the absence of an immune response, as well as can be lyophilized and reconstituted to form hydrogels. To date, there have been no reports of using decellularized ovary ECM for the study of ovarian cancers. However, the use of ovarian dECMs might benefit 3D *in vitro* ovarian models, due to the preservation of ECM proteins and growth factors found in the native ovary. A handful of studies have shown high biocompatibility with ovarian cell types grown in reconstituted dECM hydrogels and scaffolds. A mixture of sodium alginate with decellularized murine ovarian tissue supported *in vitro* follicle survival (Nikniaz et al., 2021). Preliminary studies of hydrogels derived from decellularized porcine ovarian ECM highlighted the effect of ECM stiffness on ovarian follicle development, with stiffer matrices reducing oocyte viability and triggering premature follicle release (Buckenmeyer et al., 2016), though this effect has not been investigated with ovarian cancer cells. There are nevertheless some concerns surrounding the use of dECMs, namely donor batch differences, retention of native genetic material such as DNA, and the harsh decellularization process that may result in a loss of critical downstream biological interactions with cells (Mendibil et al., 2020).

### 5.2.4 Organotypic Omental Mesothelial Model

Three-dimensional organotypic models of the human mesothelium (**Figure 3**) have been utilized for the study of early metastasis to the omentum and interactions with the tumor microenvironment (Kenny et al., 2007). Taking a layered approach to reproduce the architecture of the omentum as observed from histological staining of omental biopsies, this model consists of primary human fibroblasts with ECM, rat-tail collagen-I and human fibronectin, as a base, layered with primary human mesothelial cells. Ovarian cancer cells or ascites-derived spheroids can be added to investigate cell attachment and invasion into the omentum. Using this model, Kenny and colleagues identified MMP-2 mediated cleavage of fibronectin and vitronectin produced by mesothelial cells as an early response to omental metastasis (Kenny et al., 2009). Another study identified mir-193b downregulation as a driver of omental metastasis with this mesothelial model (Mitra et al., 2015a). Further, Henry and colleagues described the dynamic roles of the receptor tyrosine kinases ROR1 and ROR2 in different omental cell types that promote cancer cell adhesion in early metastasis (Henry et al., 2017). This model has also been adapted for high throughput drug screening of potential inhibitors of adhesion and invasion. Though the mesothelial models had fewer efficacious drug hits than traditional 2D models, similar drug responses were observed *in vivo* in PDX models (Kenny et al., 2014; Lal-Nag et al., 2017). This organotypic model was also more cost and time-efficient with similar results to *in vivo* models, when testing micellar-based nanoparticle therapies to prevent early metastasis (Lu et al., 2019). To add complexity to the static organotypic mesothelial model, it has been incorporated into a microfluidics device, enabling the study of hydrodynamic forces of ascites fluid flow on spheroid attachment and metastasis.

The use of the organotypic mesothelial model has been reviewed in depth and a standardized protocol published to enable reproducibility between research groups across the world (Peters et al., 2015; Watters et al., 2018). While this co-culture model has been quite successful, as a scalable, 3D pre-clinical model of ovarian cancer metastases, it lacks vasculature, as well as immune cells and cells from adipose tissue.

### 5.2.5 3D Ovarian Cancer Co-Cultures

In order to best recapitulate the TME of ovarian cancers, the addition of cancer-associated cell types including stromal, immune, mesenchymal, mesothelial, and endothelial cells, to ovarian cancer cells *in vitro* enables the heterotypic cell-to-cell crosstalk that may influence chemoresistance, angiogenesis, and metastasis. Two-dimensional co-cultures, while enabling intercellular contact and cross-talk, cannot mimic the multidimensional cell interactions. Three-dimensional co-cultures, particularly when combined with ECM scaffolds, are *in vitro*, biomimetic models that may better represent the *in vivo* situation and more accurately predict cellular responses in a patient. While not an exhaustive list, recently published 2D and 3D ovarian cancer co-cultures models are summarized in **Table 3**.

There are two major co-culture methodologies: indirect and direct contact models. Indirect contact co-cultures, such as by the use of transwells or conditioned media, mimic cellular signaling in the absence of physical cellular contact, and enable simple segregation of cell types for ease of downstream analyses of individual cell population behavior. Direct contact co-cultures enable the study of physical interaction of several cell types and their influence on cell behavior as an “organ-like” model. Two-dimensional culture studies showed ovarian cancer cell lines in contact with normal omental fibroblasts could drive activation to a cancer-associated fibroblast (CAF) phenotype associated with TGF- $\beta$ 1 secretion (Cai et al., 2012).

In 3D multicellular spheroid cultures, addition of fibroblasts, mesenchymal stem cells, or endothelial cells have been shown to enhance spheroid size, chemoresistance and a stem-like phenotype compared to 3D monocultures (Hedegaard et al., 2020; Tofani et al., 2021). Co-cultures of ovarian cancer cells and macrophages have identified positive feedback loops that drive stemness, chemoresistance and spheroid formation in cancer cells and M2 polarization of macrophages (Long et al., 2018; Ning et al., 2018; Raghavan et al., 2019). Three-dimensional co-culture systems of ovarian cancers and mesothelial cells, including the organotypic omental mesothelium model (described in **Section 5.2.4**) have also enabled the study of mechanisms driving peritoneal and omental metastasis (Iwanicki et al., 2011; Henry et al., 2017; Shishido et al., 2018; Loessner et al., 2019).

The number of studies utilizing 3D co-cultures of ovarian cancers at the time of this publication was limited but is growing. It is clear that with increasing model complexity through addition of multiple patient-derived cell types in conjunction with physiologically relevant ECM mimics, that the most biologically appropriate and predictive *in vitro* models will be discovered. Integration of organoids with endothelial cells could enable more biologically appropriate, predictive studies of anti-angiogenic drugs such as bevacizumab in the presence of ovarian cancers with specific mutations. Further, utilization of microfluidics devices for emulation of fluid flow and the addition of immune cell types enable the creation of a more accurate biomimetic TME.

### 5.2.6 Organoids

Patient-derived organoids are becoming an important and powerful pre-clinical model for personalized medicine (**Figure 3**). While primary patient-derived samples are the gold standard for prediction of treatment response, long-term culture of these samples in 2D often leads to phenotypic changes and differential responses to drug treatments (Kapałczyńska et al., 2018). Cryopreservation of patient-derived organoids allows for biobanking of unique samples for genotype/phenotype matching with future samples from the same patient as their cancer progresses to inform treatment decision making.

In comparison to xenograft models, organoid or tumoroid cultures require significantly shorter times for development from small starting samples, have a higher success rate and accurately reproduce the genetic and phenotypic features of the derivative tumor, allowing for personalized medicine strategies (Hidalgo

**TABLE 3 |** Indirect and direct *in vitro* ovarian cancer co-culture models.

Co-culture type	Co-culture model	Model format	References
Indirect/non-contact	Cancer-stroma	SK-OV-3 + FP-96 fibroblasts (transwell insert) OVCAR-5 + MRC-5 fibroblasts (bioprinted onto Matrigel)	Medeiros et al. (2019) <sup>a</sup> Xu et al. (2011)
	Cancer-immune (macrophage)	SK-OV-3, HEY, HO8910, A2780 in Matrigel (transwell insert) + Primary macrophages SK-OV-3 spheres (transwell insert) + THP-1 macrophages SK-OV-3 + THP-1 macrophages (transwell insert)	Yi et al. (2020) Ning et al. (2018) Wang et al. (2013) <sup>a</sup>
	Cancer-endothelial	SK-OV-3, OVCAR-3 + HUVECs on Matrigel (transwell insert) "NICO-1" transwell system—Primary OvCa stem cell spheroids (ascites, ULA plate) + HUEhT-1 endothelial cells on Matrigel	Yuan et al. (2021) <sup>a</sup> Miyagawa et al. (2020)
	Cancer-MSC	OvCa cell lines + MSC (adipocyte, bone marrow, umbilical cord) conditioned media	Khalil et al. (2019) <sup>a</sup>
Direct/contact	Cancer-stroma	SK-OV-3 on top of WI38 fibroblasts in Matrigel HEY or SK-OV-3 + NIH3T3 cells in hanging drop A2780 + Human ovarian fibroblast cell line in a microfluidic chip SK-OV-3 + mesenchymal cells (MUC-9) or fibroblasts (CCD27-Sk) in ULA plates	Lau et al. (2017) Weydert et al. (2020) Flont et al. (2020) Tofani et al. (2021)
	Cancer-immune (macrophage)	ID8 cells on top of Matrigel + TAMs from mouse ascites	Long et al. (2018)
	Cancer-adipocyte	OVCAR-3 + PBMCs in hanging drop	Raghavan et al. (2019)
	Cancer-mesothelial	ID8 cells on top of primary mouse adipocytes in Matrigel OVCA433 spheroids (created on poly-HEMA coating) on top of immortalized human lung mesothelial cells or MeT-5A mesothelial cells CAOV-3 or A2780 + Primary mesothelial cell or MeT-5A mesothelial cell spheroids on poly-HEMA coated plates OV-MZ-6 + MeT-5A mesothelial cells in PEG hydrogel	John et al. (2019) Iwanicki et al. (2011) Shishido et al. (2018) Loessner et al. (2019)
	Organotypic omental mesothelial model	OvCa cell line + Primary mesothelial cells + Primary omental fibroblasts	Kenny et al. (2009); Kenny et al. (2007); Mitra et al. (2015a); Henry et al. (2017); Lu et al. (2019); Li et al. (2017); Peters et al. (2015)
	Multicellular models	OVCAR-4 + HUVEC + hMSC in peptide-based hydrogels Patient explant orbital rotational cultures (epithelial cells, fibroblasts, tumor-infiltrating immune cells) Early passage HGSOC organoids (maintained immune cells)	Hedegaard et al. (2020) Abreu et al. (2020) Hill et al. (2018)

<sup>a</sup>Cancer cells grown in 2D

MSC, Mesenchymal stem cell; HUVEC, Human umbilical vein endothelial cell; CSC, Cancer Stem Cell; OvCa, Ovarian Cancer; TAM, tumor-associated macrophages; PBMC, primary blood mononuclear cell; PEG, polyethylene glycol.

et al., 2014). Nanki and colleagues were able to propagate primary ovarian tumor organoids from a variety of histological subtypes including HGSOC, OCCO, and EnOC with an 80% success rate and maintenance of their original tumor mutational profiles (Nanki et al., 2020). The analysis of ovarian tumor organoids derived from multiple tumor sites within the same patient showed differential drug sensitivities, emphasizing the need to account for intrapatient tumor heterogeneity (De Witte et al., 2020). When grown in a modified Matrigel bilayer, organoids from MOCs could reproduce behaviors of their derivative cancer, such as production of mucin and a cystic morphology (Maru et al., 2019).

While there is growing evidence that ovarian cancer organoids/tumoroids are becoming the new benchmark for pre-clinical models compared to traditional 2D methods, varying success rates have been reported, particularly attributed to the heterogeneity of these cancers, and propagation success has been highly dependent on starting sample volume and sample handling. In contrast to traditional organoid culture methods that utilize Wnt to maintain stem-like properties, Wnt pathway induction resulted in tumoroid growth arrest in HGSOC organoids, however was able to be rescued by

BMP signaling (Hoffmann et al., 2020). The opposite was observed in fallopian tube organoids whereby shRNA downregulation of tumor suppressor genes *TP53*, *PTEN*, and *RB*, showed stem-like changes occurring early in tumor development. Work by Maenhoudt and colleagues identified that the addition of neuregulin-1 (NRG1) to culture medium can increase the proliferation time of primary organoid cultures from fresh and cryopreserved HGSOC and LGSOC, particularly in slower-growing cultures (Maenhoudt et al., 2020). In contrast, it has been noted that organoid propagation methods tend to be selective and result in a cell population that may not be representative of the original tumor heterogeneity and in turn, treatment response, particularly in patients who have undergone previous neoadjuvant therapy (Hill et al., 2018). Therefore, care must be taken in interpretation of data and use of the correct modelling systems. Improvements in methodologies to maintain the heterogenous phenotype that exists in patient tumors are needed, such as propagation of organoids from different regions of the same tumor (Maru et al., 2019). Furthermore, the standardization of protocols and materials for organoid culture between laboratories around the world will lead to vast

improvements in reproducibility and reliability of this technique into the future.

As the initial triggers for the development of ovarian cancer is still being debated, organoids from normal ovarian tissue have also been utilized in studies of tumor development. Organoid cultures from high-risk women with germline mutations in *BRCA1* or *BRCA2* have been developed for research into early tumor development (Kopper et al., 2019). Kopper and colleagues have performed gene editing in normal non-tumor organoids established from fallopian tube or ovarian epithelium using CRISPR-Cas9 gene editing for modelling *TP53* mutations, and determined that HRD ovarian cancer organoids with fewer *RAD51* loci were more sensitive to the PARPi niraparib, analogous to responses observed *in vivo* (Kopper et al., 2019). An extension of this work has similarly used CRISPR-Cas9 genome editing to introduce common HGSOC gene defects into mouse oviduct and OSE cell organoids, showing that both organoid types could become carcinogenic and that drug sensitivities in HGSOC patients may be cell lineage-dependent (Löhmusaar et al., 2020).

### 5.3 Bioprinting of 3D OC Models

Three dimensional bioprinting presents an automated solution that combines both ECM components and high-throughput creation of ovarian cancer models in a spatially-controlled manner (Figure 3). As a relatively new approach to 3D cell model creation, the number of published studies is limited for ovarian cancer.

Droplet-based bioprinting systems enable the precise and agile fabrication of microtissue cultures by overlaying drops of biomaterial. Used mainly for deposition of scaffolds, this layer-by-layer technique has also been used for addition of drugs, growth factors and living cells. Xu and colleagues have used a droplet-based system to bioprint OVCAR-5 cells and MRF-5 normal fibroblasts on top of a Matrigel scaffold in a controlled spatial distribution for investigation of feedback mechanisms between tumor and stromal cells (Xu et al., 2011). While there are no publications to date utilizing drop-on-demand inkjet bioprinting, laser-assisted bioprinting or stereolithography with ovarian cancer cells, these are promising techniques that could enable high-throughput 3D ovarian cancer cell model development that would seamlessly integrate with existing high-throughput drug screening technologies (Mazzocchi et al., 2019).

Extrusion based bioprinting has been employed to fabricate a 3D bioprinted ovary that successfully supported oocyte growth using a GelMA-based bioink (Wu et al., 2021). While this study focused on oocyte maturation *ex vivo*, ovarian cancer cell lines were utilized during optimization of bioink biocompatibility, showing high cell viability during and after the extrusion process. Unfortunately, this was not translatable in primary murine oocytes, suggestive of the delicate nature of primary-derived cells with this technique.

An important factor of 3D bioprinting is the printability of the matrix to be deposited. The material properties of Matrigel and other natural matrices are limited in their printability as bioinks

due to temperature sensitivities and pre-determined stiffnesses, highlighting the flexibility of synthetic matrices that can be modified to best mimic *in vivo* conditions. In contrast, synthetic matrices are limited by their biocompatibility but can be biofunctionalized with peptides and full-length ECM proteins. Overall, 3D bioprinting and automation has great potential as a future staple for *in vitro* and *ex vivo* studies driving drug development and discovery for all cancer types.

## 5.4 Bioreactors

Bioreactors have largely been used to study the effects of fluid flow as a physiological mechanical stimulus on cell behavior. In the context of ovarian cancers, mechanotransduction and shear stress from ascites fluid build-up and flow in the peritoneum have been shown to drive ovarian cancer metastasis. Tumor-on-a-chip microfluidics systems have been used to model peritoneal metastases as well as vasculature in solid tumors.

### 5.4.1 Rotating Wall Vessels and Orbital Shakers

Rotating wall vessel bioreactors or rotary cell culture systems (Figure 2) utilize low shear, low turbulence biomechanical forces to influence cell differentiation and aggregation in three dimensions as a suspension (Schwarz et al., 1992). Originally designed to mimic microgravity, this technique has been important for studies of transcoelomic ovarian cancer metastases (Shield et al., 2009). Microgravity, as a biomechanical force, has been reported to reduce metastatic markers, change cell metabolism and chemosensitivity in a variety of cancer cell lines, though the *in vivo* effect is unknown (Takeda et al., 2009; Vidyasekar et al., 2015). LN1 cells, derived from a mixed Mullerian tumor, were grown in a horizontally-oriented high aspect rotating vessel (HARV) with microcarrier beads as a scaffold to investigate the potential for metastatic growth as spheroids or aggregates (Becker et al., 1993). This study also showed that there is growth selection for certain cell types from a mixed population in 3D compared to 2D. Further work confirmed the production of chondroitin sulphate in the 3D culture similar to that observed in the *in vivo* tumor; however, this was not observed in 2D culture (Goodwin et al., 1997; Grun et al., 2009). These spheroids also showed varying degree of oncogene expression not seen in 2D, although the variation was likely due to the mixed populations present. Low passage primary ovarian and endometrial cancer cell lines propagated as multicellular spheroids in a rotating cell culture system, showed similar histological markers to the primary tumor with differentially expressed markers including prohibitin, VDAC1 and annexin 4 identified in 2D *versus* 3D culture methods (Grun et al., 2009).

Orbital shakers, traditionally used for bacterial cultures, have also been employed to investigate fluid shear stress on ovarian cancer spheroid formation. Masiello and colleagues adapted the orbital shaker to rotate at physiologically relevant speeds and utilized typical culture dishes to investigate the effects of rotational speeds, cell density and well size on spheroid formation (Masiello et al., 2018). This study resulted in more rounded and consistent spheroid formation, amenable to the analyses of functional endpoints. Patient-derived explants of



multiple ovarian cancer histotypes have been propagated for up to 30 days in orbital shakers, resulting in maintenance of tumor architectures, epithelial, fibroblasts and immune cells, as well as ECM (Abreu et al., 2020). Studies using these rotational techniques have contributed to the understanding of shear stress on ovarian cancer metastasis, drivers of spheroid formation in ascites and long-term propagation of ovarian cancer cells.

#### 5.4.2 Compressive Stress Bioreactors

The majority of bioreactor-based models for ovarian cancer have been used for the study of fluid shear stress pressures on cancer invasion and proliferation. Investigation into compressive stress to model external compressive stimuli such as ascites accumulation that increases hydrostatic pressure as a driver of metastasis is a relatively new approach and its effect on treatment is still unknown. Novak and colleagues created a custom bioreactor to mimic the hydrostatic compression pressures on ovarian cancer metastasis from the primary tumor (Novak et al., 2020). This was modelled by the HGSOC cell line OVSAHO that was encapsulated in an agarose-collagen-I hydrogel on top of a membrane where air can be pumped to mimic the compressive forces from ascites fluid build-up in both a static and cyclic manner. This work identified CDC42 as a driver of chemoresistance and proliferation under compressive stimuli. Recently, Onal and colleagues developed a microfluidic platform with micro-pistons that enable the application of dynamic compression to the system, for investigations of cyclic and pressure-controlled compressive stress on SK-OV-3 cell damage (Onal et al., 2021). While this study used ovarian cancer cells as a monolayer, the authors iterate that their platform can be easily modified to include hydrogel ECM and spheroid models.

#### 5.4.3 Tumor-on-a-Chip Microfluidic Systems

Tumor-on-a-chip devices utilize microfluidics to simulate effects of vascular flow in solid tumors and more specifically in the context of ovarian cancer, mimicking the hydrodynamics that influence ascitic seeding in the peritoneum and contributing to metastases (Figure 3). Microfluidic devices consist of networks of microchannels where fluids including cell media with cells, or media with drugs or cytokines can be injected and evacuated in an automated manner, enabling nutrient and gas exchange. Microchannels may be laden with matrix and/or cells to mimic a lumen. Culture within a microfluidic system is often short-term and high-throughput.

Tumor-on-a-chip microfluidic systems have been used to model various aspects of ovarian cancer progression, both as solid primary tumors and drivers of cell survival in metastases. Microfluidic chips have been used to model 3D tumor nodule development in the peritoneum by ascitic spheroids, showing that the flow stream was a factor that drove OVCAR-5 cell attachment to Matrigel-laden walls *via* EMT (Rizvi et al., 2013). Using the same system, SK-OV-3 spheroids were flowed through a poly-HEMA-coated chamber to investigate the effects of shear stress on EMT status changes in cancer

spheroids, similarly showing that perfusion promoted spheroid viability and stemness (Ip et al., 2016). These findings were further validated when transplanted into nude mice as xenografts, with perfused spheroids forming larger subcutaneous tumors that were found to be chemoresistant, regulated by the PI3K/AKT signaling pathway. Microfluidic chips have also been used to investigate platelet extravasion in the presence of both primary endothelial cell and ovarian cancer cells, whereby platelets were found to induce cancer cell mediated disruption of the endothelial layer (Saha et al., 2020). This disruption was partially rescued by addition of atorvastatin, a statin drug used for preservation of endothelial junctions, with results reproduced using primary HGSOC cells with prior atorvastatin treatment *in vivo*. Induction of inflammatory cytokines such as MCP-1 and TNF also mirrored the pro-inflammatory vascular microenvironment observed in the vicinity of ovarian tumors *in vivo* and inferred some regulation of cancer progression.

Advantages of microfluidic chip systems include the ability to utilize small amounts of starting material, homogenous creation of large numbers of spheroids, portable sizing, and the potential to control drug or chemokine gradients with integration of multiple wells or chips. An orthogonal microfluidic chip developed for seeding into PDMS-based microwells, was superior to standard low-attachment plates and Matrigel seeding in cell viability and maintenance of patient-derived epithelial ovarian cancer cell phenotypes, even when starting with low starting cell numbers (Dadgar et al., 2020). The multi-well microfluidic chip also enabled simpler cytotoxicity measurements by imaging analyses when compared to Matrigel methods, and allowed simultaneous drug gradients in a single microfluidic chip. A direct comparison of spheroid formation and carboplatin sensitivity in four ovarian cancer cell lines in either PDMS-based microfluidic devices with microwells, ULA plates or hanging drop showed microfluidic devices created more homogeneous spheroids with similar carboplatin sensitivities to ULA-plate derived spheroids (Patra et al., 2020). Microfluidic systems have also been used to study macrophage recruitment by ovarian cancer cells *via* integration of chemokine concentration gradients to mimic macrophage infiltration into the tumor with both HGSOC cell lines and patient-derived xenografts (Scott et al., 2021). The study showed correlation between macrophage recruitment and tumor invasiveness and results were replicated in *in vivo* PDX models, with future work looking to identify correlations between macrophage infiltration and chemoresistance.

While microfluidic devices have great potential as more physiological and reproducible 3D *in vitro* models of ovarian cancer, there are still a number of drawbacks to this new technology, namely in costing. There is also a high level of variability between studies due to the majority of devices being fabricated in-house to meet specific researchers' needs, though commercially available options ranging from single to multichannel perfusion systems are becoming increasingly obtainable, that assists with method standardization.

## 6 3D *IN VITRO* OVARIAN CANCER MODELS FOR PERSONALIZED MEDICINE

The concept of a personalized medicine approach where specific treatments are tailored for individuals, is the overarching goal of cancer therapy. As already discussed, ovarian cancer is in fact an umbrella term for multiple histotypes, with differing sites of origin, different genetic and epigenetic events and survival rates. Further, ethnicity and different occurrence rates of histotypes between ethnicities adds another layer of complexity (Peres et al., 2018). Given these variables, homogenous, immortalized 2D cell lines as *in vitro* models of ovarian cancer only address few of these variables at a single given timepoint of the disease and in a defined microenvironment dissimilar to the *in vivo* situation. Therefore, there is a need for more representative *in vitro* and *ex vivo* models of ovarian cancer for a more personalized prediction of therapeutic efficacy.

There is growing evidence that 2D cultures are more divergent and 3D cultures are better models to reproduce and predict patient drug responses. Patient-derived spheroids grown in 384-well ULA plates derived from primary debulking surgery formed over 24 h and after a further 72 h of growth predicted patient response to first-line adjuvant chemotherapies with 89% accuracy (Shuford et al., 2019). A study by Jabs and colleagues documented that primary ovarian cancers cells grown as organoids had HRD scores, growth and drug cytotoxicity more strongly correlated with the original tumor compared to monolayer cultures, indicative that 3D tumoroid cultures are better mimics of patient tumor behavior (Jabs et al., 2017). Further, numerous studies have shown the utility of ovarian cancer organoids of various histotypes for drug screening, with maintenance of mutational profiles and accurate reproduction of treatment responses when challenged with FDA-approved clinically utilized drugs (Kopper et al., 2019; Maenhoudt et al., 2020; Nanki et al., 2020).

For the prediction of drug response, HGSOC tumor organoids from primary and interval debulking surgeries showed histological concordance with the original tumor and reliably predicted carboplatin sensitivity and resistance (Gorski et al., 2021). RNA sequencing of these tumoroids identified cell-specific pathways that may contribute to carboplatin sensitivity or resistance, and has potential for use in stratification of patients, to guide treatment strategies before clinical recurrence (Gorski et al., 2021). High-throughput development of patient-derived ovarian cancer organoids grown in a ring-shaped geometry of Matrigel, was able to identify responses to 240 kinase inhibitor compounds within a week of cell isolation (Phan et al., 2019). The ring-shaped geometry is particularly advantageous as it eliminates the need for sample transfer or tumoroid dissociation, and can utilize very small starting cell numbers. Further, tumoroids grown by this method were able to maintain heterogeneity with distinct cytomorphologies from mixed type carcinomas. This method could enable rapid screening and identification of clinically actionable drugs as well as identify clinical trial eligibility. Hill and colleagues employed organoids from HGSOC for DNA repair profiling and were able to predict the therapeutic sensitivity in patients

to PARP inhibitors. This valuable study highlights the use of organoids as a tool to guide treatment decisions that may have the most benefit (Hill et al., 2018).

## 7 FUTURE PERSPECTIVES

Given the high mortality and recurrence rate of ovarian cancers, there is a clear need for more physiologically relevant models that can accurately predict the likelihood that a patient will respond to a particular therapy, both at diagnosis and relapse in order to guide therapeutic strategy. These models will need to be constructed across all of the ovarian cancer histotypes, including those that are very rare, and generate results in a timeframe that facilitates rapid and targeted translation to patients. A vision for the future would encompass automated functional assays of ovarian tumoroids including tumor proliferation, metastatic spread, spheroid formation and cell death that routinely complement molecular studies to provide strong predictions of patient response to new molecular targeted therapies such as described in **Figure 4**. Furthermore, discovery-based science that will identify new drugs to treat ovarian cancer, will also be conducted in models that more strongly mimic *in vivo* condition. These studies will not only identify new therapies, but also diagnostic and prognostic markers.

The field of 3D bioprinting, currently in its infancy, is rapidly emerging as an answer to the manual, low throughput methods of creating 3D cell models, including organoids and tumoroids. In the future, the challenges of including common components missing in most 3D *in vitro* models today of ovarian cancer such as incorporation of vasculature, immune cells and hydrostatic forces will be met as models are created to best recapitulate the patient environment and to better inform the clinical management of women with ovarian cancer.

## AUTHOR CONTRIBUTIONS

CY and DJM contributed to all aspects of the article and led the team efforts. CY and K-AD created the tables, and all authors (CY, K-AD, MNM, YM, and DJM) collected the literature, provided revision suggestions, reviewed and commented on the manuscript.

## FUNDING

CY was supported by grants to DJM: Medical Research Future Fund (APP1199620) and Cancer Council NSW (2019/TPG1002).

## SUPPLEMENTARY MATERIAL

The Supplementary Material for this article can be found online at: <https://www.frontiersin.org/articles/10.3389/fbioe.2022.836984/full#supplementary-material>

## REFERENCES

- Abreu, S., Silva, F., Mendes, R., Mendes, T. F., Teixeira, M., Santo, V. E., et al. (2020). Patient-derived Ovarian Cancer Explants: Preserved Viability and Histopathological Features in Long-Term Agitation-Based Cultures. *Sci. Rep.* 10 (1), 1. doi:10.1038/s41598-020-76291-z
- Alkhouli, N., Mansfield, J., Green, E., Bell, J., Knight, B., Liversedge, N., et al. (2013). The Mechanical Properties of Human Adipose Tissues and Their Relationships to the Structure and Composition of the Extracellular Matrix. *Am. J. Physiology-Endocrinology Metab.* 305 (12), E1427–E1435. doi:10.1152/ajpendo.00111.2013
- Alsop, K., Fereday, S., Meldrum, C., deFazio, A., Emmanuel, C., George, J., et al. (2012). BRCA Mutation Frequency and Patterns of Treatment Response in BRCA Mutation-Positive Women with Ovarian Cancer: A Report from the Australian Ovarian Cancer Study Group. *Jco* 30 (21), 2654–2663. doi:10.1200/jco.2011.39.8545
- Anglesio, M. S., Wiegand, K. C., Melnyk, N., Chow, C., Salamanca, C., Prentice, L. M., et al. (2013). Type-specific Cell Line Models for Type-specific Ovarian Cancer Research. *PLoS One* 8 (9), e72162. doi:10.1371/journal.pone.0072162
- Audeh, M. W., Carmichael, J., Penson, R. T., Friedlander, M., Powell, B., Bell-McGuinn, K. M., et al. (2010). Oral poly(ADP-Ribose) Polymerase Inhibitor Olaparib in Patients with BRCA1 or BRCA2 Mutations and Recurrent Ovarian Cancer: a Proof-Of-Concept Trial. *The Lancet* 376 (9737), 245–251. doi:10.1016/S0140-6736(10)60893-8
- Auguste, A., Blanc-Durand, F., Deloger, M., Le Formal, A., Bareja, R., Wilkes, D. C., et al. (2020). Small Cell Carcinoma of the Ovary, Hypercalcemic Type (SCCOHT) beyond SMARCA4 Mutations: A Comprehensive Genomic Analysis. *Cells* 9 (6), 1496. doi:10.3390/cells9061496
- Barnes, B. M., Nelson, L., Tighe, A., Burghel, G. J., Lin, I.-H., Desai, S., et al. (2021). Distinct Transcriptional Programs Stratify Ovarian Cancer Cell Lines into the Five Major Histological Subtypes. *Genome Med.* 13 (1), 140. doi:10.1186/s13073-021-00952-5
- Beaufort, C. M., Helmijs, J. C. A., Piskorz, A. M., Hoogstraal, M., Ruigrok-Ritstier, K., Besselink, N., et al. (2014). Ovarian Cancer Cell Line Panel (OCCP): Clinical Importance of *In Vitro* Morphological Subtypes. *PLoS ONE* 9 (9), e103988. doi:10.1371/journal.pone.0103988
- Becker, J. L., Prewett, T. L., Spaulding, G. F., and Goodwin, T. J. (1993). Three-dimensional Growth and Differentiation of Ovarian Tumor Cell Line in High Aspect Rotating-wall Vessel: Morphologic and Embryologic Considerations. *J. Cel. Biochem.* 51 (3), 283–289. doi:10.1002/jcb.240510307
- Behrens, B. C., Hamilton, T. C., Masuda, H., Grotzinger, K. R., Whang-Peng, J., Louie, K. G., et al. (1987). Characterization of a cis-Diamminedichloroplatinum(II)-resistant Human Ovarian Cancer Cell Line and its Use in Evaluation of Platinum Analogues. *Cancer Res.* 47 (2), 414–418.
- Bell, D. (2011). Integrated Genomic Analyses of Ovarian Carcinoma. *Nature* 474, 609–615. doi:10.1038/nature10166
- Bernardo, A. D. M., Thorsteinsdóttir, S., and Mummery, C. L. (2015). Advantages of the Avian Model for Human Ovarian Cancer. *Mol. Clin. Oncol.* 3 (6), 1191–1198. doi:10.3892/mco.2015.619
- Boylan, K. L. M., Manion, R. D., Shah, H., Skubitz, K. M., and Skubitz, A. P. N. (2020). Inhibition of Ovarian Cancer Cell Spheroid Formation by Synthetic Peptides Derived from Nectin-4. *Ijms* 21 (13), 4637. doi:10.3390/ijms21134637
- Brooks, E. A., Gencoglu, M. F., Corbett, D. C., Stevens, K. R., and Peyton, S. R. (2019). An Omentum-Inspired 3D PEG Hydrogel for Identifying ECM-Drivers of Drug Resistant Ovarian Cancer. *APL Bioeng.* 3 (2), 026106. doi:10.1063/1.5091713
- Buechel, M. E., Enserro, D., Burger, R. A., Brady, M. F., Wade, K., Secord, A. A., et al. (2021). Correlation of Imaging and Plasma Based Biomarkers to Predict Response to Bevacizumab in Epithelial Ovarian Cancer (EOC). *Gynecol. Oncol.* 161 (2), 382–388. doi:10.1016/j.ygyno.2021.02.032
- Buick, R. N., Pullano, R., and Trent, J. M. (1985). Comparative Properties of Five Human Ovarian Adenocarcinoma Cell Lines. *Cancer Res.* 45 (8), 3668–3676.
- Burger, R. A., Brady, M. F., Bookman, M. A., Fleming, G. F., Monk, B. J., Huang, H., et al. (2011). Incorporation of Bevacizumab in the Primary Treatment of Ovarian Cancer. *N. Engl. J. Med.* 365 (26), 2473–2483. doi:10.1056/NEJMoa1104390
- Burleson, K. M., Casey, R. C., Skubitz, K. M., Pambuccian, S. E., Oegema, T. R., and Skubitz, A. P. N. (2004). Ovarian Carcinoma Ascites Spheroids Adhere to Extracellular Matrix Components and Mesothelial Cell Monolayers. *Gynecol. Oncol.* 93 (1), 170–181. doi:10.1016/j.ygyno.2003.12.034
- Cai, J., Tang, H., Xu, L., Wang, X., Yang, C., Ruan, S., et al. (2012). Fibroblasts in Omentum Activated by Tumor Cells Promote Ovarian Cancer Growth, Adhesion and Invasiveness. *Carcinogenesis* 33 (1), 20–29. doi:10.1093/carcin/bgr230
- Casagrande, N., Borghese, C., Agostini, F., Durante, C., Mazzucato, M., Colombatti, A., et al. (2021). In Ovarian Cancer Multicellular Spheroids, Platelet Release Promotes Growth, Expansion of ALDH+ and CD133+ Cancer Stem Cells, and Protection against the Cytotoxic Effects of Cisplatin, Carboplatin and Paclitaxel. *Ijms* 22 (6), 3019. doi:10.3390/ijms22063019
- Chao, A., Lai, C.-H., Wang, T.-H., Jung, S.-M., Lee, Y.-S., Chang, W.-Y., et al. (2018). Genomic Scar Signatures Associated with Homologous Recombination Deficiency Predict Adverse Clinical Outcomes in Patients with Ovarian clear Cell Carcinoma. *J. Mol. Med.* 96 (6), 527–536. doi:10.1007/s00109-018-1643-8
- Cheasley, D., Nigam, A., Zethoven, M., Hunter, S., Etemadmoghadam, D., Semple, T., et al. (2021). Genomic Analysis of Low-grade Serous Ovarian Carcinoma to Identify Key Drivers and Therapeutic Vulnerabilities. *J. Pathol.* 253 (1), 41–54. doi:10.1002/path.5545
- Cheasley, D., Wakefield, M. J., Ryland, G. L., Allan, P. E., Alsop, K., Amarasinghe, K. C., et al. (2019). The Molecular Origin and Taxonomy of Mucinous Ovarian Carcinoma. *Nat. Commun.* 10 (1), 3935. doi:10.1038/s41467-019-11862-x
- Cole, A. J., Dwight, T., Gill, A. J., Dickson, K.-A., Zhu, Y., Clarkson, A., et al. (2016). Assessing Mutant P53 in Primary High-Grade Serous Ovarian Cancer Using Immunohistochemistry and Massively Parallel Sequencing. *Sci. Rep.* 6, 26191. doi:10.1038/srep26191
- Colombo, P.-E., du Manoir, S., Orsetti, B., Bras-Gonçalves, R., Lambros, M. B., MacKay, A., et al. (2015). Ovarian Carcinoma Patient Derived Xenografts Reproduce Their Tumor of Origin and Preserve an Oligoclonal Structure. *Oncotarget* 6 (29), 28327–28340. doi:10.18632/oncotarget.5069
- Conover, C. A., Hartmann, L. C., Bradley, S., Stalboerger, P., Klee, G. G., Kalli, K. R., et al. (1998). Biological Characterization of Human Epithelial Ovarian Carcinoma Cells in Primary Culture: the Insulin-like Growth Factor System. *Exp. Cell Res.* 238 (2), 439–449. doi:10.1006/excr.1997.3861
- Crum, C. P., Drapkin, R., Kindelberger, D., Medeiros, F., Miron, A., and Lee, Y. (2007). Lessons from BRCA: the Tubal Fimbria Emerges as an Origin for Pelvic Serous Cancer. *Clin. Med. Res.* 5 (1), 35–44. doi:10.3121/cmr.2007.702
- Dadgar, N., Gonzalez-Suarez, A. M., Fattahi, P., Hou, X., Weroha, J. S., Gaspar-Maia, A., et al. (2020). A Microfluidic Platform for Cultivating Ovarian Cancer Spheroids and Testing Their Responses to Chemotherapies. *Microsyst. Nanoeng.* 6 (1), 1. doi:10.1038/s41378-020-00201-6
- Davies, B., Steele, I. A., Edmondson, R. J., Zwolinski, S. A., Saretzki, G., von Zglinicki, T., et al. (2003). Immortalisation of Human Ovarian Surface Epithelium with Telomerase and Temperature-Sensitive SV40 Large T Antigen. *Exp. Cell Res.* 288 (2), 390–402. doi:10.1016/S0014-4827(03)00218-0
- Davis, A., Tinker, A. V., and Friedlander, M. (2014). "Platinum Resistant" Ovarian Cancer: What Is it, Who to Treat and How to Measure Benefit? *Gynecol. Oncol.* 133 (3), 624–631. doi:10.1016/j.ygyno.2014.02.038
- De Haven Brandon, A., Box, G., Hallsworth, A., Court, W., Matthews, N., Herodek, B., et al. (2020). Identification of Ovarian High-Grade Serous Carcinoma Cell Lines that Show Estrogen-Sensitive Growth as Xenografts in Immunocompromised Mice. *Sci. Rep.* 10 (1), 1. doi:10.1038/s41598-020-67533-1
- De Paolis, E., Paragliola, R. M., and Concolino, P. (2021). Spectrum of DICER1 Germline Pathogenic Variants in Ovarian Sertoli-Leydig Cell Tumor. *Jcm* 10 (9), 1845. doi:10.3390/jcm10091845
- De Pauw, A., Naert, E., Van de Vijver, K., Philippe, T., Vandecasteele, K., and Denys, H. (2021). A Clearer View on Ovarian Clear Cell Carcinoma. *Acta Clinica Belgica* 17, 1–13. doi:10.1080/17843286.2021.1964051
- De Thaye, E., Van de Vijver, K., Van der Meulen, J., Taminiau, J., Wagemans, G., Denys, H., et al. (2020). Establishment and Characterization of a Cell Line and Patient-Derived Xenograft (PDX) from Peritoneal Metastasis of Low-Grade Serous Ovarian Carcinoma. *Sci. Rep.* 10 (1), 6688. doi:10.1038/s41598-020-63738-6
- De Witte, C. J., Espejo Valle-Inclan, J., Hami, N., Löhmussaar, K., Kopper, O., Vreuls, C. P. H., et al. (2020). Patient-Derived Ovarian Cancer Organoids Mimic Clinical Response and Exhibit Heterogeneous Inter- and Intrapatient Drug Responses. *Cell Rep.* 31 (11), 107762. doi:10.1016/j.celrep.2020.107762

- Dedes, K. J., Wilkerson, P. M., Wetterskog, D., Weigelt, B., Ashworth, A., and Reis-Filho, J. S. (2011). Synthetic Lethality of PARP Inhibition in Cancers lacking BRCA1 and BRCA2 mutations. *Cell Cycle* 10 (8), 1192–1199. doi:10.4161/cc.10.8.15273
- DelloRusso, C., Welch, P. L., Wang, W., Garcia, R. L., King, M.-C., and Swisher, E. M. (2007). Functional Characterization of a Novel BRCA1-Null Ovarian Cancer Cell Line in Response to Ionizing Radiation. *Mol. Cancer Res.* 5 (1), 35–45. doi:10.1158/1541-7786.Mcr-06-0234
- Dickson, K.-A., Xie, T., Evenhuis, C., Ma, Y., and Marsh, D. J. (2021). PARP Inhibitors Display Differential Efficacy in Models of BRCA Mutant High-Grade Serous Ovarian Cancer. *Ijms* 22 (16), 8506. doi:10.3390/ijms22168506
- Domcke, S., Sinha, R., Levine, D. A., Sander, C., and Schultz, N. (2013). Evaluating Cell Lines as Tumour Models by Comparison of Genomic Profiles. *Nat. Commun.* 4, 2126. doi:10.1038/ncomms3126
- Donaldson, A. R., Tanase, C. E., Awuah, D., Vasanthi Bathrinayyan, P., Hall, L., Nikkiah, M., et al. (2018). Photocrosslinkable Gelatin Hydrogels Modulate the Production of the Major Pro-inflammatory Cytokine, TNF- $\alpha$ , by Human Mononuclear Cells. *Front. Bioeng. Biotechnol.* 6 (116), 1. doi:10.3389/fbioe.2018.00116
- Dong, R., Qiang, W., Guo, H., Xu, X., Kim, J. J., Mazar, A., et al. (2016). Histologic and Molecular Analysis of Patient Derived Xenografts of High-Grade Serous Ovarian Carcinoma. *J. Hematol. Oncol.* 9 (1), 92. doi:10.1186/s13045-016-0318-6
- Evans, C. L., Abu-Yousif, A. O., Park, Y. J., Klein, O. J., Celli, J. P., Rizvi, I., et al. (2011). Killing Hypoxic Cell Populations in a 3D Tumor Model with EtNBS-PDT. *PLoS ONE* 6 (8), e23434. doi:10.1371/journal.pone.0023434
- Fan, R., Piou, M., Darling, E., Cormier, D., Sun, J., and Wan, J. (2016). Bio-printing Cell-Laden Matrigel-Agarose Constructs. *J. Biomater. Appl.* 31 (5), 684–692. doi:10.1177/0885328216669238
- Flont, M., Jastrzębska, E., and Brzózka, Z. (2020). A Multilayered Cancer-On-A-Chip Model to Analyze the Effectiveness of New-Generation Photosensitizers. *Analyst* 145 (21), 6937–6947. doi:10.1039/D0AN00911C
- Florczyk, S. J., Kievit, F. M., Wang, K., Erickson, A. E., Ellenbogen, R. G., and Zhang, M. (2016). 3D Porous Chitosan-Alginate Scaffolds Promote Proliferation and Enrichment of Cancer Stem-like Cells. *J. Mater. Chem. B* 4 (38), 6326–6334. doi:10.1039/C6TB01713D
- Ford, C. E., Werner, B., Hacker, N. F., and Warton, K. (2020). The Untapped Potential of Ascites in Ovarian Cancer Research and Treatment. *Br. J. Cancer* 123 (1), 9–16. doi:10.1038/s41416-020-0875-x
- Fujisawa, T., Joshi, B. H., and Puri, R. K. (2012). IL-13 Regulates Cancer Invasion and Metastasis through IL-13Ra2 via ERK/AP-1 Pathway in Mouse Model of Human Ovarian Cancer. *Int. J. Cancer* 131 (2), 344–356. doi:10.1002/ijc.26366
- Fuller, P. J., Leung, D., and Chu, S. (2017). Genetics and Genomics of Ovarian Sex Cord-Stromal Tumors. *Clin. Genet.* 91 (2), 285–291. doi:10.1111/cge.12917
- Ganguli, A., Mostafa, A., Saavedra, C., Kim, Y., Le, P., Faramarzi, V., et al. (2021). Three-dimensional Microscale Hanging Drop Arrays with Geometric Control for Drug Screening and Live Tissue Imaging. *Sci. Adv.* 7 (17), eabc1323. doi:10.1126/sciadv.abc1323
- Gao, J., Li, F., Liu, Z., Huang, M., Chen, H., Liao, G., et al. (2021). Multiple Genetic Variants Predict the Progression-free Survival of Bevacizumab Plus Chemotherapy in Advanced Ovarian Cancer. *Medicine (Baltimore)* 100 (35), e27130. doi:10.1097/md.00000000000027130
- George, E., Kim, H., Krepler, C., Wenz, B., Makvandi, M., Tanyi, J. L., et al. (2017). A Patient-Derived-Xenograft Platform to Study BRCA-Deficient Ovarian Cancers. *JCI Insight* 2 (1), 1. doi:10.1172/jci.insight.89760
- Gombotz, W., and Wee, S. (1998). Protein Release from Alginate Matrices. *Adv. Drug Deliv. Rev.* 31 (3), 267–285. doi:10.1016/S0169-409X(97)00124-5
- Goodwin, T. J., Prewett, T. L., Spaulding, G. F., and Becker, J. L. (1997). Three-dimensional Culture of a Mixed Mullerian Tumor of the Ovary: Expression of *In Vivo* Characteristics. *In Vitro Cell.Dev.Biol.-Animal* 33 (5), 366–374. doi:10.1007/s11626-997-0007-4
- Gorai, I., Nakazawa, T., Miyagi, E., Hirahara, F., Nagashima, Y., and Minaguchi, H. (1995). Establishment and Characterization of Two Human Ovarian clear Cell Adenocarcinoma Lines from Metastatic Lesions with Different Properties. *Gynecol. Oncol.* 57 (1), 33–46. doi:10.1006/jgyo.1995.1097
- Gorski, J. W., Zhang, Z., McCorkle, J. R., DeJohn, J. M., Wang, C., Miller, R. W., et al. (2021). Utilizing Patient-Derived Epithelial Ovarian Cancer Tumor Organoids to Predict Carboplatin Resistance. *Biomedicine* 9 (8), 1021. doi:10.3390/biomedicine9081021
- Graf, B. W., and Boppart, S. A. (2010). Imaging and Analysis of Three-Dimensional Cell Culture Models. *Methods Mol. Biol. (Clifton, N.J.)* 591, 211–227. doi:10.1007/978-1-60761-404-3\_13
- Greenaway, J., Moorehead, R., Shaw, P., and Petrik, J. (2008). Epithelial-stromal Interaction Increases Cell Proliferation, Survival and Tumorigenicity in a Mouse Model of Human Epithelial Ovarian Cancer. *Gynecol. Oncol.* 108 (2), 385–394. doi:10.1016/j.jgyo.2007.10.035
- Grun, B., Benjamin, E., Sinclair, J., Timms, J. F., Jacobs, I. J., Gayther, S. A., et al. (2009). Three-dimensional *In Vitro* Cell Biology Models of Ovarian and Endometrial Cancer. *Cell Prolif.* 42 (2), 219–228. doi:10.1111/j.1365-2184.2008.00579.x
- Gurler, H., Yu, Y., Choi, J., Kajdacsy-Balla, A., and Barbolina, M. (2015). Three-Dimensional Collagen Type I Matrix Up-Regulates Nuclear Isoforms of the Microtubule Associated Protein Tau Implicated in Resistance to Paclitaxel Therapy in Ovarian Carcinoma. *Ijms* 16 (2), 3419–3433. doi:10.3390/ijms16023419
- Hallas-Potts, A., Dawson, J. C., and Herrington, C. S. (2019). Ovarian Cancer Cell Lines Derived from Non-serous Carcinomas Migrate and Invade More Aggressively Than Those Derived from High-Grade Serous Carcinomas. *Sci. Rep.* 9 (1), 1. doi:10.1038/s41598-019-41941-4
- Hamilton, T. C., Young, R. C., McKoy, W. M., Grotzinger, K. R., Green, J. A., Chu, E. W., et al. (1983). Characterization of a Human Ovarian Carcinoma Cell Line (NIH:OVCA-3) with Androgen and Estrogen Receptors. *Cancer Res.* 43 (11), 5379–5389.
- Harris, M. A., Delap, L. M., Sengupta, P. S., Wilkinson, P. M., Welch, R. S., Swindell, R., et al. (2003). Carcinosarcoma of the Ovary. *Br. J. Cancer* 88 (5), 654–657. doi:10.1038/sj.bjc.6600770
- Hedegaard, C. L., Redondo-Gómez, C., Tan, B. Y., Ng, K. W., Loessner, D., and Mata, A. (2020). Peptide-protein Coassembling Matrices as a Biomimetic 3D Model of Ovarian Cancer. *Sci. Adv.* 6 (40), eabb3298. doi:10.1126/sciadv.abb3298
- Henry, C., Hacker, N., and Ford, C. (2017). Silencing ROR1 and ROR2 Inhibits Invasion and Adhesion in an Organotypic Model of Ovarian Cancer Metastasis. *Oncotarget* 8 (68), 112727–112738. doi:10.18632/oncotarget.22559
- Heo, E. J., Cho, Y. J., Cho, W. C., Hong, J. E., Jeon, H.-K., Oh, D.-Y., et al. (2017). Patient-Derived Xenograft Models of Epithelial Ovarian Cancer for Preclinical Studies. *Cancer Res. Treat.* 49 (4), 915–926. doi:10.4143/crt.2016.322
- Heredia-Soto, V., Redondo, A., Berjón, A., Miguel-Martín, M., Díaz, E., Crespo, R., et al. (2018). High-throughput 3-dimensional Culture of Epithelial Ovarian Cancer Cells as Preclinical Model of Disease. *Oncotarget* 9 (31), 21893–21903. doi:10.18632/oncotarget.25098
- Hernandez, L., Kim, M. K., Lyle, L. T., Bunch, K. P., House, C. D., Ning, F., et al. (2016). Characterization of Ovarian Cancer Cell Lines as *In Vivo* Models for Preclinical Studies. *Gynecol. Oncol.* 142 (2), 332–340. doi:10.1016/j.jgyo.2016.05.028
- Hidalgo, M., Amant, F., Biankin, A. V., Budinská, E., Byrne, A. T., Caldas, C., et al. (2014). Patient-derived Xenograft Models: an Emerging Platform for Translational Cancer Research. *Cancer Discov.* 4 (9), 998–1013. doi:10.1158/2159-8290.Cd-14-0001
- Hill, S. J., Decker, B., Roberts, E. A., Horowitz, N. S., Muto, M. G., Worley, M. J., Jr., et al. (2018). Prediction of DNA Repair Inhibitor Response in Short-Term Patient-Derived Ovarian Cancer Organoids. *Cancer Discov.* 8 (11), 1404–1421. doi:10.1158/2159-8290.Cd-18-0474
- Hoffmann, K., Berger, H., Kulbe, H., Thillainadarasan, S., Mollenkopf, H. J., Zemojtel, T., et al. (2020). Stable Expansion of High-grade Serous Ovarian Cancer Organoids Requires a low-Wnt Environment. *Embo J.* 39 (6), 1. doi:10.15252/embj.2019104013
- Hollis, R. L., Thomson, J. P., Stanley, B., Churchman, M., Meynert, A. M., Rye, T., et al. (2020). Molecular Stratification of Endometrioid Ovarian Carcinoma Predicts Clinical Outcome. *Nat. Commun.* 11 (1), 4995. doi:10.1038/s41467-020-18819-5
- Hopkins, T. I. R., Bemmer, V. L., Franks, S., Dunlop, C., Hardy, K., and Dunlop, I. E. (2021). Micromechanical Mapping of the Intact Ovary interior Reveals Contrasting Mechanical Roles for Follicles and Stroma. *Biomaterials* 277, 121099. doi:10.1016/j.biomaterials.2021.121099



- Hsu, P.-C., Chao, T.-K., Chou, Y.-C., Yu, M.-H., Wang, Y.-C., Lin, Y.-H., et al. (2021). AIM2 Inflammasome in Tumor Cells as a Biomarker for Predicting the Treatment Response to Antiangiogenic Therapy in Epithelial Ovarian Cancer Patients. *Jcm* 10 (19), 4529. doi:10.3390/jcm10194529
- Hughes, C. S., Postovit, L. M., and Lajoie, G. A. (2010). Matrigel: a Complex Protein Mixture Required for Optimal Growth of Cell Culture. *Proteomics* 10 (9), 1886–1890. doi:10.1002/pmic.200900758
- Ip, C. K. M., Li, S.-S., Tang, M. Y. H., Sy, S. K. H., Ren, Y., Shum, H. C., et al. (2016). Stemness and Chemoresistance in Epithelial Ovarian Carcinoma Cells under Shear Stress. *Sci. Rep.* 6 (1), 26788. doi:10.1038/srep26788
- Ivascu, A., and Kubbies, M. (2006). Rapid Generation of Single-Tumor Spheroids for High-Throughput Cell Function and Toxicity Analysis. *J. Biomol. Screen.* 11 (8), 922–932. doi:10.1177/1087057106292763
- Iwanicki, M. P., Davidowitz, R. A., Ng, M. R., Besser, A., Muranen, T., Merritt, M., et al. (2011). Ovarian Cancer Spheroids Use Myosin-Generated Force to Clear the Mesothelium. *Cancer Discov.* 1 (2), 144–157. doi:10.1158/2159-8274.cd-11-0010
- Iyer, S., Zhang, S., Yucel, S., Horn, H., Smith, S. G., Reinhardt, F., et al. (2021). Genetically Defined Syngeneic Mouse Models of Ovarian Cancer as Tools for the Discovery of Combination Immunotherapy. *Cancer Discov.* 11 (2), 384–407. doi:10.1158/2159-8290.CD-20-0818
- Jabs, J., Zickgraf, F. M., Park, J., Wagner, S., Jiang, X., Jechow, K., et al. (2017). Screening Drug Effects in Patient-derived Cancer Cells Links Organoid Responses to Genome Alterations. *Mol. Syst. Biol.* 13 (11), 955. doi:10.15252/msb.20177697
- Jamieson, S., and Fuller, P. J. (2012). Molecular Pathogenesis of Granulosa Cell Tumors of the Ovary. *Endocr. Rev.* 33 (1), 109–144. doi:10.1210/er.2011-0014
- Jelinic, P., Schlappe, B. A., Conlon, N., Tseng, J., Olvera, N., Dao, F., et al. (2016). Concomitant Loss of SMARCA2 and SMARCA4 Expression in Small Cell Carcinoma of the Ovary, Hypercalcemic Type. *Mod. Pathol.* 29 (1), 60–66. doi:10.1038/modpathol.2015.129
- Jensen, C., and Teng, Y. (2020). Is it Time to Start Transitioning from 2D to 3D Cell Culture? *Front. Mol. Biosci.* 7 (33), 1. doi:10.3389/fmolb.2020.00033
- Jin, K., Teng, L., Shen, Y., He, K., Xu, Z., and Li, G. (2010). Patient-derived Human Tumour Tissue Xenografts in Immunodeficient Mice: a Systematic Review. *Clin. Transl. Oncol.* 12 (7), 473–480. doi:10.1007/s12094-010-0540-6
- John, B., Naczki, C., Patel, C., Ghoneum, A., Qasem, S., Salih, Z., et al. (2019). Regulation of the Bi-directional Cross-Talk between Ovarian Cancer Cells and Adipocytes by SPARC. *Oncogene* 38 (22), 4366–4383. doi:10.1038/s41388-019-0728-3
- Johnson, P. A., and Giles, J. R. (2013). The Hen as a Model of Ovarian Cancer. *Nat. Rev. Cancer* 13 (6), 432–436. doi:10.1038/nrc3535
- Joshi, N., Liu, D., Dickson, K.-A., Marsh, D. J., Ford, C. E., and Stenzel, M. H. (2021). An Organotypic Model of High-Grade Serous Ovarian Cancer to Test the Anti-metastatic Potential of ROR2 Targeted Polyion Complex Nanoparticles. *J. Mater. Chem. B* 9 (44), 9123–9135. doi:10.1039/d1tb01837j
- Kaemmerer, E., Melchels, F. P. W., Holzapfel, B. M., Meckel, T., Hutmacher, D. W., and Loessner, D. (2014). Gelatine Methacrylamide-Based Hydrogels: An Alternative Three-Dimensional Cancer Cell Culture System. *Acta Biomater.* 10 (6), 2551–2562. doi:10.1016/j.actbio.2014.02.035
- Kalli, K. R., Chen, B.-K., Bale, L. K., Gernand, E., Overgaard, M. T., Oxvig, C., et al. (2004). Pregnancy-associated Plasma Protein-A (PAPP-A) Expression and Insulin-like Growth Factor Binding Protein-4 Protease Activity in normal and Malignant Ovarian Surface Epithelial Cells. *Int. J. Cancer* 110 (5), 633–640. doi:10.1002/ijc.20185
- Kapalczyńska, M., Kolenda, T., Przybyła, W., Zajackowska, M., Teresiak, A., Filas, V., et al. (2018). 2D and 3D Cell Cultures - a Comparison of Different Types of Cancer Cell Cultures. *aoms* 14 (4), 910–919. doi:10.5114/aoms.2016.63743
- Karnezi, A. N., Chen, S. Y., Chow, C., Yang, W., Hendricks, W. P. D., Ramos, P., et al. (2021). Re-assigning the Histologic Identities of COV434 and TOV-112D Ovarian Cancer Cell Lines. *Gynecol. Oncol.* 160 (2), 568–578. doi:10.1016/j.ygyno.2020.12.004
- Karst, A. M., Levanon, K., and Drapkin, R. (2011). Modeling High-Grade Serous Ovarian Carcinogenesis from the Fallopian Tube. *Proc. Natl. Acad. Sci.* 108 (18), 7547–7552. doi:10.1073/pnas.1017300108
- Kashiyama, T., Oda, K., Ikeda, Y., Shiose, Y., Hirota, Y., Inaba, K., et al. (2014). Antitumor Activity and Induction of TP53-dependent Apoptosis toward Ovarian clear Cell Adenocarcinoma by the Dual PI3K/mTOR Inhibitor DS-7423. *PLoS ONE* 9 (2), e87220. doi:10.1371/journal.pone.0087220
- Kenny, H. A., Chiang, C.-Y., White, E. A., Schryver, E. M., Habis, M., Romero, I. L., et al. (2014). Mesothelial Cells Promote Early Ovarian Cancer Metastasis through Fibronectin Secretion. *J. Clin. Invest.* 124 (10), 4614–4628. doi:10.1172/jci74778
- Kenny, H. A., Dogan, S., Zillhardt, M., Mitra, A. A., Yamada, S. D., Krausz, T., et al. (2009). “Organotypic Models of Metastasis: A Three-Dimensional Culture Mimicking the Human Peritoneum and Omentum for the Study of the Early Steps of Ovarian Cancer Metastasis,” in *Cancer Treatment and Research* (US: Springer), 335–351. doi:10.1007/978-0-387-98094-2\_16
- Kenny, H. A., Krausz, T., Yamada, S. D., and Lengyel, E. (2007). Use of a Novel 3D Culture Model to Elucidate the Role of Mesothelial Cells, Fibroblasts and Extra-cellular Matrices on Adhesion and Invasion of Ovarian Cancer Cells to the Omentum. *Int. J. Cancer* 121 (7), 1463–1472. doi:10.1002/ijc.22874
- Khalil, C., Moussa, M., Azar, A., Tawk, J., Habbouche, J., Salameh, R., et al. (2019). Anti-proliferative Effects of Mesenchymal Stem Cells (MSCs) Derived from Multiple Sources on Ovarian Cancer Cell Lines: an *In-Vitro* Experimental Study. *J. Ovarian Res.* 12 (1), 70. doi:10.1186/s13048-019-0546-9
- Kidera, Y., Yoshimura, T., Ohkuma, Y., Iwasaka, T., and Sugimori, H. (1985). Establishment and Characterization of a Cell Line Derived from Mucinous Cystadenocarcinoma of Human Ovary. *Nihon Sanka Fujinka Gakkai Zasshi* 37 (9), 1820–1824.
- Kim, S. I., Lee, J. W., Lee, M., Kim, H. S., Chung, H. H., Kim, J.-W., et al. (2018). Genomic Landscape of Ovarian clear Cell Carcinoma via Whole Exome Sequencing. *Gynecol. Oncol.* 148 (2), 375–382. doi:10.1016/j.ygyno.2017.12.005
- King, S. M., Quartuccio, S., Hilliard, T. S., Inoue, K., and Burdette, J. E. (2011). Alginate Hydrogels for Three-Dimensional Organ Culture of Ovaries and Oviducts. *JoVE* 52, 1. doi:10.3791/2804
- Köbel, M., and Kang, E. Y. (2021). The Many Uses of P53 Immunohistochemistry in Gynecological Pathology: Proceedings of the ISGyP Companion Society Session at the 2020 USCAP Annual Meeting. *Int. J. Gynecol. Pathol.* 40 (1), 32–40. doi:10.1097/pgp.0000000000000725
- Kondrashova, O., Nguyen, M., Shield-Artin, K., Tinker, A. V., Teng, N. N. H., Harrell, M. I., et al. (2017). Secondary Somatic Mutations Restoring RAD51C and RAD51D Associated with Acquired Resistance to the PARP Inhibitor Rucaparib in High-Grade Ovarian Carcinoma. *Cancer Discov.* 7 (9), 984–998. doi:10.1158/2159-8290.Cd-17-0419
- Konstantinopoulos, P. A., Spentzos, D., Karlan, B. Y., Taniguchi, T., Fountzilas, E., Francoeur, N., et al. (2010). Gene Expression Profile of BRCAness that Correlates with Responsiveness to Chemotherapy and with Outcome in Patients with Epithelial Ovarian Cancer. *Jco* 28 (22), 3555–3561. doi:10.1200/jco.2009.27.5719
- Kopper, O., de Witte, C. J., Löhmußsaar, K., Valle-Inclán, J. E., Hami, N., Kester, L., et al. (2019). An Organoid Platform for Ovarian Cancer Captures Intra- and Interpatient Heterogeneity. *Nat. Med.* 25 (5), 838–849. doi:10.1038/s41591-019-0422-6
- Kuo, K.-T., Mao, T.-L., Jones, S., Veras, E., Ayhan, A., Wang, T.-L., et al. (2009). Frequent Activating Mutations of PIK3CA in Ovarian clear Cell Carcinoma. *Am. J. Pathol.* 174 (5), 1597–1601. doi:10.2353/ajpath.2009.081000
- Kunz-Schughart, L. A., Freyer, J. P., Hofstaedter, F., and Ebner, R. (2004). The Use of 3-D Cultures for High-Throughput Screening: The Multicellular Spheroid Model. *J. Biomol. Screen.* 9 (4), 273–285. doi:10.1177/1087057104265040
- Kurman, R. J., and Shih, I.-M. (2010). The Origin and Pathogenesis of Epithelial Ovarian Cancer: a Proposed Unifying Theory. *Am. J. Surg. Pathol.* 34 (3), 433–443. doi:10.1097/PAS.0b013e3181cf3d79
- Lal-Nag, M., McGee, L., Guha, R., Lengyel, E., Kenny, H. A., and Ferrer, M. (2017). A High-Throughput Screening Model of the Tumor Microenvironment for Ovarian Cancer Cell Growth. *SLAS DISCOVERY: Advancing Sci. Drug Discov.* 22 (5), 494–506. doi:10.1177/2472555216687082
- Langdon, S. P., Lawrie, S. S., Hay, F. G., Hawkes, M. M., McDonald, A., Hayward, I. P., et al. (1988). Characterization and Properties of Nine Human Ovarian Adenocarcinoma Cell Lines. *Cancer Res.* 48 (21), 6166–6172.
- Lau, T.-S., Chan, L. K.-Y., Wong, E. C.-H., Hui, C. W.-C., Sneddon, K., Cheung, T.-H., et al. (2017). A Loop of Cancer-Stroma-Cancer Interaction Promotes Peritoneal Metastasis of Ovarian Cancer via TNFα-Tgfa-EGFR. *Oncogene* 36 (25), 3576–3587. doi:10.1038/onc.2016.509

- Lawrenson, K., Grun, B., and Gayther, S. A. (2012). Heterotypic Three-Dimensional *In Vitro* Modeling of Stromal-Epithelial Interactions during Ovarian Cancer Initiation and Progression. *JoVE* 66, e4206. doi:10.3791/4206
- Ledermann, J. A., Luvero, D., Shafer, A., O'Connor, D., Mangili, G., Friedlander, M., et al. (2014b). Gynecologic Cancer InterGroup (GCIg) Consensus Review for Mucinous Ovarian Carcinoma. *Int. J. Gynecol. Cancer* 24 (9), S14–S19. doi:10.1097/igc.0000000000000296
- Ledermann, J., Harter, P., Gourley, C., Friedlander, M., Vergote, I., Rustin, G., et al. (2014a). Olaparib Maintenance Therapy in Patients with Platinum-Sensitive Relapsed Serous Ovarian Cancer: a Preplanned Retrospective Analysis of Outcomes by BRCA Status in a Randomised Phase 2 Trial. *Lancet Oncol.* 15 (8), 852–861. doi:10.1016/s1470-2045(14)70228-1
- Ledermann, J., Harter, P., Gourley, C., Friedlander, M., Vergote, I., Rustin, G., et al. (2012). Olaparib Maintenance Therapy in Platinum-Sensitive Relapsed Ovarian Cancer. *N. Engl. J. Med.* 366 (15), 1382–1392. doi:10.1056/NEJMoal105535
- Lee, C. K., Friedlander, M. L., Tjokrowidjaja, A., Ledermann, J. A., Coleman, R. L., Mirza, M. R., et al. (2021). Molecular and Clinical Predictors of Improvement in Progression-free Survival with Maintenance PARP Inhibitor Therapy in Women with Platinum-sensitive, Recurrent Ovarian Cancer: A Meta-analysis. *Cancer* 127 (14), 2432–2441. doi:10.1002/cncr.33517
- Li, S.-S., Ip, C. K. M., Tang, M. Y. H., Sy, S. K. H., Yung, S., Chan, T.-M., et al. (2017). Modeling Ovarian Cancer Multicellular Spheroid Behavior in a Dynamic 3D Peritoneal Microdevice. *JoVE* 120, 55337. doi:10.3791/55337
- Liao, J., Qian, F., Tchabo, N., Mhawech-Fauceglia, P., Beck, A., Qian, Z., et al. (2014). Ovarian Cancer Spheroid Cells with Stem Cell-like Properties Contribute to Tumor Generation, Metastasis and Chemotherapy Resistance through Hypoxia-Resistant Metabolism. *PLoS ONE* 9 (1), e84941. doi:10.1371/journal.pone.0084941
- Liu, J. F., Palakurthi, S., Zeng, Q., Zhou, S., Ivanova, E., Huang, W., et al. (2017). Establishment of Patient-Derived Tumor Xenograft Models of Epithelial Ovarian Cancer for Preclinical Evaluation of Novel Therapeutics. *Clin. Cancer Res.* 23 (5), 1263–1273. doi:10.1158/1078-0432.Ccr-16-1237
- Liu, M., Zhang, X., Long, C., Xu, H., Cheng, X., Chang, J., et al. (2018). Collagen-based Three-Dimensional Culture Microenvironment Promotes Epithelial to Mesenchymal Transition and Drug Resistance of Human Ovarian Cancer in Vitro. *RSC Adv.* 8 (16), 8910–8919. doi:10.1039/C7RA13742G
- Loessner, D., Rockstroh, A., Shokoohmand, A., Holzapfel, B. M., Wagner, F., Baldwin, J., et al. (2019). A 3D Tumor Microenvironment Regulates Cell Proliferation, Peritoneal Growth and Expression Patterns. *Biomaterials* 190–191, 63–75. doi:10.1016/j.biomaterials.2018.10.014
- Löhmusaar, K., Kopper, O., Korving, J., Begthel, H., Vreuls, C. P. H., Van Es, J. H., et al. (2020). Assessing the Origin of High-Grade Serous Ovarian Cancer Using CRISPR-Modification of Mouse Organoids. *Nat. Commun.* 11 (1), 1. doi:10.1038/s41467-020-16432-0
- Long, L., Yin, M., and Min, W. (2018). 3D Co-culture System of Tumor-Associated Macrophages and Ovarian Cancer Cells. *Bio-protocol* 8 (8), e2815. doi:10.21769/BioProtoc.2815
- Lu, M., Henry, C. E., Lai, H., Khine, Y. Y., Ford, C. E., and Stenzel, M. H. (2019). A New 3D Organotypic Model of Ovarian Cancer to Help Evaluate the Antimetastatic Activity of RAPTA-C Conjugated Micelles. *Biomater. Sci.* 7 (4), 1652–1660. doi:10.1039/c8bm01326h
- Lutolf, M. P., Lauer-Fields, J. L., Schmoekel, H. G., Metters, A. T., Weber, F. E., Fields, G. B., et al. (2003). Synthetic Matrix Metalloproteinase-Sensitive Hydrogels for the Conduction of Tissue Regeneration: Engineering Cell-Invasion Characteristics. *Proc. Natl. Acad. Sci.* 100 (9), 5413–5418. doi:10.1073/pnas.0737381100
- Lynn, A. K., Yannas, I. V., and Bonfield, W. (2004). Antigenicity and Immunogenicity of Collagen. *J. Biomed. Mater. Res.* 71B (2), 343–354. doi:10.1002/jbm.b.30096
- Mabuchi, S., Sugiyama, T., and Kimura, T. (2016). Clear Cell Carcinoma of the Ovary: Molecular Insights and Future Therapeutic Perspectives. *J. Gynecol. Oncol.* 27 (3), e31. doi:10.3802/jgo.2016.27.e31
- Machida-Sano, I., Matsuda, Y., and Namiki, H. (2009). In Vitro Adhesion of Human Dermal Fibroblasts on Iron Cross-Linked Alginate Films. *Biomed. Mater.* 4, 025008. doi:10.1088/1748-6041/4/2/025008
- Maenhoudt, N., Defraye, C., Boretto, M., Jan, Z., Heremans, R., Boeckx, B., et al. (2020). Developing Organoids from Ovarian Cancer as Experimental and Preclinical Models. *Stem Cell Rep.* 14 (4), 717–729. doi:10.1016/j.stemcr.2020.03.004
- Maenhoudt, N., and Vankelecom, H. (2021). Protocol for Establishing Organoids from Human Ovarian Cancer Biopsies. *STAR Protoc.* 2 (2), 100429. doi:10.1016/j.xpro.2021.100429
- Makalowski, W., Zhang, J., and Boguski, M. S. (1996). Comparative Analysis of 1196 Orthologous Mouse and Human Full-Length mRNA and Protein Sequences. *Genome Res.* 6 (9), 846–857. doi:10.1101/gr.6.9.846
- Maniati, E., Berlato, C., Gopinathan, G., Heath, O., Kotantaki, P., Lakhani, A., et al. (2020). Mouse Ovarian Cancer Models Recapitulate the Human Tumor Microenvironment and Patient Response to Treatment. *Cell Rep.* 30 (2), 525–540. e527. doi:10.1016/j.celrep.2019.12.034
- Maru, Y., Tanaka, N., Itami, M., and Hippo, Y. (2019). Efficient Use of Patient-Derived Organoids as a Preclinical Model for Gynecologic Tumors. *Gynecol. Oncol.* 154 (1), 189–198. doi:10.1016/j.ygyno.2019.05.005
- Masiello, T., Dhall, A., Hemachandra, L., Tokranova, N., Melendez, J., and Castracane, J. (2018). A Dynamic Culture Method to Produce Ovarian Cancer Spheroids under Physiologically-Relevant Shear Stress. *Cells* 7 (12), 277. doi:10.3390/cells7120277
- Matsuo, K., Nishimura, M., Bottsford-Miller, J. N., Huang, J., Komurov, K., Armaiz-Pena, G. N., et al. (2011). Targeting SRC in Mucinous Ovarian Carcinoma. *Clin. Cancer Res.* 17 (16), 5367–5378. doi:10.1158/1078-0432.Ccr-10-3176
- Mazzocchi, A., Soker, S., and Skardal, A. (2019). 3D Bioprinting for High-Throughput Screening: Drug Screening, Disease Modeling, and Precision Medicine Applications. *Appl. Phys. Rev.* 6 (1), 011302. doi:10.1063/1.5056188
- McCloskey, C. W., Goldberg, R. L., Carter, L. E., Gamwell, L. F., Al-Hujaili, E. M., Collins, O., et al. (2014). A New Spontaneously Transformed Syngeneic Model of High-Grade Serous Ovarian Cancer with a Tumor-Initiating Cell Population. *Front. Oncol.* 4 (53), 1. doi:10.3389/fonc.2014.00053
- McCluggage, W. G., and Stewart, C. J. R. (2021). SWI/SNF-deficient Malignancies of the Female Genital Tract. *Semin. Diagn. Pathol.* 38 (3), 199–211. doi:10.1053/j.semdp.2020.08.003
- Mckenzie, A. J., Hicks, S. R., Svec, K. V., Naughton, H., Edmunds, Z. L., and Howe, A. K. (2018). The Mechanical Microenvironment Regulates Ovarian Cancer Cell Morphology, Migration, and Spheroid Disaggregation. *Sci. Rep.* 8 (1), 1. doi:10.1038/s41598-018-25589-0
- Medeiros, M., Ribeiro, A. O., Lupi, L. A., Romualdo, G. R., Pinhal, D., Chuffa, L. G. d. A., et al. (2019). Mimicking the Tumor Microenvironment: Fibroblasts Reduce miR-29b Expression and Increase the Motility of Ovarian Cancer Cells in a Co-culture Model. *Biochem. Biophysical Res. Commun.* 516 (1), 96–101. doi:10.1016/j.bbrc.2019.06.001
- Mehta, G., Hsiao, A. Y., Ingram, M., Luker, G. D., and Takayama, S. (2012). Opportunities and Challenges for Use of Tumor Spheroids as Models to Test Drug Delivery and Efficacy. *J. Control. Release* 164 (2), 192–204. doi:10.1016/j.jconrel.2012.04.045
- Mendibil, U., Ruiz-Hernandez, R., Retegi-Carrion, S., Garcia-Urquiza, N., Olalde-Graells, B., and Abarategi, A. (2020). Tissue-Specific Decellularization Methods: Rationale and Strategies to Achieve Regenerative Compounds. *Ijms* 21 (15), 5447. doi:10.3390/ijms21155447
- Michael, B., Yong-Hyun, S., Aleksandar, R., and Bryan, B. (2016). The Effect of ECM Stiffness on Ovarian Follicle Development. *Front. Bioeng. Biotechnol.* 4, 1. doi:10.3389/conf.FBIOE.2016.01.00303
- Mieulet, V., Garnier, C., Kieffer, Y., Guilbert, T., Nemati, F., Marangoni, E., et al. (2021). Stiffness Increases with Myofibroblast Content and Collagen Density in Mesenchymal High Grade Serous Ovarian Cancer. *Sci. Rep.* 11 (1), 1. doi:10.1038/s41598-021-83685-0
- Mitra, A. K., Chiang, C. Y., Tiwari, P., Tomar, S., Watters, K. M., Peter, M. E., et al. (2015a). Microenvironment-induced Downregulation of miR-193b Drives Ovarian Cancer Metastasis. *Oncogene* 34 (48), 5923–5932. doi:10.1038/onc.2015.43
- Mitra, A. K., Davis, D. A., Tomar, S., Roy, L., Gurler, H., Xie, J., et al. (2015b). *In Vivo* Tumor Growth of High-Grade Serous Ovarian Cancer Cell Lines. *Gynecol. Oncol.* 138 (2), 372–377. doi:10.1016/j.ygyno.2015.05.040
- Miyagawa, Y., Nagasaka, K., Yamawaki, K., Mori, Y., Ishiguro, T., Hashimoto, K., et al. (2020). Evaluating the Angiogenetic Properties of Ovarian Cancer Stem-

- like Cells Using the Three-Dimensional Co-culture System, NICO-1. *JoVE* 166, 1. doi:10.3791/61751
- Moore, K., Colombo, N., Scambia, G., Kim, B.-G., Oaknin, A., Friedlander, M., et al. (2018). Maintenance Olaparib in Patients with Newly Diagnosed Advanced Ovarian Cancer. *N. Engl. J. Med.* 379 (26), 2495–2505. doi:10.1056/NEJMoa1810858
- Morton, C. L., and Houghton, P. J. (2007). Establishment of Human Tumor Xenografts in Immunodeficient Mice. *Nat. Protoc.* 2 (2), 247–250. doi:10.1038/nprot.2007.25
- Motohara, T., Masuda, K., Morotti, M., Zheng, Y., El-Sahhar, S., Chong, K. Y., et al. (2019). An Evolving story of the Metastatic Voyage of Ovarian Cancer Cells: Cellular and Molecular Orchestration of the Adipose-Rich Metastatic Microenvironment. *Oncogene* 38 (16), 2885–2898. doi:10.1038/s41388-018-0637-x
- Motoyama, T. (1981). Biological Characterization Including Sensitivity to Mitomycin C of Cultured Human Ovarian Cancers (Author's Transl). *Nihon Sanka Fujinka Gakkai Zasshi* 33 (8), 1197–1204.
- Moujaber, T., Balleine, R. L., Gao, B., Madsen, I., Harnett, P. R., and DeFazio, A. (2022). New Therapeutic Opportunities for Women with Low-Grade Serous Ovarian Cancer. *Endocr. Relat. Cancer* 29 (1), R1–r16. doi:10.1530/erc-21-0191
- Muggia, F., and Safran, T. (2014). 'BRCAness' and its Implications for Platinum Action in Gynecologic Cancer. *Anticancer Res.* 34 (2), 551–556.
- Mullen, P., Ritchie, A., Langdon, S. P., and Miller, W. R. (1996). Effect of Matrigel on the Tumorigenicity of Human Breast and Ovarian Carcinoma Cell Lines. *Int'l J. Cancer* 67 (6), 816–820. doi:10.1002/(sici)1097-0215(19960917)67:6<816::aid-ijc10>3.0.co;2-#
- Nanki, Y., Chiyoda, T., Hirasawa, A., Ookubo, A., Itoh, M., Ueno, M., et al. (2020). Patient-derived Ovarian Cancer Organoids Capture the Genomic Profiles of Primary Tumours Applicable for Drug Sensitivity and Resistance Testing. *Sci. Rep.* 10 (1), 1. doi:10.1038/s41598-020-69488-9
- Nesic, K., Kondrashova, O., Hurley, R. M., McGehee, C. D., Vandenberg, C. J., Ho, G.-Y., et al. (2021). Acquired RAD51C Promoter Methylation Loss Causes PARP Inhibitor Resistance in High-Grade Serous Ovarian Carcinoma. *Cancer Res.* 81 (18), 4709–4722. doi:10.1158/0008-5472.Can-21-0774
- Nguyen, L., W. M. Martens, J., Van Hoeck, A., and Cuppen, E. (2020). Pan-cancer Landscape of Homologous Recombination Deficiency. *Nat. Commun.* 11 (1), 5584. doi:10.1038/s41467-020-19406-4
- Nikniaz, H., Zandieh, Z., Nouri, M., Daei-farshbaf, N., Aflatoonian, R., Gholipourmalekabadi, M., et al. (2021). Comparing Various Protocols of Human and Bovine Ovarian Tissue Decellularization to Prepare Extracellular Matrix-Alginate Scaffold for Better Follicle Development *In Vitro*. *BMC Biotechnol.* 21 (1), 8. doi:10.1186/s12896-020-00658-3
- Ning, Y., Cui, Y., Li, X., Cao, X., Chen, A., Xu, C., et al. (2018). Co-culture of Ovarian Cancer Stem-like Cells with Macrophages Induced SKOV3 Cells Stemness via IL-8/STAT3 Signaling. *Biomed. Pharmacother.* 103, 262–271. doi:10.1016/j.biopha.2018.04.022
- Nishi, Y., Yanase, T., Mu, Y.-M., Oba, K., Ichino, I., Saito, M., et al. (2001). Establishment and Characterization of a Steroidogenic Human Granulosa-like Tumor Cell Line, KGN, that Expresses Functional Follicle-Stimulating Hormone Receptor. *Endocrinology* 142 (1), 437–445. doi:10.1210/endo.142.1.7862
- Noshadi, I., Hong, S., Sullivan, K. E., Shirzaei Sani, E., Portillo-Lara, R., Tamayol, A., et al. (2017). *In Vitro* and *In Vivo* Analysis of Visible Light Crosslinkable Gelatin Methacryloyl (GelMA) Hydrogels. *Biomater. Sci.* 5 (10), 2093–2105. doi:10.1039/c7bm00110j
- Novak, C. M., Horst, E. N., Lin, E., and Mehta, G. (2020). Compressive Stimulation Enhances Ovarian Cancer Proliferation, Invasion, Chemoresistance, and Mechanotransduction via CDC42 in a 3D Bioreactor. *Cancers* 12 (6), 1521. doi:10.3390/cancers12061521
- Nowacka, M., Sterzynska, K., Andrzejewska, M., Nowicki, M., and Januchowski, R. (2021). Drug Resistance Evaluation in Novel 3D *In Vitro* Model. *Biomed. Pharmacother.* 138, 111536. doi:10.1016/j.biopha.2021.111536
- Nozawa, S., Yajima, M., Sasaki, H., Tsukazaki, K., Aoki, D., Sakayori, M., et al. (1991). A New CA125-like Antigen (CA602) Recognized by Two Monoclonal Antibodies against a Newly Established Ovarian clear Cell Carcinoma Cell Line (RMG-II). *Jpn. J. Cancer Res.* 82 (7), 854–861. doi:10.1111/j.1349-7006.1991.tb02713.x
- Odunsi, A., McGray, A. J. R., Miliotto, A., Zhang, Y., Wang, J., Abiola, A., et al. (2020). Fidelity of Human Ovarian Cancer Patient-Derived Xenografts in a Partially Humanized Mouse Model for Preclinical Testing of Immunotherapies. *J. Immunother. Cancer* 8 (2), e001237. doi:10.1136/jitc-2020-001237
- Onal, S., Alkai, M. M., and Nock, V. (2021). A Flexible Microdevice for Mechanical Cell Stimulation and Compression in Microfluidic Settings. *Front. Phys.* 9 (280), 1. doi:10.3389/fphy.2021.654918
- Orkin, R. W., Gehron, P., McGoodwin, E. B., Martin, G. R., Valentine, T., and Swarm, R. (1977). A Murine Tumor Producing a Matrix of Basement Membrane. *J. Exp. Med.* 145 (1), 204–220. doi:10.1084/jem.145.1.204
- Oza, A. M., Cook, A. D., Pfisterer, J., Embleton, A., Ledermann, J. A., Pujade-Lauraine, E., et al. (2015). Standard Chemotherapy with or without Bevacizumab for Women with Newly Diagnosed Ovarian Cancer (ICON7): Overall Survival Results of a Phase 3 Randomised Trial. *Lancet Oncol.* 16 (8), 928–936. doi:10.1016/s1470-2045(15)00086-8
- Ozols, R. F., Willson, J. K., Grotzinger, K. R., and Young, R. C. (1980). Cloning of Human Ovarian Cancer Cells in Soft agar from Malignant and Peritoneal Washings. *Cancer Res.* 40 (8), 2743–2747.
- Papp, E., Hallberg, D., Konecny, G. E., Bruhm, D. C., Adelff, V., Noë, M., et al. (2018). Integrated Genomic, Epigenomic, and Expression Analyses of Ovarian Cancer Cell Lines. *Cell Rep.* 25 (9), 2617–2633. doi:10.1016/j.celrep.2018.10.096
- Paradiso, F., Fitzgerald, J., Yao, S., Barry, F., Taraballi, F., Gonzalez, D., et al. (2019). Marine Collagen Substrates for 2D and 3D Ovarian Cancer Cell Systems. *Front. Bioeng. Biotechnol.* 7, 1. doi:10.3389/fbioe.2019.00343
- Parra-Herran, C., Bassiouny, D., Lerner-Ellis, J., Olkhov-Mitsel, E., Ismail, N., Hogen, L., et al. (2019). p53, Mismatch Repair Protein, and POLE Abnormalities in Ovarian Clear Cell Carcinoma. *Am. J. Surg. Pathol.* 43 (12), 1591–1599. doi:10.1097/pas.0000000000001328
- Patch, A.-M., Christie, E. L., Christie, E. L., Etemadmoghadam, D., Garsed, D. W., George, J., et al. (2015). Whole-genome Characterization of Chemoresistant Ovarian Cancer. *Nature* 521 (7553), 489–494. doi:10.1038/nature14410
- Patra, B., Lateef, M. A., Brodeur, M. N., Fleury, H., Carmona, E., Péant, B., et al. (2020). Carboplatin Sensitivity in Epithelial Ovarian Cancer Cell Lines: The Impact of Model Systems. *PLoS ONE* 15 (12), e0244549. doi:10.1371/journal.pone.0244549
- Pennington, K. P., Walsh, T., Harrell, M. I., Lee, M. K., Pennil, C. C., Rendi, M. H., et al. (2014). Germline and Somatic Mutations in Homologous Recombination Genes Predict Platinum Response and Survival in Ovarian, Fallopian Tube, and Peritoneal Carcinomas. *Clin. Cancer Res.* 20 (3), 764–775. doi:10.1158/1078-0432.Ccr-13-2287
- Peres, L. C., Risch, H., Terry, K. L., Webb, P. M., Goodman, M. T., Wu, A. H., et al. (2018). Racial/ethnic Differences in the Epidemiology of Ovarian Cancer: a Pooled Analysis of 12 Case-Control Studies. *Int. J. Epidemiol.* 47 (2), 460–472. doi:10.1093/ije/dyx252
- Perets, R., and Drapkin, R. (2016). It's Totally Tubular. . . Riding the New Wave of Ovarian Cancer Research. *Cancer Res.* 76 (1), 10–17. doi:10.1158/0008-5472.Can-15-1382
- Perets, R., Wyant, G. A., Muto, K. W., Bijron, J. G., Poole, B. B., Chin, K. T., et al. (2013). Transformation of the Fallopian Tube Secretory Epithelium Leads to High-Grade Serous Ovarian Cancer in Brca;Tp53;Pten Models. *Cancer Cell* 24 (6), 751–765. doi:10.1016/j.ccr.2013.10.013
- Perren, T. J., Swart, A. M., Pfisterer, J., Ledermann, J. A., Pujade-Lauraine, E., Kristensen, G., et al. (2011). A Phase 3 Trial of Bevacizumab in Ovarian Cancer. *N. Engl. J. Med.* 365 (26), 2484–2496. doi:10.1056/NEJMoa1103799
- Peters, P. N., Schryver, E. M., Lengyel, E., and Kenny, H. (2015). Modeling the Early Steps of Ovarian Cancer Dissemination in an Organotypic Culture of the Human Peritoneal Cavity. *JoVE* 106, e53541. doi:10.3791/53541
- Phan, N., Hong, J. J., Tofig, B., Mapua, M., Elashoff, D., Moatamed, N. A., et al. (2019). A Simple High-Throughput Approach Identifies Actionable Drug Sensitivities in Patient-Derived Tumor Organoids. *Commun. Biol.* 2 (1), 78. doi:10.1038/s42003-019-0305-x
- Pietilä, E. A., Gonzalez-Molina, J., Moyano-Galceran, L., Jamalzadeh, S., Zhang, K., Lehtinen, L., et al. (2021). Co-evolution of Matrisome and Adaptive Adhesion Dynamics Drives Ovarian Cancer Chemoresistance. *Nat. Commun.* 12 (1), 1. doi:10.1038/s41467-021-24009-8



- Pirker, R., FitzGerald, D. J., Hamilton, T. C., Ozols, R. F., Laird, W., Frankel, A. E., et al. (1985). Characterization of Immunotoxins Active against Ovarian Cancer Cell Lines. *J. Clin. Invest.* 76 (3), 1261–1267. doi:10.1172/JCI112082
- Provencher, D. M., Lounis, H., Champoux, L., Tétrault, M., Manderson, E. N., Wang, J. C., et al. (2000). Characterization of Four Novel Epithelial Ovarian Cancer Cell Lines. *In Vitro Cell Dev Biol Anim* 36 (6), 357–361. doi:10.1290/1071-2690(2000)036<0357:Cofneo>2.0.CO;2
- Rafehi, S., Valdes, Y. R., Bertrand, M., Mcgee, J., Préfontaine, M., Sugimoto, A., et al. (2016). TGF $\beta$  Signaling Regulates Epithelial-Mesenchymal Plasticity in Ovarian Cancer Ascites-Derived Spheroids. *Endocrine-Related Cancer* 23 (3), 147–159. doi:10.1530/erc-15-0383
- Raghavan, S., Mehta, P., Horst, E. N., Ward, M. R., Rowley, K. R., and Mehta, G. (2016). Comparative Analysis of Tumor Spheroid Generation Techniques for Differential *In Vitro* Drug Toxicity. *Oncotarget* 7 (13), 16948–16961. doi:10.18632/oncotarget.7659
- Raghavan, S., Mehta, P., Xie, Y., Lei, Y. L., and Mehta, G. (2019). Ovarian Cancer Stem Cells and Macrophages Reciprocally Interact through the WNT Pathway to Promote Pro-tumoral and Malignant Phenotypes in 3D Engineered Microenvironments. *J. Immunotherapy Cancer* 7 (1), 1. doi:10.1186/s40425-019-0666-1
- Raghavan, S., Ward, M. R., Rowley, K. R., Wold, R. M., Takayama, S., Buckanovich, R. J., et al. (2015). Formation of Stable Small Cell Number Three-Dimensional Ovarian Cancer Spheroids Using Hanging Drop Arrays for Preclinical Drug Sensitivity Assays. *Gynecol. Oncol.* 138 (1), 181–189. doi:10.1016/j.ygyno.2015.04.014
- Ricci, F., Guffanti, F., Affatato, R., Brunelli, L., Roberta, P., Fruscio, R., et al. (2020). Establishment of Patient-Derived Tumor Xenograft Models of Mucinous Ovarian Cancer. *Am. J. Cancer Res.* 10 (2), 572–580.
- Rizvi, I., Gurkan, U. A., Tasoglu, S., Alagic, N., Celli, J. P., Mensah, L. B., et al. (2013). Flow Induces Epithelial-Mesenchymal Transition, Cellular Heterogeneity and Biomarker Modulation in 3D Ovarian Cancer Nodules. *Proc. Natl. Acad. Sci.* 110 (22), E1974–E1983. doi:10.1073/pnas.1216989110
- Roby, K. F., Taylor, C. C., Sweetwood, J. P., Cheng, Y., Pace, J. L., Tawfik, O., et al. (2000). Development of a Syngeneic Mouse Model for Events Related to Ovarian Cancer. *Carcinogenesis* 21 (4), 585–591. doi:10.1093/carcin/21.4.585
- Rosales-Nieves, A. E., and González-Reyes, A. (2014). Genetics and Mechanisms of Ovarian Cancer: Parallels between Drosophila and Humans. *Semin. Cell Dev. Biol.* 28, 104–109. doi:10.1016/j.semdb.2014.03.031
- Rowley, J. A., Madlambayan, G., and Mooney, D. J. (1999). Alginate Hydrogels as Synthetic Extracellular Matrix Materials. *Biomaterials* 20 (1), 45–53. doi:10.1016/s0142-9612(98)00107-0
- Saga, Y., Saga, Y., Mizukami, H., Wang, D., Fujiwara, H., Takei, Y., et al. (2012). Cetuximab Inhibits the Growth of Mucinous Ovarian Carcinoma Tumor Cells Lacking KRAS Gene Mutations. *Oncol. Rep.* 27 (5), 1336–1340. doi:10.3892/or.2012.1626
- Saha, B., Mathur, T., Handley, K. F., Hu, W., Afshar-Kharghan, V., Sood, A. K., et al. (2020). OvCa-Chip Microsystem Recreates Vascular Endothelium-Mediated Platelet Extravasation in Ovarian Cancer. *Blood Adv.* 4 (14), 3329–3342. doi:10.1182/bloodadvances.2020001632
- Sakayori, M., Nozawa, S., Udagawa, Y., Chin, K., Lee, S. G., Sakuma, T., et al. (1990). Biological Properties of Two Newly Established Cell Lines (RMUG-S, RMUG-L) from a Human Ovarian Mucinous Cystadenocarcinoma. *Hum. Cell* 3 (1), 52–56.
- Šale, S., and Orsulic, S. (2006). Models of Ovarian Cancer Metastasis: Murine Models. *Drug Discov. Today Dis. Models* 3 (2), 149–154. doi:10.1016/j.ddmod.2006.05.006
- Samartzis, E. P., Labidi-Galy, S. I., Moschetta, M., Uccello, M., Kalaitzopoulos, D. R., Perez-Fidalgo, J. A., et al. (2020). Endometriosis-associated Ovarian Carcinomas: Insights into Pathogenesis, Diagnostics, and Therapeutic Targets-A Narrative Review. *Ann. Transl. Med.* 8 (24), 1712. doi:10.21037/atm-20-3022a
- Schwarz, R. P., Goodwin, T. J., and Wolf, D. A. (1992). Cell Culture for Three-Dimensional Modeling in Rotating-wall Vessels: an Application of Simulated Microgravity. *J. Tissue Cult. Methods* 14 (2), 51–57. doi:10.1007/bf01404744
- Scott, A. L., Ayoola, O., and Zervantonakis, I. K. (2021). Abstract PO042: Microfluidic Modeling of Tumor-Macrophage Signaling in Ovarian Cancer. *Cancer Res.* 81 (5), PO042. doi:10.1158/1538-7445.TME21-PO042
- Scott, C. L., Becker, M. A., Haluska, P., and Samimi, G. (2013). Patient-derived Xenograft Models to Improve Targeted Therapy in Epithelial Ovarian Cancer Treatment. *Front. Oncol.* 3, 295. doi:10.3389/fonc.2013.00295
- Shield, K., Ackland, M. L., Ahmed, N., and Rice, G. E. (2009). Multicellular Spheroids in Ovarian Cancer Metastases: Biology and Pathology. *Gynecol. Oncol.* 113 (1), 143–148. doi:10.1016/j.ygyno.2008.11.032
- Shield, K., Riley, C., Quinn, M. A., Rice, G. E., Ackland, M. L., and Ahmed, N. (2007).  $\alpha\beta 1$  Integrin Affects Metastatic Potential of Ovarian Carcinoma Spheroids by Supporting Disaggregation and Proteolysis. *J. Carcinog* 6, 11. doi:10.1186/1477-3163-6-11
- Shih, I.-M., and Kurman, R. J. (2004). Ovarian Tumorigenesis. *Am. J. Pathol.* 164 (5), 1511–1518. doi:10.1016/s0002-9440(10)63708-x
- Shin, H.-Y., Yang, W., Lee, E.-j., Han, G. H., Cho, H., Chay, D. B., et al. (2018). Establishment of Five Immortalized Human Ovarian Surface Epithelial Cell Lines via SV40 T Antigen or HPV E6/E7 Expression. *PLoS ONE* 13 (10), e0205297. doi:10.1371/journal.pone.0205297
- Shin, S. I., Freedman, V. H., Risser, R., and Pollack, R. (1975). Tumorigenicity of Virus-Transformed Cells in Nude Mice Is Correlated Specifically with anchorage Independent Growth *In Vitro*. *Proc. Natl. Acad. Sci.* 72 (11), 4435–4439. doi:10.1073/pnas.72.11.4435
- Shin, S., Ikram, M., Subhan, F., Kang, H. Y., Lim, Y., Lee, R., et al. (2016). Alginate-marine Collagen-Agarose Composite Hydrogels as Matrices for Biomimetic 3D Cell Spheroid Formation. *RSC Adv.* 6 (52), 46952–46965. doi:10.1039/c6ra01937d
- Shishido, A., Mori, S., Yokoyama, Y., Hamada, Y., Minami, K., Qian, Y., et al. (2018). Mesothelial Cells Facilitate Cancer Stem like properties in spheroids of ovarian cancer cells. *Oncol. Rep.* 40 (4), 2105–2114. doi:10.3892/or.2018.6605
- Shuford, S., Wilhelm, C., Rayner, M., Elrod, A., Millard, M., Mattingly, C., et al. (2019). Prospective Validation of an *Ex Vivo*, Patient-Derived 3D Spheroid Model for Response Predictions in Newly Diagnosed Ovarian Cancer. *Sci. Rep.* 9 (1), 11153. doi:10.1038/s41598-019-47578-7
- Singh, M. S., Goldsmith, M., Thakur, K., Chatterjee, S., Landesman-Milo, D., Levy, T., et al. (2020). An Ovarian Spheroid Based Tumor Model that Represents Vascularized Tumors and Enables the Investigation of Nanomedicine Therapeutics. *Nanoscale* 12 (3), 1894–1903. doi:10.1039/c9nr09572a
- Siolas, D., and Hannon, G. J. (2013). Patient-derived Tumor Xenografts: Transforming Clinical Samples into Mouse Models. *Cancer Res.* 73 (17), 5315–5319. doi:10.1158/0008-5472.CAN-13-1069
- Sodek, K. L., Brown, T. J., and Ringuette, M. J. (2008). Collagen I but Not Matrigel Matrices Provide an MMP-dependent Barrier to Ovarian Cancer Cell Penetration. *BMC Cancer* 8 (1), 223. doi:10.1186/1471-2407-8-223
- Sodek, K. L., Ringuette, M. J., and Brown, T. J. (2009). Compact Spheroid Formation by Ovarian Cancer Cells Is Associated with Contractile Behavior and an Invasive Phenotype. *Int. J. Cancer* 124 (9), 2060–2070. doi:10.1002/ijc.24188
- Song, H., Cai, G.-H., Liang, J., Ao, D.-S., Wang, H., and Yang, Z.-H. (2020). Three-dimensional Culture and Clinical Drug Responses of a Highly Metastatic Human Ovarian Cancer HO-8910PM Cells in Nanofibrous Microenvironments of Three Hydrogel Biomaterials. *J. Nanobiotechnol* 18 (1), 1. doi:10.1186/s12951-020-00646-x
- Soofi, S. S., Last, J. A., Liliensiek, S. J., Nealey, P. F., and Murphy, C. J. (2009). The Elastic Modulus of Matrigel as Determined by Atomic Force Microscopy. *J. Struct. Biol.* 167 (3), 216–219. doi:10.1016/j.jsb.2009.05.005
- Sterzyńska, K., Klejewski, A., Wojtowicz, K., Świerczewska, M., Nowacka, M., Kaźmierczak, D., et al. (2018). Mutual Expression of ALDH1A1, LOX, and Collagens in Ovarian Cancer Cell Lines as Combined CSCs- and ECM-Related Models of Drug Resistance Development. *Ijms* 20 (1), 54. doi:10.3390/ijms20010054
- Stuckelberger, S., and Drapkin, R. (2018). Precious GEMMs: Emergence of Faithful Models for Ovarian Cancer Research. *J. Pathol.* 245 (2), 129–131. doi:10.1002/path.5065
- Sugiyama, T., Kamura, T., Kigawa, J., Terakawa, N., Kikuchi, Y., Kita, T., et al. (2000). Clinical Characteristics of clear Cell Carcinoma of the Ovary. *Cancer* 88 (11), 2584–2589. doi:10.1002/1097-0142(20000601)88:11<2584:aid-cnrc22>3.0.co;2-5
- Sung, H., Ferlay, J., Siegel, R. L., Laversanne, M., Soerjomataram, I., Jemal, A., et al. (2021). Global Cancer Statistics 2020: GLOBOCAN Estimates of Incidence and



- Mortality Worldwide for 36 Cancers in 185 Countries. *CA A. Cancer J. Clin.* 71 (3), 209–249. doi:10.3322/caac.21660
- Swisher, E. M., Lin, K. K., Oza, A. M., Scott, C. L., Giordano, H., Sun, J., et al. (2017). Rucaparib in Relapsed, Platinum-Sensitive High-Grade Ovarian Carcinoma (ARIEL2 Part 1): an International, Multicentre, Open-Label, Phase 2 Trial. *Lancet Oncol.* 18 (1), 75–87. doi:10.1016/s1470-2045(16)30559-9
- Szabova, L., Bupp, S., Kamal, M., Householder, D. B., Hernandez, L., Schlomer, J. J., et al. (2014). Pathway-Specific Engineered Mouse Allograft Models Functionally Recapitulate Human Serous Epithelial Ovarian Cancer. *PLoS ONE* 9 (4), e95649. doi:10.1371/journal.pone.0095649
- Szabova, L., Yin, C., Bupp, S., Guerin, T. M., Schlomer, J. J., Householder, D. B., et al. (2012). Perturbation of Rb, P53, and Brca1 or Brca2 Cooperate in Inducing Metastatic Serous Epithelial Ovarian Cancer. *Cancer Res.* 72 (16), 4141–4153. doi:10.1158/0008-5472.CAN-11-3834
- Takeda, M., Magaki, T., Okazaki, T., Kawahara, Y., Manabe, T., Yuge, L., et al. (2009). Effects of Simulated Microgravity on Proliferation and Chemosensitivity in Malignant Glioma Cells. *Neurosci. Lett.* 463 (1), 54–59. doi:10.1016/j.neulet.2009.07.045
- Tan, T. Z., Ye, J., Yee, C. V., Lim, D., Ngoi, N. Y. L., Tan, D. S. P., et al. (2019). Analysis of Gene Expression Signatures Identifies Prognostic and Functionally Distinct Ovarian clear Cell Carcinoma Subtypes. *EBioMedicine* 50, 203–210. doi:10.1016/j.ebiom.2019.11.017
- Tofani, L. B., Sousa, L. O., Luiz, M. T., Abriata, J. P., Marchetti, J. M., Leopoldino, A. M., et al. (2021). Generation of a Three-Dimensional *In Vitro* Ovarian Cancer Co-culture Model for Drug Screening Assays. *J. Pharm. Sci.* 110 (7), 2629–2636. doi:10.1016/j.xphs.2021.04.003
- Tong, J. G., Valdes, Y. R., Barrett, J. W., Bell, J. C., Stojdl, D., McFadden, G., et al. (2015). Evidence for Differential Viral Oncolytic Efficacy in an *In Vitro* Model of Epithelial Ovarian Cancer Metastasis. *Mol. Ther. - Oncolytics* 2, 15013. doi:10.1038/mto.2015.13
- Trento, M., Munari, G., Carraro, V., Lanza, C., Salmaso, R., Pizzi, S., et al. (2020). Mutational and Immunophenotypic Profiling of a Series of 8 Tubo-Ovarian Carcinomas Revealed a Monoclonal Origin of the Disease. *Int. J. Gynecol. Pathol.* 39 (4), 305–312. doi:10.1097/pgp.0000000000000645
- Tsao, S.-W., Mok, S. C., Fey, E. G., Fletcher, J. A., Wan, T. S. K., Chew, E.-C., et al. (1995). Characterization of Human Ovarian Surface Epithelial Cells Immortalized by Human Papilloma Viral Oncogenes (HPV-E6/7 ORFs). *Exp. Cell Res.* 218 (2), 499–507. doi:10.1006/excr.1995.1184
- Tudrej, P., Kujawa, K. A., Cortez, A. J., and Lisowska, K. M. (2019). Characteristics of *In Vivo* Model Systems for Ovarian Cancer Studies. *Diagnostics* 9 (3), 120. doi:10.3390/diagnostics9030120
- Valabrega, G., Scotto, G., Tuninetti, V., Pani, A., and Scaglione, F. (2021). Differences in PARP Inhibitors for the Treatment of Ovarian Cancer: Mechanisms of Action, Pharmacology, Safety, and Efficacy. *Ijms* 22 (8), 4203. doi:10.3390/ijms22084203
- van den Berg-Bakker, C. A. M., Hagemeijer, A., Franken-Postma, E. M., Smit, V. T. H. B. M., Kuppen, P. J. K., Claasen, H. H. V. R., et al. (1993). Establishment and Characterization of 7 Ovarian Carcinoma Cell Lines and One Granulosa Tumor Cell Line: Growth Features and Cytogenetics. *Int. J. Cancer* 53 (4), 613–620. doi:10.1002/ijc.2910530415
- Varoni, E., Tschon, M., Palazzo, B., Nitti, P., Martini, L., and Rimondini, L. (2012). Agarose Gel as Biomaterial or Scaffold for Implantation Surgery: Characterization, Histological and Histomorphometric Study on Soft Tissue Response. *Connect. Tissue Res.* 53 (6), 548–554. doi:10.3109/03008207.2012.712583
- Vidyasekar, P., Shyamsunder, P., Arun, R., Santhakumar, R., Kapadia, N. K., Kumar, R., et al. (2015). Genome Wide Expression Profiling of Cancer Cell Lines Cultured in Microgravity Reveals Significant Dysregulation of Cell Cycle and MicroRNA Gene Networks. *PLoS ONE* 10 (8), e0135958. doi:10.1371/journal.pone.0135958
- Vinci, M., Gowan, S., Boxall, F., Patterson, L., Zimmermann, M., Court, W., et al. (2012). Advances in Establishment and Analysis of Three-Dimensional Tumor Spheroid-Based Functional Assays for Target Validation and Drug Evaluation. *BMC Biol.* 10 (1), 29. doi:10.1186/1741-7007-10-29
- Vukicevic, S., Kleinman, H. K., Luyten, F. P., Roberts, A. B., Roche, N. S., and Reddi, A. H. (1992). Identification of Multiple Active Growth Factors in Basement Membrane Matrigel Suggests Caution in Interpretation of Cellular Activity Related to Extracellular Matrix Components. *Exp. Cell Res.* 202 (1), 1–8. doi:10.1016/0014-4827(92)90397-q
- Wang, X., Zhao, X., Wang, K., Wu, L., and Duan, T. (2013). Interaction of Monocytes/macrophages with Ovarian Cancer Cells Promotes Angiogenesis *In Vitro*. *Cancer Sci.* 104 (4), 516–523. doi:10.1111/cas.12110
- Wang, Z. C., Birkbak, N. J., Culhane, A. C., Drapkin, R., Fatima, A., Tian, R., et al. (2012). Profiles of Genomic Instability in High-Grade Serous Ovarian Cancer Predict Treatment Outcome. *Clin. Cancer Res.* 18 (20), 5806–5815. doi:10.1158/1078-0432.Ccr-12-0857
- Ward Rashidi, M. R., Mehta, P., Bregenzer, M., Raghavan, S., Fleck, E. M., Horst, E. N., et al. (2019). Engineered 3D Model of Cancer Stem Cell Enrichment and Chemoresistance. *Neoplasia* 21 (8), 822–836. doi:10.1016/j.neo.2019.06.005
- Watkins, J. A., Irshad, S., Grigoriadis, A., and Tutt, A. N. (2014). Genomic Scars as Biomarkers of Homologous Recombination Deficiency and Drug Response in Breast and Ovarian Cancers. *Breast Cancer Res.* 16 (3), 211. doi:10.1186/bcr3670
- Watters, K. M., Bajwa, P., and Kenny, H. A. (2018). Organotypic 3D Models of the Ovarian Cancer Tumor Microenvironment. *Cancers* 10 (8), 265. doi:10.3390/cancers10080265
- Weydert, Z., Lal-Nag, M., Mathews-Greiner, L., Thiel, C., Cordes, H., Küpfer, L., et al. (2020). A 3D Heterotypic Multicellular Tumor Spheroid Assay Platform to Discriminate Drug Effects on Stroma versus Cancer Cells. *SLAS DISCOVERY: Advancing Sci. Drug Discov.* 25 (3), 265–276. doi:10.1177/2472555219880194
- Wilkinson-Ryan, I., Pham, M. M., Sergeant, P., Tafé, L. J., and Berwin, B. L. (2019). A Syngeneic Mouse Model of Epithelial Ovarian Cancer Port Site Metastases. *Translational Oncol.* 12 (1), 62–68. doi:10.1016/j.tranon.2018.08.020
- Wilson, A., Dent, M., Pejovic, T., Hubbard, L., and Radford, H. (1996). Characterisation of Seven Human Ovarian Tumour Cell Lines. *Br. J. Cancer* 74 (5), 722–727. doi:10.1038/bjc.1996.428
- Woo, M. M. M., Salamanca, C. M., Minor, A., and Auersperg, N. (2007). An Improved Assay to Quantitate the Invasiveness of Cells in Modified Boyden chambers. *In Vitro Cell.Dev.Biol.-Animal* 43 (1), 7–9. doi:10.1007/s11626-006-9002-4
- Wu, J., Zheng, Y., Tian, Q., Yao, M., and Yi, X. (2019). Establishment of Patient-derived Xenograft Model in Ovarian Cancer and Its Influence Factors Analysis. *J. Obstet. Gynaecol. Res.* 45 (10), 2062–2073. doi:10.1111/jog.14054
- Wu, T., Gao, Y. Y., Su, J., Tang, X. N., Chen, Q., Ma, L. W., et al. (2021). Three-dimensional Bioprinting of Artificial Ovaries by an Extrusion-Based Method Using Gelatin-Methacryloyl Bioink. *Climacteric* 17, 1–9. doi:10.1080/13697137.2021.1921726
- Wu, Y.-H., Chang, T.-H., Huang, Y.-F., Huang, H.-D., and Chou, C.-Y. (2014). COL11A1 Promotes Tumor Progression and Predicts Poor Clinical Outcome in Ovarian Cancer. *Oncogene* 33 (26), 3432–3440. doi:10.1038/onc.2013.307
- Xu, F., Celli, J., Rizvi, I., Moon, S., Hasan, T., and Demirci, U. (2011). A Three-Dimensional *In Vitro* Ovarian Cancer Coculture Model Using a High-Throughput Cell Patterning Platform. *Biotechnol. J.* 6 (2), 204–212. doi:10.1002/biot.201000340
- Xu, G., Yin, F., Wu, H., Hu, X., Zheng, L., and Zhao, J. (2014). *In Vitro* ovarian Cancer Model Based on Three-Dimensional Agarose Hydrogel. *J. Tissue Eng.* 5 (0), 204173141352043. doi:10.1177/2041731413520438
- Xu, S., Xu, H., Wang, W., Li, S., Li, H., Li, T., et al. (2019). The Role of Collagen in Cancer: from Bench to Bedside. *J. Transl. Med.* 17 (1), 309. doi:10.1186/s12967-019-2058-1
- Xue, Y., Morris, J. L., Yang, K., Fu, Z., Zhu, X., Johnson, F., et al. (2021). SMARCA4/2 Loss Inhibits Chemotherapy-Induced Apoptosis by Restricting IP3R3-Mediated Ca<sup>2+</sup> Flux to Mitochondria. *Nat. Commun.* 12 (1), 5404. doi:10.1038/s41467-021-25260-9
- Yamada, Y., Yoshida, C., Hamada, K., Kikkawa, Y., and Nomizu, M. (2020). Development of Three-Dimensional Cell Culture Scaffolds Using Laminin Peptide-Conjugated Agarose Microgels. *Biomacromolecules* 21 (9), 3765–3771. doi:10.1021/acs.biomac.0c00871
- Yamawaki, K., Mori, Y., Sakai, H., Kanda, Y., Shiokawa, D., Ueda, H., et al. (2021). Integrative Analyses of Gene Expression and Chemosensitivity of Patient-Derived Ovarian Cancer Spheroids Link G6PD-Driven Redox Metabolism to Cisplatin Chemoresistance. *Cancer Lett.* 521, 29–38. doi:10.1016/j.canlet.2021.08.018
- Yanagibashi, T., Gorai, I., Nakazawa, T., Miyagi, E., Hirahara, F., Kitamura, H., et al. (1997). Complexity of Expression of the Intermediate Filaments of Six New Human Ovarian Carcinoma Cell Lines: New Expression of Cytokeratin 20. *Br. J. Cancer* 76 (7), 829–835. doi:10.1038/bjc.1997.471

- Yang, C., Hillas, P. J., Baez, J. A., Nokelainen, M., Balan, J., Tang, J., et al. (2004). The Application of Recombinant Human Collagen in Tissue Engineering. *BioDrugs* 18 (2), 103–119. doi:10.2165/00063030-200418020-00004
- Yang, Z., Xu, H., and Zhao, X. (2020). Designer Self-Assembling Peptide Hydrogels to Engineer 3D Cell Microenvironments for Cell Constructs Formation and Precise Oncology Remodeling in Ovarian Cancer. *Adv. Sci.* 7 (9), 1903718. doi:10.1002/advs.201903718
- Yang, Z., and Zhao, X. (2011). A 3D Model of Ovarian Cancer Cell Lines on Peptide Nanofiber Scaffold to Explore the Cell-Scaffold Interaction and Chemotherapeutic Resistance of Anticancer Drugs. *Ijpn* 6, 303–310. doi:10.2147/IJN.S15279
- Yi, J., Lin, Y., Yicong, W., Chengyan, L., Shulin, Z., and Wenjun, C. (2020). Effect of Macrophages on Biological Function of Ovarian Cancer Cells in Tumor Microenvironment *In Vitro*. *Arch. Gynecol. Obstet.* 302 (4), 1009–1017. doi:10.1007/s00404-020-05719-8
- Yoshiya, N., Adachi, S., Misawa, Y., Yuzawa, H., Honda, T., Kanazawa, K., et al. (1989). Isolation of Cisplatin-Resistant Subline from Human Ovarian Cancer Cell Line and Analysis of its Cell-Biological Characteristics. *Nihon Sanka Fujinka Gakkai Zasshi* 41 (1), 7–14.
- Yu, J. W., Bhattacharya, S., Yanamandra, N., Kilian, D., Shi, H., Yadavilli, S., et al. (2018). Tumor-immune Profiling of Murine Syngeneic Tumor Models as a Framework to Guide Mechanistic Studies and Predict Therapy Response in Distinct Tumor Microenvironments. *PLoS ONE* 13 (11), e0206223. doi:10.1371/journal.pone.0206223
- Yuan, J., Yi, K., and Yang, L. (2021). LncRNA NEAT1 Promotes Proliferation of Ovarian Cancer Cells and Angiogenesis of Co-incubated Human Umbilical Vein Endothelial Cells by Regulating FGF9 through Sponging miR-365. *Medicine (Baltimore)* 100 (3), e23423. doi:10.1097/md.00000000000023423
- Zakarya, R., Howell, V. M., and Colvin, E. K. (2020). Modelling Epithelial Ovarian Cancer in Mice: Classical and Emerging Approaches. *Ijms* 21 (13), 4806. doi:10.3390/ijms21134806
- Zarrintaj, P., Manouchehri, S., Ahmadi, Z., Saeb, M. R., Urbanska, A. M., Kaplan, D. L., et al. (2018). Agarose-based Biomaterials for Tissue Engineering. *Carbohydr. Polym.* 187, 66–84. doi:10.1016/j.carbpol.2018.01.060
- Zhai, Y., Wu, R., Kuick, R., Sessine, M. S., Schulman, S., Green, M., et al. (2017). High-grade Serous Carcinomas Arise in the Mouse Oviduct via Defects Linked to the Human Disease. *J. Pathol.* 243 (1), 16–25. doi:10.1002/path.4927
- Zhang, L., Yang, N., Conejo Garcia, J.-R., Mohamed, A., Benencia, F., Rubin, S. C., et al. (2002). Generation of a Syngeneic Mouse Model to Study the Effects of Vascular Endothelial Growth Factor in Ovarian Carcinoma. *Am. J. Pathol.* 161 (6), 2295–2309. doi:10.1016/s0002-9440(10)64505-1
- Zhang, S., Dolgalev, I., Zhang, T., Ran, H., Levine, D. A., and Neel, B. G. (2019). Both fallopian Tube and Ovarian Surface Epithelium Are Cells-Of-Origin for High-Grade Serous Ovarian Carcinoma. *Nat. Commun.* 10 (1), 5367. doi:10.1038/s41467-019-13116-2
- Zhao, L., Xiu, J., Liu, Y., Zhang, T., Pan, W., Zheng, X., et al. (2019a). A 3D Printed Hanging Drop Dripper for Tumor Spheroids Analysis without Recovery. *Sci. Rep.* 9 (1), 1. doi:10.1038/s41598-019-56241-0
- Zhao, Y., Cao, J., Melamed, A., Worley, M., Gockley, A., Jones, D., et al. (2019b). Losartan Treatment Enhances Chemotherapy Efficacy and Reduces Ascites in Ovarian Cancer Models by Normalizing the Tumor Stroma. *Proc. Natl. Acad. Sci. USA* 116 (6), 2210–2219. doi:10.1073/pnas.1818357116
- Zhou, N., Ma, X., Bernaerts, K. V., Ren, P., Hu, W., and Zhang, T. (2020). Expansion of Ovarian Cancer Stem-like Cells in Poly(ethylene Glycol)-Cross-Linked Poly(methyl Vinyl Ether-Alt-Maleic Acid) and Alginate Double-Network Hydrogels. *ACS Biomater. Sci. Eng.* 6 (6), 3310–3326. doi:10.1021/acsbomaterials.9b01967
- Zhou, N., Ma, X., Hu, W., Ren, P., Zhao, Y., and Zhang, T. (2021). Effect of RGD Content in Poly(ethylene Glycol)-Crosslinked Poly(methyl Vinyl Ether-Alt-Maleic Acid) Hydrogels on the Expansion of Ovarian Cancer Stem-like Cells. *Mater. Sci. Eng. C* 118, 111477. doi:10.1016/j.msec.2020.111477
- Zhu, M., Wang, Y., Ferracci, G., Zheng, J., Cho, N.-J., and Lee, B. H. (2019). Gelatin Methacryloyl and its Hydrogels with an Exceptional Degree of Controllability and Batch-To-Batch Consistency. *Sci. Rep.* 9 (1), 1. doi:10.1038/s41598-019-42186-x

**Conflict of Interest:** The authors declare that the research was conducted in the absence of any commercial or financial relationships that could be construed as a potential conflict of interest.

**Publisher's Note:** All claims expressed in this article are solely those of the authors and do not necessarily represent those of their affiliated organizations, or those of the publisher, the editors, and the reviewers. Any product that may be evaluated in this article, or claim that may be made by its manufacturer, is not guaranteed or endorsed by the publisher.

Copyright © 2022 Yee, Dickson, Muntasir, Ma and Marsh. This is an open-access article distributed under the terms of the Creative Commons Attribution License (CC BY). The use, distribution or reproduction in other forums is permitted, provided the original author(s) and the copyright owner(s) are credited and that the original publication in this journal is cited, in accordance with accepted academic practice. No use, distribution or reproduction is permitted which does not comply with these terms.

# CRISPR single base-editing: *in silico* predictions to variant clonal cell lines

Kristie-Ann Dickson<sup>1</sup>, Natisha Field<sup>1</sup>, Tiane Blackman<sup>1</sup>, Yue Ma<sup>1</sup>, Tao Xie<sup>1</sup>, Ecem Kurangil<sup>1</sup>, Sobia Idrees<sup>2</sup>, Senani N.H. Rathnayake<sup>3</sup>, Rashad M. Mahbub<sup>3</sup>, Alen Faiz<sup>3</sup> and Deborah J. Marsh<sup>1,\*</sup>

<sup>1</sup>Translational Oncology Group, Faculty of Science, School of Life Sciences, University of Technology Sydney, Ultimo, NSW 2007, Australia

<sup>2</sup>Faculty of Science, School of Life Sciences, Centre for Inflammation, Centenary Institute and the University of Technology Sydney, Sydney, NSW 2007, Australia

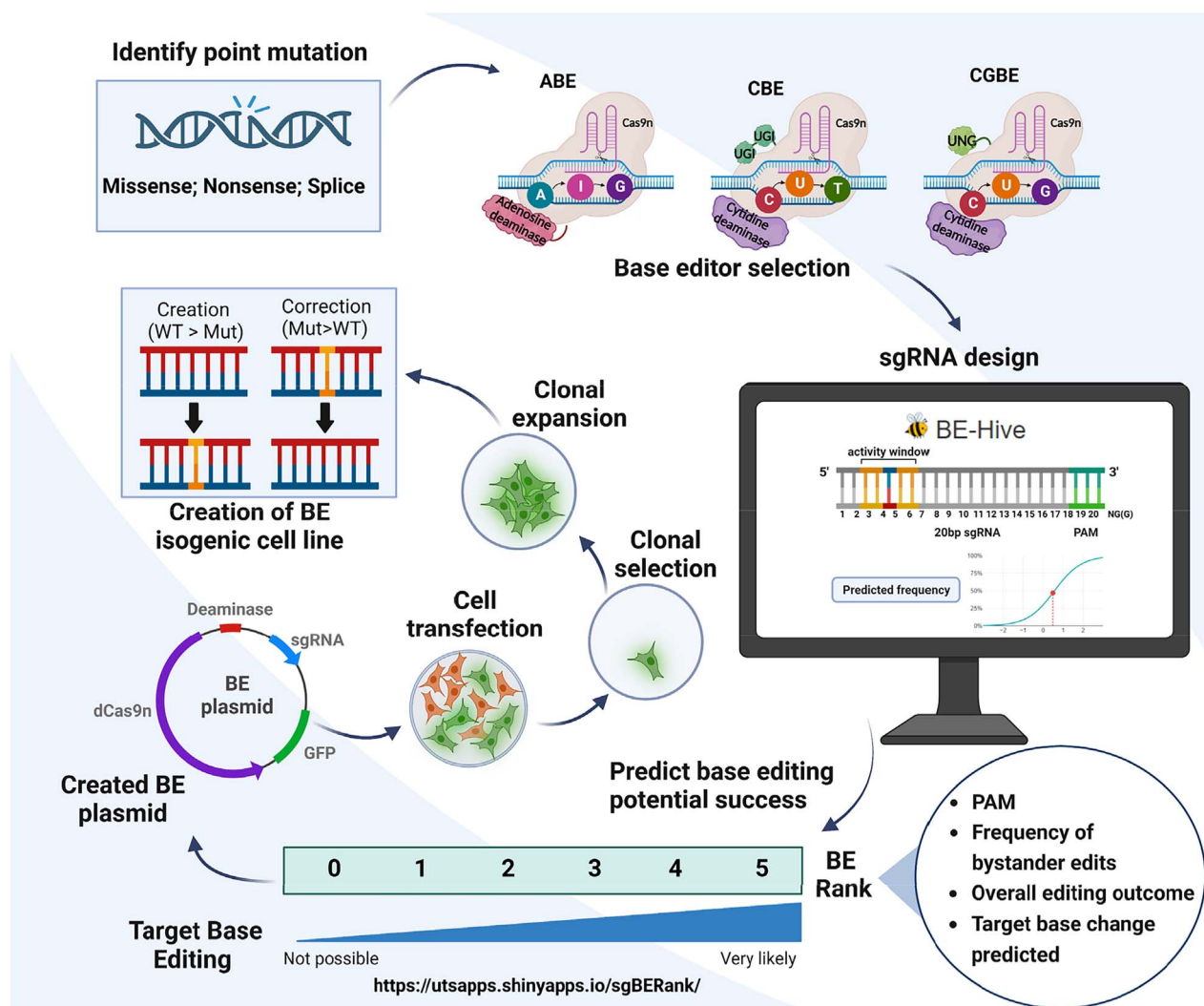
<sup>3</sup>Respiratory Bioinformatics and Molecular Biology (RBMB), Faculty of Science, School of Life Sciences, University of Technology Sydney, Ultimo, NSW 2007, Australia

\*To whom correspondence should be addressed: DJ Marsh, School of Life Sciences, Faculty of Science, University of Technology Sydney, Ultimo, NSW 2007, Australia. Tel: +61 2 9514 7574; Email: Deborah.Marsh@uts.edu.au

## Abstract

Engineering single base edits using CRISPR technology including specific deaminases and single-guide RNA (sgRNA) is a rapidly evolving field. Different types of base edits can be constructed, with cytidine base editors (CBEs) facilitating transition of C-to-T variants, adenine base editors (ABEs) enabling transition of A-to-G variants, C-to-G transversion base editors (CGBEs) and recently adenine transversion editors (AYBE) that create A-to-C and A-to-T variants. The base-editing machine learning algorithm BE-Hive predicts which sgRNA and base editor combinations have the strongest likelihood of achieving desired base edits. We have used BE-Hive and TP53 mutation data from The Cancer Genome Atlas (TCGA) ovarian cancer cohort to predict which mutations can be engineered, or reverted to wild-type (WT) sequence, using CBEs, ABEs or CGBEs. We have developed and automated a ranking system to assist in selecting optimally designed sgRNA that considers the presence of a suitable protospacer adjacent motif (PAM), the frequency of predicted bystander edits, editing efficiency and target base change. We have generated single constructs containing ABE or CBE editing machinery, an sgRNA cloning backbone and an enhanced green fluorescent protein tag (EGFP), removing the need for co-transfection of multiple plasmids. We have tested our ranking system and new plasmid constructs to engineer the p53 mutants Y220C, R282W and R248Q into WT p53 cells and shown that these mutants cannot activate four p53 target genes, mimicking the behaviour of endogenous p53 mutations. This field will continue to rapidly progress, requiring new strategies such as we propose to ensure desired base-editing outcomes.

## Graphical Abstract



## Introduction

Base-editing technology can facilitate exquisite control to the level of alteration of a single nucleotide, and when applied to cancer-related genes, can enable the expansion of *in vitro* models to study the effect of gene mutations in a range of malignancies. The use of CRISPR-Cas9 to engineer cell line knockouts (KOs) of genes-of-interest (GOIs) is now mainstream in many cancer research laboratories and large scale CRISPR KO screens to identify synthetic lethal interactions are increasingly reported (1–4). The ability to study specific cancer-related point mutations, however, either by editing them from wild-type (WT) sequence or correcting them to WT in cancer cell lines, has remained elusive until recently. The generation of isogenic cancer cell line panels where single nucleotide changes are engineered enables focus on the effect of very specific changes of known pathogenic clinical consequence under conditions where background biological ‘noise’ is effectively removed. Engineered isogenic panels that may comprise loss-of-function (LOF) mutants, gain-of-function (GOF) mutants and WT cell lines constructed on identical parental cell line backgrounds are powerful tools for drug screening and understanding cancer cell biology, including identifying synthetic lethal interactions (5–7).

Not all point mutations can currently be engineered using CRISPR-Cas9 technology, either due to the nature of the alteration or the surrounding sequence. CRISPR base-editing utilizes a deaminase enzyme and components of CRISPR-Cas9 systems to generate point mutations at specific nucleotides in cellular DNA without creating double strand breaks (DSBs) (8). Cytidine base editors (CBEs) were the first editors described, followed by adenine base editors (ABEs). CBEs enable the transition of cytosine (C) to thymine (T), whereas ABEs facilitate adenine (A) to a guanine (G) transition base substitution (9). C•G-to-G•C transversion base editors (CGBEs) have also been described (10,11). More recently, an adenine transversion base editor (BE), capable of editing A-to-C and A-to-T (AYBE), has been reported (12).

CBEs were created by fusing a catalytically inactivated Cas9 nickase (Cas9n) that retained its ability to bind to, but not cleave, double stranded DNA, with a cytidine deaminase enzyme such as apolipoprotein B mRNA editing enzyme complex-1 (APOBEC1) that is a C to uracil (U) RNA editing enzyme (9,13,14). Cas9n functions to unfold the DNA and generate a nick on one DNA strand only, forming a single-stranded DNA (ssDNA) target that allows cytidine deaminase to create a C to U edit, which is



read as a T upon DNA repair, explaining the power of CBEs to create irreversible C•G to T•A conversions. As U does not occur endogenously in DNA, uracil DNA glycosylase inhibitor domains (UGIs) are also included in CBEs to prevent the correction of the edited base (13). In CGBEs, UGIs are replaced with uracil DNA N-glycosylase (UNG) which favours C•G-to-G•C permanent conversions (10,11).

A major challenge in the development of ABEs has been that unlike for cytidine deaminase enzymes, there is no naturally occurring human adenine deaminase that acts on DNA. In order to overcome this, mutations were introduced into a tRNA adenosine deaminase (TadA) from *Escherichia coli* through challenge with kanamycin to enrich for editing efficiencies (15). This 'evolved' or mutant TadA edited adenosine to inosine (I), which is read as a G upon DNA repair. WT and mutant evolved TadA were fused to a catalytically impaired Cas9n resulting in an ABE that targets and irreversibly converts A•T into G•C using a similar process as for CBEs described above (15).

The most frequently used Cas9 nuclease is derived from *Streptococcus pyogenes* (SpCas9), and requires the presence of a protospacer adjacent motif (PAM) 'NGG', where 'N' is any nucleotide, directly following the target genomic DNA (gDNA) sequence located by a 20 base pair single-guide RNA (sgRNA). This strict requirement for an 'NGG' in order for Cas9 to recognize its targets places further restriction as to the nucleotides that can be edited by BEs. Representing a strong advance is the engineering of an 'NG' PAM site (SpCas9-NG) that can increase the range of targetable genomic loci (16). An expanded SpCas9 variant (xCas9) has also been evolved to recognize PAM sequences including 'NG', 'GAA' and 'GAT', further increasing the range of sequence that can be targeted (17). Investigation of bacteria other than *S. pyogenes* is likely to further expand the range of recognizable PAM sequences (18,19).

As noted, sgRNA recognizes the specific target gDNA region for editing, directing the Cas9 nuclease to this region. In order to edit a single nucleotide, the target base needs to be located within the editing window of the BE, usually at position 4–7 bp in the sgRNA (9). If multiple editable bases exist within or near the editing window, this can result in editing of additional bases or 'bystander' editing in addition to, or separately from, the target base. In order to limit bystander editing, BE variants have been developed. Wide-window editors increase the chance of an appropriately positioned PAM, but may compromise on purity of the desired base edit. Conversely, narrow-window editors strategically avoid bystander edits, however their position is restricted by location of the PAM (20–22). For example, the introduction of bystander variants can be reduced in CBEs by engineering the cytidine deaminase domain on APOBEC3A (the engineered deaminase referred to as eA3A) to favour deamination of cytidines in specific motifs (23). Further, next-generation CBEs that demonstrate reduced guide-independent off-target editing profiles at the same time as having the same or improved on-target editing efficiencies have also been identified (24).

An sgRNA design resource for base-editing has recently become available which predicts base-editing efficiency of a specific target base and any potential bystander edits. BE-Hive uses machine learning algorithms to determine which BE and sgRNA combinations are predicted to achieve specific genetic edits in a sequence of interest (25). This model was initially trained on actual experimental data which used 11 CBE and ABEs to generate single nucleotide edits at 38538 sites in human (HEK293T) and mouse (mESC) cell line backgrounds (25). CGBEs were recently

incorporated into the BE-Hive predictive algorithm (10); however, to date, AYBEs are yet to be included as part of this predictive modelling.

Here, we present a research pipeline from *in silico* analyses using the predictive algorithm BE-Hive, to proof-of-principle *in vitro* experiments that can be used for single nucleotide gene editing in cancer-related, and other, GOIs. As an exemplar, we chose to interrogate mutations in the p53 tumour suppressor gene, TP53, given that this gene is mutated in over 50% of different human malignancies, with the majority of mutations being missense, therefore it is of wide interest (26,27). The proof of principle cohort we have selected is one of high-grade serous ovarian cancers (HGSOC) reported in The Cancer Genome Atlas (TCGA) where approaching 100% of these tumours have a somatic mutation in TP53 (28). Using data from BE-Hive, we have developed an automated ranking system for predicting success of specific base edits, both to generate and correct mutations of interest for the purpose of discovery science, including for drug screening. Lastly, we have engineered existing CRISPR BE vectors to test the accuracy of our ranking system for creating an isogenic panel of ovarian cancer cell lines focused on the introduction of TP53 missense mutations into a WT TP53 cell line resulting in loss of regulation of p53 target genes.

## Results

### Development of a ranking system using BE-Hive to predict success of base-editing dependent upon the sgRNA design

Machine learning algorithms provide information on the prediction frequency of editing a particular target base and the frequency of any bystander edits in the editing window for different base-editing constructs, as well as overall editing efficiency based on the surrounding sequence. Additional manual determination of an appropriate PAM site (usually NGG or NG depending on the BE construct) directly following the 20-bp sgRNA is essential. We have developed a 0–5 ranking system to predict the success of editing a given target base in human sequence utilizing a distinct sgRNA design and the base-editing outcome criteria predicted by BE-Hive based on data generated in the HEK293T cell background and where available the mESC mouse cell background (Supplementary Material, Tables S2–S5). A rank of 0 states that the particular base of interest cannot be edited, whereas a rank of 5 indicates the most favourable editing outcome. Overall editing outcomes that are predicted by BE-Hive as 'above average' for a particular genetic region, are ranked higher compared with those regions predicted to have 'below average' editing outcomes. Additionally, the absence of bystander edits in the editing window, or sgRNA with bystander edits occurring at a predicted editing frequency less than the target base are more conducive to a potentially successful outcome and achieve a higher rank. Our ranking criteria are explained in detail in Table 1. We have made our ranking system's automated user-friendly online web server (<https://utsapps.shinyapps.io/sgBERank/>) available for researchers to assess the likelihood of achieving single base edits.

### *In silico* analyses of likelihood of successful base-editing to introduce or revert TP53 mutations

Next, we sought to conduct *in silico* analyses using our ranking system on TP53 mutation data from the TCGA-HGSOC cohort to

**Table 1.** Ranking system of likelihood of successful single base-editing with designed sgRNAs

Rank	Criteria
0	<ul style="list-style-type: none"> <li>No available PAM sequence, and</li> <li>High frequency of bystander edits that inhibit exclusive editing of target base, or</li> <li>Above average overall editing outcome; target base change predicted &lt;1%, or</li> <li>Average overall editing outcome; target base change predicted &lt;5%, or</li> <li>Below average overall editing outcome; target base change predicted &lt;15%</li> </ul>
1	<ul style="list-style-type: none"> <li>PAM sequence, and</li> <li>Above average overall editing outcome; target base change predicted 1–5%; bystander edits &gt; targeted base change, or</li> <li>Average editing overall editing outcome; target base change predicted 5–10%; bystander edits &gt; targeted base change, or</li> <li>Below average overall editing outcome; target base change predicted 15–40%</li> </ul>
2	<ul style="list-style-type: none"> <li>PAM sequence, and</li> <li>Above average overall editing outcome; target base change predicted 5–10%; bystander edits &gt; targeted base change, or</li> <li>Average editing overall editing outcome; target base change predicted &gt;10%; bystander edits &gt; targeted base change, or</li> <li>Below average overall editing outcome; target base change predicted &gt;40%; bystander edits &lt; targeted base change or no bystander edits &gt;10%</li> </ul>
3	<ul style="list-style-type: none"> <li>PAM sequence, and</li> <li>Above average overall editing outcome; target base change predicted &gt;10%; bystander edits &gt; targeted base change, or</li> <li>Average editing overall editing outcome; target base change predicted &gt;10%; bystander edits &lt; targeted base change, or</li> <li>Below average overall editing outcome; target base change predicted &gt;60%; no bystander edits &gt;15%</li> </ul>
4	<ul style="list-style-type: none"> <li>PAM sequence, and</li> <li>Above average overall editing outcome; target base change predicted &gt;10%; bystander edits &lt; targeted base change, or</li> <li>Average editing overall editing outcome; target base change predicted &gt;40%; no bystander edits &gt;10%</li> </ul>
5	<ul style="list-style-type: none"> <li>PAM sequence, and</li> <li>Above average overall editing outcome; target base change predicted &gt;60%, no bystander edits &gt;10%</li> </ul>

Ranking system 0 (cannot achieve the desired base edit) to 5 (high likelihood of achieving the desired base edit) is based on BE-Hive predictions (25). Automated sgRNA BE rank can be determined using sgBERank (<https://utsapps.shinyapps.io/sgBERank/>).

test the likelihood of engineering both clinically reported TP53 mutations from WT sequence, or correcting TP53 mutations to WT sequence for the purpose of fundamental discovery science. The TCGA-HGSOC cohort provides whole exome DNA sequencing data on 316 tumours, around 96% of which had a mutation in TP53 (28). Of the 187 tumours harbouring missense TP53 mutations, only 67% (126 of 187) were transition mutations, 66% (83 of 126) of which were A-to-G or T-to-C mutations and 34% (43 of 126) were C-to-T or G-to-A changes. Transversion missense mutations were found in 33% (61 of 187) of patients, with C-to-G transversion point mutations observed in only 16% of patients (10 of 61) with missense mutations (Supplementary Material, Fig. S1). In sum, 81 unique TP53 point mutations were interrogated for this study, specifically 55 missense, 11 nonsense and 15 splice site mutations.

### Predicted reversion efficiency of TP53 mutations to WT by base-editing

We have ranked the likelihood of success of engineering reversion missense, nonsense and splice site TP53 mutations reported in the TCGA-HGSOC dataset using BE-Hive and our ranking system (Table 1). The base-editing rank of reverting 55 unique TP53 missense mutations to WT sequence with ABEs (ABEmax and CP1041-ABEmax); CBEs (eA3A and BE4max) or CGBE (CG-eA3A) is shown (Fig. 1A, Supplementary Material, Table S2). Overall, reversion is more probable for A-to-G (and T-to-C) edits compared with C-to-T (and G-to-A) or C-to-G (and G-to-C) edits based on BE-Hive analyses.

Next, we sought to focus on TP53 missense mutations that occurred in four or more patients in the TCGA-HGSOC cohort given that there may be greater interest in studying these

higher frequency mutations. Pathogenic accumulation and gain-of-function (GOF) TP53 mutations R175H, C176Y, R282W and R248W were predicted to be capable of reversion to WT by base-editing (rank 4–5), whereas H179R, I195T and R248Q were unable to be edited with a rank of 0 due to the absence of an available PAM site, low or no predicted editing of the target base, a high number of bystander base edits and/or an overall 'below average' editing of the sequence region flanking the target base (Fig. 1B, Supplementary Material, Table S2).

TP53 point nonsense mutations resulting in LOF occurred in 29 patients in the TCGA-HGSOC cohort of which 69% (20 of 29) had the potential to be edited to WT with ABE, CBE or CGBE editors, while splice point mutations were reported in 34 patients of which 59% (20 of 34) had the potential to be reverted to WT. The editing rank for the 11 unique nonsense and 15 unique splice mutations are shown (Fig. 1C and D, Supplementary Material, Tables S3 and S4). All nonsense mutations require editing using an ABE for reversion to WT, with 82% (9 of 11) having a rank of  $\geq 3$ , compared with splice mutations where only 53% (8 of 15) had a rank of  $\geq 3$ . Missense mutations were predicted to be edited successfully in 64% (35 of 55) of cases that were allocated a rank of  $\geq 3$ . The selection of an optimal base-editing construct that maximizes editing potential of a specific target base and minimizes bystander edits is very important. Although both ABE editors used in our study had similar ranks for reverting TP53 missense mutations, for the CBE editors, a higher likelihood of base-editing success, as defined by our ranking system, was seen using either eA3A or BE4max BEs, with some targets displaying a similar likelihood of success using either editor (Fig. 1A, C and D). A number of ovarian cancer cell lines harbour endogenous TP53 point mutations that are also reported in the TCGA-HGSOC cohort, including TYK-nu, COV362,

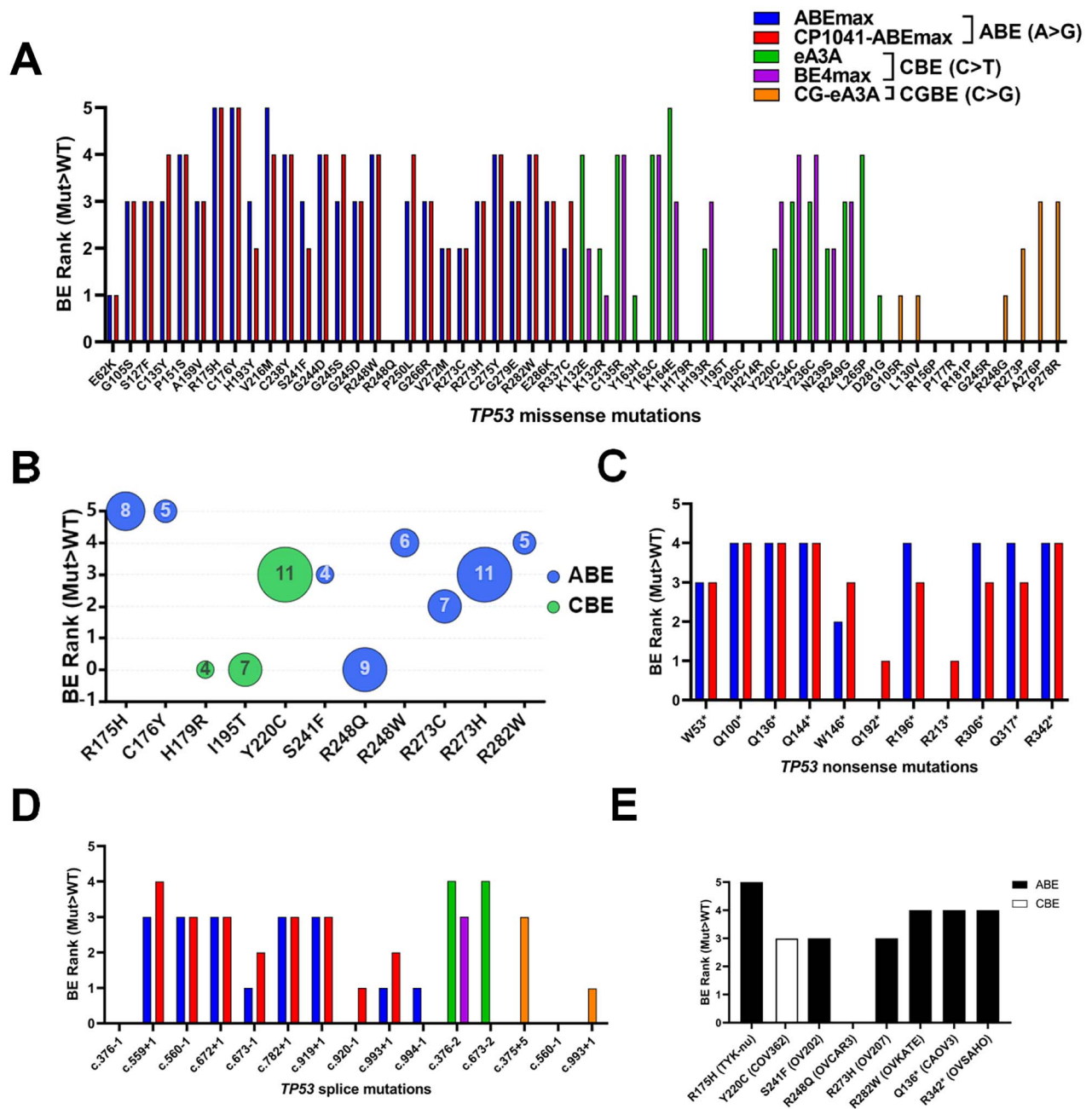


**Figure 1.** Predicted efficiencies of reverting TP53 mutations identified in the TCGA-HGSOC cohort to WT sequence using ABE, CBE and CGBE editors. (A) BE ranks (0–5 from Table 1) for converting missense TP53 mutations to WT. (B) BE ranks for reverting the most frequent TP53 missense mutations in the TCGA-HGSOC cohort to WT where the bubble size is indicative of the absolute number of tumours with a specific TP53 mutation using the best BE construct. BE ranks for reverting TP53 (C) nonsense and (D) splice site mutations to WT sequence. (E) BE ranks (0–5) for the best BE construct predicted to revert endogenous missense and nonsense TP53 mutations in ovarian cancer cell lines to WT sequence.

OV202, OVCAR-3, OV207, OVKATE, CaOV3 and OVSAHO (Fig. 1E) (29,30). The R248Q TP53 mutation in OVCAR-3 cells is the only mutation amongst these that is currently predicted to be unable to be reverted to WT due to the absence of a nearby PAM site.

### Predicted efficiency of engineering pathogenic TP53 mutations from WT sequence

Next, we used base-editing predictions to advise on the likelihood of engineering pathogenic TP53 point mutations, reported in the TCGA-HGSOC cohort, from a WT TP53 genetic background for the purpose of creating isogenic panels to be used in discovery science. A greater chance of successful introduction of a missense

mutation, a rank of  $\geq 3$ , was predicted for A-to-G edits (56%; 10 of 18), and C-to-T base substitutions (44%; 12 of 27) compared with C-to-G missense base edits (0%, 0/10) for which there were no predictions above a rank of 2. (Fig. 2A). The frequent pathogenic TP53 mutations that occurred in four or more patients in the TCGA-HGSOC cohort, R175H, I195T, Y220C and R282W had a prediction rank of 4 for engineering from WT sequence. Only R248W is predicted to be unable to be edited due to the absence of an appropriate PAM site assigning it a rank score of 0 (Fig. 2B). Endogenously, nonsense and splice mutations in the TCGA-HGSOC cohort result primarily from C-to-T base substitutions and are predicted to be engineered from WT sequence *in vitro* in 45% (5 of 11) and 50% (5

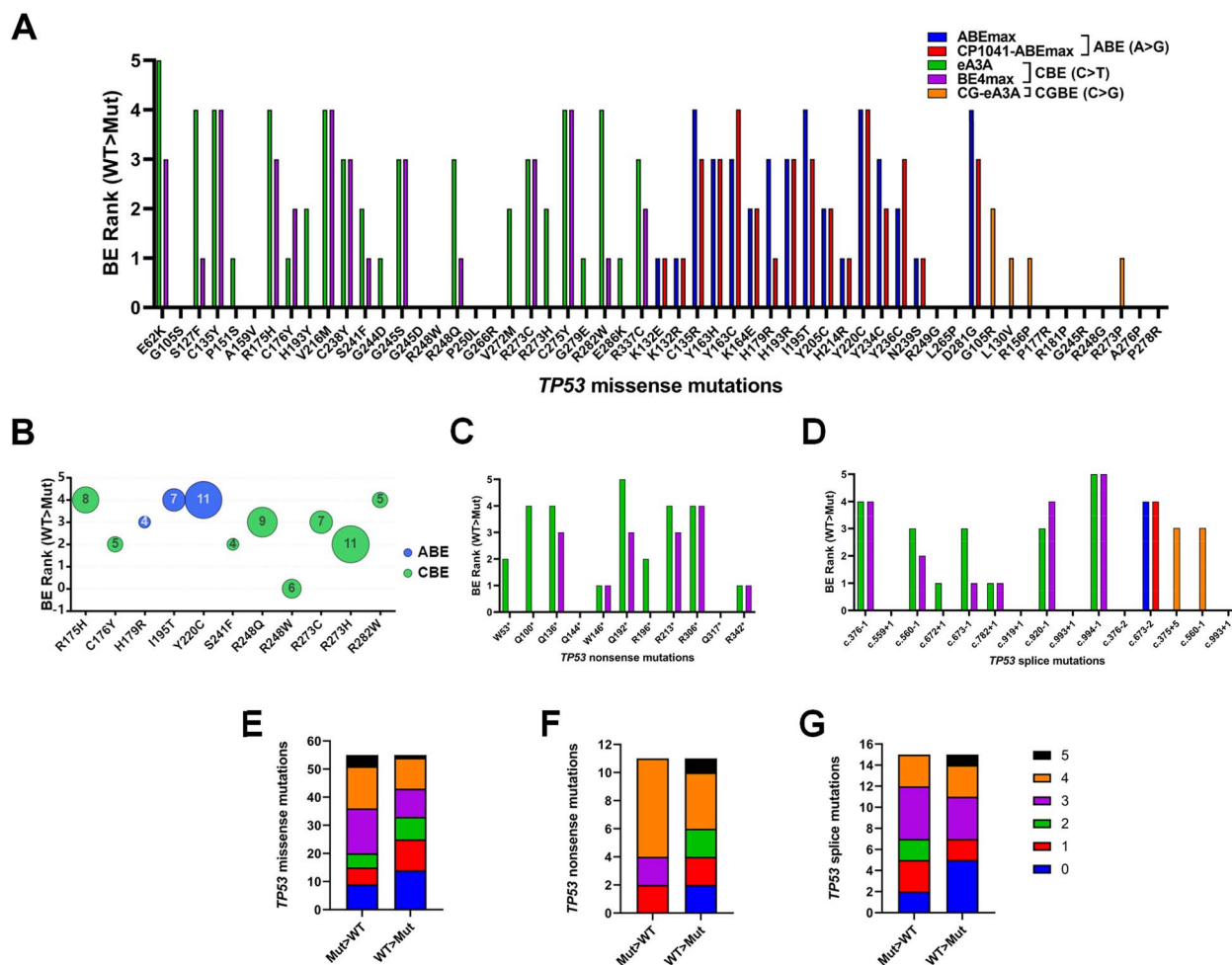


**Figure 2.** Predicted efficiencies of engineering TP53 mutations identified in the TCGA-HGSOC cohort from WT sequence using ABE, CBE and CGBE editors. (A) BE ranks (0–5 from Table 1) for engineering TP53 missense mutations from the WT sequence. (B) BE ranks for engineering the most frequent TP53 missense mutations in the TCGA-HGSOC cohort from WT sequence where the bubble size is indicative of the absolute number of tumours with a specific TP53 mutation using the best BE construct. BE ranks for engineering TP53 (C) nonsense and (D) splice site mutations from WT sequence. Rank summaries for converting WT into TP53 mutant (MUT) and TP53 MUT to WT for (E) missense, (F) nonsense and (G) splice site mutations using the optimal BE construct.

of 10) of cases, respectively (Fig. 2C and D). Overall, 53% (8 of 15) splice mutations were given a prediction rank of  $\geq 3$  (Fig. 2D).

Of interest, collectively for the three categories of TP53 point mutations; missense, nonsense and splice site, the likelihood of single bases being able to be reverted to WT sequence, was more highly ranked compared with single bases being engineered from WT to mutant sequence (Fig. 2E, F and G). Conversely, for the more frequent TP53 missense mutations occurring in  $\geq 4$  patients, 73% (8 of 11) had a prediction rank of  $\geq 2$  for reverting from mutant to WT, whereas 91% (10 of 11) had a rank of  $\geq 2$  for the likelihood of engineering these TP53 mutants into WT sequence.

### Testing predictive TP53 base edits for CBE and ABE BEs in vitro

As described, ABE and CBE plasmids containing sgRNA expression, Cas9n and base-editing deaminase were constructed by fusing base-editing machinery from pCMV-CP1041-ABEmax or pCMV-eA3A-BE5-NG with the PX458 vector backbone (minus Cas9) containing the gRNA scaffold sequence for sgRNA cloning. EGFP was subsequently cloned into these plasmids. These new BE

constructs allow for a single plasmid-based transfection, permitting base-editing machinery and sgRNA expression simultaneously, easily identified by an EGFP tag after cell transfection (Fig. 3A and B).

A highly ranked sgRNA designed to engineer the Y220C (c.659A>G) TP53 mutation was cloned into the ABE vector CP1041-ABEmax-sgRNA-EGFP. Similarly, for the R248Q (c.743G>A) and R282W (c.844C>T) TP53 mutations, sgRNA were cloned into the CBE vector eA3A-sgRNA-EGFP at *BbsI* sites (Supplementary Material, Table S1). These pathogenic missense TP53 mutations were frequently reported in HGSOCs in the TCGA-ovarian cohort (Y220C, 11 patients; R248Q, 9 patients; and R282W, 5 patients) and are present in commercially available HGSOC cell lines COV362, OVCAR3 and OVKATE respectively. Successful transfection of BE constructs determined by EGFP expression in the nuclei of cells, was observed in A2780.b1 clonal cells for all constructs after 24 h without impacting cell viability (Fig. 3C and D). Cell sorting based on EGFP expression revealed transfection efficiencies of 10.1, 13 and 11.4% for Y220C, R248Q and R282W, respectively, compared with reagent control that correlated with EGFP count determined by IncuCyte live cell imaging (Fig. 3D and E).



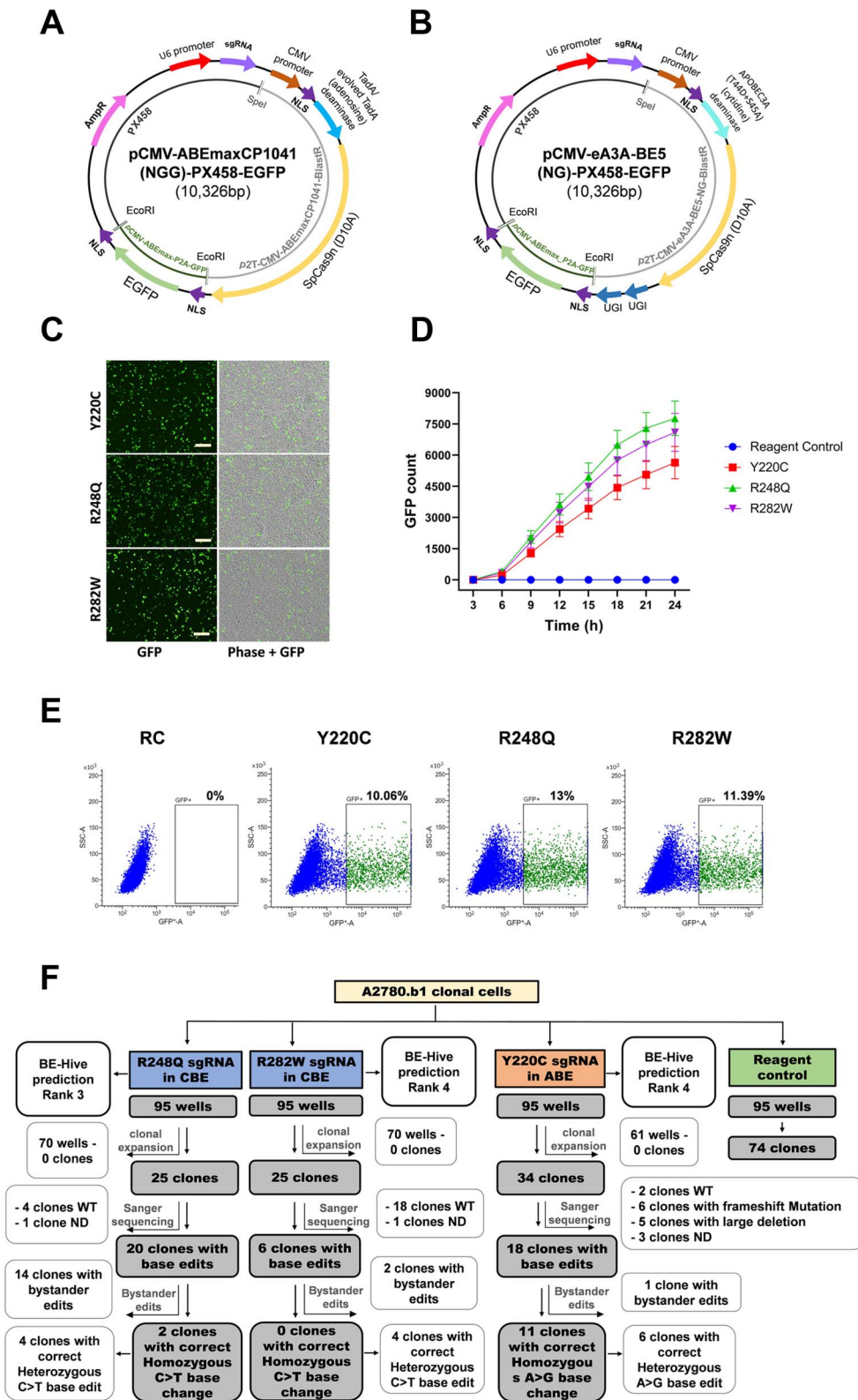


**Figure 3.** Generation of a TP53 isogenic cell line panel in A2780 parental cells. Vector maps of (A) ABE and (B) CBE plasmid constructs where we have engineered single plasmids containing base-editing machinery, sgRNA cloning backbone and enhanced green fluorescent protein (EGFP) to create pCMV-ABEmaxCP1041-(NGG)-PX458-EGFP (abbreviated to: CP1041-ABEmax-sgRNA-EGFP) and pCMV-eA3A-BE5-(NG)-PX458-EGFP (abbreviated to: eA3A-sgRNA-EGFP). (C) Cell images of EGFP nuclear expression in the A2780 clonal parental cell line (A2780.b1), and (D) number of cells with green nuclei (EGFP) measured every 3 h 24 h post transfection indicating successful transfection of base-editing plasmid constructs expressing sgRNA to engineer the p53 mutants Y220C, R248Q and R282W. Images were generated using IncuCyte live cell imaging; 4× objective, scale=200 μm. (E) Flow sorting of transfected cells based on EGFP expression. The reagent control (RC), Lipofectamine 3000 alone, showed an absence of EGFP. (F) Flow diagram summarizing the transfected clones resulting from cell sorting with either the ABE or CBE constructs and their sequencing outcomes. ND, not determined due to clones failing Sanger sequencing.

Overall, from all wells seeded with a single EGFP cell, clones emerged in 36% (34 of 95) of wells transfected with Y220C sgRNA, and 26% (25 of 95) for both R248Q sgRNA and R282W sgRNA. In comparison, 78% (74 of 95) of cells transfected with the reagent control resulted in clonal growth (Fig. 3F). gDNA extracted from expanded EGFP positive single cells and assessed by sequencing DNA regions flanking the sgRNA target sites revealed successful homozygous editing of an A-to-G conversion in 11 (32%) of Y220C clones and G-to-A conversion in 2 (8%) of R248Q clones, while for R282W a heterozygous C-to-T edit only was achieved in four clones (16%) (Figs 3F and 4A). Of note, bystander edits were higher predictions than the desired base edit to create R248Q using the selected sgRNA, correlating with a higher percentage of actual bystander edits seen when creating this mutant. Heterozygous edits were also found in 6 (18%) of Y220C and 4 (16%) of R248Q clones. In Y220C, R248Q and R282W clones, bystander edits were revealed in 1 (3%), 14 (56%) and 2 (8%) clones, respectively (Figs 3F and 4A). These base-editing results correlate with BE-Hive sgRNA predictions, where R248Q and R282W had a greater number of predicted bystander edits compared with Y220C. Heterozygous non-canonical base edits, T-to-A and C-to-G, were shown in one Y220C and four R282W clones, respectively (Fig. 4A). Of interest, five Y220C clones had large deletions and six had small indels resulting in frameshift mutations suggesting DSBs did in fact occur with this CP1041-ABE editor (Fig. 3F).

Next, we sought to demonstrate functional validation of engineered p53 mutants. Loss of the MDM2 and p21 WT p53 targets were observed upon DNA damage in cell lines engineered to express the Y220C and R248Q mutations (Fig. 4B). In the R282W engineered heterozygous mutation, a reduction in levels of MDM2 and p21 was observed in response to DNA damage compared with the clonal parental WT cell line (Fig. 4B). In cell lines harbouring endogenous p53 mutations, p53 targets were not induced in response to cisplatin as expected (Fig. 4C). Furthermore, RNA analysis revealed essentially no MDM2 mRNA expression in engineered Y220C and R248Q cell lines after DNA damage, and a significant reduction in MDM2 mRNA in cells engineered with the heterozygous R282W mutant (Fig. 4D). MDM2 was not increased in cell lines harbouring p53 mutations in response to cisplatin as expected (Fig. 4E). MDM2 protein and mRNA expression was absent in OVKATE cells that have an endogenous R282W mutation, differing in a predicted manner to engineered cells that were heterozygous for this TP53 mutation and expressed low levels of MDM2 gene and protein (Fig. 4C and E). Similar results were seen for CDKN1A in engineered and endogenous p53 mutant cell lines (Fig. 4F and G) and p53 targets BAX and GADD45A (Supplementary Material, Fig. S2) suggesting that these engineered p53 mutants were behaving in a predicted manner. We are able to conclude therefore that successful base-editing was achieved for all base-editing targets following BE-Hive predictions and that the expected functional effects based on loss of the ability to transcriptionally activate WT p53 gene targets was observed.

## Discussion

CRISPR base-editing is a rapidly evolving field with new tools for conducting base-editing and predicting the likelihood of success of a specific edit emerging to meet challenges. Still, not all base edits can be engineered with tools that are currently available and predictive algorithms do not presently exist for all base-editing tools. We have sought to provide an evidence-based approach to engineering single base changes using resources available to researchers today. We used TP53 as a model cancer gene

characterized for point mutations in the TCGA-HGSOC cohort (28) to develop a ranking system to predict success of base-editing. We have automated this system and made it available for researchers to access (<https://utsapps.shinyapps.io/sgBERank/>). Although we have targeted a single cancer gene, the strategies we present have applicability to other cancer, and non-cancer-related, genes. We focussed on ABE and CBE editors that facilitate engineering of all transition edits, respectively, A•T to G•C and C•G to T•A conversions (9), and the more recently reported CGBE editor that enables the transversion edit C•G-to-G•C (10). The BE-Hive prediction algorithm currently encompasses ABE, CBE and CGBE to inform the likelihood of success of engineering a specific base edit (25). We used this algorithm to develop a predictive 0–5 ranking system, with ranked scores  $\geq 3$  indicating a stronger likelihood of success of a specific sgRNA and BE combination achieving the desired base edit. Desired base edits receiving a predictive rank score of 1 or 2 may still be possible to achieve, however we suggest that many more clones will need to be screened to detect the intended outcome. A desired base edit with a predictive rank score of 0 based on lack of an available PAM, a high frequency of bystander edits or low to no target base editing frequency, is not possible to achieve with current technology. We have summarized a strategy for selecting the preferred sgRNA to achieve a specific base edit with an ABE, CBE or CGBE editor using BE-Hive and our ranking system (Fig. 5, Table 1). AYBE editors are not currently part of the BE-Hive prediction algorithm and so are unable to be ranked in our system.

Efficient base editing is best performed using a clonal cell line. This is especially the case for cancer cell lines given the variable aneuploidy that can be present, even in apparently homogenous cell line cultures (31). Whether base editing is able to be achieved also relies on cell lines tolerating transfection without significant cell toxicity. Numerous lipid-based transfection agents are commercially available and won't be discussed further here. We have streamlined the transfection process for ABE and CBE by engineering a single plasmid containing all the required components (base-editing machinery, a sgRNA cloning site and EGFP), avoiding the need for multiple or co-transfections that can negatively impact upon transfection efficiency. We have named these new ABE and CBE plasmids, respectively pCMV-ABEmaxCP1041-(NGG)-PX458-EGFP (CP1041-ABEmax-sgRNA-EGFP) and pCMV-eA3A-BE5-(NG)-PX458-EGFP (eA3A-sgRNA-EGFP). sgRNA informed by BE-Hive predictive analyses were cloned into these plasmids that were then used to validate our predictive strategy *in vitro*. It should be noted that while we used BE-Hive predictive analyses for a HEK293 background, our experiments were performed in the A2780 cell line, which could introduce some discrepancies. Three TP53 mutants were engineered from WT sequence with cell lines demonstrating loss of the ability to transcriptionally regulate p53 target genes for the homozygously engineered mutants Y220C and R248Q. In the case of the heterozygously engineered mutant R282W, reduction in expression of p53 target genes was observed relative to WT cells. For any GOI, the ability to functionally demonstrate an effect of an engineered base edit will strengthen the confidence that the model is behaving as predicted and is suitable for downstream analyses that may include drug discovery as part of an isogenic panel or elucidating basic cell biology interactions.

Unlike using CRISPR technology for gene knockout experiments that may target broad and different regions of a gene and result in edits involving multiple nucleotides, the requirement to either generate or revert a specific missense, nonsense or splice site mutation is highly limited by the surrounding sequence. In this scenario, the need to select sgRNAs with minimal bystander

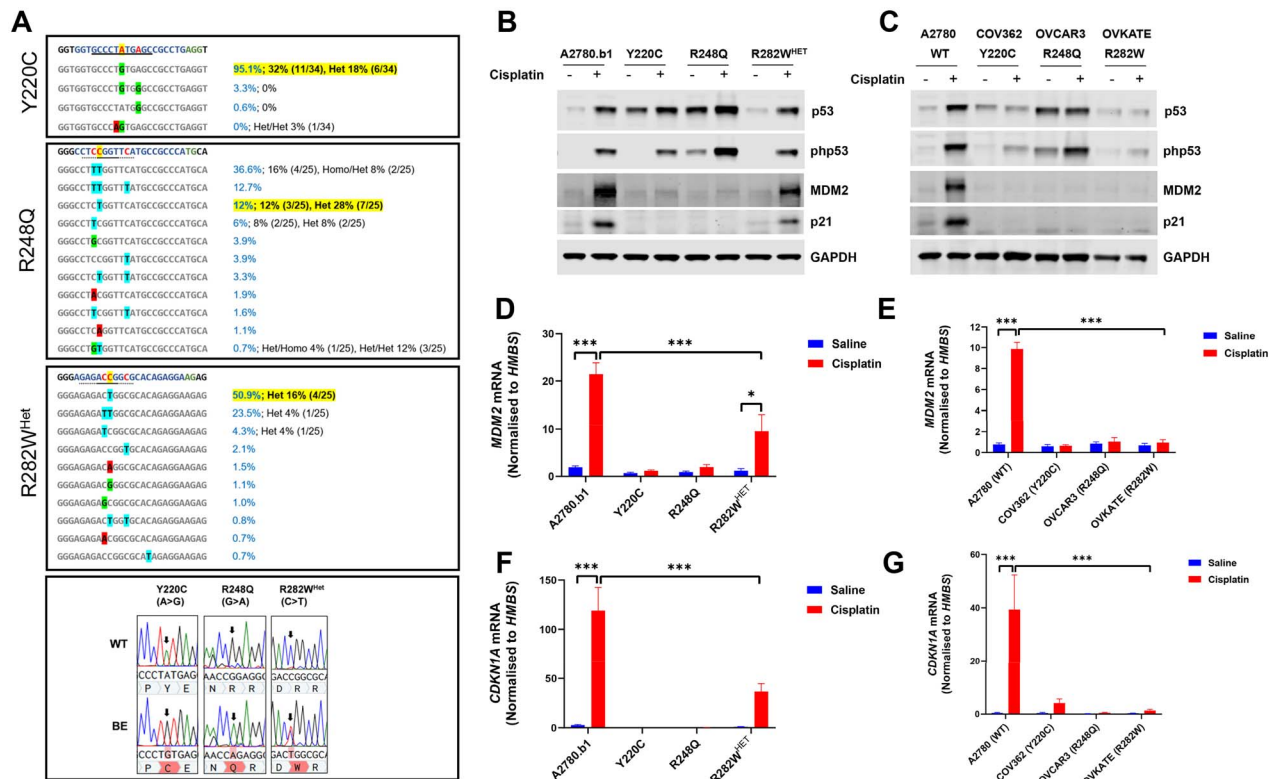


**Figure 4.** Validation of Y220C, R248Q and R282W<sup>Het</sup> TP53 base-edited A2780.b1 isogenic cell line panel. **(A)** gDNA sequence illustrating the 20 bp sgRNA predominantly in blue with exception of the target bases in the editing window depicted with red text. The adjacent PAM site is shown in green text. Yellow highlights depict successful editing of the target base (BE-Hive prediction percentages are shown in blue and black text summarizes the actual base editing outcomes, with non-highlighted percentages being bystander and other editing events, both predicted (blue) and actual (black) outcomes). Highlighted bases (G, green; T, blue; A, red) in the sequence data represent the bases predicted by BE-Hive to change. Sanger sequencing showing the homozygous A-to-G edit (engineering of Y220C), homozygous G-to-A edit (engineering of R248Q cells), and the heterozygous C-to-T edit (engineering of R282W<sup>Het</sup> cells) (WT, wild-type; BE, based-edited). **(B)** Western blot showing higher levels of basal p53 in engineered Y220C and R248Q mutants compared with WT p53, and increased phosphorylation of all p53 proteins in response to DNA damage with cisplatin. The p53 targets MDM2 and p21 were only increased in WT and R282W<sup>Het</sup> cells in response to cisplatin. GAPDH was used as an endogenous reference (blot representative of  $n = 3$ ). **(C)** Western blot showing the behaviour of p53 and p53 targets in response to cisplatin in both p53 WT and endogenous mutant cell lines (blot representative of  $n = 3$ ). **(D)** MDM2 mRNA expression was significantly increased in response to DNA damage with cisplatin in A2780.b1 WT cells, as well as in R282W<sup>Het</sup> engineered cells where some WT p53 remained. MDM2 was not induced in either Y220C and R248Q engineered mutants in response to cisplatin ( $n = 3$ ). **(E)** MDM2 levels in engineered p53 mutants were recapitulated in cells lines harbouring endogenous TP53 mutations ( $n = 3$ ). **(F)** CDKN1A mRNA expression was significantly increased in response to DNA damage with cisplatin in A2780.b1 WT cells, but not in engineered cells. **(G)** CDKN1A levels in engineered p53 mutants were recapitulated in cells lines harbouring endogenous TP53 mutations ( $n = 3$ ). \* $P < 0.05$ ; \*\*\* $P \leq 0.001$ , One-way ANOVA with Tukey's post hoc test.

edits becomes paramount and predictive algorithms assist to this end. There are some limitations, however, to the strategies that we have presented and tested. Firstly, and specifically in the cancer context, it needs to be acknowledged that correcting some cancer-associated mutations back to WT sequence in specific genes may significantly impact on the ability of cancer cells to proliferate *in vitro* due to mechanisms such as oncogene addiction, making such clonal cell lines difficult to both generate and maintain. Furthermore, in cell lines that harbour more than two copies of a GOI, achieving the desired edit might prove challenging as the edit needs to occur in each copy of the gene. Similarly, while engineering of the R282W mutation was given a predictive likelihood rank score of 4 in our system, indicating that it would be highly likely that this edit could be achieved, we were only able to create this mutation in one copy of the TP53 gene, creating a heterozygote for this mutation. While predictive software does not specifically address these issues, they must be considered when designing experiments with BEs.

Although we designed the sgRNAs used in this study with Benchling and coupled this with BE-Hive to predict the efficiency

of editing a specific target with either a CBE, ABE or CGBE, other programs are also available to design sgRNAs for use in base-editing, including BE-Designer (32–34), *beditor* (35), and others (reviewed in 36). As this field continues its rapid progress, the incorporation of machine learning based algorithms into the selection of sgRNAs that most efficiently target single base edits will enhance base-editing outcomes. Together, these tools can enable the generation of isogenic panels of base-edited cell lines for use in both basic discovery science to uncover molecular and cellular behaviours, as well as translational science in arenas including the discovery of molecular targeted drugs.

## Materials and Methods

### Cell lines

The A2780 endometroid ovarian cancer cell line was sourced from the European Collection of Authenticated Cell Cultures (ECACC; cat. #93112519), distributed by Cellbank Australia (Westmead, New South Wales, Australia) (37). The clonal cell line A2780.b1 was produced from a single A2780 parent cell by seeding individual



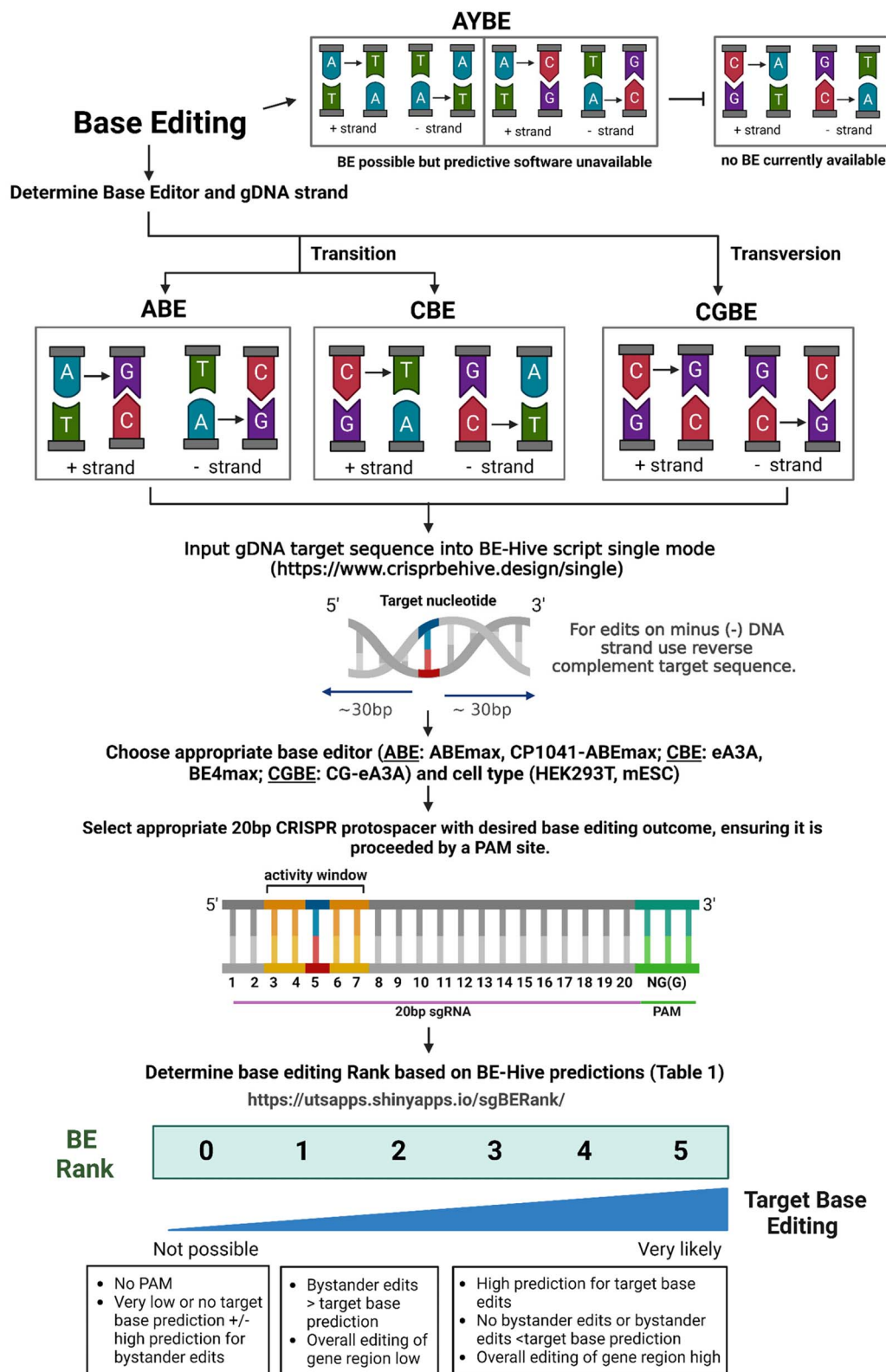


**Figure 5.** Using the BE-Hive base editing machine learning algorithm and new ranking system proposed for selection of optimal sgRNA (single-guide RNA) for successful base editing. Base edits able to be engineered with currently available BEs—ABEs, CBEs, CGBEs and most recently reported, AYBEs are summarized. AYBEs are not yet part of predictive machine learning algorithms.

cells into 96 well plates and allowing them to expand into clonal cell lines. A2780.b1 was selected as it had similar growth rate, cisplatin sensitivity and morphology to the original parent population. Cells were cultured in RPMI 1640 (cat. #42402016, Thermo Fisher Scientific, Mulgrave, VIC, Australia) plus 10% fetal bovine serum (FBS; cat. # FBSAU, AusGeneX, Molendinar, QLD, Australia) at 37°C in a humidified 5% CO<sub>2</sub> atmosphere. The HGSOC cell lines (HGSOC) used in this study were COV362 (European Collection of Authenticated Cell Cultures (ECAAC), #07071910); OVCAR3 (American Tissue Culture Collection (ATCC), VA, USA, #HTB-1610) and OVKATE (Japanese Collection of Research Biosource (JCRB), Osaka Japan #JCRB10440). COV362 were cultured in DMEM (cat. #11965084 Thermo Fisher Scientific, Mulgrave, VIC, Australia), and OVCAR3 and OVKATE in RPMI 1640 all supplemented with 10% FBS (AusGeneX). Cell line authentication was undertaken by the Australian Genome Research Facility (AGRF) Melbourne, Australia, within the last 3 years as previously (38). Mycoplasma testing was conducted using the MycoAlert™ Mycoplasma Detection Kit (cat. #LT07-318, LONZA, Walkersville, MD, USA).

## TCGA: HGSOC cohort

TP53 mutation data from 316 HGSOC patients was obtained from The Cancer Genome Atlas. TP53 mutations were identified in 96% of HGSOC tumours in this cohort. Of these TP53 mutations 61% (187 of 306) were missense, 14% (42 of 306) frameshift, 12% (37 of 306) splice site, 9% (29 of 306) nonsense, 3% (9 of 306) in-frame insertions or deletions, and 1% (2 of 306) were silent mutations (28). For this study, we used BE-Hive predictive software to analyse single base variants with transition or C-to-G transversion TP53 mutations; specifically, 136 missense, 20 nonsense and 20 splice site point mutations, for the potential to be corrected to WT sequence or be introduced into a WT cell line using base-editing CRISPR-Cas9 technology. Further, as proof-of-principle, we used base-editing CRISPR-Cas9 tools to engineer a subset of TP53 single nucleotide variants.

## BE-Hive predictive software and sgRNA design

BE-Hive predictive software (<https://www.crisprbehive.design/>) was used in single mode to design sgRNA for base-editing and determine the predicted frequency of editing a particular nucleotide, accounting for bystander edits and the overall editing efficiency of the target sequence region (25). This was determined for two ABEs, ABEmax (39) and CP1041-ABEmax (40), and two CBEs, eA3A (23) and BE4max (39), as well as CGBE CG-eA3A (10). Additional BEs are available in the BE-Hive program. In all cases, the availability of an appropriate PAM site was manually determined. For ABE and CBE, we examined predicted base-editing potential in both a human and mouse cell background, respectively, HEK293T and mESC cells (25). CGBE predictions with CG-eA3A are only currently available in the HEK293T background (10).

## Engineering base-editing plasmids (Cas9n-deaminase) to contain an sgRNA cloning site and EGFP in a single vector construct

Previously, base-editing has relied on co-expressing two plasmids, one expressing the sgRNA that targets the genomic location of interest, and the other expressing the base-editing components (Cas9n-deaminase fusion) (41). Here, we report modifying the base-editing plasmids to include an sgRNA cloning site and enhanced green fluorescent protein (EGFP) into a single plasmid construct, eliminating the challenges of co-transfection that can include lower transfection efficiency and increased cell toxicity (42).

Specifically, the ABE plasmid p2T-CMV-ABEmaxCP1041-BlastR (CP1041-ABEmax, cat. #152990, Addgene, Watertown MA, USA) and CBE plasmid p2T-CMV-eA3A-BE5-NG-BlastR (eA3A, cat. #152998, Addgene) (25) were engineered to include the sgRNA cloning backbone from the CRISPR-Cas9 KO plasmid pSPCas9(BB)-2A-GFP (PX458; cat. #48138, Addgene) (43). In brief, the Cas9n, deaminase and UGI (CBE only) BE components of CP1041-ABEmax or eA3A, and cytomegalovirus (CMV) promoter were excised using *AgeI* and *SpeI* restriction enzymes (cats. #R3552S, #R3133S, New England BioLabs, Ipswich, MA, USA). The human U6 promoter, sgRNA cloning site and ampicillin resistance gene (ampR) from PX458 were PCR amplified using AccuPrime™ Pfx DNA Polymerase (cat. #12344024, Invitrogen, Waltham, Massachusetts, USA), and the following primers containing *AgeI* and *SpeI* sites (underlined) respectively, and cloned with the *AgeI/SpeI* CP1041-ABEmax and eA3A base-editing fragments (forward primer: 5'-TAATACCGGTGGAATTCTAACTAGAGCTCGCTG-3'; reverse primer: 5'-TGCTACTACTCGCGCTAAAAACGGACTAGC-3'). In subsequent cloning, EGFP from pCMV\_ABEmax\_P2A\_GFP (ABEmax, cat. #112101, Addgene) was cloned into the *EcoRI* site giving rise to the final base-editing constructs we have named pCMV-ABEmaxCP1041-(NGG)-PX458-EGFP (CP1041-ABEmax-sgRNA-EGFP) and pCMV-eA3A-BE5-(NG)-PX458-EGFP (eA3A-sgRNA-EGFP).

## BE construct sgRNA design and cloning

As proof of principle, optimal sgRNAs were predicted using BE-Hive to introduce the accumulation and GOF TP53 missense mutations Y220C (c.659A>G), R248Q (c.743G>A) and R282W (c.844C>T) into WT sequence (26,44,45). sgRNAs were designed using Benchling (Benchling Inc, San Francisco, CA, USA) to include *BbsI* isoschizomer *BpII* (cat. #FD1314, ThermoFisher Scientific, Waltham, MA, USA) overhangs to enable cloning into the sgRNA cloning site in BE plasmids. sgRNAs were synthesized by Integrated DNA Technologies (IDT; Coralville, Iowa, USA). To engineer the Y220C mutant, designed sgRNA were cloned into the ABE plasmid construct generated by us (pCMV-ABEmaxCP1041-(NGG)-PX458-EGFP). In order to engineer both R248Q and R282W, designed sgRNAs were cloned into the CBE plasmid construct generated by us (pCMV-eA3A-BE5-(NG)-PX458-EGFP). If the target sgRNA did not start with a guanine, this base was added to the 5' end of the protospacer before cloning to increase the expression of the sgRNA from the human U6 promoter as was the case for R282W and R248Q sgRNAs (46) (Supplementary Material, Table S1). An endogenous NGG PAM located after the sgRNA target was used to facilitate engineering of the Y220C mutant, and similarly, an endogenous NG PAM was used to facilitate engineering of both the R248Q and R282W mutants.

Sanger sequencing was performed to verify cloning of the designed sgRNA using the U6 sequencing primer 5'-GACTATCATATGCTTACCGT-3' (AGRF, NSW, Australia). Base-editing constructs were transfected into A2780.b1 cells using Lipofectamine 3000 (cat. #L3000015, Life Technologies, California, USA), and single EGFP positive cells were sorted into 96 well plates using the FACS Melody cell sorter instrument (Becton Dickinson, NSW, Australia). Clones were expanded, gDNA were extracted and regions containing the edited bases were amplified by PCR with Phusion Green HS II HF (cat. #F566L, Thermo Fisher Scientific, NSW, Australia) (Supplementary Material, Table S1). Purified PCR fragments underwent Sanger sequencing to confirm base-editing events using sequencing primers listed in Supplementary Material, Table S1 (AGRF, NSW, Australia).

## Assessing protein levels of WT and mutant p53 cells, including functional consequences by western blotting of the TP53 engineered isogenic panel

In order to stimulate the DNA damage response that activates p53 and in turn its target genes such as MDM2 and CDKN1A, cell lines were treated with IC75 concentrations (A2780 parent and base-edited cell lines, 10  $\mu$ M; COV362, 15.4  $\mu$ M; OVCAR3, 4  $\mu$ M; OVKATE, 18.2  $\mu$ M) of cisplatin (cat. #P4394, Sigma-Aldrich, Sydney, NSW, Australia), or vehicle control (0.9% saline) for 24 h and protein extracted using urea buffer as previously (38). Extracts were sonicated for 15 s followed by denaturation at 95°C for 5 min. Ten  $\mu$ g of each sample was separated on a 4–12% Bis-Tris gel (cat. #NP0336BOX, Life Technologies, Thornton, NSW, Australia) at 180 V for 1 h and subsequently transferred to nitrocellulose membrane (cat. #10600016, Sigma Aldrich, St. Louis, Missouri, USA) for 1.5 h using a wet transfer system (Biorad, California, USA). Nitrocellulose membranes were blocked with 50% (v/v) Intercept Blocking Buffer/TBS (cat. #927-60-001, LI-COR Bioscience, Lincoln, NE, USA) and incubated overnight at 4°C with the following primary antibodies: p53 (DO-1) (cat. #MA5-12571, ThermoFisher Scientific, Mulgrave, VIC, Australia), and from Cell Signalling Technology (Danvers, MA, USA); phosphorylated p53 (Ser15; cat. #9284), MDM2 (D1V2Z; cat. #86943), p21 (Waf1-Cip1 (DCS60); cat. #2946) and GAPDH (D14C10) (cat. #2118). Membranes were probed with appropriate species specific near infrared (NIR) fluorescent secondary antibodies; IRDye 800CW Donkey anti-Mouse IgG (cat. #LCR-926-32212), IRDye 800CW Donkey anti-Rabbit IgG (cat. #LCR-926-32213), or IRDye 680RD Donkey anti-Rabbit (cat. #LCR-926-68073, LI-COR Bioscience, Lincoln, NE, USA) for 1 h at room temperature and fluorescent signals visualized on the Odyssey CLx imaging system (LI-COR Bioscience, Lincoln, NE, USA). Quantitation was undertaken using ImageStudio software version 5.2 (LI-COR Bioscience).

## Quantitating mRNA levels of the p53 target gene MDM2 in the TP53 engineered isogenic panel

Total RNA was extracted using the RNeasy Mini Kit (Qiagen, Chadstone, VIC, Australia) and 500 ng converted to cDNA using the SuperScript™ IV First-Strand Synthesis System (cat. #18091200, Thermo Fisher Scientific). Gene expression was analysed in triplicate with the MDM2, Hs00242813\_m1; CDKN1A, Hs00355782\_m1; BAX, Hs00180269\_m1; and GADD45A, Hs00169255\_m1 TaqMan assays (Life Technologies, Scoresby, VIC, Australia), and the HMBS, 97639748 (Integrated DNA Technologies, Baulkham Hills, NSW, Australia) reference gene, using the TaqMan Fast Advanced Master Mix Kit (cat. #444557, Thermo Fisher Scientific Laboratories, Gladesville, NSW, Australia). Analyses were performed using the QuantStudio 12K Flex Real-Time PCR System (Thermo Fisher Scientific) and relative mRNA expression determined.

## Implementation of the ranking system as an online web server

sgBERank (<https://utsapps.shinyapps.io/sgBERank/>) is a standalone application written in R (version 4.2.1). sgBERank takes the predictions from the BE-Hive web server as a CSV file and then assesses the likelihood of the success of single base edits through our ranking system. Detailed usage of the app is available in the app's help section.

## Statistical analyses

Protein and RNA data generated from isogenic panels was analysed using IBM SPSS version 28.0 (SPSS Australasia Pty Ltd, Chatswood, NSW, Australia). Data are presented as the

mean  $\pm$  SEM from three independent experiments. One-way ANOVA with Tukey's post hoc test was used to test for multiple comparisons between cell lines constituting the engineered isogenic panel.  $P < 0.05$  was considered statistically significant for all analyses.

## Supplementary Material

Supplementary material is available at HMG online.

## Acknowledgements

T.X. and Y.M. are supported by scholarships from the Chinese Scholarship Council (CSC).

Conflict of Interest statement. None declared.

## Funding

National Health and Medical Research Council (NHMRC) Australia (grant 2019296) and a University of Technology Sydney, Australia Establishment Fund (both to D.J.M.).

## Data availability

All data is available to be shared upon request.

## References

1. Das, S., Bano, S., Kapse, P. and Kundu, G.C. (2022) CRISPR based therapeutics: a new paradigm in cancer precision medicine. *Mol. Cancer*, **21**, 85.
2. Hayward, S.B. and Ciccia, A. (2021) Towards a CRISPeR understanding of homologous recombination with high-throughput functional genomics. *Curr. Opin. Genet. Dev.*, **71**, 171–181.
3. Lau, M.T., Ghazanfar, S., Parkin, A., Chou, A., Rouaen, J.R., Littleboy, J.B., Nessem, D., Khuong, T.M., Nevoltris, D., Schofield, P. et al. (2020) Systematic functional identification of cancer multi-drug resistance genes. *Genome Biol.*, **21**, 27.
4. Gimeno, M., San José-Enériz, E., Rubio, A., Garate, L., Miranda, E., Castilla, C., Agirre, X., Prosper, F. and Carazo, F. (2022) Identifying lethal dependencies with HUGE predictive power. *Cancers (Basel)*, **14**, 3251.
5. Feng, X., Tang, M., Dede, M., Su, D., Pei, G., Jiang, D., Wang, C., Chen, Z., Li, M., Nie, L. et al. (2022) Genome-wide CRISPR screens using isogenic cells reveal vulnerabilities conferred by loss of tumor suppressors. *Sci. Adv.*, **8**, eabm6638.
6. Lyu, J., Liu, Y., Gong, L., Chen, M., Madanat, Y.F., Zhang, Y., Cai, F., Gu, Z., Cao, H., Kaphle, P. et al. (2022) Disabling uncompetitive inhibition of oncogenic IDH mutations drives acquired resistance. *Cancer Discov.*, **13**, 170–193.
7. Cook, A.L., Wyhs, N., Sur, S., Ptak, B., Popoli, M., Dobbyn, L., Papadopoulos, T., Bettegowda, C., Papadopoulos, N., Vogelstein, B., Zhou, S. and Kinzler, K.W. (2022) An isogenic cell line panel for sequence-based screening of targeted anticancer drugs. *iScience*, **25**, 104437.
8. Qi, T., Wu, F., Xie, Y., Gao, S., Li, M., Pu, J., Li, D., Lan, F. and Wang, Y. (2020) Base editing mediated generation of point mutations into human pluripotent stem cells for modeling disease. *Front. Cell Dev. Biol.*, **8**, 590581.
9. Rees, H.A. and Liu, D.R. (2018) Base editing: precision chemistry on the genome and transcriptome of living cells. *Nat. Rev. Genet.*, **19**, 770–788.

10. Koblan, L.W., Arbab, M., Shen, M.W., Hussmann, J.A., Anzalone, A.V., Doman, J.L., Newby, G.A., Yang, D., Mok, B., Replogle, J.M. et al. (2021) Efficient C•G-to-G•C base editors developed using CRISPRi screens, target-library analysis, and machine learning. *Nat. Biotechnol.*, **39**, 1414–1425.
11. Kurt, I.C., Zhou, R., Iyer, S., Garcia, S.P., Miller, B.R., Langner, L.M., Grünwald, J. and Joung, J.K. (2021) CRISPR C-to-G base editors for inducing targeted DNA transversions in human cells. *Nat. Biotechnol.*, **39**, 41–46.
12. Tong, H., Wang, X., Liu, Y., Liu, N., Li, Y., Luo, J., Ma, Q., Wu, D., Li, J., Xu, C. and Yang, H. (2023) Programmable A-to-Y base editing by fusing an adenine base editor with an N-methylpurine DNA glycosylase. *Nat. Biotechnol.*, [Online ahead of print].
13. Komor, A.C., Kim, Y.B., Packer, M.S., Zuris, J.A. and Liu, D.R. (2016) Programmable editing of a target base in genomic DNA without double-stranded DNA cleavage. *Nature*, **533**, 420–424.
14. Porto, E.M., Komor, A.C., Slaymaker, I.M. and Yeo, G.W. (2020) Base editing: advances and therapeutic opportunities. *Nat. Rev. Drug Discov.*, **19**, 839–859.
15. Gaudelli, N.M., Komor, A.C., Rees, H.A., Packer, M.S., Badran, A.H., Bryson, D.I. and Liu, D.R. (2017) Programmable base editing of A•T to G•C in genomic DNA without DNA cleavage. *Nature*, **551**, 464–471.
16. Nishimasu, H., Shi, X., Ishiguro, S., Gao, L., Hirano, S., Okazaki, S., Noda, T., Abudayyeh, O.O., Gootenberg, J.S., Mori, H. et al. (2018) Engineered CRISPR-Cas9 nuclease with expanded targeting space. *Science*, **361**, 1259–1262.
17. Hu, J.H., Miller, S.M., Geurts, M.H., Tang, W., Chen, L., Sun, N., Zeina, C.M., Gao, X., Rees, H.A., Lin, Z. and Liu, D.R. (2018) Evolved Cas9 variants with broad PAM compatibility and high DNA specificity. *Nature*, **556**, 57–63.
18. Kleinstiver, B.P., Prew, M.S., Tsai, S.Q., Topkar, V.V., Nguyen, N.T., Zheng, Z., Gonzales, A.P., Li, Z., Peterson, R.T., Yeh, J.R., Aryee, M.J. and Joung, J.K. (2015) Engineered CRISPR-Cas9 nucleases with altered PAM specificities. *Nature*, **523**, 481–485.
19. Amrani, N., Gao, X.D., Liu, P., Edraki, A., Mir, A., Ibraheim, R., Gupta, A., Sasaki, K.E., Wu, T., Donohoue, P.D. et al. (2018) NmeCas9 is an intrinsically high-fidelity genome-editing platform. *Genome Biol.*, **19**, 214.
20. Tan, J., Zhang, F., Karcher, D. and Bock, R. (2019) Engineering of high-precision base editors for site-specific single nucleotide replacement. *Nat. Commun.*, **10**, 439.
21. Doman, J.L., Raguram, A., Newby, G.A. and Liu, D.R. (2020) Evaluation and minimization of Cas9-independent off-target DNA editing by cytosine base editors. *Nat. Biotechnol.*, **38**, 620–628.
22. Kim, Y.B., Komor, A.C., Levy, J.M., Packer, M.S., Zhao, K.T. and Liu, D.R. (2017) Increasing the genome-targeting scope and precision of base editing with engineered Cas9-cytidine deaminase fusions. *Nat. Biotechnol.*, **35**, 371–376.
23. Gehrke, J.M., Cervantes, O., Clement, M.K., Wu, Y., Zeng, J., Bauer, D.E., Pinello, L. and Joung, J.K. (2018) An APOBEC3A-Cas9 base editor with minimized bystander and off-target activities. *Nat. Biotechnol.*, **36**, 977–982.
24. Yu, Y., Leete, T.C., Born, D.A., Young, L., Barrera, L.A., Lee, S.J., Rees, H.A., Ciaramella, G. and Gaudelli, N.M. (2020) Cytosine base editors with minimized unguided DNA and RNA off-target events and high on-target activity. *Nat. Commun.*, **11**, 2052.
25. Arbab, M., Shen, M.W., Mok, B., Wilson, C., Matuszek, Z., Cassa, C.A. and Liu, D.R. (2020) Determinants of base editing outcomes from target library analysis and machine learning. *Cell*, **182**, 463–480.e30.
26. Biegging, K.T., Mello, S.S. and Attardi, L.D. (2014) Unravelling mechanisms of p53-mediated tumour suppression. *Nat. Rev. Cancer*, **14**, 359–370.
27. Olivier, M., Hollstein, M. and Hainaut, P. (2010) TP53 mutations in human cancers: origins, consequences, and clinical use. *Cold Spring Harb. Perspect. Biol.*, **2**, a001008.
28. Bell, D., Berchuck, A., Birrer, M., Chien, J., Cramer, D., Dao, F., Dhir, R., DiSaia, P., Gabra, H., Glenn, P. et al. (2011) Integrated genomic analyses of ovarian carcinoma. *Nature*, **474**, 609–615.
29. Domcke, S., Sinha, R., Levine, D.A., Sander, C. and Schultz, N. (2013) Evaluating cell lines as tumour models by comparison of genomic profiles. *Nat. Commun.*, **4**, 2126.
30. Cole, A.J., Dwight, T., Gill, A.J., Dickson, K.A., Zhu, Y., Clarkson, A., Gard, G.B., Maidens, J., Valmadre, S., Clifton-Bligh, R. and Marsh, D.J. (2016) Assessing mutant p53 in primary high-grade serous ovarian cancer using immunohistochemistry and massively parallel sequencing. *Sci. Rep.*, **6**, 26191.
31. Li, R. and Zhu, J. (2022) Effects of aneuploidy on cell behaviour and function. *Nat. Rev. Mol. Cell Biol.*, **23**, 250–265.
32. Hwang, G.H., Park, J., Lim, K., Kim, S., Yu, J., Yu, E., Kim, S.T., Eils, R., Kim, J.S. and Bae, S. (2018) Web-based design and analysis tools for CRISPR base editing. *BMC Bioinform.*, **19**, 542.
33. Hwang, G.H. and Bae, S. (2021) Web-based base editing toolkits: BE-designer and BE-analyzer. *Methods Mol. Biol.*, **2189**, 81–88.
34. Hwang, G.H. and Bae, S. (2023) Web-based computational tools for base editors. *Methods Mol. Biol.*, **2606**, 13–22.
35. Dandage, R., Després, P.C., Yachie, N. and Landry, C.R. (2019) beditor: a computational workflow for designing libraries of guide RNAs for CRISPR-mediated base editing. *Genetics*, **212**, 377–385.
36. Jeong, Y.K., Song, B. and Bae, S. (2020) Current status and challenges of DNA base editing tools. *Mol. Ther.*, **28**, 1938–1952.
37. Hamilton, T.C., Young, R.C. and Ozols, R.F. (1984) Experimental model systems of ovarian cancer: applications to the design and evaluation of new treatment approaches. *Semin. Oncol.*, **11**, 285–298.
38. Dickson, K.A., Xie, T., Evenhuis, C., Ma, Y. and Marsh, D.J. (2021) PARP inhibitors display differential efficacy in models of BRCA mutant high-grade serous ovarian cancer. *Int. J. Mol. Sci.*, **22**, 8506.
39. Koblan, L.W., Doman, J.L., Wilson, C., Levy, J.M., Tay, T., Newby, G.A., Maiani, J.P., Raguram, A. and Liu, D.R. (2018) Improving cytidine and adenine base editors by expression optimization and ancestral reconstruction. *Nat. Biotechnol.*, **36**, 843–846.
40. Huang, T.P., Zhao, K.T., Miller, S.M., Gaudelli, N.M., Oakes, B.L., Fellmann, C., Savage, D.F. and Liu, D.R. (2019) Circularly permuted and PAM-modified Cas9 variants broaden the targeting scope of base editors. *Nat. Biotechnol.*, **37**, 626–631.
41. Vasquez, C.A., Cowan, Q.T. and Komor, A.C. (2020) Base editing in human cells to produce single-nucleotide-variant clonal cell lines. *Curr. Protoc. Mol. Biol.*, **133**, e129.
42. Di Blasi, R., Marbahi, M.M., Siciliano, V., Polizzi, K. and Ceroni, F. (2021) A call for caution in analysing mammalian co-transfection experiments and implications of resource competition in data misinterpretation. *Nat. Commun.*, **12**, 2545.
43. Ran, F.A., Hsu, P.D., Wright, J., Agarwala, V., Scott, D.A. and Zhang, F. (2013) Genome engineering using the CRISPR-Cas9 system. *Nat. Protoc.*, **8**, 2281–2308.
44. Liu, D.P., Song, H. and Xu, Y. (2010) A common gain of function of p53 cancer mutants in inducing genetic instability. *Oncogene*, **29**, 949–956.
45. Brosh, R. and Rotter, V. (2009) When mutants gain new powers: news from the mutant p53 field. *Nat. Rev. Cancer*, **9**, 701–713.
46. Zhang, X.H., Tee, L.Y., Wang, X.G., Huang, Q.S. and Yang, S.H. (2015) Off-target effects in CRISPR/Cas9-mediated genome engineering. *Mol. Ther. Nucleic Acids*, **4**, e264.



## Review

# Targeting Homologous Recombination Deficiency in Ovarian Cancer with PARP Inhibitors: Synthetic Lethal Strategies That Impact Overall Survival

Tao Xie <sup>1</sup>, Kristie-Ann Dickson <sup>1</sup> , Christine Yee <sup>1</sup>, Yue Ma <sup>1</sup> , Caroline E. Ford <sup>2</sup> , Nikola A. Bowden <sup>3,4,5</sup>  and Deborah J. Marsh <sup>1,6,\*</sup> 

- <sup>1</sup> Translational Oncology Group, School of Life Sciences, Faculty of Science, University of Technology Sydney, Sydney, NSW 2007, Australia
- <sup>2</sup> School of Clinical Medicine, Faculty of Medicine and Health, University of New South Wales, Sydney, NSW 2052, Australia
- <sup>3</sup> Centre for Drug Repurposing and Medicines Research, University of Newcastle, Newcastle, NSW 2289, Australia
- <sup>4</sup> School of Medicine and Public Health, University of Newcastle, Newcastle, NSW 2289, Australia
- <sup>5</sup> Hunter Medical Research Institute, Newcastle, NSW 2289, Australia
- <sup>6</sup> Northern Clinical School, Faculty of Medicine and Health, University of Sydney, Camperdown, NSW 2006, Australia
- \* Correspondence: [deborah.marsh@uts.edu.au](mailto:deborah.marsh@uts.edu.au)



**Citation:** Xie, T.; Dickson, K.-A.; Yee, C.; Ma, Y.; Ford, C.E.; Bowden, N.A.; Marsh, D.J. Targeting Homologous Recombination Deficiency in Ovarian Cancer with PARP Inhibitors: Synthetic Lethal Strategies That Impact Overall Survival. *Cancers* **2022**, *14*, 4621. <https://doi.org/10.3390/cancers14194621>

Academic Editors: Péter Bay and José Yélamos

Received: 8 July 2022

Accepted: 21 September 2022

Published: 23 September 2022

**Publisher's Note:** MDPI stays neutral with regard to jurisdictional claims in published maps and institutional affiliations.



**Copyright:** © 2022 by the authors. Licensee MDPI, Basel, Switzerland. This article is an open access article distributed under the terms and conditions of the Creative Commons Attribution (CC BY) license (<https://creativecommons.org/licenses/by/4.0/>).

**Simple Summary:** Synthetic lethality approaches to cancer therapy involves combining events to cause cancer cell death. Using this strategy, major advances have occurred in the treatment of women with ovarian cancer who have defects in the Homologous Recombination Repair (HRR) pathway. When the HRR pathway is defective, due to mutations or epigenetic changes in genes such as *BRCA1* or *BRCA2*, cells can no longer accurately repair double strand breaks (DSBs). Capitalising on this weakness, pharmacological inhibition of poly (ADP-ribose) polymerase (PARP) that function to repair single strand breaks (SSBs) leads to synthetic lethality in cells with defective HRR. PARP inhibitors (PARPis) including olaparib, niraparib and rucaparib are approved for the clinical management of women with ovarian cancer. Understanding and overcoming issues of acquired resistance to PARPis, extending these strategies to benefit more patients and combining PARPis with other drugs, including immunotherapies, are of high priority in the field today.

**Abstract:** The advent of molecular targeted therapies has made a significant impact on survival of women with ovarian cancer who have defects in homologous recombination repair (HRR). High-grade serous ovarian cancer (HGSOC) is the most common histological subtype of ovarian cancer, with over 50% displaying defective HRR. Poly ADP ribose polymerases (PARPs) are a family of enzymes that catalyse the transfer of ADP-ribose to target proteins, functioning in fundamental cellular processes including transcription, chromatin remodelling and DNA repair. In cells with deficient HRR, PARP inhibitors (PARPis) cause synthetic lethality leading to cell death. Despite the major advances that PARPis have heralded for women with ovarian cancer, questions and challenges remain, including: can the benefits of PARPis be brought to a wider range of women with ovarian cancer; can other drugs in clinical use function in a similar way or with greater efficacy than currently clinically approved PARPis; what can we learn from long-term responders to PARPis; can PARPis sensitise ovarian cancer cells to immunotherapy; and can synthetic lethal strategies be employed more broadly to develop new therapies for women with ovarian cancer. We examine these, and other, questions with focus on improving outcomes for women with ovarian cancer.

**Keywords:** ovarian cancer; high-grade serous ovarian cancer; PARP; homologous recombination repair; BRCA; homologous recombination deficiency; synthetic lethal; olaparib; niraparib; rucaparib



## 1. Introduction

The application of molecular targeted therapy to treat poor outcome malignancies is revolutionising the field of cancer medicine and extending the lives of patients. Fundamental discovery science has elucidated the cellular response to DNA damage and this knowledge has been harnessed for the development of new therapies. Acknowledged as a major breakthrough, blocking poly (ADP-ribose) polymerase (PARP), a key enzyme in DNA repair, in tumours with genetic or epigenetic abrogation of proteins involved in homologous recombination repair (HRR), creates a synthetic lethal phenotype that kills cancer cells. Small molecule inhibitors of PARP are now clinically approved in many countries for the treatment of a number of malignancies including breast, ovarian and pancreatic cancers. In fact, in a relatively short time, PARP inhibitors (PARPi) have entirely altered the approach to treating a large subset of ovarian cancers. The clinical use of PARPi represents a major and impactful advance in the management of this disease. Here, we focus on women with certain types of ovarian cancer where significant extension in overall survival has been reported in response to a PARPi.

### 1.1. Ovarian Cancer and Defects in Homologous Recombination Repair (HRR)

Ovarian cancer encompasses a number of distinct malignancies that share an anatomical location, yet have different cellular origins, molecular profiles and responses to therapy [1–5]. High-grade serous ovarian cancer (HGSOC) is the most common histological subtype of epithelial ovarian cancer, with less common subtypes including ovarian clear cell carcinoma (OCCC), endometrioid ovarian cancer (EnOC), mucinous ovarian cancer (MOC) and low-grade serous ovarian cancer (LGSOC). An additional exceedingly rare subtype is small cell carcinoma of the ovary (SCCOHT). This review focuses on HGSOC, an aggressive malignancy, generally treated with a combination of surgery and platinum-taxane based chemotherapy. Despite this treatment regime, the majority of women relapse within two years and recurrent disease is generally viewed as incurable [6]. Five-year survival has remained less than 50% and, until very recently, options for treatment in addition to chemotherapy have been absent [7].

Molecular profiling is revolutionising the clinical management of HGSOC, with actionable targets now known. Mutation of the tumour suppressor gene *TP53* occurs in almost 100% of HGSOC [8,9]. Extensive research efforts are ongoing worldwide to target mutant p53 in ovarian and many other malignancies, for example using compounds that reactivate mutant p53 back to its wild-type form such as APR-246 (also known as PRIMA-1<sup>MET</sup>) [10–12]. To date, no mutant p53 targeting drug has been approved for routine clinical use. In sharp contrast to this are the recent successes of clinical targeting of molecular defects in the HRR pathway. Over 50% of HGSOC have a defect in this pathway due to mutations in *BRCA1*, *BRCA2*, *RAD51C*, *RAD51D*, *ATM* or *PALB2* [8,13–17], or methylation of genes including *BRCA1* [8,18–22] or *RAD51C* [23–25]. Mutations in HRR-associated genes have also been identified in OCCC and EnOC, albeit at lower frequencies than for HGSOC [26–28].

Collectively, tumours with a deficient HRR pathway due to genetic or epigenetic events are described as having a “BRCAness” phenotype that is frequently accompanied by higher levels of loss of heterozygosity, telomeric allelic imbalance and large-scale state transitions, due to the cell’s impaired ability to repair double strand breaks (DSBs), referred to as a genomic scar [29–31]. This genomic instability present as the result of BRCAness can be measured and used as a diagnostic tool for identifying HRR deficiency in tumours. By analysing these phenotypic effects of HRR deficiency, the involvement of defective HRR genes other than *BRCA1* or *BRCA2* can also be identified by implication. This includes HRR genes where their expression is determined by methylation. Commercial FDA-approved companion diagnostic (CDx) tests, FoundationOne<sup>®</sup> CDx (Foundation Medicine, Cambridge, MA, USA) and myChoice<sup>®</sup> CDx (Myriad, Salt Lake City, UT, USA) are now used to determine whether a woman with ovarian cancer is likely to see clinical benefit

from a PARPi based on having HRR deficiency [32,33]. These tests generate a score, above which the tumour is likely HRR deficient and below which HRR proficient.

In addition to certain ovarian cancers, BRCAness is seen in other malignancies including breast [34], prostate [35], pancreatic [36], gastric [37] and colorectal cancers [38], as well as in acute leukemias [39]. While BRCAness is a clear driver of malignancy, it can be targeted using synthetic lethal strategies that involve inhibition of PARP.

### 1.2. The PARP Family and DNA Repair

The 17-member PARP family of enzymes includes PARP1, PARP2, PARP3, PARP4 (also known as Vault PARP) and tankyrases 1 and 2 (PARP5a and PARP5b) [40–42]. PARPs are involved in many key cellular processes including regulating transcription, translation, telomere maintenance, remodelling the chromatin landscape and, importantly in the context of this review, DNA repair [43,44]. PARPs catalyse the transfer of poly (ADP-ribose) (poly(adenosinediphosphate-ribose)) to target proteins. In this process of polyADP-ribosylation, also known as PARylation, catalytic activation of PARP synthesises poly (ADP-ribose), PAR, from its substrate nicotinamide adenine dinucleotide (NAD<sup>+</sup>) to form chains of PAR polymers. These chains attach covalently to specific amino acid residues on either PARP itself, known as auto-PARylation, or other acceptor proteins [45,46]. It is understood that PARP1 is responsible for over 90% of PARylation in the context of DNA damage, with PARPs 2, 3, 4, 5a and 5b also having PARylation activity [45,47].

During the DNA Damage Response (DDR) PARPs bind to sites of single strand breaks (SSBs) undergoing base excision repair (BER), PARylating substrates in order to facilitate recruitment of DNA repair machinery [48]. PARylation also destabilises PARP1 interaction with the SSB, uncoupling these two factors that then facilitates access for BER machinery [49]. Left unrepaired, SSBs pose a risk to genetic stability and therefore to cell survival. When the DNA replication fork encounters a SSB it can stall and collapse, causing a double strand break (DSB) that requires correction via HRR [50]. This creates a pharmacological opportunity in HRR deficient cells whereby inhibition of PARP reduces the ability of cells to repair DNA damage via the BER pathway. In this case, HRR deficient cells are unable to repair DNA damage by either HRR or BER, creating a synthetic lethal phenotype resulting in cancer cell death [51–53] (Figure 1). Simply stated, the combination of HRR deficiency and PARP inhibition is fatal to the cell. Further, the scaffold protein XRCC1 assembles protein complexes containing DNA polymerase  $\beta$  and DNA ligase III, preventing PARP1 engagement and activity during BER. This flags XRCC1 as an “anti-trapper” that may have implications for genome integrity [54].

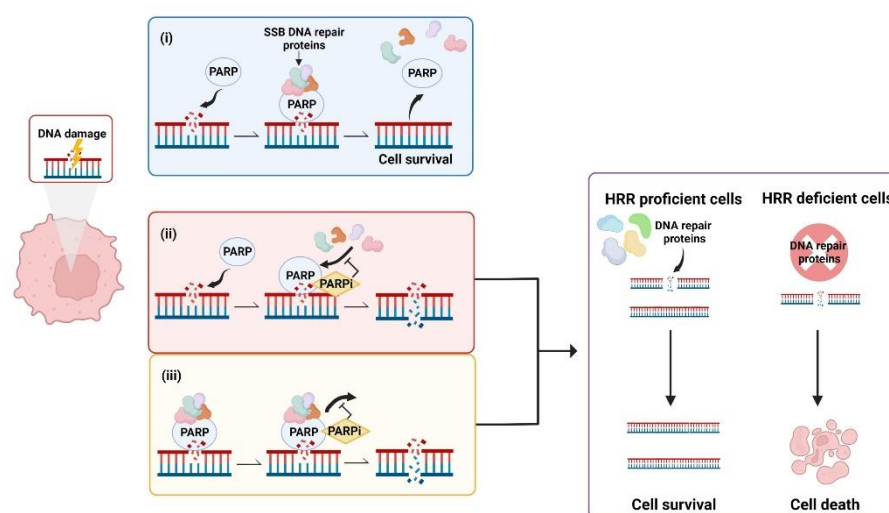


**Figure 1.** Synthetic lethality occurs when a defect in the homologous recombination repair (HRR)

pathway is combined with inhibition of poly (ADP-ribose) polymerase (PARP). (i) PARP binds to sites of single strand breaks (SSBs), PARylates substrates and recruits DNA repair proteins. (ii) PARP inhibitors (PARPis) bind PARP, preventing PARylation and blocking access of PARP to DNA lesions that results in double strand breaks (DSBs). (iii) PARPis can also work to trap PARP at the DNA, inhibiting the dissociation of PARP from DNA and leading to the generation of DSBs. In cells with defective HRR, DSBs are unable to be repaired, leading to cell death. Created with Biorender.com.

## 2. PARP Inhibitors (PARPis)—Focus on Ovarian Cancer

PARP inhibitors (PARPis) including olaparib (Lynparza®; AstraZeneca Pharmaceuticals, Cambridge, UK), rucaparib (Rubraca®; Clovis Oncology, Inc., Boulder, CO, USA) and niraparib (Zejula®; GlaxoSmithKline, Brentford, Middlesex, UK) are small molecule inhibitors of PARP that have been approved by the US Food and Drug Administration (FDA), and other regulatory authorities worldwide, for women with ovarian cancer under certain conditions, including as maintenance therapy. Talazoparib (Talzenna®; Pfizer, Inc., Manhattan, NY, USA) is approved for treatment of advanced breast cancer and veliparib (ABT-888; AbbVie, North Chicago, IL, USA) is still being evaluated. An additional two PARPis, pamiparib (Partruvix™; BeiGene Ltd., Beijing, China) and fuzuloparib (AiRuiYi®, formerly fluzoparib; Jiangsu Hengrui Pharmaceuticals Co., Ltd., Lianyungang, China), have been approved in China for the treatment of women with ovarian cancer.

### 2.1. Timeline of Discovery and Clinical Adoption of PARPis

In 1963, Chambon and colleagues reported their initial discovery that nicotinamide mononucleotide enhanced the activity of a DNA dependent enzyme [55,56]. This discovery would go on to form the basis of the PARP field as we know it today. By the early 1980s, PARP had been found to play an essential role in the repair of DNA SSBs and the first PARPi was identified [57–59]. In 2005, the landmark discovery that BRCA dysfunction greatly sensitised cancer cells to PARP inhibition was reported [60,61]. This was proof that the concept of synthetic lethality could be adopted as a therapeutic strategy by targeting BRCA-related HRR dysfunction with a DNA repair inhibitor. For malignancies such as HGSOV where *BRCA1* and *BRCA2* mutations are prevalent [14], this discovery marked a clear turning point and new hope for molecular targeted therapy.

Almost a decade later in December 2014, olaparib became the first PARPi approved by the FDA for the treatment of advanced, recurrent ovarian cancers with germline *BRCA* mutation, or suspected germline mutation, and previous treatment of three or more lines of chemotherapy [62,63]. FDA approval of rucaparib followed in 2016, for treatment of the same indication [51,64]. Niraparib was approved by the FDA in 2017 for maintenance treatment of patients with recurrent epithelial ovarian, fallopian tube, or primary peritoneal cancer who were in complete or partial response to platinum-based chemotherapy [65]. Olaparib in 2017 [66] and rucaparib in 2018 [67] were also FDA approved as maintenance therapies under the same conditions as niraparib. While not currently approved for the treatment of ovarian cancer, in 2018 talazoparib was approved for the treatment of locally advanced or metastatic *BRCA*-mutated HER2-negative breast cancers [68]. Pamiparib was approved in China in 2021 for the treatment of germline *BRCA* mutated recurrent advanced ovarian, fallopian tube and primary peritoneal cancer in women who have had two or more lines of chemotherapy [69], as was fuzuloparib [70].

Reflecting the growing understanding that HRR-deficiency was the result of more than just *BRCA1* or *BRCA2* defects, niraparib was FDA approved for HRR-deficient advanced ovarian cancer in 2019 [71]. The combination of olaparib and the anti-angiogenic bevacizumab was FDA approved in 2020 for first-line maintenance of HRR deficient advanced epithelial ovarian, fallopian tube, or primary peritoneal cancers in complete or partial response to platinum-based chemotherapy [72]. Of significance, in 2020 the FDA-approved front-line maintenance with niraparib for platinum sensitive advanced ovarian cancer regardless of HRR status [73,74]. Other PARPis, including veliparib, are currently undergoing preclinical and clinical research and may be approved for either first-line or maintenance

treatment of ovarian cancers in the future. A timeline of PARP and PARPi discovery, as well as clinical approvals is shown in Figure 2.

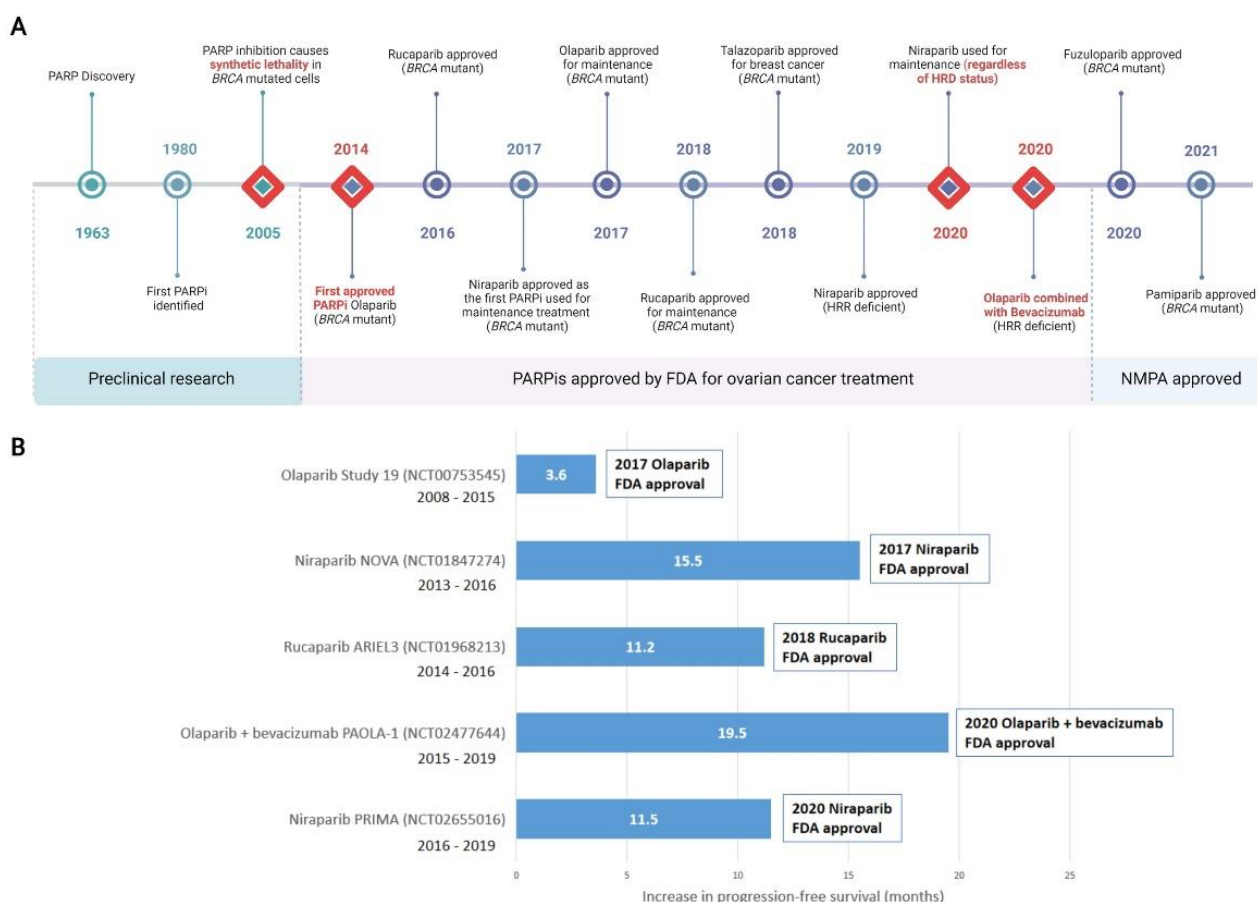


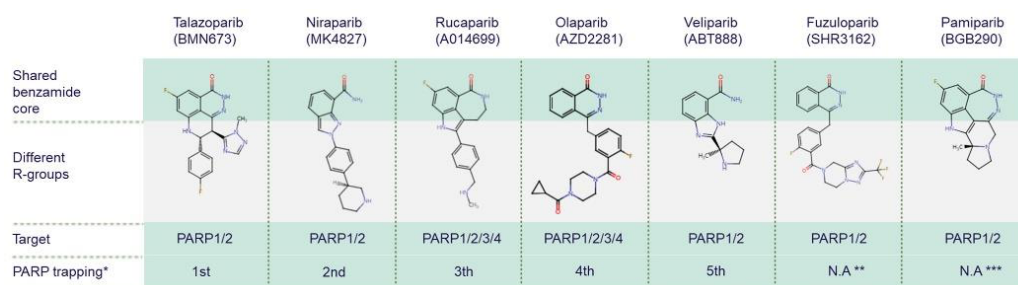
**Figure 2.** Discovery of PARP inhibitors and their introduction to the clinic. **(A)** Milestones in the discovery of PARP and clinical adoption of PARPis are recorded over time. Major milestones are indicated with a red diamond. All milestones are specific to the treatment of ovarian cancer, with the exception of talazoparib which was first approved for metastatic breast cancer and not currently approved for ovarian cancer. **(B)** Selected landmark clinical trials investigating progression-free survival (PFS) that were instrumental in clinical approval of PARPis, including in combination therapy, are shown. Increased PFS in treatment compared to placebo arms are represented. Additional months of PFS for treatment versus placebo groups are reported for the whole cohort (NCT00753545); BRCA mutant patients (NCT01847274 and NCT01968213); HRD positive patients including BRCA mutant (NCT02477644); HRD positive patients (NCT02655016). Detailed clinical trial information is reported in Supplementary Tables S1 and S2. For trials noted as active but not recruiting, the primary completion date for data collection is noted. FDA, Food and Drug Administration (US); NMPA, National Medical Products Administration (China). HRD, homologous recombination deficiency; HRR, Homologous Recombination Repair; PARPi, PARP inhibitor. Created with Biorender.com.

## 2.2. Structure and Function of PARPis

While all PARPis contain pharmacologically active nicotinamide/benzamide core structures that compete with endogenous NAD to access catalytic binding pockets of PARPs, each has a unique structure overall [75–77]. PARP1 and PARP2 are common targets for all PARPis; however, PARPis have different binding affinities for certain other PARP family members [78,79] (Figure 3). Antolin and colleagues summarise the affinity of olaparib, rucaparib, niraparib and talazoparib for different PARPs based on IC<sub>50</sub> values from the literature and the ChEMBL database ([www.ebi.ac.uk/chembl](http://www.ebi.ac.uk/chembl)) [78]. PARP



trapping potency also differs between PARPis. During PARP trapping, the PARP complex locks on at sites of DNA breakage, inhibiting the release of PARP and likely removing it from the process of DNA repair-associated PARylation, as well as inhibiting binding of DNA repair factors [80–82]. In order from highest to lowest, the PARP trapping abilities of five PARPis have been reported as talazoparib, niraparib, rucaparib, olaparib, and finally veliparib [80,81]. Pamiparib has also been reported to display PARP trapping activity [83]. It has been suggested that differences in PARP trapping activity associated with higher cytotoxicity will need to be considered when testing in combination with other cytotoxic therapies [80].

	Talazoparib (BMN673)	Niraparib (MK4827)	Rucaparib (A014699)	Olaparib (AZD2281)	Veliparib (ABT888)	Fuzuloparib (SHR3162)	Pamiparib (BGB290)
Shared benzamide core							
Different R-groups							
Target	PARP1/2	PARP1/2	PARP1/2/3/4	PARP1/2/3/4	PARP1/2	PARP1/2	PARP1/2
PARP trapping*	1st	2nd	3th	4th	5th	N.A **	N.A ***

**Figure 3.** Chemical structures of clinically used PARP inhibitors. The chemical structures of PARP inhibitors (PARPis) are from ChEMBL database ([www.ebi.ac.uk/chembl](http://www.ebi.ac.uk/chembl), accessed on 15 June 2022). \* PARPis are listed by PARP trapping potency from highest to lowest [80]. \*\* There is no currently available data (N.A) for fuzuloparib PARP trapping potency. \*\*\* There is no currently available data for pamiparib trapping potency relative to other PARPis.

In addition to roles in DNA repair, PARPs function in other critical cellular processes. A role for PARP1 and PARP2 has been described in the maintenance of T-lymphocyte number and function [84]. PARP1 trapping has been shown to result in toxicity in healthy bone marrow [85]. PARP2 has been implicated in erythropoiesis and PARP2 deficient mice (Parp2<sup>−/−</sup>) are chronically anaemic [86]. Given these additional roles of PARP family members in important cellular processes, it is perhaps not surprising that adverse events are reported by patients taking PARPis.

### 3. Clinical Trials—PARPis and Ovarian Cancer

Data from clinical trials over the last decade inform clinical decisions made today regarding the use of PARPis for women with HGSOE [87–89]. Several trials have been pivotal in gaining approval from regulatory bodies worldwide. Some of these are discussed below. Trials that have focussed on treating advanced ovarian cancer, treating patients as a maintenance therapy and combining PARPis with other drugs are listed in Supplementary Tables S1 and S2. While FDA approval is mainly referred to in this review, similar approvals have been granted from the European Medicines Agency (EMA), Therapeutic Goods Administration (TGA) in Australia and the National Medical Products Administration (NMPA) in China.

#### 3.1. Trials Informing Clinical Use of PARPis

Study 19 (NCT00753545) investigated olaparib as a maintenance treatment in women with recurrent platinum-sensitive HGSOE who had received 2 or more lines of platinum-based chemotherapy and had a partial or complete response to their latest round. Improvement in progression free survival (PFS) was seen in women allocated olaparib versus placebo, and although not formally powered to study overall survival (OS), an advantage in OS was observed [90,91]. SOLO-1 (NCT01844986) was a landmark clinical trial that randomised women with advanced ovarian cancer based on mutations in *BRCA1* or *BRCA2* to olaparib or placebo maintenance after first-line chemotherapy. PFS in women receiving olaparib showed unprecedented improvement [92,93]. SOLO2/ENGOT-ov21 (NCT01874353)

investigated women with a *BRCA* mutation and platinum-sensitive relapsed ovarian cancer, showing again, unprecedented improvement, this time in OS [94]. Olaparib is the first PARPi to be approved for use in combination therapy. The PAOLA-1 trial (NCT02477644) combined olaparib with bevacizumab to treat women with advanced ovarian cancer, observing significant improvement in PFS in patients with HRR defective tumours [95].

The outcomes of ARIEL2 (NCT01891344) saw increases in PFS in women treated with rucaparib who had platinum sensitive relapsed HGSOc with high levels of tumour loss of heterozygosity [96]. The PRIMA/ENGOT-OV26/GOG-3012 trial (NCT02655016) investigated niraparib in women with newly diagnosed advanced, platinum sensitive ovarian cancer and showed significant improvement in PFS regardless of HRR status [97]. Niraparib is the first PARPi recommended to be administered regardless of whether cells are HRR deficient or proficient. Outcomes of the clinical trial NCT03333915 has led to approval of pamiparib for recurrent advanced ovarian cancer and germline *BRCA* mutation [69,98]. Fuzuloparib has been approved for similar indications based on the outcomes of NCT03509636 and NCT03863860 clinical trials [70].

Of note, not all ovarian cancer clinical trials of new PARPis led to approval for routine use in patients. While iniparib showed early promise, it failed clinical trials in a number of malignancies including ovarian cancer, triple-negative breast cancer, squamous non-small-cell lung cancer and others, it was structurally different to other PARPis under development and was shown not to inhibit PARP at clinically relevant doses [99,100].

### 3.2. Adverse Events Associated with PARPis

The most frequent adverse events reported by patients taking a PARPi include non-haematological toxicities such as nausea, vomiting and fatigue as well as haematological side effects such as anaemia and thrombocytopenia [101–105]. Some side effects seem to be amplified with specific PARPis. In patients taking olaparib, nasopharyngitis and decreased appetite have been reported [63,106]. Neutropenia, insomnia, hypertension, tachycardia and palpitations are more often reported for patients taking niraparib [103,107,108]. Large dose reductions of niraparib can also be required to manage the effects of thrombocytopenia [109]. Patients taking rucaparib have reported dysgeusia, dyspepsia, greater sensitivity to the sun and other sources of ultra-violet light, itching and increased cholesterol [96,104,110]. While talazoparib has not been approved for patients with ovarian cancer, in patients with germline *BRCA* mutations and advanced breast cancer, shortness of breath has been reported [111,112]. Patients taking pamiparib [98] or fuzuloparib [70] report a decreased appetite, neutropenia and diarrhoea [98,113–115]. A meta-analysis has suggested that olaparib has the mildest toxicity of the PARPis, with rucaparib and niraparib reporting much higher levels of grade 3–5 adverse events [116]. Relative to the adverse events reported with platinum-based chemotherapy, PARPi-associated adverse events may, in many patients, be considered less impactful in the context of quality of life. Furthermore, some of the more common adverse effects reported in the first 6 months of PARPi treatment were able to be resolved after this time by dose interruptions or reductions, as well as supportive care [91,104,109,117].

### 3.3. Long Term Responders to PARP Inhibition

Studies are beginning to report on long term responders to PARPis. The first study to support a survival advantage for ovarian cancer patients given a PARPi was conducted by Ledermann and colleagues where 13% (18 of 136 patients) had received maintenance olaparib for 5 or more years [118]. This study reported that patients with recurrent HGSOc that was *BRCA*-mutated and platinum-sensitive who received olaparib as a sole agent for maintenance after platinum therapy achieved longer OS than patients receiving placebo, albeit not reaching statistical significance in this study. Further investigation of this, and another, cohort, classified long term responders as >2 years and short-term responders as <3 months. It was concluded that reasons for a long-term response to olaparib was likely multifactorial; however, the presence of mutations in *BRCA1* or *BRCA2* increased the

likelihood of longer survival, with *BRCA2* mutations in particular being enriched amongst the long-term responders [119].

Another study investigating long term response to rucaparib classified long term response as  $\geq 12$  months, intermediate response as  $>6$  months but  $<12$  months, and a short response as  $<6$  months. Of the responders in this study, 27.5% (38 of 138 patients) had a long-term response. Interestingly, patients with *BRCA* structural variants, such as deletions or rearrangements, were amongst the longer-term responders, in some instances up to 4 years. These types of variants are less likely to succumb to secondary reversion mutations, thereby removing at least one of the mechanisms of developing resistance to a PARPi [120]. In this study, high levels of *BRCA1* methylation also corresponded to longer OS. As with olaparib, extended treatment with rucaparib has been shown to be both safe and well tolerated [119,120]. With the accumulation of time, additional studies on long-term survivors of HGSOC treated with a maintenance PARPi will no doubt emerge and elucidate further predictive biomarkers of this sought after response.

#### 4. Understanding and Overcoming PARPi Resistance

As with platinum-based drugs, some patients with ovarian cancer have innate resistance to a PARPi and some acquire resistance during treatment. Currently there are four mechanisms thought to influence resistance to a PARPi: (i) reactivation of HRR by secondary mutations or loss of hypermethylation, (ii) stabilisation of the DNA replication fork, (iii) reduction in the efficacy of PARP trapping and, (iv) cellular availability of the inhibitor (Figure 4).

##### 4.1. Reactivation of HRR

*BRCA1/2* reversion mutations have been found in ovarian tumour tissue and cell lines from patients, with correlations or predictions made with loss of sensitivity to both platinum drugs and PARPis [13,121–123]. Furthermore, these mutations have been detected in circulating cell-free DNA (cfDNA) in plasma from patients both pre-treatment and after progression of their cancer, correlating with decreased responses to a PARPi [124]. Methylation of the *BRCA1* promoter that silences *BRCA1* gene expression has been reported in ovarian cancer tissue [8,20,125]. Loss of *BRCA1* gene silencing by methylation was investigated in HGSOC patient-derived xenografts challenged with rucaparib. This study showed that loss of methylation can occur post chemotherapy and that while methylation of both *BRCA1* alleles was associated with a response to the PARPi, heterozygous methylation was associated with resistance [18]. Another way cancer cells have been shown to restore HRR proficiency is by producing splice variants. An example of this is the *BRCA1-Δ11q* alternative splice isoform that lacks the majority of exon 11. The presence of a frameshift mutation in *BRCA1* was shown to result in nonsense mediated decay of full-length mRNA transcripts, but not of the *BRCA1-Δ11q* isoform. Subsequently, presence of the *BRCA1-Δ11q* protein isoform was linked with partial resistance to treatment with a PARPi and cisplatin [126–128].

Genetic and epigenetic events in other genes functioning in HRR have also been linked to loss of PARPi sensitivity. Secondary mutations in *RAD51C* and *RAD51D* have been observed to restore the open reading frame of these genes and negatively impact upon PARPi sensitivity [129]. Loss of *RAD51C* methylation has also been shown to impact upon cellular sensitivity to a PARPi [24]. Furthermore, loss of the DNA damage response factor p53-binding protein 1 (53BP1) in *BRCA1* mutant cells has been shown to restore HRR proficiency and inhibit sensitivity to PARP inhibition [130].

Aberrations of other genes including *REV7* and *TRIP13* can also serve to reactivate HRR. *REV7* is a member of the shieldin complex that is recruited to DSBs, where, amongst other activities, it assists non-homologous end joining (NHEJ)-dependent repair of intra-chromosomal breaks and sensitises *BRCA1*-deficient cells to PARP inhibition [131]. Loss of *REV7* in *BRCA1*-deficient cells restores HRR leading to resistance to PARPis [132]. As a negative regulator of *REV7*, the *TRIP13* ATPase, frequently upregulated in cancer, has also been implicated in restoring HRR, leading to resistance to PARP inhibition [133].

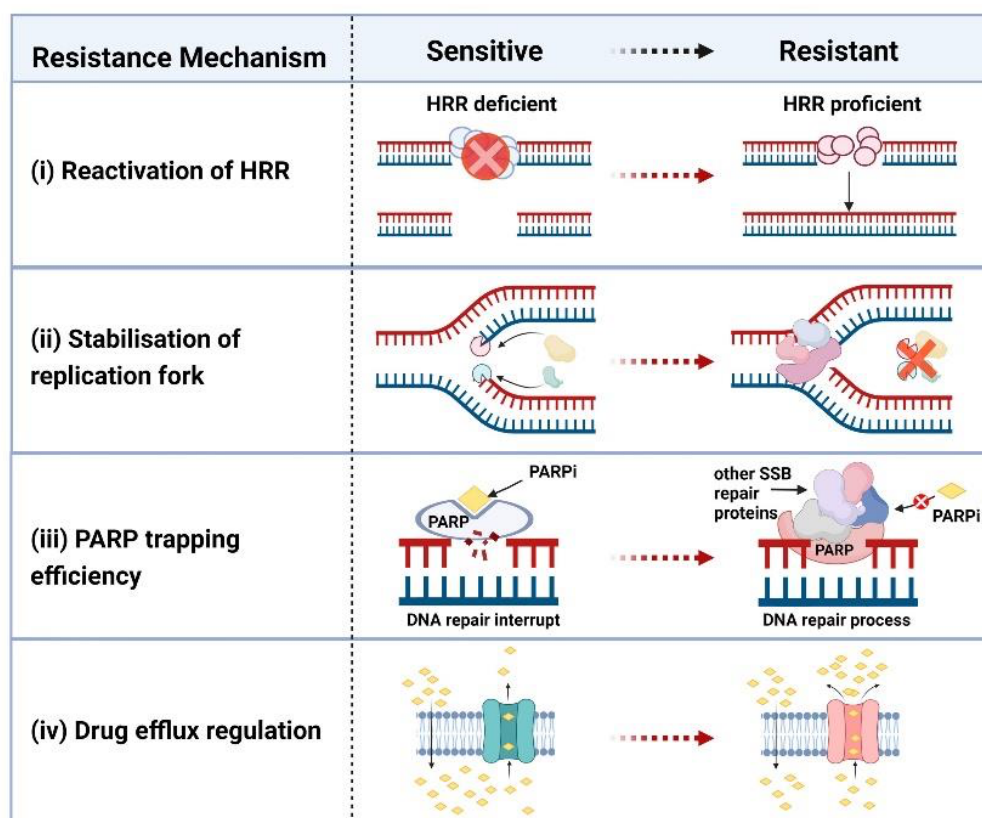


**Figure 4.** Mechanisms of PARP inhibitor resistance. There are four generally accepted mechanisms of PARPi resistance. (i) Homologous Recombination (HRR) restoration. The synthetic lethality is based on HRR deficiency and PARP inhibition. When HR reactivates in cancer cells for reasons including the occurrence of a reversion mutation, DNA damage can be repaired by the HRR pathway, cancer cells survive and become resistant to PARP inhibitors (PARPis). (ii) Stabilisation of the replication fork. Some HRR-associated proteins also function to stabilise stalled DNA replication forks. In HRR deficient cells (sensitive to PARPi), stalled replication forks will be degraded by DNA nucleases (e.g., MRE11, MUS81). PARPi resistant cells protect the replication fork by inhibiting the recruitment of DNA nucleases, therefore maintaining genomic stability. (iii) A PARP mutation can affect the ability of PARPi to bind PARP, leading to a decrease in PARP trapping. Mutated PARP can recruit other DNA repair proteins to correct single-strand breaks, leading to PARPi resistance and cell survival. (iv) Increase in drug efflux. Some PARPis (e.g., olaparib) are substrates of the transmembrane glycoprotein MDR1 (multi-drug resistance protein 1), also known as p-glycoprotein 1. By upregulating the activities of MDR1, PARPi is transported out of the cancer cells. Created with Biorender.com.

#### 4.2. Stabilisation/Destabilisation of the DNA Replication Fork

HRR-associated proteins including BRCA1, BRCA2 and RAD51, function to stabilise stalled DNA replication forks [134–137]. They do this by protecting newly transcribed DNA at stalled or reversed replication forks from degradation by the DNA repair nuclease MRE11, thus avoiding genomic instability [138]. HRR-associated proteins that become dysfunctional due to mutation or methylation lose their ability to protect against degradation of DNA at the replication fork, therefore triggering susceptibility to PARP inhibition.

As such a critical element in the maintenance of genomic stability, it is not surprising that a number of additional factors are involved in protection of the DNA replication fork. One of these other factors is the SNF2-family DNA translocase SMARCA1 that functions in BRCA1/2-deficient cells to stabilise the DNA replication fork [139]. Another of these factors is the MLL3/4 complex protein PTIP that functions to inhibit the recruitment of MRE11 to stalled replication forks, thus preventing their degradation and ensuring their



stabilisation [140]. Inhibition of the MUS81 nuclease has also been shown to restore DNA replication fork protection in *BRCA*-mutant cells [141]. In these ways, both resistance to PARPis, as well as platinum drugs, develops based on stabilisation of the DNA replication fork, even though the original events of defective HRR signaling remain.

Given that stabilisation of the stalled DNA replication fork leads to PARPi resistance in HRR-defective tumours, strategies that encourage collapse of this fork and so overcome replication fork protection should work to overcome this resistance, thus restoring sensitivity to PARP inhibition. Acetylation of histone 4 at lysine 8 (H4K8) by the histone acetyltransferase PCAF (p300/CBP-associated) recruits the MRE11 nuclease to stalled forks, but PCAF activity has been reported as low in some *BRCA2*-deficient cells [142]. The RNA polymerase 1 inhibitor CX-5461 has also been demonstrated to overcome replication fork protection in patient-derived xenograft (PDX) models of HRR-deficient HGSOV involving MRE11 degradation of replication forks [143,144]. Down-regulation of the de-ubiquitylating enzyme USP1 (ubiquitin specific peptidase 1) in *BRCA1*-deficient cells leads to replication fork destabilisation in a synthetic lethal manner and may be another strategy to address PARPi resistance in HRR deficient tumour cells that have undergone stabilisation of the DNA replication fork [145,146].

#### 4.3. PARP Trapping Efficiency

PARP trapping efficiency can be decreased by both mutations in PARP and by decreasing levels of PARP in the cell. The E3 ubiquitin ligase TRIP12 has been shown to polyubiquitinate PARP1, thus marking it for proteasomal degradation and limiting the efficacy of PARP1 trapping [147]. Furthermore, mutations in the PARP1 DNA-binding zinc-finger domains have been shown to decrease PARP1 trapping, therefore decreasing sensitivity to PARPis with a high reliance on PARP trapping to effect cytotoxicity [148].

#### 4.4. Regulation of Drug Efflux Pumps

Multi-drug resistance proteins are plasma membrane pumps that actively work to transport cytotoxic agents such as chemotherapy drugs out of the cancer cell. Upregulation of these drug efflux pumps can cause drug resistance. Multi-drug Resistance Protein 1 (MDR1), also known as p-glycoprotein 1, is a transmembrane glycoprotein belonging to the superfamily of ATP-binding cassette (ABC) transporters [149]. Upregulation of this drug efflux pump has been reported as the result of promoter fusion in patients with ovarian cancer [149]. MDR1 substrates include paclitaxel [150–152], but there appears to be a varied response to different PARPis. There is evidence that olaparib is a MDR1 substrate, with upregulation of this drug resistance pump being a mechanism of resistance to this PARPi [153,154].

Two possible strategies to overcome or avoid PARPi resistance related to drug efflux pumps are to either reduce the expression of drug transporters or employ PARPis that do not appear to be substrates of p-glycoprotein. All-trans retinoic acid (ATRA), targets activity of the cancer stem cell marker aldehyde dehydrogenase A1 (ALDH1A) and has also been shown to down-regulate p-glycoprotein [155]. Treatment of cells with diethylaminobenzaldehyde (DEAB) also results in down-regulation of p-glycoprotein [155]. Furthermore, in a genetically engineered mouse model of *Brca2*-related breast cancer, inhibition of p-glycoprotein with tariquidar was shown to partially re-sensitise some tumours to olaparib [156]. While olaparib is a substrate of p-glycoprotein, veliparib and pamiparib do not appear to be and so resistance to these PARPis should not be mechanistically related to this plasma membrane pump [153,154]. Combination therapies that minimise the activity of drug efflux pumps, while at the same time facilitate inhibition of PARP, should be considered.

### 5. Drug Repurposing for HRR Deficient Ovarian Cancer

To date, the development of PARPis for HRR deficient ovarian cancer remains focussed on identification of new drugs. Many FDA approved drugs for cancer and non-cancer

indications are pleiotropic and provide non-specific inhibition of multiple targets, including PARP, but remain under-studied for potential clinical use for HRR deficient ovarian cancer. The method of identifying new uses for approved or investigational drugs that are outside the scope of the original intended or approved medical use is termed drug repurposing [157,158]. The development of repurposed drugs that target PARP is attractive both in terms of the substantial cost and time efficiencies it offers in comparison to drug discovery [159].

The very first report of PARP inhibition was the discovery that nicotinamide has weak PARPi properties [160] and virtually all PARPis developed to date still contain the nicotinamide pharmacophore [161]. The anti-psychotic drug class, benzamides, were the second class of agents to have reported PARPi activity [162]. Analogs of both nicotinamide and benzamides have been used to extensively study the selective blocking of the NAD<sup>+</sup> catalytic domain of PARP [163] but have not been further investigated for potential clinical use due to weak PARP inhibition. Other PARP binding domains remain understudied as potential drug binding sites including the DNA-binding zinc-finger binding domains [163,164] and the WGR domain [165].

Although the PARP inhibition reported for nicotinamide and benzamides was not at therapeutically relevant levels for HRR-deficient ovarian cancer, there remains an opportunity to screen for other drug classes that inhibit PARP. To date, there are limited examples of large-scale drug repurposing screens for PARP inhibition for HRR deficient ovarian cancer. One such screen used the Prestwick chemical library that contains 1,280 FDA-approved drugs to identify the alkylating agent chlorambucil as being toxic to *BRCA1/2* deficient cells [166]. There is potential that future repurposing screens for PARP inhibition activity of FDA approved drugs, will identify cost-effective and readily available treatment options targeted at PARP inhibition in HRR deficient ovarian cancer.

## 6. Discovering New Synthetic Lethal Relationships to Treat Ovarian Cancer

Based entirely on the concept of synthetic lethality, PARPis have clearly made a major impact on the survival of women with HRR defective ovarian cancer. Can this major advance be emulated to design new approaches for the treatment of PARPi and/or platinum-resistant tumours, as well as for ovarian, and other, cancers, that are HRR proficient? Discovery tools have expanded to meet this challenge with the advent of three-dimensional cancer models, both cell lines and organoids, that can better mimic the behaviour of cancer cells in vivo in a sustained manner, including their response to molecular targeted drugs [1,167–172]. Given that *TP53* is mutated in almost all HGSOC, the development of a synthetic lethal strategy to target the effect of these mutations would have large impact. Proteins and pathways under investigation as synthetic lethal partners to mutant p53 include the DNA damage checkpoint kinase CHK1, the nuclear kinase WEE1, ATR (ataxia telangiectasia and Rad3-related protein) and components of PI3-K (phosphoinositide 3-kinase) signaling (reviewed in [173]). Knockdown of TIGAR (TP53 induced glycolysis and apoptosis regulator) was shown to down-regulate *BRCA1* and the Fanconi anemia pathway, increasing the efficacy of olaparib [174].

An increasing number of studies are focussing on achieving and/or increasing sensitivity to different PARPis, including in cancer cells that are HRR proficient. A key question being explored in these studies is can HRR deficiency in fact be induced? While many of these studies are being conducted in cancer types other than ovarian, the discoveries made have direct relevance to ovarian cancer. Using HRR proficient pancreatic cancer cells for discovery, investigators have shown that a small molecule disruptor of the *BRCA2*-*RAD51* relationship sensitised cells to olaparib at a level comparable to *BRCA2* mutated cells [175]. Continuing with a focus on *RAD51*, the LRRK2 (leucine-rich repeat kinase 2) inhibitor GSK2578215A suppressed HRR, disrupting the *BRCA2*-*RAD51* relationship in DNA repair, with cells showing increased sensitivity to olaparib [176]. Irrespective of HRR status, combinations of DNA damage response inhibitors suppressing WEE1, CHK1 and ATR have shown synergistic effects with olaparib in ID8 mouse ovarian surface epithelial cells [177].

Pre-clinical studies have also highlighted the potential of focussing on modulators of the epigenome as targets for synergistic activity with PARPis, that can induce HRR deficiency. These studies include targeting chromatin readers like bromodomain-containing proteins such as BRD4 with BET inhibitors [178–180] and chromatin writers such as the E3 ubiquitin ligase RNF20 [181]. Additionally, the DNA methyltransferase inhibitors 5-azacytidine and decitabine, have been shown to sensitise cancers with intact BRCA to PARPis by stimulating innate immune signaling that is in part mediated by STING (Stimulator of Interferon Genes) [182]. High throughput screening approaches using CRISPR-Cas9 and/or shRNA libraries are already identifying new synthetic lethal pairings with the potential to impact upon cancer therapy (reviewed in [183,184]).

## 7. PARPis and Immunotherapy

The remarkable benefits of immune checkpoint blockade seen for some tumours such as melanoma have not yet been recapitulated for ovarian cancer, a tumour that is largely viewed as “cold”. Cold tumours have few to no infiltrating T cells and are unable to mount an effective immune response [185]. Reasons for this include that compared to some other malignancies, ovarian tumours have a low tumour mutational burden (TMB), immunosuppressive functions of the tumour microenvironment (TME) and low expression of the targets of checkpoint blockade, including PD-L1 (programmed death ligand—1) [186,187].

Excitingly, combining a PARPi with an immunotherapy is showing early promise [188–190]. In preclinical models, niraparib has been shown to promote tumour immune cell infiltration by CD4<sup>+</sup> and CD8<sup>+</sup> T cells, induce activation of interferon signaling and work synergistically to decrease tumour volume when combined with the PD-L1 checkpoint inhibitor pembrolizumab [191]. Olaparib has also been shown to induce both intratumoral and peripheral effector CD4<sup>+</sup> and CD8<sup>+</sup> T cells in ovarian cancer cells lacking *Brca1* [192]. Furthermore, both niraparib and olaparib treatment has been shown to activate STING signaling that is important in mediating the proinflammatory immune response induced by DNA damage [191,192]. The addition of a STING agonist together with a PARPi in pre-clinical models of breast cancer lacking *BRCA1* increased anti-tumour immunity resulting in increased therapeutic efficacy that may also be an approach to overcoming resistance to PARP inhibition [193].

Early results of clinical trials combining niraparib and pembrolizumab show promise, including for patients with recurrent platinum-resistant ovarian cancer [194,195]. A study combining olaparib and the CHK1 (checkpoint kinase 1) inhibitor prexasertib in a small group of patients, identified partial response in some HGSOC patients with *BRCA1* mutant tumours who had demonstrated PARPi resistance [196]. Immunomodulatory effects of CHK1 inhibitors have recently been reported [197,198].

## 8. Conclusions

The synthetic lethality strategies underpinning the advent of PARPis have revolutionised the approach to clinical management of a large subset of women with HGSOC. Over the next decade, research in this field will necessarily proceed to more fully address platinum and PARPi resistant ovarian cancer. It is predicted that the field of combination therapies will expand beyond the currently approved combination of olaparib and bevacizumab, bringing the benefit of PARPis to a greater number of women with ovarian cancer. Lessons learned from targeting PARP will provide fundamental insights needed to expand synthetic lethal strategies to new combinations of genetic and/or epigenetic regulation and pharmacological inhibition.

**Supplementary Materials:** The following are available online at <https://www.mdpi.com/article/10.3390/cancers14194621/s1>, Table S1: Clinical trials of PARP inhibitors (PARPis) as a monotherapy in ovarian cancer, Table S2: Clinical trials of PARP inhibitors (PARPis) in combination therapy for ovarian cancer. References [22,69,70,88,89,93,94,97,101,103–105,114,118,194,199–232] are cited in the supplementary materials.

**Author Contributions:** Conceptualisation, D.J.M. and T.X.; data curation, K.-A.D. and Y.M.; writing—original draft preparation, D.J.M., T.X., C.Y. and N.A.B.; writing—review and editing, D.J.M., T.X., K.-A.D., C.Y., Y.M., C.E.F. and N.A.B.; visualisation, T.X. and D.J.M.; supervision, D.J.M.; project administration, D.J.M.; funding acquisition, N.A.B., D.J.M. and C.E.F. All authors have read and agreed to the published version of the manuscript.

**Funding:** T.X. and Y.M. are supported by scholarships from the Chinese Scholarship Council (CSC). C.Y. is supported by a grant to N.A.B., D.J.M. and C.E.F.: Australian Medical Research Future Fund (APP1199620). N.A.B. is supported by the Hunter Medical Research Institute Vanessa McGuigan Memorial Fellowship.

**Conflicts of Interest:** The authors declare no conflict of interest. The funders had no role in the design of the study; in the collection, analyses, or interpretation of data; in the writing of the manuscript, or in the decision to publish the results.

## References

1. Yee, C.; Dickson, K.A.; Muntasir, M.N.; Ma, Y.; Marsh, D.J. Three-Dimensional Modelling of Ovarian Cancer: From Cell Lines to Organoids for Discovery and Personalized Medicine. *Front. Bioeng. Biotechnol.* **2022**, *10*, 836984. [CrossRef] [PubMed]
2. Dion, L.; Carton, I.; Jaillard, S.; Nyangoh Timoh, K.; Henno, S.; Sardain, H.; Foucher, F.; Levêque, J.; de la Motte Rouge, T.; Brousse, S.; et al. The Landscape and Therapeutic Implications of Molecular Profiles in Epithelial Ovarian Cancer. *J. Clin. Med.* **2020**, *9*, 2239. [CrossRef] [PubMed]
3. Kurman, R.J.; Shih Ie, M. The origin and pathogenesis of epithelial ovarian cancer: A proposed unifying theory. *Am. J. Surg. Pathol.* **2010**, *34*, 433–443. [CrossRef] [PubMed]
4. Köbel, M.; Kalloger, S.E.; Boyd, N.; McKinney, S.; Mehl, E.; Palmer, C.; Leung, S.; Bowen, N.J.; Ionescu, D.N.; Rajput, A.; et al. Ovarian carcinoma subtypes are different diseases: Implications for biomarker studies. *PLoS Med.* **2008**, *5*, e232. [CrossRef]
5. Bowtell, D.D.; Böhm, S.; Ahmed, A.A.; Aspuria, P.J.; Bast, R.C., Jr.; Beral, V.; Berek, J.S.; Birrer, M.J.; Blagden, S.; Bookman, M.A.; et al. Rethinking ovarian cancer II: Reducing mortality from high-grade serous ovarian cancer. *Nat. Rev. Cancer* **2015**, *15*, 668–679. [CrossRef] [PubMed]
6. Beesley, V.L.; Green, A.C.; Wyld, D.K.; O'Rourke, P.; Wockner, L.F.; deFazio, A.; Butow, P.N.; Price, M.A.; Horwood, K.R.; Clavarino, A.M.; et al. Quality of life and treatment response among women with platinum-resistant versus platinum-sensitive ovarian cancer treated for progression: A prospective analysis. *Gynecol. Oncol.* **2014**, *132*, 130–136. [CrossRef]
7. SEER Ovarian Cancer. Available online: <https://seer.cancer.gov/statfacts/html/ovary.html> (accessed on 6 June 2022).
8. Bell, D.; Berchuck, A.; Birrer, M.; Chien, J.; Cramer, D.W.; Dao, F.; Dhir, R.; DiSaia, P.; Gabra, H.; Glenn, P.; et al. Integrated genomic analyses of ovarian carcinoma. *Nature* **2011**, *474*, 609–615.
9. Cole, A.J.; Dwight, T.; Gill, A.J.; Dickson, K.A.; Zhu, Y.; Clarkson, A.; Gard, G.B.; Maidens, J.; Valmadre, S.; Clifton-Bligh, R.; et al. Assessing mutant p53 in primary high-grade serous ovarian cancer using immunohistochemistry and massively parallel sequencing. *Sci. Rep.* **2016**, *6*, 26191. [CrossRef]
10. Fransson, Å.; Glaessgen, D.; Alfredsson, J.; Wiman, K.G.; Bajalica-Lagercrantz, S.; Mohell, N. Strong synergy with APR-246 and DNA-damaging drugs in primary cancer cells from patients with TP53 mutant High-Grade Serous ovarian cancer. *J. Ovarian Res* **2016**, *9*, 27. [CrossRef]
11. Amirtharaj, F.; Venkatesh, G.H.; Wojtas, B.; Nawafleh, H.H.; Mahmood, A.S.; Nizami, Z.N.; Khan, M.S.; Thiery, J.; Chouaib, S. p53 reactivating small molecule PRIMA-1(MET)/APR-246 regulates genomic instability in MDA-MB-231 cells. *Oncol. Rep.* **2022**, *47*, 85. [CrossRef]
12. Duffy, M.J.; Synnott, N.C.; O'Grady, S.; Crown, J. Targeting p53 for the treatment of cancer. *Semin. Cancer Biol.* **2022**, *79*, 58–67. [CrossRef] [PubMed]
13. Patch, A.M.; Christie, E.L.; Etemadmoghadam, D.; Garsed, D.W.; George, J.; Fereday, S.; Nones, K.; Cowin, P.; Alsop, K.; Bailey, P.J.; et al. Whole-genome characterization of chemoresistant ovarian cancer. *Nature* **2015**, *521*, 489–494. [CrossRef] [PubMed]
14. Alsop, K.; Fereday, S.; Meldrum, C.; deFazio, A.; Emmanuel, C.; George, J.; Dobrovic, A.; Birrer, M.J.; Webb, P.M.; Stewart, C.; et al. BRCA mutation frequency and patterns of treatment response in BRCA mutation-positive women with ovarian cancer: A report from the Australian Ovarian Cancer Study Group. *J. Clin. Oncol.* **2012**, *30*, 2654–2663. [CrossRef] [PubMed]
15. Pennington, K.P.; Walsh, T.; Harrell, M.I.; Lee, M.K.; Pennil, C.C.; Rendi, M.H.; Thornton, A.; Norquist, B.M.; Casadei, S.; Nord, A.S.; et al. Germline and somatic mutations in homologous recombination genes predict platinum response and survival in ovarian, fallopian tube, and peritoneal carcinomas. *Clin. Cancer Res.* **2014**, *20*, 764–775. [CrossRef] [PubMed]
16. Pelttari, L.M.; Heikkinen, T.; Thompson, D.; Kallioniemi, A.; Schleutker, J.; Holli, K.; Blomqvist, C.; Aittomäki, K.; Bützow, R.; Nevanlinna, H. RAD51C is a susceptibility gene for ovarian cancer. *Hum. Mol. Genet.* **2011**, *20*, 3278–3288. [CrossRef] [PubMed]
17. Loveday, C.; Turnbull, C.; Ruark, E.; Xicola, R.M.; Ramsay, E.; Hughes, D.; Warren-Perry, M.; Snape, K.; Eccles, D.; Evans, D.G.; et al. Germline RAD51C mutations confer susceptibility to ovarian cancer. *Nat. Genet.* **2012**, *44*, 475–476. [CrossRef]
18. Kondrashova, O.; Topp, M.; Nesic, K.; Lieschke, E.; Ho, G.Y.; Harrell, M.I.; Zapparo, G.V.; Hadley, A.; Holian, R.; Boehm, E.; et al. Methylation of all BRCA1 copies predicts response to the PARP inhibitor rucaparib in ovarian carcinoma. *Nat. Commun.* **2018**, *9*, 3970. [CrossRef]



19. Catteau, A.; Harris, W.H.; Xu, C.F.; Solomon, E. Methylation of the BRCA1 promoter region in sporadic breast and ovarian cancer: Correlation with disease characteristics. *Oncogene* **1999**, *18*, 1957–1965. [\[CrossRef\]](#)
20. Esteller, M.; Silva, J.M.; Dominguez, G.; Bonilla, F.; Matias-Guiu, X.; Lerma, E.; Bussaglia, E.; Prat, J.; Harkes, I.C.; Repasky, E.A.; et al. Promoter hypermethylation and BRCA1 inactivation in sporadic breast and ovarian tumors. *J. Natl. Cancer Inst.* **2000**, *92*, 564–569. [\[CrossRef\]](#)
21. Bianco, T.; Chenevix-Trench, G.; Walsh, D.C.; Cooper, J.E.; Dobrovic, A. Tumour-specific distribution of BRCA1 promoter region methylation supports a pathogenetic role in breast and ovarian cancer. *Carcinogenesis* **2000**, *21*, 147–151. [\[CrossRef\]](#)
22. Swisher, E.M.; Kwan, T.T.; Oza, A.M.; Tinker, A.V.; Ray-Coquard, I.; Oaknin, A.; Coleman, R.L.; Aghajanian, C.; Konecny, G.E.; O'Malley, D.M.; et al. Molecular and clinical determinants of response and resistance to rucaparib for recurrent ovarian cancer treatment in ARIEL2 (Parts 1 and 2). *Nat. Commun.* **2021**, *12*, 2487. [\[CrossRef\]](#) [\[PubMed\]](#)
23. Hurley, R.M.; McGehee, C.D.; Nesic, K.; Correia, C.; Weiskittel, T.M.; Kelly, R.L.; Venkatachalam, A.; Hou, X.; Pathoulas, N.M.; Meng, X.W.; et al. Characterization of a RAD51C-silenced high-grade serous ovarian cancer model during development of PARP inhibitor resistance. *NAR Cancer* **2021**, *3*, zcab028. [\[CrossRef\]](#)
24. Nesic, K.; Kondrashova, O.; Hurley, R.M.; McGehee, C.D.; Vandenberg, C.J.; Ho, G.Y.; Lieschke, E.; Dall, G.; Bound, N.; Shield-Artin, K.; et al. Acquired RAD51C Promoter Methylation Loss Causes PARP Inhibitor Resistance in High-Grade Serous Ovarian Carcinoma. *Cancer Res.* **2021**, *81*, 4709–4722. [\[CrossRef\]](#)
25. Min, A.; Im, S.A.; Yoon, Y.K.; Song, S.H.; Nam, H.J.; Hur, H.S.; Kim, H.P.; Lee, K.H.; Han, S.W.; Oh, D.Y.; et al. RAD51C-deficient cancer cells are highly sensitive to the PARP inhibitor olaparib. *Mol. Cancer Ther.* **2013**, *12*, 865–877. [\[CrossRef\]](#)
26. Goodheart, M.J.; Rose, S.L.; Hattermann-Zogg, M.; Smith, B.J.; De Young, B.R.; Buller, R.E. BRCA2 alteration is important in clear cell carcinoma of the ovary. *Clin. Genet.* **2009**, *76*, 161–167. [\[CrossRef\]](#) [\[PubMed\]](#)
27. Yao, Q.; Liu, Y.; Zhang, L.; Dong, L.; Bao, L.; Bai, Q.; Cui, Q.; Xu, J.; Li, M.; Liu, J.; et al. Mutation Landscape of Homologous Recombination Repair Genes in Epithelial Ovarian Cancer in China and Its Relationship with Clinicopathological Characteristics. *Front. Oncol.* **2022**, *12*, 709645. [\[CrossRef\]](#)
28. Cao, C.; Yu, R.; Gong, W.; Liu, D.; Zhang, X.; Fang, Y.; Xia, Y.; Zhang, W.; Gao, Q. Genomic mutation features identify distinct BRCA-associated mutation characteristics in endometrioid carcinoma and endometrioid ovarian carcinoma. *Aging* **2021**, *13*, 24686–24709. [\[CrossRef\]](#) [\[PubMed\]](#)
29. Gou, R.; Dong, H.; Lin, B. Application and reflection of genomic scar assays in evaluating the efficacy of platinum salts and PARP inhibitors in cancer therapy. *Life Sci.* **2020**, *261*, 118434. [\[CrossRef\]](#)
30. Watkins, J.A.; Irshad, S.; Grigoriadis, A.; Tutt, A.N. Genomic scars as biomarkers of homologous recombination deficiency and drug response in breast and ovarian cancers. *Breast Cancer Res.* **2014**, *16*, 211. [\[CrossRef\]](#)
31. Nguyen, L.; WM Martens, J.; Van Hoeck, A.; Cuppen, E. Pan-cancer landscape of homologous recombination deficiency. *Nat. Commun.* **2020**, *11*, 5584. [\[CrossRef\]](#)
32. Sekine, M.; Nishino, K.; Enomoto, T. BRCA Genetic Test and Risk-Reducing Salpingo-Oophorectomy for Hereditary Breast and Ovarian Cancer: State-of-the-Art. *Cancers* **2021**, *13*, 2562. [\[CrossRef\]](#) [\[PubMed\]](#)
33. Ngoi, N.Y.L.; Tan, D.S.P. The role of homologous recombination deficiency testing in ovarian cancer and its clinical implications: Do we need it? *ESMO Open* **2021**, *6*, 100144. [\[CrossRef\]](#) [\[PubMed\]](#)
34. Liu, L.; Matsunaga, Y.; Tsurutani, J.; Akashi-Tanaka, S.; Masuda, H.; Ide, Y.; Hashimoto, R.; Inuzuka, M.; Watanabe, C.; Taruno, K.; et al. BRCAness as a prognostic indicator in patients with early breast cancer. *Sci. Rep.* **2020**, *10*, 21173. [\[CrossRef\]](#) [\[PubMed\]](#)
35. Dhawan, M.; Ryan, C.J. BRCAness and prostate cancer: Diagnostic and therapeutic considerations. *Prostate Cancer Prostatic Dis.* **2018**, *21*, 488–498. [\[CrossRef\]](#) [\[PubMed\]](#)
36. Wong, W.; Raufi, A.G.; Safyan, R.A.; Bates, S.E.; Manji, G.A. BRCA Mutations in Pancreas Cancer: Spectrum, Current Management, Challenges and Future Prospects. *Cancer Manag. Res.* **2020**, *12*, 2731–2742. [\[CrossRef\]](#)
37. Wang, Y.; Zheng, K.; Huang, Y.; Xiong, H.; Su, J.; Chen, R.; Zou, Y. PARP inhibitors in gastric cancer: Beacon of hope. *J. Exp. Clin. Cancer Res.* **2021**, *40*, 211. [\[CrossRef\]](#) [\[PubMed\]](#)
38. Catalano, F.; Borea, R.; Puglisi, S.; Boutros, A.; Gandini, A.; Cremante, M.; Martelli, V.; Sciallero, S.; Puccini, A. Targeting the DNA Damage Response Pathway as a Novel Therapeutic Strategy in Colorectal Cancer. *Cancers* **2022**, *14*, 1388. [\[CrossRef\]](#)
39. Fritz, C.; Portwood, S.M.; Przespolewski, A.; Wang, E.S. PARP goes the weasel! Emerging role of PARP inhibitors in acute leukemias. *Blood Rev.* **2021**, *45*, 100696. [\[CrossRef\]](#)
40. Jubin, T.; Kadam, A.; Jariwala, M.; Bhatt, S.; Sutariya, S.; Gani, A.R.; Gautam, S.; Begum, R. The PARP family: Insights into functional aspects of poly (ADP-ribose) polymerase-1 in cell growth and survival. *Cell Prolif.* **2016**, *49*, 421–437. [\[CrossRef\]](#)
41. Cerrato, A.; Morra, F.; Celetti, A. Use of poly ADP-ribose polymerase [PARP] inhibitors in cancer cells bearing DDR defects: The rationale for their inclusion in the clinic. *J. Exp. Clin. Cancer Res.* **2016**, *35*, 179. [\[CrossRef\]](#)
42. Demény, M.A.; Virág, L. The PARP Enzyme Family and the Hallmarks of Cancer Part 2: Hallmarks Related to Cancer Host Interactions. *Cancers* **2021**, *13*, 2057. [\[CrossRef\]](#) [\[PubMed\]](#)
43. De Vos, M.; Schreiber, V.; Dantzer, F. The diverse roles and clinical relevance of PARPs in DNA damage repair: Current state of the art. *Biochem. Pharmacol.* **2012**, *84*, 137–146. [\[CrossRef\]](#)
44. Abbotts, R.; Dellomo, A.J.; Rassool, F.V. Pharmacologic Induction of BRCAness in BRCA-Proficient Cancers: Expanding PARP Inhibitor Use. *Cancers* **2022**, *14*, 2640. [\[CrossRef\]](#)

45. Kamaletdinova, T.; Fanaei-Kahrani, Z.; Wang, Z.Q. The Enigmatic Function of PARP1: From PARylation Activity to PAR Readers. *Cells* **2019**, *8*, 1625. [CrossRef] [PubMed]
46. Ray Chaudhuri, A.; Nussenzweig, A. The multifaceted roles of PARP1 in DNA repair and chromatin remodelling. *Nat. Rev. Mol. Cell Biol.* **2017**, *18*, 610–621. [CrossRef] [PubMed]
47. Beck, C.; Robert, I.; Reina-San-Martin, B.; Schreiber, V.; Dantzer, F. Poly(ADP-ribose) polymerases in double-strand break repair: Focus on PARP1, PARP2 and PARP3. *Exp. Cell Res.* **2014**, *329*, 18–25. [CrossRef]
48. Caldecott, K.W. Single-strand break repair and genetic disease. *Nat. Rev. Genet.* **2008**, *9*, 619–631. [CrossRef]
49. Satoh, M.S.; Lindahl, T. Role of poly(ADP-ribose) formation in DNA repair. *Nature* **1992**, *356*, 356–358. [CrossRef]
50. Kuzminov, A. Single-strand interruptions in replicating chromosomes cause double-strand breaks. *Proc. Natl. Acad. Sci. USA* **2001**, *98*, 8241–8246. [CrossRef]
51. del Rivero, J.; Kohn, E.C. PARP Inhibitors: The Cornerstone of DNA Repair-Targeted Therapies. *Oncology* **2017**, *31*, 265–273.
52. Nijman, S.M. Synthetic lethality: General principles, utility and detection using genetic screens in human cells. *FEBS Lett.* **2011**, *585*, 1–6. [CrossRef] [PubMed]
53. Dziadkowiec, K.N.; Gąsiorowska, E.; Nowak-Markwitz, E.; Jankowska, A. PARP inhibitors: Review of mechanisms of action and BRCA1/2 mutation targeting. *Menopause Rev./Przegląd Menopauzalny* **2016**, *15*, 215–219. [CrossRef] [PubMed]
54. Demin, A.A.; Hirota, K.; Tsuda, M.; Adamowicz, M.; Hailstone, R.; Brazina, J.; Gittens, W.; Kalasova, I.; Shao, Z.; Zha, S.; et al. XRCC1 prevents toxic PARP1 trapping during DNA base excision repair. *Mol. Cell* **2021**, *81*, 3018–3030.e5. [CrossRef] [PubMed]
55. Chambon, P.; Weill, J.D.; Mandel, P. Nicotinamide mononucleotide activation of new DNA-dependent polyadenylic acid synthesizing nuclear enzyme. *Biochem. Biophys. Res. Commun.* **1963**, *11*, 39–43. [CrossRef]
56. Kraus, W.L. PARPs and ADP-Ribosylation: 50 Years . . . and Counting. *Mol. Cell* **2015**, *58*, 902–910. [CrossRef] [PubMed]
57. Durkacz, B.W.; Omidiji, O.; Gray, D.A.; Shall, S. (ADP-ribose)<sub>n</sub> participates in DNA excision repair. *Nature* **1980**, *283*, 593–596. [CrossRef]
58. Benjamin, R.C.; Gill, D.M. ADP-ribosylation in mammalian cell ghosts. Dependence of poly(ADP-ribose) synthesis on strand breakage in DNA. *J. Biol. Chem.* **1980**, *255*, 10493–10501. [CrossRef]
59. Purnell, M.R.; Whish, W.J. Novel inhibitors of poly(ADP-ribose) synthetase. *Biochem. J.* **1980**, *185*, 775–777. [CrossRef]
60. Farmer, H.; McCabe, N.; Lord, C.J.; Tutt, A.N.; Johnson, D.A.; Richardson, T.B.; Santarosa, M.; Dillon, K.J.; Hickson, I.; Knights, C.; et al. Targeting the DNA repair defect in BRCA mutant cells as a therapeutic strategy. *Nature* **2005**, *434*, 917–921. [CrossRef]
61. Bryant, H.E.; Schultz, N.; Thomas, H.D.; Parker, K.M.; Flower, D.; Lopez, E.; Kyle, S.; Meuth, M.; Curtin, N.J.; Helleday, T. Specific killing of BRCA2-deficient tumours with inhibitors of poly(ADP-ribose) polymerase. *Nature* **2005**, *434*, 913–917. [CrossRef]
62. U.S. Food and Drug Administration. Olaparib. Available online: <http://wayback.archive-it.org/7993/20170111231644/http://www.fda.gov/Drugs/InformationOnDrugs/ApprovedDrugs/ucm427598.htm>. (accessed on 8 July 2022).
63. Kim, G.; Ison, G.; McKee, A.E.; Zhang, H.; Tang, S.; Gwise, T.; Sridhara, R.; Lee, E.; Tzou, A.; Philip, R.; et al. FDA Approval Summary: Olaparib Monotherapy in Patients with Deleterious Germline BRCA-Mutated Advanced Ovarian Cancer Treated with Three or More Lines of Chemotherapy. *Clin. Cancer Res.* **2015**, *21*, 4257–4261. [CrossRef] [PubMed]
64. U.S. Food and Drug Administration. Rucaparib. Available online: <http://wayback.archive-it.org/7993/20170111231546/http://www.fda.gov/Drugs/InformationOnDrugs/ApprovedDrugs/ucm533891.htm> (accessed on 8 July 2022).
65. U.S. Food and Drug Administration. Niraparib (Zejula). Available online: <https://www.fda.gov/drugs/resources-information-approved-drugs/niraparib-zejula> (accessed on 8 July 2022).
66. U.S. Food and Drug Administration. FDA Approves Olaparib Tablets for Maintenance Treatment in Ovarian Cancer. Available online: <https://www.fda.gov/drugs/resources-information-approved-drugs/fda-approves-olaparib-tablets-maintenance-treatment-ovarian-cancer> (accessed on 8 July 2022).
67. U.S. Food and Drug Administration. FDA Approves Rucaparib for Maintenance Treatment of Recurrent Ovarian, Fallopian Tube, or Primary Peritoneal Cancer. Available online: <https://www.fda.gov/drugs/resources-information-approved-drugs/fda-approves-rucaparib-maintenance-treatment-recurrent-ovarian-fallopian-tube-or-primary-peritoneal> (accessed on 8 July 2022).
68. FDA. FDA Approves Talazoparib for gBRCAm HER2-Negative Locally Advanced or Metastatic Breast Cancer. FDA Approves Talazoparib for gBRCAm HER2-Negative Locally Advanced or Metastatic Breast Cancer | FDA. Available online: <https://www.fda.gov/drugs/drug-approvals-and-databases/fda-approves-talazoparib-gbrcam-her2-negative-locally-advanced-or-metastatic-breast-cancer> (accessed on 22 June 2022).
69. Markham, A. Pamiparib: First Approval. *Drugs* **2021**, *81*, 1343–1348. [CrossRef] [PubMed]
70. Lee, A. Fuzuloparib: First Approval. *Drugs* **2021**, *81*, 1221–1226. [CrossRef] [PubMed]
71. U.S. Food and Drug Administration. FDA Approves Niraparib for HRD-Positive Advanced Ovarian Cancer. Available online: <https://www.fda.gov/drugs/resources-information-approved-drugs/fda-approves-niraparib-hrd-positive-advanced-ovarian-cancer> (accessed on 8 July 2022).
72. U.S. Food and Drug Administration. FDA approves Olaparib Plus Bevacizumab as Maintenance Treatment for Ovarian, Fallopian Tube, or Primary Peritoneal Cancers. Available online: <https://www.fda.gov/drugs/resources-information-approved-drugs/fda-approves-olaparib-plus-bevacizumab-maintenance-treatment-ovarian-fallopian-tube-or-primary> (accessed on 8 July 2022).
73. Lee, A. Niraparib: A Review in First-Line Maintenance Therapy in Advanced Ovarian Cancer. *Target. Oncol.* **2021**, *16*, 839–845. [CrossRef]

74. U.S. Food and Drug Administration. FDA Approves Niraparib for First-Line Maintenance of Advanced Ovarian Cancer. Available online: <https://www.fda.gov/drugs/resources-information-approved-drugs/fda-approves-niraparib-first-line-maintenance-advanced-ovarian-cancer> (accessed on 22 June 2022).
75. Ferraris, D.V. Evolution of poly(ADP-ribose) polymerase-1 (PARP-1) inhibitors. From concept to clinic. *J. Med. Chem.* **2010**, *53*, 4561–4584. [\[CrossRef\]](#)
76. Steffen, J.D.; Brody, J.R.; Armen, R.S.; Pascal, J.M. Structural Implications for Selective Targeting of PARPs. *Front. Oncol.* **2013**, *3*, 301. [\[CrossRef\]](#)
77. Min, A.; Im, S.A. PARP Inhibitors as Therapeutics: Beyond Modulation of PARylation. *Cancers* **2020**, *12*, 394. [\[CrossRef\]](#)
78. Antolin, A.A.; Ameratunga, M.; Banerji, U.; Clarke, P.A.; Workman, P.; Al-Lazikani, B. The kinase polypharmacology landscape of clinical PARP inhibitors. *Sci. Rep.* **2020**, *10*, 2585. [\[CrossRef\]](#)
79. Valabrega, G.; Scotto, G.; Tuninetti, V.; Pani, A.; Scaglione, F. Differences in PARP Inhibitors for the Treatment of Ovarian Cancer: Mechanisms of Action, Pharmacology, Safety, and Efficacy. *Int. J. Mol. Sci.* **2021**, *22*, 4203. [\[CrossRef\]](#)
80. Lord, C.J.; Ashworth, A. PARP inhibitors: Synthetic lethality in the clinic. *Science* **2017**, *355*, 1152–1158. [\[CrossRef\]](#)
81. Murai, J.; Huang, S.Y.; Das, B.B.; Renaud, A.; Zhang, Y.; Doroshow, J.H.; Ji, J.; Takeda, S.; Pommier, Y. Trapping of PARP1 and PARP2 by Clinical PARP Inhibitors. *Cancer Res.* **2012**, *72*, 5588–5599. [\[CrossRef\]](#)
82. Hopkins, T.A.; Shi, Y.; Rodriguez, L.E.; Solomon, L.R.; Donawho, C.K.; DiGiammarino, E.L.; Panchal, S.C.; Wilsbacher, J.L.; Gao, W.; Olson, A.M.; et al. Mechanistic Dissection of PARP1 Trapping and the Impact on In Vivo Tolerability and Efficacy of PARP Inhibitors. *Mol. Cancer Res.* **2015**, *13*, 1465–1477. [\[CrossRef\]](#) [\[PubMed\]](#)
83. Xiong, Y.; Guo, Y.; Liu, Y.; Wang, H.; Gong, W.; Liu, Y.; Wang, X.; Gao, Y.; Yu, F.; Su, D.; et al. Pamiparib is a potent and selective PARP inhibitor with unique potential for the treatment of brain tumor. *Neoplasia* **2020**, *22*, 431–440. [\[CrossRef\]](#) [\[PubMed\]](#)
84. Navarro, J.; Gozalbo-López, B.; Méndez, A.C.; Dantzer, F.; Schreiber, V.; Martínez, C.; Arana, D.M.; Farrés, J.; Revilla-Nuin, B.; Bueno, M.F.; et al. PARP-1/PARP-2 double deficiency in mouse T cells results in faulty immune responses and T lymphomas. *Sci. Rep.* **2017**, *7*, 41962. [\[CrossRef\]](#)
85. Hopkins, T.A.; Ainsworth, W.B.; Ellis, P.A.; Donawho, C.K.; DiGiammarino, E.L.; Panchal, S.C.; Abraham, V.C.; Algire, M.A.; Shi, Y.; Olson, A.M.; et al. PARP1 Trapping by PARP Inhibitors Drives Cytotoxicity in Both Cancer Cells and Healthy Bone Marrow. *Mol. Cancer Res.* **2019**, *17*, 409–419. [\[CrossRef\]](#)
86. Farrés, J.; Llacuna, L.; Martín-Caballero, J.; Martínez, C.; Lozano, J.J.; Ampurdanés, C.; López-Contreras, A.J.; Florensa, L.; Navarro, J.; Ottina, E.; et al. PARP-2 sustains erythropoiesis in mice by limiting replicative stress in erythroid progenitors. *Cell Death Differ.* **2015**, *22*, 1144–1157. [\[CrossRef\]](#) [\[PubMed\]](#)
87. Foo, T.; George, A.; Banerjee, S. PARP inhibitors in ovarian cancer: An overview of the practice-changing trials. *Genes Chromosomes Cancer* **2021**, *60*, 385–397. [\[CrossRef\]](#)
88. Luo, L.; Keyomarsi, K. PARP inhibitors as single agents and in combination therapy: The most promising treatment strategies in clinical trials for BRCA-mutant ovarian and triple-negative breast cancers. *Expert Opin. Investig. Drugs* **2022**, *31*, 607–631. [\[CrossRef\]](#)
89. Smith, M.; Pothuri, B. Appropriate Selection of PARP Inhibitors in Ovarian Cancer. *Curr. Treat. Options Oncol.* **2022**, *23*, 887–903. [\[CrossRef\]](#)
90. Ledermann, J.; Harter, P.; Gourley, C.; Friedlander, M.; Vergote, I.; Rustin, G.; Scott, C.; Meier, W.; Shapira-Frommer, R.; Safrá, T.; et al. Olaparib maintenance therapy in platinum-sensitive relapsed ovarian cancer. *N. Engl. J. Med.* **2012**, *366*, 1382–1392. [\[CrossRef\]](#)
91. Friedlander, M.; Matulonis, U.; Gourley, C.; du Bois, A.; Vergote, I.; Rustin, G.; Scott, C.; Meier, W.; Shapira-Frommer, R.; Safrá, T.; et al. Long-term efficacy, tolerability and overall survival in patients with platinum-sensitive, recurrent high-grade serous ovarian cancer treated with maintenance olaparib capsules following response to chemotherapy. *Br. J. Cancer* **2018**, *119*, 1075–1085. [\[CrossRef\]](#) [\[PubMed\]](#)
92. Miller, R.E.; Crusz, S.M.; Ledermann, J.A. Olaparib maintenance for first-line treatment of ovarian cancer: Will SOLO1 reset the standard of care? *Future Oncol.* **2019**, *15*, 1845–1853. [\[CrossRef\]](#) [\[PubMed\]](#)
93. Moore, K.; Colombo, N.; Scambia, G.; Kim, B.G.; Oaknin, A.; Friedlander, M.; Lisyanskaya, A.; Floquet, A.; Leary, A.; Sonke, G.S.; et al. Maintenance Olaparib in Patients with Newly Diagnosed Advanced Ovarian Cancer. *N. Engl. J. Med.* **2018**, *379*, 2495–2505. [\[CrossRef\]](#) [\[PubMed\]](#)
94. Poveda, A.; Floquet, A.; Ledermann, J.A.; Asher, R.; Penson, R.T.; Oza, A.M.; Korach, J.; Huzarski, T.; Pignata, S.; Friedlander, M.; et al. Olaparib tablets as maintenance therapy in patients with platinum-sensitive relapsed ovarian cancer and a BRCA1/2 mutation (SOLO2/ENGOT-Ov21): A final analysis of a double-blind, randomised, placebo-controlled, phase 3 trial. *Lancet Oncol.* **2021**, *22*, 620–631. [\[CrossRef\]](#)
95. Ray-Coquard, I.; Pautier, P.; Pignata, S.; Pérol, D.; González-Martín, A.; Berger, R.; Fujiwara, K.; Vergote, I.; Colombo, N.; Mäenpää, J.; et al. Olaparib plus Bevacizumab as First-Line Maintenance in Ovarian Cancer. *N. Engl. J. Med.* **2019**, *381*, 2416–2428. [\[CrossRef\]](#) [\[PubMed\]](#)
96. Swisher, E.M.; Lin, K.K.; Oza, A.M.; Scott, C.L.; Giordano, H.; Sun, J.; Konecny, G.E.; Coleman, R.L.; Tinker, A.V.; O'Malley, D.M.; et al. Rucaparib in relapsed, platinum-sensitive high-grade ovarian carcinoma (ARIEL2 Part 1): An international, multicentre, open-label, phase 2 trial. *Lancet Oncol.* **2017**, *18*, 75–87. [\[CrossRef\]](#)



97. González-Martín, A.; Pothuri, B.; Vergote, I.; DePont Christensen, R.; Graybill, W.; Mirza, M.R.; McCormick, C.; Lorusso, D.; Hoskins, P.; Freyer, G.; et al. Niraparib in Patients with Newly Diagnosed Advanced Ovarian Cancer. *N. Engl. J. Med.* **2019**, *381*, 2391–2402. [\[CrossRef\]](#)
98. Xu, B.; Yin, Y.; Dong, M.; Song, Y.; Li, W.; Huang, X.; Wang, T.; He, J.; Mu, X.; Li, L.; et al. Pamiparib dose escalation in Chinese patients with non-mucinous high-grade ovarian cancer or advanced triple-negative breast cancer. *Cancer Med.* **2021**, *10*, 109–118. [\[CrossRef\]](#)
99. Sinha, G. Downfall of iniparib: A PARP inhibitor that doesn't inhibit PARP after all. *J. Natl. Cancer Inst.* **2014**, *106*, djt447. [\[CrossRef\]](#)
100. Mateo, J.; Ong, M.; Tan, D.S.; Gonzalez, M.A.; de Bono, J.S. Appraising iniparib, the PARP inhibitor that never was—what must we learn? *Nat. Rev. Clin. Oncol.* **2013**, *10*, 688–696. [\[CrossRef\]](#)
101. Kaufman, B.; Shapira-Frommer, R.; Schmutzler, R.K.; Audeh, M.W.; Friedlander, M.; Balmaña, J.; Mitchell, G.; Fried, G.; Stemmer, S.M.; Hubert, A.; et al. Olaparib monotherapy in patients with advanced cancer and a germline BRCA1/2 mutation. *J. Clin. Oncol.* **2015**, *33*, 244–250. [\[CrossRef\]](#) [\[PubMed\]](#)
102. Pujade-Lauraine, E.; Ledermann, J.A.; Selle, F.; Gebski, V.; Penson, R.T.; Oza, A.M.; Korach, J.; Huzarski, T.; Poveda, A.; Pignata, S.; et al. Olaparib tablets as maintenance therapy in patients with platinum-sensitive, relapsed ovarian cancer and a BRCA1/2 mutation (SOLO2/ENGOT-Ov21): A double-blind, randomised, placebo-controlled, phase 3 trial. *Lancet Oncol.* **2017**, *18*, 1274–1284. [\[CrossRef\]](#)
103. Mirza, M.R.; Monk, B.J.; Herrstedt, J.; Oza, A.M.; Mahner, S.; Redondo, A.; Fabbro, M.; Ledermann, J.A.; Lorusso, D.; Vergote, I.; et al. Niraparib Maintenance Therapy in Platinum-Sensitive, Recurrent Ovarian Cancer. *N. Engl. J. Med.* **2016**, *375*, 2154–2164. [\[CrossRef\]](#) [\[PubMed\]](#)
104. Coleman, R.L.; Oza, A.M.; Lorusso, D.; Aghajanian, C.; Oaknin, A.; Dean, A.; Colombo, N.; Weberpals, J.I.; Clamp, A.; Scambia, G.; et al. Rucaparib maintenance treatment for recurrent ovarian carcinoma after response to platinum therapy (ARIEL3): A randomised, double-blind, placebo-controlled, phase 3 trial. *Lancet* **2017**, *390*, 1949–1961. [\[CrossRef\]](#)
105. Moore, K.N.; Secord, A.A.; Geller, M.A.; Miller, D.S.; Cloven, N.; Fleming, G.F.; Wahner Hendrickson, A.E.; Azodi, M.; DiSilvestro, P.; Oza, A.M.; et al. Niraparib monotherapy for late-line treatment of ovarian cancer (QUADRA): A multicentre, open-label, single-arm, phase 2 trial. *Lancet Oncol.* **2019**, *20*, 636–648. [\[CrossRef\]](#)
106. Javle, M.; Shacham-Shmueli, E.; Xiao, L.; Varadhachary, G.; Halpern, N.; Fogelman, D.; Boursi, B.; Uruba, S.; Margalit, O.; Wolff, R.A.; et al. Olaparib Monotherapy for Previously Treated Pancreatic Cancer with DNA Damage Repair Genetic Alterations Other Than Germline BRCA Variants: Findings From 2 Phase 2 Nonrandomized Clinical Trials. *JAMA Oncol.* **2021**, *7*, 693–699. [\[CrossRef\]](#)
107. Ison, G.; Howie, L.J.; Amiri-Kordestani, L.; Zhang, L.; Tang, S.; Sridhara, R.; Pierre, V.; Charlab, R.; Ramamoorthy, A.; Song, P.; et al. FDA Approval Summary: Niraparib for the Maintenance Treatment of Patients with Recurrent Ovarian Cancer in Response to Platinum-Based Chemotherapy. *Clin. Cancer Res.* **2018**, *24*, 4066–4071. [\[CrossRef\]](#)
108. Ray-Coquard, I.; Mirza, M.R.; Pignata, S.; Walther, A.; Romero, I.; du Bois, A. Therapeutic options following second-line platinum-based chemotherapy in patients with recurrent ovarian cancer: Comparison of active surveillance and maintenance treatment. *Cancer Treat. Rev.* **2020**, *90*, 102107. [\[CrossRef\]](#)
109. Berek, J.S.; Matulonis, U.A.; Peen, U.; Ghatage, P.; Mahner, S.; Redondo, A.; Lesoin, A.; Colombo, N.; Vergote, I.; Rosengarten, O.; et al. Safety and dose modification for patients receiving niraparib. *Ann. Oncol.* **2018**, *29*, 1784–1792. [\[CrossRef\]](#)
110. Tookman, L.; Krell, J.; Nkolobe, B.; Burley, L.; McNeish, I.A. Practical guidance for the management of side effects during rucaparib therapy in a multidisciplinary UK setting. *Ther. Adv. Med. Oncol.* **2020**, *12*, 1758835920921980. [\[CrossRef\]](#)
111. Hurvitz, S.A.; Quek, R.G.W.; Turner, N.C.; Telli, M.L.; Rugo, H.S.; Mailliez, A.; Ettl, J.; Grischke, E.; Mina, L.A.; Balmaña, J.; et al. Quality of life with talazoparib after platinum or multiple cytotoxic non-platinum regimens in patients with advanced breast cancer and germline BRCA1/2 mutations: Patient-reported outcomes from the ABRAZO phase 2 trial. *Eur. J. Cancer* **2018**, *104*, 160–168. [\[CrossRef\]](#) [\[PubMed\]](#)
112. Litton, J.K.; Scoggins, M.E.; Hess, K.R.; Adrada, B.E.; Murthy, R.K.; Damodaran, S.; DeSnyder, S.M.; Brewster, A.M.; Barcenas, C.H.; Valero, V.; et al. Neoadjuvant Talazoparib for Patients with Operable Breast Cancer with a Germline BRCA Pathogenic Variant. *J. Clin. Oncol.* **2020**, *38*, 388–394. [\[CrossRef\]](#) [\[PubMed\]](#)
113. Li, H.; Liu, R.; Shao, B.; Ran, R.; Song, G.; Wang, K.; Shi, Y.; Liu, J.; Hu, W.; Chen, F.; et al. Phase I dose-escalation and expansion study of PARP inhibitor, fluzoparib (SHR3162), in patients with advanced solid tumors. *Chin. J. Cancer Res.* **2020**, *32*, 370–382. [\[CrossRef\]](#) [\[PubMed\]](#)
114. Li, N.; Bu, H.; Liu, J.; Zhu, J.; Zhou, Q.; Wang, L.; Yin, R.; Wu, X.; Yao, S.; Gu, K.; et al. An Open-label, Multicenter, Single-arm, Phase II Study of Fluzoparib in Patients with Germline BRCA1/2 Mutation and Platinum-sensitive Recurrent Ovarian Cancer. *Clin. Cancer Res.* **2021**, *27*, 2452–2458. [\[CrossRef\]](#) [\[PubMed\]](#)
115. Lickliter, J.D.; Voskoboynik, M.; Mileschkin, L.; Gan, H.K.; Kichenadasse, G.; Zhang, K.; Zhang, M.; Tang, Z.; Millward, M. Phase 1A/1B dose-escalation and -expansion study to evaluate the safety, pharmacokinetics, food effects and antitumor activity of pamiparib in advanced solid tumours. *Br. J. Cancer* **2022**, *126*, 576–585. [\[CrossRef\]](#)
116. Bao, S.; Yue, Y.; Hua, Y.; Zeng, T.; Yang, Y.; Yang, F.; Yan, X.; Sun, C.; Yang, M.; Fu, Z.; et al. Safety profile of poly (ADP-ribose) polymerase (PARP) inhibitors in cancer: A network meta-analysis of randomized controlled trials. *Ann. Transl. Med.* **2021**, *9*, 1229. [\[CrossRef\]](#)



117. Matulonis, U.; Friedlander, M.; Bois, A.D.; Gourley, C.; Vergote, I.; Rustin, G.J.S.; Scott, C.L.; Meier, W.; Shapira-Frommer, R.; Safra, T.; et al. Frequency, severity and timing of common adverse events (AEs) with maintenance olaparib in patients (pts) with platinum-sensitive relapsed serous ovarian cancer (PSR SOC). *J. Clin. Oncol.* **2015**, *33*, 5550. [\[CrossRef\]](#)
118. Ledermann, J.A.; Harter, P.; Gourley, C.; Friedlander, M.; Vergote, I.; Rustin, G.; Scott, C.; Meier, W.; Shapira-Frommer, R.; Safra, T.; et al. Overall survival in patients with platinum-sensitive recurrent serous ovarian cancer receiving olaparib maintenance monotherapy: An updated analysis from a randomised, placebo-controlled, double-blind, phase 2 trial. *Lancet Oncol.* **2016**, *17*, 1579–1589. [\[CrossRef\]](#)
119. Lheureux, S.; Lai, Z.; Dougherty, B.A.; Runswick, S.; Hodgson, D.R.; Timms, K.M.; Lanchbury, J.S.; Kaye, S.; Gourley, C.; Bowtell, D.; et al. Long-Term Responders on Olaparib Maintenance in High-Grade Serous Ovarian Cancer: Clinical and Molecular Characterization. *Clin. Cancer Res.* **2017**, *23*, 4086–4094. [\[CrossRef\]](#)
120. Swisher, E.M.; Kristeleit, R.S.; Oza, A.M.; Tinker, A.V.; Ray-Coquard, I.; Oaknin, A.; Coleman, R.L.; Burris, H.A.; Aghajanian, C.; O'Malley, D.M.; et al. Characterization of patients with long-term responses to rucaparib treatment in recurrent ovarian cancer. *Gynecol. Oncol.* **2021**, *163*, 490–497. [\[CrossRef\]](#)
121. Barber, L.J.; Sandhu, S.; Chen, L.; Campbell, J.; Kozarewa, I.; Fenwick, K.; Assiotis, I.; Rodrigues, D.N.; Reis Filho, J.S.; Moreno, V.; et al. Secondary mutations in BRCA2 associated with clinical resistance to a PARP inhibitor. *J. Pathol.* **2013**, *229*, 422–429. [\[CrossRef\]](#) [\[PubMed\]](#)
122. Norquist, B.; Wurz, K.A.; Pennil, C.C.; Garcia, R.; Gross, J.; Sakai, W.; Karlan, B.Y.; Taniguchi, T.; Swisher, E.M. Secondary somatic mutations restoring BRCA1/2 predict chemotherapy resistance in hereditary ovarian carcinomas. *J. Clin. Oncol.* **2011**, *29*, 3008–3015. [\[CrossRef\]](#) [\[PubMed\]](#)
123. Stordal, B.; Timms, K.; Farrelly, A.; Gallagher, D.; Busschots, S.; Renaud, M.; Thery, J.; Williams, D.; Potter, J.; Tran, T.; et al. BRCA1/2 mutation analysis in 41 ovarian cell lines reveals only one functionally deleterious BRCA1 mutation. *Mol. Oncol.* **2013**, *7*, 567–579. [\[CrossRef\]](#) [\[PubMed\]](#)
124. Lin, K.K.; Harrell, M.I.; Oza, A.M.; Oaknin, A.; Ray-Coquard, I.; Tinker, A.V.; Helman, E.; Radke, M.R.; Say, C.; Vo, L.T.; et al. BRCA Reversion Mutations in Circulating Tumor DNA Predict Primary and Acquired Resistance to the PARP Inhibitor Rucaparib in High-Grade Ovarian Carcinoma. *Cancer Discov.* **2019**, *9*, 210–219. [\[CrossRef\]](#)
125. Kalachand, R.D.; Stordal, B.; Madden, S.; Chandler, B.; Cunningham, J.; Goode, E.L.; Ruscito, I.; Braicu, E.I.; Sehouli, J.; Ignatov, A.; et al. BRCA1 Promoter Methylation and Clinical Outcomes in Ovarian Cancer: An Individual Patient Data Meta-Analysis. *J. Natl. Cancer Inst.* **2020**, *112*, 1190–1203. [\[CrossRef\]](#)
126. Wang, Y.; Bernhardt, A.J.; Cruz, C.; Kraus, J.J.; Nacson, J.; Nicolas, E.; Peri, S.; van der Gulden, H.; van der Heijden, I.; O'Brien, S.W.; et al. The BRCA1-Δ11q Alternative Splice Isoform Bypasses Germline Mutations and Promotes Therapeutic Resistance to PARP Inhibition and Cisplatin. *Cancer Res.* **2016**, *76*, 2778–2790. [\[CrossRef\]](#) [\[PubMed\]](#)
127. Tamaro, C.; Raponi, M.; Wilson, D.I.; Baralle, D. BRCA1 exon 11 alternative splicing, multiple functions and the association with cancer. *Biochem. Soc. Trans.* **2012**, *40*, 768–772. [\[CrossRef\]](#)
128. Raponi, M.; Smith, L.D.; Silipo, M.; Stuni, C.; Buratti, E.; Baralle, D. BRCA1 exon 11 a model of long exon splicing regulation. *RNA Biol.* **2014**, *11*, 351–359. [\[CrossRef\]](#)
129. Kondrashova, O.; Nguyen, M.; Shield-Artin, K.; Tinker, A.V.; Teng, N.N.H.; Harrell, M.I.; Kuiper, M.J.; Ho, G.Y.; Barker, H.; Jasin, M.; et al. Secondary Somatic Mutations Restoring RAD51C and RAD51D Associated with Acquired Resistance to the PARP Inhibitor Rucaparib in High-Grade Ovarian Carcinoma. *Cancer Discov.* **2017**, *7*, 984–998. [\[CrossRef\]](#)
130. Bunting, S.F.; Callén, E.; Wong, N.; Chen, H.T.; Polato, F.; Gunn, A.; Bothmer, A.; Feldhahn, N.; Fernandez-Capetillo, O.; Cao, L.; et al. 53BP1 inhibits homologous recombination in Brca1-deficient cells by blocking resection of DNA breaks. *Cell* **2010**, *141*, 243–254. [\[CrossRef\]](#)
131. Gupta, R.; Somyajit, K.; Narita, T.; Maskey, E.; Stanlie, A.; Kremer, M.; Typas, D.; Lammers, M.; Mailand, N.; Nussenzweig, A.; et al. DNA Repair Network Analysis Reveals Shieldin as a Key Regulator of NHEJ and PARP Inhibitor Sensitivity. *Cell* **2018**, *173*, 972–988.e23. [\[CrossRef\]](#) [\[PubMed\]](#)
132. Xu, G.; Chapman, J.R.; Brandsma, I.; Yuan, J.; Mistrik, M.; Bouwman, P.; Bartkova, J.; Gogola, E.; Warmerdam, D.; Barazas, M.; et al. REV7 counteracts DNA double-strand break resection and affects PARP inhibition. *Nature* **2015**, *521*, 541–544. [\[CrossRef\]](#) [\[PubMed\]](#)
133. Clairmont, C.S.; Sarangi, P.; Ponnienselvan, K.; Galli, L.D.; Csete, I.; Moreau, L.; Adelmant, G.; Chowdhury, D.; Marto, J.A.; D'Andrea, A.D. TRIP13 regulates DNA repair pathway choice through REV7 conformational change. *Nat. Cell Biol.* **2020**, *22*, 87–96. [\[CrossRef\]](#) [\[PubMed\]](#)
134. Lomonosov, M.; Anand, S.; Sangrithi, M.; Davies, R.; Venkitaraman, A.R. Stabilization of stalled DNA replication forks by the BRCA2 breast cancer susceptibility protein. *Genes Dev.* **2003**, *17*, 3017–3022. [\[CrossRef\]](#)
135. Qiu, S.; Jiang, G.; Cao, L.; Huang, J. Replication Fork Reversal and Protection. *Front. Cell Dev. Biol.* **2021**, *9*, 670392. [\[CrossRef\]](#) [\[PubMed\]](#)
136. Mason, J.M.; Chan, Y.L.; Weichselbaum, R.W.; Bishop, D.K. Non-enzymatic roles of human RAD51 at stalled replication forks. *Nat. Commun.* **2019**, *10*, 4410. [\[CrossRef\]](#)
137. Schlacher, K.; Christ, N.; Siaud, N.; Egashira, A.; Wu, H.; Jasin, M. Double-strand break repair-independent role for BRCA2 in blocking stalled replication fork degradation by MRE11. *Cell* **2011**, *145*, 529–542. [\[CrossRef\]](#)
138. Schlacher, K. PARPi focus the spotlight on replication fork protection in cancer. *Nat. Cell Biol.* **2017**, *19*, 1309–1310. [\[CrossRef\]](#)

139. Taglialatela, A.; Alvarez, S.; Leuzzi, G.; Sannino, V.; Ranjha, L.; Huang, J.W.; Madubata, C.; Anand, R.; Levy, B.; Rabadan, R.; et al. Restoration of Replication Fork Stability in BRCA1- and BRCA2-Deficient Cells by Inactivation of SNF2-Family Fork Remodelers. *Mol. Cell* **2017**, *68*, 414–430.e418. [[CrossRef](#)]
140. Ray Chaudhuri, A.; Callen, E.; Ding, X.; Gogola, E.; Duarte, A.A.; Lee, J.E.; Wong, N.; Lafarga, V.; Calvo, J.A.; Panzarino, N.J.; et al. Replication fork stability confers chemoresistance in BRCA-deficient cells. *Nature* **2016**, *535*, 382–387. [[CrossRef](#)]
141. Rondinelli, B.; Gogola, E.; Yücel, H.; Duarte, A.A.; van de Ven, M.; van der Sluijs, R.; Konstantinopoulos, P.A.; Jonkers, J.; Ceccaldi, R.; Rottenberg, S.; et al. EZH2 promotes degradation of stalled replication forks by recruiting MUS81 through histone H3 trimethylation. *Nat. Cell Biol.* **2017**, *19*, 1371–1378. [[CrossRef](#)] [[PubMed](#)]
142. Kim, J.J.; Lee, S.Y.; Choi, J.H.; Woo, H.G.; Xhemalce, B.; Miller, K.M. PCAF-Mediated Histone Acetylation Promotes Replication Fork Degradation by MRE11 and EXO1 in BRCA-Deficient Cells. *Mol. Cell* **2020**, *80*, 327–344.e328. [[CrossRef](#)] [[PubMed](#)]
143. Xuan, J.; Pearson, R.B.; Sanij, E. CX-5461 can destabilize replication forks in PARP inhibitor-resistant models of ovarian cancer. *Mol. Cell. Oncol.* **2020**, *7*, 1805256. [[CrossRef](#)] [[PubMed](#)]
144. Sanij, E.; Hannan, K.M.; Xuan, J.; Yan, S.; Ahern, J.E.; Trigos, A.S.; Brajanovski, N.; Son, J.; Chan, K.T.; Kondrashova, O.; et al. CX-5461 activates the DNA damage response and demonstrates therapeutic efficacy in high-grade serous ovarian cancer. *Nat. Commun.* **2020**, *11*, 2641. [[CrossRef](#)] [[PubMed](#)]
145. Lim, K.S.; Li, H.; Roberts, E.A.; Gaudiano, E.F.; Clairmont, C.; Sambel, L.A.; Ponnienselvan, K.; Liu, J.C.; Yang, C.; Kozono, D.; et al. USP1 Is Required for Replication Fork Protection in BRCA1-Deficient Tumors. *Mol. Cell* **2018**, *72*, 925–941.e924. [[CrossRef](#)]
146. Liang, Q.; Dexheimer, T.S.; Zhang, P.; Rosenthal, A.S.; Villamil, M.A.; You, C.; Zhang, Q.; Chen, J.; Ott, C.A.; Sun, H.; et al. A selective USP1-UAF1 inhibitor links deubiquitination to DNA damage responses. *Nat. Chem. Biol.* **2014**, *10*, 298–304. [[CrossRef](#)]
147. Gatti, M.; Imhof, R.; Huang, Q.; Baudis, M.; Altmeyer, M. The Ubiquitin Ligase TRIP12 Limits PARP1 Trapping and Constrains PARP Inhibitor Efficiency. *Cell Rep.* **2020**, *32*, 107985. [[CrossRef](#)]
148. Pettitt, S.J.; Krastev, D.B.; Brandsma, I.; Dréan, A.; Song, F.; Aleksandrov, R.; Harrell, M.I.; Menon, M.; Brough, R.; Campbell, J.; et al. Genome-wide and high-density CRISPR-Cas9 screens identify point mutations in PARP1 causing PARP inhibitor resistance. *Nat. Commun.* **2018**, *9*, 1849. [[CrossRef](#)]
149. Sarkadi, B.; Homolya, L.; Szakács, G.; Váradi, A. Human multidrug resistance ABCB and ABCG transporters: Participation in a chemoinnity defense system. *Physiol. Rev.* **2006**, *86*, 1179–1236. [[CrossRef](#)]
150. Stordal, B.; Hamon, M.; McEneaney, V.; Roche, S.; Gillet, J.P.; O’Leary, J.J.; Gottesman, M.; Clynes, M. Resistance to paclitaxel in a cisplatin-resistant ovarian cancer cell line is mediated by P-glycoprotein. *PLoS ONE* **2012**, *7*, e40717. [[CrossRef](#)]
151. Crowe, A. The influence of P-glycoprotein on morphine transport in Caco-2 cells. Comparison with paclitaxel. *Eur. J. Pharmacol.* **2002**, *440*, 7–16. [[CrossRef](#)]
152. Penson, R.T.; Oliva, E.; Skates, S.J.; Glyptis, T.; Fuller, A.F., Jr.; Goodman, A.; Seiden, M.V. Expression of multidrug resistance-1 protein inversely correlates with paclitaxel response and survival in ovarian cancer patients: A study in serial samples. *Gynecol. Oncol.* **2004**, *93*, 98–106. [[CrossRef](#)] [[PubMed](#)]
153. Lawlor, D.; Martin, P.; Busschots, S.; Thery, J.; O’Leary, J.J.; Hennessy, B.T.; Stordal, B. PARP Inhibitors as P-glycoprotein Substrates. *J. Pharm. Sci.* **2014**, *103*, 1913–1920. [[CrossRef](#)] [[PubMed](#)]
154. Dufour, R.; Daumar, P.; Mounetou, E.; Aubel, C.; Kwiatkowski, F.; Abrial, C.; Vatoux, C.; Penault-Llorca, F.; Bamdad, M. BCRP and P-gp relay overexpression in triple negative basal-like breast cancer cell line: A prospective role in resistance to Olaparib. *Sci. Rep.* **2015**, *5*, 12670. [[CrossRef](#)] [[PubMed](#)]
155. Januchowski, R.; Wojtowicz, K.; Sterzyńska, K.; Sosńska, P.; Andrzejewska, M.; Zawierucha, P.; Nowicki, M.; Zabel, M. Inhibition of ALDH1A1 activity decreases expression of drug transporters and reduces chemotherapy resistance in ovarian cancer cell lines. *Int. J. Biochem. Cell Biol.* **2016**, *78*, 248–259. [[CrossRef](#)]
156. Jaspers, J.E.; Sol, W.; Kersbergen, A.; Schlicker, A.; Guyader, C.; Xu, G.; Wessels, L.; Borst, P.; Jonkers, J.; Rottenberg, S. BRCA2-deficient sarcomatoid mammary tumors exhibit multidrug resistance. *Cancer Res.* **2015**, *75*, 732–741. [[CrossRef](#)]
157. Ashburn, T.T.; Thor, K.B. Drug repositioning: Identifying and developing new uses for existing drugs. *Nat. Rev. Drug Discov.* **2004**, *3*, 673–683. [[CrossRef](#)]
158. Pushpakom, S.; Iorio, F.; Eyers, P.A.; Escott, K.J.; Hopper, S.; Wells, A.; Doig, A.; Guilliams, T.; Latimer, J.; McNamee, C.; et al. Drug repurposing: Progress, challenges and recommendations. *Nat. Rev. Drug Discov.* **2019**, *18*, 41–58. [[CrossRef](#)]
159. Islam, S.; Wang, S.; Bowden, N.; Martin, J.; Head, R. Repurposing existing therapeutics, its importance in oncology drug development: Kinases as a potential target. *Br. J. Clin. Pharmacol.* **2022**, *88*, 64–74. [[CrossRef](#)]
160. Clark, J.B.; Ferris, G.M.; Pinder, S. Inhibition of nuclear NAD nucleosidase and poly ADP-ribose polymerase activity from rat liver by nicotinamide and 5'-methyl nicotinamide. *Biochim. Biophys. Acta* **1971**, *238*, 82–85. [[CrossRef](#)]
161. Curtin, N.J.; Szabo, C. Poly(ADP-ribose) polymerase inhibition: Past, present and future. *Nat. Rev. Drug Discov.* **2020**, *19*, 711–736. [[CrossRef](#)] [[PubMed](#)]
162. Banasik, M.; Komura, H.; Shimoyama, M.; Ueda, K. Specific inhibitors of poly(ADP-ribose) synthetase and mono(ADP-ribosyl)transferase. *J. Biol. Chem.* **1992**, *267*, 1569–1575. [[CrossRef](#)]
163. Langelier, M.F.; Zandarashvili, L.; Aguiar, P.M.; Black, B.E.; Pascal, J.M. NAD(+) analog reveals PARP-1 substrate-blocking mechanism and allosteric communication from catalytic center to DNA-binding domains. *Nat. Commun.* **2018**, *9*, 844. [[CrossRef](#)] [[PubMed](#)]

164. Eustermann, S.; Wu, W.F.; Langelier, M.F.; Yang, J.C.; Easton, L.E.; Riccio, A.A.; Pascal, J.M.; Neuhaus, D. Structural Basis of Detection and Signaling of DNA Single-Strand Breaks by Human PARP-1. *Mol. Cell* **2015**, *60*, 742–754. [[CrossRef](#)]
165. Langelier, M.F.; Planck, J.L.; Roy, S.; Pascal, J.M. Structural basis for DNA damage-dependent poly(ADP-ribosyl)ation by human PARP-1. *Science* **2012**, *336*, 728–732. [[CrossRef](#)]
166. Tacconi, E.M.; Badie, S.; De Gregoriis, G.; Reisländer, T.; Lai, X.; Porru, M.; Folio, C.; Moore, J.; Kopp, A.; Baguña Torres, J.; et al. Chlorambucil targets BRCA1/2-deficient tumours and counteracts PARP inhibitor resistance. *EMBO Mol. Med.* **2019**, *11*, e9982. [[CrossRef](#)]
167. Hill, S.J.; Decker, B.; Roberts, E.A.; Horowitz, N.S.; Muto, M.G.; Worley, M.J., Jr.; Feltmate, C.M.; Nucci, M.R.; Swisher, E.M.; Nguyen, H.; et al. Prediction of DNA Repair Inhibitor Response in Short-Term Patient-Derived Ovarian Cancer Organoids. *Cancer Discov.* **2018**, *8*, 1404–1421. [[CrossRef](#)]
168. Sheta, R.; Bachvarova, M.; Plante, M.; Renaud, M.C.; Sebastianelli, A.; Gregoire, J.; Navarro, J.M.; Perez, R.B.; Masson, J.Y.; Bachvarov, D. Development of a 3D functional assay and identification of biomarkers, predictive for response of high-grade serous ovarian cancer (HGSOC) patients to poly-ADP ribose polymerase inhibitors (PARPis): Targeted therapy. *J. Transl. Med.* **2020**, *18*, 439. [[CrossRef](#)]
169. Tao, M.; Sun, F.; Wang, J.; Wang, Y.; Zhu, H.; Chen, M.; Liu, L.; Liu, L.; Lin, H.; Wu, X. Developing patient-derived organoids to predict PARP inhibitor response and explore resistance overcoming strategies in ovarian cancer. *Pharmacol. Res.* **2022**, *179*, 106232. [[CrossRef](#)]
170. Kopper, O.; de Witte, C.J.; Löhmussaar, K.; Valle-Inclan, J.E.; Hami, N.; Kester, L.; Balgobind, A.V.; Korving, J.; Proost, N.; Begthel, H.; et al. An organoid platform for ovarian cancer captures intra- and interpatient heterogeneity. *Nat. Med.* **2019**, *25*, 838–849. [[CrossRef](#)]
171. de Witte, C.J.; Espejo Valle-Inclan, J.; Hami, N.; Löhmussaar, K.; Kopper, O.; Vreuls, C.P.H.; Jonges, G.N.; van Diest, P.; Nguyen, L.; Clevers, H.; et al. Patient-Derived Ovarian Cancer Organoids Mimic Clinical Response and Exhibit Heterogeneous Inter- and Intrapatient Drug Responses. *Cell Rep.* **2020**, *31*, 107762. [[CrossRef](#)] [[PubMed](#)]
172. Appleton, K.M.; Elrod, A.K.; Lassahn, K.A.; Shuford, S.; Holmes, L.M.; DesRochers, T.M. PD-1/PD-L1 checkpoint inhibitors in combination with olaparib display antitumor activity in ovarian cancer patient-derived three-dimensional spheroid cultures. *Cancer Immunol. Immunother.* **2021**, *70*, 843–856. [[CrossRef](#)] [[PubMed](#)]
173. Chandrasekaran, A.; Elias, K.M. Synthetic Lethality in Ovarian Cancer. *Mol. Cancer Ther.* **2021**, *20*, 2117–2128. [[CrossRef](#)] [[PubMed](#)]
174. Fang, P.; De Souza, C.; Minn, K.; Chien, J. Genome-scale CRISPR knockout screen identifies TIGAR as a modifier of PARP inhibitor sensitivity. *Commun. Biol.* **2019**, *2*, 335. [[CrossRef](#)]
175. Falchi, F.; Giacomini, E.; Masini, T.; Boutard, N.; Di Ianni, L.; Manerba, M.; Farabegoli, F.; Rossini, L.; Robertson, J.; Minucci, S.; et al. Synthetic Lethality Triggered by Combining Olaparib with BRCA2-Rad51 Disruptors. *ACS Chem. Biol.* **2017**, *12*, 2491–2497. [[CrossRef](#)]
176. Chen, L.; Hou, J.; Zeng, X.; Guo, Q.; Deng, M.; Kloeber, J.A.; Tu, X.; Zhao, F.; Wu, Z.; Huang, J.; et al. LRRK2 inhibition potentiates PARP inhibitor cytotoxicity through inhibiting homologous recombination-mediated DNA double strand break repair. *Clin. Transl. Med.* **2021**, *11*, e341. [[CrossRef](#)] [[PubMed](#)]
177. Chiappa, M.; Guffanti, F.; Anselmi, M.; Lupi, M.; Panini, N.; Wiesmüller, L.; Damia, G. Combinations of ATR, Chk1 and Wee1 Inhibitors with Olaparib Are Active in Olaparib Resistant Brca1 Proficient and Deficient Murine Ovarian Cells. *Cancers* **2022**, *14*, 1807. [[CrossRef](#)]
178. Lui, G.Y.L.; Shaw, R.; Schaub, F.X.; Stork, I.N.; Gurley, K.E.; Bridgwater, C.; Diaz, R.L.; Rosati, R.; Swan, H.A.; Ince, T.A.; et al. BET, SRC, and BCL2 family inhibitors are synergistic drug combinations with PARP inhibitors in ovarian cancer. *EBioMedicine* **2020**, *60*, 102988. [[CrossRef](#)]
179. Wang, S.P.; Li, Y.; Huang, S.H.; Wu, S.Q.; Gao, L.L.; Sun, Q.; Lin, Q.W.; Huang, L.; Meng, L.Q.; Zou, Y.; et al. Discovery of Potent and Novel Dual PARP/BRD4 Inhibitors for Efficient Treatment of Pancreatic Cancer. *J. Med. Chem.* **2021**, *64*, 17413–17435. [[CrossRef](#)]
180. Sun, C.; Yin, J.; Fang, Y.; Chen, J.; Jeong, K.J.; Chen, X.; Vellano, C.P.; Ju, Z.; Zhao, W.; Zhang, D.; et al. BRD4 Inhibition Is Synthetic Lethal with PARP Inhibitors through the Induction of Homologous Recombination Deficiency. *Cancer Cell* **2018**, *33*, 401–416.e408. [[CrossRef](#)]
181. Guppy, B.J.; McManus, K.J. Synthetic lethal targeting of RNF20 through PARP1 silencing and inhibition. *Cell. Oncol.* **2017**, *40*, 281–292. [[CrossRef](#)] [[PubMed](#)]
182. McLaughlin, L.J.; Stojanovic, L.; Kogan, A.A.; Rutherford, J.L.; Choi, E.Y.; Yen, R.C.; Xia, L.; Zou, Y.; Lapidus, R.G.; Baylin, S.B.; et al. Pharmacologic induction of innate immune signaling directly drives homologous recombination deficiency. *Proc. Natl. Acad. Sci. USA* **2020**, *117*, 17785–17795. [[CrossRef](#)] [[PubMed](#)]
183. Yang, H.; Cui, W.; Wang, L. Epigenetic synthetic lethality approaches in cancer therapy. *Clin. Epigenetics* **2019**, *11*, 136. [[CrossRef](#)] [[PubMed](#)]
184. Chen, E.S. Targeting epigenetics using synthetic lethality in precision medicine. *Cell. Mol. Life Sci.* **2018**, *75*, 3381–3392. [[CrossRef](#)] [[PubMed](#)]
185. Bonaventura, P.; Shekarian, T.; Alcazer, V.; Valladeau-Guilemond, J.; Valsesia-Wittmann, S.; Amigorena, S.; Caux, C.; Depil, S. Cold Tumors: A Therapeutic Challenge for Immunotherapy. *Front. Immunol.* **2019**, *10*, 168. [[CrossRef](#)] [[PubMed](#)]



186. Chan, T.A.; Yarchoan, M.; Jaffee, E.; Swanton, C.; Quezada, S.A.; Stenzinger, A.; Peters, S. Development of tumor mutation burden as an immunotherapy biomarker: Utility for the oncology clinic. *Ann. Oncol.* **2019**, *30*, 44–56. [[CrossRef](#)] [[PubMed](#)]
187. Chardin, L.; Leary, A. Immunotherapy in Ovarian Cancer: Thinking Beyond PD-1/PD-L1. *Front. Oncol.* **2021**, *11*, 795547. [[CrossRef](#)]
188. Vikas, P.; Borchering, N.; Chennamadhavuni, A.; Garje, R. Therapeutic Potential of Combining PARP Inhibitor and Immunotherapy in Solid Tumors. *Front. Oncol.* **2020**, *10*, 570. [[CrossRef](#)]
189. Leary, A.; Tan, D.; Ledermann, J. Immune checkpoint inhibitors in ovarian cancer: Where do we stand? *Ther. Adv. Med. Oncol.* **2021**, *13*, 17588359211039899. [[CrossRef](#)]
190. Miller, R.E.; Lewis, A.J.; Powell, M.E. PARP inhibitors and immunotherapy in ovarian and endometrial cancers. *Br. J. Radiol.* **2021**, *94*, 20210002. [[CrossRef](#)]
191. Wang, Z.; Sun, K.; Xiao, Y.; Feng, B.; Mikule, K.; Ma, X.; Feng, N.; Vellano, C.P.; Federico, L.; Marszalek, J.R.; et al. Niraparib activates interferon signaling and potentiates anti-PD-1 antibody efficacy in tumor models. *Sci. Rep.* **2019**, *9*, 1853. [[CrossRef](#)] [[PubMed](#)]
192. Ding, L.; Kim, H.J.; Wang, Q.; Kearns, M.; Jiang, T.; Ohlson, C.E.; Li, B.B.; Xie, S.; Liu, J.F.; Stover, E.H.; et al. PARP Inhibition Elicits STING-Dependent Antitumor Immunity in Brca1-Deficient Ovarian Cancer. *Cell Rep.* **2018**, *25*, 2972–2980.e2975. [[CrossRef](#)] [[PubMed](#)]
193. Wang, Q.; Bergholz, J.S.; Ding, L.; Lin, Z.; Kabraji, S.K.; Hughes, M.E.; He, X.; Xie, S.; Jiang, T.; Wang, W.; et al. STING agonism reprograms tumor-associated macrophages and overcomes resistance to PARP inhibition in BRCA1-deficient models of breast cancer. *Nat. Commun.* **2022**, *13*, 3022. [[CrossRef](#)]
194. Konstantinopoulos, P.A.; Waggoner, S.; Vidal, G.A.; Mita, M.; Moroney, J.W.; Holloway, R.; Van Le, L.; Sachdev, J.C.; Chapman-Davis, E.; Colon-Otero, G.; et al. Single-Arm Phases 1 and 2 Trial of Niraparib in Combination With Pembrolizumab in Patients With Recurrent Platinum-Resistant Ovarian Carcinoma. *JAMA Oncol.* **2019**, *5*, 1141–1149. [[CrossRef](#)]
195. Färkkilä, A.; Gulhan, D.C.; Casado, J.; Jacobson, C.A.; Nguyen, H.; Kochupurakkal, B.; Maliga, Z.; Yapp, C.; Chen, Y.A.; Schapiro, D.; et al. Immunogenomic profiling determines responses to combined PARP and PD-1 inhibition in ovarian cancer. *Nat. Commun.* **2020**, *11*, 1459. [[CrossRef](#)]
196. Do, K.T.; Kochupurakkal, B.; Kelland, S.; de Jonge, A.; Hedglin, J.; Powers, A.; Quinn, N.; Gannon, C.; Vuong, L.; Parmar, K.; et al. Phase 1 Combination Study of the CHK1 Inhibitor Prexasertib and the PARP Inhibitor Olaparib in High-grade Serous Ovarian Cancer and Other Solid Tumors. *Clin. Cancer Res.* **2021**, *27*, 4710–4716. [[CrossRef](#)] [[PubMed](#)]
197. Sen, T.; Rodriguez, B.L.; Chen, L.; Corte, C.M.D.; Morikawa, N.; Fujimoto, J.; Cristea, S.; Nguyen, T.; Diao, L.; Li, L.; et al. Targeting DNA Damage Response Promotes Antitumor Immunity through STING-Mediated T-cell Activation in Small Cell Lung Cancer. *Cancer Discov.* **2019**, *9*, 646–661. [[CrossRef](#)]
198. Chaudhary, R.; Slebos, R.J.C.; Song, F.; McCleary-Sharp, K.P.; Masannat, J.; Tan, A.C.; Wang, X.; Amaladas, N.; Wu, W.; Hall, G.E.; et al. Effects of checkpoint kinase 1 inhibition by prexasertib on the tumor immune microenvironment of head and neck squamous cell carcinoma. *Mol. Carcinog.* **2021**, *60*, 138–150. [[CrossRef](#)]
199. Xu, Q.; Li, Z. Update on Poly ADP-Ribose polymerase inhibitors in ovarian cancer with non-BRCA mutations. *Front. Pharmacol.* **2021**, *12*, 743073. [[CrossRef](#)]
200. Penson, R.T.; Valencia, R.V.; Cibula, D.; Colombo, N.; Leath, C.A., 3rd; Bidziński, M.; Kim, J.W.; Nam, J.H.; Madry, R.; Hernández, C.; et al. Olaparib versus nonplatinum chemotherapy in patients with platinum-sensitive relapsed ovarian cancer and a germline BRCA1/2 mutation (SOLO3): A randomized phase III trial. *J. Clin. Oncol.* **2020**, *38*, 1164–1174. [[CrossRef](#)]
201. Gadducci, A.; Cosio, S. Randomized clinical trials and real world prospective observational studies on bevacizumab, PARP inhibitors, and immune checkpoint inhibitors in the first-line treatment of advanced ovarian carcinoma: A critical review. *Anticancer Res.* **2021**, *41*, 4673–4685. [[CrossRef](#)] [[PubMed](#)]
202. Pignata, S.; Oza, A.M.; Hall, G.; Pardo, B.; Madry, R.; Cibula, D.; Klat, J.; Montes, A.; Glasspool, R.; Colombo, N.; et al. Maintenance olaparib in patients (pts) with platinum-sensitive relapsed ovarian cancer (PSROC) by somatic (s) or germline (g) BRCA and other homologous recombination repair (HRR) gene mutation status: Overall survival (OS) results from the ORZORA study. *J. Clin. Oncol.* **2022**, *40*, 5519. [[CrossRef](#)]
203. Vanderstichele, A.; Loverix, L.; Busschaert, P.; Van Nieuwenhuysen, E.; Han, S.N.; Concina, N.; Callewaert, T.; Olbrecht, S.; Salihi, R.; Berteloot, P.; et al. Randomized CLIO/BGOG-ov10 trial of olaparib monotherapy versus physician's choice chemotherapy in relapsed ovarian cancer. *Gynecol. Oncol.* **2022**, *165*, 14–22. [[CrossRef](#)] [[PubMed](#)]
204. Poveda, A.M.; Davidson, R.; Blakeley, C.; Milner, A. Olaparib maintenance monotherapy in platinum-sensitive, relapsed ovarian cancer without germline BRCA mutations: OPINION Phase IIIb study design. *Future Oncol.* **2019**, *15*, 3651–3663. [[CrossRef](#)]
205. Kristeleit, R.; Lisyanskaya, A.; Fedenko, A.; Dvorkin, M.; de Melo, A.C.; Shparyk, Y.; Rakhmatullina, I.; Bondarenko, I.; Colombo, N.; Svintsitskiy, V.; et al. Rucaparib versus standard-of-care chemotherapy in patients with relapsed ovarian cancer and a deleterious BRCA1 or BRCA2 mutation (ARIEL4): An international, open-label, randomised, phase 3 trial. *Lancet Oncol.* **2022**, *23*, 465–478. [[CrossRef](#)]
206. Monk, B.J.; Coleman, R.L.; Fujiwara, K.; Wilson, M.K.; Oza, A.M.; Oaknin, A.; O'Malley, D.M.; Lorusso, D.; Westin, S.N.; Safra, T.; et al. ATHENA (GOG-3020/ENGOT-ov45): A randomized, phase III trial to evaluate rucaparib as monotherapy (ATHENA-MONO) and rucaparib in combination with nivolumab (ATHENA-COMBO) as maintenance treatment following frontline platinum-based chemotherapy in ovarian cancer. *Int. J. Gynecol. Cancer* **2021**, *31*, 1589–1594. [[CrossRef](#)]

207. Monk, B.J.; Parkinson, C.; Lim, M.C.; O'Malley, D.M.; Oaknin, A.; Wilson, M.K.; Coleman, R.L.; Lorusso, D.; Bessette, P.; Ghamande, S.; et al. A Randomized, Phase III Trial to Evaluate Rucaparib Monotherapy as Maintenance Treatment in Patients With Newly Diagnosed Ovarian Cancer (ATHENA-MONO/GOG-3020/ENGOT-ov45). *J. Clin. Oncol.* **2022**, JCO2201003. [\[CrossRef\]](#)
208. Braicu, E.I.; Wimberger, P.; Richter, R.; Keller, M.; Krabisch, P.; Deryal, M.; Runnebaum, I.B.; Witteler, R.; Bangemann, N.; Marmé, F.; et al. NOGGO Ov-42/MAMOC: Rucaparib maintenance after bevacizumab maintenance following carboplatin-based first line-chemotherapy in ovarian cancer patients. *J. Clin. Oncol.* **2020**, *38*, TPS6102. [\[CrossRef\]](#)
209. Park, J.; Lim, M.C.; Lee, J.K.; Jeong, D.H.; Kim, S.I.; Choi, M.C.; Kim, B.G.; Lee, J.Y. A single-arm, phase II study of niraparib and bevacizumab maintenance therapy in platinum-sensitive, recurrent ovarian cancer patients previously treated with a PARP inhibitor: Korean Gynecologic Oncology Group (KGOG 3056)/NIRVANA-R trial. *J. Gynecol. Oncol.* **2022**, *33*, e12. [\[CrossRef\]](#)
210. Manzo, J.; Puhalla, S.; Pahuja, S.; Ding, F.; Lin, Y.; Appleman, L.; Tawbi, H.; Stoller, R.; Lee, J.J.; Diergaarde, B.; et al. A phase 1 and pharmacodynamic study of chronically-dosed, single-agent veliparib (ABT-888) in patients with BRCA1- or BRCA2-mutated cancer or platinum-refractory ovarian or triple-negative breast cancer. *Cancer Chemother. Pharmacol.* **2022**, *89*, 721–735. [\[CrossRef\]](#)
211. van der Biessen, D.A.J.; Gietema, J.A.; de Jonge, M.J.A.; Desar, I.M.E.; den Hollander, M.W.; Dudley, M.; Dunbar, M.; Hetman, R.; Serpenti, C.; Xiong, H.; et al. A phase 1 study of PARP-inhibitor ABT-767 in advanced solid tumors with BRCA1/2 mutations and high-grade serous ovarian, fallopian tube, or primary peritoneal cancer. *Investig. New Drugs* **2018**, *36*, 828–835. [\[CrossRef\]](#) [\[PubMed\]](#)
212. Plummer, R.; Dua, D.; Cresti, N.; Drew, Y.; Stephens, P.; Foegh, M.; Knudsen, S.; Sachdev, P.; Mistry, B.M.; Dixit, V.; et al. First-in-human study of the PARP/tankyrase inhibitor E7449 in patients with advanced solid tumours and evaluation of a novel drug-response predictor. *Br. J. Cancer* **2020**, *123*, 525–533. [\[CrossRef\]](#) [\[PubMed\]](#)
213. Buechel, M.; Herzog, T.J.; Westin, S.N.; Coleman, R.L.; Monk, B.J.; Moore, K.N. Treatment of patients with recurrent epithelial ovarian cancer for whom platinum is still an option. *Ann. Oncol.* **2019**, *30*, 721–732. [\[CrossRef\]](#) [\[PubMed\]](#)
214. Coleman, R.L.; Fleming, G.F.; Brady, M.F.; Swisher, E.M.; Steffensen, K.D.; Friedlander, M.; Okamoto, A.; Moore, K.N.; Efrat Ben-Baruch, N.; Werner, T.L.; et al. Veliparib with first-line chemotherapy and as maintenance therapy in ovarian cancer. *N. Engl. J. Med.* **2019**, *381*, 2403–2415. [\[CrossRef\]](#) [\[PubMed\]](#)
215. Eder, J.P.; Sohal, D.; Mahdi, H.; Do, K.; Keedy, V.; Hafez, N.; Doroshow, D.; Avedissian, M.; Mortimer, P.; Glover, C.; et al. Abstract A080: Olaparib and the ATR inhibitor AZD6738 in relapsed, refractory cancer patients with homologous recombination (HR) repair mutations—OLAPCO. *Mol. Cancer Ther.* **2019**, *18*, A080. [\[CrossRef\]](#)
216. Konstantinopoulos, P.A.; Cheng, S.-C.; Supko, J.G.; Polak, M.; Wahner-Hendrickson, A.E.; Ivy, S.P.; Bowes, B.; Sawyer, H.; Basada, P.; Hayes, M.; et al. Combined PARP and HSP90 inhibition: Preclinical and Phase 1 evaluation in patients with advanced solid tumours. *Br. J. Cancer* **2022**, *126*, 1027–1036. [\[CrossRef\]](#)
217. Westin, S.N.; Coleman, R.L.; Fellman, B.M.; Yuan, Y.; Sood, A.K.; Soliman, P.T.; Wright, A.A.; Horowitz, N.S.; Campos, S.M.; Konstantinopoulos, P.A.; et al. EFFORT: EFFicacy Of adavosertib in parp ResisTance: A randomized two-arm non-comparative phase II study of adavosertib with or without olaparib in women with PARP-resistant ovarian cancer. *J. Clin. Oncol.* **2021**, *39*, 5505. [\[CrossRef\]](#)
218. Smith, G.; Alholm, Z.; Coleman, R.L.; Monk, B.J. DNA Damage Repair inhibitors-Combination therapies. *Cancer J.* **2021**, *27*, 501–505. [\[CrossRef\]](#)
219. Shah, P.D.; Wethington, S.L.; Pagan, C.; Latif, N.; Tanyi, J.; Martin, L.P.; Morgan, M.; Burger, R.A.; Haggerty, A.; Zarrin, H.; et al. Combination ATR and PARP Inhibitor (CAPRI): A phase 2 study of ceralasertib plus olaparib in patients with recurrent, platinum-resistant epithelial ovarian cancer. *Gynecol. Oncol.* **2021**, *163*, 246–253. [\[CrossRef\]](#)
220. Jo, U.; Senatorov, I.S.; Zimmermann, A.; Saha, L.K.; Murai, Y.; Kim, S.H.; Rajapakse, V.N.; Elloumi, F.; Takahashi, N.; Schultz, C.W.; et al. Novel and highly potent ATR inhibitor M4344 kills cancer cells with replication stress, and enhances the chemotherapeutic activity of widely used DNA damaging agents. *Mol. Cancer Ther.* **2021**, *20*, 1431–1441. [\[CrossRef\]](#)
221. Konstantinopoulos, P.A.; Barry, W.T.; Birrer, M.; Westin, S.N.; Cadoo, K.A.; Shapiro, G.I.; Mayer, E.L.; O'Cearbhaill, R.E.; Coleman, R.L.; Kochupurakkal, B.; et al. Olaparib and  $\alpha$ -specific PI3K inhibitor alpelisib for patients with epithelial ovarian cancer: A dose-escalation and dose-expansion phase 1b trial. *Lancet Oncol.* **2019**, *20*, 570–580. [\[CrossRef\]](#)
222. Sun, C.; Fang, Y.; Labrie, M.; Li, X.; Mills, G.B. Systems approach to rational combination therapy: PARP inhibitors. *Biochem. Soc. Trans.* **2020**, *48*, 1101–1108. [\[CrossRef\]](#) [\[PubMed\]](#)
223. Liu, J.F.; Barry, W.T.; Birrer, M.; Lee, J.M.; Buckanovich, R.J.; Fleming, G.F.; Rimel, B.; Buss, M.K.; Nattam, S.; Hurteau, J.; et al. Combination cediranib and olaparib versus olaparib alone for women with recurrent platinum-sensitive ovarian cancer: A randomised phase 2 study. *Lancet Oncol.* **2014**, *15*, 1207–1214. [\[CrossRef\]](#)
224. Harter, P.; Mouret-Reynier, M.A.; Pignata, S.; Cropet, C.; González-Martín, A.; Bogner, G.; Fujiwara, K.; Vergote, I.; Colombo, N.; Nøttrup, T.J.; et al. Efficacy of maintenance olaparib plus bevacizumab according to clinical risk in patients with newly diagnosed, advanced ovarian cancer in the phase III PAOLA-1/ENGOT-ov25 trial. *Gynecol. Oncol.* **2022**, *164*, 254–264. [\[CrossRef\]](#)
225. Lee, J.-m.; Moore, R.G.; Ghamande, S.A.; Park, M.S.; Diaz, J.P.; Chapman, J.A.; Kendrick, J.E.; Slomovitz, B.M.; Tewari, K.S.; Lowe, E.S.; et al. Cediranib in combination with olaparib in patients without a germline BRCA1/2 mutation with recurrent platinum-resistant ovarian cancer: Phase IIb CONCERTO trial. *J. Clin. Oncol.* **2020**, *38*, 6056. [\[CrossRef\]](#)
226. Wang, M.; Chen, S.; Ao, D. Targeting DNA repair pathway in cancer: Mechanisms and clinical application. *MedComm* **2021**, *2*, 654–691. [\[CrossRef\]](#)

227. Domchek, S.M.; Postel-Vinay, S.; Im, S.A.; Park, Y.H.; Delord, J.P.; Italiano, A.; Alexandre, J.; You, B.; Bastian, S.; Krebs, M.G.; et al. Olaparib and durvalumab in patients with germline BRCA-mutated metastatic breast cancer (MEDIOLA): An open-label, multicentre, phase 1/2, basket study. *Lancet Oncol.* **2020**, *21*, 1155–1164. [[CrossRef](#)]
228. Boussios, S.; Karihtala, P.; Moschetta, M.; Karathanasi, A.; Sadauskaite, A.; Rassy, E.; Pavlidis, N. Combined strategies with poly (ADP-Ribose) polymerase (PARP) inhibitors for the treatment of ovarian cancer: A literature review. *Diagnostics* **2019**, *9*, 87. [[CrossRef](#)]
229. Randall, L.M.; O'Malley, D.M.; Monk, B.J.; Coleman, R.L.; O'Cearbhaill, R.E.; Gaillard, S.; Adams, S.; Cappuccini, F.; Huang, M.; Chon, H.S.; et al. 883TiP MOONSTONE/GOG-3032: A phase II, open-label, single-arm study to evaluate the efficacy and safety of niraparib + dostarlimab in patients with platinum-resistant ovarian cancer. *Ann. Oncol.* **2020**, *31*, S646–S647. [[CrossRef](#)]
230. Ray-Coquard, I.L.; Leary, A.; Bigot, F.; Montane, L.; Fabbro, M.; Hardy-Bessard, A.-C.; Selle, F.; Chakiba, C.; Lortholary, A.; Berton, D.; et al. ROCSAN trial (GINECO-EN203b/ENGOT-EN8): A multicentric randomized phase II/III evaluating dostarlimab in combination with niraparib versus niraparib alone compared to chemotherapy in the treatment of endometrial/ovarian carcinosarcoma after at least one line of platinum based chemotherapy. *J. Clin. Oncol.* **2021**, *39*, TPS5604. [[CrossRef](#)]
231. Zimmer, A.S.; Nichols, E.; Cimino-Mathews, A.; Peer, C.; Cao, L.; Lee, M.J.; Kohn, E.C.; Annunziata, C.M.; Lipkowitz, S.; Trepel, J.B.; et al. A phase I study of the PD-L1 inhibitor, durvalumab, in combination with a PARP inhibitor, olaparib, and a VEGFR1-3 inhibitor, cediranib, in recurrent women's cancers with biomarker analyses. *J. Immunother. Cancer* **2019**, *7*, 197. [[CrossRef](#)] [[PubMed](#)]
232. Karzai, F.; VanderWeele, D.; Madan, R.A.; Owens, H.; Cordes, L.M.; Hankin, A.; Couvillon, A.; Nichols, E.; Bilusic, M.; Beshiri, M.L.; et al. Activity of durvalumab plus olaparib in metastatic castration-resistant prostate cancer in men with and without DNA damage repair mutations. *J. Immunother. Cancer* **2018**, *6*, 141. [[CrossRef](#)] [[PubMed](#)]



Article

# PARP Inhibitors Display Differential Efficacy in Models of BRCA Mutant High-Grade Serous Ovarian Cancer

Kristie-Ann Dickson <sup>1,†</sup> , Tao Xie <sup>1,†</sup> , Christian Evenhuis <sup>2</sup>, Yue Ma <sup>1</sup> and Deborah J. Marsh <sup>1,3,\*</sup>

<sup>1</sup> Translational Oncology Group, School of Life Sciences, Faculty of Science, University of Technology Sydney, Ultimo, NSW 2007, Australia; Kristie-Ann.Dickson@uts.edu.au (K.-A.D.); Tao.Xie-1@alumni.uts.edu.au (T.X.); Yue.Ma-7@student.uts.edu.au (Y.M.)

<sup>2</sup> iThree Institute, School of Life Sciences, Faculty of Science, University of Technology Sydney, Ultimo, NSW 2007, Australia; christian.evenhuis@gmail.com

<sup>3</sup> Northern Clinical School, Faculty of Medicine and Health, University of Sydney, Camperdown, NSW 2006, Australia

\* Correspondence: Deborah.Marsh@uts.edu.au; Tel.: +61-2-9514-7574

† Contributed equally to this work.

**Abstract:** Several poly (adenosine diphosphate-ribose) polymerase (PARP) inhibitors are now in clinical use for tumours with defects in BRCA1 or BRCA2 that result in deficient homologous recombination repair (HRR). Use of olaparib, niraparib or rucaparib for the treatment of high-grade serous ovarian cancer, including in the maintenance setting, has extended both progression free and overall survival for women with this malignancy. While different PARP inhibitors (PARPis) are mechanistically similar, differences are apparent in their chemical structures, toxicity profiles, PARP trapping abilities and polypharmacological landscapes. We have treated ovarian cancer cell line models of known BRCA status, including the paired cell lines PEO1 and PEO4, and UWB1.289 and UWB1.289+BRCA1, with five PARPis (olaparib, niraparib, rucaparib, talazoparib and veliparib) and observed differences between PARPis in both cell viability and cell survival. A cell line model of acquired resistance to veliparib showed increased resistance to the other four PARPis tested, suggesting that acquired resistance to one PARPi may not be able to be rescued by another. Lastly, as a proof of principle, HRR proficient ovarian cancer cells were sensitised to PARPis by depletion of BRCA1. In the future, guidelines will need to emerge to assist clinicians in matching specific PARPis to specific patients and tumours.

**Keywords:** BRCA1; BRCA2; homologous recombination repair; PARP inhibitor; olaparib; rucaparib; niraparib; talazoparib; veliparib



**Citation:** Dickson, K.-A.; Xie, T.; Evenhuis, C.; Ma, Y.; Marsh, D.J. PARP Inhibitors Display Differential Efficacy in Models of BRCA Mutant High-Grade Serous Ovarian Cancer. *Int. J. Mol. Sci.* **2021**, *22*, 8506. <https://doi.org/10.3390/ijms22168506>

Academic Editor: Valentina Silvestri

Received: 13 July 2021

Accepted: 4 August 2021

Published: 7 August 2021

**Publisher's Note:** MDPI stays neutral with regard to jurisdictional claims in published maps and institutional affiliations.



**Copyright:** © 2021 by the authors. Licensee MDPI, Basel, Switzerland. This article is an open access article distributed under the terms and conditions of the Creative Commons Attribution (CC BY) license (<https://creativecommons.org/licenses/by/4.0/>).

## 1. Introduction

The advent of pharmacological inhibitors of the DNA repair enzyme poly (adenosine diphosphate-ribose) polymerase (PARP) has heralded major therapeutic advances for malignancies that have defects in components of homologous recombination repair (HRR) pathways [1–3]. The focus of PARP inhibitors (PARPis) to date has been on BRCA1 and BRCA2 mutated tumours, with clinical benefits seen in patients with mutations in these DNA repair genes such as ovarian [4], breast [5], prostate [6] and pancreatic cancers [7]. BRCA1 methylated tumours are also sensitive to PARP inhibition [8], as are tumours with mutations in other genes that function in repair of double strand breaks (DSBs), including RAD51C, RAD51D, ATM and PALB2, where tumours are described as having a “BRCAness” phenotype [8–10]. With this broadening concept of BRCAness, other malignancies are being investigated to assess sensitivity to PARP inhibitors, including colorectal, upper gastrointestinal and acute myeloid leukemia [1,11–13].

PARP family members function in a number of cellular processes including the regulation of gene transcription, chromatin remodelling and DNA repair [14,15]. PARPs bind



to DNA at sites of single strand breaks (SSBs) undergoing base excision repair (BER) where they function to recruit DNA repair machinery. When the replication fork comes across a SSB, DSBs are generated that then need to undergo HRR [16,17]. BER is the default repair pathway for cells with defects in HRR, the preferred pathway for repair of DSBs, such as occurs in the presence of *BRCA* mutations. By inhibiting PARP function in cells with deficient HRR, cells lose their ability to choose the default BER pathway to repair DNA damage, creating synthetic lethality that leads to cell death [18–20].

PARP1, PARP2, PARP3, PARP4 (also known as Vault PARP) and tankyrases 1 and 2 (PARP5a and PARP5b) are amongst the most studied members of the PARP family [2,15]. Catalytic activation of PARP1 synthesises poly (ADP-ribose), PAR, from the substrate nicotinamide adenine dinucleotide (NAD<sup>+</sup>) in a process known as PARylation. While PARP1 is reported to conduct more than 90% of PARylation associated with DNA damage, PARPs 2, 3, 4, 5a and 5b also demonstrate PARylation activity [21,22]. Inhibition of these PARP enzymes and in turn the PARylation process has proven to be a major advancement in the treatment of HRR deficient tumours [1–3,23,24].

Olaparib (Lynparza<sup>®</sup>) was the first PARPi endorsed by the Food and Drug Administration (FDA) for the treatment of advanced germline *BRCA*-mutated ovarian cancer in 2014, followed by rucaparib (Rubraca<sup>®</sup>) for use to treat the same indication in 2016 [18,25–27]. Olaparib and rucaparib were sanctioned in 2018 for use as maintenance therapy for women with ovarian cancer following surgery. Niraparib (Zejula<sup>®</sup>) was endorsed in 2020 by the FDA as maintenance for advanced epithelial ovarian, fallopian tube or primary peritoneal cancer where patients have had complete or partial response to first-line platinum-based chemotherapy [28]. Talazoparib (Talzenna<sup>®</sup>) became licensed by the FDA in 2018 for the treatment of *BRCA*-mutated HER2-negative breast cancers [29]. Veliparib (ABT-888) is one of a number of PARPis that have not been endorsed to date for mainstream clinical use. Each of these PARPis has a unique structure and different binding affinities for PARP family members [25,30]. Furthermore, these PARPis display differential PARP trapping potencies, where the PARP complex locks onto or becomes trapped on DNA at the site of breakage, thus preventing binding of other DNA repair factors [17,31]. The PARP trapping potency of these five PARPis from highest to lowest is talazoparib, niraparib, rucaparib, olaparib, then veliparib [24]. While amongst the most efficacious molecular target drugs of recent times, tumours can display innate or acquired resistance to PARPis. The reasons for this include innate HRR proficiency, reversion of *BRCA* mutations or mutations in other HRR-related genes such as *PALB2* or *RAD51C*, loss of *BRCA1* methylation that re-establishes HRR proficiency, the increase in expression of drug efflux pumps such as the MDR1 (p-glycoprotein) gene, aberrant replication fork protection and down-regulation of PARP proteins themselves, possibly as a result of PARP trapping [32,33].

Here, we have focused on ovarian cancer, where over 50% of the most common subtype high-grade serous ovarian cancer (HGSOC) have defects in genes that function in HRR [32]. We use models of *BRCA* wild-type and mutant ovarian cancer to investigate the efficacy of five PARPis—olaparib, rucaparib, niraparib, talazoparib and veliparib—on cell viability and cell survival. Further, we have investigated whether acquired PARP resistance to veliparib can be overcome by use of other PARPis. Lastly, we manipulated HRR by down-regulating *BRCA1* in *BRCA1* wild-type cells, including in OVCAR-3 cells known to harbor a *CCNE1* amplification and be HRR proficient, to determine whether we could sensitise cells to PARP inhibitors.

## 2. Results

### 2.1. PARPis Display Differential Efficacy on Cell Viability in *BRCA* Wild-Type and Mutant Ovarian Cancer Cell Line Pairs

LC50 levels of five PARPis (olaparib, niraparib, rucaparib, talazoparib and veliparib) in PEO1 and PEO4 (Figure 1A), as well as UWB1.289 and UWB1.289+*BRCA1* cells (Figure 1B), were determined from dose curves of each drug and endpoint MTS assay (Figures S1 and S2). Doses and serial dilutions used for each PARPi in different cell lines for all experiments are summarised in Table S1. *BRCA2* mutant PEO1 cells were responsive



to olaparib, niraparib and talazoparib over the dose curve compared with wild-type (WT) PEO4 cells, but not to rucaparib and veliparib in the context of cell viability (Figure S1). Veliparib displayed the highest of all LC50s at 47.59  $\mu\text{M}$  in PEO1 cells and 28.13  $\mu\text{M}$  in PEO4, suggesting that the PEO1/PEO4 cell line pair are highly resistant to this PARPi. Both WT PEO4 and the mutant PEO1 cell pair were highly sensitive to talazoparib (LC50s of 0.0557 and 0.0729  $\mu\text{M}$ , respectively), suggesting that this sensitivity was independent of *BRCA2* status (Table 1).

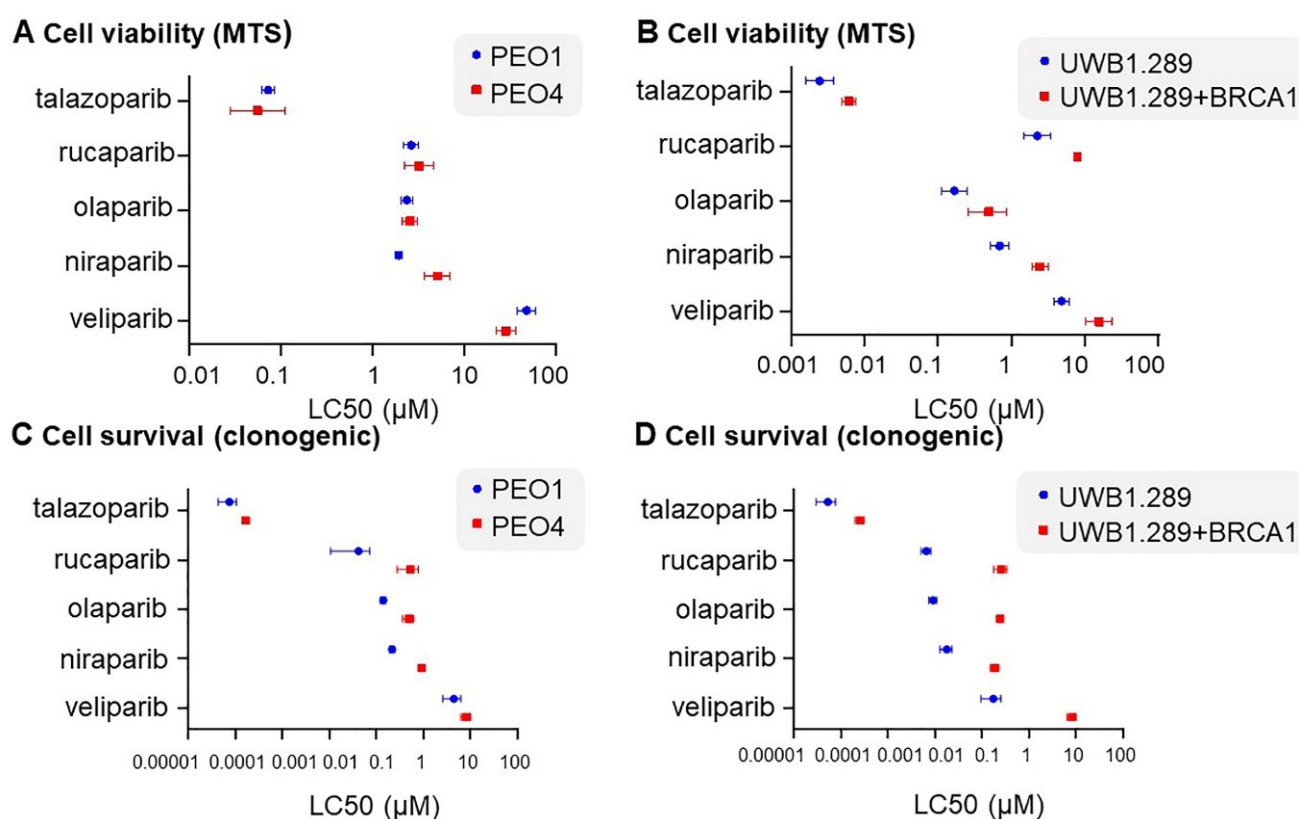


**Figure 1.** LC50 calculated from cell viability (MTS assay) data for each of five PARPis (talazoparib, rucaparib, olaparib, niraparib and veliparib) in (A) PEO1 and PEO4; (B) UWB1.289 and UWB1.289+BRCA1. LC50 calculated from cell survival (clonogenic assay) data for the identical five PARPis in (C) PEO1 and PEO4; (D) UWB1.289 and UWB1.289+BRCA1.

*BRCA1* mutant UWB1.289 cells were more responsive to all five PARPis tested based on LC50 data, compared to the paired cell line UWB1.289+BRCA1 (Table 1). Similar to the PEO paired cell lines, the UWB1.289 paired lines displayed the greatest sensitivity to talazoparib (Table 1). Niraparib showed the greatest discrimination in both cell line pairs based on the largest fold change in LC50 between mutant and WT cells, followed by rucaparib (Table 1). Further, greater fold changes based on LC50 data in response to all PARPis were seen in the *BRCA1* mutant and WT pair UWB1.289 compared with the *BRCA2* mutant and WT pair PEO1 and PEO4 (Table 1). This suggests that different *BRCA* mutations may respond differently to a range of PARPis.

**Table 1.** LC50 comparisons (cell proliferation; MTS) for PARP is in *BRCA1/2*-WT paired HGSOC cell lines and a parental-veliparib resistant endometrioid ovarian cancer cell line.

	LC50 (μM)		^ Fold Change
PARPi			
PEO1 vs. PEO4			
	PEO1	PEO4	
niraparib	1.9300	5.0640	2.62
rucaparib	2.6370	3.2140	1.22
olaparib	2.3560	2.5710	1.09
talazoparib	0.0729	0.0557	0.76
veliparib	47.5900	28.1300	0.59
UWB1.289 vs. UWB1.289 + BRCA1			
	UWB1.289	UWB1.289 + BRCA1	
niraparib	0.6936	2.4620	3.55
rucaparib	2.2560	7.9120	3.51
veliparib	4.8490	15.7200	3.24
olaparib	0.1679	0.4920	2.93
talazoparib	0.0025	0.0062	2.52
A2780 vs. A2780VeliR			
	A2780	A2780VeliR	
talazoparib	0.0024	0.0347	14.41
rucaparib	1.1440	6.3480	5.55
veliparib	16.62	57.49	3.46
niraparib	0.2934	0.8718	2.97
olaparib	0.8735	2.2230	2.54

^ fold change is displayed in descending order.

## 2.2. PARPis Display Differential Efficacy on Cell Survival in BRCA Wild-Type and Mutant Ovarian Cancer Cell Line Pairs

LC50 doses calculated using cell survival data from clonogenic assays of each PARPi in *BRCA* WT and mutant pairs were determined (Table 2, Figure 1C,D). As expected, greater sensitivity to all PARPis was seen in the *BRCA* mutant cell line of each pair (PEO1 and PEO4, Figure S3; UWB1.289 and UWB1.289+BRCA1, Figure S4) in the context of cell survival. As for cell viability, based on LC50 doses, the greatest sensitivity was observed for talazoparib in all cell lines (Table 2). Again, as for cell viability, differences in cell survival post treatment with different PARPis were seen in both of the cell line pairs tested. Veliparib showed the greatest fold change in the UWB1.289 pair, with a 47.36-fold difference in LC50 between the mutant and WT cell lines (Table 2). Curiously, veliparib showed the least fold difference in LC50 values between the mutant and WT PEO pair, with rucaparib showing the largest fold change at 12.78 (Table 2). Overall, greater fold differences in all PARPis were observed in the UWB1.289 pair compared to the PEO pair (Table 2). This observation was also true for cell viability (Table 1).

**Table 2.** LC50 comparisons (cell survival; clonogenic assay) for PARP is in *BRCA1/2*-WT paired HGSOC cell lines and a parental-veliparib resistant endometrioid ovarian cancer cell line.

LC50 (μM)			^ Fold Change
PARPi			
PEO1 vs. PEO4			
	PEO1	PEO4	
rucaparib	0.0417	0.5332	12.78
niraparib	0.2168	0.9263	4.27
olaparib	0.1405	0.4935	3.51
talazoparib	0.00008	0.00017	2.23
veliparib	4.445	8.2154	1.85
UWB1.289 vs. UWB1.289 + BRCA1			
	UWB1.289	UWB1.289 + BRCA1	
veliparib	0.1745	8.2640	47.36
rucaparib	0.0066	0.2592	39.30
olaparib	0.0091	0.2446	26.77
niraparib	0.0178	0.1889	10.63
talazoparib	0.00005	0.00026	4.86
A2780 vs. A2780VeliR			
	A2780	A2780VeliR	
olaparib	0.0052	0.1206	23.03
rucaparib	0.0071	0.0915	12.97
veliparib	0.5395	4.7707	8.84
talazoparib	0.00003	0.0001	2.99
niraparib	0.0194	0.0484	2.49

$\wedge$  fold change is displayed in descending order.

### 2.3. Veliparib Resistant A2780 Cells Retain Resistance to Other PARP Inhibitors

Given that different PARPis target PARP family members with varying efficiency, as well as show differences in their PARP trapping potency, we sought to determine whether olaparib, niraparib, talazoparib or rucaparib could rescue acquired resistance to veliparib. The A2780veliR cell line was developed in-house by the addition of increasing doses of ABT-888 and based on LC50 dose calculated from MTS assay was found to be 3.46-fold more resistant to veliparib than parental A2780 cells (Table 1, Figure 2A and Figure S5). Furthermore, based on LC50 doses calculated from cell survival data, A2780veliR cells were 8.84-fold more resistant to veliparib than A2780 (Table 2, Figure 2B and Figure S6). A2780veliR cells were between 2.54- to 14.41-fold more resistant to the other PARPis tested than parental A2780 cells based on LC50 doses calculated from MTS data (Table 1, Figure 2A and Figure S5). Furthermore, LC50 levels calculated from clonogenic assays showed that A2780veliR cells were between 2.49- to 23.03-fold more resistant to the other PARPis tested (Table 2, Figure 2A and Figure S6). These data support the conclusion that acquired veliparib resistance *in vitro* also leads to greater resistance to other PARPis. It therefore seems unlikely that PARPis will be able to rescue acquired resistance to a specific PARPi, at least in the case of resistance to veliparib.

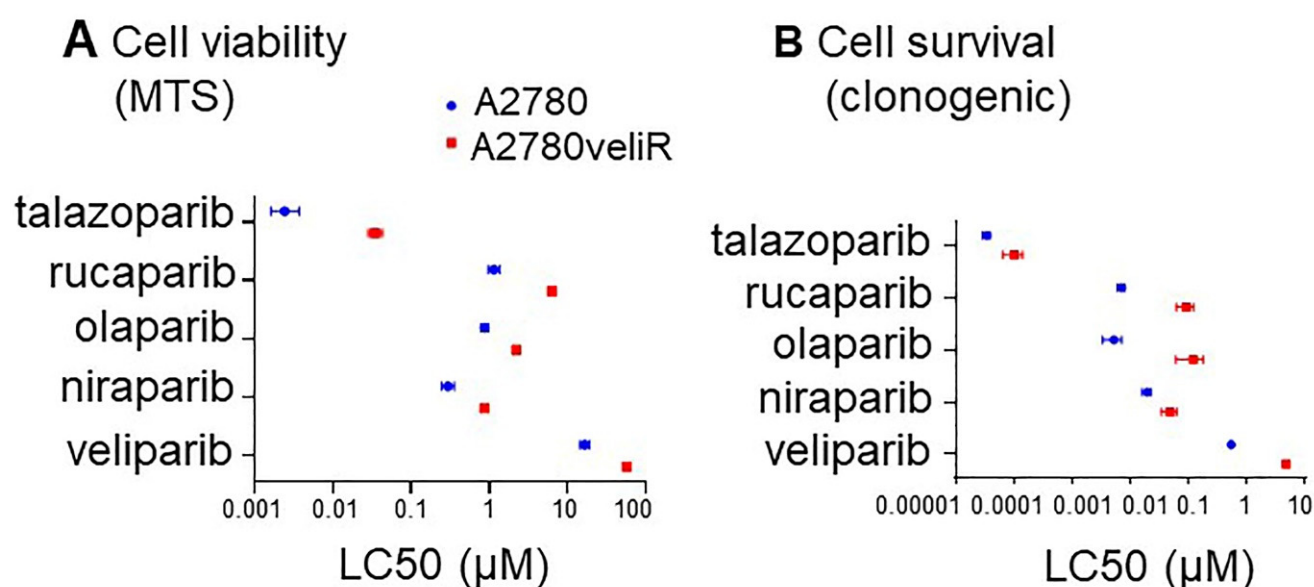


**Figure 2.** Talazoparib, rucaparib, olaparib or niraparib cannot rescue acquired veliparib resistance in the A2780veliR cell line model. **(A)** LC50 calculated from cell viability (MTS assay) data post treatment with a PARPi. **(B)** LC50 calculated from cell survival (clonogenic assay) data post treatment with a PARPi.

#### 2.4. Down-Regulation of BRCA1 in BRCA1 Wild-Type Ovarian Cancer Cell Lines Sensitises Cells to PARPis

Next, we sought to determine whether we could sensitise ovarian cancer cells to PARP inhibition by down-regulation of a key component of HR, specifically *BRCA1*. We chose two *BRCA1* WT cell lines for this purpose, specifically OVCAR-3 with a known *CCNE1* amplification frequently associated with HR proficiency [34], and A2780 that has been speculated to harbor a defect in DNA repair [35]. *BRCA1* was down-regulated using two independent siRNAs. We achieved between 56 and 62% *BRCA1* down-regulation in OVCAR-3 cells and 40–53% down-regulation in A2780 cells (Figure S7). Down-regulation of *BRCA1* alone in both cell lines decreased cell viability, by 12–33% in A2780 cells and 56–67% in OVCAR-3 cells (Figure 3). The large decrease in cell viability for OVCAR-3 cells upon down-regulation of *BRCA1* is likely due to the presence of a *CCNE1* amplification, previously reported as mutually exclusive events [36]. Down-regulation of *BRCA1* in A2780 cells (Figure 3B and Figure S8) and OVCAR-3 cells (Figure 3D and Figure S9) lowered the LC50 dose for all five PARPis, indicating that loss of *BRCA1* in these cell lines sensitised them to PARP inhibitors (Table 3).

#### 2.5. Down-Regulation of BRCA1 in BRCA1 Wild-Type Ovarian Cancer Cell Lines Decreases Cell Survival

We then sought to determine the effect of down-regulation of *BRCA1* on cell survival in A2780 and HR proficient OVCAR-3 cells. In both cases, down-regulation of *BRCA1* caused a decrease in plating efficiency, with a greater decrease seen in OVCAR-3 cells (Figure 4C) than A2780 cells (Figure 4A), indicating a significant basal effect on cell survival of down-regulating *BRCA1* in these cell line models. Dose curves of cell lines treated with PARPis did not show a significant difference between cells treated with the non-silencing control or either of two *BRCA1* siRNAs (Figures S10 and S11). This is possibly due to the fact that down-regulation of *BRCA1* alone in these cells had a large effect on cell survival and any additional effects of PARP inhibition were difficult to detect. With this in mind, small differences in LC50 dose comparing the non-silencing control to cell lines in which *BRCA1* was down-regulated were observed for most PARPis in both cell line models (Figure 4B,D, Table 3).

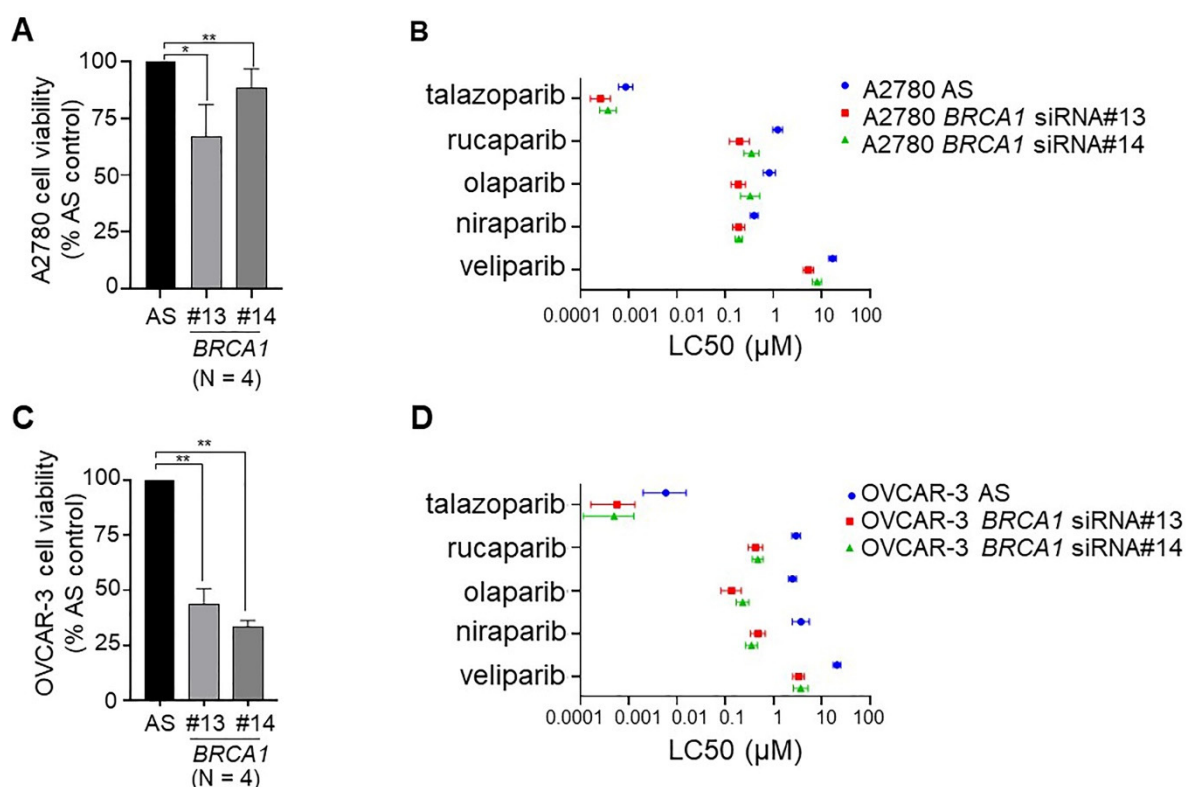


**Figure 3.** Down-regulation of *BRCA1* decreased basal cell viability and sensitised cells to PARP inhibition. Down-regulation of *BRCA1* by two distinct siRNAs (#13 and #14) in (A) A2780 cells and (C) OVCAR-3 cells decreased cell viability measured by MTS assay (N = 4; AS, AllStars control siRNA). LC50 calculated from cell viability (MTS assay) data for each of the five PARPis (talazoparib, rucaparib, olaparib, niraparib and veliparib) after *BRCA1* down-regulation in (B) A2780 cells and (D) OVCAR-3 cells. \*  $p < 0.05$ , \*\*  $p < 0.01$ .

**Table 3.** LC50 comparisons (cell survival; clonogenic assays) for PARPis in cell lines with down-regulated *BRCA1*.

	LC50 (μM)		
	AS	<i>BRCA1</i> si#13 (fold change)	<i>BRCA1</i> si#14 (fold change)
<b>PARPi</b>			
<b>A2780 <i>BRCA1</i> KD (cell viability)</b>			
olaparib	1.2330	0.1994 (6.18)	0.3539 (3.48)
rucaparib	0.8272	0.1886 (4.39)	0.3320 (2.49)
talazoparib	0.0009	0.0003 (3.32)	0.0004 (2.32)
veliparib	16.9900	5.3730 (3.16)	8.0910 (2.10)
niraparib	0.4010	0.1910 (2.10)	0.1927 (2.08)
<b>OVCAR-3 <i>BRCA1</i> KD (cell viability)</b>			
talazoparib	0.0058	0.0006 (10.24)	0.0005 (11.81)
rucaparib	2.4500	0.1345 (18.22)	0.2293 (10.68)
niraparib	3.6650	0.4730 (7.75)	0.3468 (10.57)

Table 3. Cont.

	LC50 ( $\mu$ M)		
	AS	BRCA1 si#13 (fold change)	BRCA1 si#14 (fold change ^)
olaparib	2.9110	0.4229 (6.88)	0.4687 (6.21)
veliparib	20.5600	3.2850 (6.26)	3.6540 (5.63)
<b>A2780 BRCA1 KD (cell survival)</b>			
olaparib	0.0275	0.0075 (3.67)	0.0110 (2.50)
niraparib	0.0471	0.0204 (2.30)	0.0311 (1.51)
veliparib	1.1726	0.5215 (2.25)	0.8487 (1.38)
talazoparib	0.0006	0.0003 (2.10)	0.0004 (1.26)
rucaparib	0.0283	0.0119 (2.38)	0.0229 (1.24)
<b>OVCAR-3 BRCA1 KD (cell survival)</b>			
rucaparib	0.0173	0.0085 (2.04)	0.0074 (2.33)
veliparib	1.5195	1.3455 (1.13)	0.7451 (2.04)
olaparib	0.0089	0.0062 (1.43)	0.0056 (1.59)
niraparib	0.0319	0.0263 (1.22)	0.0206 (1.55)
talazoparib	0.0003	0.0003 (0.94)	0.0003 (0.93)

^ fold change is displayed in descending order for BRCA1 si#14; KD, knock-down; AS, AllStars non-silencing control.

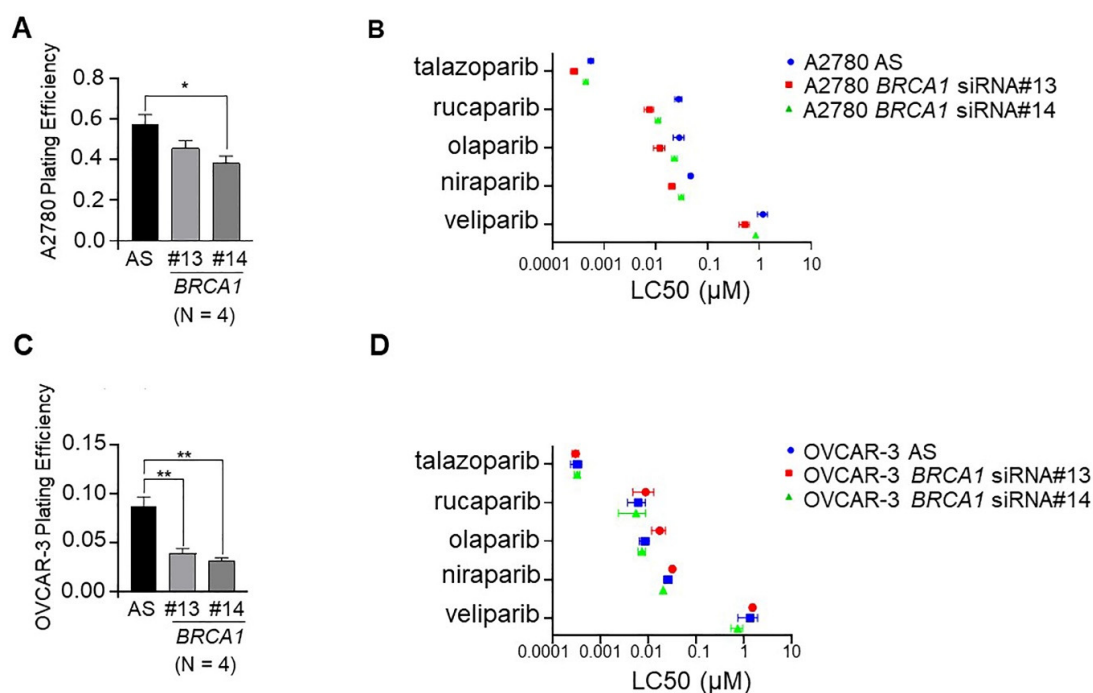


**Figure 4.** Down-regulation of *BRCA1* decreased basal cell survival, and in some cases, sensitised cells to PARP inhibition. Down-regulation of *BRCA1* by two distinct siRNAs (#13 and #14) in (A) A2780 cells and (C) OVCAR-3 cells decreased plating efficiency (N = 4; AS, AllStars control siRNA). LC50 data calculated from cell survival (clonogenic assay) for each of the five PARPis (niraparib, olaparib, rucaparib, talazoparib and veliparib) after *BRCA1* down-regulation in (B) A2780 cells and (D) OVCAR-3 cells. \*  $p < 0.05$ , \*\*  $p < 0.01$ .



### 3. Discussion

The fundamental premise of targeting the cell's DNA repair machinery has seen the development and rapid uptake of PARPis in the clinic. Specific improvements have been seen in both progression free and overall survival for women with HGSOc treated with a PARPi [37–41]. Still, currently there is no clear rationale regarding which PARPi to use, for which ovarian cancer patients beyond FDA endorsement of olaparib, rucaparib or niraparib when a mutation is present in *BRCA1* or *BRCA2* after first-line platinum-based chemotherapy or as maintenance therapy [30,42]. We show clear differences in response and sensitivity to different PARPis in our cell line models with known *BRCA* mutation status. Based on LC50 doses calculated from cell viability data, *BRCA2* mutant PEO1 cells were actually less sensitive to talazoparib and veliparib than their mutation reversion counterpart cell line, PEO4. In contrast, UWB1.289 cells lacking *BRCA1* were more sensitive to all five PARPis tested, with larger fold differences in LC50 doses observed between this cell line and its WT *BRCA1* partner line compared with the PEO1/PEO4 pair for all PARPis analysed. This larger fold difference in LC50 dose for the UWB1.289 pair compared to the PEO1/PEO4 pair was also observed for cell survival calculated from clonogenic assays for all PARPis analysed.

There are a number of possible explanations for these observations. It is possible that there are inherent differences in response to PARPis based on whether tumours have a *BRCA1* or *BRCA2* mutation. To date, few studies have explored this possibility, although differences in response to PARPis in prostate cancer have been reported based on whether the tumour was *BRCA1* or *BRCA2* mutated [43]. While PARPis are mechanistically similar in that they all interact with the substrate NAD<sup>+</sup> to inhibit PARylation and so DNA repair, they also have a number of differences. PARPis have different chemical structures and also differ in their ability to trap PARP1 on DNA, with talazoparib having the strongest PARP trapping function, followed by niraparib, rucaparib, olaparib and lastly veliparib [17,24]. This is consistent with our data that indicate talazoparib is the most cytotoxic of the PARPis tested and veliparib the least. Polypharmacology has been reported for PARP inhibitors. For example, niraparib and rucaparib have also been found to inhibit some kinases including DYRK15, CDK16 and PIM3 that may be therapeutically useful if these kinases are aberrantly expressed in specific tumours [25,44]. We cannot exclude the possibility that aberrant regulation of certain members of the kinome in cell line models used in this study may have affected the response to specific PARPis independently of *BRCA* status.

While the mechanism of acquired resistance to veliparib is currently unknown in our A2780<sup>veliR</sup> cells developed in-house from the A2780 parental cell line, we sought to investigate whether this resistance could be overcome by treatment with an alternative PARPi. The rationale for this strategy was based in the knowledge that different PARPis have been shown to display differential affinity for PARP family members, as well as different PARP trapping abilities [17,24,25,30,31]. Our data show that increased resistance to veliparib was not able to be overcome by treatment with any of olaparib, niraparib, rucaparib or talazoparib. In fact, increased resistance to veliparib led to increased resistance to all the other PARPis tested and would suggest that employing alternative PARPis would not be a successful clinical strategy to overcome acquired resistance to a PARPi. Testing of cell lines with developed resistance to other PARPis would need to be undertaken to further explore this phenomenon. Current approaches to overcoming PARPi resistance include focus on the use of inhibitors of other participants in the DNA damage repair response such as the cell cycle checkpoint regulators ATR, WEE1 and CHK1/2 [45–48].

Lastly, given the success of PARPis for women with HR deficient ovarian cancer, there is a strong need to expand these benefits to women whose tumours are HR proficient. With this in mind, in order to drive cells towards an HR deficient phenotype, we conducted a proof-of-principle experiment where we down-regulated *BRCA1* in HR proficient OVCAR-3 cells, as well as in the A2780 cell line that is *BRCA* WT but has recently been suggested to have defective DNA repair [35]. We then treated cells with all five PARPis. OVCAR-3 cells

have an amplification of *CCNE1* that has been reported as a mutually exclusive event to defective HR [36]. In spite of the combination of *CCNE1* amplification and loss of *BRCA1* likely leading to synthetic lethality that would explain the large decrease in basal cell viability in OVCAR-3 cells upon depletion of *BRCA1*, we did observe increased sensitivity to all PARPis in *BRCA1* down-regulated cells based on LC50 doses. This was not seen in cell survival assays, likely due to the effects of synthetic lethality. In A2780 cell lines that may already have defective DNA repair, increases in sensitivity to PARP inhibition was observed following down-regulation of *BRCA1* in both cell viability and cell survival assays. This observation warrants broader exploration and suggests that responses to PARPis may be amenable to further improvement by targeting of key participants in HRR, even in cells that may already suffer impaired levels of DNA repair.

With multiple PARPis available now for clinical use, and likely additional ones in development that will be endorsed for future use, stronger guidance will be required as to which PARPi to choose for a specific patient, considering factors such as tumour type, stage of disease, the involvement of HRR genes possibly down to the level of specific mutations, as well as off-target effects of different PARPis that may be efficacious. The routine incorporation of organoids generated from primary tumours or PDx models into the clinical management of patients would assist in streamlining the choice of PARPi that would best suit particular cases [49,50]. Pharmacological targeting of components of HRR in HR proficient tumours may increase the cohort of patients who currently experience the benefits of PARPi therapy beyond those whose tumours harbor defects in HRR pathways.

## 4. Materials and Methods

### 4.1. Cell Lines

The human HGSOC cell lines UWB1.289, UWB1.289+BRCA1 [51] and OVCAR-3 [52] were purchased from the American Type Culture Collection (ATCC, Virginia, USA; respectively, cat. #CRL-2945, #CRL-2946 and #HTB-161), while PEO1 and PEO4 were gifts originating from Dr Simon Langdon [53]. UWB1.289 (University of Washington-BRCA1-family 289) was derived from a recurrent human papillary serous ovarian cancer that contained the c.2594delC germline mutation in exon 11 of *BRCA1*, resulting in a premature STOP at codon 845 and a *BRCA1*-null phenotype. The corresponding WT *BRCA1* allele was also lost. UWB1.289+BRCA1 cells were created following stable transfection of WT *BRCA1*. These paired cell lines also have a mutation in *TP53*, specifically c.625delAG and loss of the *TP53* WT allele. PEO1 and PEO4 cells were derived from peritoneal ascites of the same patient who had a poorly differentiated serous adenocarcinoma. PEO1 cells were collected after the patient was treated with cisplatin, 5-fluorouracil and chlorambucil. PEO4 cells were collected after the patient demonstrated resistance to these drugs. PEO1 cells have the *BRCA2* mutation c.5193C>G, and PEO4 cells have a second mutation in *BRCA2*, c.5193C>T, that restores WT *BRCA2* [54,55]. This cell line pair also has a mutation in *TP53*, c.731G>A. The endometrioid ovarian cancer cell line A2780 was sourced from Sigma-Aldrich Pty. Ltd. (cat. #93112591, Sydney, NSW, Australia) [35,52]. Clear defects in components of HRR have not been identified in A2780 cells, although they have recently been reported to have low levels of the repair factor RAD50 compared with their counterpart cisplatin resistant line A2780cisR, suggesting they may harbour deficiencies in HRR [35]. Further, A2780 cells have previously been reported to exhibit sensitivity to a PARP inhibitor [56]. The A2780veliR cell line is resistant to the PARPi veliparib (ABT-888, cat. #ALX-270-444-M005, Sapphire Biosciences, Waterloo, NSW, Australia) and was developed in our laboratory from the parental A2780 cell line by exposure to gradual increasing concentrations of ABT-888 (10–140 µM) over a 31-week period. Cells were then grown for 6 weeks veliparib free to wash out any remaining drug.

All cell lines were grown in RPMI 1640 (cat. #42402016, Thermo Fisher Scientific, Mulgrave, VIC, Australia) supplemented with 10% FBS (AusGeneX, Molendinar, QLD, Australia), with the exception of the UWB1.289 and UWB1.289 + BRCA1 cell lines which were maintained in 50% RPMI 1640 (HyClone #SH30027, GE Healthcare Life Sciences), 50%



MEGM (Clonetics™ MEBM supplemented with SingleQuot additives cat. #CC-3150 from LONZA, Walkersville, MD, USA), supplemented with 3% FBS at 37 °C in a humidified 5% CO<sub>2</sub> atmosphere.

Cell line authentication was performed by the Australian Genome Research Facility (AGRF) Melbourne, Australia, by short tandem repeat (STR) profiling using the GenePrint-10 System which co-amplifies ten loci, including the ASN-0002 loci (TH01, TPOX, vWA, Amelogenin, CSF1PO, D16S539, D7S820, D13S317 and D5S818) as well as D21S11. All cell lines tested negative for mycoplasma with the MycoAlert™ Mycoplasma Detection Kit (cat. #LT07-318, LONZA, Walkersville, MD, USA).

#### 4.2. BRCA1 Down-Regulation, RNA Extraction and qRT-PCR

Cells were seeded into 6-well plates (600,000/well for A2780; 1,000,000/well for OVCAR-3) for 24 h followed by transfection with 20 nM BRCA1 siRNA #13 (cat. #SI02654575, Qiagen (cat. #301707), Chadstone, VIC, Australia), BRCA1 siRNA #14 (cat. #SI02664361, Qiagen) or a non-silencing negative control (Allstars, Qiagen) using HiPerfect transfection reagent (Qiagen). After 18 h, siRNA transfected cells were re-seeded for MTS or clonogenic assays. RNA was extracted 48 h post transfection using the RNeasy Mini kit (cat. #74106, Qiagen) and 500 ng converted to cDNA using the SuperScript™ IV First-Strand Synthesis System (SSIV, cat. #18091200, Thermo Fisher Scientific Australia Pty. Ltd., Scoresby, VIC, Australia). Quantitative real-time PCR (qRT-PCR) was performed using the TaqMan Fast Advanced Master Mix Kit (cat. #444557, Thermo Fisher Scientific) with Taqman assays BRCA1 (cat. #Hs01556193\_m1, Thermo Fisher Scientific) and *hydroxymethylbilane synthase* (HMBS) endogenous control (cat. #97639748, Integrated DNA Technologies, Baulkham Hills, NSW, Australia) on the QuantStudio 12K Flex Real-Time PCR System (Thermo Fisher Scientific). Each experiment was performed in triplicate and repeated at least three times, with data reported as the mean ± S.E.M.

#### 4.3. Cell Viability Assays and Calculation of LC50 Doses for PARP Inhibitors

Cells were seeded into 96-well plates (UWB1.289 2000 cells/well; UWB1.289+BRCA1 1000 cells/well; PEO1 1500 cells/well; PEO4 4000 cells/well; OVCAR-3 3000 cells/well; A2780 and A2780veliR 5000 cells/well) and treated with niraparib, olaparib, rucaparib, talazoparib (cat. #HY-10619, cat. #HY-10619, cat. #HY-10617, cat. #HY-16106, respectively; MedChemExpress, Monmouth Junction, NJ, USA) or veliparib (ABT-888; cat. #ALX-270-444-M005, Sapphire Biosciences, Waterloo, NSW, Australia) for 5 days before being assessed for cell viability using the CellTiter 96 Aqueous One Solution Cell Proliferation Assay (cat. #G3581, Promega, Madison, USA). This assay measures cellular metabolic activity and is a surrogate for cell viability. All results using this assay are described in the context of cell viability. Each experiment was performed in triplicate and repeated four times, with data reported as the mean ± SEM.

Relative lethal concentration 50 (LC50), the concentration required to bring the dose curve halfway between the top and bottom plateau of the curve, was calculated using GraphPad Prism 9. To address the issue that some of the drugs tested did not achieve total loss of cell viability at high levels, data were normalised to vehicle alone (100%) and the highest drug concentration where a plateau was observed (0%). A non-linear regression curve was fitted to the data and LC50 concentrations extrapolated [57].

#### 4.4. Clonogenic Cell Survival Analyses

Clonogenic cell survival assays measure the ability of a single cell to grow into a colony post an intervention, in this case treatment with a PARP inhibitor or down-regulation of a gene. All results using this assay are described in the context of cell survival. Cells were seeded into 6-well plates at a density of 1000 cells/well for UWB1.289+BRCA1 and OVCAR-3, 2000 cells/well for UWB1.289, 750 cells/well for PEO1, 1500 cells/well for PEO4, 200 cells/well for A2780 and 180 cells/well for A2780veliR. Cells were then treated with niraparib, olaparib, rucaparib, talazoparib or veliparib for 8–21 days. Cells were fixed

with 100% methanol for 20 min, rinsed briefly with water and stained with 0.5% *w/v* crystal violet in 25% *v/v* methanol for 5 min [58]. Colonies were counted using the GelCount imager (Oxford Optronix, Abingdon, England) and plating efficiency (PE) and surviving fraction (SF) determined [59]. A Jupyter notebook script was written in Anaconda 3 and LC50 concentrations determined based on a published method for analysis of dose-survival curves [60].

#### 4.5. Statistical Analysis

IBM SPSS software version 27.0 (SPSS Australasia Pty Ltd., Chatswood, NSW, Australia) was used for statistical analyses. All results are expressed as the mean  $\pm$  SEM from at least three independent experiments unless otherwise stated. One-sample t-tests were used to assess the efficacy of gene down-regulation. Independent samples T tests were used to compare plating efficiency in cell survival assays. Two-way ANOVA were used to compare paired cell lines over dose courses for different PARPis. One-way ANOVA with Tukey's *post hoc* test was used to test for multiple comparisons between cell lines at discrete drug dosages. For all analyses,  $p < 0.05$  was considered statistically significant.

**Supplementary Materials:** The following are available online at <https://www.mdpi.com/article/10.3390/ijms22168506/s1>.

**Author Contributions:** Conceptualisation, D.J.M. and K.-A.D.; methodology, T.X., K.-A.D., Y.M.; software, C.E.; validation, T.X. and K.-A.D.; formal analysis, D.J.M., K.-A.D., C.E.; investigation, K.-A.D., T.X., C.E.; resources, D.J.M. and K.-A.D.; data curation, K.-A.D., T.X., C.E.; writing—original draft preparation, D.J.M. and K.-A.D.; writing—review and editing, K.-A.D., T.X., C.E., Y.M., D.J.M.; visualisation, K.-A.D. and D.J.M.; supervision, K.-A.D. and D.J.M.; project administration, D.J.M.; funding acquisition, D.J.M. All authors have read and agreed to the published version of the manuscript.

**Funding:** This research received no external funding.

**Institutional Review Board Statement:** Not applicable.

**Informed Consent Statement:** Not applicable.

**Data Availability Statement:** All data presented in this study are linked through the University of Technology Sydney's research data management platform Stash and is available upon request to the corresponding author.

**Acknowledgments:** The authors would like to acknowledge the Facilities Team (M. Ballesteros, L. Beebe and S. Osvath) at the University of Technology Sydney, Australia for assisting this project to run during challenging times of COVID-19. BioRender was used in preparation of the graphical abstract (BioRender.com, accessed on 30 July 2021).

**Conflicts of Interest:** The authors declare no conflict of interest.

## References

- Schettini, F.; Giudici, F.; Bernocchi, O.; Sirico, M.; Corona, S.P.; Giuliano, M.; Locci, M.; Paris, I.; Scambia, G.; De Placido, S.; et al. Poly (ADP-ribose) polymerase inhibitors in solid tumours: Systematic review and meta-analysis. *Eur. J. Cancer* **2021**, *149*, 134–152. [CrossRef]
- Cerrato, A.; Morra, F.; Celetti, A. Use of poly ADP-ribose polymerase [PARP] inhibitors in cancer cells bearing DDR defects: The rationale for their inclusion in the clinic. *J. Exp. Clin. Cancer Res.* **2016**, *35*, 179. [CrossRef] [PubMed]
- Rose, M.; Burgess, J.T.; O'Byrne, K.; Richard, D.J.; Bolderson, E. PARP Inhibitors: Clinical relevance, mechanisms of action and tumor resistance. *Front Cell Dev. Biol.* **2020**, *8*, 564601. [CrossRef]
- Foo, T.; George, A.; Banerjee, S. PARP inhibitors in ovarian cancer: An overview of the practice-changing trials. *Genes Chromosomes Cancer* **2021**, *60*, 385–397. [CrossRef] [PubMed]
- Oh, S.Y.; Rahman, S.; Sparano, J.A. Perspectives on PARP inhibitors as pharmacotherapeutic strategies for breast cancer. *Expert Opin Pharm.* **2021**, *22*, 981–1003. [CrossRef] [PubMed]
- Xia, M.; Guo, Z.; Hu, Z. The role of PARP inhibitors in the treatment of prostate cancer: Recent advances in clinical trials. *Biomolecules* **2021**, *11*, 722. [CrossRef] [PubMed]
- Chi, J.; Chung, S.Y.; Parakrama, R.; Fayyaz, F.; Jose, J.; Saif, M.W. The role of PARP inhibitors in BRCA mutated pancreatic cancer. *Therap. Adv. Gastroenterol.* **2021**, *14*. [CrossRef] [PubMed]




8. Swisher, E.M.; Kwan, T.T.; Oza, A.M.; Tinker, A.V.; Ray-Coquard, I.; Oaknin, A.; Coleman, R.L.; Aghajanian, C.; Konecny, G.E.; O'Malley, D.M.; et al. Molecular and clinical determinants of response and resistance to rucaparib for recurrent ovarian cancer treatment in ARIEL2 (Parts 1 and 2). *Nat. Commun.* **2021**, *12*, 2487. [\[CrossRef\]](#)
9. Hu, Y.; Guo, M. Synthetic lethality strategies: Beyond BRCA1/2 mutations in pancreatic cancer. *Cancer Sci.* **2020**, *111*, 3111–3121. [\[CrossRef\]](#)
10. Lord, C.J.; Ashworth, A. BRCAness revisited. *Nat. Rev. Cancer* **2016**, *16*, 110–120. [\[CrossRef\]](#)
11. Gentles, L.; Goranov, B.; Matheson, E.; Herriott, A.; Kaufmann, A.; Hall, S.; Mukhopadhyay, A.; Drew, Y.; Curtin, N.J.; O'Donnell, R.L. Exploring the frequency of homologous recombination DNA repair dysfunction in multiple cancer types. *Cancers* **2019**, *11*, 354. [\[CrossRef\]](#) [\[PubMed\]](#)
12. Wang, Y.; Zheng, K.; Huang, Y.; Xiong, H.; Su, J.; Chen, R.; Zou, Y. PARP inhibitors in gastric cancer: Beacon of hope. *J. Exp. Clin. Cancer Res.* **2021**, *40*, 211. [\[CrossRef\]](#) [\[PubMed\]](#)
13. Fritz, C.; Portwood, S.M.; Przespolewski, A.; Wang, E.S. PARP goes the weasel! Emerging role of PARP inhibitors in acute leukemias. *Blood Rev.* **2021**, *45*, 100696. [\[CrossRef\]](#)
14. Amé, J.C.; Spencehauer, C.; de Murcia, G. The PARP superfamily. *Bioessays* **2004**, *26*, 882–893. [\[CrossRef\]](#) [\[PubMed\]](#)
15. Jubin, T.; Kadam, A.; Jariwala, M.; Bhatt, S.; Sutariya, S.; Gani, A.R.; Gautam, S.; Begum, R. The PARP family: Insights into functional aspects of poly (ADP-ribose) polymerase-1 in cell growth and survival. *Cell Prolif.* **2016**, *49*, 421–437. [\[CrossRef\]](#)
16. Kuzminov, A. Single-strand interruptions in replicating chromosomes cause double-strand breaks. *Proc. Natl. Acad. Sci. USA* **2001**, *98*, 8241–8246. [\[CrossRef\]](#)
17. Murai, J.; Huang, S.Y.; Das, B.B.; Renaud, A.; Zhang, Y.; Doroshow, J.H.; Ji, J.; Takeda, S.; Pommier, Y. Trapping of PARP1 and PARP2 by clinical PARP inhibitors. *Cancer Res.* **2012**, *72*, 5588–5599. [\[CrossRef\]](#)
18. del Rivero, J.; Kohn, E.C. PARP Inhibitors: The Cornerstone of DNA Repair-Targeted Therapies. *Oncology* **2017**, *31*, 265–273.
19. Nijman, S.M. Synthetic lethality: General principles, utility and detection using genetic screens in human cells. *FEBS Lett.* **2011**, *585*, 1–6. [\[CrossRef\]](#)
20. Dziadkowiec, K.N.; Gąsiorowska, E.; Nowak-Markwitz, E.; Jankowska, A. PARP inhibitors: Review of mechanisms of action and BRCA1/2 mutation targeting. *Prz. Menopauzalny* **2016**, *15*, 215–219. [\[CrossRef\]](#)
21. Kamaletdinova, T.; Fanaei-Kahrani, Z.; Wang, Z.Q. The enigmatic function of PARP1: From PARylation activity to PAR readers. *Cells* **2019**, *8*, 1625. [\[CrossRef\]](#)
22. Beck, C.; Robert, I.; Reina-San-Martin, B.; Schreiber, V.; Dantzer, F. Poly(ADP-ribose) polymerases in double-strand break repair: Focus on PARP1, PARP2 and PARP3. *Exp. Cell Res.* **2014**, *329*, 18–25. [\[CrossRef\]](#) [\[PubMed\]](#)
23. Pilié, P.G.; Gay, C.M.; Byers, L.A.; O'Connor, M.J.; Yap, T.A. PARP inhibitors: Extending benefit beyond BRCA-mutant cancers. *Clin. Cancer Res.* **2019**, *25*, 3759–3771. [\[CrossRef\]](#) [\[PubMed\]](#)
24. Lord, C.J.; Ashworth, A. PARP inhibitors: Synthetic lethality in the clinic. *Science* **2017**, *355*, 1152–1158. [\[CrossRef\]](#) [\[PubMed\]](#)
25. Antolin, A.A.; Ameratunga, M.; Banerji, U.; Clarke, P.A.; Workman, P.; Al-Lazikani, B. The kinase polypharmacology landscape of clinical PARP inhibitors. *Sci. Rep.* **2020**, *10*, 2585. [\[CrossRef\]](#) [\[PubMed\]](#)
26. Food and Drug Administration. Highlights of Prescribing Information: Lynparza (Revised: January 2018). Available online: [https://www.accessdata.fda.gov/drugsatfda\\_docs/label/2018/208558s001lbl.pdf](https://www.accessdata.fda.gov/drugsatfda_docs/label/2018/208558s001lbl.pdf) (accessed on 15 July 2021).
27. Food and Drug Administration. Highlights of prescribing information: Rubraca (Revised: December 2016). Available online: [https://www.accessdata.fda.gov/drugsatfda\\_docs/label/2016/209115s000lbl.pdf](https://www.accessdata.fda.gov/drugsatfda_docs/label/2016/209115s000lbl.pdf) (accessed on 15 July 2021).
28. Food and Drug Administration. Highlights of Prescribing Information: Zejula (Revised: March 2017). Available online: [https://www.accessdata.fda.gov/drugsatfda\\_docs/label/2020/208447s015s017bledt.pdf](https://www.accessdata.fda.gov/drugsatfda_docs/label/2020/208447s015s017bledt.pdf) (accessed on 15 July 2021).
29. Food and Drug Administration. Highlights of Prescribing Information: Talzenna (Revised: October 2018). Available online: [https://www.accessdata.fda.gov/drugsatfda\\_docs/label/2018/211651s000lbl.pdf](https://www.accessdata.fda.gov/drugsatfda_docs/label/2018/211651s000lbl.pdf) (accessed on 15 July 2021).
30. Valabrega, G.; Scotto, G.; Tuninetti, V.; Pani, A.; Scaglione, F. Differences in PARP inhibitors for the treatment of ovarian cancer: Mechanisms of action, pharmacology, safety, and efficacy. *Int. J. Mol. Sci.* **2021**, *22*, 4203. [\[CrossRef\]](#)
31. Hopkins, T.A.; Shi, Y.; Rodriguez, L.E.; Solomon, L.R.; Donawho, C.K.; DiGiammarino, E.L.; Panchal, S.C.; Wilsbacher, J.L.; Gao, W.; Olson, A.M.; et al. Mechanistic dissection of PARP1 trapping and the impact on in vivo tolerability and efficacy of PARP inhibitors. *Mol. Cancer Res.* **2015**, *13*, 1465–1477. [\[CrossRef\]](#)
32. Patch, A.M.; Christie, E.L.; Etemadmoghadam, D.; Garsed, D.W.; George, J.; Fereday, S.; Nones, K.; Cowin, P.; Alsop, K.; Bailey, P.J.; et al. Whole-genome characterization of chemoresistant ovarian cancer. *Nature* **2015**, *521*, 489–494. [\[CrossRef\]](#)
33. Goel, N.; Foxall, M.E.; Scalise, C.B.; Wall, J.A.; Arend, R.C. Strategies in overcoming homologous recombination (HR) proficiency and poly (ADP-Ribose) polymerase inhibitor (PARPi) resistance. *Mol. Cancer Ther.* **2021**. [Online ahead of print]. [\[CrossRef\]](#)
34. Etemadmoghadam, D.; George, J.; Cowin, P.A.; Cullinane, C.; Kansara, M.; Gorringe, K.L.; Smyth, G.K.; Bowtell, D.D. Amplicon-dependent CCNE1 expression is critical for clonogenic survival after cisplatin treatment and is correlated with 20q11 gain in ovarian cancer. *PLoS ONE* **2010**, *5*, e15498. [\[CrossRef\]](#)
35. Alblihy, A.; Alabdullah, M.L.; Toss, M.S.; Algethani, M.; Mongan, N.P.; Rakha, E.A.; Madhusudan, S. RAD50 deficiency is a predictor of platinum sensitivity in sporadic epithelial ovarian cancers. *Mol. Biomed.* **2020**, *1*, 19. [\[CrossRef\]](#)
36. Etemadmoghadam, D.; Weir, B.A.; Au-Yeung, G.; Alsop, K.; Mitchell, G.; George, J.; Davis, S.; D'Andrea, A.D.; Simpson, K.; Hahn, W.C.; et al. Synthetic lethality between CCNE1 amplification and loss of BRCA1. *Proc. Natl. Acad. Sci. USA* **2013**, *110*, 19489–19494. [\[CrossRef\]](#) [\[PubMed\]](#)

37. Ledermann, J.A. PARP inhibitors in ovarian cancer. *Ann. Oncol.* **2016**, *27* (Suppl. 1), i40–i44. [[CrossRef](#)]
38. Poveda, A.; Floquet, A.; Ledermann, J.A.; Asher, R.; Penson, R.T.; Oza, A.M.; Korach, J.; Huzarski, T.; Pignata, S.; Friedlander, M.; et al. Olaparib tablets as maintenance therapy in patients with platinum-sensitive relapsed ovarian cancer and a BRCA1/2 mutation (SOLO2/ENGOT-Ov21): A final analysis of a double-blind, randomised, placebo-controlled, phase 3 trial. *Lancet Oncol.* **2021**, *22*, 620–631. [[CrossRef](#)]
39. Poveda, A.; Floquet, A.; Ledermann, J.A.; Asher, R.; Penson, R.T.; Oza, A.M.; Korach, J.; Huzarski, T.; Pignata, S.; Friedlander, M.; et al. Final overall survival (OS) results from SOLO2/ENGOT-ov21: A phase III trial assessing maintenance olaparib in patients (pts) with platinum-sensitive, relapsed ovarian cancer and a BRCA mutation. *J. Clin. Oncol.* **2020**, *38*, 6002. [[CrossRef](#)]
40. Pujade-Lauraine, E.; Ledermann, J.A.; Selle, F.; GebSKI, V.; Penson, R.T.; Oza, A.M.; Korach, J.; Huzarski, T.; Poveda, A.; Pignata, S.; et al. Olaparib tablets as maintenance therapy in patients with platinum-sensitive, relapsed ovarian cancer and a BRCA1/2 mutation (SOLO2/ENGOT-Ov21): A double-blind, randomised, placebo-controlled, phase 3 trial. *Lancet Oncol.* **2017**, *18*, 1274–1284. [[CrossRef](#)]
41. Cecere, S.C.; Giannone, G.; Salutati, V.; Arenare, L.; Lorusso, D.; Ronzino, G.; Lauria, R.; Cormio, G.; Carella, C.; Scollo, P.; et al. Olaparib as maintenance therapy in patients with BRCA 1-2 mutated recurrent platinum sensitive ovarian cancer: Real world data and post progression outcome. *Gynecol. Oncol.* **2020**, *156*, 38–44. [[CrossRef](#)]
42. Pothuri, B.; O’Cearbhaill, R.; Eskander, R.; Armstrong, D. Frontline PARP inhibitor maintenance therapy in ovarian cancer: A Society of Gynecologic Oncology practice statement. *Gynecol. Oncol.* **2020**, *159*, 8–12. [[CrossRef](#)]
43. Markowski, M.C.; Antonarakis, E.S. BRCA1 versus BRCA2 and PARP inhibitor sensitivity in prostate cancer: More different than alike? *J. Clin. Oncol.* **2020**, *38*, 3735–3739. [[CrossRef](#)] [[PubMed](#)]
44. Antolín, A.A.; Mestres, J. Linking off-target kinase pharmacology to the differential cellular effects observed among PARP inhibitors. *Oncotarget* **2014**, *5*, 3023–3028. [[CrossRef](#)]
45. Chiappa, M.; Guffanti, F.; Bertoni, F.; Colombo, I.; Damia, G. Overcoming PARPi resistance: Preclinical and clinical evidence in ovarian cancer. *Drug Resist. Updates* **2021**, *55*, 100744. [[CrossRef](#)]
46. Kim, H.; Xu, H.; George, E.; Hallberg, D.; Kumar, S.; Jagannathan, V.; Medvedev, S.; Kinose, Y.; Devins, K.; Verma, P.; et al. Combining PARP with ATR inhibition overcomes PARP inhibitor and platinum resistance in ovarian cancer models. *Nat. Commun.* **2020**, *11*, 3726. [[CrossRef](#)] [[PubMed](#)]
47. Burgess, B.T.; Anderson, A.M.; McCorkle, J.R.; Wu, J.; Ueland, F.R.; Kolesar, J.M. Olaparib combined with an ATR or Chk1 inhibitor as a treatment strategy for acquired olaparib-resistant BRCA1 mutant ovarian cells. *Diagnostics* **2020**, *10*, 121. [[CrossRef](#)]
48. Haynes, B.; Murai, J.; Lee, J.M. Restored replication fork stabilization, a mechanism of PARP inhibitor resistance, can be overcome by cell cycle checkpoint inhibition. *Cancer Treat. Rev.* **2018**, *71*, 1–7. [[CrossRef](#)]
49. Hill, S.J.; Decker, B.; Roberts, E.A.; Horowitz, N.S.; Muto, M.G.; Worley, M.J., Jr.; Feltmate, C.M.; Nucci, M.R.; Swisher, E.M.; Nguyen, H.; et al. Prediction of DNA repair inhibitor response in short-term patient-derived ovarian cancer organoids. *Cancer Discov.* **2018**, *8*, 1404–1421. [[CrossRef](#)] [[PubMed](#)]
50. Topp, M.D.; Hartley, L.; Cook, M.; Heong, V.; Boehm, E.; McShane, L.; Pyman, J.; McNally, O.; Ananda, S.; Harrell, M.; et al. Molecular correlates of platinum response in human high-grade serous ovarian cancer patient-derived xenografts. *Mol. Oncol.* **2014**, *8*, 656–668. [[CrossRef](#)]
51. DelloRusso, C.; Welch, P.L.; Wang, W.; Garcia, R.L.; King, M.C.; Swisher, E.M. Functional characterization of a novel BRCA1-null ovarian cancer cell line in response to ionizing radiation. *Mol. Cancer Res.* **2007**, *5*, 35–45. [[CrossRef](#)] [[PubMed](#)]
52. Anglesio, M.S.; Wiegand, K.C.; Melnyk, N.; Chow, C.; Salamanca, C.; Prentice, L.M.; Senz, J.; Yang, W.; Spillman, M.A.; Cochrane, D.R.; et al. Type-specific cell line models for type-specific ovarian cancer research. *PLoS ONE* **2013**, *8*, e72162.
53. Langdon, S.P.; Lawrie, S.S.; Hay, F.G.; Hawkes, M.M.; McDonald, A.; Hayward, I.P.; Schol, D.J.; Hilgers, J.; Leonard, R.C.; Smyth, J.F. Characterization and properties of nine human ovarian adenocarcinoma cell lines. *Cancer Res.* **1988**, *48*, 6166–6172.
54. Stordal, B.; Timms, K.; Farrelly, A.; Gallagher, D.; Busschots, S.; Renaud, M.; Thery, J.; Williams, D.; Potter, J.; Tran, T.; et al. BRCA1/2 mutation analysis in 41 ovarian cell lines reveals only one functionally deleterious BRCA1 mutation. *Mol. Oncol.* **2013**, *7*, 567–579. [[CrossRef](#)] [[PubMed](#)]
55. Sakai, W.; Swisher, E.M.; Jacquemont, C.; Chandramohan, K.V.; Couch, F.J.; Langdon, S.P.; Wurz, K.; Higgins, J.; Villegas, E.; Taniguchi, T. Functional restoration of BRCA2 protein by secondary BRCA2 mutations in BRCA2-mutated ovarian carcinoma. *Cancer Res.* **2009**, *69*, 6381–6386. [[CrossRef](#)]
56. Tan, J.; Zheng, X.; Li, M.; Ye, F.; Song, C.; Xu, C.; Zhang, X.; Li, W.; Wang, Y.; Zeng, S.; et al. C/EBP $\beta$  promotes poly(ADP-ribose) polymerase inhibitor resistance by enhancing homologous recombination repair in high-grade serous ovarian cancer. *Oncogene* **2021**, *40*, 3845–3858. [[CrossRef](#)] [[PubMed](#)]
57. Sebaugh, J.L. Guidelines for accurate EC50/IC50 estimation. *Pharm. Stat.* **2011**, *10*, 128–134. [[CrossRef](#)] [[PubMed](#)]
58. Crowley, L.C.; Christensen, M.E.; Waterhouse, N.J. Measuring survival of adherent cells with the colony-forming assay. *Cold Spring Harb. Protoc.* **2016**, 721–724. [[CrossRef](#)] [[PubMed](#)]
59. Unkel, S.; Belka, C.; Lauber, K. On the analysis of clonogenic survival data: Statistical alternatives to the linear-quadratic model. *Radiat. Oncol.* **2016**, *11*, 1–11. [[CrossRef](#)] [[PubMed](#)]
60. Franken, N.A.; Rodermond, H.M.; Stap, J.; Haveman, J.; van Bree, C. Clonogenic assay of cells in vitro. *Nat. Protoc.* **2006**, *1*, 2315–2319. [[CrossRef](#)] [[PubMed](#)]



Review

# Histone Monoubiquitination in Chromatin Remodelling: Focus on the Histone H2B Interactome and Cancer

Deborah J. Marsh <sup>1,2,\*</sup> , Yue Ma <sup>1</sup>  and Kristie-Ann Dickson <sup>1</sup> 

<sup>1</sup> Translational Oncology Group, Faculty of Science, School of Life Sciences, University of Technology Sydney, Ultimo, NSW 2007, Australia; Yue.Ma-7@student.uts.edu.au (Y.M.); Kristie-Ann.Dickson@uts.edu.au (K.-A.D.)

<sup>2</sup> Kolling Institute, Faculty of Medicine and Health, Northern Clinical School, University of Sydney, Camperdown, NSW 2006, Australia

\* Correspondence: Deborah.Marsh@uts.edu.au; Tel.: +61-2-9514-7574

Received: 17 October 2020; Accepted: 17 November 2020; Published: 20 November 2020



**Simple Summary:** Post-translational modifications (PTM) of histone tails represent epigenomic regulation of the chromatin landscape, influencing gene expression and the response to DNA damage. This review focusses on cancer-associated roles of ubiquitin as a histone PTM, specifically in conjunction with an E3 ubiquitin ligase cascade that results in the addition of a single ubiquitin (monoubiquitination) to histone H2B at lysine 120 (H2Bub1). H2Bub1 has roles in chromatin accessibility important for transcriptional elongation, the DNA damage response, cellular proliferation and developmental transitions, including in stem cell plasticity. It has been implicated in inflammation and tumour progression, with examples of its loss associated with a worse prognosis for patients with some cancers. Many factors involved in the H2Bub1 interactome are well known cancer-associated proteins, including p53, BRCA1 and components of the SWI/SNF remodelling complex. Increased knowledge of H2Bub1 and its interactome offers new opportunities for therapeutic targeting of malignancy.

**Abstract:** Chromatin remodelling is a major mechanism by which cells control fundamental processes including gene expression, the DNA damage response (DDR) and ensuring the genomic plasticity required by stem cells to enable differentiation. The post-translational modification of histone H2B resulting in addition of a single ubiquitin, in humans at lysine 120 (K120; H2Bub1) and in yeast at K123, has key roles in transcriptional elongation associated with the RNA polymerase II-associated factor 1 complex (PAF1C) and in the DDR. H2Bub1 itself has been described as having tumour suppressive roles and a number of cancer-related proteins and/or complexes are recognised as part of the H2Bub1 interactome. These include the RING finger E3 ubiquitin ligases RNF20, RNF40 and BRCA1, the guardian of the genome p53, the PAF1C member CDC73, subunits of the switch/sucrose non-fermenting (SWI/SNF) chromatin remodelling complex and histone methyltransferase complexes DOT1L and COMPASS, as well as multiple deubiquitinases including USP22 and USP44. While globally depleted in many primary human malignancies, including breast, lung and colorectal cancer, H2Bub1 is selectively enriched at the coding region of certain highly expressed genes, including at p53 target genes in response to DNA damage, functioning to exercise transcriptional control of these loci. This review draws together extensive literature to cement a significant role for H2Bub1 in a range of human malignancies and discusses the interplay between key cancer-related proteins and H2Bub1-associated chromatin remodelling.

**Keywords:** histone monoubiquitination; E3 ubiquitin ligases; RNF20; p53; BRCA1; CDC73; SWI/SNF; transcriptional elongation; DNA damage

## 1. Introduction

Post-translational modifications (PTMs) of core histone proteins H2A, H2B, H3 and H4 constituting the nucleosome have driving roles in modulating the chromatin landscape in order to regulate fundamental processes such as transcription and the DNA damage response (DDR). Examples of histone PTMs include methylation, acetylation, phosphorylation, SUMOylation, proline isomerisation and ubiquitination [1,2]. The addition of a single 76 amino acid (8.5 kDa) ubiquitin, monoubiquitination, is one of the bulkier histone modifications [2,3]. A number of histone lysines (K) are monoubiquitinated in the mammalian genome, including K13, K15, K119, K127 and K129 of histone H2A; K34, K120 and K125 of histone H2B; and K31 on histone H4 (reviewed in [4]). The two most well-known mammalian histone monoubiquitination events occur on K119 of histone H2A (H2AK119ub1) linked to the Polycomb Repressor Complex 1 (PRC1) [5] and K120 of histone H2B (H2Bub1), the latter being the subject of this review. Interestingly, these events have opposing functions, with H2AK119ub1 associated with gene silencing and H2Bub1 frequently associated with active transcription [4–6].

A cascade of enzymatic events is responsible for monoubiquitination, involving an activating ATP-dependent ubiquitin enzyme E1 of which humans have a few, a ubiquitin conjugating enzyme (E2) of which humans have around 40, and a ubiquitin protein ligase (E3) of which humans have as many as 600–1000 [4,7,8]. The most prevalent of the E3 ubiquitin ligases are RING (really interesting new gene) finger domain ligases of which the E3 complex RNF20/RNF40 is the main writer enzyme complex responsible for catalysing H2Bub1 [1,9]. The H2Bub1 chromatin mark is erased by deubiquitinases (DUBs) from the ubiquitin-specific protease (USP) sub-family of DUBs, including USP44 and USP22 (reviewed in [1,10–12]) (Figure 1).

The enzymatic cascade that writes H2Bub1 is invoked to enable association of the human RNA polymerase II-associated factor 1 (PAF1) transcriptional complex with RNA polymerase II (RNA pol II) to facilitate transcriptional elongation [13]. It is also required to facilitate the accumulation of H2Bub1 at sites of double strand breaks (DSBs) where it functions as a scaffold or docking platform for the recruitment of DNA repair factors [14]. H2Bub1 has also been linked to DNA replication in yeast [15] and in both yeast and human cells, genomic stability through the maintenance of centromeric chromatin [16]. While H2Bub1 itself has been described as having tumour suppressive properties, a number of tumour suppressor proteins are also associated with H2Bub1-related processes including RNF20, CDC73, BRCA1, p53 and members of the switch/sucrose non-fermenting (SWI/SNF) chromatin remodelling complexes (also known as the BAF complexes) [17–20].

Global levels of H2Bub1 and/or its E3 ligase complex members RNF20 and RNF40, have been investigated in numerous tumours using methods including immunohistochemistry and for RNF40 and/or RNF20, assessment of transcript levels and promoter hypermethylation. Dependent upon tumour type, depleted global H2Bub1 levels have been shown to correlate with inflammatory processes that may function as precursor events to tumorigenesis, in tumour progression and in some tumour types have been correlated with a worse prognosis [21,22].

On the background of global loss of H2Bub1 in cancer cells, H2Bub1 is enriched at the coding regions of highly expressed genes in response to DNA damage, including p53 gene targets and genes involved in resistance to therapeutic drugs [23,24]. H2Bub1 therefore has a role in determining the fate of cancer cells that may be amenable to therapeutic intervention. Further evidence for a key role in determining cell fate is the role of H2Bub1 in the differentiation of stem cells, whether it be through engaging with other histone PTMs via histone cross-talk, or the enzymes involved in writing and erasing H2Bub1 [10,12]. H2Bub1 and its associated factors have also been linked to regulation of key development pathways in plants, including seed dormancy/germination and flowering time, as well as resistance to pathogen invasion [25–28]. It is clear that H2Bub1 has a significant role across species to regulate important functions through the modulation of gene expression.

In this review we discuss the role of H2Bub1 in fundamental cellular processes including gene transcription, the DDR and stem cell differentiation. We bring together the current literature on the involvement of H2Bub1 across multiple different tumour types, including links recently established

between H2Bub1 and inflammation. Lastly, we investigate the current state-of-play between H2Bub1 and members of its interactome complicit in the establishment and/or progression of malignancy.

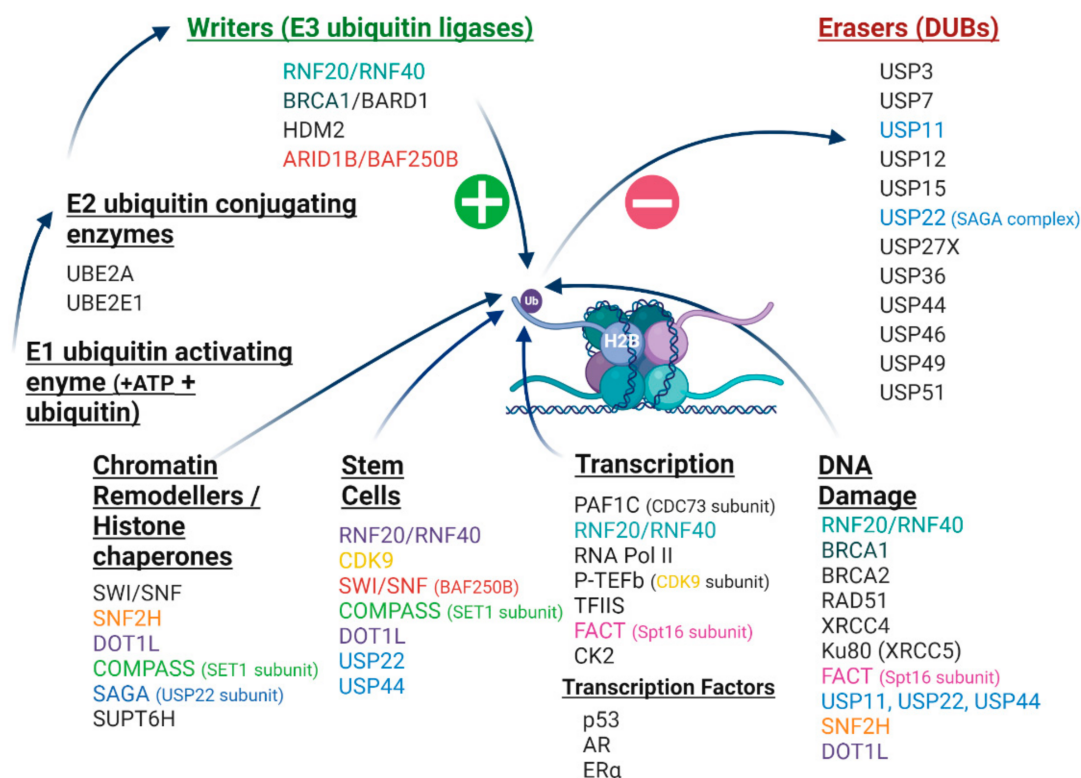


**Figure 1.** The H2Bub1 interactome. H2Bub1 can be written (green plus symbol) by multiple writer enzymes (E3 ubiquitin ligases) following an enzymatic ubiquitin cascade commencing with an E1 ubiquitin activating enzyme followed by an E2 ubiquitin conjugating enzyme. It can be removed (red minus symbol) by numerous erasing deubiquitinases (DUBs) from the Ubiquitin-Specific Protease (USP) sub-family. H2Bub1 interacts with a number of chromatin remodelling complexes and histone chaperones. Numerous components of the H2Bub1 interactome function in more than one cellular process, such as cyclin-dependent kinase 9 (CDK9) in stem cell plasticity and transcription, identified in this schematic by matching colours. The H2Bub1 interactome continues to be elucidated and is growing as new discoveries are made. Androgen receptor (AR); AT-Rich Interaction Domain 1B (ARID1B); BRG1/BRM-associated factor (BAF250B); BRCA1-Associated RING Domain 1 (BARD1); Breast Cancer Type 1 (BRCA1); Breast Cancer Type 2 (BRCA2); cyclin-dependent kinase 9 (CDK9); estrogen receptor alpha (ERα); complex of proteins associated with SET1 (COMPASS); disrupter of telomere silencing 1-like (DOT1L); facilitates chromatin transcription (FACT); Human Double Minute 2 (HDM2); X-ray Repair Cross Complementing 5 (Ku80, also known as XRCC5); RNA polymerase II-associated factor 1 complex (PAF1C); Positive Transcription Elongation Factor-b (P-TEFb); tumour protein 53 (p53); RNA polymerase II (RNA Pol II); RAD51 Recombinase (RAD51); RING Finger Protein 20 (RNF20); RING Finger Protein 40 (RNF40); Spt-Ada-Gcn5-acetyltransferase (SAGA); Su(var) 3–9 (SET1, suppressor of position effect variegation), enhancer of zeste (E(z)), and trithorax (Trx); SNF2 homologue, (SNF2H, also known as SMARCA5); Suppressor of Ty Homologue-6 (SUPT6H); Switch/sucrose non-fermenting (SWI/SNF); transcription elongation factor II S (TFIIS); ubiquitin conjugating enzyme E2 A (UBE2A); ubiquitin-conjugating enzyme E2 E (UBE2E1); Ubiquitin-Specific Protease (USP); X-ray Repair Cross Complementing 4 (XRCC4). Created with [BioRender.com](https://www.biorender.com/).

## 2. H2Bub1 and Transcriptional Elongation

Monoubiquitination isn't the only histone PTM that occurs at K120 of histone H2B. Acetylation at this site (H2BK120ac) written by the lysine acetyl transferase KAT3 is thought to act as a mark of chromatin poised to enter the active state, highlighting the temporal acetylation/ubiquitination switch working to achieve transcription [29]. H2Bub1 physically disrupts chromatin compaction, creating a more open conformation accessible to transcription factors and other proteins and/or protein complexes involved in activities such as DNA repair [30]. This is more than purely physical disruption, as replacement of ubiquitin with the even bulkier molecule small ubiquitin-like modifier (SUMO), does not result in the same functional effects [31]. K120 of histone H2B is physically located at the interface of adjacent nucleosomes, making it possible that H2Bub1 has an impact on nucleosome stacking that may affect nucleosome stability [30]. Chandrasekharan and colleagues demonstrated that nucleosome stability increases in the presence of H2Bub1 during transcription and that this negatively impacts upon cell growth [31], with a later study suggesting that this may be a modest effect [32].

H2Bub1 is enriched at the coding regions of highly expressed genes [24]. In response to stimuli such as a hormone and/or a developmental signal or DNA damaging agent, cyclin-dependent kinase 9 (CDK9), part of the Positive Transcription Elongation Factor-b (P-TEFb) [33] complex, phosphorylates both the H2Bub1 E2 enzyme UBE2A and Ser2 in the carboxy-terminal domain (CTD) of RNA Pol II [12,34]. This creates a binding domain for WAC (WW Domain-Containing Adapter Protein with Coiled-Coil) that directly links the main H2Bub1 E3 ligase complex RNF20/RNF40 to RNA pol II [12,35]. In this co-transcriptional role with H2Bub1, CDK9 has been shown in yeast to be responsible for releasing RNA pol II from promoter-proximal pausing, making it an important regulator of gene expression [1,36,37]. Notably, RNA pol II promoter-proximal pausing has been implicated in the suppression of transcription of antisense genes [38].

Both RNF20 and RNF40 have been shown to physically interact with subunits of the human PAF1C (including the PAF1 subunit itself, CDC73 and CTR9) that associates with RNA Pol II, setting the stage for interaction of all these factors that enable transcriptional elongation to proceed [39] (reviewed in [1,10,12]) (Figure 1, Figure 2A). Enrichment of H2Bub1 occupancy at highly expressed genes has been shown to correlate with the recruitment of Pol II, prior to the increase of mRNA expression and to decrease once RNA Pol II has dissociated [24]. Examples of genes with enriched H2Bub1 include those that are transcriptionally driven by hormone receptors, specifically estrogen receptor alpha (ER $\alpha$ ) [22,40,41] important in some breast and ovarian cancers, and the androgen receptor (AR), important in prostate cancer [42], as well as p53 target genes that function in the cellular response to DNA damage [10,24] (Figure 2B).

To enable transcriptional elongation, H2Bub1 recruits the histone chaperone that facilitates chromatin transcription (FACT) that works to remove the H2A-H2B dimer from the nucleosome, therefore removing the physical block to RNA pol II (Figure 2A) [43]. A FACT subunit, Spt16, functions with H2Bub1 to then enable nucleosome reassembly following RNA pol II transcriptional elongation [44]. These apparently opposing functions of H2Bub1 highlight its key roles in the kinetics of nucleosome assembly and disassembly required during and post transcription.

H2Bub1 is also central in trans-histone crosstalk, recruiting histone methyltransferase complexes that further direct chromatin configuration and gene expression [45–48]. The catalytic activity of the disrupter of telomere silencing 1-like (DOT1L) histone methyltransferase that facilitates methylation of histone H3 at K79 (H3K79me) at the proximal region of actively transcribed genes is stimulated by H2Bub1 [49–54]. Loss of H3K79me<sub>2</sub> has been correlated with genomic instability [55]. Another active chromatin mark is histone H3K4 methylation that is catalysed by SET1, the methyltransferase subunit of the complex of proteins associated with SET1 (COMPASS) after first being recruited by H2Bub1 [39,56,57]. Furthermore, Basnet and colleagues report an association between the phosphorylation of tyrosine 57 on histone H2A by casein kinase 2 (CK2) and H2Bub1 in yeast and mammalian cells. Loss of this histone H2A phosphorylation event, either by mutation at the histone H2A tyrosine site or inhibition of CK2, leads to loss of H2Bub1, H3K4me<sub>3</sub> and H3K79me<sub>3</sub>, impacting on transcriptional elongation



and likely involving the Spt-AdaGcn5 acetyltransferase (SAGA) chromatin modifying complex [58]. This is another example of how H2Bub1 functions in histone crosstalk. These patterns of trans-histone cross-talk cement the importance of H2Bub1 as a central regulator of transcription (Figure 1).

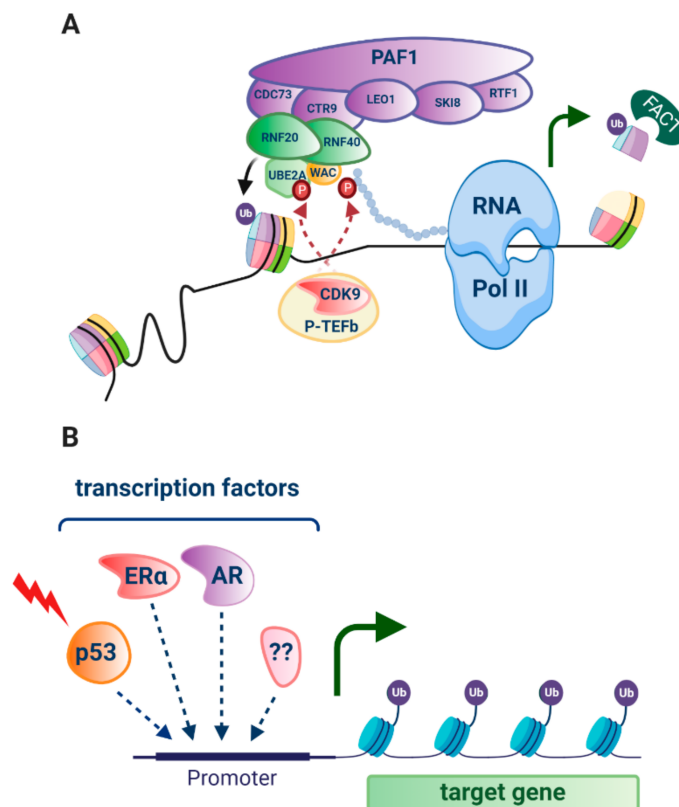


**Figure 2.** H2Bub1 in transcriptional elongation. **(A)** Following stimuli such as DNA damage, hormones or developmental signals, cyclin-dependent kinase 9 (CDK9) that is part of the Positive Transcription Elongation Factor-b (P-TEFb) complex phosphorylates Ser2 in the carboxy-terminal domain of RNA polymerase II (RNA pol II) depicted by a chain of circles, as well as the E2 ubiquitin conjugating enzyme ubiquitin conjugating enzyme E2 A (UBE2A). This dual phosphorylation shown by red circles, establishes a binding domain for the WW domain-containing adaptor with coiled-coil (WAC) and the E3 ubiquitin ligase complex RNF20/RNF40 that monoubiquitinates histone H2B at lysine 120 (H2Bub1, ubiquitin shown as a purple circle). RNF20/RNF40 physically interacts with the PAF1 complex consisting of CDC73, CTR9, LEO1, SKI8, RTF1 and PAF1 that associates with RNA pol II to establish transcriptional elongation. The chromatin remodelling factor FACT is recruited by H2Bub1, and removes a H2B-H2A dimer from the core nucleosome that takes away the physical block to RNA pol II, allowing it to move through the nucleosome, facilitating gene expression (green arrow). **(B)** A number of transcription factors have been associated with enriched H2Bub1 at target genes, including p53 (red lightning bolt depicts DNA damage that activates this tumour suppressor), the estrogen receptor (ER $\alpha$ ) and androgen receptor (AR). ?? indicates as yet unknown transcription factors. Created with BioRender.com.

While being a clear enabler of transcriptional elongation, in certain circumstances H2Bub1 can also impede it. At least in yeast, there would appear to be a positional effect determined by gene location given that H2Bub1 at promoters of genes that aren't expressed appear to inhibit the formation of transcriptional complexes [59]. The H2Bub1 writer enzyme RNF20 has been demonstrated to obstruct binding of the transcription elongation factor transcription elongation factor II S (TFIIS) to the PAF1C, so blocking the ability to relieve stalled RNA pol II on chromatin [60]. In this way, RNF20 works to selectively inhibit the transcription of pro-oncogenic genes located in condensed chromatin, supportive of a tumour suppressor function for this E3 ligase. H2Bub1 occupancy is, therefore, complex and likely

tissue, genomic position and contextually specific, as not all genes require H2Bub1 enrichment for their expression [61]. One study combining RNA sequencing and Assay for Transposase Accessible Chromatin (ATAC-seq) in fallopian tube epithelial cell lines suggested an association between loss of H2Bub1 and a more open chromatin configuration [62]. In summary, H2Bub1 is a master regulator of transcription, controlling gene expression in response to acute stimuli and developmental signals in a context specific manner and occupying a central role in histone cross-talk directing gene expression.

### 3. H2Bub1 and the DNA Damage Response (DDR)

H2Bub1 accumulates after DNA damage at sites of DSBs as part of the cellular DDR [14,63,64]. Upon DNA damage, the ATM (ataxia telangiectasia mutated) kinase phosphorylates (red circles) RNF20 and RNF40, facilitating the recruitment of this E3 ligase complex to DSBs where it acts to catalyse H2Bub1 [14]. DNA damage-associated H2Bub1 then acts as a platform to recruit the chromatin remodelling factor SNF2H and other proteins required for homologous recombination repair (HRR) including BRCA1, BRCA2 and RAD51, as well as non-homologous end joining, including XRCC4 and Ku80 (Figures 1 and 3) [14,63,65].

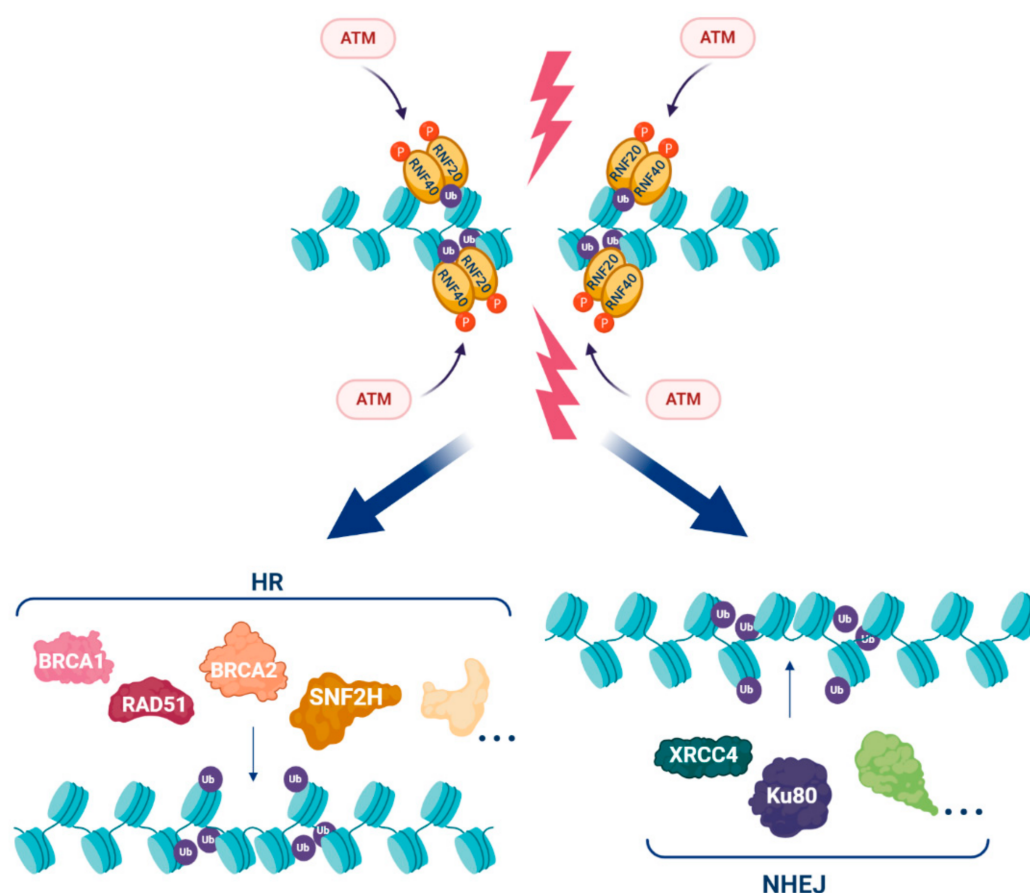


**Figure 3.** H2Bub1 in the DNA damage response. In the presence of double strand breaks (DSBs), ATM (ataxia telangiectasia mutated) phosphorylates (red circles) RNF20 and RNF40 that localise to DSBs where they function as an E3 ligase complex to write H2Bub1 (purple circles). H2Bub1 acts as a platform to attract proteins that work in both homologous recombination (HRR: BRCA1, BRCA2, RAD51, SNF2H and additional proteins) and non-homologous end joining (NHEJ: XRCC4, Ku80 (XRCC5) and additional proteins) to enable DNA repair. Created with BioRender.com.

Numerous factors that have a role in H2Bub1-related transcription also have a role in H2Bub1-related DNA repair. One of these is the histone chaperone FACT complex subunit Spt16 that binds to RNF20 to enable recruitment of SNF2H as well as the DNA repair proteins BRCA1 and RAD51

at DSBs to initiate HRR [66]. RNF40 was shown to have a similar role and interaction with Spt16 at sites of DSBs [67]. A number of the H2Bub1 DUBs have also been implicated in the DNA damage response through modulation of chromatin, including USP11 [68], USP22 [69,70] and USP44 [71]. Furthermore, the DOT1L histone methyltransferase known to engage in trans-histone cross-talk with H2Bub1 is important for HRR at DSBs [72].

Global loss of H2Bub1 has been observed in cancer cell line models following treatment with DNA damaging agents including doxorubicin, neocarzinostatin and cisplatin [14,23,24]. On the background of this global loss, H2Bub1 is enriched in the coding regions of specific highly expressed genes, including p53 target genes such as *CDKN1A* and *MDM2* [23,24]. It is likely in these cases that many genes that display enriched H2Bub1 following DNA damage are required for decisions regarding cellular fate [23].

#### 4. H2Bub1 and Cellular Proliferation in Cancer

It is well established that cellular proliferation is dependent upon access to chromatin to regulate the expression of oncogenes and tumour suppressors that when aberrantly expressed can lead to a malignant phenotype. Loss of H2Bub1 has been associated with tumour progression consistent with a tumour suppressive function of this histone PTM [1,10,12]. The role of H2Bub1 in cellular proliferation has been studied predominantly through manipulation of its key writer and eraser enzymes. For example, siRNA (short interfering RNA) down-regulation of RNF20 and RNF40 has been reported to inhibit proliferation of prostate cancer cells [42]. Of note, RNF40 has been implicated in the control of key apoptotic genes in colorectal cancer cells [73].

RNF20 has also been identified as necessary for proliferation, both in vitro in mixed-lineage leukemia (MLL)-rearranged human acute myeloid leukemia (AML) cell lines and in vivo, being important for disease progression in a genetically engineered mouse model of AML [74]. RNF20 and USP44 have different effects on the proliferation and migration of breast cancer cells dependent on subtype, i.e., basal-like versus luminal [22]. H2Bub1-associated DUBs USP22, USP51 and USP27X have been shown in vitro to be required for normal growth, with in vivo depletion suppressing tumour growth in a mouse xenograft model of breast cancer cells [75]. Down-regulation of USP36 in lung cancer cells has also been shown to negatively impact on cell proliferation [76]. A number of these associations are discussed elsewhere in this review.

#### 5. H2Bub1 is a Key Regulator of Developmental Transitions

##### 5.1. H2Bub1 and Stem Cell Plasticity

Histone PTMs are important for maintaining stem cell self-renewal and the plasticity of stem cells, as well as facilitates stem cell differentiation into different cell lineages [77–81]. H2Bub1 levels have been shown to increase during the differentiation of embryonic stem cells (ESCs) and embryonal carcinoma stem cells (ECSCs) [82], as well as in human mesenchymal stem cells (hMSCs) after differentiation into osteoblasts and adipocytes [83]. Numerous components of the H2Bub1 interactome have been implicated in the maintenance of stem cell pluripotency and differentiation, including the writers RNF20 [82] and RNF40 [83], cyclin-dependent kinase CDK9 [83], the BAF250b (BRG1/BRM-Associated Factor) subunit of the SWI/SNF chromatin remodelling complex [84], H2Bub1-interacting histone methyltransferase complexes including COMPASS [85] and DOT1L [86–88], as well as the DUBs USP22 [89–92] and USP44 [82,93]. As for DNA damage, H2Bub1 and many of its regulatory factors that modulate chromatin play a central role in determining cellular fate as part of key signalling required for differentiation. In the case of cancer stem cells that are linked with tumour initiation, relapse and drug resistance, targeting specific components of the H2Bub1 interactome may offer new therapeutic strategies for drug resistant malignancies [88,90,91,93].

## 5.2. H2Bub Regulates Developmental Pathways and the Immune Response in Plants

Drawing parallels between the human and the plant world, H2Bub1 and the E2 and E3 ligases involved in its writing have been shown to have major roles in the control of gene expression linked to developmental and immune functions in a range of plant species. E2 and E3 ligases that write H2Bub1 in *Arabidopsis thaliana* are pivotal in controlling expression of *FLOWERING LOCUS C* (*FLC*) that is the main repressor of flowering, thus dictating flowering time [25,94]. H2Bub1 in *Arabidopsis* has also been linked to the regulation of circadian clock genes [26]. Down-regulation of the E3 ligase encoding flowering-related RING Protein 1 (*FRRP1*) in rice, *Oryza sativa*, has been shown to regulate flowering time and yield potential, most likely through H2Bub1 [95]. Seed germination is another key developmental transition for plants. H2Bub1 controlled by E3 ligases has been shown to control the expression of genes involved in seed dormancy in *Arabidopsis thaliana* [27]. Further, variation in monoubiquitination of histone H2A and H2B variants has been linked to the innate immune response against fungal attack in rice, and H2Bub1 has been shown to have a role in defence against the fungus *Botrytis cinerea* in tomato, again via its E3 ubiquitin ligases [28,96].

Considered together, H2Bub1 has a significant role in the plant ubiquitin chromatin landscape with regulatory influence over the expression of genes in developmental programs including the circadian clock, flowering time, seed dormancy and germination, as well as in pathogen defence. The role of H2Bub1 spans multicellular eukaryotes and key cellular processes, establishing its importance as a major epigenomic regulator of gene expression in both the animal and plant kingdom.

## 6. Global Loss of H2Bub1 in Human Malignancy

Global loss of H2Bub1 in primary tumours or early lesions has been detected using immunohistochemistry by us and others across a range of malignancies. H2Bub1, RNF20 and/or RNF40 have been investigated in numerous cancer tissues, including breast [22,40,41,97,98], ovarian [62,99], colorectal [21,97,100], lung [97,101], gastric [102], kidney [103] and parathyroid [18]. Where clear numbers have been reported in publications, we have summarised this data; for H2Bub1 (Table 1) and RNF20/RNF40 (Table 2). In some cancers, H2Bub1 loss by way of loss of RNF20 has been implicated in an early inflammatory response, while in others it has been linked to progression of the tumour and in some cases, a worse prognosis.

**Table 1.** H2Bub1 loss in primary tumours.

Tissue Type	Cohort Size	% H2Bub1 Loss	Reference
Breast—normal mammary duct epithelial cells (adjacent tissue)	8	0%	[40]
Breast—benign tumour	18	0%	[40]
Breast—cancer	64	67%	[40]
Breast—cancer	34	97%	[97]
Colon—normal mucosa	55	0%	[100]
Colon—cancer	36	86%	[97]
Colon—cancer	1584	21% <sup>^</sup> 26% <sup>^^</sup>	[100]
Gastric cancer (well differentiated)	23	4% <sup>^</sup> 30% <sup>^^</sup>	[102]

Table 1. Cont.

Tissue Type	Cohort Size	% H2Bub1 Loss	Reference
Gastric cancer (moderately differentiated)	55	13% <sup>^</sup> 40% <sup>^^</sup>	[102]
Gastric cancer (poorly differentiated)	81	21% <sup>^</sup> 77% <sup>^^</sup>	[102]
Lung—cancer	36	97%	[97]
Lung—adenocarcinoma (well differentiated)	28	31%	[101]
Lung—adenocarcinoma (moderately differentiated)	76	46%	[101]
Lung adenocarcinoma—(poorly differentiated)	59	54%	[101]
HGSOC	407	77% <sup>^</sup> 19% <sup>^^</sup>	[99]
HGSOC	18	44% <sup>^</sup> 56% <sup>^^</sup>	[62]
Fallopian tube STIC	25	24% <sup>^</sup> 76% <sup>^^</sup>	[62]
Normal FTE	23	9% <sup>^</sup> 74% <sup>^^</sup>	[62]
Parathyroid tumours (CDC73-associated)	11	55% <sup>^</sup> 45% <sup>^^</sup>	[18]

Where H2Bub1 data was reported both as total loss or weak to moderate immunohistochemical levels, it is identified as follows: <sup>^</sup> total loss of H2Bub1 (no nuclear H2Bub1 present detected by immunohistochemistry); <sup>^^</sup> weak to moderate H2Bub1 detected by immunohistochemistry. HGSOC, High-grade serous ovarian cancer; STIC, Serous Tubal Intraepithelial Carcinoma; FTE, fallopian tube epithelium.

Table 2. RNF20 and RNF40 loss in primary tumours.

Tumour Type	Cohort Size	RNF20 <sup>^</sup>	RNF20 <sup>^^</sup>	% Tumours with RNF20 Loss	Reference
HGSOC	424	√		6% <sup>^^^</sup> 7% <sup>^^^^</sup>	[99]
HGSOC	579		√	53%	[62]
Lung adenocarcinoma	517		√	~25% <sup>*</sup>	[101]
Tumour Type	Cohort Size	RNF40 <sup>^</sup>	RNF40 <sup>^^</sup>	% Tumours with RNF40 Loss	Reference
HGSOC	579		√	36%	[62]
HCC	130	√		50% <sup>**</sup>	[104]

<sup>^</sup> protein levels assessed by immunohistochemistry; <sup>^^</sup> gene transcript levels; <sup>^^^</sup> total loss (immunohistochemical score of 0); <sup>^^^^</sup> intermediate staining; <sup>\*</sup> refers to lower RNF20 levels in malignant lung tissue versus normal lung tissue. <sup>\*\*</sup> the remainder of this cohort was described as staining high for RNF40. HGSOC, High-grade serous ovarian cancer; HCC, hepatocellular carcinoma.

### 6.1. H2Bub1 Loss is Associated with an Inflammatory Response that may Increase Risk of Developing Cancer

The ability to mount an appropriate inflammatory response is part of our key defence mechanisms against pathogens and disease; however, it is when inflammation becomes chronic that problems can arise, including acting as a trigger for tumorigenesis [105]. Chronic inflammation, such as that seen in

inflammatory bowel disease (IBD) and ulcerative colitis (UC), is driven by inflammatory mediators such as nuclear factor (NF)- $\kappa$ B and signal transducer and activator of transcription 3 (STAT3), cytokines such as interleukin 6 (IL-6) and prostaglandins, and has been linked to an increased risk of developing cancer [106–110]. Using a model of *Rnf20* heterozygous mice to drive depleted H2Bub1, as well as human samples of UC and colorectal cancer, Tarcic and colleagues have shown that loss of H2Bub1 creates a tumour promoting microenvironment in the colon centred on the chronic inflammatory response [21]. The mechanism of up-regulation of genes associated with inflammation such as IL-6 and IL-8 in conjunction with depleted H2Bub1 is through the pro-inflammatory cytokine tumour necrosis factor alpha (TNF- $\alpha$ ), itself mediated through NF- $\kappa$ B activation [110]. In non-cancerous epithelial cells in this model, depletion of *Rnf20* and as a result H2Bub1, fostered a pro-inflammatory transcriptional response. Furthermore, gene expression of both *RNF20* and *RNF40*, along with down-regulation of H2Bub1, was identified in epithelial and stromal colonic tissue from patients with UC and was inversely correlated with inflammatory cytokines *IL6* and *IL8* [21].

Studies comparing basal-like cells of triple negative breast cancer (TNBC) that are aggressive and poorly differentiated tumours, with breast tumours of luminal origin with a more favourable prognosis showed that TNBCs had expression of a greater number of inflammatory genes, including *IL6* and *IL8* [22,111]. Down-regulation of *RNF20* further increased the expression of *IL6* and *IL8* via NF- $\kappa$ B signalling in basal-like breast cancer cells and depleted the repressive chromatin mark H3K9me3 at their promoters [22]. In luminal breast cancer cells, however, *RNF20* down-regulation was associated with a decrease in expression of ER gene targets that drive proliferation and migration including *PGR*, *CXCL12* and *FOXA1* [22]. This finding goes some way towards explaining the apparent opposite roles of RNF20 and H2Bub1 in basal and luminal breast cancers, whereby RNF20 and H2Bub1 appear to function in a tumour-suppressive role in basal-like breast cancer cells and be pro-oncogenic in luminal breast cancer cells, driving tumorigenesis. Further supporting this phenomenon of a breast cancer subtype-specific function of RNF40 and H2Bub1, Wegwitz and colleagues have shown that the RNF40-H2Bub1 axis actually supports growth of HER2-positive (HER2+) breast cancers, both in vitro and in vivo, via transcriptional activation of genes involved in maintenance of the actin cytoskeleton. This important work highlights the opportunity for therapeutic intervention that targets RNF40 and/or H2Bub1 in the HER2+ breast cancer subtype [112].

In addition to discoveries linking H2Bub1 and its ligation machinery to inflammatory conditions of the colon with an increased risk of malignancy and developing TNBC, Hooda and colleagues discovered modulation of H2Bub1 levels in pre-cursor cells of ovarian cancer with links to inflammatory genes [62]. Here, upon depletion of *RNF20* and concomitant loss of H2Bub1 in fallopian tube epithelial cells, the presumed site of origin of many high-grade serous ovarian cancers (HGSOCs), IL6 was elevated and enhanced migration observed [62]. It is likely that additional tumour cell types will be discovered to increase the production of inflammatory cytokines in response to depletion of RNF20 and H2Bub1, contributing to a microenvironment conducive to initiating malignancy and/or driving tumorigenesis.

## 6.2. Global Loss of H2Bub1 Is an Early Event in Some Cancers

Two studies support that H2Bub1 loss is a very early event in ovarian tumorigenesis, with loss detected in serous tubal intraepithelial carcinomas (STICs) now known to be the precursor lesion for a large proportion of HGSOC [62,113,114], and also equally across all stages (I-IV) of HGSOC [99]. Dickson and colleagues demonstrated global loss of nuclear H2Bub1 in 77% (313 of 407) of HGSOC [99]. No correlation was made between loss of H2Bub1 and either progression free or overall survival. Furthermore, no correlation was detected between the presence of a *BRCA1* or *BRCA2* mutation and H2Bub1 loss. In the same tumour cohort, complete loss of RNF20 assessed using immunohistochemical staining was seen in only 6% of tumours (26 of 424) and did not correlate with loss of H2Bub1, implying that abrogation of RNF20 function does not explain the majority of H2Bub1 loss present in these tumours. Of note, no HGSOC had both a *BRCA1* mutation and RNF20 loss, suggesting that functional abrogation of both of these E3 ligases in the same cell may be lethal [99].



In apparent contrast to this earlier study of RNF20 immunohistochemistry in HGSOE, Hooda and colleagues reported that over half of HGSOE in The Cancer Genome Atlas (TCGA;  $n = 579$ ) are heterozygous for *RNF20* and that 36% were heterozygous for *RNF40* [62]. RNF20 protein expression would need to be interrogated in TCGA HGSOE samples to definitively correlate RNF20 and H2Bub1 in this cohort. A complete picture of the factors responsible for the maintenance of H2Bub1 in ovarian and fallopian tube epithelia remains to be elucidated; however, it would appear that H2Bub1 E3 ubiquitin ligase writers, of which there are multiple [1,10] (Figure 1), can functionally substitute for one another in some circumstances. Levels of RNF20 and RNF40 have also been reported to be lower than normal tissue in testicular seminomas, with the suggestion that their loss occurs prior to development of the invasive phenotype [115].

### 6.3. Global Loss of H2Bub1 Is Linked to Tumour Progression and a Worse Prognosis

One of the earliest immunohistochemical studies of global H2Bub1 levels in primary tumours was conducted in breast cancer, where a clear increase in H2Bub1 loss was observed over tumour progression, from no loss in normal adjacent tissue and benign tumours, to 67% loss in malignant tumours and 84% loss in breast cancer metastatic deposits [40]. While this study did not analyse tumours based on sub-type, Tarcic and colleagues have subsequently investigated H2Bub1 and its ligation machinery in basal-like (TNBC) and luminal breast cancers [22]. Here, the correlation between H2Bub1 levels and patient outcome was dependent on breast tumour subtype. For women with breast tumours that were ER positive (ER+) and of a luminal subtype, higher levels of H2Bub1 correlated with shorter survival times, while in TNBCs of a basal-like subtype, higher levels of H2Bub1 were associated with longer survival [22]. Basal-like tumours had lower H2Bub1 levels relative to other breast sub-types, and are well known to have a worse prognosis. As already noted, in vitro experiments interrogating cell migration and proliferation showed that depleting RNF20 that reduced H2Bub1 levels, acted to increase proliferation and migration of basal-like breast cancer cells, yet decreased these functional endpoints in luminal-type cells. These growth patterns were recapitulated in a mouse model, whereby down-regulation of RNF20 in basal-like cells resulted in faster growing mammary tumours relative to control cells, while down-regulation of RNF20 in luminal type cells led to slower growth than control cells [22]. Further in these preclinical models, metastases to the lung reflected the rate of tumour growth, with down-regulation of RNF20 resulting in an increase of lung metastases from basal-like cells only. Therefore at least in breast cancer, the role of RNF20 and H2Bub1 is highly dependent on cell type of origin; in fact this role is dichotomous in basal-like versus luminal breast cancer cells.

H2Bub1 loss has been strongly associated with a worse prognosis in colorectal cancer independent of nodal stage; however, loss of H2Bub1 alone was not an independent prognostic marker [100]. Patients with gastric cancer that stain positively for H2Bub1 had a higher 5 year survival compared to patients where H2Bub1 was lost; in fact, H2Bub1 was an independent prognostic factor for survival in this cancer type [102]. Here, loss of H2Bub1 was increasingly associated with more poorly differentiated tumours [102]. This was also the case for lung tumours and further, lung cancer patients whose tumours were positive for H2Bub1 displayed a trend towards increased survival compared with patients whose tumours had lost H2Bub1 [101]. Decreasing levels of tumour differentiation in parallel with loss of H2Bub1 has also been reported in breast tumours, consistent with a role for H2Bub1 in maintaining a differentiated phenotype [41]. Hahn and colleagues demonstrated global loss of H2Bub1 in familial and sporadic parathyroid tumours associated with mutation of a gene encoding a member of the PAF1C, *CDC73* [18]. Benign parathyroid tumours with wild-type *CDC73* did not demonstrate loss of H2Bub1.

## 7. Cancer-Related Proteins and the H2Bub1 Interactome

The interplay between complexes and factors that regulate the epigenome and cancer-related proteins is important for chromatin modelling and gene expression. Understanding this interplay,

both in healthy cells and in malignancy where tumour suppressors are frequently mutant and/or silenced is an emerging and intricate field. There is a growing list of cancer-related proteins, many of which have a tumour suppressive function, that either interact with, or constitute the ubiquitin ligation machinery of H2Bub1, including RNF20 and RNF40, p53, BRCA1, CDC73, members of the SWI/SNF chromatin remodelling complex, members of histone methyltransferase complexes involved in cross-talk with H2Bub1 including DOT1L and COMPASS, and numerous deubiquitinases including USP22 and USP44 (Figure 1). Below we discuss a number of these interactors, including their genetic or epigenetic abrogation in malignancy, and acknowledge that there are likely many more that remain to be discovered.

### 7.1. RNF20 and RNF40 E3 Ubiquitin Ligases

The majority of reports in the literature describe RNF20 in a manner consistent with being classified as a tumour suppressor; however, some reports suggest a pro-oncogenic activity. While the RNF20/RNF40 complex is accepted as the main E3 ligase complex responsible for writing H2Bub1, substrates other than K120 on histone H2B have been reported. For instance, RNF20 polyubiquitinates the ErbB3 receptor binding protein Ebp1 [116] and ZSCAN4 (Zinc Finger and SCAN Domain Containing 4) that is involved in telomere maintenance, genomic stability and mouse embryonic stem cells [117]. The RNF20/RNF40 complex can also monoubiquitinate the motor protein Eg5, a protein belonging to the kinesin-like family with roles in spindle dynamics and assembly associated with mitosis [118]. The rat orthologue of RNF40, Staring, polyubiquitinates the nervous system specific protein Syntaxin 1 marking it for proteasomal degradation [119].

In line with a tumour suppressive function, copy number loss of *RNF20* has been reported in HGSOc [62] and pre-invasive dysplastic airway lesions [120]. A low frequency of *RNF20* and *RNF40* mutations have been reported in colorectal cancer [121,122]. *RNF20* and/or *RNF40* transcript levels are depleted in a number of malignant or pre-malignant tissues, including in colonic tissue from patients with UC [21], in metastatic prostate cancer cells when compared with benign disease [123] and is lower in testicular germ cell cancer seminoma relative to normal testis [115]. Hypermethylation of the *RNF20* promoter has also been discovered in primary breast cancers, consistent with a tumour suppressive role for RNF20 [98]. Indirectly, RNF20 may function in a tumour suppressive capacity to obstruct the expression of oncogenes including *MYC* and *FOS* located in regions of compacted chromatin by interfering with recruitment of TFIIS that would usually function to relieve stalled RNA pol II [60]. RNF20 does this by obstructing the interaction between TFIIS and PAF1C.

In apparent contrast and already discussed in this review, a pro-oncogenic role for RNF20 has been reported in breast cancer cells of luminal, but not basal cell-type origin [22]. RNF20 also has an oncogenic role in MLL fusions that drive aberrant gene expression in haematopoietic cells and are initiators of leukemogenesis. H2Bub1 enrichment correlating with transcriptional elongation is observed in MLL-fusion target genes [74]. Furthermore, in colorectal cancer, RNF40 has been reported to promote inflammatory signalling through NF- $\kappa$ B signalling [124] and in hepatocellular carcinoma, RNF40 has been shown in a large cohort ( $n = 130$ ) to be almost equally expressed at high or low levels, with higher levels correlating with a worse prognosis [104].

Considering more broadly the cellular turnover of RNF20 and the role of additional factors, the HECT-domain E3 ubiquitin ligase Smad ubiquitin regulatory factor 2 (Smurf2) that itself has tumour suppressive roles, polyubiquitinates RNF20, marking it for proteasomal degradation, and in this way is linked in with the regulation of H2Bub1 [125]. The relationship between Smurf2 and RNF20 is likely the mechanism that accounts for the role of Smurf2 in regulating the chromatin landscape and maintaining genomic stability [126]. It is also involved in determining levels of RNF20 available to participate at sites of DSBs as part of the DDR [125].

RNF40 also has interaction partners, an important one being the histone chaperone human Suppressor of Ty Homologue-6 (SUPT6H) that likely works in a functional complex with RNF40 and RNF20 to control H2Bub1 levels [41]. All of SUPT6H, RNF20, RNF40 and ER $\alpha$  have been shown to



form a complex together at phosphorylated Ser 2 on the carboxy-terminal domain (CTD) of RNA Pol II [41]. This relationship provides a platform for estrogen modulation of the chromatin landscape, driving transcriptional elongation of ER $\alpha$  target genes important for proliferation and differentiation of the mammary epithelium. Like H2Bub1 levels, SUPT6H levels were shown to decrease over the course of breast tumorigenesis, with more malignant breast tumours with a worse prognosis demonstrating less SUPT6H and H2Bub1 [41]. In addition to association with ER $\alpha$  and regulation of ER target genes, RNF20 and RNF40 have been shown to physically associate with the AR, with the H2Bub1/RNF20/RNF40 axis implicated in AR-associated gene transcription and affecting the growth of prostate cancer cells [42]. Of note, both RNF20 and RNF40 have been linked to the maintenance of genomic stability [104,115,125,127].

### 7.2. p53 Associates with the E3 Ubiquitin Ligase RNF20

The tumour suppressor p53 is encoded by the most frequently mutated gene in human malignancy, being mutated in over 50% of all cancers, and referred to as the guardian of both the genome and the epigenome [128,129]. p53 has been shown to directly interact with RNF20 and furthermore, RNF20 and/or the RNF20/RNF40 complex have been identified as transcriptional co-activators at the promoters of p53 target genes including *CDKN1A* (encoding p21), *MDM2*, and *BBC3* (encoding PUMA) [17,130]. Loss of the RNF20/RNF40 complex correlated with depleted levels of H2Bub1 in the coding regions of these genes and reduced transcript levels [24,130]. A recent study investigating H2Bub1 enrichment at p53 target genes in p53 wild-type and gain-of-function (GOF) mutant cell line models showed absence of enrichment in the presence of *TP53* mutations [23]. It will be interesting to determine whether GOF mutant p53 cells can drive tumorigenesis by mechanisms such as H2Bub1 enrichment and correlated increased gene expression at GOF mutant p53 target genes.

Furthermore, while the oncoprotein Human Double Minute 2 (HDM2), also frequently referred to in the literature as MDM2, is well known as both a p53 target gene and the RING domain E3 ubiquitin ligase that polyubiquitinates p53 for degradation via the proteasome [131], it has also been reported to function as an enzymatic writer for H2Bub1 [132]. This would appear to be; however, on free histone H2B, and not when H2B is part of the native nucleosome core where the RNF20/RNF40 complex dominates as the main E3 ubiquitin ligase for H2Bub1 [12,133].

### 7.3. CDC73 Is a Binding Partner of RNF20 and RNF40

CDC73 (Cell Division Cycle 73; also known as parafibromin) is a classic tumour suppressor and core member of the human PAF1C [13]. It is also present in *Drosophila* (dCdc73) where it is more commonly referred to as Hyrax [134] and in yeast (yCdc73) [135]. In humans, mutations in *CDC73* (also known as *HRPT2*, Hyperparathyroidism 2) are present in germline DNA of patients with the inherited conditions Hyperparathyroidism Jaw Tumour Syndrome (HPT-JT; OMIM 145001) and Familial Hyperparathyroidism (FIHP; OMIM 145000) [136] reviewed in [137]. Somatic *CDC73* mutations are also observed in parathyroid carcinoma [138,139]. Surrogate detection of *CDC73* mutations by nuclear loss of immunohistochemical staining for CDC73 (parafibromin) in parathyroid neoplasms is a recognised diagnostic for HPT-JT and/or parathyroid cancer [140–144].

Using a yeast two-hybrid assay, CDC73 was shown to directly bind to both E3 ubiquitin ligases RNF20 and RNF40 [18]. Furthermore, loss of nuclear CDC73 in primary parathyroid tumours as the result of *CDC73* mutation led to significant depletion of H2Bub1, suggesting that CDC73 functions as a key protein associating the PAF1C with the ligase machinery that synthesises H2Bub1 [18]. It is likely that global loss of H2Bub1 and the entailing abrogation of gene expression is a major mechanism by which mutant CDC73 exerts its tumorigenic effect.

### 7.4. BRCA1-BARD1 Is an E3 Ubiquitin Ligase for H2Bub1

Germline mutations in *BRCA1* are well known to increase the risk of developing breast and/or ovarian cancer, with somatic mutations of this tumour suppressor also identified in sporadic tumours [145–151].

The BRCA1 Associated RING Domain 1 (BRCA1-BARD1) heterodimer is one of a number of E3 ligase complexes reported to write H2Bub1 [19]. In fact, BRCA1-BARD1 has been shown to ubiquitinate all core histones and the histone variant H2AX [152]. Despite this clear function of the BRCA1-BARD1 complex as a writer of H2Bub1, a large study previously discussed in this review that analysed primary HGSC characterised for *BRCA1* mutation was unable to demonstrate any correlation between *BRCA1* mutation and loss of H2Bub1 [99]. Given that there are multiple E3 ligases/ligase complexes that write H2Bub1, it is likely that these enzymes may be able to work in concert to compensate for loss of one in order to maintain this important histone modification.

#### 7.5. SWI/SNF Chromatin Remodelling Complexes, Including ARID1B/BAF250b

Initially discovered in yeast, the SWI/SNF complexes are members of the family of adenosine triphosphate (ATP) dependent chromatin remodelling complexes [153,154]. There are almost 30 known genes encoding subunits of the SWI/SNF complexes, comprised of three distinct complexes with unique and overlapping subunits (canonical BAF (cBAF), polybromo-associated BAF (PBAF) and non-canonical BAF (ncBAF) (reviewed in [155]). Around 20% of all human malignancies harbour a mutation in a gene encoding a SWI/SNF complex member [155,156]. Members of the SWI/SNF complex, including BAF155, BAF170, BRG1 and BRM were all shown to associate with H2Bub1 enriched chromatin [20]. Furthermore, SWI/SNF was shown to be required for optimal transcriptional elongation for genes reliant on RNF20 and H2Bub1 for their expression [20]. In this way, H2Bub1 appears to act as a recruitment scaffold or docking platform for the SWI/SNF chromatin remodelling complex to ensure optimal gene expression. Further demonstrating a key relationship between SWI/SNF and H2Bub1 is the discovery that the SWI/SNF complex member BAF250b/ARID1b form part of an E3 ubiquitin ligase complex along with elongin C (Elo C), Cullin-2 and Roc-1 to write H2Bub1 [157].

#### 7.6. H2Bub1 Deubiquitinases—USP22 and USP44

Ubiquitin is erased from histone H2B by DUBs of which there are at least twelve, not all in the mammalian setting, reported in the USP family that can perform this function—USP3 [158], USP7 [159], USP11 [68], USP12 [160], USP15 [161], USP22 [162], USP27X [75], USP36 [76], USP44 [82,163], USP46 [160], USP49 [164] and USP51 [75]. Many of these DUBs have previously been reviewed in the context of erasing H2Bub1 [1,10,12], therefore the focus here will be on recent discoveries, and specifically on USP22 and USP44.

USP22 is perhaps the most well studied of the H2Bub1-associated DUBs [165]. It has been implicated as part of the “death-from-cancer” signature, a stem cell gene expression signature consisting of 11 genes prognostic of rapid relapse and resistance to therapy in different solid tumours [92,166]. Expression of USP22 has been associated with stemness in cancer. In addition to its links with H2Bub1, USP22 also has non-histone substrates with important links to cancer. One of these is with the oncogene c-Myc where USP22 has been reported to function as a DUB to increase c-Myc stability in breast cancer cell lines with implications for the progression of this malignancy [167]. USP22 also been shown to deubiquitinate the transcriptional regulator far upstream element (FUSE)-binding protein 1 (FBP1), directly affecting the expression of p21 and impacting upon cell proliferation and tumorigenesis [168].

USP22 functions as a subunit of the SAGA chromatin modifying complex that is a complex capable of mediating deubiquitination and acetylation of histone and non-histone substrates [162,169]. The deubiquitinating module within SAGA consists of USP22, ATXN7L3, ATXN7 and ENY2 [165,170]. In humans, this deubiquitinating SAGA module is co-located with H2Bub1 within actively transcribed genes and is classified as a global transcriptional activator important for all RNA Pol II transcription [171,172]. USP22 has been associated with increased angiogenesis, cancer cell proliferation and metastasis, cisplatin and irradiation resistance and DNA damage signalling [173]. Targeting of USP22 is being explored as a cancer therapeutic [90,173]. Of particular interest, USP22 has recently been implicated as a regulator of PD-L1, marking it as a potential key factor in immune evasion that facilitates tumorigenesis [174]. Additional evidence that USP22 is involved in the immune response is its opposing role with RNF20 in

determining expression of the transcription factor FOXP3 (Forkhead box protein P3) that determines the development and function of regulatory T ( $T_{reg}$ ) cells that are important for the maintenance of self-tolerance and immune homeostasis [175].

Of note, USP44, co-operating with USP7, has also been identified as a DUB for FOXP3, linking these DUBs to  $T_{reg}$  cells and the immune response and flagging them as possible therapeutic targets for malignancy [176]. Furthermore, USP44 has recently been implicated in the innate immune response mounted against DNA viruses as a positive regulator of the Stimulator of Interferon Genes (STING) protein [177]. USP7 has also been implicated in destabilisation of the HDM2/p53 axis that is fundamentally important in malignancy [178].

In basal-like TNBCs, there is an inverse relationship between USP44 and RNF20/RNF40 with USP44 being more highly expressed, concomitant with lower levels of H2Bub1 in these tumours [22]. In cell line models of basal-like TNBC, down-regulation of USP44 leading to higher levels of H2Bub1 showed decreased proliferation and migration; however, the opposite was true for proliferation in luminal cell line models, highlighting the importance of consideration of cell type when determining therapeutic targeting of the H2Bub1 interactome [22]. As noted earlier, USP44 has been identified at sites of DSBs [71].

## 8. Conclusions

H2Bub1 is a key histone modification influencing fundamental cellular activities including transcriptional elongation, the DDR and stem cell plasticity. It is increasingly recognised as a central histone PTM given its influence and/or interactions with other chromatin remodelling complexes such as COMPASS, DOT1L, SAGA and SWI/SNF. The association of H2Bub1 with a growing list of cancer-related proteins affirms its clear connection to cancer. Changes in H2Bub1 enrichment levels have been implicated at all stages of tumour progression, from early lesions to metastatic disease, including association with inflammation that may increase the risk of developing malignancy in some tissues.

The importance of H2Bub1 and its modifying enzymes is now clearly established in both normal cellular processes and in malignancy, yet we do not have clear explanations regarding some apparent anomalies. Enrichment of H2Bub1, or lack thereof, in gene bodies does not always correlate with gene expression. In fact depletion of the main H2Bub1 writers RNF20 and RNF40 only influences the expression of a subset of genes [61,98]. This may be explained by selective regulation based on H2Bub1 levels, with only those genes with low to moderate H2Bub1 enrichment affected [61]. The high level of degeneracy or compensatory functions offered by multiple H2Bub1 writers and erasers likely also plays a role in maintaining the necessary levels of H2Bub1 enrichment for the maintenance of healthy tissue and during development.

Stimulus-specific gene expression, such as seen in p53 target genes in response to DNA damage, appear to have a strong correlation with H2Bub1 enrichment [23,24]. This would also seem to be true for hormonally stimulated gene expression, including genes relying on the transcription factors ER $\alpha$  and the AR [40,42]. The dynamic nature of histone PTMs, and specifically H2Bub1 in rapid chromatin remodelling, is likely crucial for the high-speed responses needed for expression of many of these genes. This is likely also true in developmental programming, including in the differentiation of mesenchymal and embryonic stem cells. Yet another complexity of H2Bub1 and its associated writers and erasers discussed in this review is seen in the context of different cellular subtypes of malignancy, with clear examples of opposing proliferative and migratory effects of manipulating H2Bub1 ligation machinery in luminal versus basal-like breast cancers [22]. It would appear that H2Bub1 and its associated factors can function as drivers of tissue specific transcription patterns associated with distinct cellular types.

Taken together, it is clear that the complexities of H2Bub1 and its associated machinery must be considered in a context specific fashion. Continued expansion and elucidation of the H2Bub1 interactome offers new insights into cellular processes and extends our opportunities for therapeutic targeting of malignancy based on the epigenome and ubiquitin chromatin modelling.

**Author Contributions:** D.J.M. conceptualised and prepared the original draft. Y.M. summarised aspects of the literature. D.J.M., Y.M. and K.-A.D. undertook review and editing of this manuscript. All authors have read and agreed to the published version of the manuscript.

**Funding:** This research received no external funding.

**Acknowledgments:** Y.M. is supported by a scholarship from the China Scholarship Council (CSC).

**Conflicts of Interest:** The authors declare no conflict of interest.

## References

1. Fuchs, G.; Oren, M. Writing and reading H2B monoubiquitylation. *Biochim. Biophys. Acta* **2014**, *1839*, 694–701. [[CrossRef](#)] [[PubMed](#)]
2. Dawson, M.A.; Kouzarides, T.; Huntly, B.J. Targeting epigenetic readers in cancer. *N. Engl. J. Med.* **2012**, *367*, 647–657. [[CrossRef](#)] [[PubMed](#)]
3. Dawson, M.A.; Kouzarides, T. Cancer epigenetics: From mechanism to therapy. *Cell* **2012**, *150*, 12–27. [[CrossRef](#)] [[PubMed](#)]
4. Marsh, D.J.; Dickson, K.A. Writing histone monoubiquitination in human malignancy—The role of RING finger E3 ubiquitin ligases. *Genes* **2019**, *10*, 67. [[CrossRef](#)]
5. Margueron, R.; Reinberg, D. The Polycomb complex PRC2 and its mark in life. *Nature* **2011**, *469*, 343–349. [[CrossRef](#)]
6. Fang, J.; Chen, T.; Chadwick, B.; Li, E.; Zhang, Y. Ring1b-mediated H2A ubiquitination associates with inactive X chromosomes and is involved in initiation of X inactivation. *J. Biol. Chem.* **2004**, *279*, 52812–52815. [[CrossRef](#)]
7. Lipkowitz, S.; Weissman, A.M. RINGs of good and evil: RING finger ubiquitin ligases at the crossroads of tumour suppression and oncogenesis. *Nat. Rev. Cancer* **2011**, *11*, 629–643. [[CrossRef](#)]
8. Deshaies, R.J.; Joazeiro, C.A. RING domain E3 ubiquitin ligases. *Annu. Rev. Biochem.* **2009**, *78*, 399–434. [[CrossRef](#)]
9. Budhidarmo, R.; Nakatani, Y.; Day, C.L. RINGs hold the key to ubiquitin transfer. *Trends Biochem. Sci.* **2012**, *37*, 58–65. [[CrossRef](#)]
10. Cole, A.J.; Clifton-Bligh, R.; Marsh, D.J. Histone H2B monoubiquitination: Roles to play in human malignancy. *Endocr.-Relat. Cancer* **2015**, *22*, T19–T33. [[CrossRef](#)]
11. Cao, J.; Yan, Q. Histone ubiquitination and deubiquitination in transcription, DNA damage response, and cancer. *Front. Oncol.* **2012**, *2*, 26. [[CrossRef](#)] [[PubMed](#)]
12. Johnsen, S.A. The enigmatic role of H2Bub1 in cancer. *FEBS Lett.* **2012**, *586*, 1592–1601. [[CrossRef](#)] [[PubMed](#)]
13. Jaehning, J.A. The Paf1 complex: Platform or player in RNA polymerase II transcription? *Biochim. Biophys. Acta.* **2010**, *1799*, 379–388. [[CrossRef](#)] [[PubMed](#)]
14. Moyal, L.; Lerenthal, Y.; Gana-Weisz, M.; Mass, G.; So, S.; Wang, S.Y.; Eppink, B.; Chung, Y.M.; Shalev, G.; Shema, E.; et al. Requirement of ATM-dependent monoubiquitylation of histone H2B for timely repair of DNA double-strand breaks. *Mol. Cell* **2011**, *41*, 529–542. [[CrossRef](#)] [[PubMed](#)]
15. Trujillo, K.M.; Osley, M.A. A role for H2B ubiquitylation in DNA replication. *Mol. Cell* **2012**, *48*, 734–746. [[CrossRef](#)]
16. Sadeghi, L.; Siggens, L.; Svensson, J.P.; Ekwall, K. Centromeric histone H2B monoubiquitination promotes noncoding transcription and chromatin integrity. *Nat. Struct. Mol. Biol.* **2014**, *21*, 236–243. [[CrossRef](#)]
17. Kim, J.; Hake, S.B.; Roeder, R.G. The human homolog of yeast BRE1 functions as a transcriptional coactivator through direct activator interactions. *Mol. Cell* **2005**, *20*, 759–770. [[CrossRef](#)]
18. Hahn, M.A.; Dickson, K.A.; Jackson, S.; Clarkson, A.; Gill, A.J.; Marsh, D.J. The tumor suppressor CDC73 interacts with the ring finger proteins RNF20 and RNF40 and is required for the maintenance of histone 2B monoubiquitination. *Hum. Mol. Genet.* **2012**, *21*, 559–568. [[CrossRef](#)]
19. Thakar, A.; Parvin, J.; Zlatanova, J. BRCA1/BARD1 E3 ubiquitin ligase can modify histones H2A and H2B in the nucleosome particle. *J. Biomol. Struct. Dyn.* **2010**, *27*, 399–406. [[CrossRef](#)]
20. Shema-Yaacoby, E.; Nikolov, M.; Haj-Yahya, M.; Siman, P.; Allemann, E.; Yamaguchi, Y.; Muchardt, C.; Urlaub, H.; Brik, A.; Oren, M.; et al. Systematic identification of proteins binding to chromatin-embedded ubiquitylated H2B reveals recruitment of SWI/SNF to regulate transcription. *Cell Rep.* **2013**, *4*, 601–608. [[CrossRef](#)]
21. Tarcic, O.; Pateras, I.S.; Cooks, T.; Shema, E.; Kanterman, J.; Ashkenazi, H.; Bocholez, H.; Hubert, A.; Rotkopf, R.; Baniyash, M.; et al. RNF20 Links Histone H2B Ubiquitylation with Inflammation and Inflammation-Associated Cancer. *Cell Rep.* **2016**, *14*, 1462–1476. [[CrossRef](#)] [[PubMed](#)]



22. Tarcic, O.; Granit, R.Z.; Pateras, I.S.; Masury, H.; Maly, B.; Zwang, Y.; Yarden, Y.; Gorgoulis, V.G.; Pikarsky, E.; Ben-Porath, I.; et al. RNF20 and histone H2B ubiquitylation exert opposing effects in Basal-Like versus luminal breast cancer. *Cell Death Differ.* **2017**, *24*, 694–704. [\[CrossRef\]](#) [\[PubMed\]](#)
23. Cole, A.J.; Dickson, K.A.; Liddle, C.; Stirzaker, C.; Shah, J.S.; Clifton-Bligh, R.; Marsh, D.J. Ubiquitin chromatin remodelling after DNA damage is associated with the expression of key cancer genes and pathways. *Cell. Mol. Life Sci.* **2020**. [\[CrossRef\]](#) [\[PubMed\]](#)
24. Minsky, N.; Shema, E.; Field, Y.; Schuster, M.; Segal, E.; Oren, M. Monoubiquitinated H2B is associated with the transcribed region of highly expressed genes in human cells. *Nat. Cell Biol.* **2008**, *10*, 483–488. [\[CrossRef\]](#)
25. Cao, Y.; Dai, Y.; Cui, S.; Ma, L. Histone H2B monoubiquitination in the chromatin of FLOWERING LOCUS C regulates flowering time in Arabidopsis. *Plant. Cell* **2008**, *20*, 2586–2602. [\[CrossRef\]](#)
26. Woloszynska, M.; Le Gall, S.; Neyt, P.; Boccardi, T.M.; Grasser, M.; Längst, G.; Aesaert, S.; Coussens, G.; Dhondt, S.; Van De Slijke, E.; et al. Histone 2B monoubiquitination complex integrates transcript elongation with RNA processing at circadian clock and flowering regulators. *Proc. Natl. Acad. Sci. USA* **2019**, *116*, 8060–8069. [\[CrossRef\]](#)
27. Liu, Y.; Koornneef, M.; Soppe, W.J. The absence of histone H2B monoubiquitination in the Arabidopsis hub1 (rdo4) mutant reveals a role for chromatin remodeling in seed dormancy. *Plant Cell* **2007**, *19*, 433–444. [\[CrossRef\]](#)
28. Zhang, Y.; Li, D.; Zhang, H.; Hong, Y.; Huang, L.; Liu, S.; Li, X.; Ouyang, Z.; Song, F. Tomato histone H2B monoubiquitination enzymes SIHUB1 and SIHUB2 contribute to disease resistance against Botrytis cinerea through modulating the balance between SA- and JA/ET-mediated signaling pathways. *BMC Plant Biol.* **2015**, *15*, 252. [\[CrossRef\]](#)
29. Gatta, R.; Dolfini, D.; Zambelli, F.; Imbriano, C.; Pavesi, G.; Mantovani, R. An acetylation-mono-ubiquitination switch on lysine 120 of H2B. *Epigenetics* **2011**, *6*, 630–637. [\[CrossRef\]](#)
30. Fierz, B.; Chatterjee, C.; McGinty, R.K.; Bar-Dagan, M.; Raleigh, D.P.; Muir, T.W. Histone H2B ubiquitylation disrupts local and higher-order chromatin compaction. *Nat. Chem. Biol.* **2011**, *7*, 113–119. [\[CrossRef\]](#)
31. Chandrasekharan, M.B.; Huang, F.; Sun, Z.W. Ubiquitination of histone H2B regulates chromatin dynamics by enhancing nucleosome stability. *Proc. Natl. Acad. Sci. USA* **2009**, *106*, 16686–16691. [\[CrossRef\]](#) [\[PubMed\]](#)
32. Fierz, B.; Kilic, S.; Hieb, A.R.; Luger, K.; Muir, T.W. Stability of nucleosomes containing homogenously ubiquitylated H2A and H2B prepared using semisynthesis. *J. Am. Chem. Soc.* **2012**, *134*, 19548–19551. [\[CrossRef\]](#) [\[PubMed\]](#)
33. Paparidis, N.F.; Durvale, M.C.; Canduri, F. The emerging picture of CDK9/P-TEFb: More than 20 years of advances since PITALRE. *Mol. Biosyst.* **2017**, *13*, 246–276. [\[CrossRef\]](#)
34. Pirngruber, J.; Shchebet, A.; Schreiber, L.; Shema, E.; Minsky, N.; Chapman, R.D.; Eick, D.; Aylon, Y.; Oren, M.; Johnsen, S.A. CDK9 directs H2B monoubiquitination and controls replication-dependent histone mRNA 3'-end processing. *EMBO Rep.* **2009**, *10*, 894–900. [\[CrossRef\]](#) [\[PubMed\]](#)
35. Zhang, F.; Yu, X. WAC, a functional partner of RNF20/40, regulates histone H2B ubiquitination and gene transcription. *Mol. Cell* **2011**, *41*, 384–397. [\[CrossRef\]](#) [\[PubMed\]](#)
36. Sansó, M.; Lee, K.M.; Viladevall, L.; Jacques, P.; Pagé, V.; Nagy, S.; Racine, A.; St Amour, C.V.; Zhang, C.; Shokat, K.M.; et al. A positive feedback loop links opposing functions of P-TEFb/Cdk9 and histone H2B ubiquitylation to regulate transcript elongation in fission yeast. *PLoS Genet.* **2012**, *8*, e1002822. [\[CrossRef\]](#)
37. Kwak, H.; Lis, J.T. Control of transcriptional elongation. *Annu. Rev. Genet.* **2013**, *47*, 483–508. [\[CrossRef\]](#) [\[PubMed\]](#)
38. Sansó, M.; Parua, P.K.; Pinto, D.; Svensson, J.P.; Pagé, V.; Bitton, D.A.; MacKinnon, S.; Garcia, P.; Hidalgo, E.; Bähler, J.; et al. Cdk9 and H2Bub1 signal to Clr6-CII/Rpd3S to suppress aberrant antisense transcription. *Nucleic Acids Res.* **2020**, *48*, 7154–7168. [\[CrossRef\]](#)
39. Kim, J.; Guermah, M.; McGinty, R.K.; Lee, J.S.; Tang, Z.; Milne, T.A.; Shilatifard, A.; Muir, T.W.; Roeder, R.G. RAD6-Mediated transcription-coupled H2B ubiquitylation directly stimulates H3K4 methylation in human cells. *Cell* **2009**, *137*, 459–471. [\[CrossRef\]](#)
40. Prenzel, T.; Begus-Nahrmann, Y.; Kramer, F.; Hennion, M.; Hsu, C.; Gorsler, T.; Hintermair, C.; Eick, D.; Kremmer, E.; Simons, M.; et al. Estrogen-dependent gene transcription in human breast cancer cells relies upon proteasome-dependent monoubiquitination of histone H2B. *Cancer Res.* **2011**, *71*, 5739–5753. [\[CrossRef\]](#)
41. Bedi, U.; Scheel, A.H.; Hennion, M.; Begus-Nahrmann, Y.; Rüschhoff, J.; Johnsen, S.A. SUPT6H controls estrogen receptor activity and cellular differentiation by multiple epigenomic mechanisms. *Oncogene* **2015**, *34*, 465–473. [\[CrossRef\]](#) [\[PubMed\]](#)

42. Jääskeläinen, T.; Makkonen, H.; Visakorpi, T.; Kim, J.; Roeder, R.G.; Palvimo, J.J. Histone H2B ubiquitin ligases RNF20 and RNF40 in androgen signaling and prostate cancer cell growth. *Mol. Cell. Endocrinol.* **2012**, *350*, 87–98. [[CrossRef](#)] [[PubMed](#)]
43. Pavri, R.; Zhu, B.; Li, G.; Trojer, P.; Mandal, S.; Shilatifard, A.; Reinberg, D. Histone H2B monoubiquitination functions cooperatively with FACT to regulate elongation by RNA polymerase II. *Cell* **2006**, *125*, 703–717. [[CrossRef](#)] [[PubMed](#)]
44. Fleming, A.B.; Kao, C.F.; Hillyer, C.; Pikaart, M.; Osley, M.A. H2B ubiquitylation plays a role in nucleosome dynamics during transcription elongation. *Mol. Cell* **2008**, *31*, 57–66. [[CrossRef](#)] [[PubMed](#)]
45. Janna, A.; Davarinejad, H.; Joshi, M.; Couture, J.F. Structural paradigms in the recognition of the nucleosome core particle by histone lysine methyltransferases. *Front. Cell Dev. Biol.* **2020**, *8*, 600. [[CrossRef](#)] [[PubMed](#)]
46. Worden, E.J.; Wolberger, C. Activation and regulation of H2B-Ubiquitin-dependent histone methyltransferases. *Curr. Opin. Struct. Biol.* **2019**, *59*, 98–106. [[CrossRef](#)]
47. Wood, A.; Schneider, J.; Shilatifard, A. Cross-talking histones: Implications for the regulation of gene expression and DNA repair. *Biochem. Cell Biol.* **2005**, *83*, 460–467. [[CrossRef](#)]
48. Smith, E.; Shilatifard, A. The chromatin signaling pathway: Diverse mechanisms of recruitment of histone-modifying enzymes and varied biological outcomes. *Mol. Cell* **2010**, *40*, 689–701. [[CrossRef](#)]
49. Ng, H.H.; Xu, R.M.; Zhang, Y.; Struhl, K. Ubiquitination of histone H2B by Rad6 is required for efficient Dot1-mediated methylation of histone H3 lysine 79. *J. Biol. Chem.* **2002**, *277*, 34655–34657. [[CrossRef](#)]
50. Valencia-Sánchez, M.I.; De Ioannes, P.; Wang, M.; Vasilyev, N.; Chen, R.; Nudler, E.; Armache, J.P.; Armache, K.J. Structural basis of Dot1L stimulation by histone H2B lysine 120 ubiquitination. *Mol. Cell* **2019**, *74*, 1010–1019.e1016. [[CrossRef](#)]
51. McGinty, R.K.; Kim, J.; Chatterjee, C.; Roeder, R.G.; Muir, T.W. Chemically ubiquitylated histone H2B stimulates hDot1L-mediated intranucleosomal methylation. *Nature* **2008**, *453*, 812–816. [[CrossRef](#)] [[PubMed](#)]
52. Min, J.; Feng, Q.; Li, Z.; Zhang, Y.; Xu, R.M. Structure of the catalytic domain of human DOT1L, a non-SET domain nucleosomal histone methyltransferase. *Cell* **2003**, *112*, 711–723. [[CrossRef](#)]
53. Steger, D.J.; Lefterova, M.I.; Ying, L.; Stonestrom, A.J.; Schupp, M.; Zhuo, D.; Vakoc, A.L.; Kim, J.E.; Chen, J.; Lazar, M.A.; et al. DOT1L/KMT4 recruitment and H3K79 methylation are ubiquitously coupled with gene transcription in mammalian cells. *Mol. Cell. Biol.* **2008**, *28*, 2825–2839. [[CrossRef](#)]
54. Worden, E.J.; Hoffmann, N.A.; Hicks, C.W.; Wolberger, C. Mechanism of Cross-talk between H2B Ubiquitination and H3 Methylation by Dot1L. *Cell* **2019**, *176*, 1490–1501.e1412. [[CrossRef](#)] [[PubMed](#)]
55. Guppy, B.J.; McManus, K.J. Mitotic accumulation of dimethylated lysine 79 of histone H3 is important for maintaining genome integrity during mitosis in human cells. *Genetics* **2015**, *199*, 423–433. [[CrossRef](#)] [[PubMed](#)]
56. Worden, E.J.; Zhang, X.; Wolberger, C. Structural basis for COMPASS recognition of an H2B-ubiquitinated nucleosome. *eLife* **2020**, *9*. [[CrossRef](#)] [[PubMed](#)]
57. Shilatifard, A. The COMPASS family of histone H3K4 methylases: Mechanisms of regulation in development and disease pathogenesis. *Annu. Rev. Biochem.* **2012**, *81*, 65–95. [[CrossRef](#)]
58. Basnet, H.; Su, X.B.; Tan, Y.; Meisenhelder, J.; Merkurjev, D.; Ohgi, K.A.; Hunter, T.; Pillus, L.; Rosenfeld, M.G. Tyrosine phosphorylation of histone H2A by CK2 regulates transcriptional elongation. *Nature* **2014**, *516*, 267–271. [[CrossRef](#)]
59. Batta, K.; Zhang, Z.; Yen, K.; Goffman, D.B.; Pugh, B.F. Genome-wide function of H2B ubiquitylation in promoter and genic regions. *Genes Dev.* **2011**, *25*, 2254–2265. [[CrossRef](#)]
60. Shema, E.; Kim, J.; Roeder, R.G.; Oren, M. RNF20 inhibits TFIIIS-facilitated transcriptional elongation to suppress pro-oncogenic gene expression. *Mol. Cell* **2011**, *42*, 477–488. [[CrossRef](#)]
61. Xie, W.; Nagarajan, S.; Baumgart, S.J.; Kosinsky, R.L.; Najafova, Z.; Kari, V.; Hennion, M.; Indenbirken, D.; Bonn, S.; Grundhoff, A.; et al. RNF40 regulates gene expression in an epigenetic context-dependent manner. *Genome Biol.* **2017**, *18*, 32. [[CrossRef](#)] [[PubMed](#)]
62. Hooda, J.; Novak, M.; Salomon, M.P.; Matsuba, C.; Ramos, R.I.; MacDuffie, E.; Song, M.; Hirsch, M.S.; Lester, J.; Parkash, V.; et al. Early loss of histone H2B monoubiquitylation alters chromatin accessibility and activates key immune pathways that facilitate progression of ovarian cancer. *Cancer Res.* **2019**, *79*, 760–772. [[CrossRef](#)]
63. Nakamura, K.; Kato, A.; Kobayashi, J.; Yanagihara, H.; Sakamoto, S.; Oliveira, D.V.; Shimada, M.; Tauchi, H.; Suzuki, H.; Tashiro, S.; et al. Regulation of homologous recombination by RNF20-dependent H2B ubiquitination. *Mol. Cell* **2011**, *41*, 515–528. [[CrossRef](#)] [[PubMed](#)]

64. So, C.C.; Ramachandran, S.; Martin, A. E3 Ubiquitin ligases RNF20 and RNF40 are required for double-stranded break (DSB) repair: Evidence for monoubiquitination of histone H2B lysine 120 as a novel axis of DSB signaling and repair. *Mol. Cell. Biol.* **2019**, *39*. [\[CrossRef\]](#) [\[PubMed\]](#)
65. Shiloh, Y.; Shema, E.; Moyal, L.; Oren, M. RNF20-RNF40: A ubiquitin-driven link between gene expression and the DNA damage response. *FEBS Lett.* **2011**, *585*, 2795–2802. [\[CrossRef\]](#) [\[PubMed\]](#)
66. Oliveira, D.V.; Kato, A.; Nakamura, K.; Ikura, T.; Okada, M.; Kobayashi, J.; Yanagihara, H.; Saito, Y.; Tauchi, H.; Komatsu, K. Histone chaperone FACT regulates homologous recombination by chromatin remodeling through interaction with RNF20. *J. Cell Sci.* **2014**, *127*, 763–772. [\[CrossRef\]](#) [\[PubMed\]](#)
67. Kari, V.; Shchebet, A.; Neumann, H.; Johnsen, S.A. The H2B ubiquitin ligase RNF40 cooperates with SUPT16H to induce dynamic changes in chromatin structure during DNA double-strand break repair. *Cell Cycle* **2011**, *10*, 3495–3504. [\[CrossRef\]](#)
68. Ting, X.; Xia, L.; Yang, J.; He, L.; Si, W.; Shang, Y.; Sun, L. USP11 acts as a histone deubiquitinase functioning in chromatin reorganization during DNA repair. *Nucleic Acids Res.* **2019**, *47*, 9721–9740. [\[CrossRef\]](#)
69. Ramachandran, S.; Haddad, D.; Li, C.; Le, M.X.; Ling, A.K.; So, C.C.; Nepal, R.M.; Gommerman, J.L.; Yu, K.; Ketela, T.; et al. The SAGA deubiquitination module promotes DNA repair and class switch recombination through ATM and DNAPK-mediated  $\gamma$ H2AX formation. *Cell Rep.* **2016**, *15*, 1554–1565. [\[CrossRef\]](#)
70. Li, C.; Irrazabal, T.; So, C.C.; Berru, M.; Du, L.; Lam, E.; Ling, A.K.; Gommerman, J.L.; Pan-Hammarström, Q.; Martin, A. The H2B deubiquitinase Usp22 promotes antibody class switch recombination by facilitating non-homologous end joining. *Nat. Commun.* **2018**, *9*, 1006. [\[CrossRef\]](#)
71. Mosbech, A.; Lukas, C.; Bekker-Jensen, S.; Mailand, N. The deubiquitylating enzyme USP44 counteracts the DNA double-strand break response mediated by the RNF8 and RNF168 ubiquitin ligases. *J. Biol. Chem.* **2013**, *288*, 16579–16587. [\[CrossRef\]](#) [\[PubMed\]](#)
72. Kari, V.; Raul, S.K.; Henck, J.M.; Kitz, J.; Kramer, F.; Kosinsky, R.L.; Übelmesser, N.; Mansour, W.Y.; Eggert, J.; Spitzner, M.; et al. The histone methyltransferase DOT1L is required for proper DNA damage response, DNA repair, and modulates chemotherapy responsiveness. *Clin. Epigenet.* **2019**, *11*, 4. [\[CrossRef\]](#) [\[PubMed\]](#)
73. Schneider, D.; Chua, R.L.; Molitor, N.; Hamdan, F.H.; Rettenmeier, E.M.; Prokakis, E.; Mishra, V.K.; Kari, V.; Wegwitz, F.; Johnsen, S.A.; et al. The E3 ubiquitin ligase RNF40 suppresses apoptosis in colorectal cancer cells. *Clin. Epigenet.* **2019**, *11*, 98. [\[CrossRef\]](#) [\[PubMed\]](#)
74. Wang, E.; Kawaoka, S.; Yu, M.; Shi, J.; Ni, T.; Yang, W.; Zhu, J.; Roeder, R.G.; Vakoc, C.R. Histone H2B ubiquitin ligase RNF20 is required for MLL-rearranged leukemia. *Proc. Natl. Acad. Sci. USA* **2013**, *110*, 3901–3906. [\[CrossRef\]](#)
75. Atanassov, B.S.; Mohan, R.D.; Lan, X.; Kuang, X.; Lu, Y.; Lin, K.; McIvor, E.; Li, W.; Zhang, Y.; Florens, L.; et al. ATXN7L3 and ENY2 coordinate activity of multiple H2B deubiquitinases important for cellular proliferation and tumor growth. *Mol. Cell* **2016**, *62*, 558–571. [\[CrossRef\]](#)
76. DeVine, T.; Sears, R.C.; Dai, M.S. The ubiquitin-specific protease USP36 is a conserved histone H2B deubiquitinase. *Biochem. Biophys. Res. Commun.* **2018**, *495*, 2363–2368. [\[CrossRef\]](#)
77. Lapinska, K.; Faria, G.; McGonagle, S.; Macumber, K.M.; Heerboth, S.; Sarkar, S. Cancer progenitor cells: The result of an epigenetic event? *Anticancer Res.* **2018**, *38*, 1–6. [\[CrossRef\]](#)
78. Tee, W.W.; Reinberg, D. Chromatin features and the epigenetic regulation of pluripotency states in ESCs. *Development* **2014**, *141*, 2376–2390. [\[CrossRef\]](#)
79. Vincent, A.; Ouelkdite-Oumouchal, A.; Souidi, M.; Leclerc, J.; Neve, B.; Van Seuning, I. Colon cancer stemness as a reversible epigenetic state: Implications for anticancer therapies. *World J. Stem Cells* **2019**, *11*, 920–936. [\[CrossRef\]](#)
80. Wang, X. Stem cells in tissues, organoids, and cancers. *Cell. Mol. Life Sci.* **2019**, *76*, 4043–4070. [\[CrossRef\]](#)
81. Onder, T.T.; Kara, N.; Cherry, A.; Sinha, A.U.; Zhu, N.; Bernt, K.M.; Cahan, P.; Marcarci, B.O.; Unternaehrer, J.; Gupta, P.B.; et al. Chromatin-modifying enzymes as modulators of reprogramming. *Nature* **2012**, *483*, 598–602. [\[CrossRef\]](#)
82. Fuchs, G.; Shema, E.; Vesterman, R.; Kotler, E.; Wolchinsky, Z.; Wilder, S.; Golomb, L.; Pribluda, A.; Zhang, F.; Haj-Yahya, M.; et al. RNF20 and USP44 regulate stem cell differentiation by modulating H2B monoubiquitylation. *Mol. Cell* **2012**, *46*, 662–673. [\[CrossRef\]](#)
83. Karpiuk, O.; Najafova, Z.; Kramer, F.; Hennion, M.; Galonska, C.; König, A.; Snaidero, N.; Vogel, T.; Shchebet, A.; Begus-Nahrman, Y.; et al. The histone H2B monoubiquitination regulatory pathway is required for differentiation of multipotent stem cells. *Mol. Cell* **2012**, *46*, 705–713. [\[CrossRef\]](#)

84. Yan, Z.; Wang, Z.; Sharova, L.; Sharov, A.A.; Ling, C.; Piao, Y.; Aiba, K.; Matoba, R.; Wang, W.; Ko, M.S. BAF250B-associated SWI/SNF chromatin-remodeling complex is required to maintain undifferentiated mouse embryonic stem cells. *Stem Cells* **2008**, *26*, 1155–1165. [[CrossRef](#)] [[PubMed](#)]
85. Sze, C.C.; Cao, K.; Collings, C.K.; Marshall, S.A.; Rendleman, E.J.; Ozark, P.A.; Chen, F.X.; Morgan, M.A.; Wang, L.; Shilatifard, A. Histone H3K4 methylation-dependent and -independent functions of Set1A/COMPASS in embryonic stem cell self-renewal and differentiation. *Genes Dev.* **2017**, *31*, 1732–1737. [[CrossRef](#)] [[PubMed](#)]
86. Wang, X.; Wang, H.; Xu, B.; Jiang, D.; Huang, S.; Yu, H.; Wu, Z.; Wu, Q. Depletion of H3K79 methyltransferase Dot1L promotes cell invasion and cancer stem-like cell property in ovarian cancer. *Am. J. Transl. Res.* **2019**, *11*, 1145–1153. [[PubMed](#)]
87. Breindel, J.L.; Skibinski, A.; Sedic, M.; Wronski-Campos, A.; Zhou, W.; Keller, P.J.; Mills, J.; Bradner, J.; Onder, T.; Kuperwasser, C. Epigenetic reprogramming of lineage-committed human mammary epithelial cells requires DNMT3A and loss of DOT1L. *Stem Cell Rep.* **2017**, *9*, 943–955. [[CrossRef](#)] [[PubMed](#)]
88. Bourguignon, L.Y.; Wong, G.; Shiina, M. Up-regulation of histone methyltransferase, DOT1L, by matrix hyaluronan promotes microRNA-10 expression leading to tumor cell invasion and chemoresistance in cancer stem cells from head and neck squamous cell carcinoma. *J. Biol. Chem.* **2016**, *291*, 10571–10585. [[CrossRef](#)] [[PubMed](#)]
89. Sussman, R.T.; Stanek, T.J.; Estes, P.; Gearhart, J.D.; Knudsen, K.E.; McMahon, S.B. The epigenetic modifier ubiquitin-specific protease 22 (USP22) regulates embryonic stem cell differentiation via transcriptional repression of sex-determining region Y-box 2 (SOX2). *J. Biol. Chem.* **2013**, *288*, 24234–24246. [[CrossRef](#)]
90. Yun, X.; Zhang, K.; Wang, J.; Pangen, R.P.; Yang, L.; Bonner, M.; Wu, J.; Wang, J.; Nardi, I.K.; Gao, M.; et al. Targeting USP22 suppresses tumorigenicity and enhances cisplatin sensitivity through ALDH1A3 downregulation in cancer-initiating cells from lung adenocarcinoma. *Mol. Cancer Res.* **2018**, *16*, 1161–1171. [[CrossRef](#)]
91. Jiang, S.; Song, C.; Gu, X.; Wang, M.; Miao, D.; Lv, J.; Liu, Y. Ubiquitin-specific peptidase 22 contributes to colorectal cancer stemness and chemoresistance via Wnt/ $\beta$ -catenin pathway. *Cell. Physiol. Biochem.* **2018**, *46*, 1412–1422. [[CrossRef](#)] [[PubMed](#)]
92. Glinsky, G.V.; Berezovska, O.; Glinskii, A.B. Microarray analysis identifies a death-from-cancer signature predicting therapy failure in patients with multiple types of cancer. *J. Clin. Invest.* **2005**, *115*, 1503–1521. [[CrossRef](#)] [[PubMed](#)]
93. Liu, T.; Sun, B.; Zhao, X.; Li, Y.; Zhao, X.; Liu, Y.; Yao, Z.; Gu, Q.; Dong, X.; Shao, B.; et al. USP44+ cancer stem cell subclones contribute to breast cancer aggressiveness by promoting vasculogenic mimicry. *Mol. Cancer Ther.* **2015**, *14*, 2121–2131. [[CrossRef](#)] [[PubMed](#)]
94. Gu, X.; Jiang, D.; Wang, Y.; Bachmair, A.; He, Y. Repression of the floral transition via histone H2B monoubiquitination. *Plant J.* **2009**, *57*, 522–533. [[CrossRef](#)]
95. Du, Y.; He, W.; Deng, C.; Chen, X.; Gou, L.; Zhu, F.; Guo, W.; Zhang, J.; Wang, T. Flowering-related RING protein 1 (FRRP1) regulates flowering time and yield potential by affecting histone H2B monoubiquitination in rice (*Oryza Sativa*). *PLoS ONE* **2016**, *11*, e0150458. [[CrossRef](#)]
96. Li, X.; Jiang, Y.; Ji, Z.; Liu, Y.; Zhang, Q. BRHIS1 suppresses rice innate immunity through binding to monoubiquitinated H2A and H2B variants. *EMBO Rep.* **2015**, *16*, 1192–1202. [[CrossRef](#)]
97. Urasaki, Y.; Heath, L.; Xu, C.W. Coupling of glucose deprivation with impaired histone H2B monoubiquitination in tumors. *PLoS ONE* **2012**, *7*, e36775. [[CrossRef](#)]
98. Shema, E.; Tirosh, I.; Aylon, Y.; Huang, J.; Ye, C.; Moskovits, N.; Raver-Shapira, N.; Minsky, N.; Pirngruber, J.; Tarcic, G.; et al. The histone H2B-specific ubiquitin ligase RNF20/hBRE1 acts as a putative tumor suppressor through selective regulation of gene expression. *Genes Dev.* **2008**, *22*, 2664–2676. [[CrossRef](#)]
99. Dickson, K.A.; Cole, A.J.; Gill, A.J.; Clarkson, A.; Gard, G.B.; Chou, A.; Kennedy, C.J.; Henderson, B.R.; Fereday, S.; Traficante, N.; et al. The RING finger domain E3 ubiquitin ligases BRCA1 and the RNF20/RNF40 complex in global loss of the chromatin mark histone H2B monoubiquitination (H2Bub1) in cell line models and primary high-grade serous ovarian cancer. *Hum. Mol. Genet.* **2016**, *25*, 5460–5471. [[CrossRef](#)]
100. Melling, N.; Grimm, N.; Simon, R.; Stahl, P.; Bokemeyer, C.; Terracciano, L.; Sauter, G.; Izibicki, J.R.; Marx, A.H. Loss of H2Bub1 Expression is Linked to Poor Prognosis in Nodal Negative Colorectal Cancers. *Pathol. Oncol. Res.* **2016**, *22*, 95–102. [[CrossRef](#)]



101. Zhang, K.; Wang, J.; Tong, T.R.; Wu, X.; Nelson, R.; Yuan, Y.C.; Reno, T.; Liu, Z.; Yun, X.; Kim, J.Y.; et al. Loss of H2B monoubiquitination is associated with poor-differentiation and enhanced malignancy of lung adenocarcinoma. *Int. J. Cancer* **2017**, *141*, 766–777. [\[CrossRef\]](#) [\[PubMed\]](#)
102. Wang, Z.J.; Yang, J.L.; Wang, Y.P.; Lou, J.Y.; Chen, J.; Liu, C.; Guo, L.D. Decreased histone H2B monoubiquitination in malignant gastric carcinoma. *World J. Gastroenterol.* **2013**, *19*, 8099–8107. [\[CrossRef\]](#) [\[PubMed\]](#)
103. Lee, J.H.; Jeon, Y.G.; Lee, K.H.; Lee, H.W.; Park, J.; Jang, H.; Kang, M.; Lee, H.S.; Cho, H.J.; Nam, D.H.; et al. RNF20 suppresses tumorigenesis by inhibiting the SREBP1c-PTTG1 axis in kidney cancer. *Mol. Cell. Biol.* **2017**, *37*. [\[CrossRef\]](#)
104. Zheng, X.; Chen, K.; Liu, X.; Pan, Y.; Liu, H. High RNF40 expression indicates poor prognosis of hepatocellular carcinoma. *Int. J. Clin. Exp. Pathol.* **2018**, *11*, 2901–2906.
105. Medzhitov, R. Inflammation 2010: New adventures of an old flame. *Cell* **2010**, *140*, 771–776. [\[CrossRef\]](#) [\[PubMed\]](#)
106. Abdalla, L.F.; Chaudhry Ehsanullah, R.; Karim, F.; Oyewande, A.A.; Khan, S. Role of using nonsteroidal anti-inflammatory drugs in chemoprevention of colon cancer in patients with inflammatory bowel disease. *Cureus* **2020**, *12*, e8240. [\[CrossRef\]](#)
107. Kimmel, J.; Axelrad, J. The complex interplay between inflammatory bowel disease and malignancy. *Curr. Gastroenterol. Rep.* **2020**, *22*, 13. [\[CrossRef\]](#) [\[PubMed\]](#)
108. Hirano, T.; Hirayama, D.; Wagatsuma, K.; Yamakawa, T.; Yokoyama, Y.; Nakase, H. Immunological mechanisms in inflammation-associated colon carcinogenesis. *Int. J. Mol. Sci.* **2020**, *21*, 3062. [\[CrossRef\]](#)
109. Greuter, T.; Vavricka, S.; König, A.O.; Beaugerie, L.; Scharl, M. Malignancies in inflammatory bowel disease. *Digestion* **2020**, 1–10. [\[CrossRef\]](#)
110. Ben-Neriah, Y.; Karin, M. Inflammation meets cancer, with NF- $\kappa$ B as the matchmaker. *Nat. Immunol.* **2011**, *12*, 715–723. [\[CrossRef\]](#)
111. Hartman, Z.C.; Poage, G.M.; den Hollander, P.; Tsimelzon, A.; Hill, J.; Panupinthu, N.; Zhang, Y.; Mazumdar, A.; Hilsenbeck, S.G.; Mills, G.B.; et al. Growth of triple-negative breast cancer cells relies upon coordinate autocrine expression of the proinflammatory cytokines IL-6 and IL-8. *Cancer Res.* **2013**, *73*, 3470–3480. [\[CrossRef\]](#) [\[PubMed\]](#)
112. Wegwitz, F.; Prokakis, E.; Pejkovska, A.; Kosinsky, R.L.; Glatzel, M.; Pantel, K.; Wikman, H.; Johnsen, S.A. The histone H2B ubiquitin ligase RNF40 is required for HER2-driven mammary tumorigenesis. *Cell Death Dis.* **2020**, *11*, 873. [\[CrossRef\]](#) [\[PubMed\]](#)
113. Labidi-Galy, S.I.; Papp, E.; Hallberg, D.; Niknafs, N.; Adleff, V.; Noe, M.; Bhattacharya, R.; Novak, M.; Jones, S.; Phallen, J.; et al. High grade serous ovarian carcinomas originate in the fallopian tube. *Nat. Commun.* **2017**, *8*, 1093. [\[CrossRef\]](#) [\[PubMed\]](#)
114. Zhang, S.; Dolgalev, I.; Zhang, T.; Ran, H.; Levine, D.A.; Neel, B.G. Both fallopian tube and ovarian surface epithelium are cells-of-origin for high-grade serous ovarian carcinoma. *Nat. Commun.* **2019**, *10*, 5367. [\[CrossRef\]](#) [\[PubMed\]](#)
115. Chernikova, S.B.; Razorenova, O.V.; Higgins, J.P.; Sishc, B.J.; Nicolau, M.; Dorth, J.A.; Chernikova, D.A.; Kwok, S.; Brooks, J.D.; Bailey, S.M.; et al. Deficiency in mammalian histone H2B ubiquitin ligase Bre1 (Rnf20/Rnf40) leads to replication stress and chromosomal instability. *Cancer Res.* **2012**, *72*, 2111–2119. [\[CrossRef\]](#)
116. Liu, Z.; Oh, S.M.; Okada, M.; Liu, X.; Cheng, D.; Peng, J.; Brat, D.J.; Sun, S.Y.; Zhou, W.; Gu, W.; et al. Human BRE1 is an E3 ubiquitin ligase for Ebp1 tumor suppressor. *Mol. Biol. Cell* **2009**, *20*, 757–768. [\[CrossRef\]](#)
117. Portney, B.A.; Khatri, R.; Meltzer, W.A.; Mariano, J.M.; Zalzman, M. ZSCAN4 is negatively regulated by the ubiquitin-proteasome system and the E3 ubiquitin ligase RNF20. *Biochem. Biophys. Res. Commun.* **2018**, *498*, 72–78. [\[CrossRef\]](#)
118. Duan, Y.; Huo, D.; Gao, J.; Wu, H.; Ye, Z.; Liu, Z.; Zhang, K.; Shan, L.; Zhou, X.; Wang, Y.; et al. Ubiquitin ligase RNF20/40 facilitates spindle assembly and promotes breast carcinogenesis through stabilizing motor protein Eg5. *Nat. Commun.* **2016**, *7*, 12648. [\[CrossRef\]](#)
119. Chin, L.S.; Vavalle, J.P.; Li, L. Staring, a novel E3 ubiquitin-protein ligase that targets syntaxin 1 for degradation. *J. Biol. Chem.* **2002**, *277*, 35071–35079. [\[CrossRef\]](#)
120. Nakachi, I.; Rice, J.L.; Coldren, C.D.; Edwards, M.G.; Stearman, R.S.; Glidewell, S.C.; Varella-Garcia, M.; Franklin, W.A.; Keith, R.L.; Lewis, M.T.; et al. Application of SNP microarrays to the genome-wide analysis of chromosomal instability in premalignant airway lesions. *Cancer Prev. Res.* **2014**, *7*, 255–265. [\[CrossRef\]](#)

121. Barber, T.D.; McManus, K.; Yuen, K.W.; Reis, M.; Parmigiani, G.; Shen, D.; Barrett, I.; Nouhi, Y.; Spencer, F.; Markowitz, S.; et al. Chromatid cohesion defects may underlie chromosome instability in human colorectal cancers. *Proc. Natl. Acad. Sci. USA* **2008**, *105*, 3443–3448. [[CrossRef](#)] [[PubMed](#)]
122. Tahara, T.; Yamamoto, E.; Madireddi, P.; Suzuki, H.; Maruyama, R.; Chung, W.; Garriga, J.; Jelinek, J.; Yamano, H.O.; Sugai, T.; et al. Colorectal carcinomas with CpG island methylator phenotype 1 frequently contain mutations in chromatin regulators. *Gastroenterology* **2014**, *146*, 530–538.e535. [[CrossRef](#)] [[PubMed](#)]
123. Varambally, S.; Yu, J.; Laxman, B.; Rhodes, D.R.; Mehra, R.; Tomlins, S.A.; Shah, R.B.; Chandran, U.; Monzon, F.A.; Becich, M.J.; et al. Integrative genomic and proteomic analysis of prostate cancer reveals signatures of metastatic progression. *Cancer Cell* **2005**, *8*, 393–406. [[CrossRef](#)] [[PubMed](#)]
124. Kosinsky, R.L.; Chua, R.L.; Qui, M.; Saul, D.; Mehlich, D.; Ströbel, P.; Schildhaus, H.U.; Wegwitz, F.; Faubion, W.A.; Johnsen, S.A. Loss of RNF40 Decreases NF- $\kappa$ B Activity in Colorectal Cancer Cells and Reduces Colitis Burden in Mice. *J. Crohn's Colitis* **2019**, *13*, 362–373. [[CrossRef](#)]
125. Blank, M.; Tang, Y.; Yamashita, M.; Burkett, S.S.; Cheng, S.Y.; Zhang, Y.E. A tumor suppressor function of Smurf2 associated with controlling chromatin landscape and genome stability through RNF20. *Nat. Med.* **2012**, *18*, 227–234. [[CrossRef](#)]
126. Fu, L.; Cui, C.P.; Zhang, X.; Zhang, L. The functions and regulation of Smurfs in cancers. *Semin. Cancer Biol.* **2019**. [[CrossRef](#)]
127. Chernikova, S.B.; Brown, J.M. R-loops and genomic instability in Bre1 (RNF20/40)-deficient cells. *Cell Cycle* **2012**, *11*, 2980–2984. [[CrossRef](#)]
128. Prives, C.; Lowe, S.W. Cancer: Mutant p53 and chromatin regulation. *Nature* **2015**, *525*, 199–200. [[CrossRef](#)]
129. Liptenko, O.; Prives, C. p53: Master of life, death, and the epigenome. *Genes Dev.* **2017**, *31*, 955–956. [[CrossRef](#)]
130. Wu, C.; Cui, Y.; Liu, X.; Zhang, F.; Lu, L.Y.; Yu, X. The RNF20/40 complex regulates p53-dependent gene transcription and mRNA splicing. *J. Mol. Cell Biol.* **2020**, *12*, 113–124. [[CrossRef](#)]
131. Argentini, M.; Barboule, N.; Wasylyk, B. The contribution of the acidic domain of MDM2 to p53 and MDM2 stability. *Oncogene* **2001**, *20*, 1267–1275. [[CrossRef](#)] [[PubMed](#)]
132. Minsky, N.; Oren, M. The RING domain of Mdm2 mediates histone ubiquitylation and transcriptional repression. *Mol. Cell* **2004**, *16*, 631–639. [[CrossRef](#)] [[PubMed](#)]
133. Zhu, B.; Zheng, Y.; Pham, A.D.; Mandal, S.S.; Erdjument-Bromage, H.; Tempst, P.; Reinberg, D. Monoubiquitination of human histone H2B: The factors involved and their roles in HOX gene regulation. *Mol. Cell* **2005**, *20*, 601–611. [[CrossRef](#)] [[PubMed](#)]
134. Mosimann, C.; Hausmann, G.; Basler, K. Parafibromin/Hyrax activates Wnt/Wg target gene transcription by direct association with beta-catenin/Armadillo. *Cell* **2006**, *125*, 327–341. [[CrossRef](#)]
135. Wade, P.A.; Werel, W.; Fentzke, R.C.; Thompson, N.E.; Leykam, J.F.; Burgess, R.R.; Jaehning, J.A.; Burton, Z.F. A novel collection of accessory factors associated with yeast RNA polymerase II. *Protein Expr. Purif.* **1996**, *8*, 85–90. [[CrossRef](#)]
136. Carpten, J.D.; Robbins, C.M.; Villablanca, A.; Forsberg, L.; Presciuttini, S.; Bailey-Wilson, J.; Simonds, W.F.; Gillanders, E.M.; Kennedy, A.M.; Chen, J.D.; et al. HRPT2, encoding parafibromin, is mutated in hyperparathyroidism-jaw tumor syndrome. *Nat. Genet.* **2002**, *32*, 676–680. [[CrossRef](#)]
137. Marsh, D.J.; Hahn, M.A.; Howell, V.M.; Gill, A.J. Molecular diagnosis of primary hyperparathyroidism in familial cancer syndromes. *Expert Opin. Med. Diagn.* **2007**, *1*, 377–392. [[CrossRef](#)]
138. Howell, V.M.; Haven, C.J.; Kahnoski, K.; Khoo, S.K.; Petillo, D.; Chen, J.; Fleuren, G.J.; Robinson, B.G.; Delbridge, L.W.; Philips, J.; et al. HRPT2 mutations are associated with malignancy in sporadic parathyroid tumours. *J. Med. Genet.* **2003**, *40*, 657–663. [[CrossRef](#)]
139. Shattuck, T.M.; Välimäki, S.; Obara, T.; Gaz, R.D.; Clark, O.H.; Shoback, D.; Wierman, M.E.; Tojo, K.; Robbins, C.M.; Carpten, J.D.; et al. Somatic and germ-line mutations of the HRPT2 gene in sporadic parathyroid carcinoma. *N. Engl. J. Med.* **2003**, *349*, 1722–1729. [[CrossRef](#)]
140. Gill, A.J.; Clarkson, A.; Gimm, O.; Keil, J.; Dralle, H.; Howell, V.M.; Marsh, D.J. Loss of nuclear expression of parafibromin distinguishes parathyroid carcinomas and hyperparathyroidism-jaw tumor (HPT-JT) syndrome-related adenomas from sporadic parathyroid adenomas and hyperplasias. *Am. J. Surg. Pathol.* **2006**, *30*, 1140–1149. [[CrossRef](#)]
141. Howell, V.M.; Gill, A.; Clarkson, A.; Nelson, A.E.; Dunne, R.; Delbridge, L.W.; Robinson, B.G.; Teh, B.T.; Gimm, O.; Marsh, D.J. Accuracy of combined protein gene product 9.5 and parafibromin markers for

- immunohistochemical diagnosis of parathyroid carcinoma. *J. Clin. Endocrinol. Metab.* **2009**, *94*, 434–441. [[CrossRef](#)] [[PubMed](#)]
142. Gill, A.J.; Lim, G.; Cheung, V.K.Y.; Andrici, J.; Perry-Keene, J.L.; Paik, J.; Sioson, L.; Clarkson, A.; Sheen, A.; Luxford, C.; et al. Parafibromin-deficient (HPT-JT Type, CDC73 Mutated) parathyroid tumors demonstrate distinctive morphologic features. *Am. J. Surg. Pathol.* **2019**, *43*, 35–46. [[CrossRef](#)] [[PubMed](#)]
  143. Pyo, J.S.; Cho, W.J. Diagnostic and prognostic implications of parafibromin immunohistochemistry in parathyroid carcinoma. *Biosci. Rep.* **2019**, *39*. [[CrossRef](#)] [[PubMed](#)]
  144. Juhlin, C.C.; Nilsson, I.L.; Lagerstedt-Robinson, K.; Stenman, A.; Bränström, R.; Tham, E.; Höög, A. Parafibromin immunostainings of parathyroid tumors in clinical routine: A near-decade experience from a tertiary center. *Mod. Pathol.* **2019**, *32*, 1082–1094. [[CrossRef](#)]
  145. Bell, D.; Berchuck, A.; Birrer, M.; Chien, J.; Cramer, D.; Dao, F.; Dhir, R.; DiSaia, P.; Gabra, H.; Glenn, P.; et al. Integrated genomic analyses of ovarian carcinoma. *Nature* **2011**, *474*, 609–615. [[CrossRef](#)]
  146. Alsop, K.; Fereday, S.; Meldrum, C.; deFazio, A.; Emmanuel, C.; George, J.; Dobrovic, A.; Birrer, M.J.; Webb, P.M.; Stewart, C.; et al. BRCA mutation frequency and patterns of treatment response in BRCA mutation-positive women with ovarian cancer: A report from the Australian Ovarian Cancer Study Group. *J. Clin. Oncol.* **2012**, *30*, 2654–2663. [[CrossRef](#)]
  147. Moschetta, M.; George, A.; Kaye, S.B.; Banerjee, S. BRCA somatic mutations and epigenetic BRCA modifications in serous ovarian cancer. *Ann. Oncol.* **2016**, *27*, 1449–1455. [[CrossRef](#)]
  148. Koboldt, D.C.; Fulton, R.S.; McLellan, M.D.; Schmidt, H.; Kalicki-Veizer, J.; McMichael, J.F.; Fulton, L.L.; Dooling, D.J.; Ding, L.; Mardis, E.R.; et al. Comprehensive molecular portraits of human breast tumours. *Nature* **2012**, *490*, 61–70. [[CrossRef](#)]
  149. Shiovitz, S.; Korde, L.A. Genetics of breast cancer: A topic in evolution. *Ann. Oncol.* **2015**, *26*, 1291–1299. [[CrossRef](#)]
  150. Yoshida, R. Hereditary breast and ovarian cancer (HBOC): Review of its molecular characteristics, screening, treatment, and prognosis. *Breast Cancer* **2020**. [[CrossRef](#)]
  151. Alenezi, W.M.; Fierheller, C.T.; Recio, N.; Tonin, P.N. Literature Review of BARD1 as a Cancer Predisposing Gene with a Focus on Breast and Ovarian Cancers. *Genes* **2020**, *11*, 856. [[CrossRef](#)] [[PubMed](#)]
  152. Mallery, D.L.; Vandenberg, C.J.; Hiom, K. Activation of the E3 ligase function of the BRCA1/BARD1 complex by polyubiquitin chains. *EMBO J.* **2002**, *21*, 6755–6762. [[CrossRef](#)] [[PubMed](#)]
  153. Masliah-Planchon, J.; Bièche, I.; Guinebretière, J.M.; Bourdeaut, F.; Delattre, O. SWI/SNF chromatin remodeling and human malignancies. *Ann. Rev. Pathol.* **2015**, *10*, 145–171. [[CrossRef](#)] [[PubMed](#)]
  154. Alfert, A.; Moreno, N.; Kerl, K. The BAF complex in development and disease. *Epigenet. Chromatin* **2019**, *12*, 19. [[CrossRef](#)] [[PubMed](#)]
  155. Centore, R.C.; Sandoval, G.J.; Soares, L.M.M.; Kadoch, C.; Chan, H.M. Mammalian SWI/SNF Chromatin Remodeling Complexes: Emerging Mechanisms and Therapeutic Strategies. *Trends Genet.* **2020**. [[CrossRef](#)] [[PubMed](#)]
  156. Kadoch, C.; Hargreaves, D.C.; Hodges, C.; Elias, L.; Ho, L.; Ranish, J.; Crabtree, G.R. Proteomic and bioinformatic analysis of mammalian SWI/SNF complexes identifies extensive roles in human malignancy. *Nat. Genet.* **2013**, *45*, 592–601. [[CrossRef](#)]
  157. Li, X.S.; Trojer, P.; Matsumura, T.; Treisman, J.E.; Tanese, N. Mammalian SWI/SNF—a subunit BAF250/ARID1 is an E3 ubiquitin ligase that targets histone H2B. *Mol. Cell. Biol.* **2010**, *30*, 1673–1688. [[CrossRef](#)]
  158. Nicassio, F.; Corrado, N.; Vissers, J.H.; Areces, L.B.; Bergink, S.; Marteijn, J.A.; Geverts, B.; Houtsmuller, A.B.; Vermeulen, W.; Di Fiore, P.P.; et al. Human USP3 is a chromatin modifier required for S phase progression and genome stability. *Curr. Biol.* **2007**, *17*, 1972–1977. [[CrossRef](#)]
  159. van der Knaap, J.A.; Kumar, B.R.; Moshkin, Y.M.; Langenberg, K.; Krijgsveld, J.; Heck, A.J.; Karch, F.; Verrijzer, C.P. GMP synthetase stimulates histone H2B deubiquitylation by the epigenetic silencer USP7. *Mol. Cell* **2005**, *17*, 695–707. [[CrossRef](#)]
  160. Joo, H.Y.; Jones, A.; Yang, C.; Zhai, L.; Smith, A.D.t.; Zhang, Z.; Chandrasekharan, M.B.; Sun, Z.W.; Renfrow, M.B.; Wang, Y.; et al. Regulation of histone H2A and H2B deubiquitination and Xenopus development by USP12 and USP46. *J. Biol. Chem.* **2011**, *286*, 7190–7201. [[CrossRef](#)]
  161. Long, L.; Thelen, J.P.; Furgason, M.; Haj-Yahya, M.; Brik, A.; Cheng, D.; Peng, J.; Yao, T. The U4/U6 recycling factor SART3 has histone chaperone activity and associates with USP15 to regulate H2B deubiquitination. *J. Biol. Chem.* **2014**, *289*, 8916–8930. [[CrossRef](#)] [[PubMed](#)]

162. Zhang, X.Y.; Varthi, M.; Sykes, S.M.; Phillips, C.; Warzecha, C.; Zhu, W.; Wyce, A.; Thorne, A.W.; Berger, S.L.; McMahon, S.B. The putative cancer stem cell marker USP22 is a subunit of the human SAGA complex required for activated transcription and cell-cycle progression. *Mol. Cell* **2008**, *29*, 102–111. [\[CrossRef\]](#) [\[PubMed\]](#)
163. Lan, X.; Atanassov, B.S.; Li, W.; Zhang, Y.; Florens, L.; Mohan, R.D.; Galardy, P.J.; Washburn, M.P.; Workman, J.L.; Dent, S.Y.R. USP44 Is an Integral Component of N-CoR that Contributes to Gene Repression by Deubiquitinating Histone H2B. *Cell Rep.* **2016**, *17*, 2382–2393. [\[CrossRef\]](#) [\[PubMed\]](#)
164. Zhang, Z.; Jones, A.; Joo, H.Y.; Zhou, D.; Cao, Y.; Chen, S.; Erdjument-Bromage, H.; Renfrow, M.; He, H.; Tempst, P.; et al. USP49 deubiquitinates histone H2B and regulates cotranscriptional pre-mRNA splicing. *Genes Dev.* **2013**, *27*, 1581–1595. [\[CrossRef\]](#) [\[PubMed\]](#)
165. Jeusset, L.M.; McManus, K.J. Ubiquitin Specific Peptidase 22 regulates histone H2B mono-ubiquitination and exhibits both oncogenic and tumor suppressor roles in cancer. *Cancers* **2017**, *9*, 167. [\[CrossRef\]](#)
166. Schrecengost, R.S.; Dean, J.L.; Goodwin, J.F.; Schiewer, M.J.; Urban, M.W.; Stanek, T.J.; Sussman, R.T.; Hicks, J.L.; Birbe, R.C.; Draganova-Tacheva, R.A.; et al. USP22 regulates oncogenic signaling pathways to drive lethal cancer progression. *Cancer Res.* **2014**, *74*, 272–286. [\[CrossRef\]](#)
167. Kim, D.; Hong, A.; Park, H.I.; Shin, W.H.; Yoo, L.; Jeon, S.J.; Chung, K.C. Deubiquitinating enzyme USP22 positively regulates c-Myc stability and tumorigenic activity in mammalian and breast cancer cells. *J. Cell. Physiol.* **2017**, *232*, 3664–3676. [\[CrossRef\]](#)
168. Atanassov, B.S.; Dent, S.Y. USP22 regulates cell proliferation by deubiquitinating the transcriptional regulator FBP1. *EMBO Rep.* **2011**, *12*, 924–930. [\[CrossRef\]](#)
169. Baker, S.P.; Grant, P.A. The SAGA continues: Expanding the cellular role of a transcriptional co-activator complex. *Oncogene* **2007**, *26*, 5329–5340. [\[CrossRef\]](#)
170. Morgan, M.T.; Haj-Yahya, M.; Ringel, A.E.; Bandi, P.; Brik, A.; Wolberger, C. Structural basis for histone H2B deubiquitination by the SAGA DUB module. *Science* **2016**, *351*, 725–728. [\[CrossRef\]](#)
171. Lang, G.; Bonnet, J.; Umlauf, D.; Karmodiya, K.; Koffler, J.; Stierle, M.; Devys, D.; Tora, L. The tightly controlled deubiquitination activity of the human SAGA complex differentially modifies distinct gene regulatory elements. *Mol. Cell. Biol.* **2011**, *31*, 3734–3744. [\[CrossRef\]](#) [\[PubMed\]](#)
172. Bonnet, J.; Wang, C.Y.; Baptista, T.; Vincent, S.D.; Hsiao, W.C.; Stierle, M.; Kao, C.F.; Tora, L.; Devys, D. The SAGA coactivator complex acts on the whole transcribed genome and is required for RNA polymerase II transcription. *Genes Dev.* **2014**, *28*, 1999–2012. [\[CrossRef\]](#) [\[PubMed\]](#)
173. Zhang, K.; Yang, L.; Wang, J.; Sun, T.; Guo, Y.; Nelson, R.; Tong, T.R.; Pangen, R.; Salgia, R.; Raz, D.J. Ubiquitin-specific protease 22 is critical to in vivo angiogenesis, growth and metastasis of non-small cell lung cancer. *Cell Commun. Signal.* **2019**, *17*, 167. [\[CrossRef\]](#) [\[PubMed\]](#)
174. Wang, Y.; Sun, Q.; Mu, N.; Sun, X.; Wang, Y.; Fan, S.; Su, L.; Liu, X. The deubiquitinase USP22 regulates PD-L1 degradation in human cancer cells. *Cell Commun. Signal.* **2020**, *18*, 112. [\[CrossRef\]](#)
175. Cortez, J.T.; Montauti, E.; Shifrut, E.; Gatchalian, J.; Zhang, Y.; Shaked, O.; Xu, Y.; Roth, T.L.; Simeonov, D.R.; Zhang, Y.; et al. CRISPR screen in regulatory T cells reveals modulators of Foxp3. *Nature* **2020**, *582*, 416–420. [\[CrossRef\]](#)
176. Yang, J.; Wei, P.; Barbi, J.; Huang, Q.; Yang, E.; Bai, Y.; Nie, J.; Gao, Y.; Tao, J.; Lu, Y.; et al. The deubiquitinase USP44 promotes Treg function during inflammation by preventing FOXP3 degradation. *EMBO Rep.* **2020**, *21*, e50308. [\[CrossRef\]](#)
177. Zhang, H.Y.; Liao, B.W.; Xu, Z.S.; Ran, Y.; Wang, D.P.; Yang, Y.; Luo, W.W.; Wang, Y.Y. USP44 positively regulates innate immune response to DNA viruses through deubiquitinating MTA. *PLoS Pathog.* **2020**, *16*, e1008178. [\[CrossRef\]](#)
178. Nicholson, B.; Suresh Kumar, K.G. The multifaceted roles of USP7: New therapeutic opportunities. *Cell Biochem. Biophys.* **2011**, *60*, 61–68. [\[CrossRef\]](#)

**Publisher's Note:** MDPI stays neutral with regard to jurisdictional claims in published maps and institutional affiliations.



© 2020 by the authors. Licensee MDPI, Basel, Switzerland. This article is an open access article distributed under the terms and conditions of the Creative Commons Attribution (CC BY) license (<http://creativecommons.org/licenses/by/4.0/>).